UTM
UNIVERSITI TEKNOLOGI MALAYSIA
Faculty of
Electrical Engineering

# Proceedings of 2017 Electrical Engineering Symposium (EES2017) - Vol. 2

# PROCEEDINGS OF 2017 ELECTRICAL ENGINEERING SYMPOSIUM (EES2017)

## VOLUME 2

First Edition 2017



Diterbitkan oleh: Fakulti Kejuruteraan Elektrik, Universiti Teknologi Malaysia, 81310 Johor Bahru Johor, Malaysia

# PREFACE

This book introduces several research works from final year undergraduate project till the level of master project by taught course. The projects have been evaluated by industries as well as academician to ensure that its fulfill the standard of each level before it can be published. The text emphasizes the combination of the research material in different field of engineering generally in power, electronic, communication, control and mechatronic which hampered by three main program offered by Faculty of Electrical Engineering.

This book is generally suitable as an accompaniment to students and researchers that generally involved with different field of study including modeling and control design for various example of application. There are also research on hardware design implementation which integrate both for simulation and experimental study as well as laboratory sessions available at a particular institution.

Mohamad Kamal A. Rahim
Md. Pauzi Abdullah
Faculty of Electrical Engineering
Universiti Teknologi Malaysia

# 2017 ELECTRICAL ENGINEERING SYMPOSIUM COMMITTEE

**GENERAL CHAIR**

PROFESSOR DR. MOHAMAD KAMAL A. RAHIM

**CO-CHAIR**

IR. DR. MD. PAUZI ABDULLAH

**2017 ELECTRICAL ENGINEERING SYMPOSIUM MEMBERS**

DR. KAMALUDIN MOHD. YUSOF

DR. SHAHARIN FADZLI ABD. RAHMAN

DR. YUSMEERAZ YUSOF

DR. MOHD. HAFIZI AHMAD

DR. NURUL EZAILA ALIAS

DR. ZULKARNAIN AHMAD NOORDEN

DR. MOHD. AFZAN OTHMAN

DR. MOHD. AMRI MD. YUNUS

DR. MOHD. RASHIDI SALIM

**2017 ELECTRICAL ENGINEERING SYMPOSIUM SECRETARIAT STAFF**

SABRINA ZAINAL ABIDIN

AZLINA MOHD. LAZIM

# Dual Band Antenna Array Incorporated With Hexagonal-Slotted Patch Electromagnetic Band Gap Structure

Nur Zurina Bt Mohd Jasmi
*Faculty of Electrical Engineering*
*Universiti Teknologi Malaysia*
*Johor Bahru, Malaysia.*
*zurina5628@gmail.com*

Osman bin Ayop
*Department of Communication Engineering*
*Faculty of Electrical Engineering*
*Universiti Teknologi Malaysia*
*Johor Bahru, Malaysia.*
*osman@fke.utm.my*

***Abstract*— In this paper, the new structure of electromagnetic band gap (EBG) is introduced which namely hexagonal-slotted patch electromagnetic band gap (hexagonal-spEBG) due to its hexagon shape. This hexagonal-spEBG structure is being incorporated with a dual band antenna operating at frequency of 2.4 GHz and 5.8 GHz. The result of this structure is presented in term of return loss $S_{11}$ and radiation pattern for dual band antenna array and forward transmission coefficient, $S_{21}$ for the hexagonal-spEBG structure. The simulations of the designed structures are done using CST software. The new shape of EBG is capable to reject dual frequency bands compared to the conventional mushroom-EBG structure which is rejecting only one frequency band. The hexagonal-spEBG structure has been simulated to operate at 2.4 GHz and then the size is altered to operate at 5.8 GHz. From the simulated result, a promising result is obtained when incorporate the hexagonal-spEBG structure with the dual-band antenna array.**

***Keywords—Dual Band Antenna Array; Electromagnetic Band Gap; Band Rejector; Gain enhancement***

## I. INTRODUCTION

Nowadays, researches on dual band antenna arrays are very popular. This is due to its ability to work at two frequency bands so that different communication standards can be used for the same device. The application of wireless communication system such as IEEE 802.11n systems requires at least two frequencies to simultaneously transmit and receive signals. This is quite challenging when there are two different types or shapes of radiating elements working at two different frequencies are being integrated as one array formation. The results for having accurate reading in certain frequency and uniform radiation patterns are tricky to achieve.

The mutual coupling for the microstrip patch antennas exist other than acting as parasitic elements when it is not resonating. This is because the lower band radiating elements shows a higher (harmonics) resonant frequencies and it will degrades the antennas radiation pattern if there is another resonance at the intended second band frequency operation with a different phase [1]. This matter will occur in dual band microstrip patch antenna array and to solve this problem, the innovative technique is introduced by incorporating the new structure of electromagnetic band gap into the antenna array as a band rejecter.

The selection of EBG structure for incorporation with dual band antenna array is due to its special behavior, which is the rejection band capability. The research on electromagnetic band gap structures, since many years have been increased among the electromagnetic and antenna community. This is due to its huge potential and their advantages toward antenna such as to suppress the surface wave current, increase the antenna efficiency and improve the radiation pattern. [2, 3]. The electromagnetic properties of the EBG unit cells can be described using lump-circuit elements that are capacitors and inductors as shown in Figure 1 [4]. The EBG structure for the Figure 1 is also known as mushroom-like EBG structure [5] with a unit cell as shown in Figure 2.

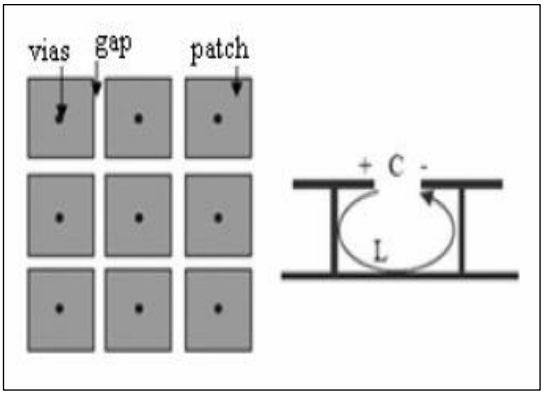


**Figure 1: 2D mushroom like-EBG structure [4]**

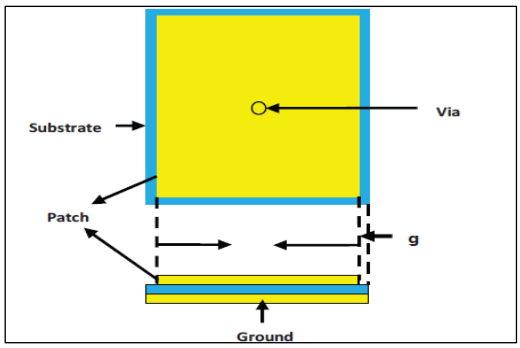


**Figure 2: A unit cell of mushroom-like EBG structure [5]**

## II. DUAL BAND ANTENNA ARRAY

One of the examples of dual band antenna array is a multi-layer antenna microstrip structure for the whole build-up. The upper layer composite is an aperture coupled microstrip antenna array operating at the high frequency band while the bottom layer is operating at the lower frequency [6]. In order to separate the upper array feeding network and the lower radiating array elements, a dielectric material is inserted between the sub-antenna arrays and the array are arranged cross-polarizationally stacked. Then the sub-antennas have separated feeding networks and the antennas are operated independently. The main objective of the discussed dual band antenna array is to minimize the mutual coupling between the sub-antennas [7]. In this research, the dual band antenna array which can operate at 2.4 GHz and 5.8 GHz is proposed using the combination of insert fed microstrip patch antenna.

## III. DESIGN CONSIDERATION

### *A. Dual band antenna array*

The proposed dual band antenna array has been designed using 1.6 mm thick FR4 board with relative permittivity of 4.6 and tangent loss of 0.019. The dual band antenna is designed using double layer FR4 substrate with the same thickness which means 3.2 mm because this antenna will be incorporated hexagonal-spEBG later on. Figure 3 is presenting the overall simulated dual band antenna array structure and also their dimensions.

This Figure 3 also shows the dual band antenna array is designed using a combination of 2 insert fed microstrip patch antenna at the frequency of 2.4 GHz and 2 inset fed microstrip patch antenna at the frequency 5.8 GHz. The patch is combined together and corporate using transmission line feeds. The initial configuration of dual band microstrip antenna array is initially designed separately to their respective frequency of operation at 2.4 GHz and 5.8 GHz, and then they are combined together to form one array formation upon optimization.

A single sub-miniature version A (SMA) port is also designed as its main feed connecting the branch of combined non-symmetry corporate insert feed network. The 50 Ohm transmission line feed that is connecting to the 5.8 GHz patches has been introduced. The approximation of the microstrip patch antenna size is obtained using specific formula and then the size has been adjusted as shown in Figure 3 to obtain the desired operating frequency.

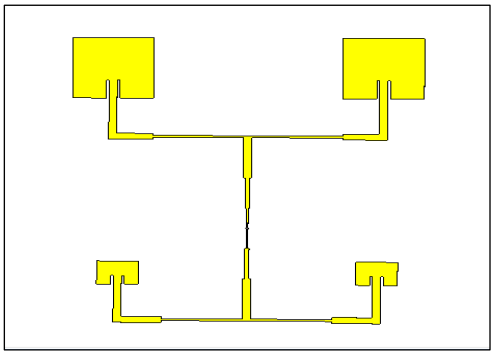

**Figure 3: Dual band antenna array**

After obtain the optimize shape of dual band antenna array through simulation process using CST software, the antenna is then incorporated with hexagonal-spEBG structure to achieve the objective of this research.

### *B. The single hexagonal-spEBG structure at 2.4 GHz*

The hexagonal-spEBG has been designed as dual band rejecter as shown in Figure 4. The new shaped of slotted patch EBG has been proposed in the hexagon shape patch with double C slots. This structure has been placed between the transmission line and the ground plane of the dual band antenna array. The substrate used is FR4 with the same specification as dual band antenna array. It has been designed at two operating frequencies which is 2.4 GHz and 5.8 GHz. The hexagonal-spEBG patches are placed beneath a transmission line. The hexagonal-spEBG is grounded to the ground plane of the dual band antenna array with metallic via. The overall size of the substrate with the hexagonal-spEBG structure is the same with the overall antenna size. This is because this structure will be used as artificial ground plane of the dual band antenna array structure when the structure is combined together. The size of the ground plane is 50 × 50 mm. For the single slot of 2.4 GHz, the size of the hexagon shape hexagonal-spEBG is 6.9 mm for the outer radius, 6 × 6 mm for the inner patch and 1 mm for the slot width with the C shapes. The 3 mm width transmission line has been used to transmit EM waves using two SMA connectors and the $S_{21}$ value is determined.

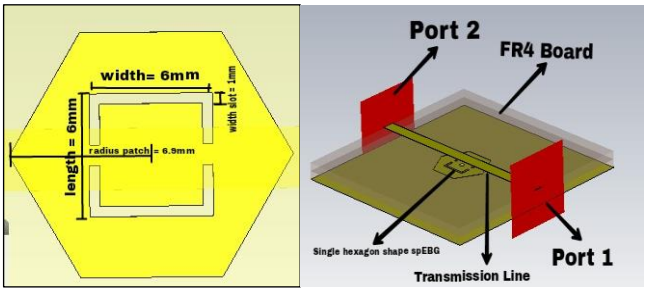


**Figure 4: A unit cell of hexagonal-spEBG structure at 2.4GHz**

*C. 3 by 3 slotted patches EBG at 5.8 GHz*

For this structure, the specification of the substrate used is same with single hexagonal-spEBG except the size of the hexagonal-spEBG patches. In Figure 5, the single slot of 5.8 GHz, the size of the hexagon shape spEBG is 1.9 mm for the outer radius, 2 × 2 mm for the inner patch, 1 mm for the slot width with the C shapes and the gap between element is 1mm. The 3 mm width transmission line was used to transmit EM waves using two SMA connectors and the $S_{21}$ value was determined.

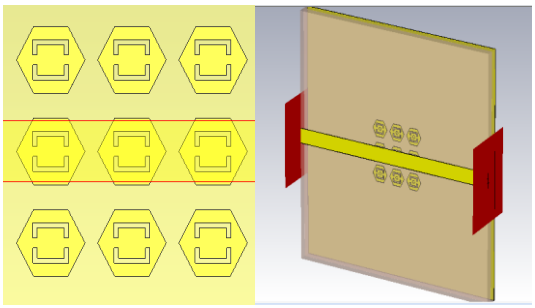

**Figure 5: 3 by 3 hexagonal-spEBG structure at 5.8GHz**

*D. Dual band antenna array with hexagonal-spEBG structure*

The last part of the work is the incorporation of the hexagon-spEBG structure together with dual band antenna array. The configuration of the structure is shown in Figure 6. The hexagonal-spEBG structures are placed beneath the transmission line as same as the simulation of single hexagonal-spEBG patch. Then, the structure is simulated and the $S_{11}$ value is compared with the dual band antenna array without incorporated with hexagon-spEBG structure.

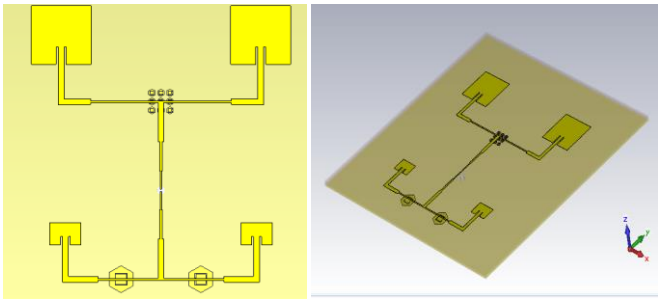

**Figure 6: Dual band antenna array with hexagonal-spEBG structure**

## IV. Result and Discussion

The simulation results of the structures have been done using CST software. The structure of the dual band antenna array has been simulated to investigate the performance of return loss, $S_{11}$. The return loss value provides the information of the impedance bandwidth which is the ranges of the operating frequency of dual band antenna array. The -10dB impedance bandwidth is used in this design where at least 90% of the power will be radiated by the antenna patch. For the hexagonal-spEBG structure, the analysis of forward transmission coefficient $S_{21}$ has been conducted to determine the frequency stop band for band rejection of dual band antenna array

*A. Dual band antenna array*

Figure 7 shows the simulated return loss, $S_{11}$ of dual band antenna array without incorporation with hexagonal-spEBG structure. From the simulated result, the dual band antenna array resonates at 2.4 GHz and 5.8 GHz. The same size of this dual band antenna array is used during the incorporation with the hexagon-spEBG later on and the result will be presented.

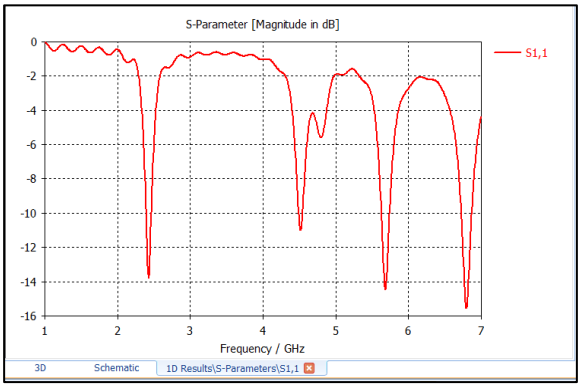


**Figure 7: The simulated $S_{11}$ for dual band antenna array**

*B. Single Hexagonal-spEBG at 2.4 GHz*

Figure 8 below shows the simulated result of forward transmission line, $S_{21}$ for single hexagon-spEBG structure. From the simulation, the resonance frequency of hexagonal-spEBG structure is 2.4GHz.

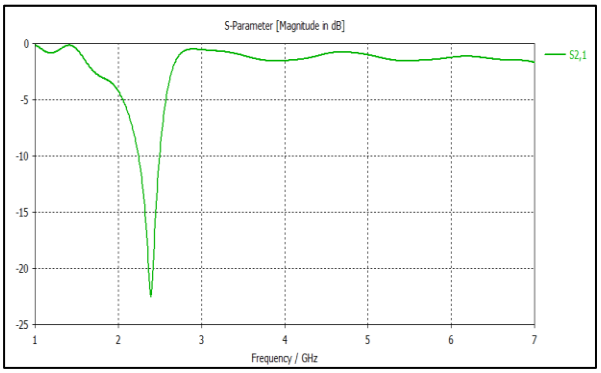


**Figure 8: Transmission coefficient $S_{21}$ (dB) of hexagonal-spEBG at 2.4GHz**

### *C. 3 by 3 Hexagonal-spEBG at 5.8 GHz*

Figure 9 shows the simulated result of forward transmission line, $S_{21}$ for 3 by 3 hexagon-spEBG structure. From the simulation, the resonance frequency of the hexagonal-spEBG structure is 5.8GHz.

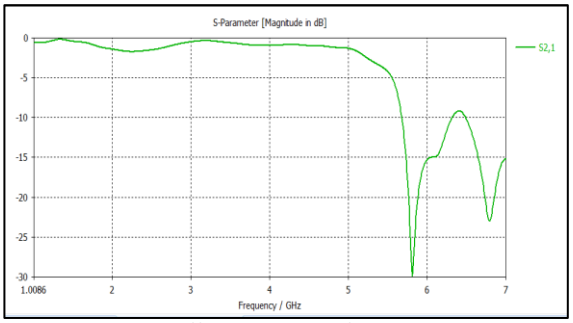


**Figure 9: Transmission coefficient $S_{21}$ (dB) of 3x3 slotted patch EBG at 5.8GHz**

### *D. Incorporation of Dual Band Antenna Array with Hexagonal-spEBG*

Figure 10 shows the simulated return loss $S_{11}$ for dual band antenna array with and without hexagonal-spEBG structure. From the figure, it can be seen that the resonant frequencies at 2.4 GHz and 5.8 GHz of the dual band antenna array has been improved by incorporating the antenna with the hexagonal-spEBG.

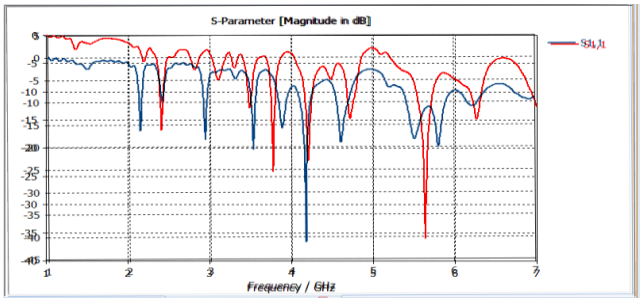


**Figure 10: Simulation return loss $S_{11}$ for dual band antenna array with and without hexagonal-spEBG (Red-with; blue-without)**

| | E FIELD | H FIELD |
|---|---|---|
| Dual band antenna array with spEBG | 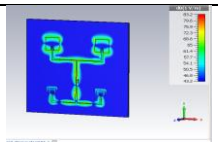 2.4GHz | 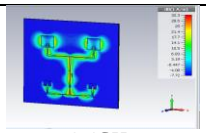 2.4GHz |
| | 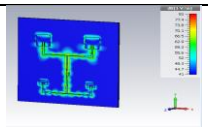 5.8GHz | 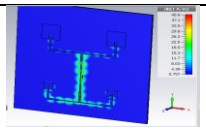 5.8GHz |
| Dual band antenna array without spEBG | 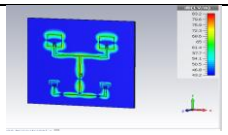 2.4GHz | 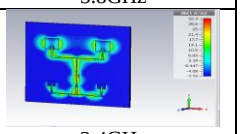 2.4GHz |
| | 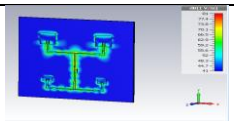 5.8GHz | 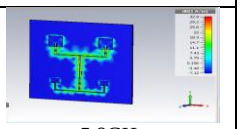 5.8GHz |

**Table 1: E-field and H-field current distribution for dual band antenna array with and without spEBG**

The comparisons between dual band antenna array with and without hexagonal-spEBG structure are made in term of E-field and H-field current distribution. From the Table 1, it shows that the E field and H-field current distribution are strong at all the antenna patches for 2.4 GHz and 5.8 GHz resonant for dual band antenna array. For dual band antenna array incorporated with hexagonal-spEBG, at 2.4 GHz resonant, the current only strong at larger patches array (designed for 2.4 GHz) because the hexagonal-spEBG is rejecting the frequency band of 2.4 GHz from flowing at the smaller patches array (designed for 5.8 GHz). The same case happened at resonant frequency of 5.8 GHz.

## V. CONCLUSION

The new application of electromagnetic band gap (EBG) structure has been discussed in this paper. Other than suppressing surface waves, reducing mutual coupling, provides in phase reflection for antenna design and the other, the unique properties of EBG structure especially their band gap frequency make it possible for other antenna application.

## AKNOWLEDGEMENTL

The authors thanks to her supervisor, Dr. Osman bin Ayop, her parent and her fellow friend for their guidance and support to conduct this research.

## REFERENCES

[1] T. Masri, M. K. A. Rahim and O. Ayop, "Dual band microstrip array antenna radiation characteristics enhancement via novel band rejection technique using EBG structures," *2008 Asia-Pacific Microwave Conference*, Macau, 2008, pp. 1-4..

[2] Fan Yang and Yahya Rahmat-Samii, "Mutual Coupling Reduction of Microstrip Antennas Using Electromagnetic Band-Gap Structure",*2001 IEEE AP-S Digest*, vol. 2, pp. 478-481, July 2001.

[3] Fan Yang, Chul-Sik Kee, and Yahya Rahmatsamii, “Step-Like Structure and EBG Structure to Improve the Performance of Patch Antennas on High Dielectric Substrate”, *2001 IEEE AP-S Digest*. vol 2, pp. 482-485, July 2001

[4] Fan Yang and Yahya Rahmat-Samii, “A Mushroom-Like Electromagnetic Band-Gap (EBG) Structure: Band Gap Characterization and Antenna Applications”, *2002 URSI digest*, pp. 225, June 2002

[5] S. M. Umar, F. Ahmad, W. U. R. Khan and S. Ullah, "Specific absorption rate analysis of a WLAN antenna using mushroom-type electromagnetic bandgap (EBG) structure," *2016 13th International Bhurban Conference on Applied Sciences and Technology (IBCAST)*, Islamabad, 2016, pp. 631-635

[6] Tungshing Chan and Yeongming Hwang, "A dual-band microstrip array antenna," *IEEE Antennas and Propagation Society International Symposium. 1995 Digest*, Newport Beach, CA, USA, 1995, pp. 2132-2135 vol.4

[7] O. Ayop, M. K. A. Rahim and T. Masri, "Dual band Electromagnetic Band Gap (EBG) structure," *2007 Asia-Pacific Conference on Applied Electromagnetics*, Melaka, 2007, pp. 1-3.

[8] T. Masri and M. K. A. Rahim, "Dual-band microstrip antenna array with a combination of mushroom, modified Minkowski and Sierpinski electromagnetic band gap structures," in *IET Microwaves, Antennas & Propagation*, vol. 4, no. 11, pp. 1756-1763, November 2010.

[9] O. Ayop, M. K. A. Rahim, M. R. Kamarudin, M. Z. A. A. Aziz and M. Abu, "Dual band electromagnetic band gap structure incorporated with ultra-wideband antenna," *Proceedings of the Fourth European Conference on Antennas and Propagation*, Barcelona, Spain, 2010, pp. 1-4.

# Highly Efficient Power Amplifiers

Reuban Rao Radhakrishnan
*Faculty of Electrical Engineering*
*Universiti Teknologi Malaysia*
*Johor Bahru, Malaysia.*
*reubanrao93@gmail.com*

Farid Zubir
*Department of Communication Engineering*
*Faculty of Electrical Engineering*
*Universiti Teknologi Malaysia*
*Johor Bahru, Malaysia.*
*faridzubir@utm.my*

***Abstract*—Sustainability is currently becoming a trend in technologies such as telecommunications. The goal is to reduce power consumption and increase the battery life of mobile nodes. The highest power consumer in the telecommunication module, the power amplifiers were designed using inefficient configurations as the older emphasization is only to achieve highest linearity possible at the output. This dissertation proposes designs for Class E power amplifiers operating at 2.4 GHz based on nonlinear SPICE FET models using two different Sokal's empirical equations. One emphasizes considerations of output power with loaded quality factor, the other does not. Clear differences can be observed through simulation results as the newer Sokal's equation proved to be more efficient. This analytical solution can be used to design future power amplifiers where efficiency is the prime concern.**

***Keywords—ClassE; SPICE Models; Field Effect Transistors; 2.4Ghz***

## I. INTRODUCTION

With the world moving towards the era of 5G networks where the means of communication can soon extend between 50 billion devices, technological trends are now looking into better coverage, low power consumption and more connected devices [1]. In concurrent to this future, power wastages are tackled vigorously and key components in the communication modules which are heavily power dependent are introduced with new types of highly efficient configurations. From these modules, the highest power consumer is the power transistor in the power amplifier [2]. Qin [3] stated that power amplifiers that are highly efficient always sought for because of these devices tend to have longer battery life, reduced power dissipation and are generally smaller in size. Conventional classes of power amplifiers are used in current generation RF and microwave systems wastes most of its input power in forms of energy dissipation of heat which cannot be avoided due to the very nature of power components used to drive amplification models [4]. Switching mode amplifier such as the Class E has potential to provide a solution to the above as it has a theoretical efficiency of 100%. This would reduce the power wastage compared to conventional power amplifiers. This work looks into aspects of switching mode power amplifiers which is theoretically able to achieve 100% efficiency. In comparison, commercial power amplifiers used in the current designs only can operate with the highest achievable power added efficiency, (PAE) of merely 50%. Switching mode amplifiers such as Class E or Class F are not preferred by RF circuit designers due to its highly non-linear behaviour. However, this disadvantage can be solved by using linearization techniques such as pre-distortion or feedback/feed forward techniques. In practicality, there is always tradeoffs between achieving high PAE and output power which will be proved in this paper. Besides that, investigations towards intermodulation distortion, (IMD) will be conducted across power amplifier configurations. It would be such a waste to discard a power amplifier that has very high potential in conserving energy such as the switching mode amplifier.

## II. ANALYTICAL SOLUTION

### A. Class E Power Amplifier Background

The general approach designing a Class E amplifier is by looking into the works of Nathan O. Sokal, one of the key founders of the Class E configuration. Nathan has introduced several empirical equations which has been fine-tuned over the years to achieve a much more reliable and accurate result. These equations give the value of passive components in ($R_{load}$,$L_s$,$C_s$and $C_p$) which induces a non-overlapping current and voltage waveform, vital to sustain a high PAE [2]. Figure 1 illustrates the general schematic of the Class E amplifier.

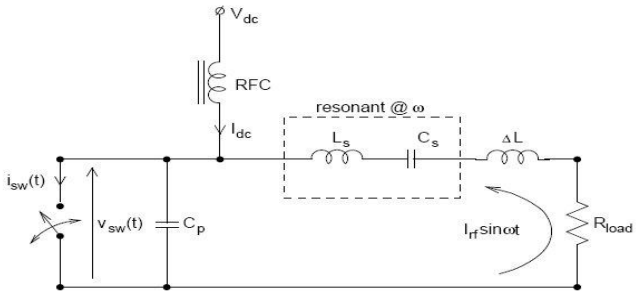


Fig. 1. Basic arrangement of a Class E power amplifier.

### B. Passive Element Design

Iruan [5], has designed the passive components based on older version of Sokal's empirical equation listed below as equations (1) to (3). All values of passive components can be calculated except for $R_{load}$. By practicality, designer would prefer to choose $R_{load}$= 50Ω. Sokal [2] claimed, output power deteriorates between 10% to 38% of expected result for values of $Q_L$ from 1.7678 to 5 using the older equations prior to his. In

the newer formula, the values of $Q_L$ should be chosen above 1.7678 to avoid zero division for resonator capacitor, $C_S$.

$$C_P = \frac{1}{2\pi f R\left(\frac{\pi^2}{4}+1\right)\left(\frac{\pi}{2}\right)} \quad (1)$$

$$C_S = C_P\left(\frac{5.447}{Q_L}\right)\left(1+\frac{1.153}{Q_L-1.153}\right) \quad (2)$$

$$L_S = \frac{Q_L R}{\omega} \quad (3)$$

Sokal's new equations put heavy consideration to output power with correlation to quality factor to produce a much accurate result. However, the equation to calculate $L_S$ is similar with the older equation.

$$R_{LOAD} = 0.5786\left(\frac{{V_{DD}}^2}{P_{OUT}}\right)\left(1-\frac{0.451759}{Q_L}-\frac{0.402444}{{Q_L}^2}\right) \quad (4)$$

$$C_P = \frac{1}{5.44668\omega R}\left(1+\frac{0.91424}{Q_L}-\frac{1.03175}{{Q_L}^2}\right)+\frac{0.6}{\omega^2 L_S} \quad (5)$$

$$C_S = \frac{1}{\omega R}\left(\frac{1}{Q_L-0.104823}\right)\left(1+\frac{1.101468}{Q_L-1.7879}\right)-\frac{0.2}{\omega^2 L_S} \quad (6)$$

In this work, the aim is to build a Class E power amplifier with the design specifications tabulated in Table I. Input power ranging from -20dBm to 50dBm is injected to the circuit to identify which specific input power can produce either high PAE (between 60% to 100%), high output power, or even both. However, there will be tradeoffs between high output power and high PAE which will be discussed in the later sections.

TABLE I. DESIGN SPECIFICATION FOR CLASS E AMPLIFIERS

| Parameters | Proposed Class E Circuit Specifications |
|---|---|
| Operating Frequency | 2.4Ghz |
| FET Models | STAZ, CURTICE2, TQ_MATRK |
| Minimum PAE | 60% - 100% |
| Loaded quality factor | 7 |
| Input power | -20dBm to 50dBm |

The values for passive components are calculated using equations (1) to (6) as shown in Table II. As discussed in the previous section, the value for the passive component. $R_{load}$ is chosen as 50Ω and the resonator inductor,$L_s$ are same for both equations. By rule of thumb, RFC should be at least 30 times more than the resonator inductor, $L_s$ [6].

TABLE II. CALCULATED PASSIVE COMPONENT VALUE BASED ON PRIOP AND NEWER VERSION

| Passive component values | Passive component values based on equations (1) - (3) | Passive component values based on equations (4) - (6) |
|---|---|---|
| $R_{load}$ | 50Ω | 50Ω |
| $L_s$, | 23.21nH | 23.21nH |
| $C_s$ | 0.2433pF | 0.2701pF |
| $C_p$ | 0.22685pF | 0.23299pF |

To control the harmonics, the resonator circuit denoted by $L_s$ and $C_s$ provides a condition of circuit where it is short at the fundamental frequency and open at the harmonics. As a comparison, a Class B configurations requires to be short circuited at the harmonics [7, 8]. Based on Figure 1 there is a requirement for selecting a type of switching device. We have decided to use the field effect transistor (FET) as the switching device of choice because of ease of use and high ratio of ON and OFF state resistance [3]. Power amplifiers generally are designed with FETs thus it best in this dissertation the FET is used as the switching device to understand how suitable is this element in a Class E configuration. To determine whether a configuration is operating in Class E, we can look at the output waveform as a conclusive factor besides a high PAE. Due to the switching nature of Class E power amplifier, there can be no coexisting current and voltage at any instantaneous time resulting in the theoretical efficiency of 100%. The circuit should either conducts maximum current swing during the transistor ON period with voltage almost zero, charging the parallel capacitor, $C_s$. After presumably 50% duty cycle, transistor goes to OFF state where capacitor, $C_s$ discharges to the load resulting in maximum voltage swing, with current almost zero. One important criteria worth mentioning is the simplicity of the Class E design compared to other switching power amplifiers such as the Class F or Class $F^{-1}$. The small number of reactive capacitance of Class E amplifier can be easily absorbed as part of the output matching network. Figure 2 shows the typical output waveform of a Class E amplifier which shows no over-lapping between voltages and currents waveforms. Thus, there is no product of power (P = VI) which results in no power dissipation hence efficiencies reach 100%, theoretically.

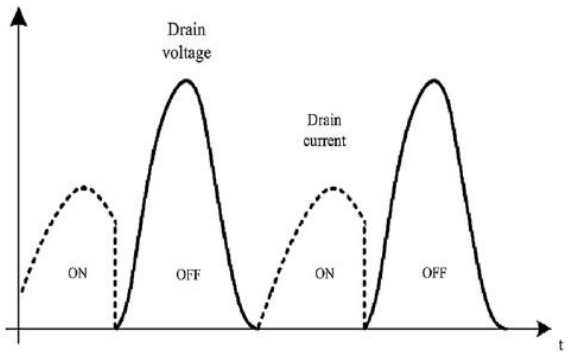


Fig. 2. Class E output waveforms.

## III. SIMULATION AND ANALYSIS

### A. Simulator Circuit Design

By rule of thumb, the FET must be driven in the saturation region to function in switching mode. $V_{GS}$ was chosen at the saturation level on the load line with highest $V_{DS}$ curve to achieve maximum output voltage and current swings. However, it is important to make sure $V_{GS}$ value chosen is not too low (below threshold voltage) which causes the FET to not even turn on. Each of the FET stated above have their own specific $V_{GS}$ and $V_{DS}$ with swept input power (-20dbm to 50dBm) and

operating at 2.4 GHz matched with Class E passive elements calculated (Table II). Figure 3 illustrates the STAZ Class E power amplifier designed using the AWR MWO simulator. An HBTuner is used to replace the input matching network for ease and simplicity. Values of passive component calculated in Section 2.3 are loaded as the output matching network (OMN).

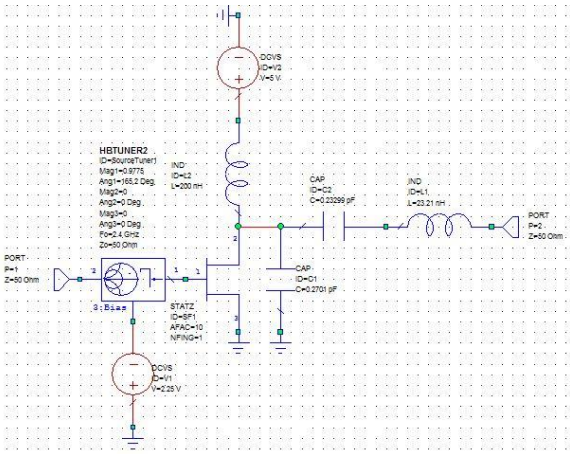


Fig. 3. SSTAZ Class E circuit topology with HBTUNER IMN and calculated OMN.

A reference model without the passive elements is also designed as a comparison with other circuits. All three circuits will be compared for their performances which are the circuit designed based on older equations, the circuit designed based on Sokal's newer equation and the reference circuit with no OMN.

### *B. Simulation Result*

Figure 4 shows the PAE with swept input power for the STAZ FET circuit for all three types of configurations. This circuit is able to achieve PAE as high as 97.2% for the input power (Pin) of 30dBm at 2.4 GHz utilizing Sokal's newer equations. Non-overlapping current waveforms can also be observed on the FET's output as shown in Figure 5. Current swing for the STAZ amplifier peaks at 144.6mA and voltage swing peaks at 17.831V with little overlapping. In all three FET Class E designs, the newer Sokal's equations produces the highest PAE. However, performance varies across the other FET models. Table III displays comparisons between the three models. The CURTICE 2 circuit has a PAE of 68.21% as its highest providing injection power is set at 26dBm.

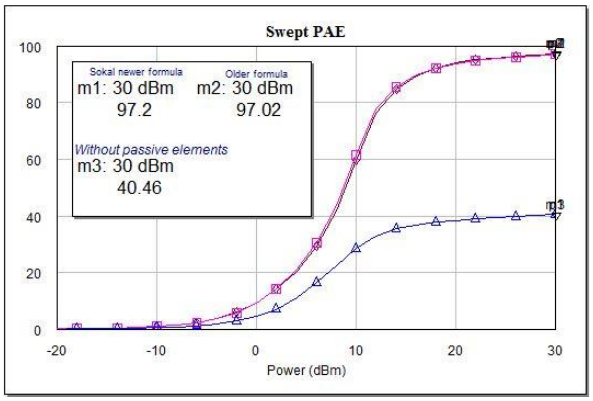


Fig. 4. PAEs for STAZ model with 30dBm injection power.

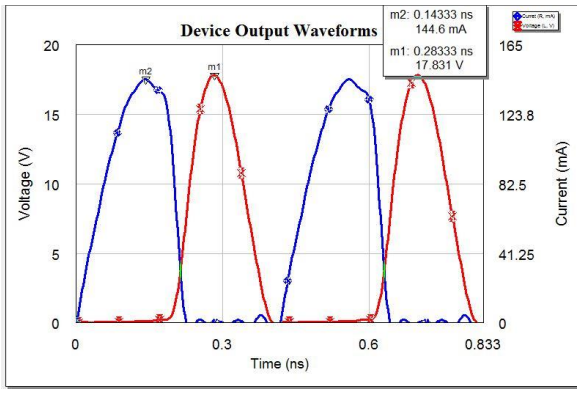


Fig. 5. STAZ non-overlapping waveform output.

The TQ_MATRK requires a much lower input power of 4dBm for the device to operate at its highest PAE of 74.61%. This FET may be suitable to be used as a Low Noise Amplifier (LNA) at the receiver side which usually receives very low input power. On the contrary, even though TQ_MTRK has the lowest PAE among all three FETs, it has the highest gain of all the FETs which is 21.03dB, an important consideration that might be vital during a power amplifier design.

TABLE III. PAE COMPARISON BETWEEN FET MODELS IN AWR MWO LIBRARY.

| **Passive component values** | **STAZ Pin = 30dBm** | **CURTICE2 Pin = 26dBm** | **TQ_MATRK Pin = 6dBm** |
|---|---|---|---|
| Reference circuit PAE | 40.46% | -34.97% | 24.53% |
| Sokal's older equation PAE | 97.02% | 61.32% | 72.52% |
| Sokal's newer equation PAE | 97.2% | 68.21% | 74.61% |
| Output power | 48.07dBm | 28.4dBm | 25.55dBm |
| Amplifier gain | 18.07dB | 2.4dB | 19.55dB |

There is always a tradeoff between PAE and output power for a FET. We can achieve a high PAE but not without adverse effect to the output power. Table IV shows the highest output power

achievable across all three models with its effect on their PAEs. Note that all FET models in this section are simulated from circuits designed from Sokal's newer formula. Just like in achieving highest PAE in the previous section, each FET model requires its own specific input power shown in Table IV. The STAZ configuration suffers a PAE deterioration by 11.14% from its maximum PAE if the circuit is driven to produce a high output power of 54.07dBm. CURTICE 2 suffers with PAE deteriorating by 50.19% for a mere amplification output of 32.38dBm. CURTICE 2 has only a 2.38dB gain which may be a problem in some design specifications as there may be insufficient amplification. On the contrary, once again the TQ_MATRK device shows its capability of producing a very high gain amongst the FETs which is 19.56dB. With the input power of 8.304dBm which is lowest among the 3 FET models, TQ_MTRK is able to produce output power of 27.86dBm but with cost of PAE to drop by 66.26%. It's the highest PAE deterioration and lowest instantaneous PAE among the FETs. Another interesting criteria to look into is the IMD existing at the output gate of FETs. IMD or simply known as neighboring distortion occurs due to non-linear characteristic that exist at the FET gate node. This causes other nearby frequencies besides than the fundamental such as harmonics to have unwanted powers and gains, reducing overall performance since the goal is to operate at one frequency band solely which is at 2.4 GHz.

TABLE IV. PAE AND OUTPUT POWER COMPARISON ACROSS FET DEVICES.

| **Passive component values** | **STAZ Pin=36dBm** | **CURTICE2 Pin=30dBm** | **TQ_MATRK Pin=8.304dBm** |
|---|---|---|---|
| Highest Output Power | 54.07dBm | 32.38dBm | 27.86dBm |
| Amplifier gain | 18.07dB | 2.38dB | 19.56dB |
| Instantaneous PAE | 85.88% | 18.02% | 8.35% |
| PAE deterioration | 11.14% | 50.19% | 66.26% |

However, IMD is not necessarily bad. It really depends on what type of operation that this circuit was designed to achieve; either wideband or narrowband. For narrowband operations, IMD is catastrophic as it introduces unwanted noises which leads to higher bit error rate due to intersymbol interference. But for wideband, IMD is rather a lucrative as the FET can operate in a much higher bandwidth giving way for usage of wideband techniques such as orthogonal frequency-division multiple access, OFDMA which is widely being discussed to be implemented in upcoming 5G systems [3]. Table V displays the frequencies range for the three types of FET models. STAZ has the widest band amongst the three with a leeway of 200 MHz and CURTICE 2 has the narrowest band with only 50 MHz gap.

TABLE V. INTERMODULATION RANGE COMPARISON

| **FET types** | **STAZ** | **CURTICE2** | **TQ_MATRK** |
|---|---|---|---|
| Frequency Range | 2.3Ghz-2.5Ghz | 2.4Ghz-2.45Ghz | 2.35Ghz-2.5Ghz |

In previous measurements, we have chosen $\boldsymbol{Q_L}$ value of 7 to design the Class E circuit's OMN. Now we would reduce the $\boldsymbol{Q_L}$ to 3.5 for each FET and evaluate their performance at fundamental power and intermodulation products, (IMD) power contributions. For comparison purposes, we decided to use the newer Sokal's equation circuits in this section. Hence we can observe performance deterioration within circuits that previously produce a high PAE as we tweak the $\boldsymbol{Q_L}$ values. Typically if the device has a larger bandwidth, IMD should have higher power compared to IMD in narrow bandwidth amplifiers. Table VI shows the values of power components with the original $\boldsymbol{Q_L}$ of 7. Table VII which shows values for $\boldsymbol{Q_L}$ of 3.5 which is half of the previous value. We can observe how reduction of $\boldsymbol{Q_L}$ can affect performance of amplifiers.

TABLE VI. POWER OUTPUT COMPONENTS WITH $Q_L$ OF 7

| **Frequency range (GHz)** | **STAZ with $Q_L$ of 3.5 (dBm) PAE: 97.2%** | **CURTICE2with $Q_L$ of 3.5 (dBm) PAE: 68.21** | **TQ_MTRK with $Q_L$ of 3.5 (dBm) PAE: 74.61%** |
|---|---|---|---|
| 2.39 (second IMD) | 7.143 | 9.566 | -12.41 |
| 2.395 (1st IMD) | 9.09 | 13.73 | -1.258 |
| 2.4 fundamental frequency | 19.6 | 24.27 | 17.95 |
| 2.405 (1st IMD) | 19.55 | 24.57 | 18.01 |
| 2.41 (second IMD) | 11.16 | 13.54 | -1.06 |

TABLE VII. POWER COMPONENTS WITH $Q_L$ OF 3.5

| **Frequency range (GHz)** | **STAZ with $Q_L$ of 3.5 (dBm) PAE: 87.7%** | **CURTICE2with $Q_L$ of 3.5 (dBm) PAE: 56.52%** | **TQ_MTRK with $Q_L$ of 3.5 (dBm) PAE: 70.04%** |
|---|---|---|---|
| PAE reduction | -9.5% | -11.69% | -4.57% |
| 2.39 (second IMD) | 6.215 | 11.26 | -10.23 |
| 2.395 (1st IMD) | 9.467 | 15.46 | -3.441 |
| 2.4 fundamental frequency | 20.39 | 25.89 | 18.18 |
| 2.405 (1st IMD) | 20.94 | 26.24 | 18.27 |
| 2.41 (second IMD) | 11.8 | 15.4 | -3.069 |

In this study, each FET behaves differently, but overall proves that reducing $Q_L$ can increase bandwidth. Typically a lower $Q_L$ would produce a larger bandwidth. From Table VI, we can observe the increase of power in all IMDs and fundamental power for the SPICE models. Even though power in fundamental and IMDs increased for STAZ model, however there is a reduction of PAE from 97.2% to 87.7%. The CURTICE 2 model shows similar improvement in terms of power. Both fundamental and IMD increased in power indicating a wider gap of bandwidth where the amplifier can extend its operation. However, as before this power amplifier also suffers losses in efficiencies as PAE degrades from 68.21% to 56.52%. The TQ_MTRK response is rather different. The fundamental's and majority of the IMD's power level are higher

in $Q_L$ of 3.5. However, there is much higher power in IMDs such as at 2.395 GHz and at 2.41 GHz in $Q_L$ value of 7. But it important to highlight that these values are negative PAE. Negative value occurs when the input power exceeds the saturated output power meaning that the amplifier is actually wasting power rather than to amplify it. Thus the range is only suffice for positive values of PAE. There no change of bandwidth for different values of $Q_L$ for the TQ_MTRK.

## IV. Conclusion

In this contribution, high efficiencies can be achieved using SPICE FET models using Sokal's equations. Simulations results were compared to prove validity that Sokal's newer equations is able to achieve higher efficiency. However considerations must be taken between tradeoffs that exist between PAE and output power. These Class E circuits can be used as either PAs or LNAs depending on the bandwidth, PAE or output power considerations and functionality of FET in Class E configuration. Future works can look into harmonic terminations for Class E PAs which may improve performance.

## References


[1] T. Ashtom, "Lauching of UTM Ericsson Innovation Centre for 5G", Dewan Azman Hisham, Universiti Teknologi Malaysia, Kuala Lumpur, (2016)

[2] N. Sokal and A. Sokal, "Class E-A new class of high-efficiency tuned single-ended switching power amplifiers", *IEEE Journal of Solid-State Circuits*, vol. 10, no. 3, pp. 168-176, (1975)

[3] Y. Qin, S. Gao, A. Sambell and E. Korolkiewicz, "Design of low-cost broadband class-E power amplifier using low-voltage supply", *Microwave and Optical Technology Letters*, vol. 44, no. 2, pp. 103-106, (2004)

[4] F. Norouzian, "Dual-Band and Switched-Band Highly Efficient Power Amplifiers", (2014).

[5] Udin, Mohd. "RF LDMOS Power Amplifier Class E for Wireless Communication", pp. 52-55, (2006)

[6] Steve Cripps, "RF Power Amplifiers for Wireless Communications", 1st ed. Norwood: Artech House, pp. 192-196, (2006).

[7] F.Zubir and P.Gardner, "A New Power Combiner using Aperture Coupling Technique for Push-Pull Class B Power Amplifier", IEEE, pp.1-4, (2013).

[8] F.Zubir and P.Gardner, *"Differentially fed multilayer antennas with harmonic filtering for push-pull Class B Power Amplifier integration*" IET, pp.96-99, (2013)

# Acoustic Metamaterial for Image Detection

Nur Farah Hanis Bt. Daud
*Faculty of Electrical Engineering*
*Universiti Teknologi Malaysia (UTM)*
*Johor, Malaysia.*
*farahhanis_daud@yahoo.com.my*

Siti Zaleha Abdul Hamid
*Department of Communication Engineering.*
*Faculty of Electrical Engineering*
*Universiti Teknologi Malaysia (UTM)*
*szaleha@utm.my*

***Abstract*— Metamaterial have developed in acoustic to control, manipulate the sound waves which have the physic properties with beyond the limit from its conventional. Acoustic metamaterial shown it ability to restore the propagative and evanescent waves and produce subwavelength imaging. This capability able to simplify the several area of technology especially in medical, underwater sonar and non-destructive. However, in order to detect an image, Image processing is the fundamental tool that used to implement arithmetic operations on images and have many function to simulate causes added time and complexity. This research was conducted to investigate the holey structure of 3D metamaterial transmits evanescent field components of object efficiently due to the formation of Fabry- Parot inside the holey structure and detect the image of the object. In this case, the structural design of the metamaterial give the formation of image by vary the size of hole, thickness plate and the frequency used.**

***Keywords— metamaterial; acoustic; evanescent field; Fabry-Perot; imaging device;***

## I. INTRODUCTION

Image detection is one of the important tools in image processing that applied in several area of science and technology especially in medical, non- destructive testing and computer vision. Image detection algorithm is used to extract data of an object and finding the boundaries of the objects by reduces the amount of data to be process. On the other words, this technique is known as high pass filter as it remove the spatial frequency and then enhancing those area of image which contain edges. The edge of an object is clarified by evanescent waves that scattered from the object due to the formation of Fabry-Perot transmission resonances. A device capable creating image with only evanescent waves would generate only the significant information contained in image which is the edge of an object.

The evanescent wave has several ways detected to overcome the diffraction limit of classical wave such as light or sound. The previous study proved that diffraction limit can be overcome by superlenses [1], time reversal techniques [2]. These approach evanescent wave can be restored and the details of an object can be provided on its image. This paper report a metamaterial design able to create image of object as the information carried by evanescent wave is successfully transmitted through the metamaterial. The metamaterial was designed with perforate structure in repeated pattern. The characteristics of the holey plate structure is defined with the ability of the metamaterial to transfer its input impedance to the output of the metamaterial.

## II. LITERATURE REVIEW

### *A. Hyperlens and Superlens Overcome Diffraction Limit*

Recent theories discussed that acoustic superlenses or magnified hyperlenses resolve the diffraction limit of conventional imaging device where the evanescent wave of the acoustic hyperlens converted to propagating wave and significantly magnified the subwavelength of the object. The research demonstrated that the fabricated acoustic hyperlens relies on straightforward cut-off free propagation and achieve deep subwavelength resolution with low loss over a broad frequency bandwidth [3]. It was shown that special properties of the engineered metamaterial hyperlens able to overcome diffraction limit by providing smaller than half of the operating wavelength. However, the capability of the device not only transmits information which carried by evanescent wave, it also magnify it as the information travels to the far-field outside the lens [4]. Another research also demonstrated hyperlens with added metalenses realize the super-resolution imaging such transfer the information to the far-field by magnification phenomenon while the metalenses able to achieve detail image and also provide optical Fourier transforms.

A practical superlens or super lenses which is uses metamaterial to go beyond diffraction limit. Diffraction limit is a feature of conventional lenses and microscopes that limits the finest of their resolution. There are many length design have been proposed that go beyond the diffraction limit in some way, but there are constraints and obstacles involved in realizing each of them as the Ernt Abby report an 1873 the lens of the camera or microscope is incapable of capturing some very fine details of any given image the superlens. On the other hand is intended to capture these fine details consequently conventional lens limitation has inhibited progress in certain areas of the biological science. This is because of virus or DNA molecule is out of visual range with highest power microscopes also this limitation inhibits seeing the processes of cellular proteins moving along side microtubules of a living in their natural environments. Additionally computer chips and the related microelectronics are manufactured as smaller and smaller this requires specialized optical equipment which is also limited because these use the conventional lens hence the principles governing a superlens show that it has potential for imaging a DNA molecule and

cellular protein processes or aiding in the manufacture of even smaller computer chips and microelectronics. Furthermore conventional lenses capture only the propagating light waves there are waves that travel from a light source for an object to a lens or the human eye[5]. This can alternatively be studied as the far-field in contrast superlens captures propagating light wave and light waves that stay on top of the surface of an object which alternatively can be studied as both the far field and the near field.

### *B. Properties and Classification of Metamaterial*

The term of metamaterial is come from Greek word which are "meta" and "material". Meta is defined as something ability that can be beyond, altered, and change or something advance [6]. Metamaterial is manmade structure to have a property that is not found in nature which arranged in repeating pattern and provide the less scale than wavelength of phenomenon they influence. By having these smart properties, they are able to manipulate the electromagnetic waves by blocking, absorbing, enhancing and bending wave to achieve better performance that go beyond the limit of conventional materials.

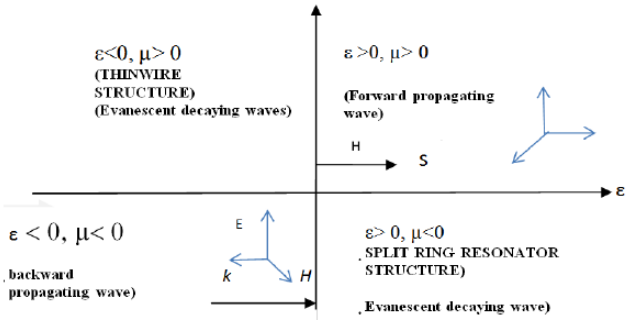


Fig. 1 Classification of metamaterial.

The right handed material (RHM) was represented at the first quadrant (μ>0, Ɛ>0). It is commonly used material where the forward propagation of wave take placed [7]. The second quadrant (Ɛ<0, μ>0) describes the evanescent waves supported by electric plasmas. The third quadrant shows metamaterial properties as double negative material . The propagation waves follows the left hand rule. Regarding to the relationship from the equation refractive index, the permittivity and permeability are in negative region cause the refractive index of the medium also became negative. While the fourth quadrant (Ɛ>0, μ<0) also supports evanescent.

## III. PROJECT METHODOLOGY

The initiation phase of the beginning the designation of metamaterial is understands of design requirement. In order to design metamaterial, the scale of arrangement in repeating pattern of the materials must smaller than the operating wavelength. In physics, wave transfer energy through oscillation can either be longitudinal, that is when the oscillations are in the direction of the movement of the wave, or they could be transverse. That is when the oscillations are perpendicular. In either case, the distance or the repeat distance between those oscillations is called a wavelength and we used lamda, λ to represent wavelength. In this case, the medium that the waves travel through is air, the sound wave in air or known as the speed of sound in air at room temperature and atmospheric pressure which is 343 m/s. The wavelength of the sounds that send out continuous sinusoidal waves travelling at the constant speed v is given by [8]

$$\lambda = v/f \quad (1)$$

The metamaterial is designed with repeated structured of cells as shown in the figure below.

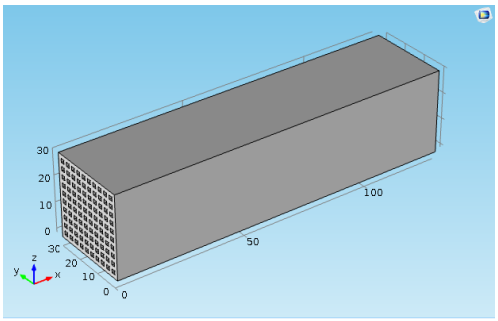


Fig. 2 3D metamaterial.

The schematic of the figure above shows the holey structure of metamaterial and filled with air inside the holes. The separation between hole to hole is β for horizontal and vertical line where the size of each hole is a and the height is known as h. The type of material that be used as the wall for the holes is brass alloy. Hence, the geometrical parameter in the experimental was chosen are: a= 1.5mm, β=3mm, h= 130mm and number of holes=100 (10x10)

### *A. Software Simulation*

In order to further corroborate our results on holey structure, the metamaterial designed is sketched based on the parameters needed and simulated the response of the designed by using COMSOL Multiphysics. From the simulation, it demonstrated as we setting the physical properties and the position as in the real experiment.

The experiment in the COMSOL was conducted in air where the most front of boundary was set as sound source with initial pressure 20 Pa. The metamaterial is place 20 cm from the source and the rectangular plate as the input object is 3 mm from the input of metamaterial. The another end of the metamaterial is the output region where the image of the object is formed. The arrangement of the experiment in COMSOL as shown in the figure 3.

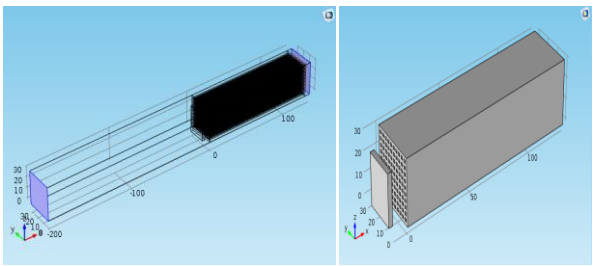

Fig. 3 Experimental diagram in COMSOL

The experiment was repeated by varying the size of square of hole, with 3mm x 3mm, thickness of the metamaterial, and

also run the same test but replacing the holey plate with square long wire as in electromagnetic case.

## IV. RESULT AND ANALYSIS

The simulated result was compared the output image of the object. The results were varied with the size of hole, thickness plate and frequency.

### A. *Comparison between size of hole,a*

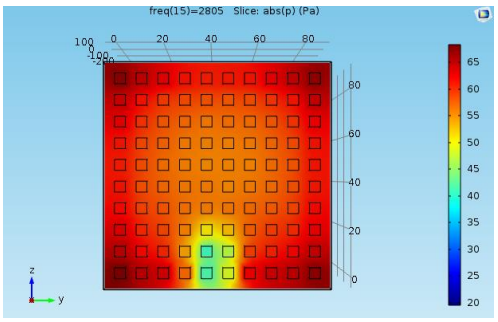


Fig. 4 a=4.5 mm

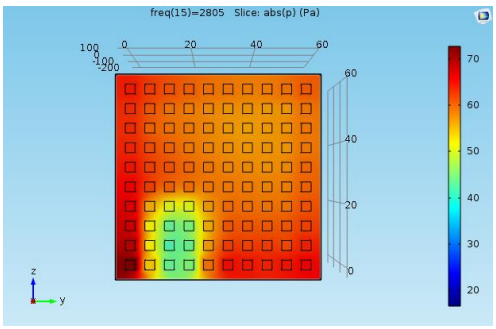


Fig. 5 a=3 mm

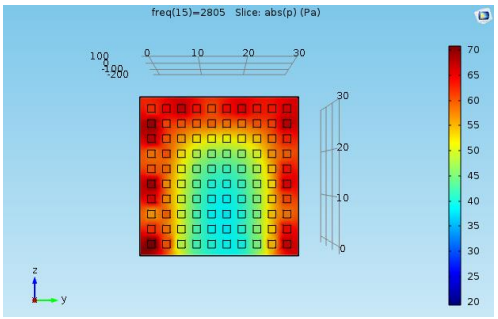


Fig. 6 a=1.5 mm, h= 130 mm, f= 2805 Hz

### B. *Comparison between thickness of the metamaterial,h*

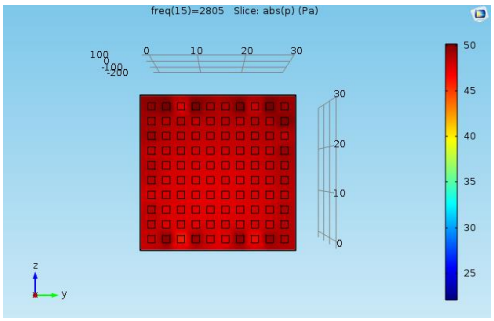


Fig. 7 h=135 mm

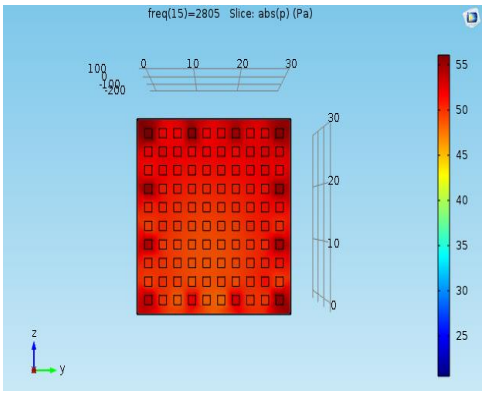


Fig. 8 h=133 mm

### C. *Comparation between frequency*

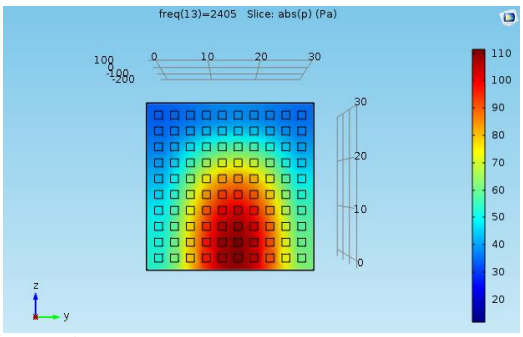


Fig. 9 frequency= 2405 Hz

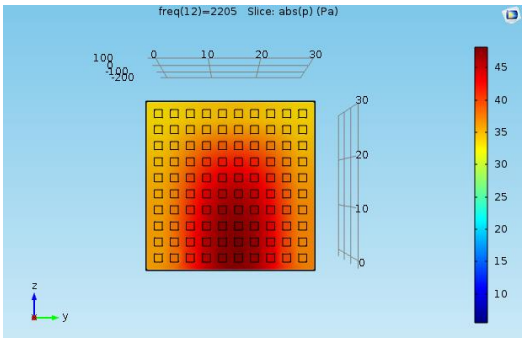


Fig. 10 frequency = 2205 Hz

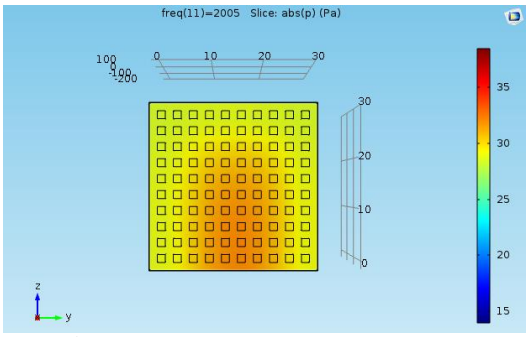


Fig. 11 frequency = 2005 Hz

The result in figure 6 is the better result compare to the others. From the result we can see that the concentration of distribution pressure is slightly higher at smallest range of pressure value which is around 45 Pa to 50 Pa. This behavior result showed capability of this holey structure metamaterial to resolve the spatial information as in figure 6. It demonstrated that the diffraction effect is neglected because significant mode propagation dominate the transmission information through the holey plate which is the wavelength is much smaller than size of hole and thickness of wall ($\lambda >> \beta, a$). The phenomenon take place in transmission when there is zero order transmission coefficient for an acoustic wave with parallel momentum $b_{\|}=(b_x^2+b_y^2)^{1/2}$ can be defined as [9]:

$$t(\lambda, b_{\|}) = \frac{4|S00|^2 Y exp(iqh)}{(1+Y|S00|^2)^2-(1-Y|S00|^2)^2 \exp(2\, iq_z\, h)} \qquad (2)$$

where the propagation contanst, $q_z=b_0=2\pi/\lambda$
waveguide mode, $S_{00} = a/\lambda$
$Y=b_0/(b_02+b_{\|}2)^{1/2}$
At the standing wave excitation is there is resonance condition where $q_zh=m\pi$ ($m>0$) provide unity transmission coefficient for all b|| including evanescent waves. This result proved that if an object is place infront of the metamaterial, the image of the object is transfer through the holey plate and formed at the output of the metamaterial. The parallel momentum is not affected the dispersion inside the hole, so $\varrho_{eff}^z=1/K_{eff}^z=\infty$. While for x and y direction, the metamaterial is defined as equal denstity which is $\varrho_{eff}^x= \varrho_{eff}^y= \varrho_{eff}= \varrho_{air}\beta^2/a^2$ and bulk modulus $K_{eff}^x= K_{eff}^y= K_{eff}= K_{air}\beta^2/a^2$ and also the velocity of sound is consider equal to air.

The figure 12 showed the point graph of sound pressure level at the edge and middle of the image.

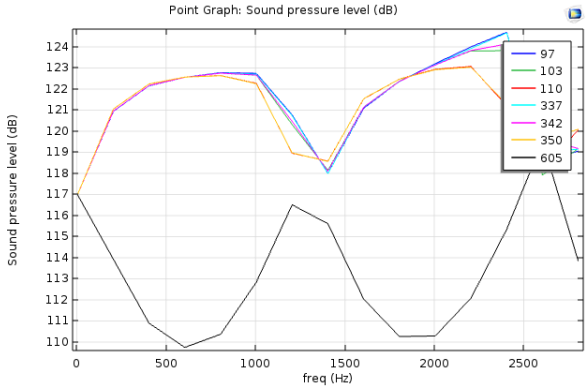


Fig. 12 Point graph of image; line 97,103,110, 337, 342, and 350 are point at the edge of output image. Line 605 is the point at the middle of the suface.

The line graphs are going up and down uniformly for each holes illustrated that the holey plate act as perfect mirror for acoustic wave and hence it possible to have the formation of Fabry-Perot resonance.

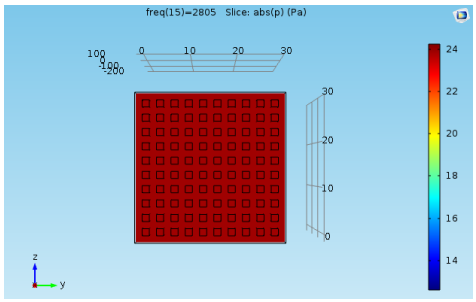


Fig. 13 simulation result periodic of array square wire.

Next, the result from the electromagnetic case portrayed that there is no image can be formed at the output of metamaterial. The square of wire array do not formed the Fabry-Perot inside the structure because there is difference propagation through structure between acoustic wave and electromagnetic and it is not possible the multiple scattering event in electromagnetic case. The result clearly shown that the periodic array of long wire could not transfer the information from input to output.

## V. CONCLUSION

The experimental results confirm that the holey structure of metamaterial able to detect image and act as imaging device by reproducing the image of an object. This device is perfectly operated at lower frequency with less attenuation in propagation system. This device can be enhances its performance by using the smallest scale of the geometrical parameter. The 3D metamaterial can be used to improve the technologies nowadays especially in medical area, non-destructive detection, underwater and other applications.

## VI. REFERENCES


[1] Pendry, J. B. Negative refraction makes a perfect lens. Phys. Rev. Lett. 85, 3966–3969 (2000).

[2] Lerosey, G., de Rosny, J., Tourin, A. & Fink, M. Focusing beyond the diffraction limit with far-field time reversal. Science 315, 1120–1122 (2007).

[3] He, Z., Cai, F., Ding, Y. & Liu, Z. Subwavelength imaging of acoustic waves by a canalization mechanism in a two-dimensional phononic crystal. Appl. Phys. Lett. 93, 233503 (2008).

[4] Li, J., Fok, L., Yin, X., Bartal, G. & Zhang, X. Experimental demonstration of an acoustic magnifying hyperlens. Nat. Mater. 8, 931–934 (2009).

[5] Jia, H. et al. Subwavelength imaging by a simple planar acoustic superlens. App. Phys. Lett. 97, 173507 (2010).

[6] A.Sihvola . Metamaterials in electromagnetics, Metamaterials1.2007. 2-11

[7] S Anantha Ramakrishna. Physics of negative refractive index materials, 2005. 453-467.S. Raghavan , Rajesh Kumar . An Overview of Metamaterials in Biomedical Applications, PIERS Proceedings. 2013.490-495.

[8] David C. Cassidy, Gerald James Holton, Floyd James Rutherford . Understanding physics. Birkhäuser. 339: 2002.

[9] Zhu, J. et al. A holey-structured metamaterial for acoustic deep-subwavelength imaging. Nat. Phys. 7, 52–55 (2011).

# Heart Rate Monitoring System on Android Platform

Nuralia E'zzati bt Yusop
*Department of Communication*
*Faculty of Electrical Engineering*
*Universiti Teknologi Malaysia*
*Johor Bahru, Malaysia*
*nuraliaezzati17@gmail.com*

Norazan bin Mohd Kassim
*Department of Communication Engineering*
*Faculty of Electrical Engineering*
*Universiti Teknologi Malaysia*
*Johor Bahru, Malaysia*
*norazan@utm.my*

***Abstract*—This paper discusses the process of developing a practical heart monitoring system using Arduino UNO as the microcontroller on an Android platform. The first phase of the project involves literature review on journals and theses related to heart rate monitoring system. This was followed by the development of hardware fragment using Arduino UNO, pulse sensor, ESP8266 and also software fragment by developing Android application using Android Studio. The final phase involves integration between hardware and software fragment. Through this project, patient will be allowed to monitor their heart rate and store the data wirelessly. This will increase patients' access to the device as it is an affordable alternative to others in the market.**

***Keywords—heart rate; Arduino UNO; Android; monitor; wireless***

## I. INTRODUCTION

In current times, heart disease has become one of the critical health problems globally. In fact, heart disease is the leading cause of death in the world and is expected to escalate continuously throughout the next few decades. Heart disease is sometimes called coronary heart disease which is the term defined when there is an accumulation of plaque in the lining and inner layers of coronary arteries causing blockage of blood returning to the heart [1]. The causes for this are usually people's lifestyle factors and eating habits [2]. In the event of severe heart problems, constant check-up is needed at least once a year with proper health care arranged for heart disease patients. This can be accomplished by constant monitoring of their heart condition and heart rate. Heart rate or pulse is described by the speed or the number of times your heat contracts of beats per minute (bpm).

### *A. Problem Statement*

Lately, it has been found that there are numerous complications for heart disease patients in keeping up with their cardiologists' appointments for a proper check-ups. Also, the current machines are cost ineffective which would be unaffordable to low-income society hence limiting access to them.

### *B. Objectives*

- To provide a practical heart monitoring system for patient using Arduino UNO as the microcontroller and Android as the platform.
- To introduce an affordable alternative allowing more people to have access to the developed equipment.
- To create an Android platform which enables patient to store data from the device wirelessly and for the doctor to have an up-to-date data from the patient.

### *C. Scope of Work*

The development of this project requires the integration work between hardware and software parts. Pulse sensor is connected to Arduino Uno to measure heart rate. Arduino UNO will be programmed to count the heart rate from the sensor the result displayed on Android. The Arduino uses C/C++ language for programming. Furthermore, Android Studio is used as the tool while JAVA language is used as the programming code. After the integration process, the system was analysed and verified.

## II. LITERATURE REVIEW

### *A. Related Research*

Studies about heart rate monitoring system from many papers have been carried out for the development of this project. The purpose of this study is to identify the platform used in existing projects, identify their and find alternative ideas for the purpose of improving them.

*1) Development of Electrocardiogram (ECG) Wireless Sensors Board for Medical Healthcare Application 2009 by Nor Syahidatul Nadiah binti Ismail, Universiti Teknologi Malaysia*

This project developed ECG wireless sensors board with wireless transmission as the transmission medium between the manufactured hardware and the display unit [3]. The drawback is that the XBEE module used in this project is limited to only 100m.

*2) Handheld NIBP and Heart Beat Monitoring System for Home Use 2012 by Ruhaizan binti Ismail, Universiti Teknologi Malaysia*

This project designed a blood pressure and heart beat monitoring system. However, this project is not portable thus diminishing its practicality. This project also contains fault in the systolic and diastolic measuring that causes compilation error on behalf of the display part could not be compiled with the circuit [4]. Moreover, the Cytron Bluebee Module range is also limited to only 20m.

*3) Sustainable Wireless Sensor Device for Heartbeat Monitoring with Energy Harvester 2012 by Sin Tong Kok, Universiti Teknologi Malaysia*

This project developed a self-sustained wireless sensor device to measure heartbeat and the data from the sensor will be gathered and displayed in numerical order on GUI Android application [5].

*4) Heartbeat Monitoring for Office Worker 2013 by Nur Hidayu binti Zainal, Universiti Teknologi Malaysia*

This project was designed to allow office workers in monitoring their own heart rate because of its portability. However, there is no warning system for the employers in case of escalated heart rate reading beyond the normal range [6].

*5) Mobile Telecardiology Application Development for Connected Heart Care 2015 by Vineetha A/P G. Jaya Kumaran, Universiti Teknologi Malaysia*

This project established a Windows-based smartphone telecardiology application [7]. The problem with this application is patients are supposed to manually input their data and buy a separate hardware device to check on their heart rate and health.

## III. METHODOLOGY

The development of this project was divided into 3 phase. The first phase involves decisions regarding the project title as well as defining problem statements and objectives. This phase also includes conducting literature review on journals and theses relevant to the heart rate monitoring system.

The second phase introduces the proposed design which includes the hardware and software development of the project. For hardware developments, all components were installed and developed with Arduino UNO. Meanwhile, Android application was developed in fulfillment of the software requirement.

Next, the third phase includes the integration between the hardware and software components to form a complete system. The system was tested and underwent troubleshooting should any error occurs.

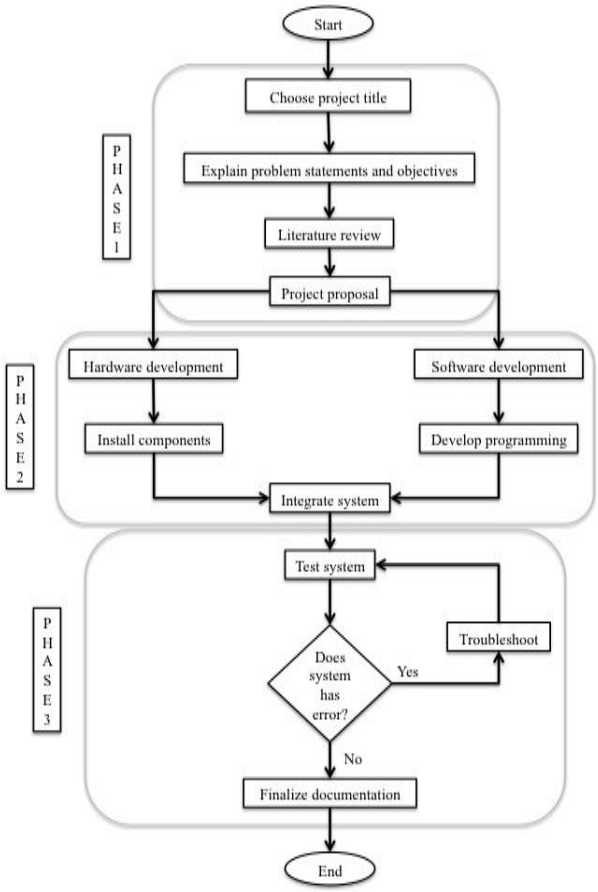


Fig. 1. Work Flow of The Project.

### A. Hardware Development

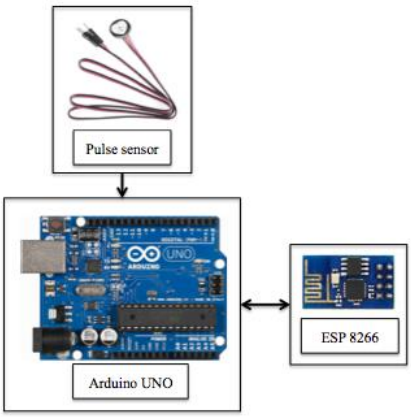


Fig. 2. System Block Diagram

Pulse will be detected from the finger using the Pulse Sensor that was developed using Arduino UNO. Arduino UNO was thusly programmed to count the heart rate and ESP8266 acted as transmission module to send the data to the Android application.

*1) Arduino UNO*

Arduino UNO is a microcontroller featuring the Atmel Atmega328P [8]. The board is reasonably priced and the library

can be downloaded for free. The programming language used in Arduino UNO is C/C++.

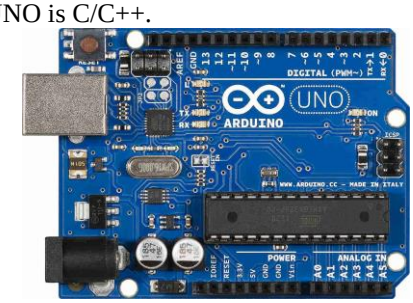


Fig. 3. Arduino UNO

*2) ESP8266*

ESP8266 is a WiFi module that was designed by Espressif System. It inserts WiFi functionality to a present microcontroller board and the pins are compatible with Arduino. This WiFi module acts as a transmission module between Arduino UNO and Android application.

Fig. 4. ESP8266

*3) Pulse Sensor*

This sensor used the concept of photoplethysmograph (PPG) by detecting the relative changes in light intensity during each pulse.

Fig. 5. Pulse Sensor

## B. Software Development

The software development began with the General User Interface (GUI) development. This process involved the structuring, mapping and designing of page as well as the flow of application. Android Studio was utilized for these tasks.

Subsequently, system integration with the database that was developed with the Microsoft SQL Server.

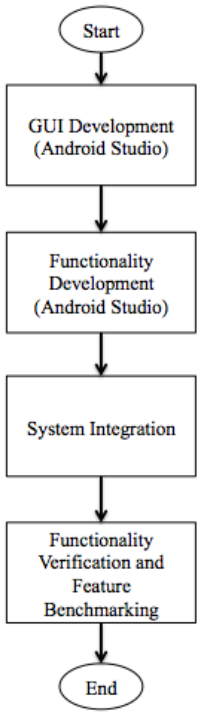


Fig. 6. Software Development Flow Chart

# IV. Result and Discussion

## A. Hardware Development

Pulse will be detected from finger using the Pulse Sensor. Then, the pulse sensor was developed using Arduino UNO. Arduino UNO has been programmed to count the heart rate and ESP8266 will act as the WiFi module allowing internet connection for Arduino UNO.

Figure 7 shows bpm reading from serial monitor on Arduino IDE. Readings were taken every 2 miliseconds. These readings were sent to the local database, phpMyAdmin.


Fig. 7. Serial Monitor from Arduino

### B. *Software Development*

The software development of this project is divided into two parts. The first part would be the programming code in Arduino UNO using C/C++ as the programming language.

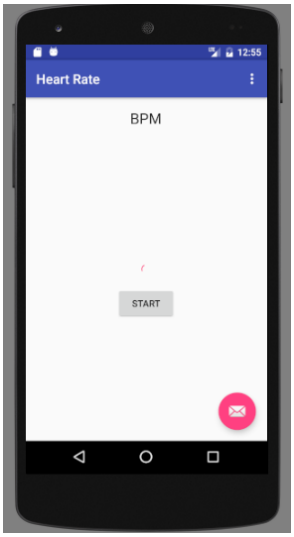


Fig. 8. GUI for Android Application

The next part is the programming in developing Android application which utilised Android Studio as the tool and JAVA as the language. As shown in the figure above, start button will be pressed to load the bpm reading from the database that have been sent from ESP8266 in hardware fragment.

## V. CONCLUSION

As a conclusion, this heart rate monitoring system has been successfully developed with Arduino UNO as the microcontroller, a pulse sensor and ESP8266 as the Wi-Fi module. This project used Android interface (GUI) by using a smartphone which displayed the bpm reading from the pulse sensor. This practical heart rate monitoring system also provides affordable alternative to other devices in the market.

## REFERENCES

[1] P.S. Douglas, M.A. Daubert, "Heart Disease in Women," vol. 133, issue 1, American Heart Association Journals, 2015.

[2] S. Sasayama, "Heart Disease in Asia," vol. 118, issue 25, American Heart Association Journals, 2008.

[3] N.S.N. Ismail, " Development of Electrocardiogram (ECG) Wireless Sensor Board for Medical Healthcare Application, Universiti Teknologi Malaysia, 2009.

[4] R. Ismail, "Handheld NIBP and Heart Beat Monitoring System for Home Use, Universiti Teknologi Malaysia, 2012.

[5] T.K. Sin, "Sustainable Wireless Sensor Device for Heartbeat Monitoring with Energy Harvester, Universiti Teknologi Malaysia, 2012.

[6] H.N. Zainal, "Heartbeat Monitoring for Office Worker," Universiti Teknologi Malaysia, 2013.

[7] V.G.J.Kumaran, "Mobile Telecardiology Application Development for Connected Heart Care," Universiti Teknologi Malaysia, 2015.

[8] W. Durfee, "Arduino Microcontroller Guide," University of Minnesota, 2011.

# Performance Characterization of BiDirectional Wavelength Division Multiplexing Passive Optical Network (WDM-PON)

Nur Amirah Binti Aidulfetri
Department of communication
Faculty of Electrical Engineering UTM
81310 Johor Bahru, Johor
amirahaidulfetri@gmail.com

Prof Dr Sevia Mahdaliza Idrus Sutan Nameh
Department of communication
Faculty of Electrical Engineering UTM
81310 Johor Bahru, Johor
sevia@fke.utm.my

***Abstract*—Optical fiber has become the most crucial and fastest transmission media in the communication. With increment number of broadband applications such as high definition television (HDTV) and broadband internet access has created a growing interest among service providers by improving networks to supply broadband services to residential and small business. This project was conducted to present and design of a passive optical network (PON). From the simulation, PON has introduce a good data transmission rate and large bandwidth. The wavelength division multiplexing passive optical network (WDM-PON) is a technology that can fulfil users' requirement in the future like high data rate, faster speed and more secure. In this project all the design simulate using Optisystem software. The data rate for downstream signal equals to 10Gbps while for upstream equals to 5Gbps and the signal transmit in optical bidirectional single mode fiber (SMF). Two types of models have been proposed in this project. The performance of the system can be obtained by using eye diagram and Bit error rate (BER) with various input power. It is found that PON based on reflective semiconductor optical amplifier RFB give lowest BER for downstream and upstream.**

***Keywords—Wavelength Division Multiplexing, Passive Optical Network, Bit Error Rate, Reflective Semiconductor Optical Amplifier, single mode fiber, Downstream, Upstream***

## I. INTRODUCTION

The communication system in the world was revolutionizing by the deployment of optical fiber. Higher bandwidth requirement has brought the rapid growth in the development of fiber-to-the-x (FTTx) technology which is based on the broadband access networks. The explosive growth on the demand for higher bandwidth has introduce to fiber-to-the-home (FTTH) based broadband access networks. It's related to the installation of optical fiber from central point to the users such as residences, apartment buildings and businesses which can provide unprecedented high speed internet access. In addition, by introducing FTTH based on wavelength division multiplexing (WDM) it can support future services [1]. WDM operates by depending on the optical carrier signals. It works by multiplexing a number of optical carrier signals to a single fiber optic using different wavelengths or color of the laser light. WDM-PON systems which employ Reflective Semiconductor Optical Amplifiers (RSOA) for colorless ONU's traditional employ On-Off Keying (OOK) modulation because it easy in implementation and exploitation of a non-linear gain characteristics of the RSOA compression which can minimize the downstream modulation. Intensity noise was experienced during upstream transmission which is due to the imperfect erasure residual of the upstream signal. There are some techniques which can eliminate the residual effect. Spectral location for upstream and downstream have studied; a scheme with a phase modulated downstream signal uses separate fibers for upstream and downstream [2].

The deployment of single bidirectional optical fiber in WDM-PON can make it into two way direction of communications which is downstream and upstream. The deployment of single bidirectional optical fiber can reduce the cost of maintenance and also complexity during installation. However, it can degrade the system performance of downstream and upstream and also leading to degrade of signal to noise ratio (SNR) at the receiver. This is due to the back-reflection exist from the downstream which beats with the opposite propagation upstream as both transmission use the same wavelength. The deployment of the single strand of bidirectional optical fiber also can introduce losses. Rayleigh and material absorption are two major losses in optical fiber and will degrade the system performance. Material absorption can be reduce by using dehydration and vapor phase oxidation techniques. While for Rayleigh, it cannot be eliminate because it is natural losses happen in the optical fiber. It only can be reduce by using suitable wavelength which is 1550nm. The higher the wavelength, the lower the losses occur in the optical fiber.

## II. LITERATURE REVIEW

### *A. Fundamentals of WDM-PON*

#### *1) Optical Fiber*

Optical fiber is one way of transmitting signal to the users in form of light. It will act like optical waveguide for the photons as they travel down the optical path toward the receiver. From the source its' has many characteristics which can provide very high speed communication. It also has very low attenuation over

high frequencies range compare to the other medium which can give as low as 0.2dB/Km in between the range of 1300nm to 1500nm for the wavelength. It often used for long distance communication because it can give low attenuation and higher bandwidth compare with traditional methods.

*2) Optical circulator*

Optical circulator is a passive components to deliver signals with minimum loss. It is use to separate signals travel in opposite directions in an optical fiber. Deployment of circulator in optical communication system can support a bidirectional transmission over a single fiber. Optical circulator can give low level of loss. Commonly it can give 0.3dB and 1.5dB port to port loss while for isolation typically between 20dB to 40dB. It very functional devices that can be used in many applications such as a bidirectional link consisting of two fiber strands is multiplexed onto a single strand of fiber.

*B. Limitations in WDM-PON*

*1) Attenuation*

Attenuation is the reduction in power of the light signal as it transmitted toward the users. This is because, in the fiber optic communication systems, there are passive media components such as cables, cable splices and connectors. The major cause of attenuation is scattering. Scattering occurs when transmitted light hits with individual atoms in the glass and is an isotropic. It happens in the low absorption window between infrared and ultraviolet. When light that is scattered outside the angle of numerical aperture of the fiber, it will absorb into the cladding. Thus, for long distance transmission, it is advantageous to use the longest practical wavelength for minimal attenuation and maximum distance between repeaters. Attenuation can be calculate by using equation as below.

$$YL = 10 \log (Pi/Po) \quad (1)$$

*2) Dispersion*

Dispersion is the phenomenon in which the phase velocity of a wave depends on its frequency. Dispersion is the spreading of the signal over time. It causes distortion for both analog and digital transmission along optical fibers [3]. It will broaden optical pulses of individual signal along the propagation direction. Pulse optical broadening can lead to corruption of the transmitted signals as optical pulse spread across to another allocated bit slots.

*C. Passive Optical Network (PON)*

Passive Optical Network (PON) is a telecommunications technology which provide point-to-multipoint architecture by using the fiber optic splitter to enable a single optical fiber to serve to the user without using individual fibers between the hub and customer. There are several types of PON such as APON, GPON, BPON, EPON or GEPON and 10G-PON. The usage of PON depend on the data rates in upstream and downstream transmission and also depend on the distance between OLT and ONU. APON stands for Asynchronous Passive Optical Network which is used for business applications. Characteristics of APON is that it can define different types of services which is suitable for carrying various types of traffic, including voice, video and data. Table 1 below shows the summary of three common standard.

*Table 1: Common PON standards*

| Technology | Standard | Distance (km) | Splitting radio (max) | Downstream (Mbps) | Upstream (Mbps) |
|---|---|---|---|---|---|
| BPON | G.983 | 20 | 1:32 | 155,622,1244 | 155,622 |
| EPON | 802.3 | 10 | 1:32 | 1244 | 1244 |
| GPON | G.984 | 20 | 1:64 | 1244,2488 | 155 to 2488 |

*1) TDM-PON*

TDM-PON is one way which can achieve higher bandwidth. However this technique cannot cope with the requirements of future network evolution with respect to aggregated bandwidth [4]. Recently, Telecom was standardized and deployed TDM-PON such as Ethernet PON, Broadband PON, Gigabit PON and 10G Ethernet PON for access network applications. Nowadays, the rate for upstream TDM-PON is 25 GB/s while for downstream is 25 GB/s and 40 GB/s. The current capacities for TDM-PON cannot satisfy the bandwidth for the future multiple user services like voice, video, internet and mobile connections. Fig 1 shows the TDM-PON diagram. This technique is based on the uses of the discrete time slot allocation sequence for into different slots with each subscribers will allocate the time slot over data transmission.

*Fig. 1. TDM-PON Diagram*

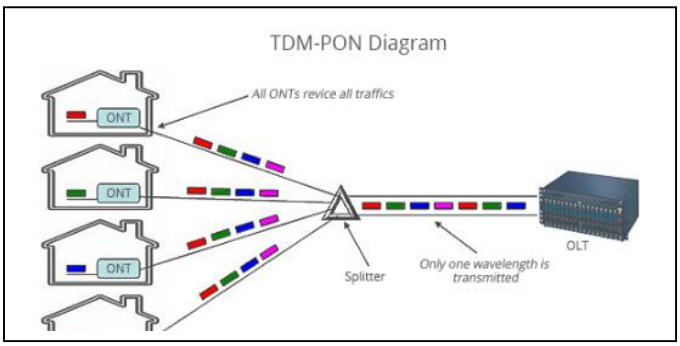


*2) WDM-PON*

WDM-PON is a fiber to the home (FTTH) solution characterized by the use of a PON structure plus the use of many wavelengths that can be dedicated for each user or shared among the group of users. It can allow the multiple and different wavelength pass through over the single fiber cable which known as bidirectional optical fiber. It can provide much higher bandwidth compare to current technology and also can carry multiple number of different wavelength over a single optical fiber which use of single mode fiber [5]. For downstream and upstream transmission, it used different wavelength. Based on

the figure below, the service provider is act like central office (CO) which is generate the downstream wavelength when the different wavelength are being transmitted using multiplexer to multiple ONU over a single fiber. While, de-multiplexer is located at the remote nodes (RN) which will distribute the different wavelength to the end users. Fig 2 shows WDM-PON diagram to subscriber.

*Fig. 2. WDM-PON Diagram*

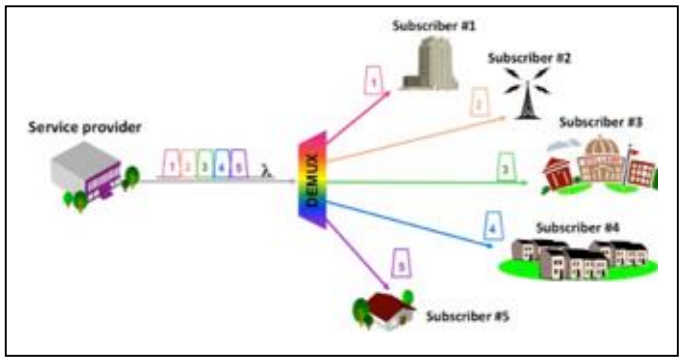


*a) Arrayed Waveguide Grating (AWG)*

AWG are being greatly used in communication system which is used as optical multiplexers and demultiplexers especially in WDM systems. It is capable to combine multiple different number of wavelengths over a single optical fiber and separate it to the end users [6], [7]. By using AWG, the number of transmission capacity will increase and the system will be more efficient and also will reduce cost.

.

*b) Reflective Semiconductor Optical Amplifier*

RSOA is the device use in WDM-PON to reprocess of downstream wavelength and reuse for upstream. RSOA is one of the method which can increase the speed for upstream transmission [8]. Usually, the speed for upstream transmission is lower than speed of downstream. This is due to the users commonly download compare to upload something. To further increase the speed of RSOA, the certain method is required such as utilize the multilevel modulation formats and electronic equalization techniques [8]. RSOA component is a cost effective since it can be modulator (no need for local laser source) and amplifier. It also suitable for long reach directional [9]. The value of the injection current in RSOA is an input signal which is allow the modulation of optical signal by SOA.

## III. METHODOLOGY

The proposed WDM-PON architecture is reported in fig. 3. We have implemented a bidirectional WDM-PON in Optisystem software. 1550 nm was used as default wavelength. The downstream signal has been detected using PIN photodetector receiver and sent to low pass Bessel filter to filter unwanted noise and sent to bit error rate (BER). We are using PRBS which generate random binary data of 10 Gbps. All data will be passing through NRZ modulator and the output is electrical signal which is information signal superimposed on light which is carrier. It is knows as external modulation. The MZM is used as external modulator. The output coming from MZM is optical signal which is carrying 10 Gbps and multiplex using WDM mux and passing through on single optical bidirectional. There are three types of models in the proposed scheme which is located at ONUs side; i) Bidirectional GPON system for upstream and downstream by deployment of RSOA at RN ii) Bidirectional PON system using AWG at RN and with RSOA. iii) Bidirectional PON system with AWG and reflective filter bidirectional at user. The length of SMF is 60km. All optical signal from OLT with 10 Gbps is split by demuultiplexer.

10 Gbps downstream signal is received and the performance of the signal is done by comparing the transmitted power and receive power. Q-factor, BER, eye diagram and eye height can be measured by using eye diagram analyzer. The remaining 50% optical signal is given to RSOA which is use for upstream transmission. RSOA consist of two input which are optical signal and electrical signal. For upstream transmission, the modulated data is multiplexed by WDM mux and transmitted through SMF. PIN photodetector will detect incoming signal and filter unwanted noise and the performance of the signal can be analyzed by eye diagram analyzer. Fig 3 shows the basic system block diagram of WDM-PON.

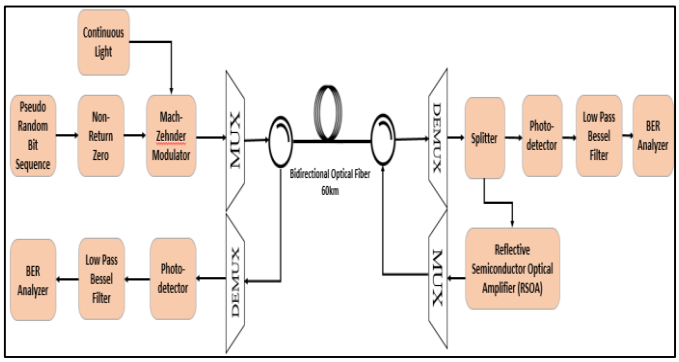


*Fig. 3. System Block Diagram*

## IV. RESULTS AND DISCUSSION

We estimated the BER from the recovered data Fig. shows the results for downstream data for a default wavelength which is 1550 nm and transmitted power by continuous wave to the system is 0 dBm. There are a few parameter need to be set in this design like wavelength, power, length and others. There are three different type of models use with different component.

*A) Bidirectional GPON system by deployment of RSOA at ONU's side.*

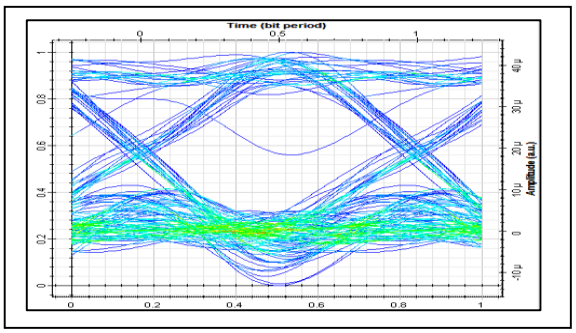


*Fig. 4. Downstream*

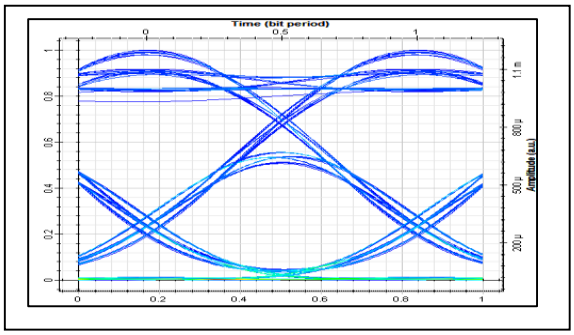


*Fig. 5. Upstream*

At receiver stage, there are few components used such as PIN photo detector, LPBF, 3R regenerator, RSOA, NRZ, PRBS and delay. The function RSOA in this side is to reflect and amplify the sending signal from central office (CO). It was used to reflect 50% of the received signal to go to downstream and other percent to upstream. Min BER for downstream transmission is $7.340 \times 10^{-9}$ which is shown in figure 4. Figure 5 shows Min BER for upstream transmission at OLT side which equal to $1.28 \times 10^{-32}$.

*B) Bidirectional PON system using RFB at RN*

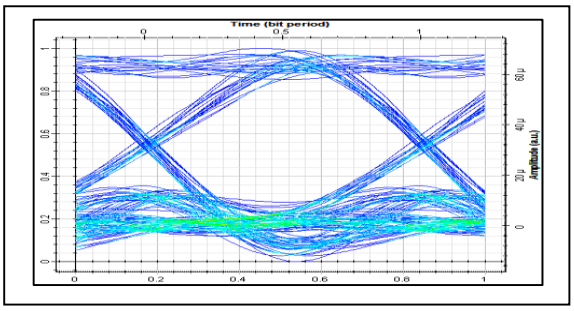


*Fig. 6. Downstream*

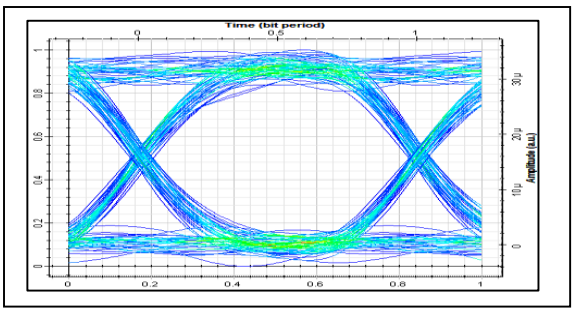


*Fig. 7. Upstream*

The receiver stage for case II is difference with case I. At receiver stage, case II using RFB component which is have quite similar function as RSOA. Fig. 6 and 7 show the Min BER for downstream and upstream transmission. Min BER for downstream is $1.239 \times 10^{-14}$ and upstream is $2.348 \times 10^{-36}$. By comparing with case I, the BER for downstream and upstream is much better in case II. This is due to the parameters of the simulation is not fulfill the system requirement used in this system.

*C) Comparison on the Results between RSOA and RFB.*

In this part, we will take a look the differences results between RSOA and RFB for both transmission. This section will investigate the effect of CW laser power (0 dBm) on bit error rate analyzer and also at the end user part for both downstream and upstream transmission. When RSOA was used in the system at ONU, min BER of downstream signal is equal to $7.34 \times 10^{-9}$ while min BER of downstream signals using Reflective filter bidirectional equals to $1.239 \times 10^{-14}$. We can see that the system based on RFB has better value of min BER than the system based on the RSOA on the downstream case. Now, let's take a look at the effect of using RSOA and RFB on the upstream signal at central office. Min BER of upstream signal when using RSOA is equal to $1.282 \times 10^{-32}$ while min BER of upstream when using RFB is equal to $2.348 \times 10^{-36}$. So the

system based on RFB has better value of min BER than RSOA for both transmissions because RFB can filter noise before send to the users and used for upstream transmission. Table 2 below shows the comparison between RSOA and RFB on PON.

Based on the existing project by Alaa Hamza Khander, they found that, when using RFB it shows better performance for downstream while when using RSOA can give better performance for upstream. This is we used EDFA in this design which is to amplify the signal. The reason of using EDFA in this design is to improve the downstream and upstream transmission performance due to the using longer distance and also higher bit rates for upstream transmission.

*Table 2: Comparison between RSOA and RFB on PON.*

| **Models** | **Min BER for Downstream** | **Min BER for Upstream** | **Pr at downstream (dBm)** | **Pr at upstream (dBm** |
|---|---|---|---|---|
| **PON based on RSOA** | $7.340 \times 10^{-9}$ | $1.282 \times 10^{-32}$ | -23.097 | -17.839 |
| **PON based on RFB** | $1.239 \times 10^{-14}$ | $2.348 \times 10^{-36}$ | -21.085 | -18.033 |

## V. CONCLUSION

The simulation was successfully demonstrated that wavelength division multiplexing passive optical network (WDM-PON) system can be implemented for 60 km. The system can deliver 10 Gbps for downstream and 5 Gbps for upstream data on a single bidirectional optical fiber. Among two types of models, the best result for downstream and upstream transmission is when the system using RFB at the ONUs side.

## REFERENCES


[1] Kwanil Lee, Seung Beom Kang, Dong Sung Lim, Hak Kyu Lee and W. V. Sorin, "Fiber link loss monitoring scheme in bidirectional WDM transmission using ASE-injected FP-LD," in IEEE Photonics Technology Letters, vol. 18, no. 3, pp. 523-525, Feb. 1, 2006.

[2] M.A. Akosu, “Mitigation Techniques of Backreflection in Bi-Directional Optical Colorless WDM-PON,” M.S. thesis, Dept Elect. Eng., Universiti Teknologi Malaysia, Skudai Johor, 2015

[3] M.S. AB-Rahman and F.M. Shaltami “Colorless and sourceless optical network units in passive optical networks,” in Journal of Theoretical and Applied Information Technology, Vol 75, No 3, pp. 293-300,2015.

[4] K. Grobe and J. P. Elbers, "PON in adolescence: from TDMA to WDM-PON," in IEEE Communications Magazine, vol. 46, no. 1, pp. 26-34, January 2008.

[5] S. H. Cho et.al, “Reducing the Back Reflection-Induced Penalty by Using a Receiver with an Optimized Decision Level in a lambda-Reuse Single Fiber Bidirectional WDM-PON,” in Optical Communication (ECOC), 2007 33rd European Conference and Ehxibition of, pp 1-2, 2007

[6] B. Raobawale and S.K. Sudhansu, “ WDM-PON Delivering 5-G-bps Downstream/2.5G-bps Upstream Data,” in Internationa Journal of Computer Application 90975-8887, vol 72, no 4, pp 27-31, 2013

[7] M. Surya and P.G. Gokul, “ Performance Evaluation of ONU in Bidirectional WDM-PON,” in International Journal of Engineering Research & Technology (IJERT), vol 4, no2, pp 71-74,2015

[8] Y. C. Chung, "High-speed coherent WDM PON for next-generation access network," 2013 15th International Conference on Transparent Optical Networks (ICTON), Cartagena, 2013, pp. 1-4.

[9] N. Pethkar et.al, “A Long Reach Bidirectional WDM-PON Upstream and Downstream Data Rate 10Gbps by using Mode Locked Laser and RSOA,” in International Journal on Recent and Innovation Trends in Computing and Communication, vol 3, no 3, pp 1533-1537, 2015

# The Design of Small Theater Hall for Local Music Performances

Nadiah Binti Mohammad
*Faculty of Electrical Engineering*
*Universiti Teknologi Malaysia, Skudai*
*Nadiah_mohd23@yahoo.com*

Mohammad Ngasri Bin Dimon
*Department of Communication Engineering*
*Faculty of Electrical Engineering*
*Universiti Teknologi Malaysia, Skudai*
*ngasri@utm.my*

***Abstract*—In theater, audiences may have enjoyed the experience of the music performance, but they were unaware of how sound reflections and acoustics that actually increased the enjoyment of the musical listening experience. The purpose of this project is to design the architectural of the theater hall and investigate the reverberation time (RT60) quality as a function of surface materials. Architectural design drawing and simulations of RT60 for an octave frequency of 250 Hz, 500 Hz, 1 kHz, 2kHz, and 4kHz using EASE 4.4 software perform the data acquisition. Therefore, the data analysis was conducted based on the findings to come up with solution to improve the acoustic quality of the theater hall. By comparing the designed RT60 with optimum RT60, this design was practically fulfill good acoustic criteria. The analysis shows that this theater hall able to deliver the sound of the performance smoothly to the audience regardless of the angle or position of the audiences.**

***Keywords—Acoustic theater hall design; reverberation time (RT60); sound pressure level (SPL);***

## I. INTRODUCTION

Acoustic is a science that dealing with all studies of mechanical waves in solids, liquids and gases also including studying of vibration and sound. Person who works in the field of acoustic technology is called an acoustical engineer. In every building, acoustics engineer played an important role as they specialized in noise control solution in every architectural, commercial and industrial market. Acoustical analysis is required to improve the acoustic and sound quality of the architecture for a better hearing of the audiences.

A theater hall is one cultural building with stage which act as performance venue and a hall filled with seats. A good theater hall is where the sound of the performance delivered smoothly to all audience regardless of the angle or position of the audience. Thus, to design a good theater hall will need a good understanding of parameters required and its acoustic properties.

In designing a theater hall, the most important parameter that should be considered is the Reverberation Time (RT60). This parameter should meet the optimum RT60 in order for audience to experience a good sound quality. Acoustic properties deal with volume and the architecture of the theater hall to provide a good reflection and absorption of the sound waves.

## II. LITERATURE REVIEW

This literature review will discuss on the theories related to the acoustic properties that need to be considered in designing a theater hall and how the sound been absorbed and reflected in building design.

### *A. Types and Forms of Theater*

A musical drama or the classical drama usually is performed in various types of theaters that involved a warehouse, outdoors, stairwells or other unfamiliar places. But in this discussion, the scope has been minimized into two sizes of drama spaces, small drama spaces and enormous drama spaces. For small drama theater are the courtyard n flexible stage while proscenium, thrust and open stage are for enormous theaters.

In small theaters, usually the stages are in the level as the audience in the first row. This is the unique feature of the small theater where it creates good intimacy relationship between the audiences and the actors. The suitable types of stages for the small theaters are the arena, thrust, end stage, flexible theaters and environmental theater [1].

Arena is a theatre where the performance stage would be in the center of the hall and surrounded by the audiences. Example of arena theatre is shown in Figure 1(a). While for the thrust theatre is the extended stage where the audience surrounds the stage in three sides and providing a space for the background scenery. But theses types of stages limit the audience view of the performance. Figure 1(b) shows the example of thrust theatre.

As for the end stage types, is a theatre where the stage and the audiences were on the same level. The stage will be placed at the end of the hall while the audience seated facing the stage. Example of the end stage is the Studio Theater, Salford UK shown in Figure 1(c). Other than that, flexible theater is also a common stage used for small drama theater. Flexible theater is a non-fixed seating interchangeable depending on the performance requirement. This theater can be change into the end stage, thrust or arena stage forms as been described above.

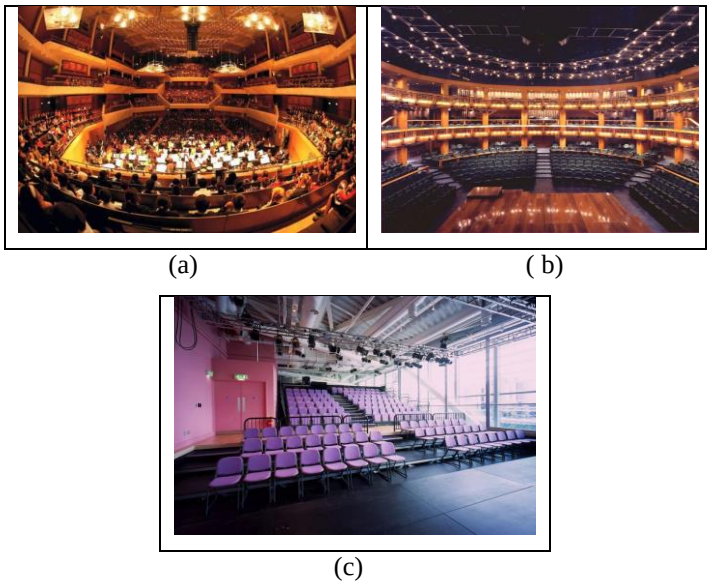

(a) ( b)

(c)

Fig. 1. a) Royal Exchange Manhester, UK.

b) Chicago Shakespeare Theater, USA.

c) Studio Theater, Salford, UK.

Enormous drama theatres usually for range of 350 to 1000 of audience seats. Mostly, enormous drama theatres are in proscenium form but in some features it were in open stage and thrust form. Proscenium theatre is where the stage of the performance was placed at the end of the hall and the audiences were physically separated from the stage by one proscenium wall called apron. This situation is also known as a "two-box" arrangement- the stage and the hall filled up the two "boxes". Example of proscenium stage is shown in Fig. 2. (a).

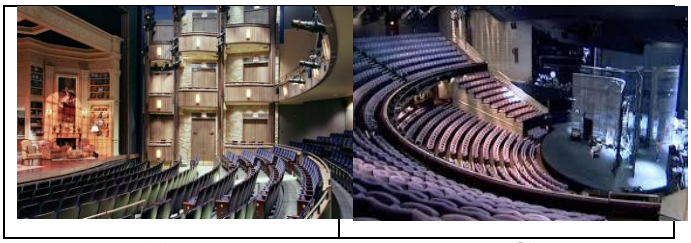

(a) (b)

Fig. 2. a) Goodman Theater, Albert Ivar Theater, Chicago.

b)Olivier Theater. Royal National Theater, UK.

Certain enormous drama theatres used the thrust open stage form, with three sides audience surround the performance stage. The term of open stage meaning that the stage can be configured into thrust form, but indicates a more frontage arrangement as shown in figure 2 (b).

## B. *Hall Capacity*

In designing a theater hall. The most important acoustic properties that should be considered are the number of the audiences in the hall. The numbers of audiences determine the volume and dimension of the hall. This is why in designing a theatre hall, the capacity should be a primary consideration.

Hall capacity usually depends on various factors covering from estimated potential audience and the required performance range characteristic. Usually, large or small theatre hall have at least 150 seats of audiences. Table 2.1 shows the range of capacity in Malaysia's theatre halls.

TABLE I. THE RANGE OF HALL CAPACITY OF MALAYSIA'S THEATERS

| THEATRE | CAPACITY (SEATS) |
|---|---|
| Panggung Bandaraya KL | 327 |
| PJ Live Arts, Jaya One | 450 |
| Experimental Theater, UPM | 500 |
| Auditorium Dewan Bandaraya KL (DBKL) | 600 |
| Bentley Music Auditorium, PJ | 800 |
| Philharmonic Theater KLCC | 885 |
| Dewan Sivik MBPJ – Civic centre | 1000 |
| Istana Budaya | 1700 |
| KLPAC Pentas 1 | 1700 |
| Kuala Lumpur Convention Centre | 3000 |
| Arena of Stars Genting Highland | 6000 |

## C. *Seating Arrangement*

The seating arrangement of one comfortable theater hall has to be user friendly yet with accurate length and distance for a perfect view of the performances and reflection of sound. There are several types of seating arrangement for theater hall such as three sides seating where the audience were divided in three areas- left, center and right area as shown in figure 2.1. In deciding the seating arrangement of the hall, the most important consideration is the safety precaution of the audiences incase of emergency. If fire or any emergency situation occurs in the hall, the audience can easily be evacuated[4].

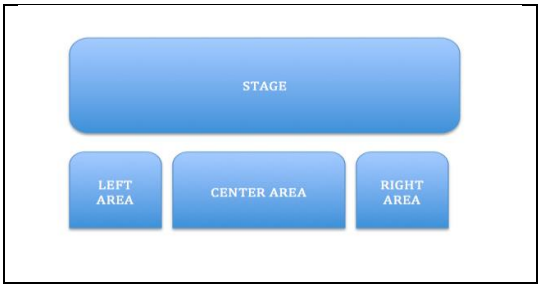


Fig. 3. Seating arrangement with three side audiences.

## D. *Reverberation Time (RT60)*

Basically, every closed room has reverberation. Reverberation time is a time taken for a sound waves produced in a room to completely die away due to absorption of the walls and other surfaces of the room. For example, when audience makes applause in an enclosed room, it takes around 10 seconds for the sound generated to die away completely. This means that the enclosed room has a RT60 of 10 seconds [7]. For the RT60 calculation, please refer to equation 2.1

$$RT60 = \frac{0.16V}{A} \qquad (2.1)$$

$A = S_n \alpha_n$

V = Volume, $m^3$

S = Surface Area

$\alpha$ = Sound absorption coefficient of the surface

## III. METHODOLOGY

Methodology used in this project consists of analysis of every aspect of architectural design of the theater hall and the measurements of the Reverberation Time (RT60). In designing a good theater hall, should have a good architectural design where absorption and reflection parameters should be considered.

### *A. Hall Shape*

The most frequent shapes used in theater hall design were summarized in Figure 4. The mostly encountered performers were the shoebox floor and rectangular plan. Based on Beranek's review on theater hall stated that halls with A+ rated have this kind of form because shoebox hall provides good side reflections. For this small project, shoebox hall shaped were used in terms of sound reflections.

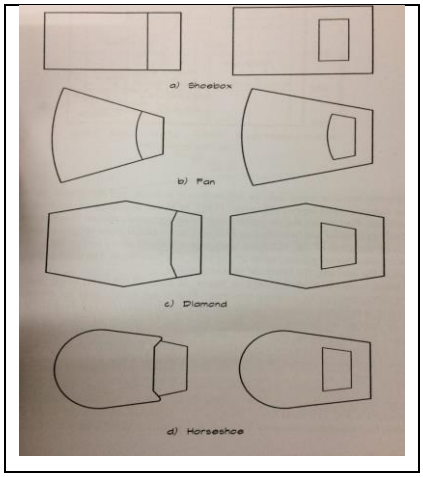


Fig. 4. Plan forms for concert halls.

### *B. Hall Seating and Capacity*

To produce a comfortable theater hall, the seating arrangement has to be user friendly yet with accurate length and distance for a perfect view of the performances and reflection of sound. Different types of seating provide different feelings and viewing of the audiences during the performance. There are two designs of seating in theater hall, which are low cost budget seating and generous seating. The different between these two designs is the row spacing as shown in Figure 5. Generous seat provide more row spacing for comfortable environment to the audience while enjoying the performance. Capacity for a small theater hall is in the range of 150 to 300 seats. Average capacities with 200 seats were used in designing the theater hall.

TABLE II. CHAIR SPECIFICATIONS

| Type | Measurement (m) |
|---|---|
| Total height | 0.98 |
| Width | 0.56 |
| Length | 0.74 |
| Height from handle to floor | 0.60 |
| Height from seat to floor | 0.44 |

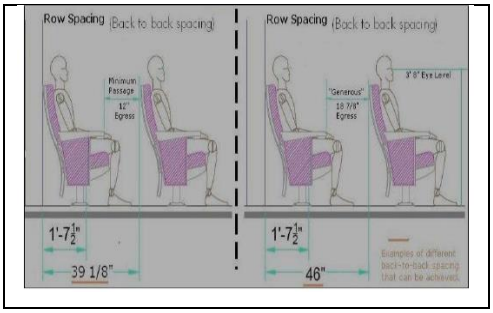


Fig. 5. Row spacing

### *C. Hall Volume and Dimension*

Volume of the hall depends on the room gain and reverberation time. Small theater hall required large volume per seat to limit excessive loudness of the theater hall. While for large theater hall need small volume per seat as it helps conserver the acoustic energy. For this volume measurement, KLPAC Pentas 2 was taken as reference. The volume of the theater hall is 2293.5 $m^3$ with room surface of 1197 $m^{2.}$

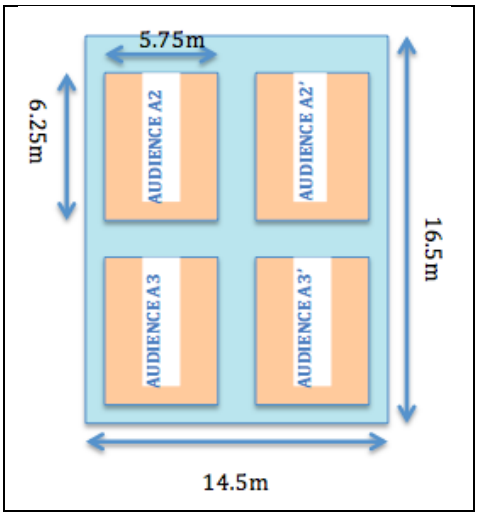


Fig. 6. Top plan of the audience area.

TABLE III. HALL DIMENSION

| Types | Measurement (m) |
|---|---|
| Audience Area Length | 16 |

| | |
|---|---|
| Audience Area Breadth | 14.5 |
| Audience Area Height | 8 |
| Stage Depth | 7 |
| Stage Breadth | 12.5 |
| Stage Height | 5 |
| Step Height | 1 |

### *D. Architectural Drawing using EASE 4.4*

EASE software is the Enhance Acoustic Simulator for Engineers. EASE provides consultants and system designers with valuable set of equipment and tools for professional practice, from realistic modeling, details and simulation of acoustic venues. In this EASE drawing design, the author used pre-existed model in the EASE as reference. The original design hall is as shown in Figure 7.

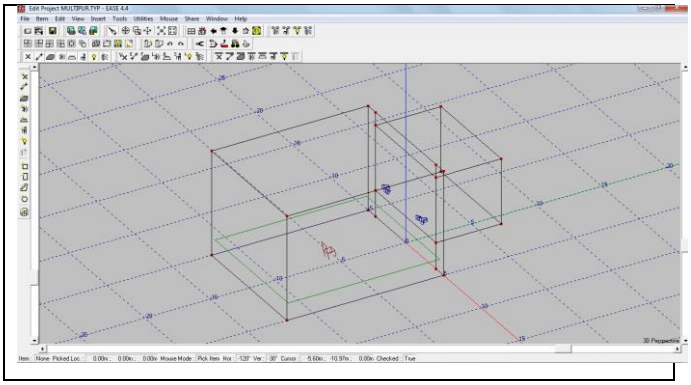

Fig. 7. The original drawing design of the theater hall.

### *E. Optimum Reverberation Time (RT60)*

The optimum reverberation time can be achieved depends on the volume and purpose of hall. Based on research stated, the reverberation time can determine the suitability of the area for a particular purpose. RT60 for the use of theater and music depending on its type as shown in Figure 8.

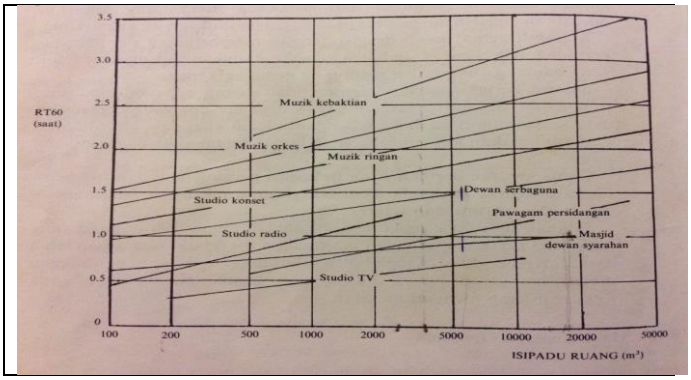


Fig. 8. The optimum reverberation time for theater hall of various volume and functions at a frequency of 1KHz.

Based on Figure 8, for volume of 2293.5 $m^3$ with studio concert type, the suitable optimum value of RT60 is in range of 1.6s to 1.7s at 1khz. For this theater hall design, the targeted value of RT60 that should be achieved is in range of 1.6s to 1.7s.

## IV. Result and Analysis

Methodology used in this project consists of analysis of every aspect of architectural design of the theater hall and the measurements of the Reverberation Time (RT60). In designing a good theater hall, should have a good architectural design where absorption and reflection parameters should be considered.

### *A. EASE Drawing*

EASE software is advance acoustic software for engineers that provide simulation of any acoustic venues. Using EASE software easier for the engineers to design the venue and analyze the acoustic parameters as the EASE software equip with complete tool set of acoustic parameters such as reverberation time (RT60), direct sound pressure level, total sound pressure level (SPL), C80, C50 and speech transmission index (STI). EASE drawing can be designate using CAD module, assigned absorption coefficient to the venue surfaces, and listener position as well as the sound sources can easily be included to the design model.

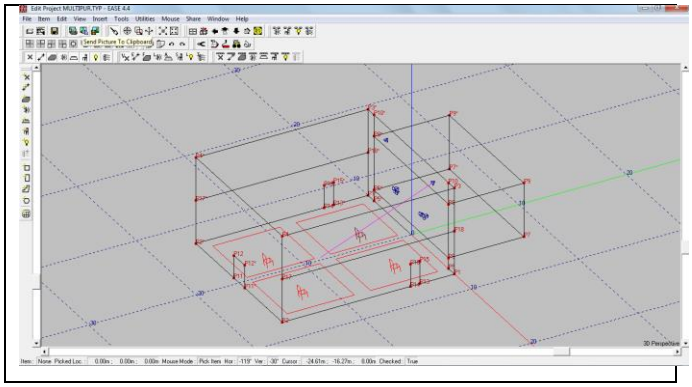

Fig. 9. EASE drawing of the Theater hall.

This theater hall drawing consists of 18 points with its own coordinates, 14 faces of wall, 4 audiences area and 1 loudspeaker installation as shown in Figure 9. While in Figure 10 shows the omniview of the concert hall drawing using EASE software with side view, end view and plan view.

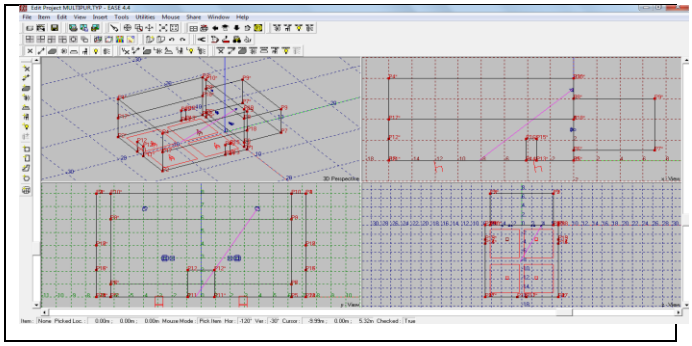

Fig. 10. The omniview of the concert hall drawing.

### *B. Reverberation Time (RT60)*

Each time a sound waves meets the surface, part of the energy absorbed and partly were being reflected. This reflected wave encounters another surface repeatedly until it disappears if it is not replaced with another wave. The reverberation time of the hall can be calculated as surface and volume of the hall have been determined. Based on the EASE architectural drawing of the theater hall, the RT60 were calculated using formula shown in equation 4.1

$$RT60 = \frac{0.16V}{A} \qquad (4.1)$$

$A = S_n \alpha_n$

V = Volume, $m^3$

S = Surface Area

$\alpha$ = Sound absorption coefficient of the surface.

The materials of each surface have to be determined before the reverberation time were calculated. Table IV shows the surface materials of each wall partition in the theater hall design.

TABLE IV. SURFACE MATERIALS OF THEATER HALL

| | Hall Partition | Materials | Surface Area, $m^2$ | Absorption Coefficient, $\alpha$ |
|---|---|---|---|---|
| **Audience Area** | Floor | WOOD FLR | 232.00 | 0.08 |
| | Upper Side Wall | PLYWD 1/2 | 64.00 | 0.17 |
| | Lower Side Wall | WOOD GRID0 | 64.00 | 0.99 |
| | Ceiling | GYP 2X 5/8 | 232.00 | 0.07 |
| | Back Wall | WDPANEL 16 | 116.00 | 0.10 |
| **Stage Area** | Floor | WOODFLR LN | 87.50 | 0.05 |
| | Side Wall | WDPANEL 18 | 35.00 | 0.08 |
| | Ceiling | GYP5/8CEIL | 87.50 | 0.04 |
| | Front Wall | WDPANEL 16 | 62.50 | 0.10 |
| **Small Wall** | Side Wall | $\alpha$ = 20% | 8.00 | 0.20 |
| | Lower Wall | $\alpha$ = 20% | 12.50 | 0.20 |
| | Upper Wall | $\alpha$ = 20% | 25.00 | 0.20 |
| **Volume** | 2293.5 $m^3$ | | | |

With the obtained volume and the surface materials of the theater hall, the design was simulated and RT60 were measured. Figure 11 shows the RT60 of the design hall from 100Hz up to 10kHz. Using the Malaysian acoustic standard, to obtained optimum RT60 should be observed at 1Khz. Based on the data collected, the RT60 of this hall design is 1.67s at 1khz. This shows that the reverberation time of this design hall is in good reverberant room because achieved the optimum value of RT60 for 2000$m^3$ room volume.

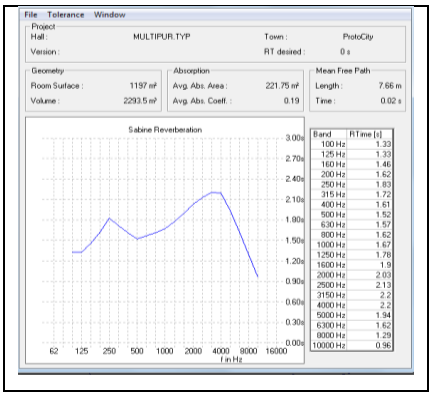


Fig. 11. The RT60 of the design hall.

### *C. Sound Pressure Level (SPL)*

The sound pressure level is commonly used parameter in acoustic wave strength. Its correspond well with human's hearing pressure. Reference sound pressure for a person is set at human threshold hearing about 1000Hz. The resultant level is 0dB when the reference pressure is equal to the sound pressure. The sound pressure level can be defined as in equation 4.2.

$$L_p = 10 \log \frac{p^2}{p_{ref}{}^2} \qquad (4.2)$$

Where p = root-mean-square sound pressure (pa)

$P_{ref}$ = reference pressure, 2 x $10^{-5}$ Pa

In this theater hall design, the results of the sound pressure level (SPL) were tabulated in Table V and Table VI.

TABLE V. DIRECT SPL OF THE AUDIENCE AREA

| No | Audience Area | Reading on the Respective Frequency (dB) | | | | |
|---|---|---|---|---|---|---|
| | | *250Hz* | *500Hz* | *1kHz* | *2kHz* | *4kHz* |
| 1 | A2 | 83.88 | 87.34 | 85.46 | 85.77 | 85.81 |
| 2 | A2' | 83.88 | 87.34 | 85.46 | 85.77 | 85.81 |
| 3 | A3 | 81.71 | 85.22 | 83.97 | 83.99 | 83.76 |
| 4 | A3' | 81.71 | 85.22 | 83.97 | 83.99 | 83.76 |

TABLE VI. TOTAL SPL OF THE AUDIENCE AREA

| No | Audience Area | Reading on the Respective Frequency (dB) | | | | |
|---|---|---|---|---|---|---|
| | | *250Hz* | *500Hz* | *1kHz* | *2kHz* | *4kHz* |
| 1 | A2 | 95.03 | 93.66 | 93.90 | 94.73 | 94.83 |
| 2 | A2' | 95.03 | 93.66 | 93.90 | 94.73 | 94.83 |
| 3 | A3 | 94.82 | 93.37 | 94.64 | 94.48 | 94.63 |
| 4 | A3' | 94.82 | 93.37 | 94.64 | 94.48 | 94.63 |

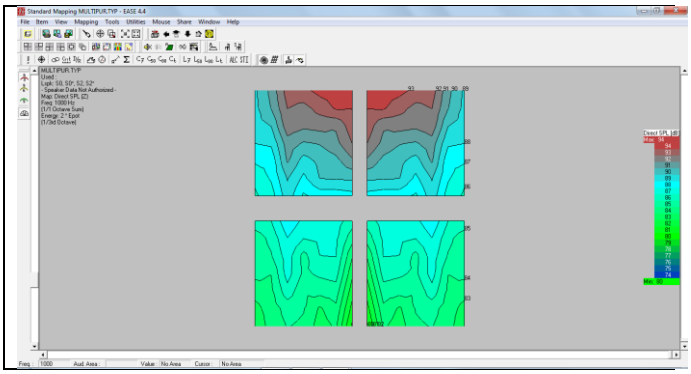

Fig. 12. Direct SPL standard mapping at audience area.

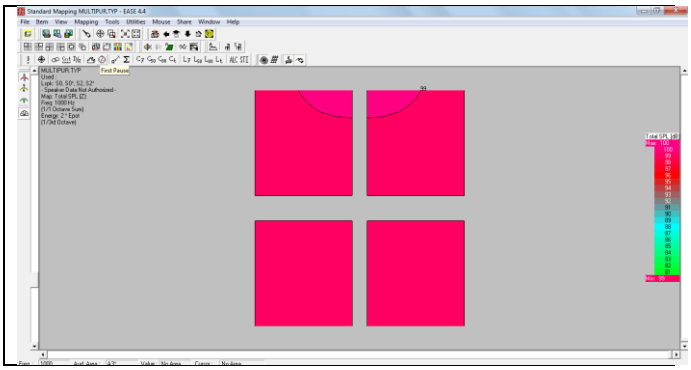

Fig. 13. Total SPL standard mapping at audience area.

The average sound pressure level at audience area A2 and A3 was found around 83dB. For theater hall design, the optimum value for SPL at audiences area with 1W inject power to loudspeaker should be in range of 80dB to 90dB at every sittings. This shows that this theater hall design results a good sound received by the audiences in the hall.

## V. CONCLUSION

In order to experience good sound quality in a theater hall, all acoustic properties and parameters should be taken into consideration. Sound qualities of one theater hall were measured in term of reverberation time (RT60). Thus, reverberation time (RT60) quality was investigated as a function of a surface area. There were six main steps in theater hall design for optimum acoustic. The early step required is deciding the room usage. Then, determine the volume of the hall. With usage and volume are known, the optimum reverberation time can be determined from the establish chart. Next, determine the surface area and finishes of the hall to check for sound absorption coefficient of every finishes. After completing the steps as stated before, the reverberation time of the hall from hall's volume, surface area and absorption coefficient were determined. Lastly, compare the optimum RT60 value with the designed RT60 value. Acoustic software EASE 4.4 was used to draw the architectural design of the theater hall model and simulation of the acoustic parameters. The reverberation time of the theater hall design were obtained through simulation of EASE software which results in RT60 equal to 1.67s at 1kHz frequency. This concluded that the reverberation time in the theater hall is good and objective of this project studies has been achieved.

## REFERENCES


[1] *Types And Forms Of Theatre*. 1st ed. Theatre Projects Consultants (pp. 3–8 ).

[2] *Types And Forms Of Theatre*. 1st ed. Theatre Projects Consultants (pp. 8–10 ).

[3] *Types And Forms Of Theatre*. 1st ed. Theatre Projects Consultants (pp. 11).

[4] Fauza, Arinal. *The Seating Design In Medium Size Of Auditorium*. Universiti Teknologi Malaysia, 2013.

[5] Nur Zhahran, Aulia. Investigation Of Acoustic And Sound Quality Of Taman Putri Kulai Multipurpose Hall. Universiti Teknologi Malaysia, 2016.

[6] Zhahran, Aulia Nur. Investigation of Acoustic and Sound of Taman Putri Kulai Multipurpose Hall (2016): 2.

[7] Nur Zhahran, Aulia. Investigation Of Acoustic And Sound Quality Of Taman Putri Kulai Multipurpose Hall(pp. 7 – 8). Universiti Teknologi Malaysia, 2016.

[8] Furness, Hannah. "'Shoe-Box Shaped' Concert Halls Make Music More Emotional"(2016, 24th March). *The Telegraph* 2016:

[9] Jaffe, J. Christopher. *The Acoustics Of Performance Halls*. 1st ed. New York: W.W. Norton & Co., 2010.

[10] Jordan, Vilhelm Lassen. *Acoustical Design Of Concert Halls And Theatres*. 1st ed. London: Applied Science Publishers, 1980.

[11] The Kuala Lumpur Performing Arts Centre (2016). *Technical Data Sheet of Pentas 2* [Brochure]

# Entrance System for Masjidil Haram (Prototype)

Nor 'Afifah Binti Awang
*Faculty of Electrical Engineering*
*Universiti Teknologi Malaysia*
*Johor Bahru, Malaysia.*
*norafifahawang94@gmail.com*

Mohd. Haniff bin Ibrahim
*Department of Communication Engineering*
*Faculty of Electrical Engineering*
*Universiti Teknologi Malaysia*
*Johor Bahru, Malaysia.*
*hanif@fke.utm.my*

***Abstract*—The entrance system (gate control) of Masjidil Haram is not really systematic. The gate will be closed by the guards although the prayers' areas are still not fully occupied. Jamaah have to pray outside the mosque under the hot sun (in summer) although more Jamaah are supposedly permitted to enter the mosque. An earlier system of entrance control system already exists but no one ever implement it to the Masjidil Haram. In this project, LED is use to replace the gate itself as a prototype. Green LED indicates gate is open while red LED indicates gate closed. While the sensor, it will sense the number of person in and out of the room. Therefore, it is expected that by having this system, the entrance of the Masjidil Haram will be systematically controlled and more Jamaah will have a chance to calmly perform their ibadah in the mosque.**

***Keywords—arduino programming;***

## I. INTRODUCTION

As we all know, Masjidil al-Haram is the very important place for Muslims. It is the largest mosque in the world and located in the city of Makkah Al Mukharamah, Saudi Arabia. Non-Muslims are not permitted to enter Makkah as it is considered as a Haram area.

Recently, the demand was increasing rapidly since our Islamic populations are growing in a bigger circle. The numbers of visitors to the holy city of Makkah are increasing each year and more needs to be done to provide them an enough space [1]. The current size is very limited and not enough to fulfill the current request. That is why there is a quota to control the number of visitors from every country especially during the Hajj season and Ramadhan season. The Saudi government is currently doing something to overcome this problem [2].

## II. LITERATURE REVIEW

### A. Introduction

In the beginning of this project, a lot of researches about entrance control system have been doing to achieve the objectives of this project. In order to fulfill the goal set, much information from various sources has been gathered such as journal, thesis and website on the internet. Several methods that related to this project are included in this chapter. The topics discussed in this chapter are about hardware and software used in completing this project.

### B. Medium Range Infrared Sensor

Basically, an IR sensor is an electronic instrument which is used to detect any certain characteristics happened along the beam of the infra red ray by either emitting or detecting the radiation. It also can measure the emitted heat by any object and also a motion detector [3]. This Medium Range IR sensor is user friendly and able to detect fast obstacle using infrared. Its implementation of modulated IR signal is very sensitive to the interferences and we can adjust the sensing distance manually.

Fig. 1. Medium Range IR Sensor

### C. Light-Emitting Diode

A light-emitting diode (LED) is a semiconductor light source. LEDs are used as indicator lamps in many devices and are increasingly used for other lighting. Appearing as practical electronics components in 1962, early LEDs emitted low-intensity red light, but modern versions are available across the visible, ultraviolet, and infrared wavelengths, with very high brightness [4].

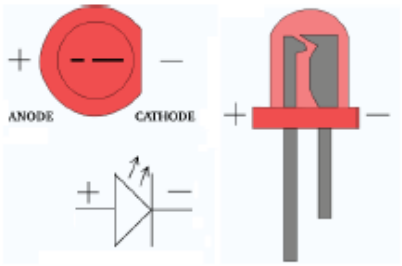


Fig. 2. LED

### D. Principle of Arduino

This project will be focused on Arduino UNO as a microcontroller which is a board based on ATmega328P [5]. It contains 14 digital input/output pins which 6 of them can be used as PWM outputs. It also has 6 analog inputs with a clock speed of 16 MHz, a power jack, a reset button, a USB

connection and an ICSP header. Everything that required for supporting the microcontroller is there. To get started, just connect the board to a computer or power it using an AC-to-DC adapter. In Italian, UNO means one which is chosen to release of Arduino Software (IDE) 1.0. It is recommended to use the input voltage in the range of 7V to 12V and the operating voltage is 5V.

Fig. 3. Arduino UNO Board

TABLE 1 ARDUINO UNO SPECIFICATION

| | |
|---|---|
| Microcontroller | ATmega328P |
| Operating Voltage | 5V |
| Input Voltage (recommended) | 7-12V |
| Input Voltage (limit) | 6-20V |
| Digital I/O Pins | 14(of which 6 provide PWM output) |
| PWM Digital I/O Pins | 6 |
| Analog Input Pins | 6 |
| DC Current per I/O Pin | 20 mA |
| DC Current for 3.3V Pin | 50 mA |
| Flash Memory | 32 KB (ATmega328P) of which 0.5 KB used by bootloader |
| SRAM | 2 KB (ATmega328P) |
| EEPROM | 1 KB (ATmega328P) |
| Clock Speed | 16 MHz |
| LED_BUILTIN | 13 |
| Length | 68.6 mm |
| Width | 53.4 mm |
| Weight | 25 g |

### *E. Research on Software*

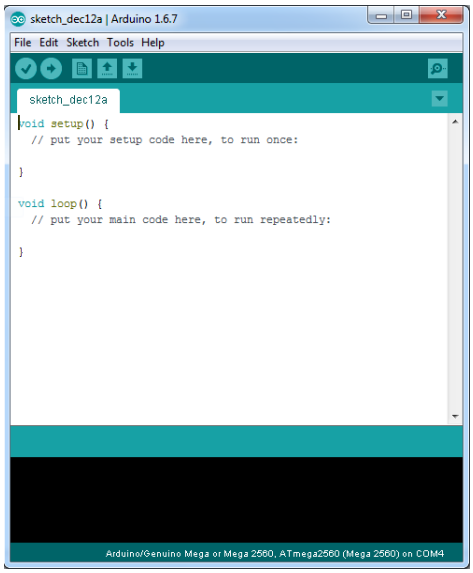


Fig. 4. Arduino sketch for Arduino software

Fig. 4. shows the Arduino Software (IDE), a software use to run the program. This software use high language which is C or C++ programming. The codings are divided into three parts. The first part is to include all the libraries that suit the desirable program and declaration of all parameters. The second part is void setup ( ). To run the code only once in the program, the code should be written in this part. The last one is void loop ( ) where this loop will run the code repeatedly. So, in this loop, all the main code should be write here

## III. METHODOLOGY

### *A. Introduction*

In this chapter, it will briefly discuss the methodology used in the process of completing this project and also how this project going to be realized based from previous chapter.

### *B. Design Methodology*

This design methodology consists of three phase. The first phase is the literature review part which is based on the related problem to collect some data and information on how to make this project can be successfully done at the end. The next phase is the compilation of the programming part. After the completion of the programming, analysis and test for all the components, then it will be interface with the Arduino by connecting all the components to the Arduino board to check either the coding are able to function or not.

When the second phase is successfully done without any errors, then the final phase could be done. This phase is where the prototype is making. After that, the system is ready to be tested. If there are any changes or improvement, the process will be repeated at the right phase until the system is ready to be tested again.

### C. Summary

Basically, this chapter is one of the most important parts in completing this project. Based on the flowchart above, the methodology parts cover all the hardware and software implementation. All the steps following the Gantt chart should be completed in this chapter.

## IV. Result and Discussion

Arduino UNO was used as the main controller to interface all the hardware components used in order to complete the system. First of all, this project require a cost to buy all the components hence, to save cost as many as possible, this project will present by using concept. Instead of using a servo motor to control the closing and the opening of the gate, this project only use two LEDs to represent the gate. Only can be explained by using the concept of prototype to make other understand about how this project and also can show how actually the project works.

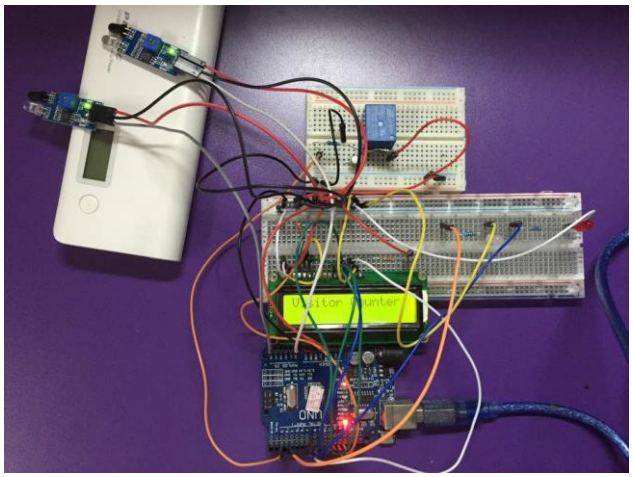

Fig. 5. Overall look of the project

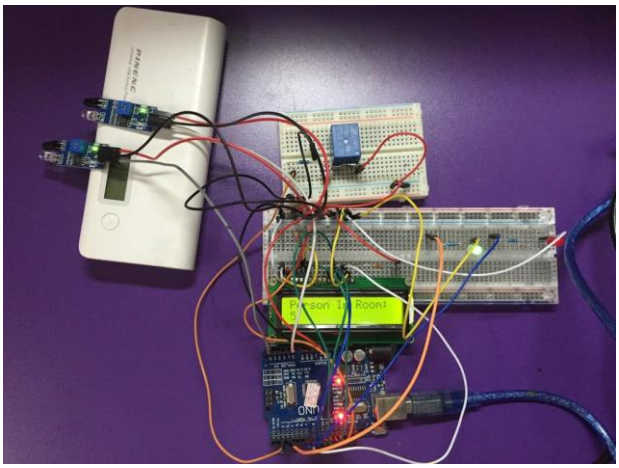

Fig. 6. Condition for gate open

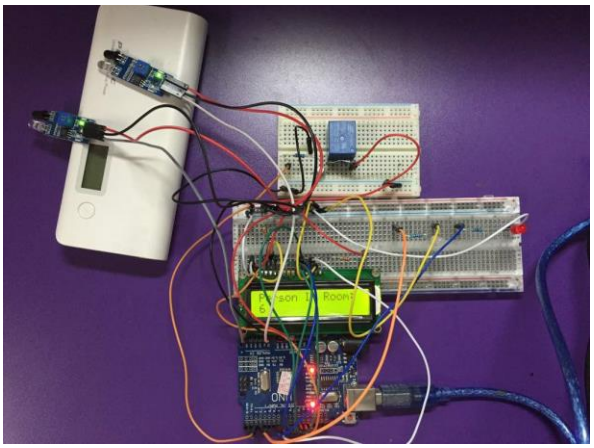

Fig. 7. Condition for gate close

Fig. 5. shows the overall look of the project before it being installed properly in a prototype case. This project is using two infrared sensors in order to sense the number of people entering and exiting the room as representation for Jamaah enters and exit the mosque.

The sensor would observe an interruption and provide an input to controller which would run the counter increment and decrement depending on entering or exiting of the person. The counted number is displayed on a 16x2 LCD through the controller which is the Arduino. When any one enters in the room, infrared sensor will get interrupted by the object then other sensor will not work because of the delay.

The condition for this project is, the gate will be closed once the number of person entered the room is exceeding limit which is when the number of person is greater than five. As can be seen from Fig. 2. the green LED is turn on because number person still in range and not exceeding the limits yet. This condition represents that the gate is still open. While for Fig. 3. is the condition when the gate is closed, the red LED is turns on but we can barely see the redness of the red LED. This condition is true when the room is actually full or exceeds the limit.

## V. Conclusion

There are several limitations in this project and the direction of future development is discussed. Further study needs to be done in order to eliminate the challenges and improve the upcoming result.

Project had been done according to the Gantt chart. The objectives of the project were accomplished at the end of the project. It is expected that by having this system, the entrance of the Masjidil Haram will be systematically controlled and more Jamaah will have a chance to calmly perform their ibadah in the mosque.

## REFERENCES

[1] Sarmady, S., Haron, F., Mohd Salahudin, M. and Talib, A. Z. H. Evaluation of existing software for simulating of crowd at Masjid Al-Haram. Jurnal Pengurusan Jabatan Wakaf Zakat & Haji, 2007. 1(1): 83–95.

[2] Kucer, S. and Friedman, N. Entrance control system, 2013. US Patent 8,453,382.

[3] Benet, G., Blanes, F., Simó, J. E. and Pérez, P. Using infrared sensors for distance measurement in mobile robots. Robotics and autonomous systems, 2002. 40(4): 255–266.

[4] Schubert, E. F., Gessmann, T. and Kim, J. K. Light emitting diodes. Wiley Online Library. 2005.

[5] Monk, S. Programming Arduino. McGraw-Hill Companies, USA. 2012.

# Non Destructive Method of Detecting Counterfeit Medicine

Nuraliza Binti Alias
*Faculty of Electrical Engineering*
*Universiti Teknologi Malaysia*
*Johor Bahru, Malaysia.*
*alizabtalias@gmail.com*

Ameruddin Bin Baharom
*Department of Communication Engineering*
*Faculty of Electrical Engineering*
*Universiti Teknologi Malaysia*
*Johor Bahru, Malaysia.*
*amer@fke.utm.my*

***Abstract*—Counterfeit medicines are widespread increasingly especially in poor countries. Authorities such as the World Health Organization (WHO) has taken some methods and technologies to identify the counterfeiting. This research was conducted to investigate the new method of detecting counterfeit medicine through its dielectric constant. A network analyzer of E5701C with open-ended coaxial probe and frequency range from 10MHz to 20GHz with 100 sample points was used to determine the dielectric constant. Samples of authentic medicines such as tablet medicine from brand of Panadol, Uphamol 650, Ponstan, Synflex and Hydrosil are being tested. A home made tablet sample of counterfeit medicine from rice flour and glutenous rice flour is use to show its content of dielectric constant difference with the authentic medicine. It is found that the various type of ingredients gave difference number of dielectric constant. Thus, the value of dielectric constant found in authentic medicine can be use as the benchmark of the drug.**

***Keywords—Dielectric constant; Network Analyzer; Dielectric Properties; Panadol; Medicine***

## I. INTRODUCTION

For the past few years, the technology has grown rapidly to ease people life. Therefore, medicine was created in a form of solid and liquid in comparison with the traditional medicine which will need more effort to consume it. However, people's lives and health are put in danger because of counterfeiting. In poor country estimated that one out of four packets medicine being sold by unregistered pharmacies was faked. About 50 % of counterfeit medicine can be found in the internet [1] which concern by many responsible parties.

In order to tackling these problems, there are many ways that have been introduced. Based on Intertek Pharmaceutical Services [2], their expertise in falsified medicine has discovered many ways with different technologies to analytic counterfeit medicine. Some of the technologies that assist the investigation are liquid chromatography - mass spectrometry (LC-MS), RAMAN spectroscopy, nuclear magnetic resonance (NMR) spectroscopy, as mass spectrometry (MS), chromatography - mass spectrometry (GC-MS) and, infra-red (FTIR) spectroscopy.

In addition to that technology, measuring dielectric constant of the counterfeit medicine using network analyzer is introduced. It using non-destructive method to measure the API's and gives scientific values of element between fake and authentic medicines.

The easiest way to detect counterfeit medicines are by analyzed it physical appearance using visual inspection. For examples, holograms examination, weight, colour, size, bar codes, crimping and printing [3]. Using this method, advance technology can fake it exactly with the original but with different contents. Thus, advance approaches are introduce which concerned the quality of medicines. However, the technology needs to destroy the medicines and using strong chemical to know the difference of quantity content between fake and original.

To overcome the weaknesses, a method of measuring the dielectric constant of the medicines without destroy it or using any chemical is introduced. Network analyzer spectrum is used to measure the dielectric constant with suitable frequency and measurement technique and fixtures.

## II. LITERATURE REVIEW

### *A. Analysis of Counterfeit Drugs by Thin Layer Chromatography*

A plate of plastic, aluminum or glass covered with thin layer of silica is use to place a sample of medicine. Then, the plate is inserted into a developing chamber contain a mixture of solvent. By a chemical reaction, the solvent will be dissolves in the sample. Before, the sample had consist of medicine and inactive components, thus, the mixture will have different affinities with the adsorbent matrix and will travel with the solvent at individual speeds. According to the characteristic, it is effective to isolate the mixture and compound. Ultraviolet (UV) radiation or chemical treatment can be used to visualized the individual component after the migration of solvent is complete.

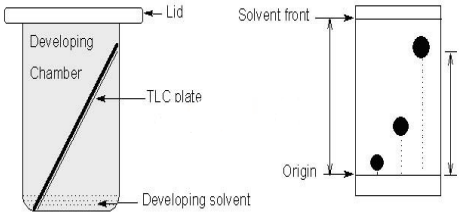


Fig. 1. Thin Layer Chromatogrpahy

The distance of travel (RF value) between the authentic and sample spot can determine the characteristic of each compound. It can be detected by comparing the size, colour and intensity of sample spot and reference spot. Therefore, an active ingredient of a medicine can be recognized by compared to a drug standard. The distance of travel (RF value) between the authentic and sample spot can determine the characteristic of each compound. It can be detected by comparing the size, colour and intensity of sample spot and reference spot. Therefore, an active ingredient of a medicine can be recognized by compared to a drug standard.

### *B. An Analysis of Dielectric Constant of Pharmaceutical Medicines using Microwave Radiation Exposure*

The sample used for this experiment is Cloperastine and Alucid. These samples are in tablet form and need to be crash into powder. Then, they are mix with moisture content which is water at 5ml, 10ml, 15ml, 20ml, 25ml and 30ml. An open ended coaxial probe is choose to perform the measurement. With the help of Vector Network Analyzer and software the dielectric can be collect easily.

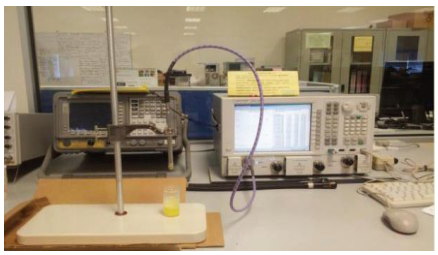

Fig. 2. Experiment setup

Figure 2 shows the measurement setup of this experiment.The end of performance probe used was inserted into the sample and measurement was taken. The vector network will supply a microwave signal and the wave reflected by the material was measured. Dielectric properties data was recorded by software in the analyzer. The software (85071E) has capability to calculate the dielectric constant and dielectric loss. The result was display in a function of frequency.

### *C. Exposure Broadband Dielectric Properties Measurement of Some Vegetables and Fruits Using Open Ended Coaxial Probe Technique*

The fruits and vegetables samples are being kept in two different air conditioned room at 16℃ and 25℃ for about five hours. Open ended coaxial probe is connected to the vector network analyzer (VNA) to measure the dielectric constant. Before, the probe system must undergo a calibration system to ensure that the measurement of reflection coefficient refer to the probe's aperture. Then, the end of Agilent 85070E open ended coaxial probe is immersed or contact to the sample as shown in Figure 3.In order to get the dielectric constant, the software of this network analyzer must be install in external computer. The dielectric constant is measured at a frequency range from 200MHz to 8Ghz for 101 samples on logarithmic scale.

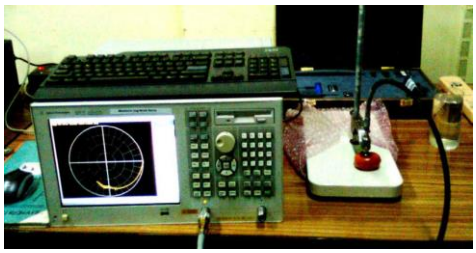

Fig. 3. Measurement setup for fruit sample

## III. METHODOLOGY

The aim of this project methodology is to give details on process used to get the dielectric constant by using equipment and apparatus needed. Network analyzer is an instrument that can provide accurate measurement with proper usage and handling [9]. It is always used to measure linear characteristic of radio frequency (RF) devices and components. Vector network analyzer is being chosen compared to the scalar network analyzer because it is easy to fabricate and lower cost. Before time, network analyzer was large, limited of external components and has complex set of instruments. Revolution of this network analyzer has created software-define, flexible, and modular instrument platform. With this innovation, it gives more precise measurement of magnitude and phase parameters.

### *A. List of Equipment*

The equipment used was supply by the Laboratory of Vector Network Analysis in Universiti Teknologi Malaysia

TABLE I. LIST OF EQUIPMENT

| **Item** | **Equipment** |
|---|---|
|  | Network Analyzer E5071C with frequency range from 10MHz to 20GHz |
|  | Open-ended coaxial probe cable |

| | |
|---|---|
|  | Open-ended coaxial probe |
|  | Shorting probe |
|  | External computer |

### *B. List of Material*

Material used in this experiment is taken from various kind of medicine. As for authentic medicine, a brand of Panadol is used. The type of panadol medicine experimented is Panadol Regular, Panadol Activefast, Panadol Soluble, Panadol Mesntrual and Panadol Chewable for Kids. Other than that, Hydrosil, Uphamol and also being used. As to differentiate the content of material to be a fake medicine, glutinous rice flour and rice flour is used to resemble it.

### *C. Procedure*

A vector network analyzer E5017C is used in this experiment. The first step to conduct this experiment is to connect the open-ended coaxial cable to the Port 1 of Network Analyzer. Then, connect the open-ended coaxial cable to the cable. Before testing samples, a calibration process during open system, short system and load system must be done to get accurate measurement reading. Load system is tested the probe into distilled water and ensure there are no bubbles in it to get the correct calibration. After the calibration, connect the sample to the probe and secure that the probe's surface aperture is touching the sample without any gap between it as in Figure 4. At the external computer, 85070 software is used to get the data. Microwave frequency from 1MHz to 20GHz at 100 sample points is used. The data is plotted graphically in the software with dielectric constant against frequency.

Fig. 4. Experiment setup

## IV. Result And Discussion

For this experiment, in order to get accurate data of dielectric constant of samples use. The measurement of medicines have been taken in ten times for every samples to get the average reading of dielectric constant.

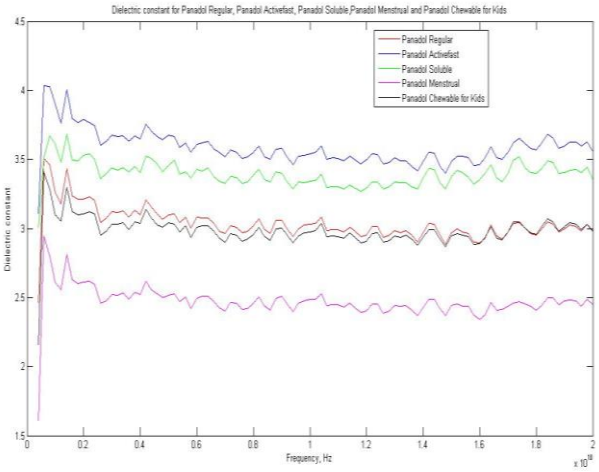


Fig. 4. Dielectric constant for Panadol Regular, Panadol Activefast, Panadol Soluble, Panadol Menstrual and Panadol Chewable for Kids

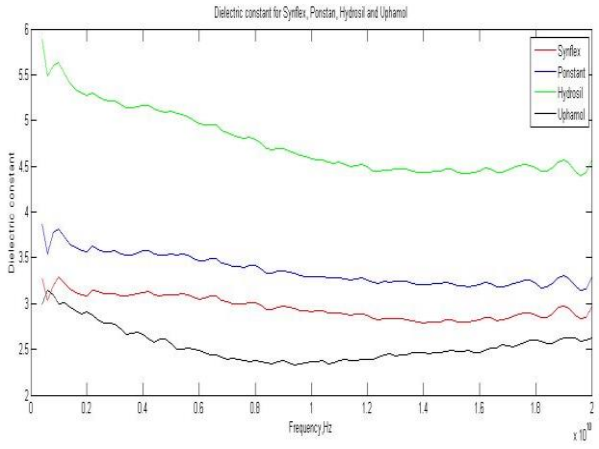


Fig. 5. Dielectric constant for Uphamol 650, Hydrosil, Synflex and Ponstan.

Authentic medicine is tested. The medicine use is from brand of Panadol which contain Paracetamol as the main element of active ingredient. From Fig. 4 it shown the dielectric constant of the medicine use that is Panadol regular, Panadol activefast, Panadol soluble, Panadol menstrual and Panadol chewable for kids. The graph shows the energy from external field is reflect the polarization of the material and stored the energy in material through the frequency range from 10MHz to 20GHz is different depending on the content of the medicines. As for Panadol Activefast, the dielectric constant of its contents is much higher with range from 3.50683 to 3.55349 , Panadol Soluble range from 3.35485 to 3.39386 , Panadol Regular range from 3.02298 to 3.03229, Panadol Chewable for Kids range from 2.88927 to 2.97748 and the lowest is Panadol Menstrual range from 2.44906 to 2.47385.

To strengthen the theory on every material has thier on dielectric constant, another samples of authentic medicine is being experimented. As show in Fig. 5, the samples used is Uphamol 650 contains acetaminophen, Hydrosil contain Magnesium Hydroxide, Synflex sample is made from naproxen sodium and Ponstan is contain mefenamic acid. From the graph, the dielectric constant for Hydrosil is higher than the other three with value from 4.69182 to 5.04017, Ponstan value range from 3.25493 to 3.38259 Synflex value range from 2.85232 to 2.96597 and the lowest value of dielectric constant is Uphamol 650 with range from 2.49635 to 2.54798.

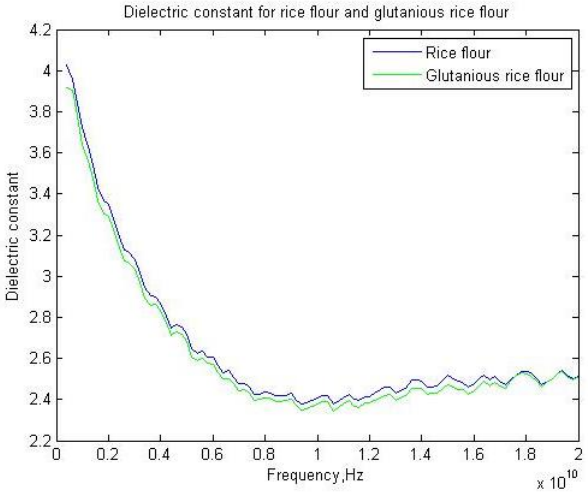


Fig. 6. Dielectric constant for rice flour and glutenous rice flour

To determine the counterfeit medicine, a home made pill was made from rice flour and glutenous rice flour. The dimension of the drug is resemble of the Panadol regular. From fig. 6 the result shows the differences of dielectric constant between these two substances. The dielectric constant for rice flour is range from 2.60846 to 2.64839 and glutenous rice flour from 2.60298 to 2.68236.

All the data collected from authentic and home made fake medicine is calculated to know the average dielectric constant. The value is tabulated as in Table I and Table II.

TABLE II. AVERAGE DIELECTRIC CONSTANT FOR AUTHENTIC MEDICINE

| Type of medicine | Average dielectric constant, $\mathcal{E}$ |
|---|---|
| Panadol Regular | 3.035804545 |
| Panadol Activefast | 3.586897172 |
| Panadol Soluble | 3.394320202 |
| Panadol Menstrual | 2.471695253 |
| Panadol Chewable for Kids | 2.985140202 |
| Uphamol 650 | 2.54847000 |
| Hydrosil | 4.77437680 |
| Ponstant | 3.37363800 |
| Synflex | 2.96496800 |

TABLE III. AVERAGE DIELECTRIC CONSTANT FOR HOME MADE COUNTERFEIT MEDICINE

| Type of home made counterfeit medicine | Average dielectric constant, $\mathcal{E}$ |
|---|---|
| Rice flour | 2.6723968 |
| Glutenous rice flour | 2.6373729 |

## V. CONCLUSION

For this experiment, in order to know the dielectric constant between authentic medicine and fake medicine a vector network analyzer type E5071C is used. The microwave frequency is set from a range of 20MHz to 20GHz with 100 sample points. Before the measurement, calibration action must be done to ensure that the data collected is accurate. Samples of authentic medicine is taken from Panadol as it is the common drug that people bought to be used as temporary treatment. The main element in Panadol is Paracetamol. Few types of tablet panadol is chose such as Panadol regular, Panadol Activefast, Panadol Soluble, Panadol Menstrual and Panadol chewable for kids. Other than that, Uphamol 650, Ponstan, Synflex and Hydrosil is being tested as authentic medicine. As a resemblance of counterfeit medicine, a pill is made up from rice flour and glutenous rice flour is tested to know its dielectric constant. The results shows that, every medicine tested has different value of dielectric constant.

For Panadol regular its dielectric constant is 3.0358, Panadol Activefast is 3.5868, Panadol Soluble is 3.3943, Panadol Menstrual is 2.4716 and Panadol chewable for kids is 2.9851. The other authentic medicine, the value of dielectric constant for Uphamol 650 is 2.5484, Ponstan is 3.37363, Synflex is 2.9649 and Hydrosil is 4.7743. The value for dielectric constant of home made fake medicine is 2.6723 for rice flour and 2.6373 for rice glutenous flour.

The dielectric constant data collected from the experiment shows data every element has their own value. The value dielectric constant of authentic medicine tested can be the threshold to differentiate it with counterfeit medicine.

This indestructible method to detect counterfeit medicine by measure its dielectric constant can be used as another technology using microwave frequency with the help of vector network analyzer.

## REFERENCES


[1] D. Taylor, Trading in False Hope, The School of Pharmacy,University of London, 2009.

[2] Prevalence and Detection of Counterfeit Pharmaceuticals: A Mini Review Facundo M. Fernandez,*,† Michael D. Green,‡ and Paul N. Newton§

[3] Application note 380-1, Basics of Measuring the Dielectric Properties of Materials, Agilent literature number 5950-2390.

[4] Application note 1287-1, Understanding the Fundamental Principles of Vector Network Analysis, Agilent literature number 5965-7707E

[5] Theory of dielectric constant and energy loss in solids and liquids, h. frohlich.f, 10th november, 1943

[6] Analysis of counterfeit drugs By thin layer chromatography J. Sherma

[7] M. A. Othman et al., "An analysis of dielectric constant of pharmaceutical medicines using microwave radiation exposure," 2013 3rd International Conference on Instrumentation, Communications, Information Technology and Biomedical Engineering (ICICI-BME), Bandung, 2013, pp. 80-84

[8] Kundu and B. Gupta, "Broadband dielectric properties measurement of some vegetables and fruits using open ended coaxial probe technique," Proceedings of The 2014 International Conference on Control, Instrumentation, Energy and Communication (CIEC), Calcutta, 2014, pp. 480-484.

[9] D.V, Blackham, R.D, Pollard, An improved Technique for Permittivity measurement using a coaxial probe, IEEE Trans. On Instr. Measr, vol 46, No 5 Oct, 1997, pp. 1093-1099

# Effect of Malay Words on Different Type of Reverberant Environment

Mohammad Syazreen Bin Ismail
*Faculty of Electrical Engineering*
*Universiti Teknologi Malaysia*
*Johor Bahru, Malaysia.*
*mr.syazreen@gmail.com*

Mokhtar Bin Harun
*Department of Communication Engineering*
*Faculty of Electrical Engineering*
*Universiti Teknologi Malaysia*
*Johor Bahru, Malaysia.*
*mokhtarharun@utm.my*

***Abstract* — To achieve success in education and to understand academic knowledges first is the environment of the knowledge been delivered itself. By other means, as for university, the lecture hall would be one of the most main thing that need to be considered to make their students to understand what had been delivered by their lecturers. This research was conducted to investigate the parameters of sound signal that can be relate to degrading of speech intelligibility in different reverberant environment. The parameters that had been measured in this paper were the sound power level, phase differences and sound frequencies. As for the room samples, P16-Demo 2 which is lecture hall in Universiti Teknologi Malaysia. The room itself is been measured while all the utilities inside it were turned on. This is because to make the situation or to record the data based on the real situation where the utilities like aircond and LCD projector were used during the lecture. This make things more difficult to find and measured the accurate value for sound power level from the sound source. Three types of cardinal vowels which are vowel I, A and U were chosen as a selective word for this project. Those words are ibu, ini, itu, pada, masa, sama, juga, bulan and dua. Using MATLAB, the sound signal that been recorded in that room were analyzed. It shows that the sound power level were affected by the background noise surround it. Position where the microphone was closed to the aircond shows the highest value. Due to the mixing sound source, the value of it increase compares to others.**

***Keywords— speech intelligibility; sound source; reverberation environment;phase differences; sound power level***

## I. INTRODUCTION

In the past, many systems design does not care about the basic parameters that affect speech intelligibility. Over the past 20 to 25 years, the understanding of loudspeakers and room interact acoustically and how it may affect intelligibility, has grown considerably [2].

Reverberation reduces Speech Intelligibility and cause problems to the listener to understand every word that been spoken in the hall or room. It is an acoustic phenomenon described by the persistence of sound in space, through physical environment it is produced by the interaction of sound from a source [8]. The causes of this degraded sound can be measured throughout its

Acoustic parameters can provide important information about their acoustic environment, and the speech quality and intelligibility observed in that environment. As for different room, have different type of noise or reverberation time, will causes different value on terms of these parameters. The parameters that can be considered as the room specification are the sound power, phase and frequency.

Reverberated speech signals in noisy acoustical environments cause problems such as reducing speech intelligibility, distinguishing speakers, locating source, quality for hands-free telephony, hearing aid, etc. [1][7][9][10]. Automatic Speech Recognition (ASR) devices could have problems which causes by reverberation [3].

### *A. Direct and Reverberant Sound*

Sound is a mechanical wave which it can travels through a medium from one spot to another. The definition of the direct sound wave is signals that not been reflected by any boundaries near it, hence produce the best quality of sound coming out from the source. Nearly as without any noise. In enclosed spaces, however, listeners also receive speech via reverberation.

Reverberation refers to the persistence of sound in a room because of multiple repeated, reflections from the boundaries [9].

### *B. Reverberation Time ($RT_{60}$)*

The reverberation sound dies away with time, because it will be absorbed by multiple interactions with the boundaries or surfaces of the room. As the reverberation time get longer, it means that the time taken for the sound to die is long. As for anechoic room, the time taken for the sound to die is way faster than the reflective room samples, hence its $RT_{60}$ is low. When the sound source stops, the reverberant sound level begins to fall but it takes some time for it to become inaudible [8 [9][10].

The time taken for the fall by 60 dB is known as the reverberation time ($RT_{60}$). Reverberation time can be calculated using Sabine's formula as stated below.

Sabine's formula:

$$\mathrm{RT60\ (s)} = \frac{0.161V}{\sum S\alpha} \quad (1)$$

The volume, V ($m^3$) is the measured volume of that room sample, which were conducted at P16-Demo 2. Surface area of the room, S ($m^2$) for walls, floor and ceiling. As for the absorption coefficient, $\alpha$ based on material used for the room, because different room might have different material used. Summation of all sound absorber for all surfaces in the room to be divided with.

### C. Critical Distance

It is a distance where the energy of the direct sound and reverberant sound becomes equal. Reverberation occurs beyond the Critical Distance while Direct Sound can be found before it reaches critical distance [12]. It can be said that the more a reverberant a room is, the lesser, closer it's critical distance. When it goes to a more absorbent a room is, the higher it's Critical Distance, longer from the sound source. As for good acoustic design, the critical distance should be as far as possible from the sound source, so that it can gain wider and longer direct sound [13]. The direction of sound from the speaker system diminishes in level as a function (inverse square law) whereas reverberation constantly spreads throughout the room, hence the listener would have trouble in listening clear sound signal [15].

## II. METHODOLOGY

In this project, the room samples used were at P16-Demo 2 at Faculty of Electrical Engineering. Before doing any play and record measurement, first, the room need to be measured. Different room have different reverberation time ($RT_{60}$) and noise level, hence by doing it so, we can see the differences that can affect our records Malay words. When it comes to words, there are plenty of words that can be the subject of this project, hence with the cardinal vowels.

### A. Selection of Words

In describing the sounds of languages, cardinal vowels were used as a reference vowel. A cardinal vowel is a vowel sound produced when the tongue is in an extreme position, either front or back, high or low. Cardinal vowels are not vowels of any particular language, but a measuring system. However, some languages such as Malay contain vowel or vowels that are close to the cardinal vowels [5].

As for this project, three types of cardinal vowels were chosen, I, A and U. This cardinal vowels have articulatory definitions.

Table 1: Chosen Word based on three type of Cardinal Vowel

| **"I"** | **"A"** | **"U"** |
|---|---|---|
| Ibu | Pada | Juga |
| Ini | Masa | Bulan |
| Itu | Sama | Dua |

As for vowel "I", produced with the tongue as far forward and as high in the mouth as is possible, with spread lips. The vowel "A" is produced with the tongue as low and as far back in the mouth as possible while vowel "U" is produced with the tongue as far back and as high in the mouth as is possible with protruded lips. Malay words as shown above, consist of multi vowel in one word, for example, IBU, contain the first "I" vowel and "U" vowel at the end of it. The cardinal vowel of it were determined based on the loudness of the word been spoken, as the vowel "I" were heard much louder than the vowel "U".

### B. Equipment and Room Specification

The source that need to be measured in that room were its reverberation time, noise level, and also recording the Malay words from the speaker. The equipment that needed in this project to get the data from the sound signals are, Real Wave Pocket Analyzer (RPA), Sound Meter Device (SOLO),Laser Distance Meter, Speaker, Microphone, and Laptop.


Figure 1: Sound Meter Device (SOLO) and Laser Distance Meter

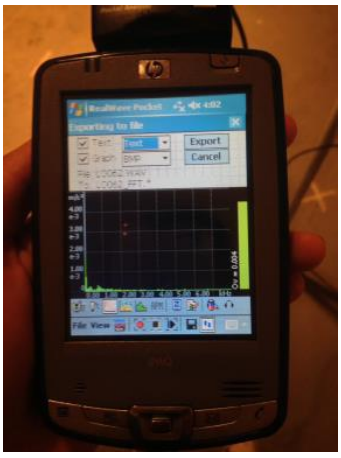


Figure 2: Real Pocket Wave Analyzer (RPA)

By using the Laser Distance Meter, the volume of that lecture hall can be measure accurately. Sound Meter Device (SOLO) were used to determine the room reverberation time ($RT_{60}$). From … (1), we can calculate the critical distance of that room sample. It is important to acknowledge the critical distance of that room because if the recorded sound was measured below the critical distance, there will be no reverberant sound from the sound sources.

Table 2: Room Specifications

| Acoustic characteristic / Room specifications | Location: P16-Demo 2 |
|---|---|
| Volume, ($m^3$) | 648 |
| $RT_{60}$, (s) | 1.84 |
| Critical Distance, $d_c$ (m) | 1.1 |

## III. RESULTS

The measurements were taken with Real Wave Pocket Analyzer, Microphone, Speaker, and also audio played by a computer. The recorded sound is played in that room sample, and save it as .wav file. The sound signal is then been analyze using MATLAB software to get the value for the sound power level, through frequencies and the phase differences.

Figure 3 shows the data of the sound signal from the recorded Malay words. All nine words are combined and play within five seconds gap between it, so that the reverberant doesn't interfere with the next sound signal from the audio. All vowels using the selection of words were played and recorded. Analyzing the sound signal with MATLAB, separating the words according to vowel, and categorized it accordingly. As for the Sound Power Level, the data taken is from frequency of 1k Hz.

Table 3: Sound Power Level of Malay words with vowel "I"

| Position of microphone | Sound Power Level (dB) | | |
|---|---|---|---|
| | Ibu | Ini | Itu |
| 1 | 2.9 | 4.7 | 4.8 |
| 2 | 0.1 | -20.2 | 5.2 |
| 3 | -12.4 | -11.9 | -10.9 |
| 4 | -6.1 | -5.5 | -6.7 |
| 5 | -20.2 | -11.3 | -9.9 |
| 6 | -24.5 | -29.8 | -6.1 |
| 7 | -2.4 | -13.5 | 2.4 |
| 8 | 0.2 | 14.8 | 4.1 |
| 9 | -0.3 | -4.6 | 3.2 |

Table 4: Sound Power Level of Malay words with vowel "A"

| Position of microphone | Magnitude (dB) | | |
|---|---|---|---|
| | Pada | Masa | Sama |
| 1 | 23.9 | 22.1 | 20.4 |
| 2 | 22.4 | 16.9 | 11.2 |
| 3 | 14.3 | 9.3 | 3.7 |
| 4 | 6.5 | -6.3 | 4.5 |
| 5 | 12.9 | 2.4 | -1.2 |
| 6 | 12.9 | 8.7 | 1.9 |
| 7 | 16.1 | 9.4 | 7.2 |
| 8 | 18.9 | 13.0 | 7.9 |
| 9 | 22.9 | 17.9 | 13.3 |

Table 5: Sound Power Level of Malay words with vowel "U"

| Position of microphone | Magnitude (dB) | | |
|---|---|---|---|
| | Juga | Bulan | Dua |
| 1 | 16.5 | 19.7 | 17.8 |
| 2 | 0.8 | 11.7 | 8.0 |
| 3 | -2.1 | 2.0 | 1.6 |
| 4 | -14.6 | 1.1 | -0.4 |
| 5 | -14.0 | 0.9 | -1.0 |
| 6 | -2.8 | 1.5 | 4.0 |
| 7 | 4.1 | 3.6 | 4.1 |
| 8 | 6.7 | 10.3 | 6.3 |
| 9 | 6.1 | 10.8 | 9.6 |

Any particle that vibrate have its maximum displacement from mean position, hence it is called Amplitude. Sound will reflects within the room by the objects inside it, whenever a source speech signal propagates in a noisy indoor environment. The microphone receives the direct sound, the reflected sound waves and the additive noise which can be anywhere even outside of reverberant environment. The desired noisy reverberated speech signals is much smaller than the amplitude of the source signal [1].

The phases of the sound signal, can be measured, and get the value for specific frequencies, as for this project, the value of the phase were taken at the frequency of 1k Hz also.

The figure above shows the signal of the phase changes of Malay word with vowel "I", the phase were identical for different position of the microphone.

**Table 6: Phase Difference of the Malay Words**

| | | | |
|---|---|---|---|
| Position of microphone 1 - 9 | Phase | | |
| | Ibu | Ini | Itu |
| | -3344 | -2485 | -2974 |
| | Phase | | |
| | Pada | Masa | Sama |
| | -2994 | -2728 | -2596 |
| | Phase | | |
| | Juga | Bulan | Dua |
| | -3025 | -2860 | -3020 |

From the output of the analyzing the sound signal through MATLAB, the phase were constant, or same even though the reverberant environment were difference. From position one to nine, the value of the phase of the same word will be identical.

## IV. CONCLUSION

In conclusion, as the data that been taken at the room samples, the outcome shows the vowel A mostly have the highest amount of power level, compared to others. The differences between different positions of the microphone were not quite accurate due to the background noise of that room. The aircond were open to make sure the data were measured according to the real situations where the utilities inside it were all used during the lectures. As for the phase differences, the data shows identical values across the same vowel played with different position of microphones.

## V. REFERENCE


[1] Joorabchi, M., et al. (2014). *Enhancement of reverberant speech in noisy acoustical environments*. 2014 Sixth International Conference on Wireless Communications and Signal Processing (WCSP)

[2] Borwick J. (2001). Loudspeaker and Headphone Handbook. Third Edition. Woburn, Massachusetts: Reed Educational and Professional Publishing LTD

[3] Y. Takata and A.K. Nabelek, English consonant recognition in noise and in reverberation by Japanese and American listeners, J. Acoust. Soc. Amer., vol. 88, pp. 663-666, 1990

[4] P.A. Naylor and N.D. Gaubitch, Speech dereverberation. London: Springer-Verlag, 2010

[5] Shao, Yang, et al. A computational auditory scene analysis system for speech segregation and robust speech recognition Computer Speech & Language 24.1 (2010): 77-93.

[6] D. Talkin, "A robust algorithm for pitch tracking (RAPT)," Speech Coding Synth., vol. 495, p. 518, 1995

[7] A. de Cheveigne and H. Kawahara, "YIN, a fundamental frequency estimator for speech and music," J. Acoust. Soc. Am., vol. 111, no. 4, pp. 1917–1930, April 2002

[8] Boothroyd, A. (1985). Evaluation of speech production in the hearing-impaired: some benefits of forced-choice testing. Journal of Speech & Hearing Research, 28, 185-196

[9] R. Meddis and L. O'Mard, A unitary model of pitch perception, J. Acoust. Soc. Am., vol. 102, pp. 1811–1820, 1997

[10] Si, S. and Q. Hu (2016). Research on two methods of acoustic isolation. 2016 IEEE/OES China Ocean Acoustics (COA)

[11] Aydogan, H. (2016). EEG response of different sound waves and frequencies. 2016 24th Signal Processing and Communication Application Conference (SIU)

[12] Mikulka, J., et al. (2016). Parametric array as a source of audible signal. 2016 Progress in Electromagnetic Research Symposium (PIERS)

[13] Khwaja, M. K., et al. (2015). Pitch tracking in reverberant environments. 2015 IEEE International Symposium on Signal Processing and Information Technology (ISSPIT)

[14] Leglaive, S., et al. (2016). Autoregressive moving average modeling of late reverberation in the frequency domain. 2016 24th European Signal Processing Conference (EUSIPCO)

[15] Liu, Y., et al. (2015). Restoration of instantaneous amplitude and phase of speech signal in noisy reverberant environments. 2015 23rd European Signal Processing Conference (EUSIPCO)

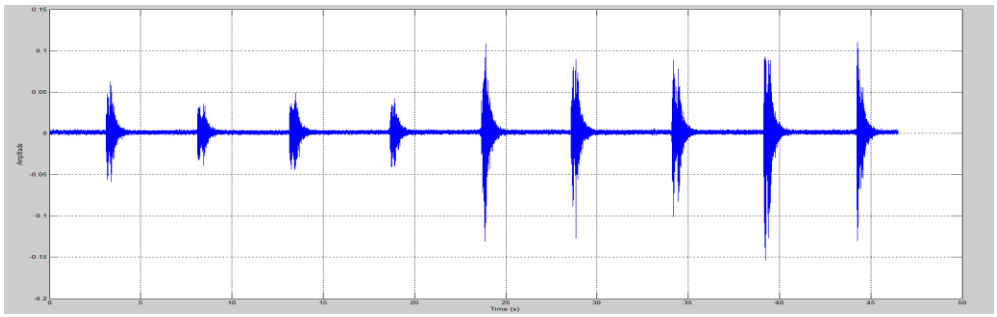

Figure 3: Recorded sound analyzed with MATLAB

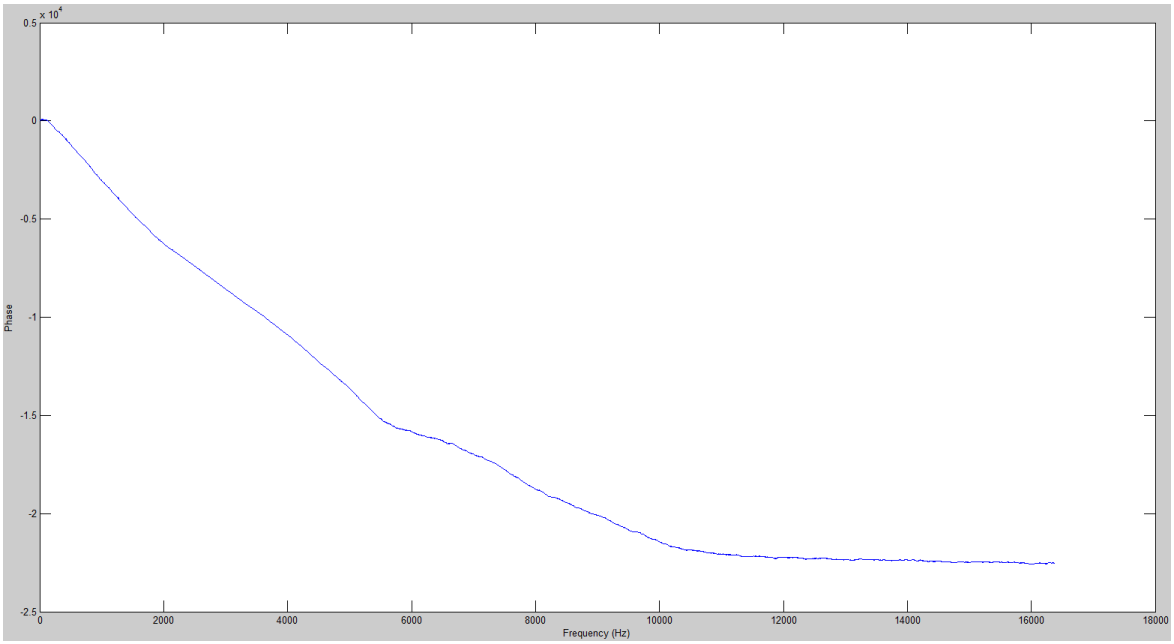


Figure 4: Phase difference of type vowel “I”

# A Compact Wilkinson Power Divider for MMIC Applications

Nurulhasikin Binti Sarip
*Faculty of Electrical Engineering*
*Universiti Teknologi Malaysia*
*Johor Bahru, Malaysia*
*nurulhasikinsatip@gmail.com*

Yusri Bin Md. Yunos
*Department of Communication Engineering*
*Faculty of Elctrical Engineering*
*Universiti Teknologi Malaysia*
*Johor Bahru, Malaysia*
*yusri@utm.my*

*Abstract*—**This paper presents a compact Wilkinson Power Divider using coupled line with high performance in order to provide low cost system for millimeter microwave integrated circuit applications. The coupled line power divider was analyzed and designed using Advanced Design System (ADS2015.01) software before compare its size and performance with conventional power divider. A conventional Wilkinson power divider with an area of 5cm$^2$ is designed with coupled line power divider with an area 0.62cm$^2$ at 2.6GHz using the same substrate which is FR4 substrate. The matching output and isolation for both power divider are slightly the same. The coupled line power divider layout is compact with more than 80% reduction compared to the conventional Wilkinson power divider**.

***Keywords—Wilkinson power divider; couple line; millimeter microwave integrated circuit.***

## I. INTRODUCTION

Power divider is widely used for antenna array in order to divide the input microwave signal into two or more antennas with the same amplitude. Antenna array for millimeter microwave integration circuit (MMIC) application requires a compact power divider with low cost system and high performance. Therefore, in this paper, a compact power divider is designed to fulfill the requirement.

There are a lot of research that have been done on power divider. T-junction power divider was designed but it has poor isolation between output ports [1]. A Wilkinson power divider was designed by employing a lumped isolation resistor of $2Z_o$ to provide high isolation between output ports using coaxial cable in [2]. Then 2 way conventional Wilkinson power divider was designed and fabricated on FR4 substrate has been presented in [3]. Conventional Wilkinson power divider was designed by employing $\lambda/4$ impedance transformer and a lumped isolation resistor so that good matching for all three port and high isolation between output ports can be achieved.

However, this conventional power divider has limitation on its sizing make it not suitable for MMIC applications. Therefore, research on compact Wilkinson power dividers have done by various method in order to comprehend the limitations. Power divider with microstrip electromagnetic band gap element for miniaturization was developed using beeline compact microstrip resonant cell in [4]. The BCMRC design is more compact with reduction in size is 39% compared to the conventional power divider. In [5], a compact Wilkinson Power divider was designed using CMOS technology. The area of the power divider circuit is 1.5cm$^{2.}$. A compact Wilkinson power divider was design using capacitive loading technology as shown in [6] - [8]. New design of compact Wilkinson power divider have good measurement result in return loss, isolation loss and insertion loss. In [9], zigzag configuration was implemented in order to reduce size of Wilkinson power divider. The area of the design is 0.04cm$^2$ with return loss of -3db.

In this paper, a compact Wilkinson power divider with small layout using coupled line is presented for MMIC applications. The output line in this design are spaced closely to achieve more compact size while maintaining the performance [10]. Figure 1(a) shows 2 way conventional Wilkinson power divider. The proposed compact Wilkinson power divider shown in Figure 1(b)

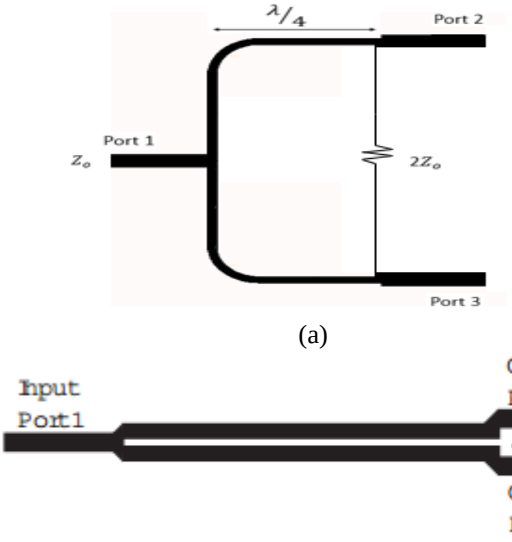


Fig. 1. (a) Conventional Wilkinson power divider and (b) proposed Wilkinson power divider using coupled line.

## II. Design Methodology

As mentioned, coupled line layout is proposed in order to reduce the size of Wilkinson power divider. The parallel line employing $\lambda/4$ impedance transformer to provide good matching port and FR4 ($\varepsilon_r$ = 4.4, H = 1.6mm) is used as a substrate. Basically, the performance of Wilkinson power divider is influenced by even-odd mode impedance.

### A. Even-Odd Mode Impedance Analysis

To use coupled line design, even-odd mode impedance ($Z_{oe}$ and $Z_{oo}$) should be analyzed. The normalized even-odd mode impedance shown as follows:

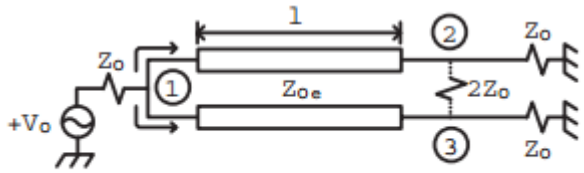


Fig. 2. Input impedance analysis

$$\bar{Z}_{in1} = \bar{Z}_{Oe}\,\frac{2+j\bar{Z}_{Oe}\tan\beta l}{\bar{Z}_{Oe}+2\tan\beta l} \quad (1)$$

$S_{11}$ determined by input impedance, $Z_{in}$. Based on input impedance formula above, returned power, $S_{11}$ influenced by $Z_{oe}$. By assuming the coupled lines are lossless, the input power is related to the transmitted power, $S_{21}$ and $S_{31}$, therefore, $S_{11}$, $S_{21}$ and $S_{31}$ influenced by $Z_{oe}$. when $\beta l = \pi/2$, (1) can be reduced to $Z_{in} = Z_{oe}^2/2Z_o$. In order to obtain perfect port matching, $Z_{in} = Z_o$ and $Z_{oe}$ should be fixed at $\sqrt{2}Z_o$.

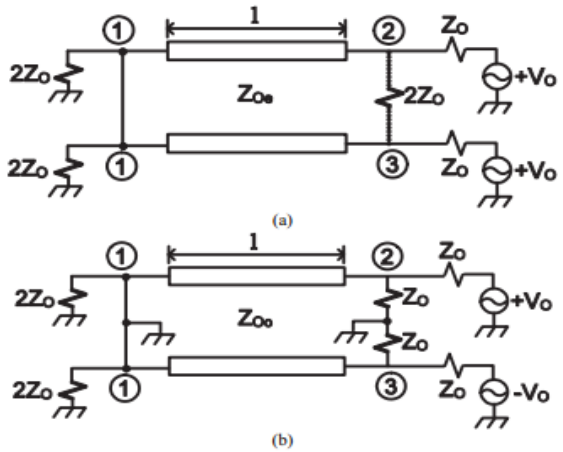


Fig. 3. (a) Even and (b) odd mode impedance analysis.

The normalized even and odd mode impedance shown as

$$\bar{Z}^{e}_{in2} = \bar{Z}_{0e}\,\frac{2+j\bar{Z}_{0e}\tan\beta l}{\bar{Z}_{0e}+j2\tan\beta l}$$
$$\bar{Z}^{o}_{in2} = \frac{j\bar{Z}_{0o}\tan\beta l}{1+j\bar{Z}_{0o}\tan\beta l} \quad (2)$$

The reflection coefficients and $S_{22}$ is:

$$\Gamma_2^{e,o} = \frac{\bar{Z}^{e,o}_{in2}-1}{\bar{Z}^{e,o}_{in2}+1} \quad (3)$$

$$S_{22} = \frac{1}{2}(\Gamma_2^e + \Gamma_2^o) \quad (4)$$

The power from port 2 to port 3 is given by

$$|S_{32}|^2 = 1-2\left|\frac{\bar{Z}^{e,o}_{in2}-1}{\bar{Z}^{e,o}_{in2}+1}\right|^2 - |S_{22}|^2 - |S_{21}|^2 \quad (5)$$

From the equation (2) – (5), it can be concluded that $S_{22}$ and $S_{32}$ are influenced by both impedance mode which is even and odd mode impedance. From [1], $Z_o = \sqrt{Z_{oe}Z_{oo}}$. Coupled line Wilkinson power divider was designed by using the formula presented. The parameters of conventional and coupled line Wilkinson power divider are shown in Table I.

TABLE I. Parameters of Conventional and Coupled Line Wilkinson Power Divider

| Parameters | Conventional Wilkinson power divider | Coupled line Wilkinson power divider |
|---|---|---|
| Relative dielectric, $\varepsilon_r$ | 4.4 | |
| Height of substrate, h (cm) | 0.16 | |
| Characteristics impedance, $Z_o$ (Ω) | 50 | |
| $Z_{oe}$ (Ω) | 70.17 | 70.17 |
| $Z_{oo}$ (Ω) | 70.17 | 35.3 |
| Length of transmission line, *l* (cm) | 1.7 | 1.6 |
| Width of copper, W (cm) | 0.15 | 0.15 |
| Spacing between two transmission line (cm) | 3.4 | 0.05 |
| Circuit area ($cm^2$) | 5.12 | 0.64 |

## III. Simulation Results

Both of 2 way Wilkinson power divider (Conventional and coupled line power divider) are designed at 2.6GHz using ADS2015.01 software and their performances are comparable. Since both designs using the same $\lambda/4$ impedance transformers, the performance for both designs are quite close.

Figure 4(a) and Figure 5(a) show the insertion loss are -3dB. In other words, the input signal is divided equally to output ports. The isolation loss indicate how output port affect another output port. In this design, isolation loss of coupled line is -32.15dB. This tell us that power at output ports are not dissipated by resistor. From the results, it shows that input power are fully transferred to the output port since the return loss is too small.

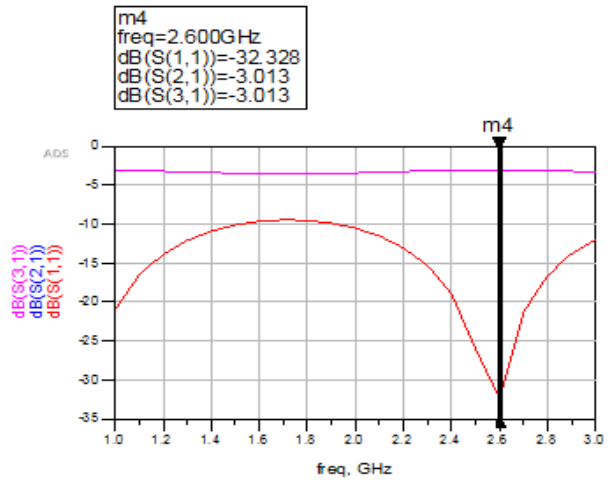


(a)

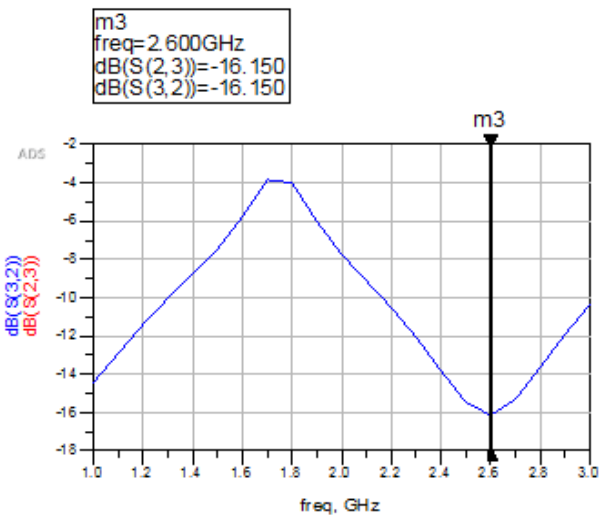


(b)

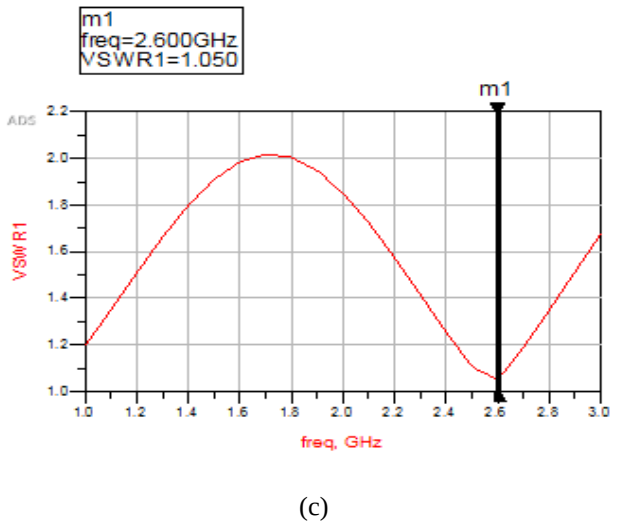


(c)

Fig. 4. (a) Insertion loss, $S_{11}$ and insertion loss, $S_{21}$ $S_{13}$ and (b) isolation loss and (c) VSWR for conventional Wilkinson power divider.

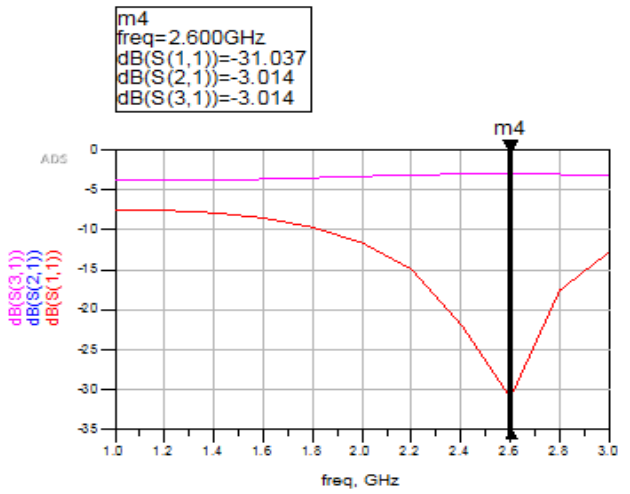


(a)

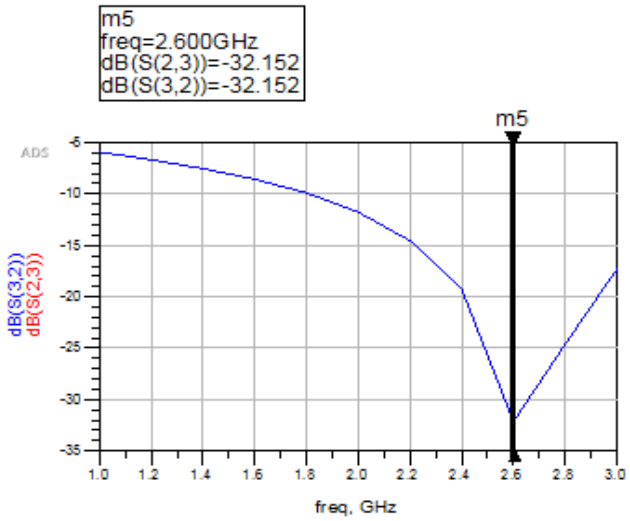


(b)

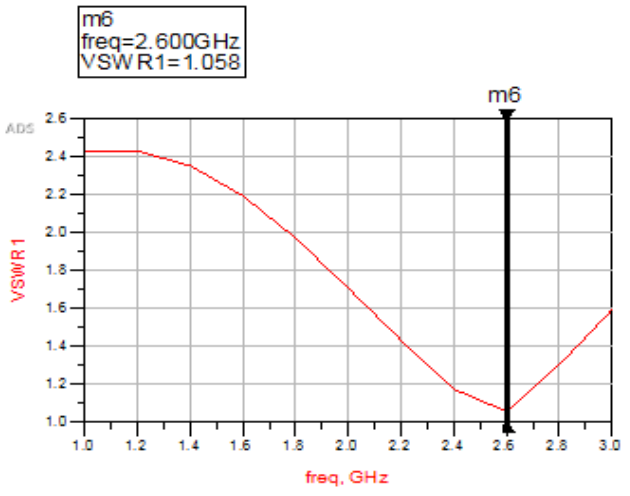


(c)

Fig. 5. (a) Return loss, $S_{11}$ and insertion loss, $S_{21}$, $S_{31}$ (b) isolation loss and (c) VSWR for Wilkinson power divider using coupled line.

TABLE II. PERFORMANCES OF CONVENTIONAL AND COUPLED LINE WILKINSON POWER DIVIDER

| | Conventional Wilkinson power divider | Coupled line Wilkinson power divider |
|---|---|---|
| Return loss, $S_{11}$ (dB) | -32.33 | -31.04 |
| SWR | 1.05 | 1.05 |
| Isolation loss, $S_{23}$, $S_{32}$ (dB) | -16.15 | -32.15 |
| Insertion loss, $S_{21}$, $S_{31}$ (dB) | -3.01 | -3.01 |

Table II shows the summary of conventional and coupled line Wilkinson power divider's performances. Table I and Table II show that the size of Wilkinson power divider can be reduced while maintain its performance using coupled line as transmission line.

## IV. CONCLUSION

Coupled line Wilkinson power divider is used to design a compact power divider with high performance for MMIC applications. The influences of $Z_{oe}$ and $Z_{oo}$ are analyzed and the conventional and coupled line Wilkinson power divider was designed using the formula presented and the simulation show comparable results for the two power divider. The area of coupled line circuit is reduced by more than 80% compared to conventional Wilkinson power divider.

## REFERENCES


[1] Pozar, D. M., "Microwave Engineering", 3rd edition, John Wiley & Son, 2005.

[2] Ernest J. Wilkinson, "An N-Wat Hybrid Power Divider", 1960.

[3] Taufiqqurrachman, Deni Permana Kurniadi, "Design and Realization Wilkinson Power Divider at Frequency 2400MHz for Radar S-band", IOSR Journal of Electronics and Communication Engineering (IOSRJECE), Vol. X, Issue X (Nov-Dec 2012).

[4] F. Zhang and C. F.Li, "Power Divider with Microstrip electromagnetic Bandgap Element for Miniturisation and harmonic rejection," 2007.

[5] Liung-Hung Lu, "A miniaturized Wilkinson Power Divider with CMOS Active Inductors," *IEEE Microwave and Wirelees Components Letter*, vol. 15, no.11, November 2005.

[6] Maximilian C. Scardelletti et.al., "Enhanced Miniaturized Wilkinson Power Divider," *IEEE Microwave and Wirelees Components Letter*, vol. 12, no.1, Januari 2002.

[7] B. Piernas and M. Hirata., "Miniaturized Wilkinson Power Dividers Utilizing Capacitive loading," 2003.

[8] Junsong Ning et.al., "A New Design of Compact Microstrip wilkinson Power Dividers," *IEEE International Symposium on Radio-Freq. Tech*, 2014.

[9] Majeed A. S Alkanhal, "Reduced size Dual Band Wilkinson Power Dividers," 2008.

[10] Mark K. Karage et.al, "Charactewristics of Coupled Microstrip Transmission line," *IEEE Trans. On Microwave theory and tech,* April 1997

# Curvature Fiber Sensor based on Multimode Fiber

Nurul Izzati binti Mohd Najid@Zakaria
Department of Communication
Faculty of Electrical Engineering
Universiti Teknologi Malaysia, Skudai, Malaysia
izzatinajid94@gmail.com

Muhammad Yusof Bin Mohd Noor
Department of Communication
Faculty of Electrical Engineering
Universiti Teknologi Malaysia, Skudai, Malaysia
yusofnor@fke.utm.my

***Abstract*— This paper introduces a fiber optic curvature sensor based on the single-mode-multimode-single-mode fiber structure developed. The multimode fiber is spliced without cladding. This curvature sensor using physio clear plastic goniometer angle ruler joint bend measure to ensure the sensor can measure a larger degree of measurement to apply in medical treatment for measure human join movement. By using different type of core diameter MMF, the transmitted spectra of the multimode interface were analyzed based on peak wavelength and power. From the analysis, the peak wavelength shifts of the sensor for curvatures changes. The findings show that a curvature sensor can be used in medical application but in small range because this fiber is very sensitive.**

***Keywords—Curvature, fiber-optic sensor, multimode interference.***

## I. INTRODUCTION

Nowadays, fiber optic is not act as medium to transmit data but it can use as a sensor in many applications. Fiber-optic sensors based on multimode fibers have been extensively investigated in recent years due to the advantages of easy fabrication, immunity from electromagnetic interference, high sensitivity, low cost and long distance between signal generation and detection [1]-[13]. By using single-mode-multimode-single-mode (SMS) structure has been used to fabricate the fiber sensors in recent years [6]. When cladding MMF was remove, experimentally was prove that SMS sensors were sensitive to temperature, strain, displacement and refractive index.

Based on the number of incidents regarding health issue has increase, demands for device to measure rapid movement of human joints under recovery is very high. Because of that, SMS sensor can be as a curvature sensor to measure movements of human joints. There are several curvature sensor designed by using variety of type multimode fiber, presented in the literature review based on technique of experiment [2]. Technique of experiment by using multimode fiber is shown in Fig.1. The overall findings, this kind of sensor can measure the curvature with high sensitivity in a relatively large scale and is capable of measuring small bend curvatures [2].

In this paper, the author is focusing a new method to design curvature sensor by using SMS sensor. The curvature sensor easy to setup but it is very sensitive to the curvature changes based cause multimode interference.

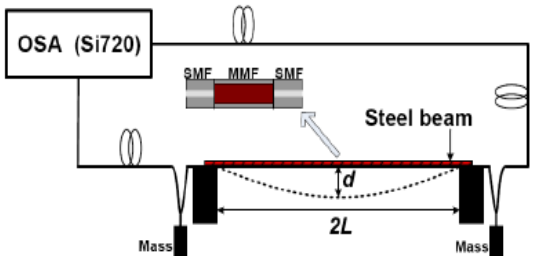


Fig. 1. Schematic diagram of the experimental setup for measuring the curvature by the SMS fiber sensor. [2]

## II. WORKING PRINCIPLE AND EXPERIMENTAL SETUP

Based on multimode interference (MMI) theory, equation [7] below can calculate the length of MMF.

$$L = p\,(\tfrac{3L_\pi}{4}) \qquad \text{with} \quad p = 0,1,2,.... \tag{1}$$

Where $p$ is the self-image number and $L_\pi$ define as the beat length,

$$L_\pi = \frac{4n_{MMF}D^2_{MMF}}{3\lambda_0} \tag{2}$$

Where $n_{MMF}$ and $D_{MMF}$ correspond respectively to the refractive index and the diameter of the multimode fiber and $\lambda_0$ is the free space wavelength. When combine Eq. (1) and Eq. (2), the free space wavelength can be calculated from the following equation:

$$\lambda_0 = p\left(\frac{n_{MMF}D^2_{MMF}}{L}\right) \qquad \text{with} \quad p = 0,1,2\ldots \tag{3}$$

In this experiment, MMF was spliced without cladding and between two SMF as shown in Fig. 2. Two different value of diameter of the MMF core used, experiment 1 is 105µm and experiment 2 is 50µm. By using steel ruler, the MMF length roughly measured about 30 mm for each fiber. The experimental setup for measuring curvature is schematically shown in Fig. 2. An optical spectrum analyzer (OSA) integrated with a narrowband swept laser was used to record the transmitted spectra [2]. For curvature measurement, the

bending curvature can be obtained by using Physio Clear Plastic Goniometer Angle Ruler Joint Bend Measure as shown in Fig. 3. The bending radius for curvature fiber was happened when the fiber rotating between 0˚ until 10˚. LabView software on computer connected with optical spectrum analyzer (OSA) displayed the results spectrum of multimode interface.

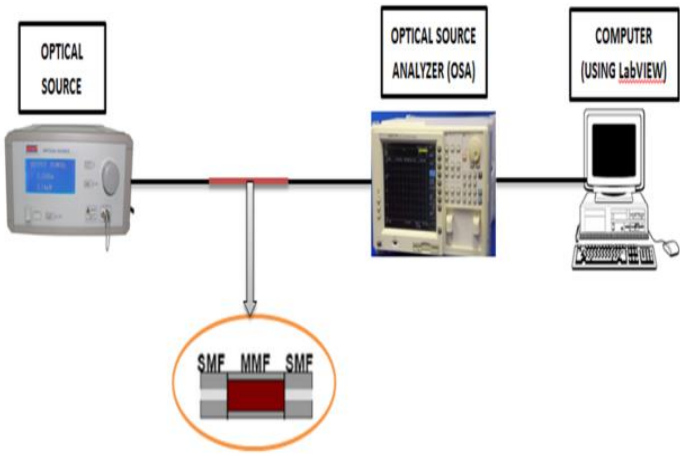


Fig. 2. Schematic diagram for experimental setup

Fig. 3. Physio Clear Plastic Goniometer Angle Ruler Joint Bend Measure

According to [6], the peak wavelength shifted when the curvature changed. The transmission spectra of the MMI sensor under different bending curvature are shown in Fig. 4(a). When applied curvature became larger, the peak wavelength shifted to shorter wavelength as shown in Fig. 4(b). Here we can see from Fig. 4(c) that the light intensity response also exhibited a linear response when the bending curvature was bigger. This characteristic of the sensor is more convenient to be used to measure the bending curvature because the light intensity is easier to be monitored compared to transmission spectra of the sensor.

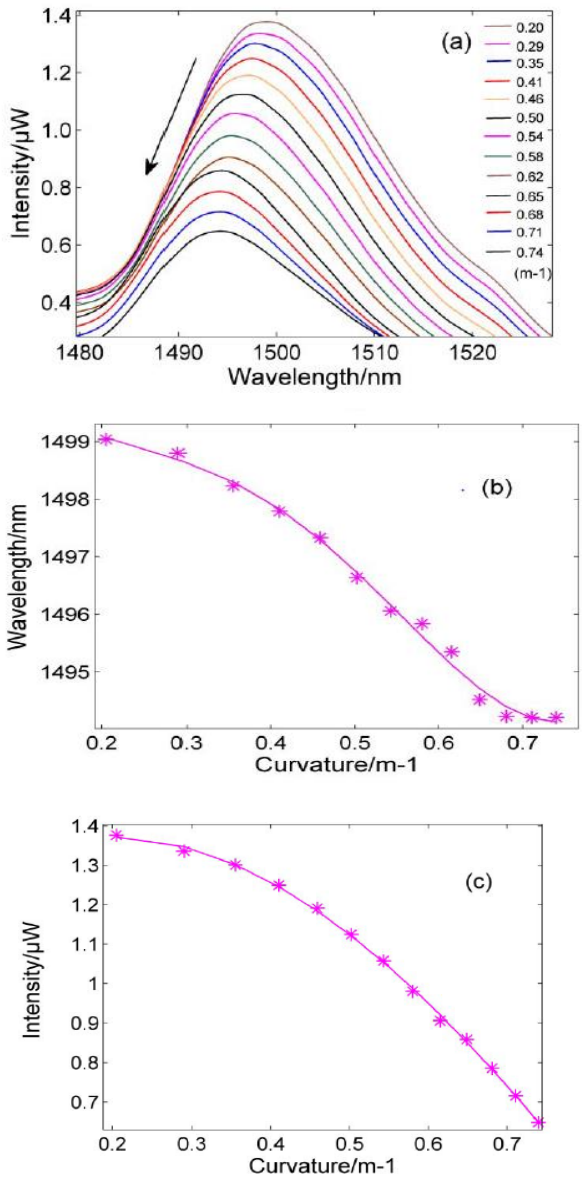


Fig. 4. (a) The transmitted spectra of the MMI sensor, (b) the peak wavelength response for curvature, and (c) the light intensity response.

## III. RESULTS AND DISCUSSIONS

### A. *Results 1*

By using core diameter 105μm, the results shown in Fig. 5, there will be shift to the peak wavelength of the SMS sensor when the curvature changed. The transmission spectra of the MMI sensor under different bending curvature are shown in Fig. 5(a). By adjusting the value of degree, the bending curvature sensor was changing. The value of degree used in this experiment between 0˚ until 10˚ but MMI spectrum formed only between 0˚ until 5˚. This proved that MMF is very sensitive because sellotape was using to stick the fiber on equipment not glue. This method affects the degree reading. When the curvature was changed, the peak wavelength shifted in Fig. 5(b). This phenomenon also can be explained by the Eq. 3. When the curvature changed, there would be a little change

for the length of MMF. Fig. 5(c), the value of power became lower when the applied degree curvatures become larger.

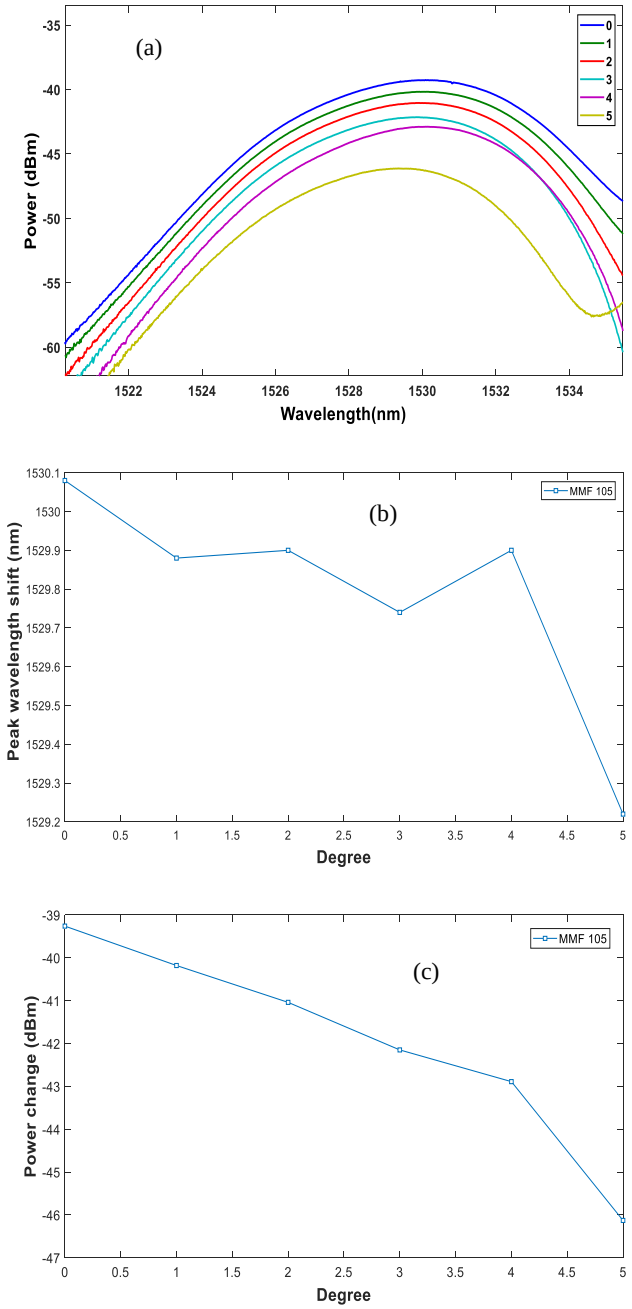


Fig. 5. (a) The transmitted spectra of the MMI sensor, (b) the peak wavelength response for curvature, and (c) the power response.

## B. *Results 2*

The length of MMF in this experiment was 30mm and the diameter core is 50µm. By adjusting the degree of curvature measurement, the value of peak wavelength was not changed between 1˚ to 4˚ and 5˚ to 10˚ in Fig. 6(b). However, Fig. 6(a) shown no multimode interference appeared in transmission spectrum of different curvature. According Fig. 6(c), the value of power almost remain unchanged because between 1˚ and 9˚ the value same.

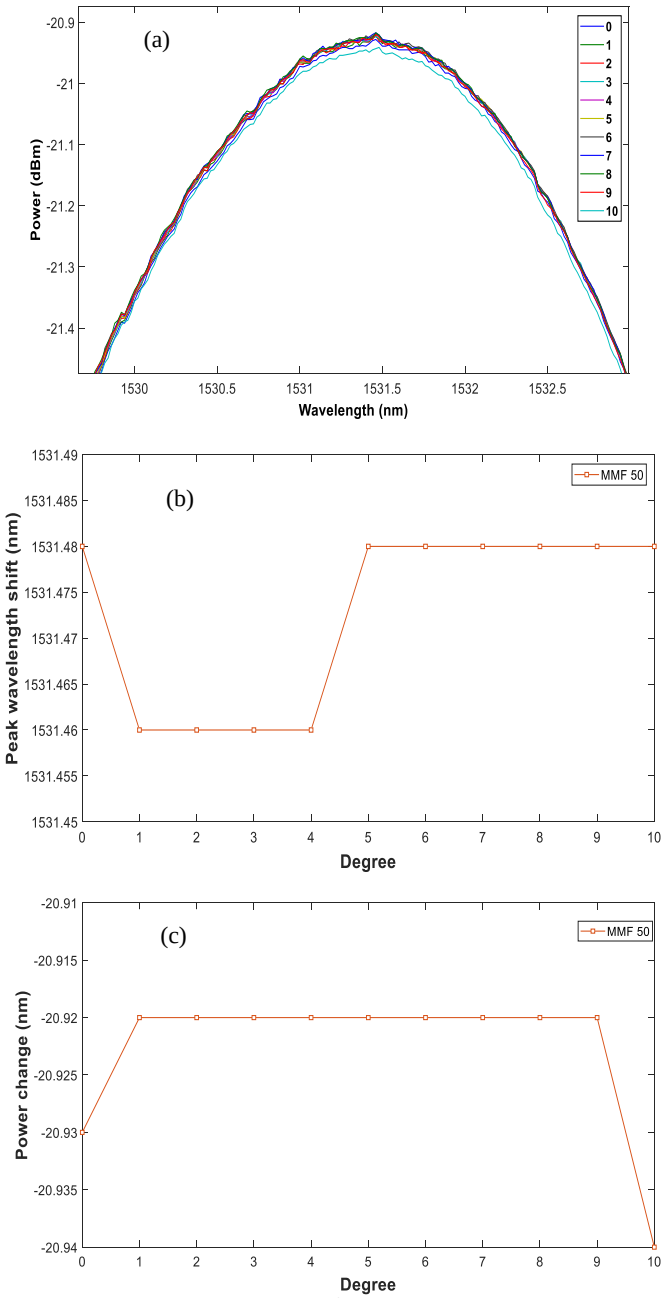


Fig. 6. (a) The transmitted spectra of the MMI sensor, (b) the peak wavelength response for curvature, and (c) the power response.

## C. *Results 3*

Based on results 1 and results 2, compared the two different type of MMF by comparison the peak wavelength and power for each MMF. In Fig. 7(a), the peak wavelength of MMF core 105µm shifted to shorter wavelength when applied curvature became larger rather than MMF cores 50µm almost remain unchanged. In addition, the value of power of MMF core 105µm slowly decreased with the value of degree curvature

measurement. Other than that, MMF core 50µm remains unchanged for the value of power and this compares shown in Fig. 7(b). Multimode fiber is very sensitive by using method in Fig. 2.

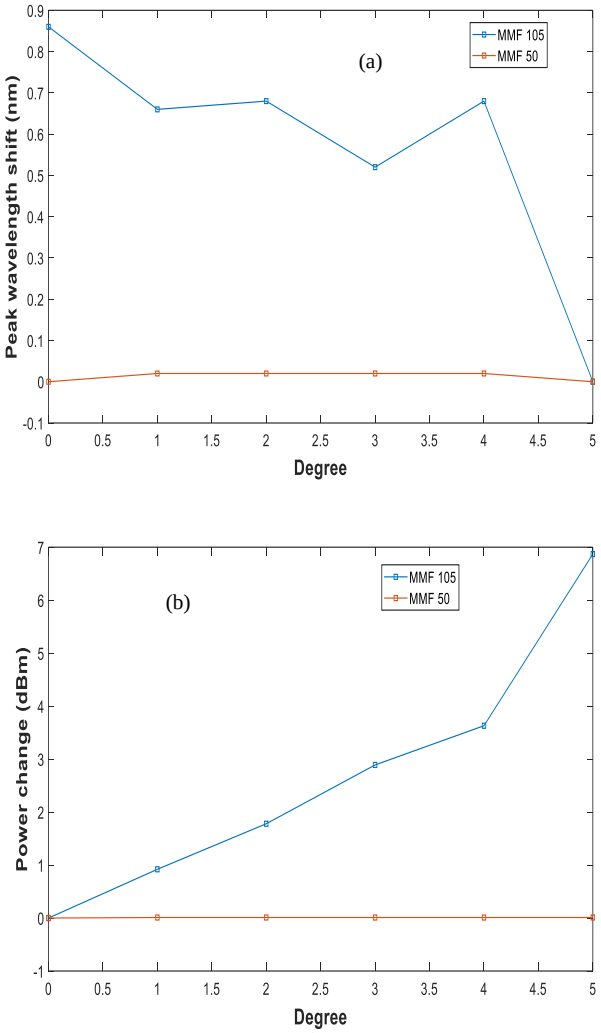


Fig. 7. (a) The peak wavelength response for curvature, and (b) the power response.

## *D. Results 4*

By using MMF core 50µm with length 30mm, this results appearance MMI pattern between degree 0˚ and 10˚ (Fig. 8(a)). The peak wavelength slowly gradually shifted when the curvature measurement was changed in Fig. 8(b). Between 0˚ and 4˚, the peak wavelength increased while at 5˚ until 10˚ the results decreased. For power change, the results same with peak wavelength when 4˚ is the highest value of power changed based on Fig. 8(c).

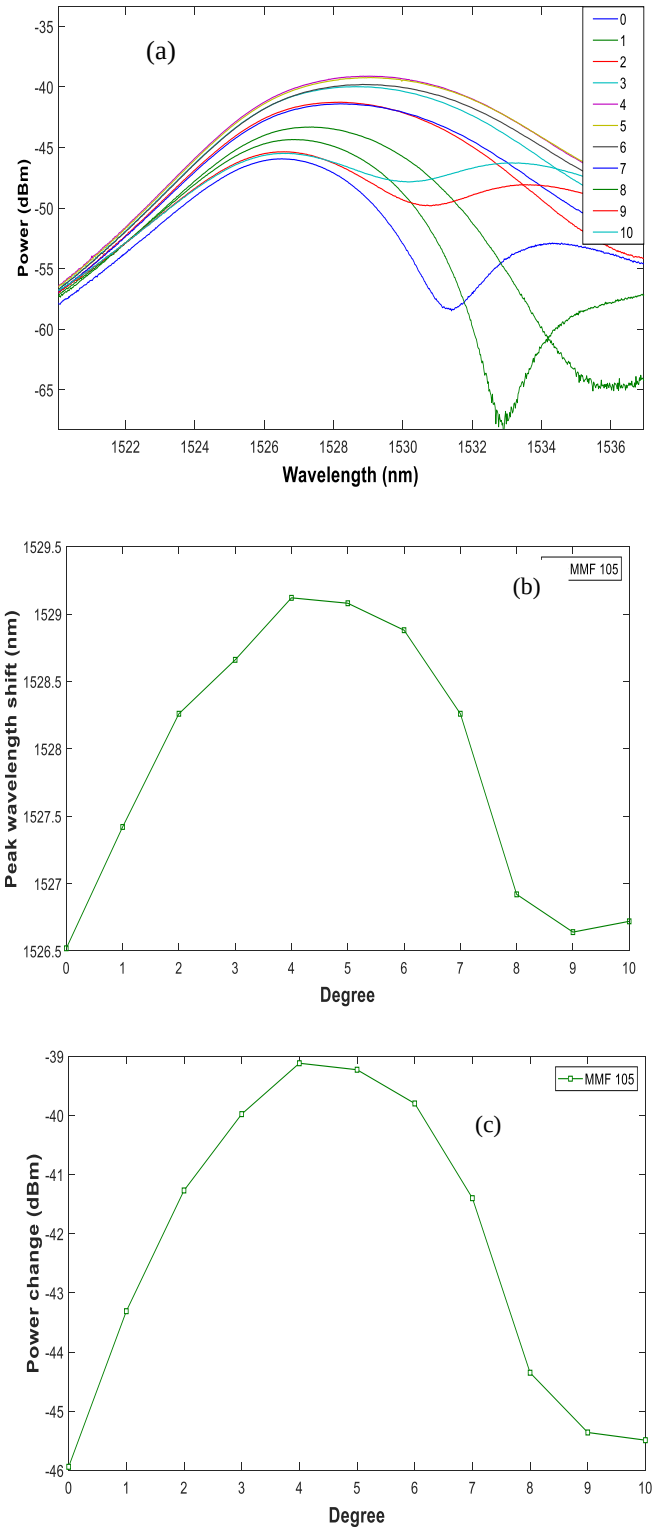


Fig. 8. (a) The transmitted spectra of the MMI sensor, (b) the peak wavelength response for curvature, and (c) the power response.

## IV. CONCLUSION

The curvature sensor was proved that the sensor can measure in limited range which is 1˚ and 10˚. This sensor can apply in medical application but in small range of measurement. Also, this method used is not suitable for this sensor because MMF is very sensitive. This sensor can use another method suitable and also can use the larger core diameter MMF. Also, this experiment will conduct by reduce the length of MMF.

## ACKNOWLEDGMENT

Foremost, I would like to express my sincere gratitude to my supervisor, Dr. Yusof Mohd Noor for the continuous support of my report project, for his patience, motivation, enthusiasm, and immense knowledge. His guidance helped me in all the time of research and writing report. Furthermore, I would like to acknowledge with mush appreciation the crucial role of the staff of Optical Communication Lab, who gave the permission to use all required equipment and the necessary material to complete my project. I have to appreciation the guidance given by other supervisor as well as the panel especially in my project presentation that has improved my presentation skills thanks to their comment and advices. Last but not least, I would like to thank my family: my father Mohd Najid@Zakaria bin Nawi, my mother Nor Anita binti Latif and also my siblings, for believing in me at the first place and supporting me spiritually throughout my life.

## REFERENCES

[1] Wenjun Zhou, Yan Zhou, Xinyong Dong,Li-Yang Shao, Jia Cheng, and Jacques Albert, " Fiber Optic Curvature Sensor Based on Cladding-Mode Bragg Grating Excited by Fiber Multimode Interferometer," IEEE Photon. Lett, vol.4, no3, pp. 1051-1056, June 2012

[2] Yuan Gong, Tian Zhao, Yun-Jiang Rao, and Yu Wu, "All-Fiber Curvature Sensor Based On Multimode Interference," IEEE Photon. Lett, vol.23, no3, pp. 679-681, June 2011.

[3] Chao Luo, Ping Lu, Xin Fu, Jing Chen, Shun Wang, Chi Zhang, Deming Liu, and Jiangshan Zhang, "All-Fiber Sensor Based On Few-Mode Fiber Offset Splicing Structure Cascaded with Long-Period Fiber Grating for Curvature and Acoustic Measurement," Photon Newt Com., 32: 224-229, February 2016K. Elissa, "

[4] Luca Palmieri, "Coupling mechanism in multimode fibers," Invited Paper, Vol.9009, 2014.

[5] Dr. Asrul Izam bin Azmi, " Slide Note Optical Communication", Universiti Teknologi Malaysia, 2016

[6] Lin Ma, Yanhui Qi, Zexin Kang, and Shuisheng Jian, "All-Fiber Strain and Curvature Sensor Based on No-Core Fiber," IEEE Sensors Journal, vol. 14, pp. 1514-1517, May 2014

[7] L. B. Soldano and E. C. M. Pennings, "Optical multi-mode interference devices based on self-imaging: Principles and applications," *J. Lightw. Technol.*, vol. 13, no. 4, pp. 615–627, 1995.

[8] A.Castillo-Guzman, J. E. Antonio-Lopez, R. Selvas-Aguilar, D. A. May "Widely tunable erbium- doped fiber laser based on multimode interference effect," *Opt. Exp.*, vol. 18, no. 2, pp. 591–597, 2010.

[9] M. Donno, E. Palange, F. D. Nicola, G. Bucci, and F. Ciancetta, "A new flexible optical fiber goniometer for dynamic angular measurements: Application to human joint movement monitoring," IEEE Trans. Instrum.Meas., vol. 57, no. 8, pp. 1614–1620, Aug. 2013.

[10] An Sun, Yuliya Semenova, Qiang Wu, Agus Muhamad Hatta and Gerald Farrell, "A Novel High Sensitive Optical Fiber Microphone Based on a Singlemode-Multimode-Singlemode Structure," Microwave and Optical Technology Letters, Vol. 53, no. 2, Pages: 442–445,2011

[11] Simon Pevec and Denis Donlagic, "All-fiber, long-active-length Fabry-Perot strain sensor," Optics Express, Vol. 19, No. 16, August 2011

[12] Yu-Cheng Lin, Woo-Hu Tsai, Yu-Chia Tsao, and Jiu-Kai Tai, "An Enhanced Optical Multimode Fiber Sensor Based on Surface Plasmon Resonance With Cascaded Structure," IEEE PHOTONICS TECHNOLOGY LETTERS, VOL. 20, NO. 15, AUGUST 2008

[13] Yu Liu and John Lit, "Fiber comb filters based on UV-writing Bragg gratings in graded-index multimode fibers," Optics Express, Vol. 13, No. 21, October 2005

# Modelling of Open-Ended Rectangular Waveguides using Polynomial Regression Technique

Muhamad Farid Bin Mohd Izazi and You Kok Yeow
*Faculty of Electrical Engineering*
*Universiti Teknologi Malaysia (UTM)*
*Johor Bahru, Malaysia.*
*muhamadfaridiz@gmail.com*

***Abstract*— This paper presents a critical study on the use of an open-ended rectangular waveguide aperture contacted with different kind of materials. By doing so, the determination of permittivity of materials can be accomplished based on the input frequency, magnitude and phase of materials. The sensor was study based on the calculation of reflection coefficient using regression method. In this work, the computation of reflection coefficient of rectangular waveguide was realized using COMSOL Multiphysics software and MATLAB software for determine the required data. Then, the result was compared with the measured reflection coefficient using *Thru Reflec Line* (TRL) method. The sensor operating between 8.2GHz until 12.4GHz.**

**Keywords—COMSOL; regression method; MATLAB; Thru Reflec Line method (TRL).**

## I. INTRODUCTION

Science and technology are beyond the limit to expect for. In recent year, this technology has been advance at an explosive rate and overcome the tradition performed by electronics and mankind. Another day another device been designed, investigated and demonstrated in research laboratories across the globe. It's all started when optic signals as a means for carrier in telecommunication after the invention of laser in 1960[1]. A decade later, Miller introduced 'integrated optics' as a term involved in realization of the optic and electro optic element which perhaps can be integrated in a huge number in one chip similarly to the processing techniques that have been used to fabricated integrated electronic circuits [2]. This development is keen to gradually increase in demand with several improving is done. Thus, the continuity of development in term of accuracy and efficiency methods for analysis of devices is more crucial.

Dielectric waveguide are fundamental components of devices and system both in microwave and optics, and such, a full understanding of how electromagnetic wave propagate in complicated waveguiding structures is essential. Recently, the advances of materials in demand and processing technologies in refractive index, geometric profile and theoretical analysis its of propagation properties just explode in interest [3].

## II. LITERATURE REVIEW

Waveguide is a special type of transmission line used at high frequencies that control the propagation of an electromagnetic wave so that the wave is forced to follow a path defined by the physical structure of the guide.

It can be used to transmit power or signal in the form of waves while minimizing power loss. Waveguides transmit energy by propagating transmitted electromagnetic wave through the inside of a tube to a receiver at the other end. Common examples are metallic tube, coaxial cables and optical fibers. Waveguide which are useful at microwave frequencies in such application as connecting the output amplifier of radar set to its antenna, typically take the form of rectangular hollow metal tubes but have also been built into integrated circuits.

A waveguide will not propagate electromagnetic waves lower than the cut off frequency. The electric and magnetic fields of an electromagnetic wave have a number of possible arrangements when the wave is travelling through a waveguide. Each of these arrangements is known as mode propagation.

## III. PROJECT METHODOLOGY

There are 3 parts in this project. The first methodology shows the overall process work in summary as in Figure 3.1. The second flow chart in Figure 3.2 show how the actual process works in COMSOL simulation software. Thus, in this chapter will only discuss about this two work process and next agenda will explain about the process of designing the rectangular waveguide. The Simulation result determine from the COMSOL will be as below:

1) Energy density across the simulated waveguide
2) Simulation works on developing the rectangular waveguide
3) Comparison result of rectangular waveguide with different geometries and frequency.

### A. *Pre-Process Module*

The first module of the proposed works as the preparation for the analysis of open-ended rectangular waveguide before getting the required equation is by analysis and getting the data from software. This is desired for the next consecutive steps where the data from the Comsol will be analyze as mathematical modelling. The modelling properties takes part in Comsol Multiphysics and the designation of open-ended rectangular waveguide will be simulated.

### B. *Anayzing the data of rectangular waveguide*

Analyzing the data is proceeded using MATLAB software. There are 3 stages taken for analysis. The first part is to analysis the correlation between frequency and permittivity based on analysis data in Comsol. Second stage is to define the value of magnitude and phase based on previous data. Lastly, the data is simulated again to determine the relation based group of magnitude and phase based on regression method. Final expression is determined between two group permittivity, $\varepsilon_r$- magnitude and phase angle. The flowchart for second stage is shown as below.

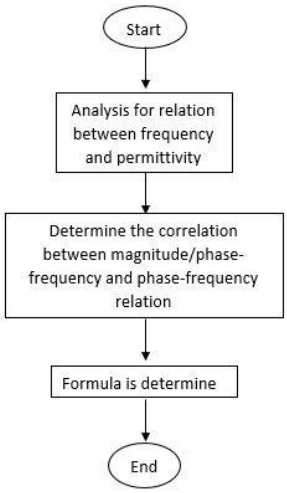


Figure 1: Methodology process for analysis

### C. *Thru Reflect Line (TRL) Method*

The final stage is where the predetermine formula is about to verified whether it is valid or not. In order to verified, several experiments are taken in real live. The method for verifying is called Thru Reflect Line (TRL) method.[4]
Some frequency and cut-off frequency is set based on x-band. This is because to make similarities between software analysis based on Stage 1.

There are two sample were taken for undergo this project. First sample is oil. Both sample has its own value of relative permittivity. The result from this experiment, again, will be analysis using software analysis, MATLAB to determine the correctness of relative permittivity's equation. The result then compared between 3 different result which is permittivity value based on magnitude, Permittivity value based on phase angle and Permittivity value based on reality.

## IV. RESULT AND ANALYSIS

The measurement results are presented in term of permittivity equation against frequency input. The input frequencies are limited to x-band which range are indicates from 8.2ghz and end at 12.4ghz. However, there are selected frequency have been selected to complete this analysis. The frequency is 8.006ghz, 8.504ghz, 9.003ghz, 9.501ghz, 10ghz, 10.504ghz, 11.003ghz, 11.5ghz, 12.006ghz and 12.504ghz. Section 4.2 describe the result from waveguide simulation for proceeding to the next steps analysis. The first section focusing on estimation of lossless of relative permittivity, $\varepsilon_r$ in magnitude and phase of selected permittivity. Second Section discuss about the equation from in the first section compared to the sample of experiment. Overall, it will present the application of dielectric measurement using open-ended rectangular waveguide.

### A. *Simulation of Open-ended rectangular waveguide*

For the simulation process, COMSOL Multiphysics software is chosen to do the simulation. This is because COMSOL have more graphical and user friendly. The output of the simulation.

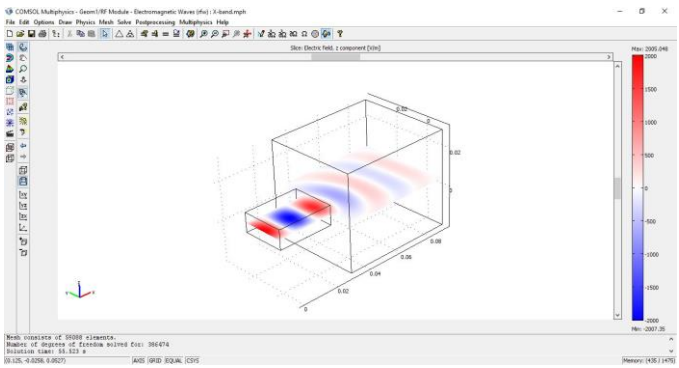

Fig.2. Rectangular Waveguide simulation using COMSOL

### B. *Regression method*

All the required data from the Comsol then will be drafted and tabulated. Next step is determining the correlation between phase of relative permittivity-frequency, $f$ and magnitude of relative permittivity-frequency, $f$. the result shown in table 1 and table 2.

**Table 1: The value of ∅ for 8GHz, 8.5GHz, 9GHz, 9.5GHz, 10GHz, 10.5GHz, 11GHz, 11.5GHz, 12GHz and 12.5GHz.**

| fq1=x*fc (GHz) | \|S11\|^4 | \|S11\|^3 | \|S11\|^2 | \|S11\|^1 | \|S11\|^0 |
|---|---|---|---|---|---|
| 8.006 | 13.6031 | 113.5623 | 347.0395 | 457.6583 | 219.7999 |
| 8.504 | 12.3429 | 101.8672 | 307.4124 | 399.8011 | 189.3035 |
| 9.003 | 12.4719 | 103.0155 | 311.315 | 405.7994 | 192.8142 |
| 9.501 | 13.4983 | 112.5145 | 343.572 | 453.3253 | 218.3615 |
| 10 | 15.0082 | 127.2273 | 395.8226 | 533.4183 | 262.9763 |
| 10.504 | 16.9826 | 145.1702 | 456.0692 | 621.833 | 310.709 |
| 11.003 | 18.7651 | 162.235 | 516.2141 | 714.1874 | 362.7246 |
| 11.5 | 21.3449 | 186.8052 | 602.3377 | 845.685 | 436.3822 |
| 12.006 | 23.5849 | 208.0785 | 676.9865 | 960.2884 | 501.2304 |
| 12.504 | 24.3 | 216.5 | 711 | 1019.1 | 538.2 |

This corresponding data indicated that 4th order polynomial expression provided a closer fit which frequency is in GHz. Similarly, the same procedure is implemented in order to find out the relationship between Phase for $\varepsilon_r$ and frequency, *f*. The values of phase $\varepsilon_r$ in table 1 above are plotted against corresponding frequency, *f*. from the figure, the best relationship between phase $\varepsilon_r$ and *f* are best represented by 5th order polynomial expression as illustrated in table 2.

**Table 2 : The relationship between phase $\varepsilon_r$ and *f* are best represented by 5th order polynomial**

| | |
|---|---|
| B1 = | $1.676218612833789e^{-1}*f^5$-$8.396191269750878e^{0}*f^4$ +$1.673881676143067e^{2}*f^3$-$1.660466640000565e^{3}*f^2$ +$8.196340794337571e^{3}*f^1$-$1.610956351388734e^{4}$ |
| B2 = | $2.096346474057691e^{0}*f^5$-$1.050143756973177e^{2}*f^4$ +$2.093767548162763e^{3}*f^3$-$2.077191792438277e^{4}*f^2$ +$1.025455243368221e^{5}*f^1$-$2.015738473739705e^{5}$ |
| B3 = | $1.041827999691639e^{1}*f^5$-$5.219294841423420e^{2}*f^4$ +$1.040697561492126e^{4}*f^3$-$1.032549596225998e^{5}*f^2$ +$5.097963610099516e^{5}*f^1$-$1.002221483258456e^{6}$ |
| B4 = | $2.571230238577420e^{1}*f^5$-$1.288200044702058e^{3}*f^4$ +$2.568768741551143e^{4}*f^3$-$2.548856337827955e^{5}*f^2$ +$1.258555597647088e^{6}*f^1$-$2.474483585979220e^{6}$ |
| B5 = | $3.150622836689462e^{1}*f^5$-$1.578562772545598e^{3}*f^4$ +$3.147955586747359e^{4}*f^3$-$3.123766611786021e^{5}*f^2$ +$1.542560596634158e^{6}*f^1$-$3.033157484249565e^{6}$ |
| B6 = | $1.533042213678925e^{1}*f^5$-$7.681384734350269e^{2}*f^4$ +$1.531890052137511e^{4}*f^3$-$1.520208122068902e^{5}*f^2$ +$7.507559157883278e^{5}*f^1$-$1.476343257907985e^{6}$ |

Final relationship between B1, B2, B3, B4, B5, B6 and Phase P11 in table are best represented as equation below. The equation (3) can accept frequency from range 8.5GHz to 12.5GHz.

$$\varepsilon_r = 10^{B1*P11^5+B2*P11^4+B3*P11^3+B4*P11^2+B5*P11+B6} \quad (2)$$

The same procedure again, will be reanimate to determine the relationship between Magnitude S11m correspond to the frequency, *f*.

**Table 3: The value of Magnitude S11m for 8GHz, 8.5GHz, 9GHz, 9.5GHz, 10GHz, 10.5GHz, 11GHz, 11.5GHz, 12GHz and 12.5GHz.**

| fq1=x*fc (GHz) | \|S11\|^4 | \|S11\|^3 | \|S11\|^2 | \|S11\|^1 | \|S11\|^0 |
|---|---|---|---|---|---|
| 8.0060 | 325.463 | -435.6461 | 221.3136 | -43.6221 | 3.8267 |
| 8.5040 | 320.956 | -393.6350 | 181.4210 | -28.9676 | 2.0238 |
| 9.0030 | 142.100 | -67.9897 | -25.9597 | 27.9180 | -3.6032 |
| 9.5010 | -30.4489 | 230.1932 | -207.3999 | 75.4972 | -8.0809 |
| 10.0000 | 57.0189 | 74.0052 | -102.2301 | 45.7097 | -5.0213 |
| 10.5040 | 53.0995 | 78.4195 | -99.6709 | 43.6843 | -4.6358 |
| 11.0030 | 37.2158 | 90.6994 | -95.9420 | 40.2489 | -4.0519 |
| 11.5000 | 201.644 | -151.4366 | 34.4392 | 10.1846 | -1.4671 |
| 12.0060 | -64.9123 | 234.8328 | -164.1680 | 53.5933 | -4.8015 |
| 12.5040 | -248.737 | 507.0909 | -309.0293 | 86.3922 | -7.3725 |

This corresponding data indicated that 4th order polynomial expression provided a closer fit which frequency is in GHz. Similarly, the same procedure is implemented in order to find out the relationship between magnitude S11m and its frequency, f. The values of magnitude S11m in table 3 above are plotted against corresponding frequency, f. from the figure, the best relationship between S11m and f are best represented by 4th order polynomial expression as illustrated in equation below:

**Table 4: The relationship between Magnitude of reflection coefficient, S11m and f are best represented by 4th order polynomial**

| | |
|---|---|
| A1 = | $-2.221930809565195e^{1}*f^{4}+8.804637010520395e^{2}*f^{3}$ $-1.294179615954564e^{4}*f^{2}+8.352725573437846e^{4}*f-$ $1.993285825665145e^{5}$ |
| A2= | $3.434833649994334e^{1}*f^{4}$ $-1.357533765638927e^{3}*f^{3}$ $+1.988103695761341e^{4}*f^{2}$ $-1.276744441980034e^{5}*f$ $+3.027920179452276e^{5}$ |
| A3= | $-1.922017948341966e^{1}*f^{4}$ $+7.572588650516070e^{2}*f^{3}$ $-1.104332410674241e^{4}*f^{2}$ $+7.052865409907891e^{4}*f$ $-1.661215006437706e^{5}$ |
| A4= | $4.591695809187982e^{0}*f^{4}$ $-1.801882598816952e^{2}*f^{3}$ $+2.613773740481315e^{3}*f^{2}$ $-1.657664200853354e^{4}*f$ $+3.870517422566917e^{4}$ |
| A5= | $-3.933230054659379e^{-1}*f^{4}$ $+1.535278432645848e^{1}*f^{3}$ $-2.211320864602528e^{2}*f^{2}$ $+1.389466174734368e^{3}*f$ $-3.205558132904536e^{3}$ |

$\varepsilon_{r1}$ = A1*S11m$^4$+A2*S11m$^3$+A3*S11m$^2$+A4*S11m+A5 (3)

The equation (3) can accept frequency from range 8.5GHz to 12.5GHz.

## V. CONCLUSION

A simulation method of open ended rectangular waveguide aperture with different kinds of materials and regression method is proposed in this paper. The measurement of the reflection-coefficient of open-ended rectangular waveguide's is valid for modelling. The further research should focus on the effectiveness determination for loss waveguide with regards to the complex part of relative permittivity.

## ACKNOWLEDGMENT

The author wishes to thank for Dr. You Kok Yeow for many helpful, guidance during the work of experiment is held.

## REFERENCES

[1] Palais, J,C..*Fibre Optic communication. Prentice Hall,Inc*. A Simon & Schuster, Englewood Ciffs, New Jersey,1992.

[2] Miller, S.E.1969. Integrated optics: An introduction. Bell System Technical Journal, 48(7):2059-2069.

[3] Abu Sahmah Mohd Supa'at, Abu Bakar Mohammad & Norazan Mohd Kassim.2002."Modelling techniques for rectangular dielectric waveguide-Rib Waveguides".Jurnal Teknologi, 36(D) 129-143.

[4] Glenn F.Engen.*Thru-Reflect-Line: An improved technique for calibrating the Dual Six-Port Automatic Network Analyzer.Vol.27.December 17.*

[5] Y. Yorozu, M. Hirano, K. Oka, and Y. Tagawa, "Electron spectroscopy studies on magneto-optical media and plastic substrate interface," IEEE Transl. J. Magn. Japan, vol. 2, pp. 740-741, August 1987 [Digests 9th Annual Conf. Magnetics Japan, p. 301, 1982].

[6] M. Young, The Technical Writer's Handbook. Mill Valley, CA: University Science, 1989.

# Indoor Location Tracking System using Euclidean Distance Estimation (LTS-ED)

Jee Chun Hian
*Faculty of Electrical Engineering*
*Universiti Teknologi Malaysia*
*Johor Bahru, Malaysia.*
*jeechunhian@gmail.com*

Sharifah Hafizah Syed Ariffin
*Department of Communication Engineering*
*Faculty of Electrical Engineering*
*Universiti Teknologi Malaysia*
*Johor Bahru, Malaysia.*
*sharifah@fke.utm.my*

***Abstract*—Indoor location tracking system is needed to support location based service such as indoor navigation system or indoor crowd monitoring system in an indoor environment. In this paper, the focus will be on the implementation of indoor location tracking system using Wi-Fi signal strength. However, there are several techniques for indoor location tracking such as triangulation, trilateration, and fingerprinting. The development of the proposed system is based on fingerprinting technique. The system consists of two main components which are the server which is based on Java and an Android-based client. The client side application is responsible for the Wi-Fi RSSI scanning, filtering out weak received signal strength (RSSI), specifically lower than -85dBm while the server provides the closest match of the location ID based on offline training data stored in database. The indoor location tracking system will be solely based on the software algorithm which is supported by MySQL. The results show that location tracking within small area gives better accuracy than bigger area.**

**Keywords—indoor location tracking; Wi-Fi; RSSI; fingerprinting, data filtering**

## I. INTRODUCTION

Navigation applications are widely used in outdoor location positioning with the aids of Global Positioning System (GPS). By using GPS and maps information, users can easily track their current real-time location and the direction to their desired destination. On the other hand, indoor positioning technology could be the future trend as day-by-day expanding of the size of buildings. Realizing location based service (LBS) in indoor environment, it could truly benefit the community because navigation system within building or indoor crowd monitoring could be enabled. However, GPS usage in indoor environment remains as a challenge as its signal travel by line-of-sight (LOS), passing through internet cloud and glass materials (as wall) but blocked by solid objects such as building [1]. To solve these issues, indoor location positioning using Wi- Fi signal is adopted as most buildings nowadays are equipped with Wi-Fi network and Wi-Fi signal could penetrate walls within acceptable RSSI.

Wi-Fi radio waves propagates over a long range in an indoor environment but experienced disturbance such as reflection, diffraction, scattering and multipath loss, resulting dynamic signals and difficult to predict using mathematical model [2]. RSSI variation in signal strength dependents upon the surrounding physical environment, which can be classified into static elements such as geometrical boundaries and dynamic element comprise mobile object such as people movement and oscillating fan [2]. Hence, signal fingerprinting method is proposed as it does not depend on the distance calculated by the mathematical model.

Main objective of this project is to provide a reliable indoor location tracking system which can used to further develop location based services in indoor environment such as indoor navigation or indoor crowd monitoring system. The objectives of this work are to develop a server for indoor location tracking system using Java platform and a client application for the system in Android-based platform. In addition, a filtering algorithm is applied in between the software to improve the accuracy of the detected mobile unit.

From the system, the client provides an automatic data collection and entry to the MySQL database through the server in its offline phase (training phase). In online phase, Java server is capable to find its closest match in database and retrieve its real-time location information. This could largely reduce the work done of the developers in the related project in near future by using this software-orientated system.

The remaining part of this paper is structured as follows. In section II, the related works are visited. In section III, methodology of the project is discussed. Section IV includes results and discussion after performing the accuracy test while Section V concludes the finding of the works.

## II. RELATED WORKS

Indoor location tracking has been developed with the advancement of technology, seeking improvement of the performance in location tracking system. This section presents different technologies used to develop different type of techniques for indoor location tracking, comparing different functionality of the technologies. Several technologies can be used as the tool in indoor location tracking system. It includes Radio Frequency Identification (RFID), Bluetooth, Cricket, and Wi-Fi. Each technology has its constraint and limitation when implement in indoor environment.

The basic working principle of RFID is based on the emitted radio frequency as the medium. Reader and tags are the essential

elements in RFID system, communicating in short distance without contact between these two elements. The most significant benefits of using RFID is its functioning capability without external power source [3]. Work from [3] aims to guide people using combination of QR-Code and active RFID in an indoor environment, building navigation service for assisting to reach their destination via shortest path in unfamiliar building. In other studies such as in [4] it uses RFID technology to develop an indoor navigation system by placing grid of passive tags located on the ceiling. By implementing RFID technology, LANDMARC algorithms uses weighted algorithms based on residual error between target tag and reference tag, achieving higher location accuracy [5].

Bluetooth is often a favorite choice in an indoor location positioning system, using wireless technology standard for exchanging data over short distance in the ISM band from 2.4 to 2.485 GHz. Utilizing the Bluetooth modules equipped in smartphones, location tracking can be used by users that are carrying smartphone in buildings. Latest Bluetooth which is version 4 aims to transmit at higher rate and less power consumption embedded in smartphone is used as tool for indoor location positioning in [6] and [7]. Work from [6] proposed an algorithm using measurement of RSSI as the input to an algorithm which utilizes the use of neural network algorithms such as I^3 BM and environmental adaptive algorithms while [7] pointed out algorithms such as trilateration, triangulation, proximity sensing and fingerprinting.

Cricket uses beacon nodes in location positioning, utilizing radio frequency signal and ultrasonic signal. Receiving multiple signals from different beacons, the current position of the user can be calculated by performing time-difference-of-arrival based distance ranging from radio frequency signal and ultrasonic signal transmitted at same time from the beacon nodes by passive receiver. Using Cricket nodes and inertial sensors, indoor localization system for human tracking is developed in [8]. By adding inertial navigation, the Cricket based accuracy is significantly improved by the system in [8]. The work in [9] used Cricket to track the indoor pedestrian which is also a good and useful application.

Connecting by radio frequency in IEEE 802.11 standard, Wi-Fi is a technology used in Wireless Local Area Network (WLAN). WLAN establishes network with a range of 70 to 300 feet by radio frequency waves at 2.4GHz ISM band, implemented by IEEE802.11 standard. It is famous in indoor location tracking because it works in longer range and it provides network to the users of mobile unit at the same time. By using its RSSI, research work done by [10] comparing accuracy using algorithms such triangulation and fingerprinting while [11] has done accuracy performance analysis using triangulation technique in 3D (x, y and z coordinates) for 2 levels building.

Technique using Wi-Fi signal is usually depending on time-of-arrival (TOA), time-difference-of-arrival (TDOA), received-signal-strength (RSS) and angle of arrival (AOA) [12]. This section will only discuss the technique using RSSI since it is simpler than obtaining delays or angle measurement. Algorithms using RSSI includes trilateration, triangulation, and fingerprinting algorithms. Trilateration and triangulation are propagation based algorithm which uses power distance loss formula in estimating distance between transmitter and receiver while fingerprinting method is an algorithm which based on pattern recognition of Wi-Fi signal strength.

Distance finding in trilateration or any other propagation-based algorithms is a crucial step in locating position, modelled by the value of RSSI which is given by power distance formula 1 in [13]:

$$P_r = \alpha - 10 * n * \log_{10}(d) + X \qquad (1)$$

X denotes by Gaussian random variable with zero mean caused by shadowing, α is a constant, n is the path loss exponent and d is the distance between transmitter and receiver. According to [13], α is a constant which depends on several factors: average fast and slow fading. Therefore, work from [13] uses measurements taken in a reference place and it can be used as a constant value in all environments. Eventually, it gives the distance formula in [11] as shown in equation 2. In [2], $d_0$ is the reference distance, WAF is the Wall Attenuation Factor while T is the number of walls between transmitter and receiver.

$$d = e^{\left(\frac{P_r(d_o) - P_r(d) - T*WAF}{10*n}\right)} \qquad (2)$$

By deploying a few routers, position of mobile unit can be located by finding the intersection of all calculated distance using trilateration. By using geometric properties of triangle, location of interest is estimated in triangulation technique. Triangulation technique is also a propagation based algorithm, applying same mathematical model in distance finding as shown in equation 2. Finding angle α using distance between the AP, mobile unit can be located by triangulation algorithm [10].

Work in [10], [11], [14] involves fingerprinting method in its algorithms to locate real time position of the mobile unit. According to [14], algorithm which uses fingerprinting technique assumes that the mobile unit which receive Wi-Fi signals always receive similar signal strength at the certain location. By storing the Wi-Fi signal strength with their respective coordinates, the position of the mobile unit can be located by comparing the scanned signal strength with the signal strength stored in database. Implementing fingerprinting technique, it can work with the K-Nearest Neighbour (K-NN), neural networks, support vector machine (SVM), probabilistic method and Gaussian Process (GP).

After applying Gaussian process in fingerprinting algorithm in [14], the paper also introduces Bayesian filter to do decision on the mobile unit location. Applying the posterior distribution of RSSI at each location determined by GP, the measurement likelihood model can be calculated by the posterior mean and variance.

## III. Location Tracking System Server & Client Module

. In this section, implementation of this project using Java programming language in the server side and Android-based in

the client side will be discuss by illustrating the system flow. As discussed, this project focuses at fingerprinting method with filter which uses Wi-Fi signal as the tool in determining the position of the mobile unit. In addition, the decision rule in fingerprinting method also will be discussed.

The system can be divided into two components, server module and client module. The client module is usually a mobile unit which will only responsible for RSSI scanning and displaying the resultant location, reducing the processing power of the mobile unit. The calculation of the location based on the chosen algorithm will be done by the server module, optimizing the energy efficiency of the mobile unit.

### *A. Offline Process / Data Training Phase*

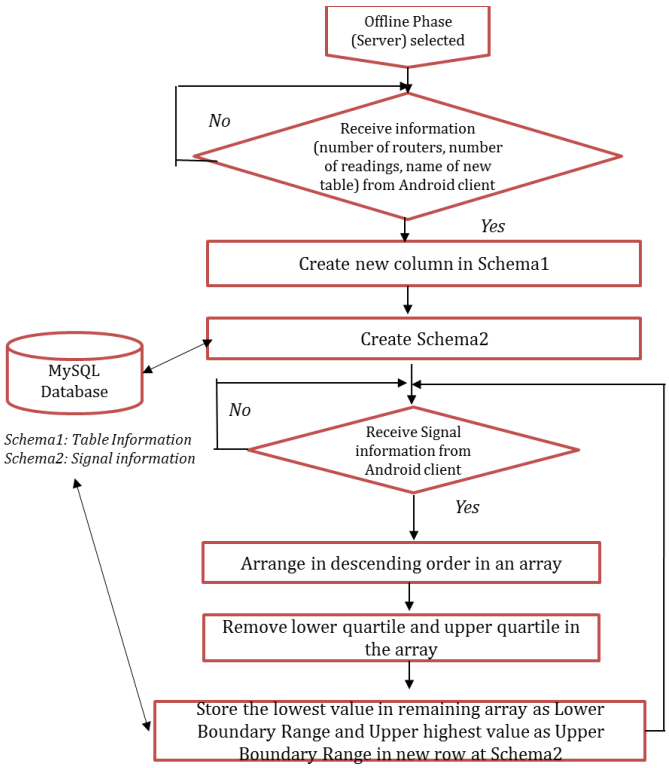


Figure 1. Server Module Offline Process

Figure 1 illustrates the server offline process. During the offline phase, the calibrated area is divided into numbered area with location ID according to the uniqueness of its RSSI fingerprints. In addition, server provides automatic entry of data based on the collection of data made by the client module.

To get a better representation of the data of the signal, data in upper quartile and lower quartile are removed to get rid of signal fluctuations. Assuming the RSSI signal fluctuations are at the extremely high or extremely low values which exists in the data set during sampling of the signal. These unusual RSSI data set values can be removed after sorting it in ascending order. In this project, the outliers which are the top 15% (Upper Quartile) and bottom 15% (Lower Quartile) will be remove from the data set. This process is illustrated in Figure 1. After removing the upper quartile and lower quartile, the remaining highest and lowest value are treated as the upper boundary and lower boundary of range of the RSSI signals respectively for each router. Then, these values are stored in the MySQL database's Schema2 (signal information).

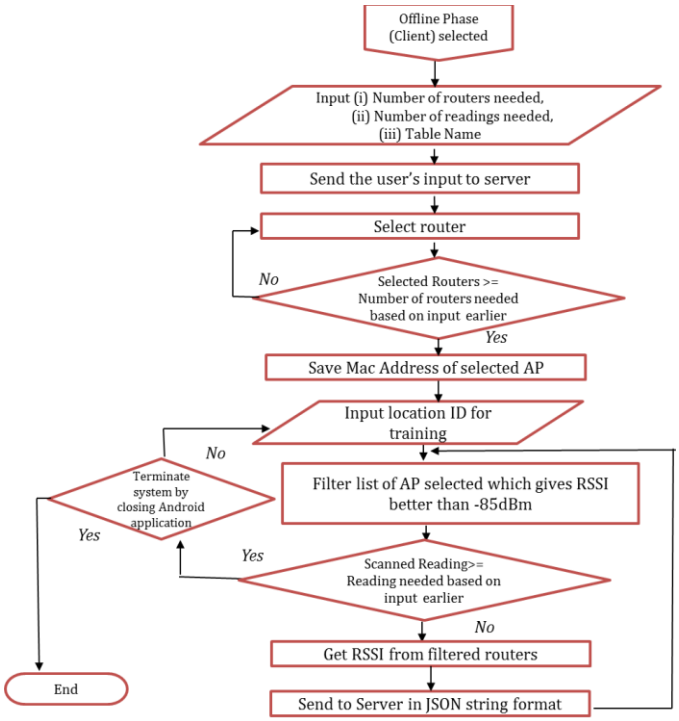


Figure 2. Client Module Offline Phase

The client module is developed using Android application. Clients can choose the routers to calibrate the routers, number of readings to be collected from each router and the name for the new table in the database. This will provide high flexibility in performing the data training process. In the data training phase, RSSI fingerprint of each location are collected by performing walk-around within the calibration area. This phase is conducted after the development of the Android-based client module and the client module is able to sample the RSSI transmitted by the access point (AP).

The RSSI values of the routers will reduce with the increment of distance from the transmitted source [15] and [16]. Apart from distance, building materials such as wood, glass, and brick also will attenuate the signal strength in an indoor environment [17]. The working range of Wi-Fi adapter highly depends on the power gain of the antenna [18], several routers are needed to cover throughout the entire office area. This is due to attenuation, indoor environment obstacles and limitation of the antenna power gain. For typical Wi-Fi receivers, RSSI value of -75dBm will provide a reasonable service, -85dBm provides an acceptable service while -100 dBm provides a barely usable service [18].

To improve accuracy of the location tracking system, filtering algorithm is applied to the fingerprinting before the scanning process taken place in a specific calibration area. During RSSI collection, AP(s) which gives signal value lower than -85dBm will be ignore for the scheduled scanning of training process. The specific AP will be given 0 value, labelling

it as an irrelevant AP at the area. The weak RSSI usually gives fluctuate values and this will fail to reflect the location ID for the specific area. By applying filtering, the system is expected to provide better accuracy in the Online Process / Position Locating Phase.

### *B. Online Process/ Position Locating Phase.*

In the online phase, the mobile unit will scan for signal strength for all calibrated APs then send it to the server for performing location positioning calculation. Before scanning process, same filtering algorithm in offline phase is applied. Comparing the signal strength from the client unit, the server will choose the closet match from the database signal strength stored during offline phase.

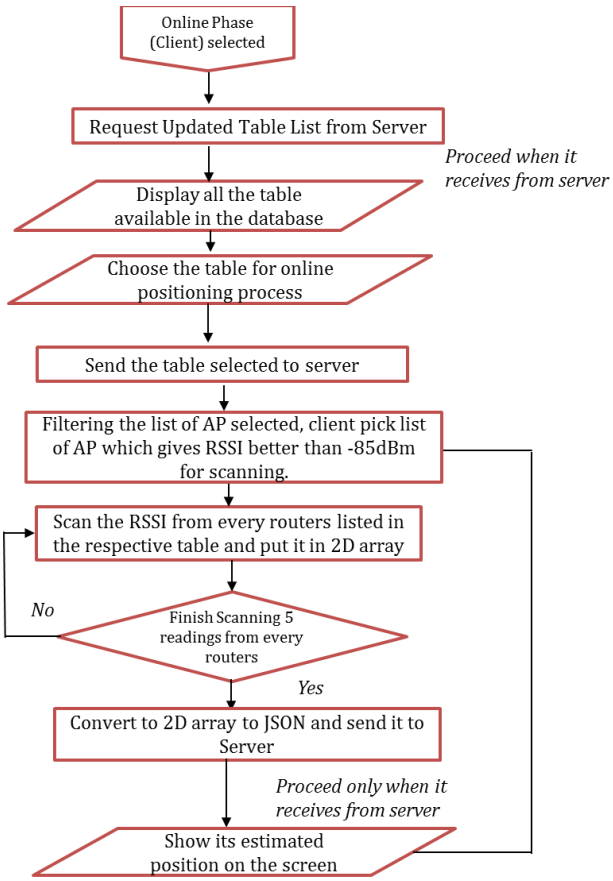


Figure 3. Client Online Phase

For the server side, K-NN algorithm is used in finding closest match of the location ID with the RSSI scanning results. K-NN algorithms stands form K-Nearest Neighbour algorithm where K is the number of nearest neighbour need to be classified. Assuming every location ID in the floor plan is unique, K=1. Hence, K-NN algorithm is used. To find its nearest neighbour, Euclidean distance is used in this project. The location ID which gives the shortest Euclidean distance is the location of the client. Euclidean distance sums up the difference of client current signal ( $A_o$ , $B_o$ , $C_o$ , ….) and the upper boundary and lower boundary for each attributes (routers) as in ( $A_L$ , $A_H$ , $B_L$ , $B_H$ , $C_L$ , $C_H$, ….). Euclidean distance is given by equation 6:

$$Distance = \sqrt{((A_o - A_L)^2 + (A_o - A_H)^2 + (B_o - B_L)^2 + (B_o - B_H)^2 + (C_o - C_L)^2 + (C_o - C_H)^2 + \cdots)} \quad (6)$$

## IV. Result and Discussion

The experiment of the indoor location tracking system is conducted at Bangunan Siswazah, F54, UTM Academic Leadership which is located in Universiti Teknologi Malaysia, Johor Bahru. Figure 4 shows the floor plan of the experimental area with the predetermined location ID.


Figure 4. Floor Plan of Experimental Area

Using Ekahau HeatMapper (Wi-Fi site survey software tool), Wi-Fi heatmap is generated to show the RSSI fingerprints shown by each router. Figure 5 and Figure 6 shows examples of Wi-Fi heatmap generated by Ekahau HeatMapper after performing walk-around in the office. Router A's SSID is dlinkUTMLED with mac address 00:22:b0:f3:e2:cb while Router B's SSID is Hotspot@UTM with mac address f8:e7:1e:1d:fd:38.

Based on user manual of Ekahau Site Survey user guide in [19], red colour indicates very weak signal strength while green colour is a symptom of strong signal strength. From the colour of the Wi-Fi heat map, signal strength and coverage of each router can be observed based on the colour changes.

Average of unit position


Figure 5. Wi-Fi heatmap generated by Router A


Figure 6. Wi-Fi heatmap generated by Router B

Figure 5 and Figure 6 shows the access point (AP) which are located at different location. These APs generate different Wi-Fi RSSI values at different location. In this experiment, 10 existing AP are chosen to be used in the location tracking algorithm. Two types of testing are done, namely corridor testing and room testing.

## A. *Corridor Testing*

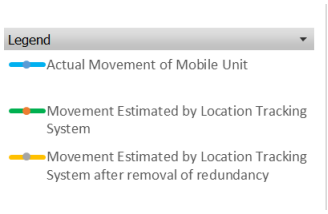



Figure 7. Comparison of LTS-ED in corridor area with and without redundancy.

Figure 7 shows the result of location tracking in corridor area after performing the walk-around from location ID 1, 2, 5, 7, 6, 10, 11 by sequence. The results are taken for actual movement, LTS-ED with redundancy (green line) and LTS-ED without redundancy (yellow). It shows that the accuracy at position 1 until 6 gives and accurate results at position 6 until 14 has some errors. LTS without redundancy is done by scanning RSSI from the AP and the ones which are less than -80dBm are remove manually to gives acceptable result as shown in the yellow legend. The error is due to the location being in low values of RSSI.

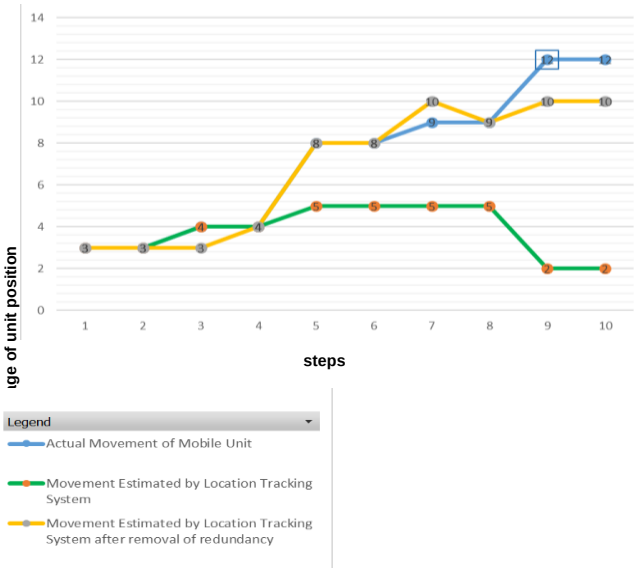


Figure 8: Comparison of LTS-ED in rooms with and without redundancy.

## B. *Rooms Testing*

Testing is also conducted in each room as shown in the floor plan in Figure 4 from location ID 3, 4, 8, 9, 12 in sequence. Similar to the testing conducted in the corridor, which only gives satisfactory results when redundancy data of -80dBm is removed from the scan result. In this experiment, it shows that the accuracy at position 1 until 6 gives accurate results, however at

position 6 until 10 gives some errors for LTS-ED without redundancy and the actual movement.

Locations which shares same values of RSSI fingerprints causes error because they give similar Euclidean distance when applying the NN-algorithm and due to the location being in low values of RSSI.

## V. Conclusion and Future works

Using Euclidean distance estimation in fingerprinting technique, RSSI fluctuation remains as challenge to apply in an indoor location tracking algorithm. To solve this issue, signal weaker than -80dBm RSSI need to be filter out to avoid redundancy of data caused by fluctuation instead of -85dBm. RSSI fingerprints at calibrated areas need to be unique for ensuring uniqueness of the fingerprints compared to other calibrated area. This is important because the location of the mobile unit is located by using Euclidean distance estimation. Similar Euclidean distance calculated using scanning result could cause error in detecting the location of the mobile unit. LTS-ED without redundancy shows acceptable performance since the infrastructure used for the experiment is using the existing infrastructure and not experimental set-up infrastructure.

## References


[1] Patrick Bertaga, "How does a GPS tracking system work", http://www.eetimes.com/document.asp?doc_id=1278363, 26 October 2010 [Accessed December 5, 2016].

[2] John C.Stein, "Indoor Radio WLAN Performance", Palm Bay, Florida, Harris Semiconductor.

[3] Saleh Alghamdi, R.V. Schyndel, A.Alahmadi, "Indoor Navigation Aid using RFID and QR Code For Sighted and Blind People", La Trobe University, Melbourne, IEEE,2013.

[4] E.Di Giampaolo, "A passive rfid based indoor navigation system for visually impaired people", Università dell'Aquila, Italy, IEEE,2010

[5] Zhong Hua Li, Z.Zijing, H.ChunHui, X.Huang, "Advances in RFID-ILA: The Past, Presents and Future of RFID-based Indoor Location Algorithms", Sun Yat-Sen University, GuangZhou,IEEE,2012.

[6] A.M.A.Hassan, "Indoor Location Tracking System using Neural Network Based on Bluetooth", October University for Modern Science and Arts, Eygpt, International Conference on Electrical , Electronics, and Optimization Technique (ICEEOT) 2016

[7] Senan M.H, S.Zickau, " Indoor Mapping for Location-based Policy Tooling Using Bluetooth Low Energy Beacons", Technische Universitat Berlin, 2015 Eight International Workshop on Selected Topics in Mobile and Wireless Computing.

[8] M.Popa, J.Ansari, J.Riihijarvi, P.M., "Combining Cricket System and Inertial Navigation for Indoor Human Tracking", RWTH Aachen University, Germany.

[9] G.Qinfeng, W.W.Choong, " Tracking Indoor Pestrian using Cricket Indoor Location System", National University of Singapore, 2012 IEEE.

[10] Sazzad Hossain, "Application Independent in Location Tracking Framework",Faculty of Electrical Engineering, Universiti Teknologi Malaysia, March 2013

[11] Norhidayu Shahila Binti Abu Hassan, "Three Dimension Positioning Based Location Tracking Technique for Indoor Environment", Universiti Teknologi Malaysia, 2014 May.

[12] F.Gustafsson and F.Gunnarsson, "Mobile positioning using wireless networks : Possibilities and fundamental limitations based on available wireless network measurement" , IEEE Signal Process. Mag., vol. 22, no. 4, pp. 41–53, Jul. 2005.

[13] S.Mazuelas, A.Bahillo, Ruben M.Lorenzo, P.Fernandez, F.A.Lago, E.Garcia, J.Blas, E.J. Abril ," Robust Indoor Positioning Provided by Real Time RSSI Values in Unmodified WLAN Networks", IEEE Journal Of Selected Topics In Signal Processing, Vol. 3, No. 5, October 2009.

[14] Xiang He, S.Badiei, Daniel Aloi, Jia Li, "Wifi Based Indoor Localization for Smartphone", Ookland University , USA.

[15] Lui, Gough, et al. "Differences in RSSI readings made by different Wi-Fi chipsets: A limitation of WLAN localization." Localization and GNSS (ICL-GNSS), 2011 International Conference on. IEEE, 2011.

[16] "Distance and Inverse Square Law," [Online]. Available: http://emfwise.com/distance.php , [Accessed May 10, 2017]

[17] Ahsan S, Zeeshan A, Iftikhar A, " Analysis And Measurement of Wi-Fi Signal in Indoor Environment", International Jornal of Advances in Engineering & Technology (IJAET), May 2013, ISSN: 2231-1963

[18] Venkatakrishnan Raghavan, Raj Jain, "Performance Analysis of Wireless Transmitters", May 1 2015, [Online] Available: http://www.cse.wustl.edu/~jain/cse567-15/ftp/wireless/index.html

[ Accessed May 10, 2017]

[19] "Ekahau Site Survey user guide: Wi-Fi planning, verification, troubleshooting", Ekahau Inc, 2012 [Online] Available: www.ekahau.com/wpcontent/uploads/2017/04/Ekahau_Site_Survey_DS.pdf, [Accessed May 10, 2017].


.

# Dual-band Microstrip Patch Antenna for LTE and WiFi Applications

Wong Soon Yaw[1]
*Faculty of Electrical Engineering*
*Universiti Teknologi Malaysia*
*Johor Bahru, Malaysia*
*sywong24@live.utm.my*

Muhammad Ramlee Kamarudin[2]
*Wireless Communication Centre*
*Faculty of Electrical Engineering*
*Universiti Teknologi Malaysia*
*Johor Bahru, Malaysia*
*ramlee@fke.utm.my*

***Abstract*—The current communication system is developing rapidly. This is the reason why developing multi-band antenna is a must. In this research, a dual-band microstrip patch antenna for Long Term Evolution (LTE) and Wireless Fidelity (WiFi) applications is presented. This antenna can operate at 2.6Giga Hertz for LTE and 5.0Giga Hertz for WiFi. The dual-band microstrip patch antenna designed consists of FR-4 as the dielectric substrate. Microstrip line feeding together with insect feeding were used to increase the bandwidth of the antenna designed. The dual-band frequencies are generated by adding 2 inverted U-slots on the radiating patch. Computer Simulation Technology (CST) was used for the simulation of the antenna designed. The fabrication of the dual-band microstrip patch antenna has been done. Analysis of the results for simulations has been discussed as well.**

***Keywords—Multi-band; Microstrip Patch; Feeding; Slots; CST***

## I. INTRODUCTION

Communication is the transfer of information from one point to another point [1]. The examples of applications for communication are LTE and WiFi. It is true that multi-band antenna can provide larger bandwidth [2]. Thin profile, light weight, low fabrication cost, easy to fabricate as well as compatible with integrated circuitry [3] are the advantages of using microstrip. There are increasing demand for a better communication system and this demand has triggered the development of antenna design. It is a must to design and fabricate a new antenna that comes with smaller size, wider bandwidth and higher directivity. The objective of this research is to design a dual-band microstrip patch antenna for LTE and WiFi applications. This scopes of this research includes the design, simulation, fabrication and analysis of the antenna designed.

## II. PRINCIPLE OF PATCH ANTENNA

A patch antenna consists of radiating patch, substrate and ground plane, where radiating patch is on top surface of the substrate and ground plane is on bottom surface of the substrate. Radiating patch will act as resonant cavity, where short circuit will occur on the top and bottom surfaces and open circuit will occur on the other sides except top and bottom surfaces. Only certain modes are allowed to exist at different resonant frequencies in a cavity [4]. A strong field will be set up inside the cavity when the antenna is excited at resonant frequencies. Also, strong current will be on the bottom surface of the radiating patch. This will allow very good radiation and the patch antenna is a very good antenna.

## III. GEOMETRY OF MICROSTRIP PATCH ANTENNA

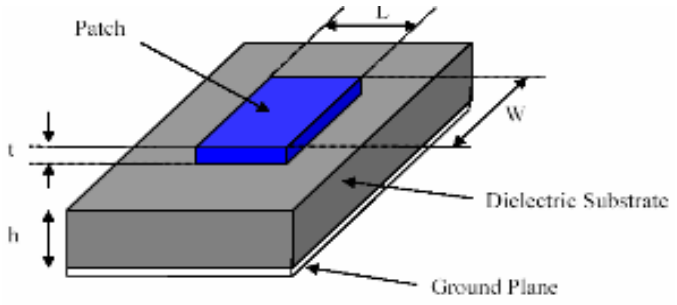


Fig. 1. Geometry of microstrip patch antenna [5]

Fig. 1 shows the geometry of microstrip patch antenna. Based on transmission line model (TEM) approximation, the parameters of the antenna, included the length and width of the radiating patch, substrate and ground plane can be calculated [6]. The radiating patch is viewed as transmission line resonator with no transverse field variation [7].

The width of the radiating patch, $W$ is calculated by,

$$W = \frac{c}{2f_o}\sqrt{\frac{2}{\varepsilon_r+1}} \quad (1)$$

The effective relative constant, $\varepsilon_{reff}$ is calculated by,

$$\varepsilon_{reff} = \frac{\varepsilon_r+1}{2} + \frac{\varepsilon_r-1}{2}(1+12\frac{h}{W})^{\frac{-1}{2}} \quad (2)$$

The effective length, $L_{eff}$ is calculated by,

$$L_{eff} = \frac{c}{2f_o\sqrt{\varepsilon_{reff}}} \quad (3)$$

The effective length due to fringing effects, $\Delta L$ is calculated by,

$$\Delta L = 0.412h\frac{(\varepsilon_{reff}+0.300)(\frac{W}{h}+0.264)}{(\varepsilon_{reff}-0.258)(\frac{W}{h}+0.800)} \quad (4)$$

The length of the radiating patch, $L$ is calculated by,

$$\mathrm{L} = \mathrm{L_{eff}} - 2\Delta\mathrm{L} \quad (5)$$

The length of the ground, $L_g$ is calculated by,

$$L_g = 6h + L \quad (6)$$

The width of the ground, $W_g$ is calculated by,

$$W_g = 6h + W \quad (7)$$

## IV. Feeding Technique And Slotting Technique

The use of feed line is to excite and to radiate. For microstrip line feeding, a conducting strip is used to connect with the edge of the microstrip patch directly. Typically, the width of the conducting strip is smaller than the radiating patch. The advantage of using microstrip line feeding is this feed line can be etched on the same dielectric substrate in order to provide a planar structure [8]. Furthermore, microstrip line feed is easy to fabricate compared to other feeding techniques. This is due to the reason of this feed line is just a conducting strip connected to the edge of the radiating patch. Moreover, microstrip line feeding is simple to model.

There are few shapes of slots that can be used. For example, U-shaped slots, L-shaped slots, C-shaped slots and E-shaped slots. Slots in microstrip patch antenna can be used to create dual-band frequencies [9]. Also, slots can be applied in microstrip patch antenna to improve the size of the bandwidth. Besides, the size of the microstrip patch antenna can be reduced by loading certain shaped slots in the radiating patch. This is because meandering of the excited patch surface current paths caused by loading of certain shaped slots in the radiating patch. As a result, the fundamental resonant frequency of the microstrip patch antenna will be lowered. Longer slot length will lower resonant frequency. This means there will be a reduction in the size of the microstrip patch antenna.

## V. Parameters Of Design

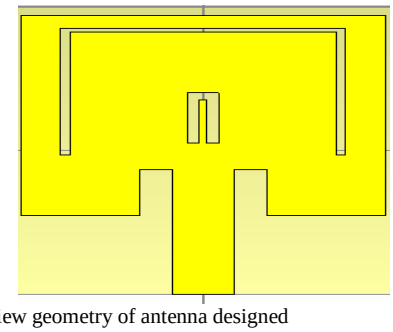

Fig. 2. Front view geometry of antenna designed

Fig. 2 shows the front view geometry of the antenna designed for LTE and WiFi applications. Some parameters for the antenna designed were calculated using (1) – (7) and presented Table I after optimization.

TABLE I. Parameters for the antenna designed after optimization.

| | |
|---|---|
| Dielectric constant of dielectric substrate ($\varepsilon_r$) | 4.30 |
| Thickness of dielectric substrate (t) | 1.60mm |
| Length of radiating patch (L) | 13.92mm |
| Width of radiating patch (W) | 18.40mm |
| Length of substrate ($L_s$) | 42.00mm |
| Width of substrate ($W_s$) | 50.00mm |
| Length of ground ($L_g$) | 42.00mm |
| Width of ground ($W_g$) | 50.00mm |
| Length of microstrip line feeding | 9.01mm |
| Width of microstrip line feeding | 3.10mm |
| Length of insect feeding | 3.22mm |
| Width of insect feeding | 1.65mm |
| Length of smaller inverted U-slot | 3.50mm |
| Width of smaller inverted U-slot | 1.60mm |
| Thickness of smaller inverted U-slot | 0.60mm |
| Length of bigger inverted U-slot | 8.80mm |
| Width of bigger inverted U-slot | 14.40mm |
| Thickness of bigger inverted U-slot | 0.50mm |

TABLE I shows the parameters for the antenna designed after optimization. The antenna designed will operate at 2.6GHz for LTE and 5.0GHz for WiFi. FR-4 ($\varepsilon_r$=4.30) is chosen as the dielectric substrate due to FR-4 dielectric substrate is available easily. Higher dielectric constant of dielectric substrate is used to reduce the size of the antenna designed. The thickness of the FR-4 dielectric substrate is kept at standard 1.6mm as this thickness is suitable for wideband applications.

## VI. Fabrication Of Antenna

The materials and equipment required for fabrication of the antenna are FR-4 board ($\varepsilon_r$=4.30), SMA connector, glossy paper, solder gun and lead. The fabrication process starts with exporting the optimized design of the antenna from CST to AutoCAD in the form of DXF file. Next, the design need to be printed on glossy paper by using AutoCAD. After that, the large FR-4 board need to be cut into the desired dimension by using cutter. Next, the FR-4 board need to be exposed to UV light by using UV light exposure machine. After that, the FR-4 board is immersed in the developer for positive photoresist. The next step of fabrication process is etching. Etching is a process to remove any unwanted copper from unshielded region and left only the wanted copper from shielded region. Next step is to solder the 50Ω SMA connector onto the fabricated antenna using solder gun and lead. The last step is to check the connection between port and antenna using digital multimeter.

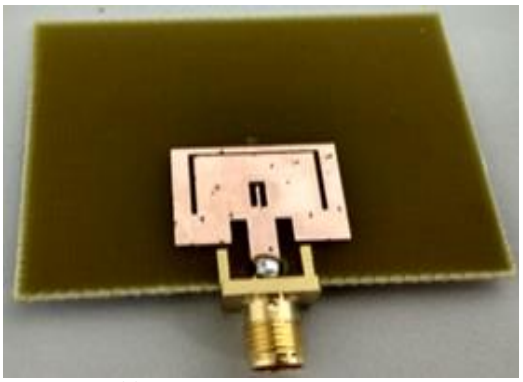

Fig. 3(a). Front view of fabricated antenna

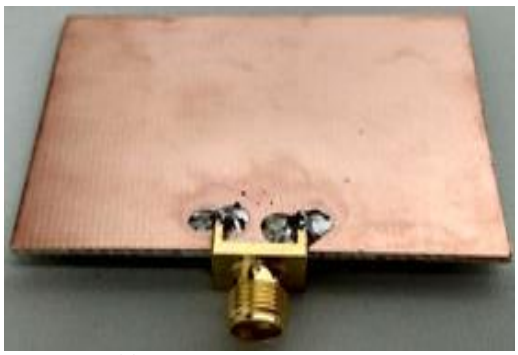

Fig. 3(b). Back view of fabricated antenna

Fig. 3(a) shows the front view of fabricated patch antenna. Fig. 3(b) shows the back view of fabricated patch antenna.

## VII. Result And Discussion

The performance of the dual-band microstrip patch antenna in terms of operating frequency, reflection coefficient magnitude ($S_{11}$), bandwidth, radiation pattern of E-Field and H-Field as well as surface current and directivity of the antenna proposed have been analysed.

### A. *Reflection Coefficient Magnitude ($S_{11}$)*

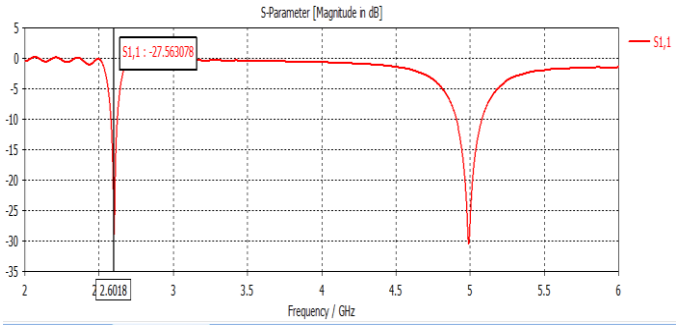


Fig. 4(a). Reflection coefficient magnitude ($S_{11}$) for 2.6GHz LTE antenna

Fig. 4(a) shows reflection coefficient magnitude ($S_{11}$) for 2.6GHz LTE antenna. The reflection coefficient magnitude ($S_{11}$) is -27.56dB, which is very good. This value met the requirement of the design, which is less than -10.0dB and is equal to more than 90% power feed absorbed. In fact, more than 99% power feed absorbed and less than 1% power loss for this 2.6GHz LTE antenna. The matching of the antenna is very good.

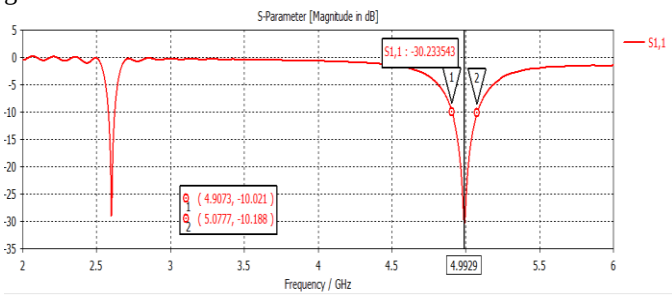


Fig. 4(b). Reflection coefficient magnitude ($S_{11}$) for 5.0GHz WiFi antenna

Fig. 4(b) shows reflection coefficient magnitude ($S_{11}$) for 5.0GHz WiFi antenna. The reflection coefficient magnitude ($S_{11}$) is -30.23dB, which is very good. This value met the requirement of the design, which is less than -10.0dB and is equal to more than 90% power feed absorbed. In fact, more than 99% power feed absorbed and less than 1% power loss for this 5.0GHz WiFi antenna. The matching of the antenna is very good.

### B. *Bandwidth*

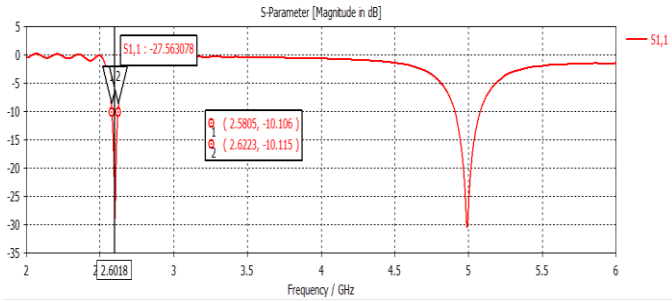


Fig. 5(a). Upper and lower frequencies for 2.6GHz LTE antenna.

Fig. 5(a) shows the upper and lower frequencies for 2.6GHz LTE antenna. The bandwidth of the 2.6GHz LTE antenna proposed has been calculated based on the frequencies operating at -10dB. The lower frequency that operated at -10dB is 2.5805GHz. Whereas the upper frequency that operated at -10dB is 2.6223dB. The bandwidth calculated is 42MHz or 1.62%. The bandwidth of this 2.6GHz LTE antenna satisfied the requirement of the design, which is 40MHz. The range of frequency, where this antenna can operate is 42MHz.

Bandwidth = ((2.6223GHz-2.5805GHz)/2.6GHz) x 100%
= (0.042GHz/2.6GHz) x 100%
= 1.62%

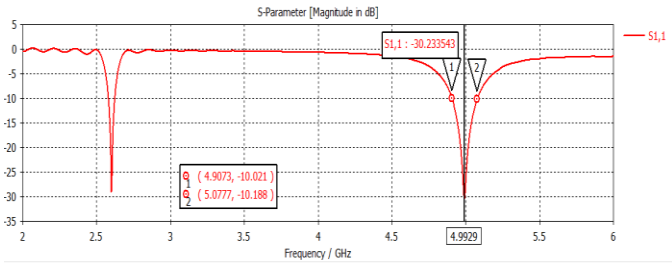


Fig. 5(b). Upper and lower frequencies for 5.0GHz WiFi antenna

Fig. 5(b) shows the upper and lower frequencies for 5.0GHz WiFi antenna. The bandwidth of the 5.0GHz WiFi antenna proposed has been calculated based on the frequencies operating at -10dB. The lower frequency that operated at -10dB is 4.9073GHz. Whereas the upper frequency that operated at -10dB is 5.0777dB. The bandwidth calculated is 170MHz or 3.40%. The bandwidth of the 5.0GHz WiFi antenna satisfied the requirement of the design, which is 160MHz. The range of frequency, where this antenna can operate is 170MHz.

Bandwidth = ((5.0777GHz-4.9073GHz)/5.0GHz) x 100%
= (0.170GHz/5.0GHz) x 100%
= 3.40%

*C. Radiation Pattern (E-Field and H-Field)*

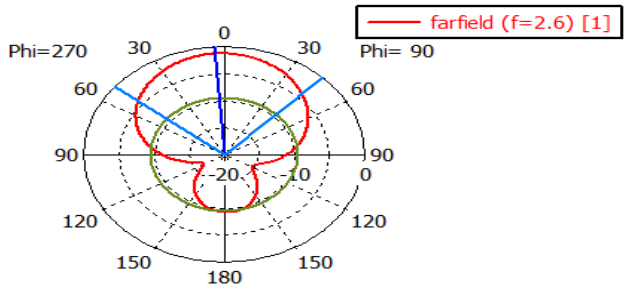


Fig. 6(a). Radiation pattern of E-Field at 2.6GHz

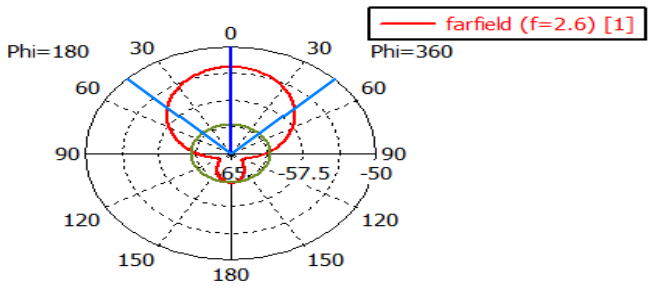


Fig. 6(b). Radiation pattern of H-Field at 2.6GHz

Fig. 6(a) shows the radiation pattern of E-Field at 2.6GHz. Fig. 6(b) shows the radiation pattern of H-Field at 2.6GHz.

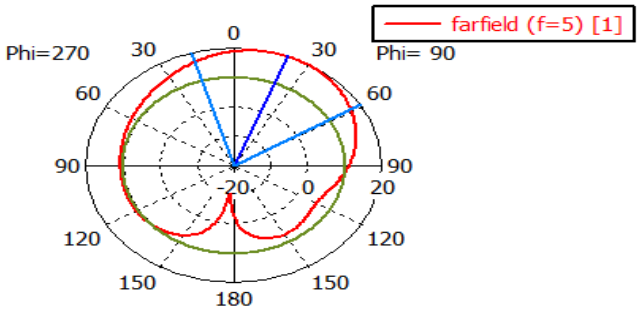


Fig. 7(a). Radiation pattern of E-Field at 5.0GHz

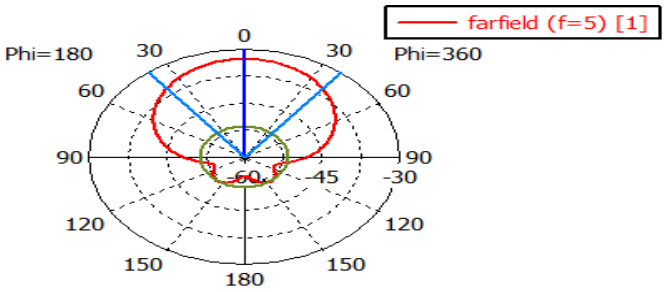


Fig. 7(b). Radiation pattern of H-Field at 5.0GHz

Fig. 7(a) shows the radiation pattern of E-Field at 5.0GHz. Fig. 7(b) shows the radiation pattern of H-Field at 5.0GHz.

*D. Surface current*

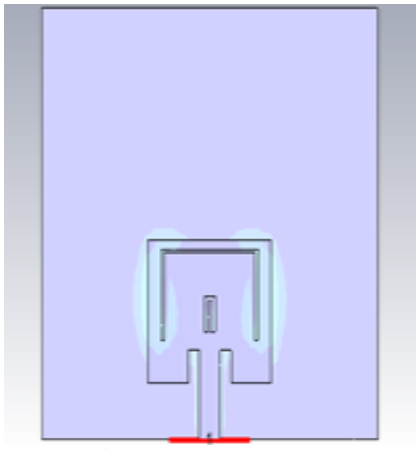

Fig. 8(a) Surface current of 2.6GHz LTE antenna

Fig. 8(a) shows the surface current of 2.6GHz LTE antenna. The maximum surface current for the antenna is 427.2A/m.

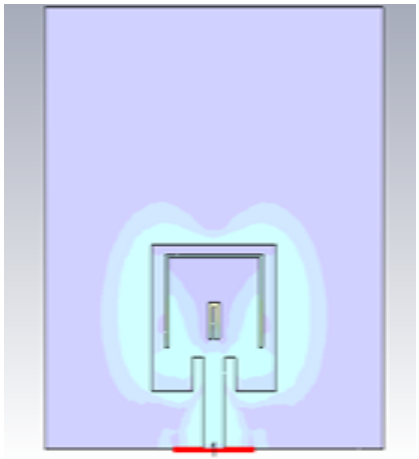

Fig. 8(b) Surface current of 5.0GHz WiFi antenna

Fig. 8(b) shows the surface current of 5.0GHz WiFi antenna. The maximum surface current for the antenna is 68.57A/m.

### *E. Directivity*

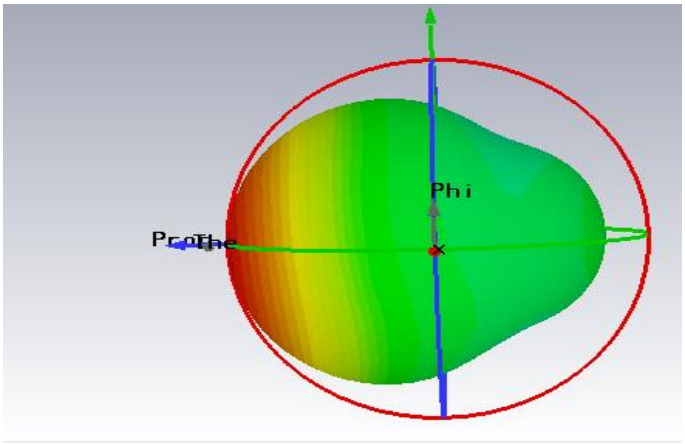


Fig. 9(a). Directivity of 2.6GHz LTE antenna

Fig. 9(a) shows the far field radiation pattern together with the directivity for 2.6GHz LTE antenna. The directivity for the 2.6GHz LTE antenna is 6.016dBi and this satisfied the requirements of the antenna proposed, which is 6dBi. The antenna has good ability to concentrate energy in a specific direction when transmitting.

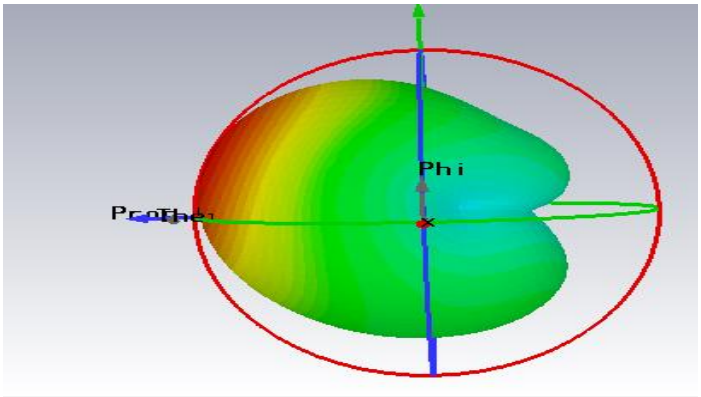


Fig. 9(b). Directivity of 5.0GHz WiFi antenna

Fig. 9(b) shows the far field radiation pattern together with the directivity for 5.0GHz WiFi antenna. The directivity for the 5.0GHz WiFi antenna is 7.542dBi and this satisfied the requirements of the antenna proposed, which is 6dBi. The antenna has good ability to concentrate energy in a specific direction when transmitting.

## CONCLUSION

The objective of this research has been achieved. This dual-band antenna was designed using CST and fabricated onto the FR-4 board. The parameters of the antenna have been optimized and better performance of the antenna proposed has been obtained. All calculations, simulation and fabrication have been completed successfully. Analysis for the performance of the antenna proposed in terms of operating frequency, reflecion coefficient magnitude ($S_{11}$), bandwidth, radiation pattern, surface current and directivity have been made. To conclude, the antenna proposed has met and satisfied the requirement of this research. The antenna proposed can operate for LTE and WiFi application at 2.6GHz and 5.0GHz.

## ACKNOWLEDGMENT

The authors would like to thank Faculty of Electrical Engineering (FKE) and Wireless Communication Centre (WCC) for their financial support of this research. Also, sincere appreciation to researchers, Mr. Raghuraman Selvaraju and Mr. Low Ching Yu for their help in this research.

## REFERENCES

[1] K.T Ahmed, M.B Hossain and M.J Hossain, “Designing a high bandwidth patch Antenna comparison with the former patch Antenna”, Canadian journal on multimedia and wireless network Vol.2, No. 2 April, 2011.

[2] Mak, C.L, “Experimental study of a microstrip patch antenna with an L-shaped probe”, Antennas and Propagation, IEEE Transactions on, 2000. 48(5): p. 777-783.

[3] M. Ali. Soliman1, T.E. Taha, W.E. Swelam, A.M. Gomaa, “A Wearable Dual-Band Dielectric Patch Antenna for LTE and WLAN”, Journal of Electromagnetic Analysis and Applications, pp. 305-309, 2012.

[4] Wagh, T. R., Bormane, D. S, “Dual Band Microstrip Antenna for WLAN Applications”, Advances in Computational Sciences & Technology;2011 Supplement 2, Vol. 4, p209.

[5] Atser A. Roy, Joseph M. Môm, Gabriel A. Igwue, “Enhancing the Bandwidth of a Microstrip Patch Antenna using Slots Shaped Patch”, American Journal of Engineering Research (AJER), Volume-02, Issue-09, pp-23-30.

[6] A. Balanis, “Antenna Theory Analysis and Design Constantine”, chapter no. 14-microstrip antenna, pg.no. 722.

[7] Vidhi Sharma and Dwjendra Arya,“Dual band Microstrip Patch Antenna using Dual feed for wireless communication”, in IJECSE Vol. 1, No.2.

[8] Gurdeep Singh, Jaget Singh. “Comparative Analysis of Microstrip Patch Antenna With Different Feeding Techniques”, International Conference on Recent Advances and Future Trends in Information Technology (iRAFIT2012) Proceedings published in International Journal of Computer Applications® (IJCA).

[9] Lu, J. H., “Single-feed dual-frequency rectangular microstrip antenna with pair of step-slots," Electronics Letters, Vol. 35, 354-355, 1999.

# Investigation of Specific Absorption Rate (SAR) at Frequency Higher Than 20GHz

Muhammad Afiq Bin Abdul Aziz
*Faculty of Electrical Engineering*
*Universiti Teknologi Malaysia*
*Johor Bahru, Malaysia.*
*Muhammadafiq6271@gmail.com*

Assoc. Prof. Dr. Norhudah Binti Seman
*Department of Communication Engineering*
*Faculty of Electrical Engineering*
*Universiti Teknologi Malaysia*
*Johor Bahru, Malaysia.*
*huda@fke.utm.my*

***Abstract*—The experiment has conducted to study of various frequency used in mobile phone in terms of the Specific Absorption Rate (SARs). The rectangular patch antenna design will used in 25.875GHz operating frequency and sample human head as spherical model are designed and simulated. The various plots such as the S-parameter, radiation patterns and SAR values are generated to investigate results. All simulations are done in CST software. The high frequency antenna design slightly high in SAR value that currently not suitable for used in mobile phone. The SAR value can be reduce by improving the design of antenna and follow the health safety standards.**

***Keywords—antenna, patch, SAR, human head, mobile phone, spherical model, electromagnetic field.***

## I. INTRODUCTION

Mobile phones are a smart device with high technology that all people need and bring it along wherever go. The mobile phones can produce energy emitted that can concern to the users. Thus, thermal heat and electromagnetic field generated from mobile phones that exposed to the human body that important for commit to investigation and studies further.

Specific absorption rate (SAR) is a measure of the rate energy absorbed by the human body when bare to a radio frequency (RF) electromagnetic field. Other than that, it can also refer to absorption of other forms of energy by tissues such as ultrasound [1]. It can defined as the power absorbed per mass of tissue and has unit of watts per kilogram (W/Kg) [2].The energy emitted will converted into heat which is then to transfer to the human body when it contact the device. The parameter to quantify the absorption of this EMF in human body is SAR. The value for SAR limit in Europe 2.0 W/Kg in 10g of tissue and the SAR limit in United State and Australian are 1.6 W/Kg in 1g of tissue. SAR values can various parameter like antenna positions relative to human body, radiation patters of the antenna, radiated power and type of antenna used. There are several method to calculate the SAR using finite element method or simulation using software.

Wireless communication was introduced in the 19th century and wireless communication technology has developed over the subsequent years. Wireless communication is one of the most important mediums of transmission of information from one device to another devices. In this technology, the information can be transmitted through the air without requiring any cables, wires or an electrical conductor. This operations permit services such as long-range communications that are impossible or impractical to implement with using of wires. The wireless communication technology are an expands rapidly from First Generation (1G) in year 1979 until currently used for Forth Generation (4G) in year 2008. Besides that, the researches about Fifth Generation (5G) are starting in year 2015 until now. This 5G technology can make faster internet connection speed with higher capacity and allowing higher number of mobile broadband users per unit area. In addition, it can improve support to machine-to-machine communication, lower cost, lower battery consumption and lower latency.

From the World Radio Communication Conference (Geneva, 2015) had considers that the frequency range must between 24.25 GHz and 86GHz for the future development in International Mobile Telecommunications (IMT) for year 2020 and beyond. The frequency bands which have been allocated to the mobile service are 24.25-27.5 GHz, 37-40.5 GHz, 42.5-43.5 GHz, 45.5-47 GHz, 47.2-50.2 GHz, 50.4-52.6 GHz, 66-76 GHz and 81-86 GHz.

## II. LITERATURE REVIEW

### *A. Specific Absorption Rate*

Specific absorption rate (SAR) is an established mechanism for evaluating the human body exposure to the electromagnetic (EM) radiation or radio frequency (RF)[3]. For the wireless device, the SAR value must not exceed at standardization guidelines. There are two organization that make standardization guidelines for limit the SAR value for wearable antennas.

The Federal Communication Commission (FCC) is functional to adopted limits for safety exposure to radio frequency (RF) energy in United State. This limits refers to Specific Absorption Rate (SAR) which is a measure the amount of radio frequency energy absorbed by the body when using a mobile phone or other wireless devices.

In Europe, the Commission on Non-Ionizing Radiation Protection (ICNIRP) will references for standard used for SAR limit. The updated published for reference in purpose of measuring the SAR value was "ICNIRP Guidelines For Limiting Exposure to Time-Varying Electric, Magnetic and Electromagnetic Fields (Up to 300 GHZ)".

### B. *Mobile Communication Technologies*

There are several mobile communication technologies used to implement in wireless devices based on the frequency used. This communication technology starting from 1G until the latest now 4G for lower frequency but for higher frequency also in researches about 5G. The frequency operation for each communication technologies in each generation are shown in TABLE I.

TABLE I. THE DIFFERENT COMMUNICATION TECHNOLOGIES GENERATION

| Communication Technologies | Frequency Operation (GHz) |
|---|---|
| 1G | 0.8 – 0.9 |
| 2G | GSM: 0.9 & 1.8 ; CDMA: 0.8 |
| 3G | 0.9 – 2.1 |
| 4G | 1.8 -2.6 |
| 5G | 3 – 300 |

### C. *SAR Simulation*

There is a software that can be implement to simulate and obtain the SAR value. The numeral method such as finite-difference time-domain (FDTD) and finite element method (FEM) at any specific adequate software for analyzing the interaction between living matter and electromagnetic field such as Computer Simulation Technology (CST) software can be used. SAR value can be obtained by comparing simulation for real life situation with the different type of exposure [7].

### D. *Previous Research*

Specific absorption rate (SAR) Reduced Mobile Phone Antenna Designs be analyze to compared in half-wave dipole antenna, rectangular patch antenna and Planar Inverted F antenna (PIFA) reported in TABLE II. This SAR value measured using sample of head model. The frequency operation used in dipole antenna is 0.835 GHz that produce high SAR values. Meanwhile, the rectangular patch antenna and PIFA used 0.8 GHz for operating frequency that give the lower SAR values. As a conclusion, the maximum SAR value is 0.00757 W/Kg in rectangular patch antenna because its size and bulkiness not realized as a mobile phone[8].

TABLE II. THE DIFFERENT TYPE OF ANTENNA IN DIFFERENT SAR VALUE

| Type of Antenna | Frequency Operation (GHz) | SAR Value (W/Kg) |
|---|---|---|
| Half-Wave Dipole Antenna | 0.835 | 11.1034 |
| Rectangular Patch Antenna | 0.800 | 0.00757 |
| Planar Inverted F Antenna (PIFA) | 0.800 | 0.03200 |

## III. METHODOLOGY

This experiment to design the rectangular patch antenna for simulation with using CST software and measured SAR value at sample of phantom model. This simulation done in order to determine S-parameter plot, radiation pattern, gain and SAR value (1g and 10g tissues of averaging mass) for frequency operation at 25.875GHz. There were several methods that required to use in order to design rectangular patch antenna and measured SAR value:

### A. *Steps to test each antenna design and measure SAR value*

- Create the rectangular patch antenna design with choosing the operating frequency that stated in IMT standard for mobile services.
- Make calculation to determine all the parameter included the length and width for antenna design.
- Using all parameter in order to design rectangular patch antenna in form 3D using CST software.
- Create the phantom model as the human head model using spherical model with diameter is 20mm or radius is 10mm.
- Place the antenna design with 10mm of gap between spherical model.
- Choose the frequency range for review the result simulation and run the simulation.
- Analyze the data from simulation of S-parameter, return loss, gain, radiation pattern and SAR values.

### B. *Parameter to design rectangular patch antenna*

To design rectangular patch antenna need to require the several parameter such as length, L and width, W as shown in Figure 1.

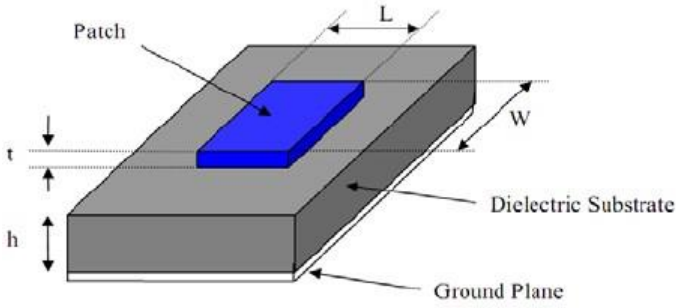


Fig. 1. The sample dimension design for rectangular patch antenna

The dielectric substrate use is RT/Duroid 5880 with thickness of substrate, h=0.254 mm. The substrate for patch antenna and ground plane use are copper with thickness, t=0.017 mm and permittivity, εr=2.2. The operation frequency used is 25.875GHz. Then, with all parameter given can used to determine the dimension of length, L using (1) and dimension of width, W using (2). The other parameter in (3) and (4) needed to used in (2) to make calculation.

$$L = \frac{c}{2f\sqrt{\varepsilon_{eff}}} - 2\Delta l \quad (1)$$

$$W = \frac{c}{2f}\left(\frac{\varepsilon_r + 1}{2}\right)^{-1/2} \quad (2)$$

$$\varepsilon_{eff} = \frac{\varepsilon_r + 1}{2} + \frac{\varepsilon_r - 1}{2}\left(1 + \frac{10h}{W}\right)^{-1/2} \quad (3)$$

$$\frac{\Delta l}{h} = \frac{0.412\left(\varepsilon_{eff} + 0.3\right)\left(\frac{W}{h} + 0.264\right)}{\left(\varepsilon_{eff} - 0.258\right)\left(\frac{W}{h} + 0.8\right)} \quad (4)$$

### C. *Sample patch antenna design at 26GHz*

The rectangular patch antenna was design as shown in Fig.2. at uv-plane view with the all parameter needed in TABLE III.

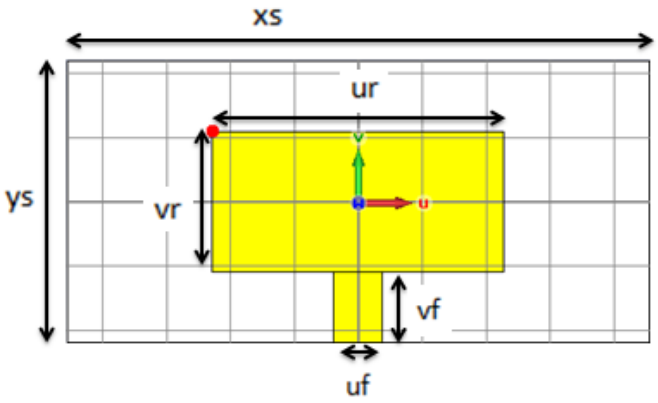


Fig. 2. Sample rectangular patch antenna design

TABLE III. THE PARAMETER TO DESIGN RECTANGULAR PATCH ANTENNA

| Name | Parameter | Value (mm) |
|---|---|---|
| Width of Substrate | xs | 9.122 |
| Length of substrate | ys | 4.4 |
| Thickness of substrate | h | 0.254 |
| Thickness of copper | t | 0.017 |
| Width of feed | uf | 0.7606 |
| Length of feed | vf | 4.829 |
| Width of radiating element | ur | 4.561 |
| Length of radiating element | vr | 2.2 |

### D. *Antenna design with spherical model*

The rectangular patch antenna design with spherical model shown in Fig. 3. In order to calculate the SAR value for the design, the reference tissues averaging mass at the spherical model need to choose in 1g and 10g that stated in the standard for telecommunication technologies devices. The size for spherical model is around 20mm radius.

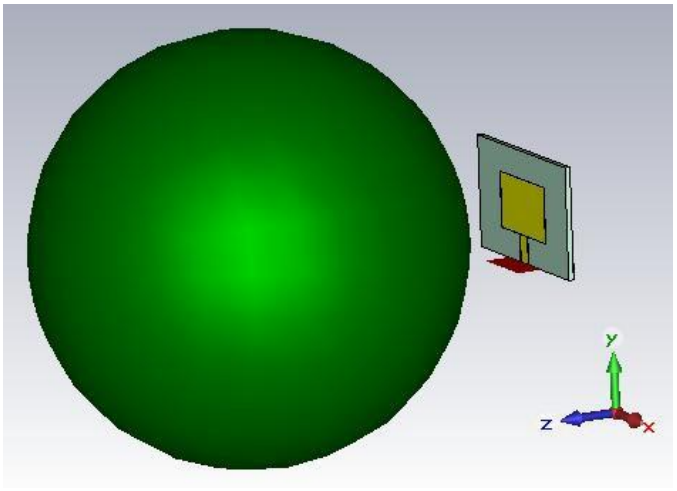


Fig. 3. Antenna design with spherical model design

The port must be supply with the impedance is 50 ohm to get best result and matching circuits when simulate the design. The gap between antenna and spherical model is 10mm.

## IV. RESULT AND DISCUSSION

The return loss for rectangular patch antenna design can be determine by S11 response or S-parameter plot graph. This response occur when the power losses at 90% that show in the S-parameter at the range -10dB. The frequency band and bandwidth can measured from this S-parameter plot.

### A. *Design of rectangular patch antenna*

Based on the simulation result for rectangular patch antenna design only, Fig. 4. show that the cut-off frequency or the result for narrow band frequency at 26GHz after making optimization the design to get best result. The bandwidth for this design is 11.006GHz.

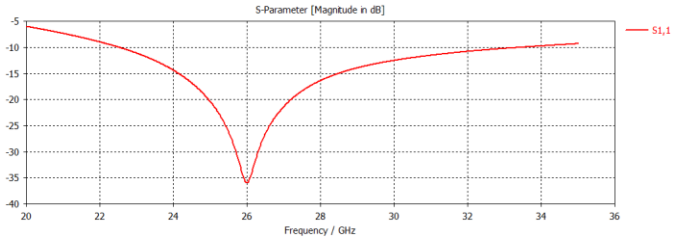


Fig. 4. S-parameter plot for rectangular patch antenna design

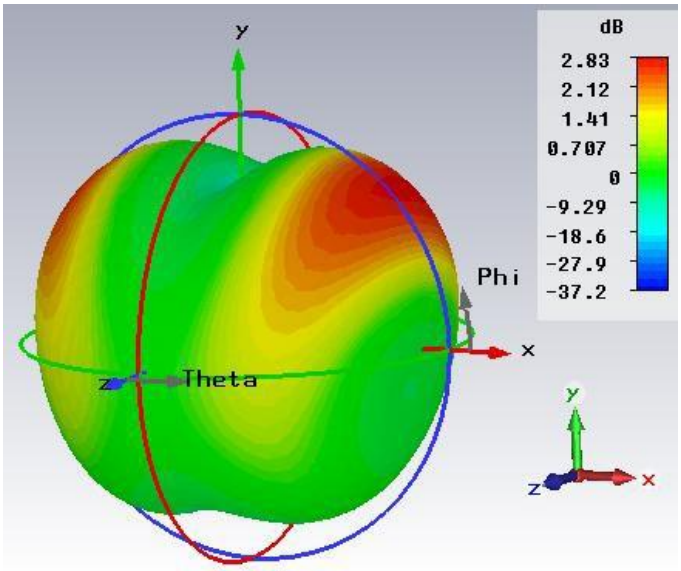


Fig. 5. 3D radiation pattern for patch antenna design

Based on the 3D radiation pattern in Fig. 5. stated the gain from this antenna is 2.829dB at operating frequency 25.875GHz. The radiation efficiency is -0.1082dB and the Total efficiency also equal to -0.1108dB. The directivity for this antenna is 2.937dBi.

*B. Antenna design with spherical model*

The simulation result for rectangular patch antenna design with spherical model in Fig. 6. show that the cut-off frequency or the result for narrow band frequency at 26.464GHz. The bandwidth for this design is 11.645GHz.

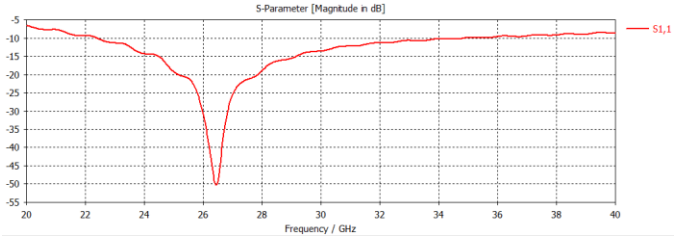


Fig. 6. S-parameter plot for rectangular patch antenna design with spherical model

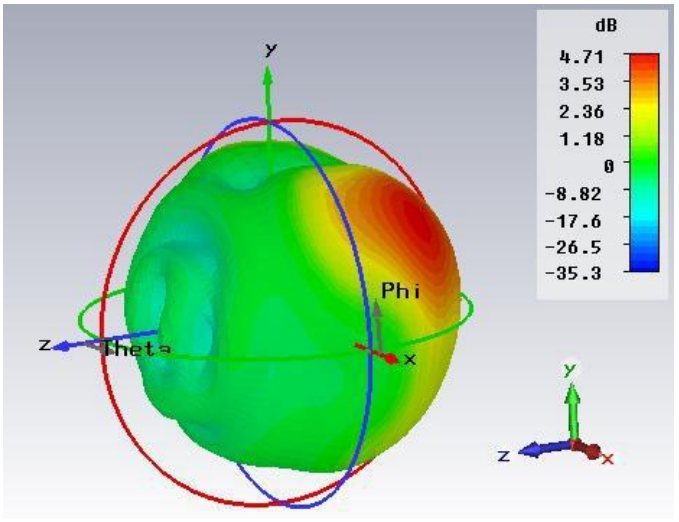


Fig. 7. 3D radiation pattern for patch antenna design with phantom model

Based on the 3D radiation pattern in Fig. 7. stated the gain from this antenna is 4.712dB at operating frequency 25.875GHz. The radiation efficiency is -0.4469dB and the Total efficiency also equal to -0.4497dB. The directivity for this antenna is 5.158dBi.

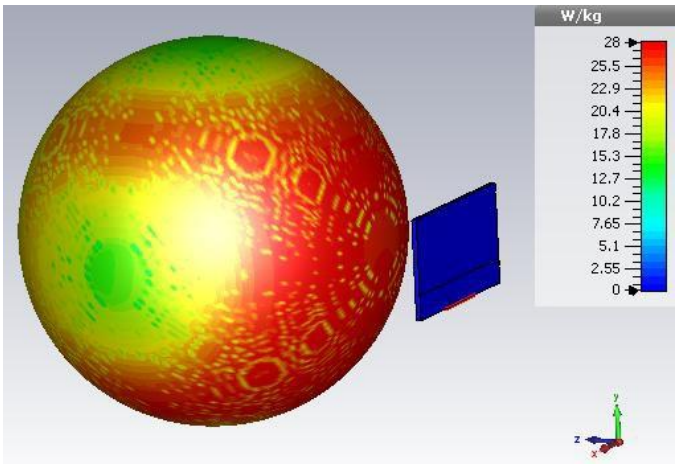


Fig. 8. SAR result at 1g tissues

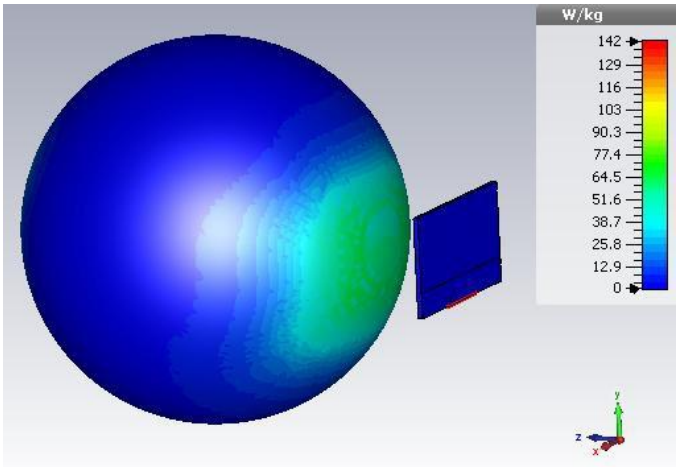


Fig. 9. SAR result for 10g tissues

From Fig. 8. show the result for 1g tissues of averaging mass is 28.04W/Kg slightly higher than the standard from IMT. However, the SAR value for 10g tissues of averaging mass is 141.8W/Kg shown in Fig. 9. This design and operating frequency were really dangerous for human uses for mobile phone.

## V. CONCLUSION

The Specific Absorption Rate of rectangular patch antenna design with spherical model is studied in this paper. This experiment show the result that the value of SAR are very high that can give high risk or dangerous toward human cells/tissues especially in high frequency antenna design are implement in the mobile phone. High frequency antenna design can avoid the risk by taking an improvement toward antenna design in order to reduce the SAR value and achieve standardize limit SAR value from IMT.

## REFERENCES

[1] Jie Sun and Kullervo Hynynen (1998), "Focusing of therapeutic ultrasound through a human skull: A numerical study," The Journal of the Acoustical Society of America , vol. 104, no. 3 [10.1121/1.424383].

[2] Jianming Jin (1998), "Electromagnetic Analysis and Design in Magnetic Resonance Imaging," CRC Press., pp. 226.

[3] Jovanche Trajkovikj and Anja K. Skrivervik (2016), "Comparison of SAR of UHF Wearable Antennas," LEMA, EPFL, Lausanne, Switzerland, pp.1-4.

[4] G. Ziegelberger (1998), "ICNIRP GUIDELINES for limiting exposure to time-varying electric, magnetic and electromagnetic fields (up to 300 GHz)," Health Phys., vol. 74, no. 4, pp. 494–522.

[5] Federal Communications Commission Office of Engineering and Technology (2001), "Evaluating Compliance with FCC Guidelines for Human Exposure to Radiofrequency Electromagnetic Fields," Supplement C, pp. 1–42.

[6] Anu Tharakan, Deepthi J, Divya Sebastian A, Gobika J and D. D. Krishna (2015), "Specific Absorption Rate (SAR) Reduced Mobile Phone Antenna Designs," IEEE Trans., pp. 250-253.

[7] Mohammad Rashed Iqbal Faruque, Mohammad Tariqul Islam and Norbahiah Misran (2010), "SAR Analysis in Human Head Tissues for Different Types of Antennas," World Applied Science Journal, vol. 11, no. 9, pp. 1089-1096.

[8] Shivalingappa M Baligar, Rajendra Soloni and Dr. Chandrappa D. N (2016), "Analysis of Specific Absorption Rate (SAR) of Microstrip Patch Antenna for Wireless Application," IJARCCE, vol. 5, no. 5, pp. 1-3.

[9] Prabir Kumar Dutta, Pappu Vankata Yasoda Jayasree and Viriyala Satya Surya Narayan Srinivasa Baba (2016), "SAR reduction in the modelled human head for mobile phone using different material shields," IEEE journals, pp. 1-4.

[10] M. T Islam, M. R. I. Faruque and N. Misran (2010), "Study of Specific Absorption Rate (SAR) in the human head by metamaterial attachment," IEICE Electronics Express, Vol. 7, No. 4, pp. 240-246.

[11] Salini. M. Chandran, J. Jayakumari (2015), "Design of Printed Antenna for Low Sar and Multiband Services," GCCT, pp. 441-445.

# Smart Birdhouse Management System using Internet of Thing (IoT)

Ahmad Salihin Amir
Faculty of Electrical Engineering
Universiti Teknologi Malaysia
Johor, Malaysia
asalihinamir@gmail.com

Nor Hisham Khamis
Faculty of Electrical Engineering
Universiti Teknologi Malaysia
Johor, Malaysia
hisham@utm.my

***Abstract*—The main aim of this project is to develop a system that will provide remote control for birdhouse. This project is mainly concerned with the control of temperature, humidity, lighting and relay module using internet. The project is made using Wi-Fi module that employs the integration of cloud networking to provide the user with remote control of the birdhouse and storing the data in the cloud. The various devices connected to the Arduino and the sensors are connected using wireless network. The sensor such as DHT22 and PIR are used to get the data and then send the data to the smart phone. In this system, to make sure all the equipment operates 24 hours continuously, a solar tracking is used to provide continuous electricity to the birdhouse. An Android application was developed by using software design as a user interface, where the user will be able to get the information such as number of swiftlet enter the birdhouse, the real-time video inside birdhouse and value of temperature and humidity. The birdhouse also completed with the security system because it has a door locking system and IP camera that can be control and monitor remotely using smart phone to prevent from intruders. This birdhouse system is designed to be low cost and flexible to be implement at another birdhouse.**

***Keywords*—Wi-Fi module, IP camera, Solar tracking, Android application, Security system, low cost**

## I. INTRODUCTION

Swiftlet industry are done by creating birdhouse building in order to attract the swiftlets to enter. The design of the birdhouse is important as the presence of swiftlets sound to attract the swiftlets. Swiftlets are attracted to 5 factors which are aroma, light, temperature, humidity and sound.

Nowadays, one of the most welcomed businesses is swiftlet nest business. Swiftlet's nest is the nest made by swiftlet by using its saliva. The nest being 'sewed' can be consumed and eaten by human being because of the healthy effect being offered for extra nutritious and maintaining health. Most people who dive into this business tend to build a cave-environmental birdhouse for the swiftlets in order they will stay and make the nesting there.

The thumb rules in constructing the ideal swiftlet birdhouse are temperature, humidity and light intensity. These requirements must be met in order for the business to be successful. Many facts have shown that the unregulated swiftlet birdhouse led to failure at the end. This problem due to the unproductive area where the owner lives which means that the birdhouse should be build out of town. Thus, the owner need to travel a long way in order to monitor and control the swiftlet birdhouse. It is considered ineffective and make the owner losses because they need to sacrifice the valuable time and money in travelling to the birdhouse.

An idea of smart management monitoring and controlling system can solve the problem that the owner faced. Both monitoring and controlling condition can be done through any electronic devices which connect to the internet. The application of Wi-Fi for swiftlet birdhouse monitoring will have variety of potential benefits for society and communities. This application will enable remote management and long term monitoring. Interconnectivity with the physical environment at a swiftlet birdhouse will allow temperature and humidity sensors to provide measurements and detailed information that is hard to obtain through traditional method. Lastly, it is hoped to be able increase the quality and quantity of the nest being produced with this smart management system.

## II. LITERATURE REVIEW

### *A. Introduction*

This section explains about the review of the papers from other researches that were related to the development of this project, which is "Smart Birdhouse Management System using Internet of Things (IoT)".

### *B. Related Study*

(i). Study on Swiftlet [12]

Swiftlets are very unique because they can make nests by using its own saliva. Swiftlet nest has a lot of nutritious which is good for the health make them special from other species. Swiftlets have four genera which are Aerodramus, Hydrochous, Schoutedenapus and Collocalia. Mostly swiftlet can be found in the South-East regions such as Malaysia, Indonesia, North Australia and Thailand. Swiftlets are the type of bird that have weak feet and not able to roost well. However, it can fly for 12 hours long from the early morning until midnight. Swiftlets can catch aerial insects in position of 1,500 meters from sea level because they have very sharp vision.

(ii). The Existing Swiftlet Birdhouse [5]

The swiftlet industry has the potential to grow into a profitable industry for edible birds' nests by wealthy nations. Malaysia is among the largest producer (7%) of edible birds' nest in the world behind Thailand (20%) and Indonesia (60%) while the main markets are Hong Kong (50%), China (8%), Taiwan (4%), Macau (3%), Japan, and South Korea.

More than 1,500 swiftlet birdhouses in Sarawak, Malaysia has been setup but none of the birdhouses has the real-time monitoring. These birdhouses are mostly equipped with electrical equipment including humidifier, audio system and timers, thermometer and humidity tester.

Every four to six weeks, the temperature and humidity of the birdhouses are monitored manually only once. The swiftlets will frighten with this manual monitoring and controlling of equipment in the birdhouses. The production of birds' nests will be affect according to all the above problems.

(iii). Suitable Temperature and Humidity for Swiftlet [15]

The quality of the swiftlets nest depends mostly on the micro habitat in the nesting birdhouse. Both temperature and humidity plays an important role in determining the quality of nest. The ideal temperature ranges from 27$^{O}$C - 29$^{O}$C while the humidity is from 80% - 90%. With this configuration, the nest will have a strong bond with solid and unbroken shape. If the temperature and humidity are below the set point, the nest will suffer from breakage and the colour will be yellow. On the other hand, if the temperature and humidity are over the indication value, the nest will mildew and the swiftlets will have difficulties in making the nest foundation because it is difficult for the nest to harden.

Swiftlet nest is being cultivated because of the benefits being offered, which makes this kind of business expands greatly especially throughout Malaysia. But in order to get a good quality nest, the micro habitat must be preserved within the ideal temperature and humidity.

(iv). Swiftlet Birdhouse [15]

The origin habitat of the swiftlets is cave. As the demand of the bird nest increases and the supplies from the cave cannot longer accommodate, people then make a 'look-alike cave' nesting birdhouse or swiftlet birdhouse.

There are some important parameters that need to be taken care of in building a nesting birdhouse.

i. The micro habitat for an ideal swiftlet birdhouse

The measured temperature is around 27$^{O}$C - 29$^{O}$C and humidity starts from 80% - 90%.

ii. The location of the swiftlet birdhouse

It is recommended to build a nesting birdhouse close to rivers, ocean, forest, rice fields, or swamps.

iii. The facilities inside the birdhouse

Nowadays swiftlet birdhouse is equipped with good sound system to attract the swiftlets. Besides sound system, there is also a system to control the room temperature and humidity.

iv. Design of the birdhouse

An ideal nesting birdhouse should contain several main parts, namely the entry hole, the roving room, nesting room, interconnecting hole, and the air circulation system.

(v). Smart Management System using Internet of Things (IoT) [16][17][18][19][20][21][22][23][24][25][26][27]

The Internet of Things (IoT) means people and things to be connected anytime, anyplace, with anyone using network (Vaishnavi & Pratibha, 2016). IoT focused on several technologies like ubiquitous, pervasive computing, ambient intelligence, sensors, actuators, communications technologies, Internet technologies and embedded systems.

In this research paper, the system consists of Arduino Ethernet acts as a micro Web-server and an Android through smart phone app. This system allows users to control and monitor with connected devices at home using any Wi-Fi or 3G/4G through smart phone. The devices at home can access and control through server real IP using graphical user interface (GUI) provides by the smart phone app. The architecture is divided into three layers which are Home Environment, Home Gateway and Remote Environment.

(vi). Solar Tracking [29]

Photovoltaic (PV) is the field of technology of solar system that converting sunlight directly into electricity. In order to get the maximum efficiency from the solar panel, the control system should be able to rotate the solar panel to be in 90 degree with the sun light. Solar tracking is necessary to be able to satisfy this condition. To achieve this purpose various methods can be used which are Traditional control method, PID control method and Solar Orientation based on Location and Time.

Solar Orientations based on Location and Time method gives high precision results and allow to the system to perform with high efficiency because the stability of the system will be high and the error probability low so clearly this method is the best to be used in the field of solar tracking system.

## III. RESEARCH METHODOLOGY

### *A. Introduction*

In this section, most of the discussion is about the methods that were being used to develop a smart birdhouse management system. The flow of the methodology consists of planning, designing of the system, software developing and testing.

### *B. Project Planning*

Systematic planning is needed to ensure that projects are completed on time and run effectively. Systematically project planning will produce good results in project.

There are a few stages that needed to be obeyed for this project to be completed. It includes literature review, identifying problem statement, proposing the system design including for hardware design and software design, system integration and testing and lastly is documentation.

### *C. Propose System Design*

In this project, the system was designed using suitable size component to make a prototype of the birdhouse and easy to installation. This birdhouse has one floor only for swiftlet

nesting. The flat at the top of the birdhouse to make the solar tracking can move easily.

This system architecture had three main parts. The first part is the birdhouse environment that has the input from the video camera, temperature sensor, humidity sensor and motion sensor. The second part is the internet of things that has act as a cloud to access point that connect to the internet and transfer data to hosting server or smartphone. The last part is remote environment that has the user to receive the data such as temperature and humidity in the birdhouse, number of swiftlets and the real-time video camera. The architecture system of the smart birdhouse management system as shown in Fig. 1.

The main idea of this project is the Wi-Fi module get the source from the solar tracking to make sure the data can transfer to cloud along 24 hours without power breakdown. If the Arduino Wi-Fi is suddenly breakdown due to lightning or burning, the user will know that the system disconnected.

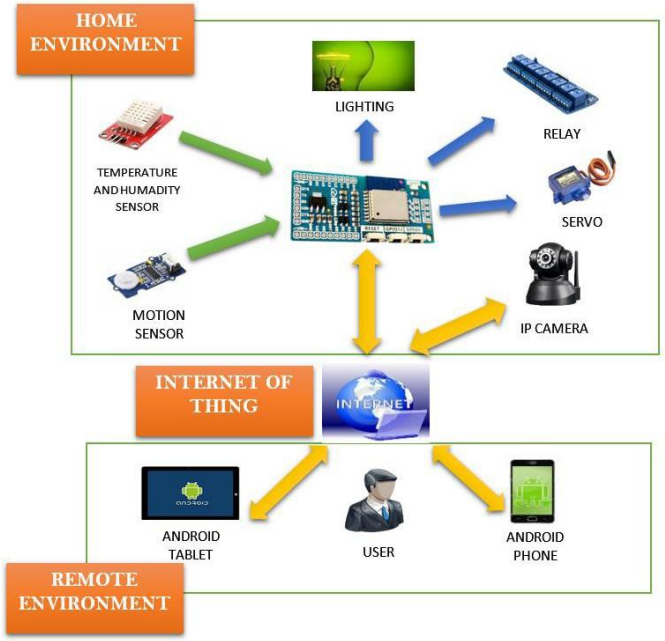


Fig. 1. Architecture System of the Smart Birdhouse Management System.

### D. Hardware Design

The design of the hardware part is an important for combining all devices to develop embedded systems in producing a good product, safe, functional, and user-friendly. The Solar Panel is used in order to generate electricity, Lead-Acid battery is used as a storage system for the electricity energy, while an inverter is used as a converter from DC to AC. Relay Module is used for all switching such as amplifier, lighting, tweeter and speaker. The function of Arduino Wi-Fi Module as a microcontroller is used to control the switching of the relay to other components. The Arduino Wi-Fi also can send and receive the data through the cloud directly without using the router.

The component of the smart birdhouse management system consists of solar panel, charge controller, lead-acid battery, inverter, Arduino Wi-Fi module, relay module, IP camera, Passive Infrared (PIR) motion sensor, DHT22, servo motor, Light Dependent Resistor (LDR), router and strip board.

### E. Software Design

Software design for development of embedded system will be discuss in this topic. Software design is actually a process to transform user requirements into the embedded system in order for the hardware part to work properly according to the user demand. The software design that were being used in this project is Arduino 1.6.9 IDE, MIT App Inventor, Proteus 8 and SketchUp.

## IV. Discussion and Result

### A. System Implementation

The Wi-Fi module and IP camera connect to router using Wi-Fi to access the internet. All information from the module can be access from the cloud using the real-time database. The IP camera can be access in the same network when smartphone connected to the router by using internal IP address. The IP camera can be access outside the network by using external IP address. The system implementation as shown in Fig. 2.

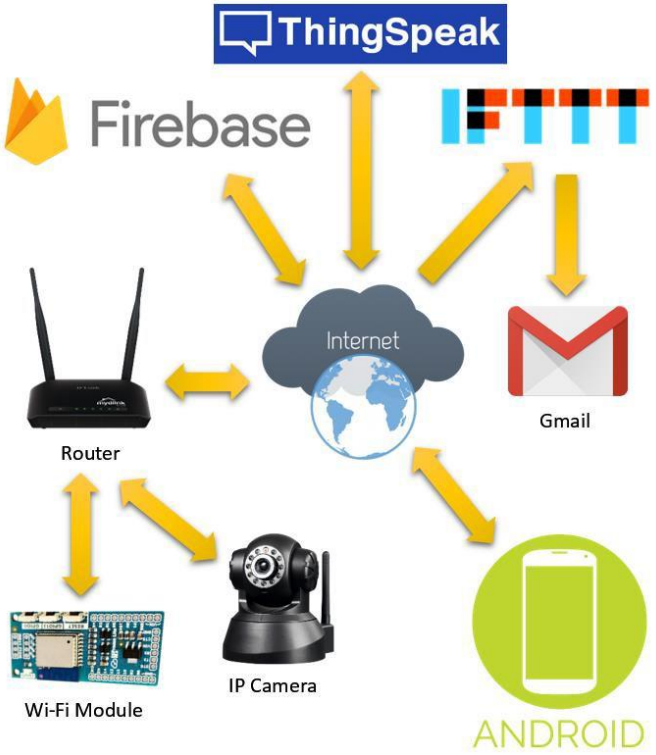


Fig. 2. System Implementation.

### B. Software Development

Software of the smart birdhouse management system is divided into two parts which are application software and microcontroller firmware. Microcontroller firmware is the library that support the Firebase database, ThingSpeak, IFTTT and HTTP. The application software is the software that can create an Android application. The application for the system is created by using MIT App Inventor. The flowchart for Wi-Fi

module sends data to Android app as shown in Fig. 3 and the flowchart for Android app sends data to Wi-Fi module as shown in Fig. 4.

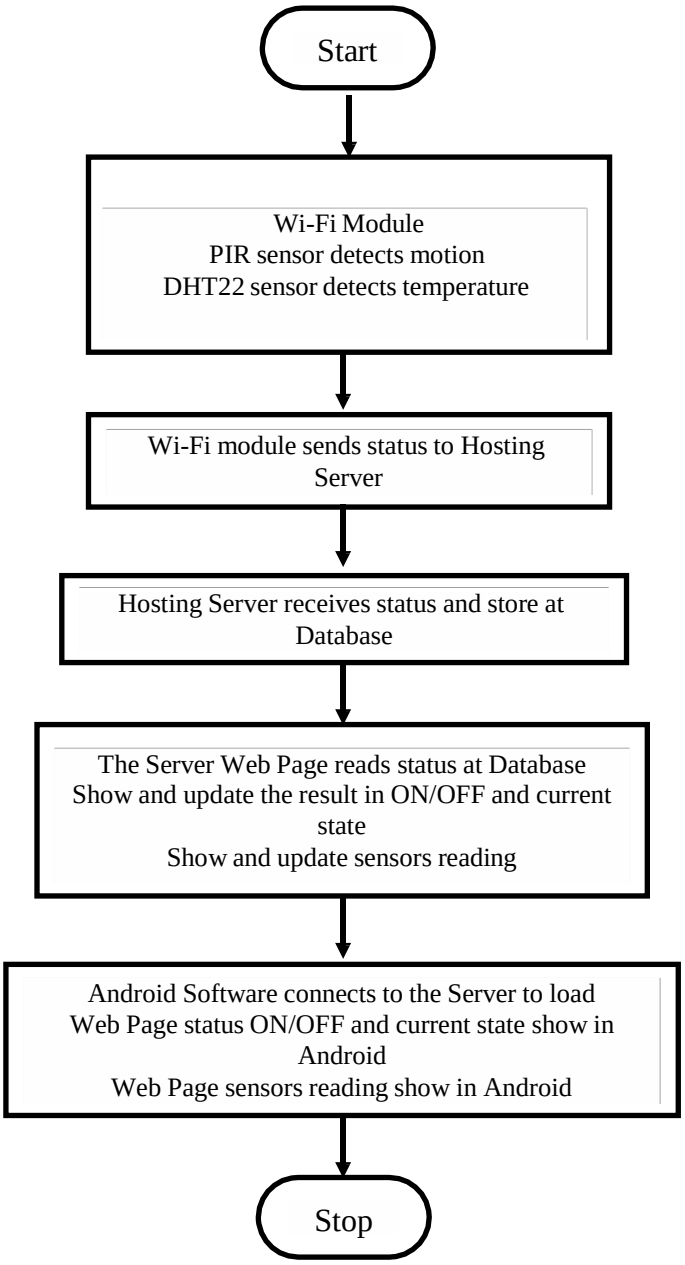


Fig. 3. Flowchart for Wi-Fi module sends data to Android app.

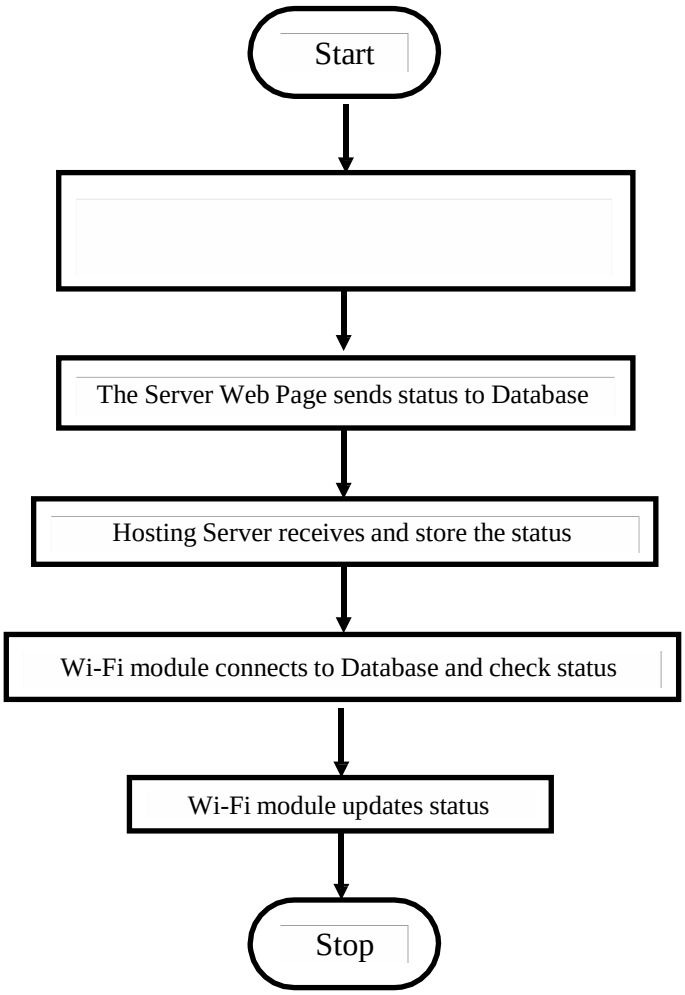


Fig. 4. Flowchart for Android app sends data to Wi-Fi module.

### *C. Android Application and Features*

The Android app for smart birdhouse management system provides the functionalities to the user such as remote connection to the database, controlling, monitoring and viewing from the camera. The MIT App Inventor is used to create the application to monitor and control the system. The interface of MIT App Inventor as shown in Fig. 5. The graphical user interface for controlling and managing the smart birdhouse management system using IoT as shown in Fig. 6.

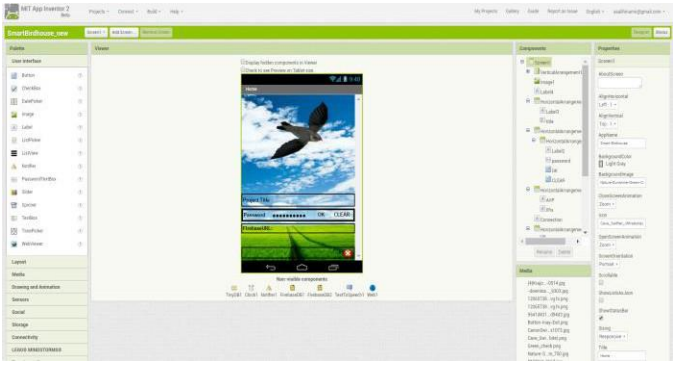

Fig. 5. The Interface of MIT App Inventor.

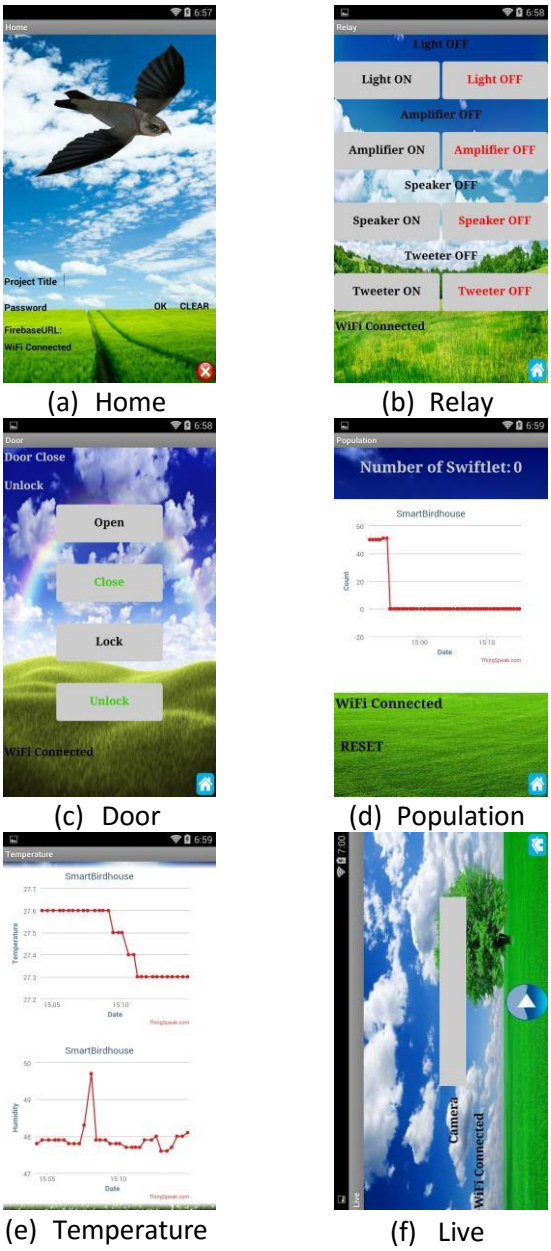


Fig. 6. Graphical User Interface for Smart Birdhouse Management System.

## V. CONCLUSION

The smart birdhouse management system is designed to be low cost and flexible to implement the system at another birdhouse. Any android smartphone can be used to monitor and control the system. When a Wi-Fi disconnected, mobile network 3G or 4G can be used to access the system. Future work will focus on creating camera detection recognition of swiftlet to avoid predator enter the birdhouse.

## REFERENCES

[1] Ibrahim, S. H., Teo, W. C., and Baharun, A. (2009, August). A Study on Suitable Habitat for Swiftlet Farming. *UNIMAS E-Journal of Civil Engineering*. 1(1), 1-7.

[2] Mohd Fakarudin Abdul Manan (2011). *Swiftlet Bird Building Temperature and Humidity Control*. Bachelor Thesis, Universiti Teknologi Malaysia, Skudai.

[3] Yaacob, M. R. and Ibrahim, W. K. W. (2015). A Proposed Study on Malay Entrepreneurship in Edible Bird Nest Industry in Malaysia: Self-Efficacy Theory as a Research Approach. *International Journal of Management Sciences*. 5(4), 256-260.

[4] Othman, A. K., Abidin, W. A. W. Z., Lee, K. M., Zen, H., Zulcaffle, T. M. A., and Kipli, K. (2009). Wireless Sensor Networks for Swiftlet Farms Monitoring. *International Journal of Electrical, Computer, Energetic, Electronic and Communication Engineering*. 3(12), 2378-2384.

[5] Mamduh, S. M., Shakaff, A. Y. M., Saad, S. M., Kamarudin, K., Kamarudin, L. M., Zakaria, A., Kamarudin, H., Ezanuddin, A. M. M., Saad, F. S. A., Nooriman, W. M. and Abdullah, A. H. (2012). Odour and Hazardous Gas Monitoring System for Swiftlet Farming using Wireless Sensor Network (WSN). *Chemical Engineering Transactions*. 30, 331-336.

[6] Zaini, S. N. Z. H., Sunardi, Ghazali, K. H. and Tajuddin, S. N. (2013). Application of Speech Recognition for Swiftlet Vocalizations. *Proceeding of the International Conference on Artificial Intelligence in Computer Science and ICT (AICS 2013)*. 25-26 November. Langkawi, Malaysia, 260-264.

[7] Zaini, S. N. Z. H., Sunardi, Ghazali, K. H. and Tajuddin, S. N. (2013). Attraction Sound in the Swiftlets House. *Proceeding of the Second International Conference on Advances in Electronic Devices and Circuits (EDC 2013)*.

[8] Lim, C. K. (2011). Opportunity and Sustainability of Swiftlet Farming in Malaysia. *International Conference of Swiftlet Ranching (ICOTOS 2011)*.

[9] Frezzal Faisal (2010). *Designing Swiftlet Farming Using Energy Plus*. Bachelor Thesis, Universiti Malaysia Sarawak.

[10] Aida Shafina Shofi (2012). *Sound Identification in the Swiftlet House*. Bachelor Thesis, Universiti Malaysia Pahang.

[11] Mohd. Syazril Amri Mohd. Bakri (2012). *Performance of Swiftlet House*. Bachelor Thesis, Universiti Teknologi Malaysia, Skudai.

[12] Muhammad Hafiz Firdaus Azmi (2015). *Sound Analysis of Swiftlet Echolocation*. Bachelor Thesis, Universiti Teknologi Malaysia, Skudai.

[13] Amirul Rasyid Zabidi (2016). *Analysis of Swiftlets Acoustic Sound*. Bachelor Thesis, Universiti Teknologi Malaysia, Skudai.

[14] Ong Foo Kheng (2012). *Swiftlet Ranching*. Bachelor Thesis, Universiti Malaysia Pahang.

[15] Wong Tung Yuen (2012). Designing and Constructing Automated Control System for Ideal Swiftlet House Environmental Condition. Bachelor Thesis, Swiss German University.

[16] Per B. Lynggaard (2014). *Artificial Intelligence and Internet of Things in a "Smart Home" Context*. Ph.D Thesis, Aalborg University Copenhagen, Denmark

[17] Nasrin Amri (2015). *Smart Renewable Energy Management System*. Bachelor Thesis, Universiti Teknologi Malaysia, Skudai.

[18] Fatima Ezzahra Barnicha (2015). *Smart Home Energy Management System*. Bachelor Thesis, Al Akhawayn University.

[19] Vinay, S. K. N. and Kusuma, S. M. (2015). Home Automation Using Internet of Things. *International Research Journal of Engineering and Technology*. 2(3), 1965-1970.

[20] ElShafee, A. and Hamed, K. A. (2012). Design and Implementation of a WiFi Based Home Automation System. *International Journal of Computer, Electrical, Automation, Control, and Information Engineering*. 6(8), 1074-1080.

[21] Jabbar, Z. A. and Kawitkar, R. S. (2016). Implementation of Smart Home Control by Using Low Cost Arduino & Android Design. *International Journal of Advanced Research in Computer and Communication Engineering*. 5(2), 248-256.

[22] Hadwan, H. H. and Reddy, Y. P. (2016). Smart Home Control by Using Raspberry Pi & Arduino Uno. *International Journal of Advanced Research in Computer and Communication Engineering*. 5(4), 283-288.

[23] Nathan, D., Abafor, C., Aronu, U., & Edoga, O. (2015). Design of a Home Automation System Using Arduino. *International Journal of Scientific & Engineering Research*. 6(6), 795-801.

[24] Pooja, P., Mitesh, P., Vishwa, P., & Vinit, N. (2016) Home Automation Using Internet of Things. *Imperial Journal of Interdisciplinary Research*. 2(5), 648-651.

[25] Rajeev, P. (2013). Internet of Things: Ubiquitous Home Control and Monitoring System using Android based Smart Phone. *International Journal of Internet of Things*. 2(1), 5-11.

[26] Pandikumar, S., & Vetrivel, R.S. (2014). Internet of Things Based Architecture of Web and Smart Home Interface Using GSM. *International Journal of Innovative Research in Science, Engineering and Technology*. 3(3), 1721-1727.

[27] Vaishnavi, S. G., & Pratibha, S. Y. (2016). Smart Home Automation: A Literature Review. *International Journal of Computer Applications*. 6-10.

[28] Ibrahim, W. K. W., Yaccob, M. R. and Abdullah, A. (2015). The Importance of Technical Knowledge in Sustainability of Malay Bird's Nest Industry in Malaysia. *Journal of Applied Environmental and Biological Sciences.* 5(4), 190-196.

[29] Ozerdem, O. C., and Shahin, A. (2014). A PV Solar Tracking System Controlled by Arduino/MATLAB/Simulink. *International Journal on Technical and Physical Problems of Engineering (IJTPE).* 6(21), 5-10.

[30] Varun, Prakash, R., and Bhat, I. K. (2010). A Figure of Merit for Evaluating Sustainability of Renewable Energy Systems. *Renewable and Sustainable Energy Reviews, Elsevier.* 14, 1640-1643.

[31] Balabel, A., Mahfouz, A. A., and Salem, F. A. (2013). Design and Performance of Solar Tracking Photo-Voltaic System. *Research and Education, International Journal of Control, Automation and Systems.*

[32] Ban, C. H. (2011, November 12). Swift Action on Bird's Nest Issue. *The Star Online*

[33] Lim, C. (2007). Introduction to Swiftlets. *Make Millions from Swiftlet Farming: A Definitive Guide* (pp. 3). Kuala Lumpur: TRUEWEALTH PUBLISHING.

[34] J. Boman, J. Taylor and A. H. Ngu, "Flexible IoT middleware for integration of things and applications," *10th IEEE International Conference on Collaborative Computing: Networking, Applications and Worksharing*, Miami, FL, 2014, pp. 481-488.

[35] N. K. Walia, P. Kalra and D. Mehrotra, "An IOT by information retrieval approach: Smart lights controlled using WiFi," *2016 6th International Conference - Cloud System and Big Data Engineering (Confluence)*, Noida, 2016, pp. 708-712.

[36] V. Gokul and S. Tadepalli, "Implementation of a WiFi based plug and sense device for dedicated air pollution monitoring using IoT," *2016 Online International Conference on Green Engineering and Technologies (IC-GET)*, Coimbatore, India, 2016, pp. 1-7.

[37] A. I. Abdul-Rahman and C. A. Graves, "Internet of Things Application Using Tethered MSP430 to Thingspeak Cloud," *2016 IEEE Symposium on Service-Oriented System Engineering (SOSE)*, Oxford, 2016, pp. 352-357.

[38] Y. Zhang, J. Wen and F. Mo, "The Application of Internet of Things in Social Network," *2014 IEEE 38th International Computer Software and Applications Conference Workshops*, Vasteras, 2014, pp. 223-228.

[39] B. Xie and H. Abelson, "Skill progression in MIT app inventor," *2016 IEEE Symposium on Visual Languages and Human-Centric Computing (VL/HCC)*, Cambridge, 2016, pp. 213-217.

[40] C. P. R. Sai, V. S. Datta and Sudheera, "Design of a Smart remote," *2016 International Conference on Circuit, Power and Computing Technologies (ICCPCT)*, Nagercoil, 2016, pp. 1-4.

[41] A. H. Sabani and R. Jailani, "Android based control and monitoring system for leg orthosis," *2015 IEEE 11th International Colloquium on Signal Processing & Its Applications (CSPA)*, Kuala Lumpur, 2015, pp. 40-45.

[42] A. Howedi and A. Jwaid, "Design and implementation prototype of a smart house system at low cost and multi-functional," *2016 Future Technologies Conference (FTC)*, San Francisco, CA, 2016, pp. 876-884.

[43] K. Roy, W. C. Rousse and D. B. DeMeritt, "Comparing the mobile novice programming environments: App Inventor for Android vs. GameSalad," *2012 Frontiers in Education Conference Proceedings*, Seattle, WA, 2012, pp. 1-6.

[44] D. Tristanto and H. P. Uranus, "Microcontroller based environmental control for swiftlet nesting with SMS notification," *Proceedings of the 2011 International Conference on Electrical Engineering and Informatics*, Bandung, 2011, pp. 1-5.

[45] F. S. A. Saad, A. Y. M. Shakaff, A. Zakaria, M. Z. Abdullah, A. H. Adom and A. A. M. Ezanuddin, "Edible Bird Nest Shape Quality Assessment Using Machine Vision System," *2012 Third International Conference on Intelligent Systems Modelling and Simulation*, Kota Kinabalu, 2012, pp. 325-329.

[46] A. Daramas, S. Pattarakitsophon, K. Eiumtrakul, T. Tantidham and N. Tamkittikhun, "HIVE: Home Automation System for Intrusion Detection," *2016 Fifth ICT International Student Project Conference (ICT-ISPC)*, Nakhon Pathom, 2016, pp. 101-104.

# Evaluation of Rain Cell Models (EXCELL and HYCELL) using Rainfall Data of Bangladesh

Shamsur Rahman Akash
*Faculty of Electrical Engineering*
*Universiti Teknologi Malaysia*
*Johor Bahru, Malaysia.*
*rashamsur2@live.utm.my*

Nor Hisham Khamis
*Department of Communication Engineering*
*Faculty of Electrical Engineering*
*Universiti Teknologi Malaysia*
*Johor Bahru, Malaysia.*
*hisham@fke.utm.my*

***Abstract*— Frequencies above 10 GHz are strongly affected by attenuation phenomena due to atmospheric impairments, among which rain plays the dominant role. Horizontal structure of rain fields is very complex due to its high space-time variability. Considering modeled cells which are described by a small number of parameters that would allow reduced computing time, storage problems, and multiply the system simulations to optimally define the system parameters. In this paper rainfall data of Bangladesh Meteorological Department have been used and the peak of rain intensity and the distances along elliptic shape of rain cells is obtained and also each model parameters. The EXCELL and HYCELL model has been fitted and compared to every rain cell. The result shows HYCELL model has good performance than EXCELL model.**

***Keywords—Evaluation of rain cell size models, EXCELL model, HYCELL model, rain attenuation analyze of Dhaka, .***

## I. INTRODUCTION

Wireless networks have significantly impacted the world, since their initial deployment. Wireless networks have continued to develop and their uses have significantly grown. Cellular phones are nowadays part of huge wireless network systems and people use mobile phones on a daily basis in order to communicate with each other and exchange information. Before planning wireless network for communication, it is necessary to determine the path loss and broadcast signal coverage for the location. The demand for increased data rates and greater bandwidths has required systems to use radio frequencies in the microwave and millimetric wave bands. Fog attenuation dominates in infrared and optical bands whereas rain attenuation plays havoc at millimetric wave bands. The microwave propagation is affected by changes in lower atmosphere; presence of hydrometeors such as rain, fog, water vapor, and oxygen in radio wave path can produce an extremely significant effect in energy absorption. In the designing of a microwave link, there are several points to be considered like system reliability, economical designs, present and future frequency selection, site planning, and multilevel systems. With respect to these hydrometeors, the path loss due to rain attenuation has been recognized as major obstacles in design of microwave communication link operating at frequencies above 10 GHz. In tropical rainfall area like Bangladesh where excessive rainfall is a common phenomenon throughout the year and rainfall rate varies very much in small location over a small distance, rain attenuation is more significant in causing propagation loss and can cause much havoc for millimetric and microwave signals. Rain attenuation degrades the system performance and limits the usage of higher frequencies for terrestrial LOS communication system.

## II. ANALYSIS

### A. Input Data

Daily rain data (in millimeter, mm) have been collected from Bangladesh Meteorological Department (BMD) of 2015. We have chosen the Capital of Bangladesh 'Dhaka' zone for rain attenuation prediction in Bangladesh. It is shown in fig 1.


Fig.1: Bangladesh map showing Dhaka zones (middle)

In our work, we have used Intelsat satellite 906 that is stationed at 64.15°E on Indian Ocean Region (IOR). This satellite has footprint over Bangladesh and provides telecommunications and broadcasting services for our country. This Dhaka site with its major parameters is given in Table 1.

Table 1. Site Information

| Location | Position | | Look Angles | | Height above sea level (m) |
|---|---|---|---|---|---|
| | *Lat. (N)* | *Long. (E)* | *Elev.* | *Az.* | |
| Dhaka | 23.78 | 90.41 | 49.51 | 230.82 | 8.45 |

*B. EXCELL Model*

The main Characteristic of this model is its exponential shape. Monoaxial model and biaxial model were suggested whereas the cell is assumed round and elliptical respectively. Mathematical expression for this biaxial EXCELL model of distributing horizontal rate of rainfall within a cell is given bellow:

$$R(x,y) = R_M \exp\left[-\left(\frac{x^2}{a_E^2}+\frac{y^2}{b_E^2}\right)^{\frac{1}{2}}\right] R \geq R_2 \quad (1)$$

Where $R_M$ is the Peak rain rate, R(x,y) The peak rainfall rate at x and y coordinates. $a_E$, $b_E$ are the distances along the axes. The area over which $R \geq R_2$, mean value of R(x,y), mean value of R(x,y), rms value and mean value of the horizontal gradient where E is the elliptic integral of second kind is given bellow respectively;

$$A_{ex} = \pi a_E b_E \ln^2 \frac{R_E}{R_2} \quad (2)$$

$$\overline{R}_{ex} = 2\pi a_E b_E \left[R_E - R_2\left(1+\ln\frac{R_E}{R_2}\right)\right] \quad (3)$$

$$Rrms_{ex} = \frac{\pi}{2} a_E b_E \left[R_E^2 - R_2^2\left(1+2\ln\frac{R_E}{R_2}\right)\right] \quad (4)$$

$$\overline{G}_{ex} = 4b_E E\left[\frac{\pi}{2}, \left(1-\frac{a_E^2}{b_E^2}\right)^{\frac{1}{2}}\right]\left[R_E - R_2\left(1+\ln\frac{R_E}{R_2}\right)\right] \quad (5)$$

Rms Value of the Horizontal Gradient of R(x,y) ,

$$Grms_{ex} = \frac{\pi}{4}\left(\frac{b_E}{a_E}+\frac{a_E}{b_E}\right)\left[R_E^2 - R_2^2\left(1+2\ln\frac{R_E}{R_2}\right)\right] \quad (6)$$

*C. HYCELL Model*

The HYCELL model is basically a hybridization process of EXCELL model and the way of determining this model is also in a similar manner to that of the EXCELL model. By using the equation (2) and (3) successively the cell area and mean rainfall rate can be obtained. The main characteristics of this model are it gives an explanation of the horizontal rainfall rate distribution whereas exponential and Gaussian shapes are combined. The mathematical expressions are;

$$R(x,y) = R_G \exp\left[-\left(\frac{x^2}{a_G^2}+\frac{y^2}{b_G^2}\right)\right]; if \rightarrow R_2 \geq R_1 \quad (8)$$

$$= R_E \exp\left[-\left(\frac{x^2}{a_E^2}+\frac{y^2}{b_E^2}\right)^{1/2}\right]; if \rightarrow R_2 \leq R < R_1, \quad (9)$$

Here $R_G$ is peak rainfall rate of the gaussian component, $a_G$ distances along x axis, $b_G$ distance along y axis and $R_1$ is the different rainfall rate so that the gaussian and exponential components can be separated. Where the parameter $R_G$, $a_G$, and $b_G$ define the Gaussian component. Respectively, they are the peak of the rain intensity, and the distances along the x and y axes for which the rain rate decays by the factor of 1/e with respect to $R_G$. Similarly, the parameters $R_E$, $a_E$, and $b_E$ define the exponential part as in the EXCELL model. $R_1$ is the crossover point between the Gaussian and the exponential regions. The validity domain for this hybrid model is $R \geq R_2$, with $R_2 = 1$ mm $h^{-1}$

In the EXCELL model, one cell is completely characterized by means of three parameters, $R_E$, $a_E$, and $b_E$ . However, the HYCELL model requires seven parameters, i.e. $R_G$, $a_G$, $b_G$, $R_E$, $a_E$, $b_E$, and $R_1$. The area ($A_{hy}$) over which $R \geq R_1$, Mean Value of R(x,y), Rms value of R(x,y), Mean Value of the Horizontal Gradient of R(x,y), where E is the elliptic integral of second kind and the Rms Value of the Horizontal Gradient of R(x,y) is given bellow accordingly;

$$A_{hy} = \pi a_G b_G \ln^2 \frac{R_G}{R_1} \quad (11)$$

$$\overline{R}_{hy} = \pi a_G b_G \left(R_G - R_1\right) \quad (12)$$

$$Rrms_{hy} = \frac{\pi}{2} a_G b_G \left(R_G^2 - R_1^2\right) \quad (13)$$

$$\overline{G}_{hy} = 4b_G E\left[\frac{\pi}{2}, \left(1-\frac{a_G^2}{b_G^2}\right)^{\frac{1}{2}}\right]\left[\frac{R_G \pi^{\frac{1}{2}}}{2} erf\left(\ln^{\frac{1}{2}}\frac{R_G}{R_1}\right) - R_1 \ln^{\frac{1}{2}}\frac{R_G}{R_1}\right] \quad (14)$$

$$Grms_{hy} = \frac{\pi}{2}\left(\frac{b_G}{a_G}+\frac{a_G}{b_G}\right)\left[R_G^2 - R_1^2\left(1+2\ln\frac{R_G}{R_1}\right)\right] \quad (15)$$

*D. Measured Rainfall Parameters*

Data Average rain rate ( $\overline{R}$ ), data peak rain rate (Rmax), excell model peak rain rate ($R_E$) and gaussian model peak ($R_G$) rain rate is determined to compare between the peak rain intensity of model and data.

Table 2. Rain Cell Parameters of the year 2015

| *Months* | $\overline{R}$ *(mm/h)* | $R_{max}$ *(mm/h)* | $R_E$ *(mm/h)* | $R_G$ *(mm/h)* |
|---|---|---|---|---|
| Jan | 12.168 | 41.38 | 40.87 | 41.10 |
| Feb | 8.92 | 15.32 | 28.63 | 15.80 |
| Mar | 10.92 | 31.56 | 29.89 | 33.56 |
| Apr | 13.68 | 52.80 | 61.35 | 42.68 |
| May | 10.88 | 58.80 | 35.260 | 42.36 |
| Jun | 14.92 | 41.91 | 70.36 | 33.65 |
| Jul | 9.08 | 18.90 | 22.62 | 17.326 |
| Aug | 2.3 | 9.89 | 0.368 | 13.82 |
| Sep | 4.859 | 5.68 | 4.65 | 5.25 |
| Oct | 9.363 | 19.90 | 18.76 | 24.64 |
| Nov | 16.56 | 49.84 | 56.93 | 44.03 |
| Dec | 12.5 | 48.54 | 51.06 | 47.69 |

## III. Results

The figure below shows, the EXCELL model of rain cell model. $R_E$ value was derived from average rain rate of radar observations from December 2015. Analytical expression of rain rate horizontal distribution within the cell is given in the horizontal plane (Oxy). aE and bE are the distance along the axes Ox and Oy, 1.2 km and 2.2 km respectively.

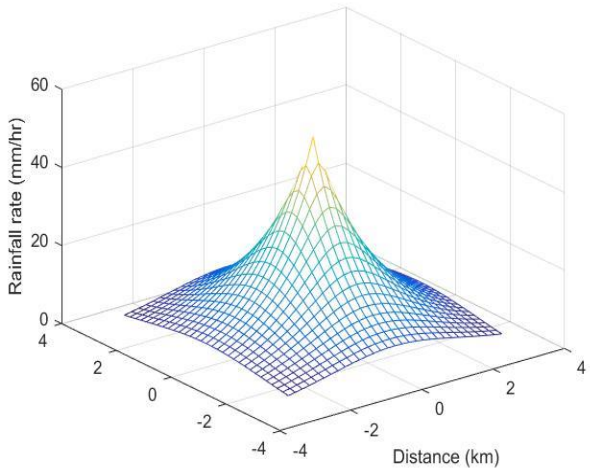


Figure 2: Model of EXCELL rain cell with the parameter $R_E$= 51 mm/h, $a_E$=1.2 km, $b_E$=2.2 km.

Seven parameters of HYCELL model was defined purely Gaussian $R_G$, $a_G$, $b_G$ and purely exponential component $R_E$, $a_E$ and $b_E$. Figure 3 show the HYCELL modeling of the rain cell. The HYCELL models approximately have same value of rain rate, Rr.

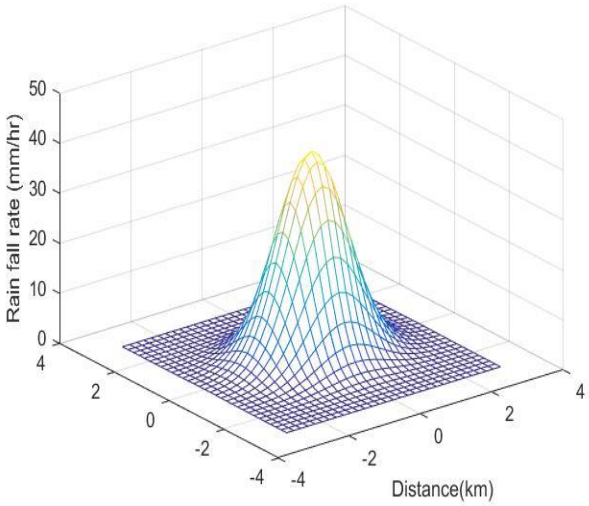


Figure 3: Model of HYCELL rain cell with the parameter Rg=41 mm/h, $a_G$=1. 22 km, $b_G$=1.02 km.

From rain cell model, rain intensity error was conducted in order to compare the result of modelled cells and actual one.

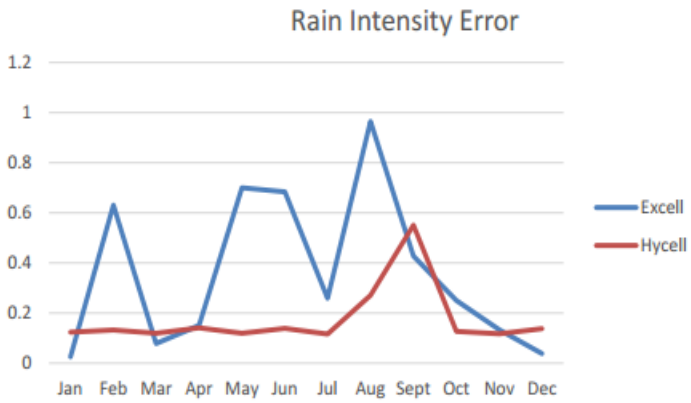


Figure 4: Rain intensity error HYCELL and EXCELL.

From Figure 4, it can be seen that HYCELL model has the small error in modeled the peak rain intensity.

## IV Conclusions

Rainfall data of Dhaka of the year 2015 measured using the rain gauge of BMD has been analyzed. The EXCELL and HYCELL model have been fitted to each rain cell measured. Both HYCELL and EXCELL have unique advantages. HYCELL model has the small error in modeled the peak rain intensity. Gaussian function give realistic value for the higher intensity in the center of the cell because horizontal distribution of intensity in the vicinity of the peak does not reality decay abruptly as an exponential function. Further work will include comparison of raindrop size distribution parameters from disdrometer data and other meteorological effects with the rain cell models.

## REFERENCES

[1] A. Paraboni, P. Gabellini, A. Martellucci, C. Capsoni, M. Buti, S. Bertorelli, N. Gatti, and P. Rinous, “Performance of a reconfigurable satellite antenna front-end as a countermeasure against tropospheric attenuation,” presented at the 13th Ka and Broadband Communications Conf., Torino, Italy, Sep. 2007.

.[2] V. Pastoriza, A. Nunez, P. Marino, F.P. Fontan, and U.-C. Fiebig, “Rain-Cell Identification and Modeling for Propagation Studies from Weather Radar Images”, IEEE Antennas and Propagation Magazine, 52, 5, October 2010, pp. 117-130.

[3] L. Castanet, “Fade mitigation techniques for new satcom systems at Ka and V bands,” Ph.D. dissertation, Department of electromagnetism and Radar, Toulouse, 2011.

[4] C. Capsoni, F. Fedi, C. Magistroni, A. Paraboni, and A. Pawlina, “Data and theory for a new model of the horizontal structure of rain cells for propagation applications,”Radio Sci., vol. 22, no. 3, pp. 395–404, 1997.

[5] L. Feral, H. Sauvageot, L. Castanet, and J. Lemorton, “Hycell - a new hybrid model of the rain horizontal distribution for propagation studies:1. modeling of the rain cell,”Radio Science, vol. 38, no. 3, p. 1056, 2013.

[6] L. Feral, F. Mesnard, H. Sauvageot, L. Castanet, and J. Lemorton, “Rain cells shape and orientation distribution in south-west of france,”Phys.Chem. Earth B, vol. 25, no. 10-12, pp. 1073–1078, 2014.

# Suspended Air-Substrate Patch Antenna for Millimeter Wave Application

Nurul Izzati Binti Khairuddin
*Faculty of Electrical Engineering*
*University of Technology Malaysia*
*Johor, Malaysia*
*Izzatikhairuddin94@gmail.com*

Noor Asniza binti Murad
*Department of Communication Engineering*
*University of Technology Malaysia*
*Johor, Malaysia*
*asniza@fke.utm.my*

***Abstract*— This paper present a suspended air substrate patch antenna for millimeter wave frequency. The antenna was operates at 30GHz and stimulated using CST. The antenna consisted of coplanar waveguide(CPW) feed line, quater wavelength feed line ,patch , supporting line, and the frame. The suspended air substrate was used to eliminate the dielectric loss as the relative permittivity for the air is unity. The material that have been used for the patch antenna is the lossy material. Since the antenna substrate was air the radiation pattern, gain and the bandwidth were increased. In this paper the CPW The bandwidth of the designed antenna is 3.31%,the simulated return loss is -27.12dB and the realized gain is 9.58dB.**

***Keywords—air substratet; suspended; millimeter wave; unity; patch antenna;gain;dielectric loss***

## I. INTRODUCTION

Recently, the millimeter wave antenna have drawn the attention of many researchers over the past year because of it attraction features[1]. In last few years, a lot of application that used the millimeter-wave frequencies have been developed. Millimeter waves antenna is the antenna that operates at the high frequency (30GHz300GHz) and usually used for the millimeter wave application[3]. The example of the application are in telecommunication, telemetry, navigation, radar and etc[4. There are lots of advantages by using the application that has an extremely high frequencies which are large bandwidth. In the telecommunication field the millimeter waves have been studied since 1970's[7]. The millimeter wave gives a lot of benefits especially terrestrial and wireless data transmission field which is the data rate may reach 40 to 100 times higher than wireless LAN[5]. The range of frequencies of the bandwidth for open communication is about 3GHz-7GHz depending the upon country[6]. In addition, the frequency for the 5G is 28GHz. As the millimeter wave gives a lot of benefits, there are a lot of antenna have been designed to operate the millimeter waves. As the frequencies increase, the size or the dimension antenna and the bandwidth will reduce. But for the high loss will occur. For the good performance of the antenna, a low dielectric substrate is needed since its provide better efficiency. According to the studies on the air-substrate, the antenna gives a low loss and the better radiation.

At extremely high frequencies, there is high significant loss[2]. To reduce the loss of the antenna, this paper suggest or designed the suspended air substrate patch antenna. This antenna is stimulated using CST and operating at 30GHz. The several designed were proposed such as CPW feed line, quater wavelength and the patch antenna. The several design were appraoched to observed the radiation pattern,gain and return loss. Since the frequency is high and the antenna size or dimension is small[3]. At the high frequencies, the antenna's bandwidth will be narrow[3]due to the triggering of the unwanted surface wave at high frequency [2]. To improve the performance of the antenna is suppressing the surface waves[2].

## II. LITERATURE REVIEW

### A. Dimension of The Antenna

To determine the length and width of the antenna the dielectric constant, εr and the height,h of the substrate must fix. The operating frequency,fo must be determined in order to design antenna. The width of the patch, W can be calculated using following equation[5].

When the W is obtained the length of patch can be obtained by

$$w := \frac{c}{2 \cdot f \cdot \sqrt{\frac{(\varepsilon r + 1)}{2}}} \tag{1}$$

calculated the ΔL first[5].

$$\Delta L := 0.412 \cdot h \cdot \left[ \frac{\left[ (\varepsilon r + 0.3) \cdot \left[ \left( \frac{w}{h} \right) + 0.264 \right] \right]}{\left[ (\varepsilon r - 0.258) \cdot \left[ \left( \frac{w}{h} \right) + 0.8 \right] \right]} \right] \tag{2}$$

After the value of the ΔL is obtaned the length of the patch can be determined by using the formula below.

$$L := \left( \frac{1}{2 \cdot f \cdot \sqrt{\varepsilon r} \cdot \sqrt{\varepsilon \cdot \mu}} \right) - 2 \cdot \Delta L \tag{3}$$

When the dimension of the patch are determined the effective can be calculated using following formula

$$\varepsilon_{eff} = \frac{\varepsilon_r + 1}{2} + \frac{\varepsilon_r - 1}{2}\left[1 + 12\frac{h}{W}\right]^{-\frac{1}{2}}. \qquad (4)$$

### B. *Findings of The Previous Reseached*

From the findings of the previous reseached the antenna was designed to operate at very high frequency which 60GHz. The antenna was designed layer by layer because it was fabricated using the SU-8. The cavity was etched at the substrate to remove the material under the patch. The dielectric constant was unity as the patch was hung in the air. The result from this paper showed the return loss was very low. The frequency that obtained from the simulation was approximately the desired frequency. The gain was very high and the return loss was very low. But the real situation, the antenna was not suitable as there will be the vibration when the antenna is radiate. The antenna will be not stable as the vibration is occured. The antenna from this paper was only stimulated and not fabricated. So the performance of the antenna in the real was not observed and profiled.

For the next reseached the antenna was designed to operate at the extremely high frequency which is at 63GHz by suspended the air. The supporting system was invented to support the patch. The supporting lines was invented at the point where voltage and current is minimum so the performance of the antenna was not effect. The supporting line was designated at the ground to the patch. The bandwidth of the of the design was very small but the radiation was direct horizontal and the return loss was small. The dimension of the patch was very small which is in micrometer and the designed antenna As the conclusion,most of the patch antenna at low frequency perform well with a commercially well known substrate. However, at high frequency, the performance was deteriorate. Therefore, most of the research try to reduce or eliminate the dielectric loss by removing partly or all the substrate.

## III. METHODOLOGY

The basic idea antenna's structure is shown in the Figure 1 below. It consists of the patch antenna, ground,feeding line and the frame. Noticed that the rectangular patch is hanging in the air. The air is actually substrate of the antenna. The air substrate underneath the parch have a low dielectric permitivity constant. The thickness of the air substrate,h is 1 mm. The thickness of the antenna is 3mm. The specificaton of the antenna are shown below.

TABLE I. SPECIFICATION OF ANTENNNA

| Parameter | Specification |
|---|---|
| Dielectric constant | 1 |
| Center frequency | 30GHz |
| Reflection coefficient | <-20dB |

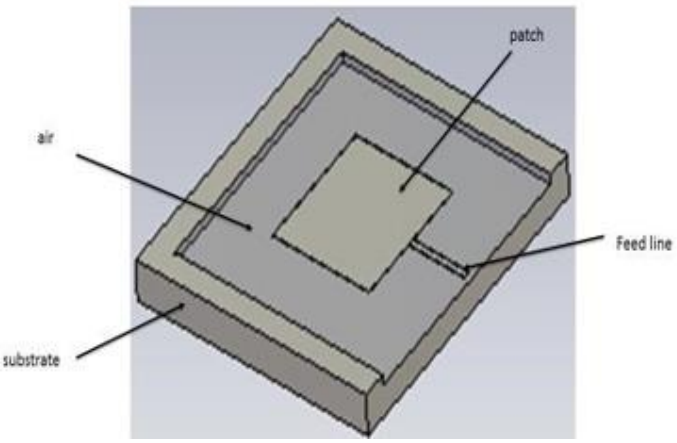


Figure 1 Antenna's Structure

The patch is hanging in the air so the air substrate can be formed underneath the patch. By using the formula that state in the literature review, the dimension of the antenna structure was obtained.

## IV. RESULT AND DISCUSSION

### A. *Quater Wavelength Feeding Line*

The simulation of the antenna was stimulated using CST followed the specification of the the proposed antenna. The antenna was using the quater wavelength feeding line. The structure of the antenna was followed exactly the basic idea of the antenna. The antenna consist of patch, feeding line, and the ground as below. The height of the substrate,thickness of the patch and the ground were 1mm.

Figure 2 Antenna's Structure

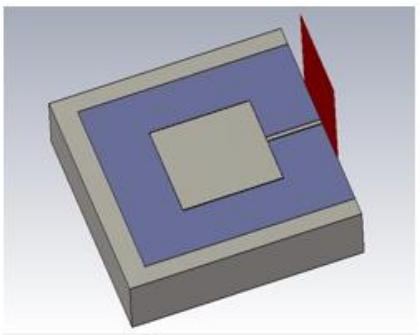

The result of the antenna are shown below.

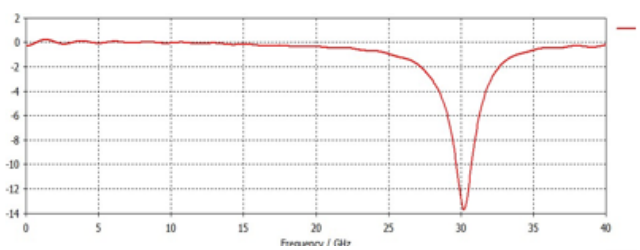


Figure 3: stimulated Return Loss

From the figure 3, it can be seen the curve drop about 30GHz. This curve shows the resonant or the frequency of the antenna. However, the return loss was about at -14dB. Eventhough the return loss are below than -10dB the loss are not consider good for the antenna. The less the loss the better the antenna. Therefore, the adjustment of the width of the feed kine and the size of the port is required to acquire the small return loss. From the s-paramete we can also observe the bandwidth of the antenna. By using the equation that have been discuss, the result of bandwidth can be seen as in below diagram. The value $f_L$ and $f_H$ are 29.685GHz and 30.74GHz. The bandwidth of the antenna is 3.51 % .

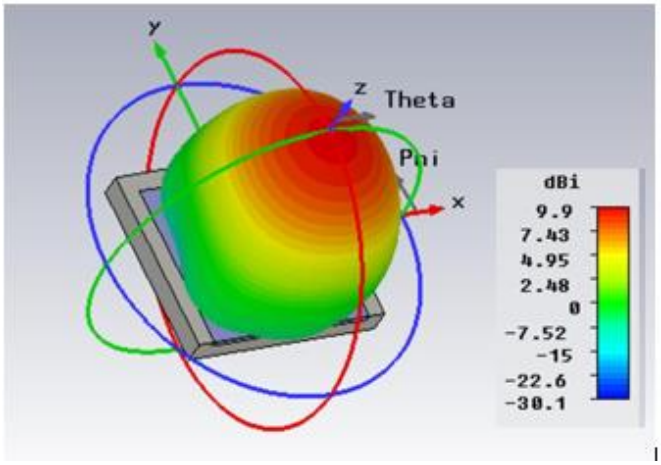


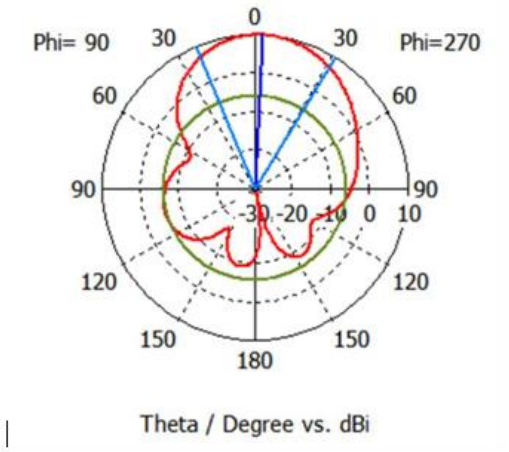


Theta / Degree vs. dBi

The radiation pattern acquired from the simulation are shows above. From the result we can observe that the direction of the antenna is almost undirectional and on direction of antenna patch. Futhermore, the gain that obtained from the simulation of the antenna that operates at 30GHz in the direction of maximum power is 9.9dBi which is equivalent to about 10dBi. An H-plane half power beamwidth (HPBW) of antenna is 54.4º. The main lobe direction 3.0º and the side lobe level is at -15.8dB.

*B. Quater Wavelength and Supporting Lines*

From the designed (A), the patch was hanging and it is impossible to make the patch is hang by itselves. Hence , to make the antenna become realistic the supporting line was designed to support the patch. The supporting line was important to make sure the height of the dielectric does not changed. The supporting line was designed at the low surface current to avoid the effection of the performance of the antenna.

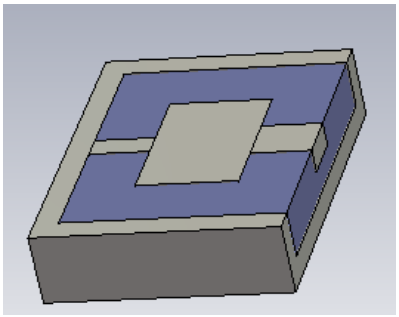

Figure 5: Antenna Design

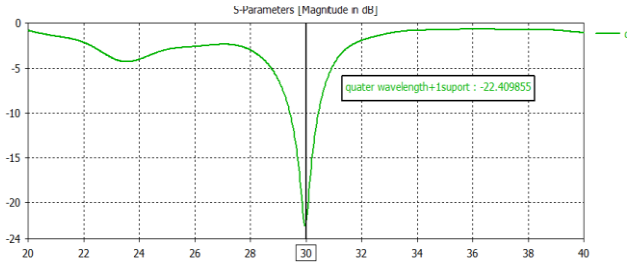


Figure 6: Stimulated Return Loss

The result of the antenna shows that the improvement of the return loss. The return loss that obtained was -22.41dB. However, The radiation pattern of the antenna was decreased after the support line was installed. The value that obtained 9.58dBi and omni directional. The bandwidth of the antenna is 3.42%

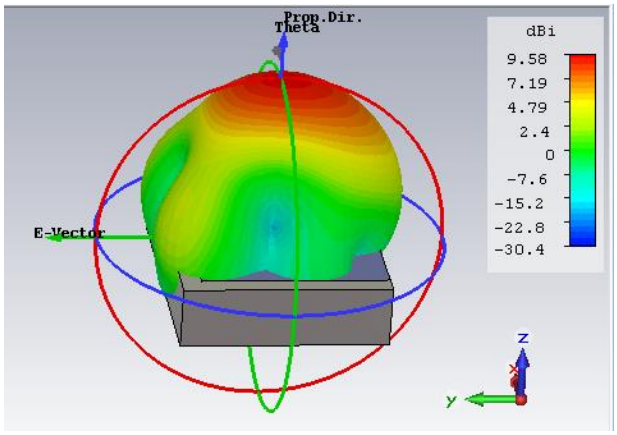


Figure 7: Radiation Pattern 3D View and Polar View

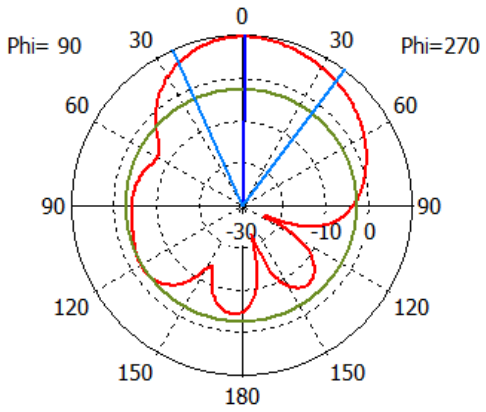


The main lobe direction of the antenna is 1° and the HPBW is 60.8°.

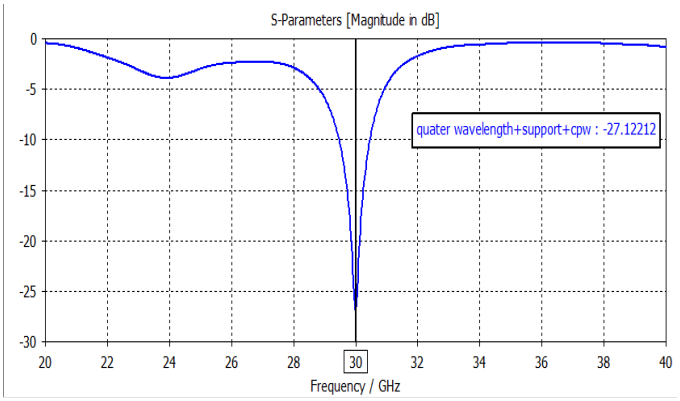


Figure 9: Stimulated Return Loss

### C. *CPW Feeding Line with Three Supporting Lines*

As the return loss and the gain that designed in (A) and (B) were not good enough the CPW feeding line was introduced. The length of the CPW was half wavelength to make sure the antenna radiate in optimum condition. From the designed (B), the patch and the feeding line were hanging and only depends on the one supporting line. To make sure the antenna become more stable as the length of feeding line increase the number of supporting line was increased to support the patch and feeding line. Figure below shows the antenna structure with three supporting line and the CPW feeding line.

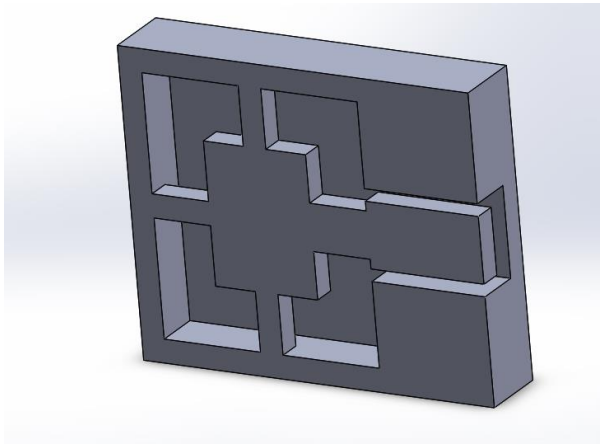

Figure 8: Antenna Design

The result of the antenna from the simulation are shown below.

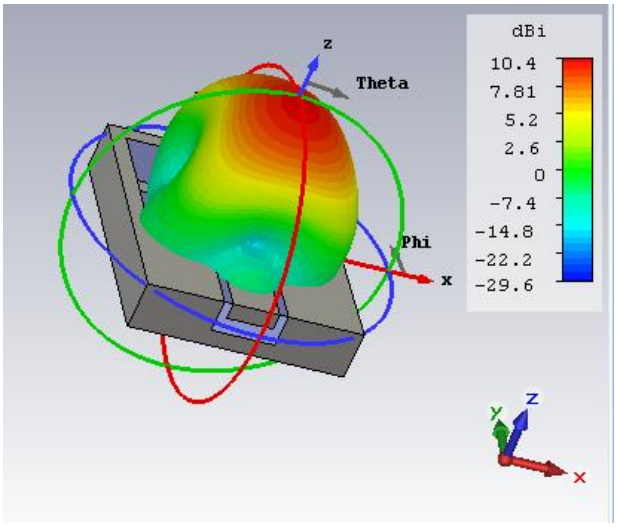


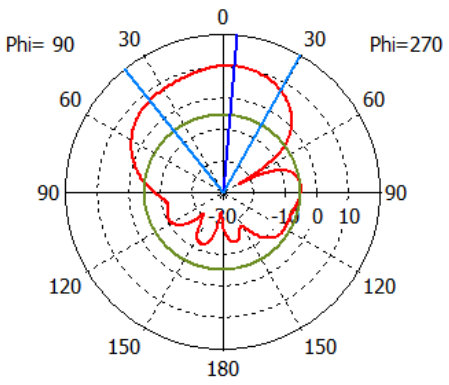


Theta / Degree vs. dB

the result shows the improvement of return loss and the gain. The return loss of the antenna is -27.12dB an the gain 10.4dBi. the stimulated return loss where the bandwidth is at -10dB is 3.31%. The main lobe direction is 5º and the HPBW is 68.3º.

## V. CONCLUSION

A single suspended air patch antenna that operates at 30GHz is designed and stimlated. The air substrate seems to be worth to use to reduce the dielectric loss.,as the dielectric constant of the air is unity The method is to enhance the performances of the antenna as the frequency of the antenna high the loss also high. The antenna have three supporting line to make sure the position of the patch is stabele. Futhermore, the supporting line is to make sure the height of the air substrate is not changed. The bandwidth that obtained is 3.31% and the result shows the gain is 10.4dBi. The stimulated return loss is -27.12dB. Therefore, as the antenna using the air substrate and CPW feeding line, it shows that the antena radiates well.

## REFERENCES


[1] Jagdish. M. Rathod, Member, IACSIT, IETE (I), IE (I), BES (I) "Comparative Study of Microstrip Patch Antenna for Wireless Communication Application", International Journal of Innovation,Management and Technology, Vol. 1, No. 2, June 2010.

[2] Noor Asniza Murad, "Micromachined Millimeterwave Circuits",University of Birmingham,2011

[3] David M, Pozar,"Microwave Engineering 4th Edition", John Wiley & Sons,2011.

[4] D. M. Pozar, Microwave Engineering, Third ed.: John Wiley & Sons, 2005.

[5] http://www3.ntu.edu.sg/home/eccboon/DIP%20website/Milimeter.html

[6] P. Adhikari, Understanding Millimeter Wave Wireless Communication, M. Young, The Technical Writer's Handbook. Mill Valley, CA: University Science, 1989.

[7] H. H. Mainel, "Commercial Applications of Millimeterwaves: History, PresentStatus, and Future Trends," IEEE Transactions on Microwave Theory and Techniques, vol.43,1995.

# 5G-Gigabit Passive Optical Network Backhaul

Nur Syahirah binti Abd Rahim
*Faculty of Electrical Engineering*
*Universiti Teknologi Malaysia*
*Johor Bahru, Malaysia.*
*nursyara2013@gmail.com*

Nadiatulhuda binti Zulkifli
*Department of Communication Engineering*
*Faculty of Electrical Engineering*
*Universiti Teknologi Malaysia*
*Johor Bahru, Malaysia.*
*nadiatulhuda@utm.my*

***Abstract*—In telecommunication, it is found that access network consumes more power compared to the other network domains since it have more active components. Recently, the fifth generation of wireless network over Gigabit Passive Optical Network (5G-GPON) backhaul has been proposed as a promising candidate for future access networks that take advantage of wireless mobility and optical link's high capacity. In this paper, this study aims to model and investigate the power consumption model and energy efficiency of this network. With optimum power consumption, energy efficiency of access network will improve since it is inversely proportional to the power consumption.**

***Keywords—backhaul;gigabit passive optical network;5G***

## I. INTRODUCTION

Nowadays, the emerging communication networks technologies and the rapid growth of internet users lead to stronger demands in terms of higher data rate, larger bandwidth and better coverage. Currently the research regarding 5G networks becomes a hot topic to be discussed where its advantages have attracted many parties. Hence, people highly anticipate to have 5G in future which by mean, the new era of technology for the mankind. However, the development of this kind of technology has come along with drawbacks in the terms of power consumption and the energy efficiency. Recent studies have indicated that wireless access network contribute to the huge amount of CO2 emissions of ICT that is dominated from the base stations of wireless access networks [1].

In the meantime, a suitable backhaul for access network employment which can be wireless or wired should be chosen wisely in order to minimize the power consumption and having a great energy efficiency. The implementation of the backhaul depends on few factors which are the type of technologies used, the surface area of deployment network and the amount of subscriber peak rate at the area. Since wireless networks is growing tremendously, the power consumption of networks is rising too. This phenomena will lead to the global warming and climate change. Hence, the awareness about power consumption in communication networks and its energy efficiency are rising which eventually become a research issue. One of the promising solutions is a hybrid access network architecture such as 5G-GPON which uses a passive, high speed optical link as the backhaul for wireless networks.

In this paper, the power consumption and energy efficiency of this integrated access network will be calculated and modeled in order to make sure it is suitable for deployment in the future. GPON offers low power consumption and very high data rate and capacity which can cater the advancement of 5G network. Besides, by reducing the power consumption of the access network, it helps in minimizing cost of network operation and will appear to be affordable to the consumer. In terms of energy efficiency, an optimum power consumption can raise the energy efficiency of every communication network. Somehow, energy efficiency is related to power consumption where the decreasing of power consumption will make the energy efficiency better. Therefore, to fight with climate change and support green technology, the suitable access network architecture should be chosen in order to obtain excellent energy efficiency as well as low power consumption.

This paper studies power consumption and energy efficiency of the integrated network which combines GPON and 5G networks as a whole network. 5G will be implemented at the front end; near to user while GPON act as the backhaul of the access network. The modelling and simulation of both power consumption and energy efficiency also are presented. The outline of this paper is as follows. Section II discusses the background of the study, Section III shows the power consumption modeling and Section IV discusses the obtained results. Finally, this paper is concluded in Section V.

## II. BACKGROUND OF THE STUDY

### *A. 5G network architecture*

Fifth generation mobile network (5G) is the evolvement of the current 4G Long Term Evolution (LTE) network and it is promising to furnish a multiple access which includes connection of machine to machine (M2M) and also device to device (D2D). In order for Internet of Things (IoT) to modernize within the rapid development of communication and electronic technologies, fifth generation of wireless is a crucial element in providing a higher bandwidth since the current bandwidth is limited in the conventional sub 6 GHz bands [2]. Apart from that, it also provides a better coverage, higher subscriber peak-rates and lower latencies. Besides, 5G transport is said to be a tool in order to accommodate a wide range of service requirements and providing a more diverse range of transport services [3]. As the traffic keeps increasing, additional spectrum is required to support mobile wireless communication. In [4], it reported that in 2015 World Radio Conference (WRC-15), the additional spectrum for 5G must not exceed 6.5GHz. However, to achieve and provide the higher demand of long-term traffic, 6.5 GHz seem insufficient. Therefore, for next WRC-18/19 the discussion is about the additional spectrum which is targeting to be 10 GHz and above. In spite of the fact that massive spectrum

can support 5G technology, it also comes with some drawbacks which are the problems that deal with propagation characteristics, aspects of implementation, and compatibility with technology's legacy. All these problems might influence the radio interface design. Figure 1 below show the future spectrum range for deployment of 5G mobile technology while Figure 2 shows the future of communication network that involve 5G and the application of it that will benefit to all mankind.

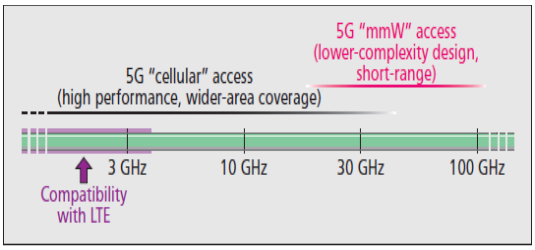


Fig. 1. Spectrum range to be contemplate for 5G [4]

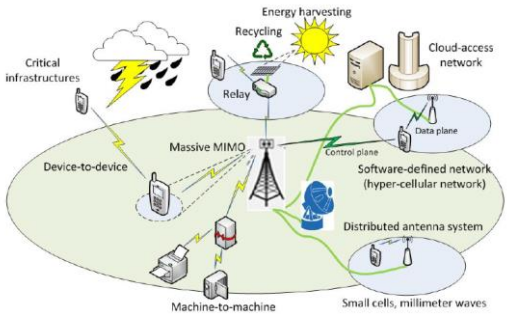


Fig. 2. Revolutionary technologies for 5G [5]

In an integrated access network, wireless medium is suitable to be put at the end (near to user) of access network terminal because it have more advantages compared to wired network as it can be connected by multiple end user, wide range of connectivity, and easy for deployment in the suburban areas. To catch up with the rapid development of communication technology, the latest of cellular network 5G is considered to be implemented in the integrated access network and there are some of research studies had been conducted already. In this research, small cells were used as the wireless part at the front haul of the 5G-GPON integrated access network. Small cells are low-powered radio access nodes, with range of a few meters to a mile diameter and it can be divided into three types. Ranging from largest to smallest they are named micocells, picocells and femtocells.

In microcells, the radius of the cell can reach up to 2 km and it provides users with high traffic densities. This type of cells are suitable for indoor and outdoor at the suburban area as well as the urban area. Meanwhile for picocells, the cell radius is 200 meters or less which can support around 100 user with its high traffic densities and high data rate. Picocells are mainly deployed indoors such as in building where it can improve the low connectivity of wireless and cellular coverage of the building. Last but not least, femtocells with a radius around 10m are little bit different from microcells and picocells where it only support a handful of users and able to manage a few simultaneous calls. To conclude, small cells are valuable in this era of telecommunication where it can provide higher capacity, speed and also as higher frequency. Small cells also beneficial in the indoors area like building since it can be deployed quickly, solve the coverage issue within the building and also come with a reasonable price which can minimize the cost of installation.

From the power consumption perspective, wireless access network consumes more power than wired network but somehow the demand for higher traffic and the upcoming development of technology must not be neglected. Therefore, the integrated of access network between wireless and wired medium should be implemented for the sake of swift development and also to conserve the environment.

### *B. Gigabit Passive Optical Network (GPON) as Mobile Backhaul*

The ultra-dense and abundant traffic cells supposedly be connected to the core network through the backhaul, often with great requirements in terms of latency, capacity, availability, energy and also as cost efficiency [6]. Therefore, for this 5G-GPON integrated access network, GPON was chosen to be the backhaul of the network since it offers a lot of advantages for the deployment of 5G mobile networks.

GPON network architecture consists of two parts which are Optical Line Termination (OLT) and Optical Network Unit (ONU). Both OLT and ONU are connected by a passive splitter which is in a form of ratio 1:*N* where *N* varies from 2 to 64. Since splitter does not consume any power, power consumption of network can be significantly reduced. A study from Vereecken (2011) shows that, GPON consumes only 0.2-0.8 Watt per subscriber whereas other medium like VDSL and ADSL consume power 3-5 W/Subs and 1-2 W/Subs respectively [7].

Besides, to be implemented as a mobile backhaul, GPON is assured to provide a very high capacity and low transmission loss as well as low bit error rates. Since it can reach up to 20 km distance, GPON is more desirable compared to others wired network. Apart from that, according to [8], GPON also promising high confidentiality, potential of strong anti-jamming and small maintenance cost.

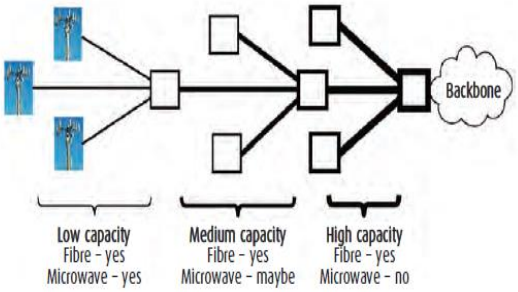


Fig. 3. Schematic diagram of a mobile backhaul network

In Fig. 3, the bold line indicates the fact that higher link capacity is required as more signal are aggregated closer to the backbone network. In addition, the abilities of PON access architecture in sharing fibers, central office equipment, and bandwidth among end terminals had make it applicable to backhaul small cells with reasonable cost. With all the advantages discussed before, GPON is suitable as an access

network backhaul since it consumes less cost, low bit error and the crucial thing is it consume small amount of power.

### C. The Power Consumption of Access Network Based on Different Network Technologies

Power consumption is the amount of power used per time during the working of appliances and generally the power exceeds the required amount for most of operations. According to Tombaz et al, the total network power consumption is known to be the sum of the power consumptions of all base stations. "Nonetheless, the selection of specific deployment of the network also bring the effect to the exact implementation of backhaul network, and hence its power consumption which is needed to pay an attention when devising energy efficiency deployment" [9]. In order to understand more about power consumption in the telecommunication network, a research by [1] has been reviewed. The result of the work are presented in table 1.

TABLE I. POWER CONSUMPTION PER USER FOR DIFFERENTS TECHNOLOGIES

| | $P^u_{home}$ [W] | $P^u_{access}$ [W] | $P^u_{core}$ [W] | $P^u_{total}$ [W] |
|---|---|---|---|---|
| **Mobile WiMAX** | 2.5 | 34.0 | 0.28 – 0.44 | 36.78 – 36.94 |
| **HSPA** | 2.5 | 462.3 | 0.28 – 0.44 | 465.08 – 465.24 |
| **LTE** | 2.5 | 83.5 | 0.28 – 0.44 | 86.28 – 86.44 |
| **ADSL2** | 3.8 – 5.0 | 1.95 | 0.28 – 0.44 | 6.03 – 7.39 |
| **VDSL2** | 6.0 – 7.5 | 3.0 | 0.28 – 0.44 | 9.28 – 10.94 |
| **PtP fibre (1Gbps)** | 5.6 – 7.1 | 4.5 – 7.5 | 0.28 – 0.44 | 10.38 – 15.04 |
| **GPON** | 7.7 – 9.7 | 0.35 – 0.47 | 0.28 – 0.44 | 8.33 – 10.61 |

Based on the above Table 1, seven type of technologies had been tested for their respective power consumption at different networks which are; $P^u_{home}$, the power consumption of CPE (Customer Premises Equipment), $P^u_{access}$ is the power consumption of access network and $P^u_{core}$ is the power consumption of core network. Since this project focuses on access network, the power consumption per user at access network will be discussed in advanced while the power consumption per user at home network and core network are neglected. For wireless access network, the power consumption for WiMAX is the lowest which is 34.0 Watt compared to HSPA and LTE which are 462.3 Watt and 83.5 Watt respectively. It can be deduced that the power consumption of the technologies in wireless network are improving from time to time.

In fix line (wired) access network, comparison of the power consumption of three different technologies like Asymmetric Digital Subscriber Loop 2 (ADSL2), Very high speed Digital Subscriber Line 2 (VDSL2) and Gigabit Passive Optical Network (GPON) proves that GPON is the best solution in terms of power saving. It provides the lowest power consumption and allow for both higher bit rates and ranges. Since GPON can offer up to 10Gb/s of bit rate and 20km distance coverage, it suit to be use as a mobile backhaul where it can aggregate a huge amount of traffic. For wireless access network, a research had conducted to determine the power consumption of three different type of wireless technologies which are mobile Worldwide Interoperability for Microwave Access (WiMAX), High Speed Packet Access (HSPA) and Long Term Evolution (LTE). In a research paper by Deruyuck [1], a scenario was created to fulfil the requirement of the research and the result are explained and revealed. Based on that research, it shown that in access network, mobile Wi-MAX has the least power consumption, followed by LTE and lastly is HSPA. It found that the access network devote the most power consumption to the telecommunication network compared to home and core network for the wireless access case. Hence, an approach to use integrated network 5G-GPON in the access network is being proposed to deal with this issue.

### D. The Energy Efficiency

Energy efficiency is defined as the amount of information bits transmitted to or received from users per unit of energy (power) consumption of access network in bit/Joule [10]. Recently, the total of energy is rising vigorously along the massive growth in requirements of service and it is expected to keep increasing in the future. Therefore, many researches were conducted in order to solve this problem. As mention before, the base station is the huge contributor of power consumption in wireless access network. In regards to this issue, wise network planning should be implemented. In [11], it a number of plans such as Energy Aware Radio and Network Technologies (EARTH) has been assigned to come up with more architecture and techniques regarding EE. Workshops on green radio also had been conducted and it aims to identify and establish innovative techniques or ways for the reduction of the overall energy required to run a radio access network [12]. Last but not least, another solution for energy efficiency is by minimizing the cell size in the network, where lower size of cell can rise up the amount of delivered data bits per unit energy for given user density and total power in service area. In implementation of GPON, as the average of data rate increases, the efficient energy used is decreases. According to [13], for access rate below 300 Mbps, PON is proven to be the best energy-efficient access network.

Meanwhile, in [14], some methods to reduce energy consumption in PON is been discussed. Those steps involved physical, data link and joint approaches as illustrated in Figure 4. Firstly is the physical layer which can be divided into two categories: device oriented and service oriented. For device oriented, the method is focusing at the reduction of energy consumption of the devices and for service oriented method, it target at enhancing the performance of the service. Second way is data link approach where it focus at data link layer of the IEEE 802.3 architecture and depending on ability of switching network elements to minimum power mode. There are three types of power saving standard which are power shedding, dozing and sleeping. Third step is joint approach where it combining the first and second step as one. For instance, combination of adaptive link rate and sleep mode for the purpose of energy saving in facing the demand of real traffic. Another example is combination of modified ONU with dynamic sleep mode in order to improve the clock recovery after ONU wake up [15]. For integrated 5G-GPON access network, both energy efficiency in wireless and wired network can be combined to produce a better performance of access.

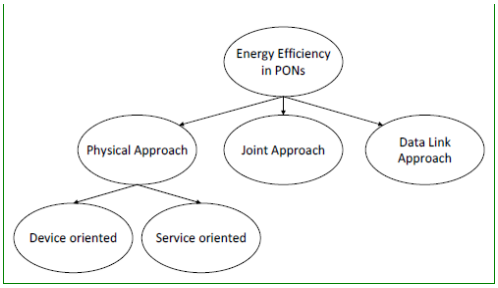


Fig. 4. Taxonomy of approaches for energy efficient

### E. The Integrated Network

Integrated network is the combination of two different type of networks in one new network architecture. For 5G-GPON integrated network, GPON act as a backhaul and 5G is put at the front end, closer to user. GPON somehow makes a good backhaul since it can cope with high data rate which is desirable to deploy 5G network. With low power consumption offered, GPON backhaul and 5G networks make a great combination in order to optimize power consumption and have a better energy efficiency.

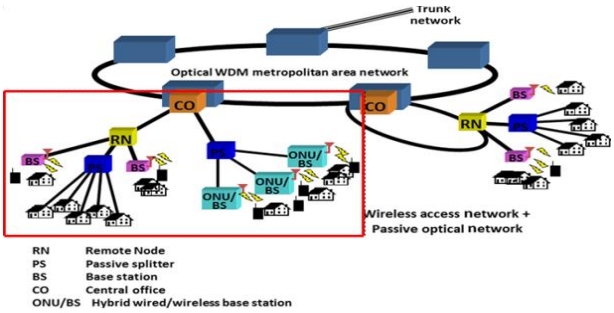


Fig. 5. The integrated network of wireless access network and PON

## III. Power Consumption Modeling

In this section, equation of power consumption as well as energy efficiency of the access network is introduced. Power consumption and energy efficiency are calculated separately for 5G and GPON before combining to become a total network consumption for hybrid 5G-GPON network.

### A. Power Consumption of 5G-GPON Integrated Access Network

As mentioned earlier, the idea of 5G-GPON integrated access network is still new and unexplored. Therefore, for easier understanding the proposed network was presented in an architecture form as shown in Figure 6.

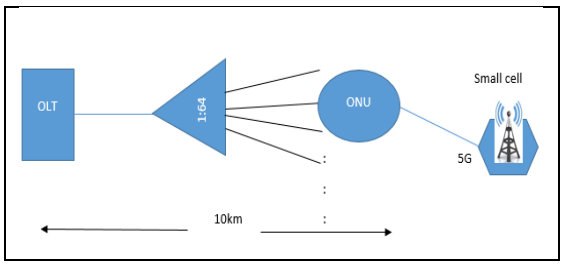


Fig. 6. Model of integrated access network

In order to obtain the power consumption of 5G-GPON integrated access network P5G-GPON, power consumption of OLT POLT, power consumption of ONU PONU and power consumption of picocell base station (PBS) PPBS are needed to be calculated. The power consumption of the integrated network can be calculated by using this equation:

$$P_{5G\text{-}GPON} = P_{OLT} + P_{ONU} + P_{PBS} \quad (1)$$

### B. Power Consumption of OLT

An OLT is the endpoint hardware device in a PON that connect with a network service provider. For this cases, the power consumption of OLT was assumed to be independent from the traffic load but it somehow related to some factors like electronics component, ambient temperature and power conversion efficiency. For power consumption of OLT, few aspects like uplink port, switching module and OLT line cards are being considered and are presented as shown below:

$$P_n^{OLT} = (P_{ports} + P_{control} + P_{UL}) \times (1 + \eta_{DC/DC}) \times SF \text{ [15]} \quad (2)$$

### C. Power Consumption of ONU

An ONU is a device that implies a multiple-subscriber device and implements a PON protocol. Power consumption of ONU based on traffic load can be obtained from

$$P_n^{ONU} = \alpha_o r_o + \gamma_o \text{ [15]} \quad (3)$$

where $\alpha_o$ is the power consumption of ONU in order to transmit or receive 1 bit of information, $r_o$ is the average access data rate per ONU and $\gamma_o$ is the power consumed by the ONU in idle condition.

### D. Power Consumption of PBS

A picocell is a small cell which is low-powered radio access nodes, with radius 200 meters or less that can support around 100 user with its' high traffic densities and high data rate. Picocells are mainly deployed indoors such as in building where it can improve the low connectivity of wireless and cellular coverage of the building. In this integrated network, power consumption for PBS can be calculated by

$$P_n^{PBS} = \alpha \times P_{TX} + b \text{ [16]} \quad (4)$$

where $\alpha$ is power depending on load, b is power without load and $P_{TX}$ is PBS transmission power.

### E. Theoretical Model of Energy Efficiency

For the energy efficiency of 5G and GPON backhaul, achievable data rate, $R_o$ is being used. Energy efficiency can be obtained by dividing $R_o$ with total power consumption, $P_T$. The equations were shown below:

$$EE = \frac{Ro}{PT} \quad (5)$$

TABLE II. Achievable Data Rate for Gpon and 5G

| | |
|---|---|
| **GPON** | $R_{GPON} = r_{DS}.B + [r_{DS}(1\text{-}B) + r_{US}] \times \frac{1}{SR}$ |
| **5G** | $R_{5G} = BW.\log_2(1+SNR)$ |

where $r_{DS}$ is GPON downstream data rate, GPON broadcast factor,B $r_{US}$ is GPON upstream data rate, BW is bandwidth and signal to ratio, SNR.

## IV. Results and Discussion

Matlab software is used for the simulation of power consumption and energy efficiency in the integrated 5G-GPON access network. Parameters required for this simulation are stated in tables below. The effects of parameters such as coverage area of network, split ratio (SR) of GPON and density of PBS per km$^2$ on power consumptions are depicted in this section.

TABLE III. Simulation Parameter

| Simulation Parameter | Value (Unit) |
|---|---|
| OLT PON port network, $P_{ports}$ | 41.5 W |
| OLT general function power, $P_{control}$ | 33.3 W |
| OLT uplink port power, $P_{UL}$ | 2.3 W |
| OLT power conversion efficiency, $\eta_{DC/DC}$ | 0.9 |
| OLT site factor, *SF* | 1.7 |
| ONU power per 1 bit, $\alpha_o$ | 0.00208 W/Mbps |
| ONU idle power, $\gamma_o$ | 11.51 W |
| PBS load power, $\alpha$ | 7.85 |
| PBS without load, b | 71.5W |
| PBS transmission power, $P_{TX}$ | 6.3mW |

### A. Simulation Power Consumption of OLT

The first simulation is OLT power consumption where the SR is 64, coverage area, A is 50 km$^2$ and density PBS is 45/km$^2$. Figure 7 show the graph obtained from the simulation is unsmooth, lumpy since the power consumption remain unchanged even though the number of ONU are different. This situation happened due to sharing same number of OLT. As an ONU connect directly to a single picocells, the number of ONU per km$^2$ is the same as density of PBS, which is 45/km$^2$. For example,

TABLE IV. Power Consumption of Olt at Different Area

| Area (km$^2$) | 40 | 41 | 43 | 44 |
|---|---|---|---|---|
| No of ONU | 1800 | 1845 | 1935 | 1980 |
| No of OLT | 29 | 29 | 30 | 30 |
| Total $P_{OLT}$ (kW) | 4.22 | 4.22 | 4.37 | 4.37 |

[a] $P_{OLT}$ = 145.66 W

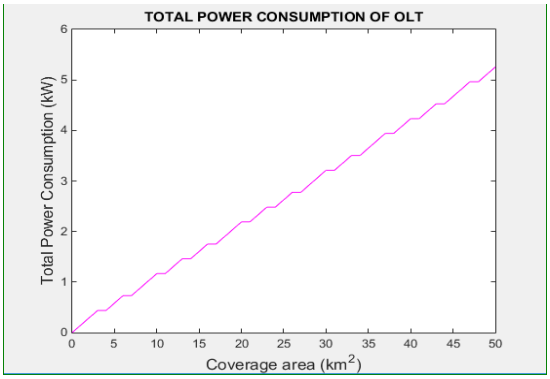


Fig. 7. The Power Consumption of OLT for 50km$^2$

### B. Simulation Power Consumption of ONU

For power consumption of ONU's simulation, the exact same parameter in A. were used. Figure 8 shows that power consumption of ONU linearly increasing as the coverage area increases. With the increasing coverage area, density of PBS/km$^2$ also increased as long as number of ONU per area.

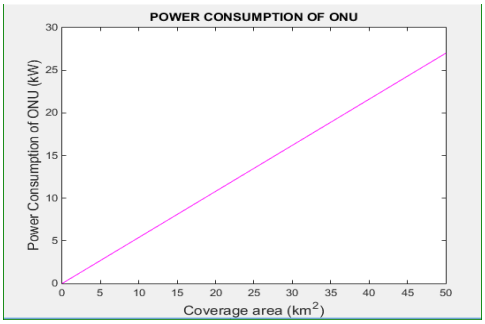


Fig. 8. The Power Consumption of ONU for 50km$^2$

### C. Simulation Power Consumption of PBS

From figure 9, result shows the power consumption of PBS is increasing linearly as the coverage become wider. Somehow, it can be seen that PBS power is a lot higher than ONU even though the number of ONU and PBS is same.

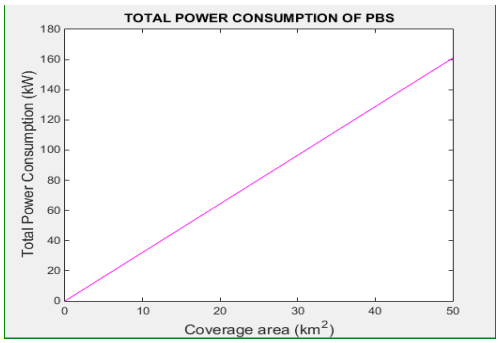


Fig. 9. The Power Consumption of PBS for 50km$^2$

### D. Total Power Consumption of Integrated Network

In this section, the density of PBS is being tested with different value like 40/km$^2$, 45/km$^2$ and 50/km$^2$ and the result is taken at same coverage area which is 30km$^2$. From figure 10, it

can be conclude that, the higher the density of PBS, the more power is consumed which is due to the increment number of ONU and OLT that contributed to power consumption respectively.

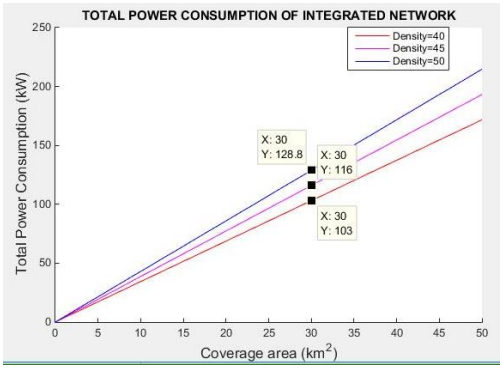


Fig. 10. Total Power Consumption of Integrated Network for Different Densities.

Meanwhile, in figure 11, total power consumption of every part of integrated network were presented. In this simulation, SR was being varied; 16, 32, 64. Result obtained show that the most consuming power between all three parts is PBS (5G). Besides, it can be deduce that, power consumption is lower when lower SR is used.

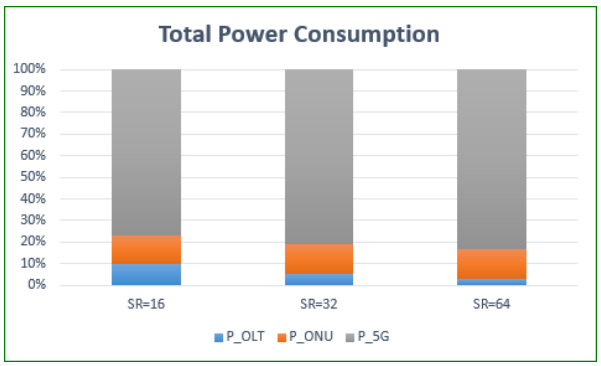


Fig. 11. Total Power Consumption of Integrated Network

## V. Conclusion

In conclusion, 5G mobile network will cater people with great of higher capacity, fast connectivity and much more. To be able implemented it, GPON is suit to play the role as backhaul of the 5G access network as well as can save a lot of power consumption. It clearly shown in Figure 11 that GPON only contribute 20% of power consumption for the integrated network. Thus, it can counter the higher power consumed by 5G network. Despite that, 5G-GPON backhaul is a good combination in power saving since a picocell (5G) is a small cell that low in consuming power while GPON with less number of active component. Based on the results obtained, it can be concluded that, with wide coverage area and higher density of PBS, more power will be consumed. Lastly, by using higher split ratio in GPON backhaul, power consumption of integrated access network can be reduce.

## References

[1] M. Deruyck et al., "Comparison of power consumption of mobile WiMAX, HSPA and LTE access networks," 2010 9th Conference of Telecommunication, Media and Internet, Ghent, 2010, pp. 1-7.

[2] Yilmaz, Turker, Gokce Gokkoca, and Ozgur B. Akan. "Millimetre Wave Communication for 5G IoT Applications." Internet of Things (IoT) in 5G Mobile Technologies. Springer International Publishing, 2016. 37-53.

[3] B. Skubic, G. Bottari, A. Rostami, F. Cavaliere, and P. Öhlén, "Rethinking Optical Transport to Pave the Way for 5G and the Networked Society," J. Lightwave Technol. 33, 1084-1091 (2015).

[4] E. Dahlman et al., "5G wireless access: requirements and realization," in IEEE Communications Magazine, vol. 52, no. 12, pp. 42-47, December 2014.

[5] F. Boccardi, R. W. Heath, A. Lozano, T. L. Marzetta and P. Popovski, "Five disruptive technology directions for 5G," in IEEE Communications Magazine, vol. 52, no. 2, pp. 74-80, February 2014.

[6] M. Jaber, M. A. Imran, R. Tafazolli and A. Tukmanov, "5G Backhaul Challenges and Emerging Research Directions: A Survey," in IEEE Access, vol. 4, no. , pp. 1743-1766, 2016.

[7] W. Vereecken et al., "Power consumption in telecommunication networks: overview and reduction strategies," in IEEE Communications Magazine, vol. 49, no. 6, pp. 62-69, June 2011.

[8] W. Zhaoqing, "Research on the Application of GPON Technologies," 2011 International Conference on Multimedia and Signal Processing, Guilin, China, 2011, pp. 61-63.

[9] S. Tombaz, P. Monti, K. Wang, A. Vastberg, M. Forzati and J. Zander, "Impact of Backhauling Power Consumption on the Deployment of Heterogeneous Mobile Networks," 2011 IEEE Global Telecommunications Conference - GLOBECOM 2011, Houston, TX, USA, 2011, pp. 1-5.

[10] A. Abrol and R. K. Jha, "Power Optimization in 5G Networks: A Step Towards GrEEn Communication," in IEEE Access, vol. 4, no. , pp. 1355-1374, 2016.

[11] G. Y. Li et al., "Energy-efficient wireless communications: tutorial, survey, and open issues," in IEEE Wireless Communications, vol. 18, no. 6, pp. 28-35, December 2011.

[12] C. Han et al., "Green radio: radio techniques to enable energy-efficient wireless networks," in IEEE Communications Magazine, vol. 49, no. 6, pp. 46-54, June 2011.

[13] Y. Zhang, P. Chowdhury, M. Tornatore and B. Mukherjee, "Energy Efficiency in Telecom Optical Networks," in IEEE Communications Surveys & Tutorials, vol. 12, no. 4, pp. 441-458, Fourth Quarter 2010.

[14] L. Valcarenghi, D. Pham Van and P. Castoldi, "How to save energy in Passive Optical Networks," 2011 13th International Conference on Transparent Optical Networks, Stockholm, 2011, pp. 1-5.

[15] A. Ramli, “Power Consumption Modelling in Integrated Optical-Wireless Access Network,” in Ph.D. Thesis, Universiti Teknologi Malaysia, 2017.

[16] X. Ge, S. Tu, G. Mao, C. X. Wang and T. Han, "5G Ultra-Dense Cellular Networks," in IEEE Wireless Communications, vol. 23, no. 1, pp. 72-79, February 2016.

# IOT-based Vehicle Access Management System

Mohamad Nor Azam bin Hassan
*Faculty of Electrical Engineering*
*Universiti Teknologi Malaysia*
*Johor Bahru, Malaysia.*
*mohamadnorazamhassan@gmail.com*

Mohd Adib bin Sarijari
*Advanced Telecommunication Technology*
*Faculty of Electrical Engineering*
*Universiti Teknologi Malaysia*
*Johor Bahru, Malaysia.*
*madib@utm.my*

***Abstract*—Internet of Things (IOT) is an evolving technology that has attracted a lot of researcher to study its potential in our environment. One of its potential application is the IOT-based vehicle access system in which the system that provides access management to parking area. The system will provide real-time information to the administrator and automatically update the information to database. This paper proposed an IOT framework for vehicle access management system that consists of three main parts which is the things, the cloud and the networks. The system is included with Advanced Encryption Algorithm (AES) for security data transfer from gateway device to the cloud. At the end of this project, the overall system performance is analyzed to determine its reliability and stability.**

***Keywords—Internet of Things; network security; framework; system model; Vehicle Access System***

## I. INTRODUCTION

The development of Internet technology is having a rapid growth due to increase of connected devices around the world- this is called Internet of Things (IOT). With the large number of connected devices, an appropriate networking hardware, software, and processors will be needed for deploying IOT system in the coming years. These include analyzing data and also improving cyber security against new threats. These devices can be almost anything including home appliances, gadgets and vehicles [1].

The term IOT was first coined by Kevin Ashton in 1999 [2]. Kevin Ashton is an innovator and consumer sensor expert and now known as the Father of IOT. Previously, many devices were unable to communicate that causes a huge limitations where devices could not be controlled or monitored remotely by the owner. With the introduction of IOT, these devices were able to interact, monitor and controlled ubiquitously. An example for that event is GPS-based location sensing and GPS system [3]. With the rapid development and capability of the Internet service, which was introduced in the mid-2000s, the IOT is becoming an interesting subject all around the world. IOT is also becoming a related technology that is used to improve technical, social and economic.

Based on K. Rose (2015), the general term for IOT can be refers to allowing all existing objects and devices to exchange and consume data requiring network connectivity and computing capability with minimal human intervention [4]. Potential applications of IOT are health care, transport, emergency services, defense, crowd monitoring, environment monitoring, building management and water quality monitoring [5]. In addition, the rapid development in this technology has attracted many companies from different industries to develop and do research on this technology. This has led to a bigger potential markets size. The companies include Cisco, Google, Dell and other big well-known hi-tech industries.

In essence, IOT concept is actually complimented to the existing network architectures in the present day. Due to this criteria, the development of this IOT related technology is seamless where it is easy to implement and will not be a nuisance as IOT will be built on top of the existing infrastructure without the needs to change the existing network architecture and structure [6][7]. By transforming into IOT deployment, developer will be able to evolve machine-to-machine strategies to innovate, drive new customer experiences and increase revenue through more sophisticated customer-facing connected products and services. Furthermore, IOT can help to strengthen customer experience through personalization, smarter payment method and digital signage. All future devices should be included and implemented this IOT technology, and it is expected that the use of IOT applications will be dominant across industries in the future.

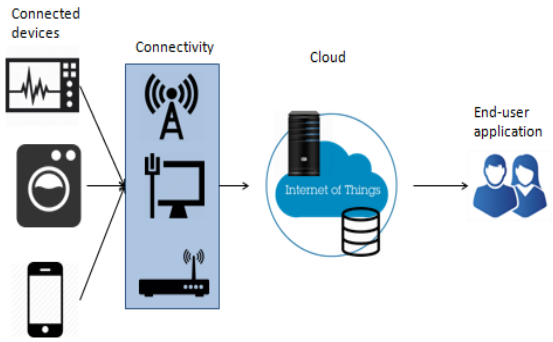


Fig.1. Block diagram of IOT architecture

As can be seen in Fig.1, the remote communication between end-user with devices or devices-to-devices will be performed via network, typically through the internet cloud. Thus, identification with unique address must be implemented on each device to provide an accurate and enable the communication between devices. By implementing unique address to devices, it will allow devices to have tracker characteristics for monitoring and identification. Depending on its application, the designers can choose whether to have a wired or wireless connection to their system. By this means, each connected devices can interact

with each other as long they are connected to the network. In addition, it will allow remote access across existing network infrastructure. Thus, objects that contain embedded hardware technology for communication, sensing or interaction with their internal or external environment can be regarded as IOT [8].

The structure of this thesis consisted of five main sections. Section one is the introduction to related technology which is IOT. The literature review of the technologies and security issues are discussed in the Section two of this thesis. Methodology and design process of vehicle access system is discussed in the section three. In section three, components and hardware details will be shown as a working design. Moreover, results and discussion for the simulation and testing of the project will be illustrated in section four. Last but not least, the conclusion of finding for this project will be constructed in chapter five.

## II. LITERATURE REVIEW

### A. *Vehicle Access System*

Conventional access system required a guard to manually collect the information and monitor the area. Thus, it is required a time and manpower to keep all the records. The proposed vehicle access system will be compared with existing system that is on the market. The review was done from the survey that has been conducted related to this project. The product comparison is presented in the Table I between the proposed system and existing products.

TABLE I. Comparison with the existing system

| **Features** | **MAGNET** | **HALIRA** | **Vehicle Access System Ltd.** | **IOT-Based Vehicle Access System** |
|---|---|---|---|---|
| Long range access | Yes | N/A | N/A | Yes |
| Access medium | RFID | N/A | Biometric/Token | NFC |
| Cloud-based system | No | No | No | Yes |
| Web-based system | No | No | No | Yes |
| Integration with UTM-SMIS | No | No | No | Yes |
| Customizable and upgradable | No | No | No | Yes |
| Supported user | Limited | Limited | Limited | Unlimited |

### B. *Security in IOT*

Most of the security issues in IOT focusing on information transfer, individual privacy and sensor data security. Bing Zhang et al [12], proposed security architecture at Perception, Network and Application Layer. Implemented a light-level cryptographic based on ECC algorithm at perception layer. Moreover, a CPK chip will be embedded for authentication purposes at network layer. The trusted access control is implementing at application layer. However, trusted database is required for authentication purposes at network layer for further protection.

Lan Li [13], states that security issue of IOT is mainly referred to sensor technology. In order to build a secured sensor networks, there is a need to combine multiple security mechanism to develop a complete security framework. However, there is a need for major changes in the devices in order to develop secure devices.

White paper [14], it demonstrates that developing a secure IOT network must be throughout the device lifecycle which is from when the power is applied until it is in operation. However, it is an evolution technique that has been proven successful using state-of-the-art of IT security.

R. Roman et al [15], there are a need to develop powerful devices using highly constrained devices that used low-bandwidth such as 802.15.4. It also required using an optimal cryptography algorithm and adequate key management systems. However, highly constrained devices must enable a secure communication channel with an economical cost and convenient to be used.

In the proposed IOT-based vehicle access system, the researcher focused on the data integrity during information transfer. It is to avoid data corruption or changes due to cyber attack from the outside of the system. Moreover, AES is implemented to improve the overall system security of the system.

## III. VEHICLE ACCESS SYSTEM

The proposed vehicle access system is for managing the parking space at UTM's Chancellery building. It also functioned to collect user information from the access card for reference and static purposes. The system also provides event logging that will be stored in the "in" and "out" vehicle access activities to a cloud database. It will allowed the administrator to view this information from anywhere at any time. The proposed IOT-based vehicle access system is shown in Fig.2.

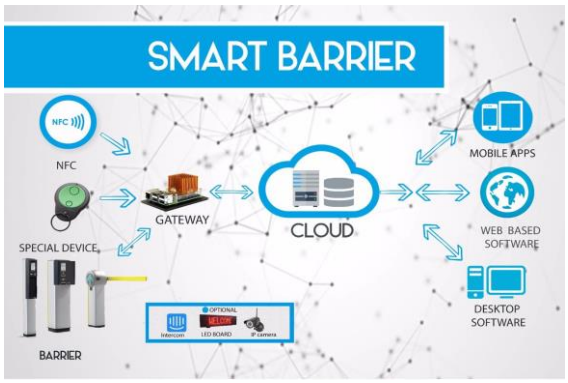


*Fig.2. System model of the system*

The system can be classified into several components such as user's interface, hardware configuration and database. all of these components will be linked with cloud server to enable and

interconnection of the user interface and hardware configuration through database. The details discussion will be shown in the next sub section of this topic.

*1. Graphical User's Interface*

User's interface consists of several static pages that were designed using Hypertext Markup Language (HTML). Moreover, the pages was designed to be a user-friendly and also as an interface to display all information collected and stored in database. Furthermore, there are several languages platform that were used to provide a fully functional user's interface for this system such as PHP and Java Script. Additional languages are used to create dynamic pages that were run as background process but will not be displayed to the users.

*2. Hardware's Configuration*

The configuration of the hardware is focus on interconnecting of the sensor nodes to the gateway device. Each of these nodes will be an input or output of the system. Peripheral units for this configuration would be NFC detector, barrier gate and other additional devices. Furthermore, the Raspberry-pi 3 would need to be programmed to enable certain function as to fulfill its design specification. Then, the gateway device would be able to collect data from the sensor and also pushing it into the cloud database through cloud server.

*3. Database*

Moreover, database can be divided into two different sections which are interconnection between GUI and server and interconnection between The Things and server. The database is used to collect inserted information from GUI and stored into the database. In addition, the GUI will use the database to retrieve certain data and display it to the user.

Another database section is the interconnection between The Things and server. In this section, the database will store all information collected by the sensor via gateway device which is Raspberry-pi 3. In this case, NFC detector will read data in the tagged NFC card and store it into the database through gateway device. The barrier gate will used the stored information in database to give an authorization for the registered user to use the parking area through cloud server.

## *A. Framework*

The IOT framework used in this paper is called IOTWave that was developed by the Advanced Telecommunication Technology (ATT), Universiti Teknologi Malaysia. It consists of three main components which are the Things, the Cloud and the Network as shown in Fig.3. The first component contains the sensor nodes and gateway device. In this part, the information will be collected at the gateway device which focuses on interconnecting sensor and actuator to the Raspberry-Pi. In order to utilize this part, sensors use will be introduce a unique addressing for identification and monitoring purpose of this system.

The second component of this model is the Cloud used to controls the information received which is collected at the Things. It consists of database for information storage and server to provide services including analyzing capabilities of the received data and enterprise services. The Cloud also consists of enterprise services. It will provide user's interface service that allows the administrator to monitor recorded information at anytime and anywhere. In addition, the Cloud also functioned as a link between user's interface (enterprise services) and the Things.

The third component is the Network is used to define the communication protocols and technologies of the proposed system. This component defines the interconnecting between each device in fulfilling the system objective.

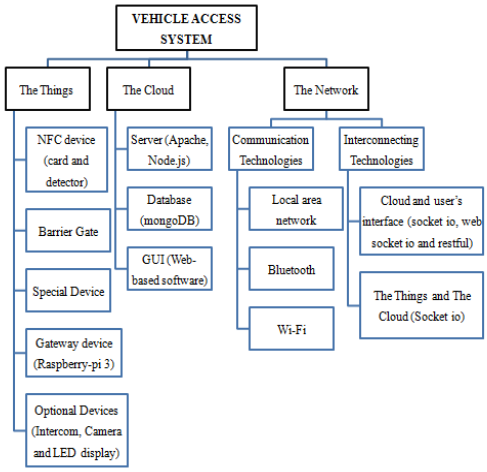


*Fig.3. Framework of the system*

## *B. Installation Location*

The proposed solution is designed to be implemented at UTM Chancellery building. The barrier will be placed at the entry and exit of the Chancellery building to monitor an authorized access to the parking area. Loop detectors are placed before and after the barrier to detect a vehicle arrival and departure from the barrier. Other services that can be implemented in that area are LED billboard display, intercom, camera and etc that can provide better user experience of the proposed system. The design of the location to implement the proposed system is illustrated in Fig.4.

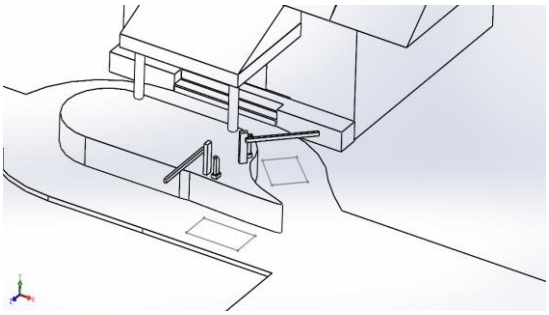

*Fig.4. Location of the system*

## *C. System's Operation*

The operation of the proposed system is shown in Fig.5. As can be seen in this figure, there are three possible scenarios in using this IOT-based vehicle access system which is

registration, entering and exiting. From the system design, the system will provide an access to the authorized user only. The unauthorized user will be taken further action or unable to use the parking space available in that area. Taken action will be taken through intercom and camera or the security will need to take action at the location. In addition, activity of the user will be limited by their authorization level as user, admin or super admin. Any guests that want to use this system are also eligible that requires them to fill all details needed and limited to one-time use only. For the first time user, it is recommended for them to scan their NFC card (IC or UTM matric card) before entering the parking area to avoid contingency of the bad service for the users. This is due to the NFC card number still unavailable for the user to provide identification and future monitoring for security purpose. Thus, it will allow the designer to set up new database for the particular purpose in order to create an innovative and friendly system around the university.

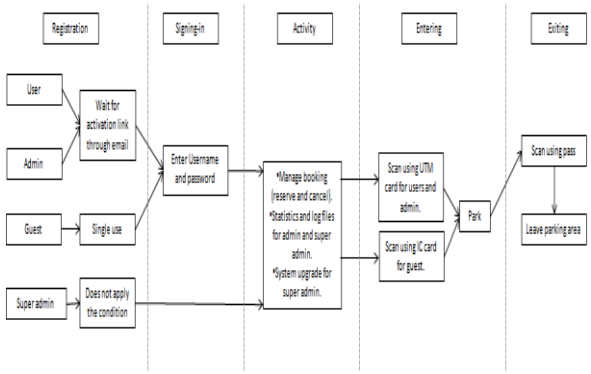


*Fig.5. User's scenario of the system*

### D. Network Security

In this paper, network security is focusing on the reliability of the transmission of information from one terminal to another. It is used to maintain integrity of data by avoiding unauthorized access from the outside into the designed system. However, the system can be further extended by looking into the wireless sensor network technology used to improved overall security performance. As mentioned, AES is the chosen standard that is used for the network security in this system. In addition, AES is the simple algorithm that introduces encryption in the data transfer that will be determine by the block size. Thus, it has higher probability of uniqueness compared to other security standard.

## IV. Results & Discussion

### A. Graphical User's Interface

The process of constructing GUI (enterprise services) is using Dreamweaver as a compiler for the coding. In figures below, it is several pages that have been designed by using HTML coding. It is examples of static pages that provide interface to the user of the system.

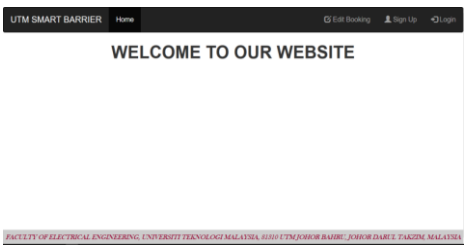


*Fig.6. Main page of GUI*


*Fig.7. Register page of GUI*


*Fig.8. Login page of GUI*

### B. Database

In Fig.9, the database that is created for this system is "BarrierDB" which will be used to accommodate the overall design objective of the system. The data storage known as collection which is "Register" that created to provide data logging of the system. Moreover, it illustrated some of the data that have been inserted through GUI. This data is used by the user to login or booking their parking space.


*Fig.9. Configuration of database using mongoDB*

### C. Network Security Algorithm

Network security introduced an encryption of data from database to gateway device and vice versa. The chosen algorithm for network security is based on Advanced Encryption Standard (AES). Moreover, the standard has been

used to develop different encryption code that can be considered a matured platform. Moreover, AES support larger key sizes which are about 128-bits block size. It is making the standard to be less susceptible on attacks or invasions into the system. In addition, AES is considered to be efficient in both hardware and software in terms of resources consumption. Thus, the level of security introduced by AES is considerably secure to be implemented in the system.

### *D. Web-based Software as Interface*

The implementation of web-based software as interface will be convenience to the users. It is due to the ease of access on any computer with an internet connection. In addition, any computer that run on different operating system such as Mac, Linux and windows would gain an access to the web-based software. However, developed apps need to be installed on the device before it can be used. The device with different operating system might not be able to use the developed apps such as android. Moreover, some of the apps might come in CD or downloaded from internet that need to be paid.

Despite its convenient to be used, web-based software also has some disadvantage which is the tendency of unavailable access due to server is down. It is because the web-based software will be installed into the cloud server with a given IP address. Thus, it will prevent all the users to access the interface when the server is going down. Moreover, web-based software requires higher maintenance cost to sustain the server from going down.

### *E. mongoDB as Server Database*

First of all, the database that was used for this system is MongoDB which is a document oriented database that provide high performance, high availability and easy scalability. In addition, a single MongoDB is able to manage multiple databases at once [16]. Due to that, MongoDB would be an excellence choice over MySQL to manage high data traffic and also faster processing time. Moreover, implementation of IOT-based system will introduce many devices that required faster operation time. Thus, it will cause traffic congestion in the system especially during a peak time.

## V. CONCLUSION

Internet of things is an enabling technology that has been used in a wide range of application such as health, home and industry. This technology is seen as the changer on how devices conventionally operate. With the advancement of this technology, it will lead to the design of an intelligent system in our environment that is able to provide an informed decision making.

In this paper, an IOT-based vehicle system was presented with new features that are not presence in the conventional system. This system is able to collect real-time vehicle access activities logging. Hence, it is provide ubiquitous monitoring to an area. It is designed with a graphical user interface for seamless access to the database for monitoring and control.

In addition, it is well recognized that in IOT, a reliable security algorithm to support high data transfer and also provide a reliable data transmission is of highly important. Therefore, it is necessary to equip the system with security algorithm for a reliable data storage and transmission. Hence, the design of this system also is equipped with AES security algorithm to provide a reliable transmission of data.

## REFERENCES


[1] L. Sun, "*Internet of Things in 2016: 6 Stats Everyone Should Know,"* [Online]. Available: http://www.theinternetofthings.eu/what-is-the-internet-of-things#iotcouncil-contact [Accessed January, 2016]

[2] K. Ashton, "*That "Internet of Things" Thing,"* [Online]. Available: http://www.rfidjournal.com/article/print/4986 [Accessed June, 2009]

[3] G. Arik (2015, January), "*Kevin Ashton Describes "the Internet of Things,"* [Online]. Available: http://www.smithsonianmag.com/innovation/kevin-ashton-describes-the-internet-of-things-180953749/?no-ist [Accessed Jnuary, 2015]

[4] K. Rose, S. Eldridge and L. Chapin, "*The Internet of Things: An Overview*," The Internet Society, Geneva, Switzerland, October, 2015.

[5] Statista, "*Internet of Things (IOT) : number of connected devices worldwide from 2012 to 2020 (in billions),"* [Online]. Available: https://www.statista.com/statistics/471264/IOT-number-of-connected-devices-worldwide/ [Accessed 2016]

[6] M. Andrew,"*2016 Predictions: M2M and IOT to Transform Operations,"* [Online]. Available: http://www.rcrwireless.com/20160105/internet-of-things/2016-predictions-m2m-and-IOT-to-transform-operations-tag2 [Accessed January, 2015]

[7] TechWeekEurope Staff, "*How will The Internet of Things and M2M Change in 2016?,"* [Online]. Available: http://www.techweekeurope.co.uk/networks/m2m/vodafone-m2m-IOT-predictions-2016-182715 [Accessed December, 2015]

[8] G. Tsaramirsis, I. Karamitsos and C. Apostolopoulos, "Smart parking: An IOT application for smart city," *2016 3rd International Conference on Computing for Sustainable Global Development (INDIACom)*, New Delhi, pp. 1412-1416, 2016.

[9] R. Gupta and R. Gupta, "ABC of Internet of Things: Advancements, benefits, challenges, enablers and facilities of IOT," *2016 Symposium on Colossal Data Analysis and Networking (CDAN)*, Indore, pp. 1-5, 2016.

[10] J. Gubbi, R. Buyya and S. Marusic and M. Palaniswami,"*Internet of Things (IOT): A vision, architectural elements and future directions*," Future Generation Computer Systems, 2013, pp. 1645-1660.

[11] Toh Jun Hao, *"IOT-Based Smart Guard Touring System (T-Rec System),"* FYP Thesis, Telecom Lab, UTM, Johor Bahru, Malaysia, 2016.

[12] Bing Zhang, Xin-Xin Ma and Zhi-Quang Qin, "*Security Architecture on the Trusting Internet of Things*", Journal of Electronic Science and Technology, Vol.9 No. 4, 2011, pp. 364-367.

[13] Lan Li, "*Study on Security Architecture in the Internet of Things*", 2012 International Conference on Measurement, Information and Control (MIC), 2012, pp. 374-377.

[14] White Paper, "*Security in the Internet of Things*", Wind River Systems Inc, 2015.

[15] R. Roman, P. Najera and J. Lopez, "Securing the Internet of Things," in *Computer*, vol. 44, no. 9, pp. 51-58, Sept. 2011.

[16] L. Stanescu, M. Brezovan and D.D Burdescu, *"Automatic Mapping of MySQL Databases to NoSQL MongoDB"*, 2016 Federated Conference on Computer Science and Information Systems (FedCSIS), 2016, pp. 837-840.

# Ku-Band Satellite Communication Availability in Malaysia

Muhammad Yusri Mahmud
*Faculty of Electrical Engineering*
*Universiti Teknologi Malaysia*
*Johor Bahru, Malaysia.*
*Muhammadyusry36@gmail.com*

Jafri Din
*Department of Communication Engineering*
*Faculty of Electrical Engineering*
*Universiti Teknologi Malaysia*
*Johor Bahru, Malaysia.*
*jafri@fke.utm.my*

***Abstract*—Malaysia is located at equatorial region, experiences heavy rain intensity. Thus, the usage of satellite for communication system and broadcast services will be significant affected, especially when operating at higher operating frequencies, such as at Ku-band. This paper is aimed investigating the availability of satellite broadcasting at Ku-band frequency using satellite TV receiver. The recorded rain attenuation has been evaluated along with rain intensity database of one-year. The outcome of this paper provide the service provider with the required information to improve the customer satisfaction which will reduce the effect of link outage.**

***Keywords— equatorial region; satellite communication system; ku band; rain attenuation.***

## I. INTRODUCTION

Satellite communication is a communication channel to send information to different place on earth. Basically signal from one place been transfer by the help of satellite communication. In order to ensure good signal strength during transmission, it is crucial to ensure the propagation path from the satellite is free from any obstacle. In a satellite communication, signal from satellite to ground station experience losses due to atmospheric effect, such as rain, cloud and snow[1]. Attenuation due to rain in path contribute to signal loss result in degradation of signal quality and link availability, thus making it an important factor for satellite signal communication design. The degradation in communication is reduction or loss in signal strength during propagates through free space[2]. Determination of attenuation due to rainfall plays a significant role satellite transmission transmitting on higher frequency band above 10 GHz in design of earth-satellite link[1].

Modern satellite communication system are operate at frequencies above 10GHz. This may lead to outages that compromise the availability and service quality, due to heavy rain[3]. This is a critical issue for Malaysia which located in equatorial region and suffering extremely high rainfall rates[4]. The rain attenuation effect always been major issue in satellite link design. The aim of this paper is to study the satellite availability characteristics during rain event and possible effect between different values of rainfall rate and their corresponding values of rain attenuation in equatorial region derived from receive signal and rain gauge data at Johor Bahru, Malaysia.

## II. LITERATURE REVIEW

### A. Rain attenution and satellite availabilty

Rain fade are more often happened during downlink location, because of the signal does have enough power for up conversion it will easy loss during rain, however for uplink for down conversion easier control the power for transmission [5]. The outage of signal are particularly prevalent at frequencies above 10 GHz [6]. Availability can be influenced by several factors. The most caused was the location and the surrounding environment, that might mask part or all of the satellites link path in the sky. In the determination satellite availability often required such an experiment to ensure the effect of rain attenuation that causes losses in communication link. However rain intensity measurement have been performed for many years in many countries hence their data is readily available for many places[1]. Rain attenuation measurement experiment in Johor Bahru have been done using satellite TV and a tipping bucket rain gauge.

### B. Rainfall in Malaysia

Rain is one of the biggest contributions to signal loss in Ku band depending on the rate rainfall. Basically, most of rain attenuation studies in different region will acquire difference value of rain attenuation. This is because different location experiences difference rainfall [7]. Malaysia as a tropical climate, is suffering extremely high rainfall rate throughout the year [9]. Rainfall database at Johor Bahru were taken from the weather station located at Wireless Communication Center (WCC), Universiti Teknologi Malaysia.

### C. Ku-Band difficulties

Satellite TV often operating using Ku-Band system between 12-18 GHz. In this experiment at UTM P18 lab are using Ku-band operating at 12.2 GHz. Furthermore, studies also show that more power for transmitting Ku-band satellites are required compared to similar system at the C band [8]. However, Ku band use smaller dishes between ranging size from 2 to 5 in diameter [7]. Generally, Ku band was used because it could offer more flexibility.

## III. MEASUREMENT SETUP

Measurement system is carried out at rooftop of P18 building, faculty of electrical engineering, Universiti Teknologi Malaysia (UTM) Johor Bahru. The receiver was set up in an open area away for obstacle that could cause attenuation in signal received. Details of the experimental setup can be found in [10]. While the rainfall were recorded through hobo rain gauge, that already been setup at roof-top of P18. The rain rate were measured by using resolution and integration time of the rain gauge is 1 minute and 0.2 mm/tip, respectively. The collected rain tips have been processed according to the procedures described in [11]. The experimental are summarized and shown in Table 1 and Fig. 1, respectively.

Table.1: Satellite, site and antenna specifications[10].

| **Satellite specifications** | | **Site and antenna specifications** | |
|---|---|---|---|
| Satellite | MEASAT-3 | Station location | 103.64˚ E, 1.55˚ N. |
| Satellite position | 91.5˚ E | Antenna elevation | 75.61˚ |
| Frequency | 12.2 GHz | Antenna height a.m.s.l | 50 m |
| Downlink polarization | Vertical | Antenna azimuth angle | 262˚ |
| Satellite EIRP | 58 dBW | Antenna diameter | 90 cm |
| | | Slant path length | 5 km |
| | | Horizontal projection of slant path length | 1.2 km |

Received signal level was collected from MEASAT-3 direct broadcast receiver. The Ku-band signal then been amplify, down converted to 1GHz intermediate by Low noise block (LNB). The down converted signal is subsequently fed to the indoor unit of receiving system. The signal enter 2-way microwave splitter that split the signal into a decoder and a spectrum analyser. Output of spectrum analyser is sent to computer display the received signal strength in the frequency domain interfaces to a personel computer via FSX Record Play software was programmed with every 1s interval to record the received signal and these data were systematically stored according to date.

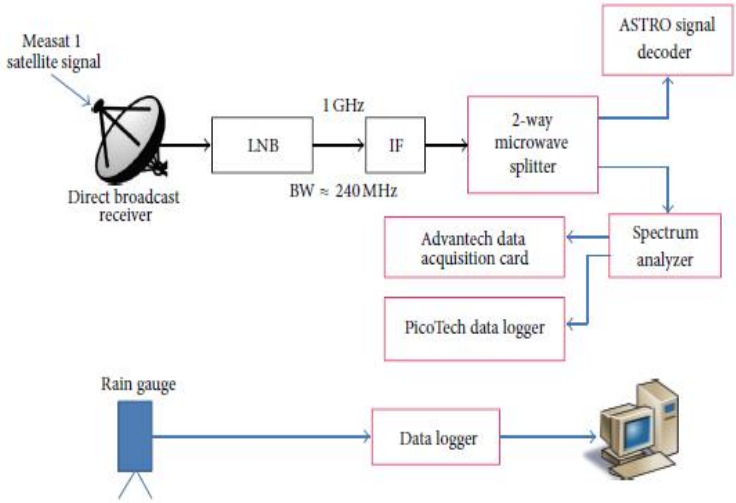


Fig.1; Experimental Setup at UTM to measure receive signal level from MEASAT 3.

## IV. DATA PROCESSING

In order to define the attenuation reference level, there were some issues related are primarily due to the effect of earth atmosphere and their impact on system availability and margin. The atmospheric effects at the millimeter wavelengths are tropospheric scintillation, cloud attenuation, gaseous absorption, and rain attenuation. During raining events, received signal contains two main components occurring concurrently such as rain attenuation and scintillation phenomena[3]. The phenomena demonstrate an additive effect on the satellite signal level variation, filtering with appropriate cut off frequency is an effective technique to separate out the two propagation effects [5].

In this work, one year data of the received signal recorded in 2013 has been used. First, the data has been filtered from atmospheric effect primarily due to scintillation [6]. The dynamic range of the measurable attenuation level is found to be approximately about 40dB.

## V. METHODOLY

An evaluation on the propagation of earth-satellite signal operating at Ku-band is carried out. The receiving signal was collected for 12 months during 18 January 2013 to 17 January 2014 and has already been

processed. The signals from MEASAT 3 satellites downlink was recorded for each 1s in one- year duration. The rain rate data were obtained from hobo rain gauge that recorded rainfall during the experimental duration. Hobo rain gauge using concept of tipping bucket rain gauge of 0.2 mm and was converted to 1 minute interval. Therefore to synchronize with time of attenuation logging system to measure rainfall rate and determines raining events the receiving signal was converted to 1 signal per 60 second. The received signal level and rain rate has been extracted according to month and day in one year period. A plot of minute against rain rate and rain attenuation in dB been plotted. High rain rate considerate has been chosen, as it will produce higher rain attenuation. The experiment carried out which has been used to determine a direct relationship between different values of rainfall rate and their corresponding values of rain attenuation In order to obtain the satellite availability, various values of rain attenuation margin has been chosen between 7dB and 15dB. The setup rain margin were used to find the total downtime of the link that been used to find satellite availability. It is found that, during the recording period, the system experiences very few equipment downtimes.

## VI. RESULT AND DISCUSSION

### *A. Rain event*

In this work, 40 rain events were considered. Based on the chosen precipitation rate, the attenuation may occur during the events categorized as heavy rain, very heavy rain and extreme rain as shown in Table 2, Fig.3, and Fig. 4, respectively.

Table 2.Rainfall categories .

| **Type of rain** | **Precipitation** |
|---|---|
| Very light rain | precipitation rate is < 0.25 mm/hour |
| Light rain | precipitation rate is between 0.25mm/hour and 1.0mm/hour |
| Moderate rain | precipitation rate is between 1.0 mm/hour and 4.0 mm/hour |
| Heavy rain | precipitation rate is between 4.0 mm/hour and 16.0 mm/hour |
| Very heavy rain | precipitation rate is between 16.0 mm/hour and 50 mm/hour |
| Extreme rain | precipitation rate is > 50.0 mm/hour |

The attenuation reference level were first determined. The clear sky level was carefully determined by averaging the samples of 30 minutes before and after a given rain event. The analyzed data consists of 4 heavy rains, 13 very heavy rains and 23 extreme rains. During extreme rain, attenuation could exceed up to 10dB. This could be considered as significant signal degradations phenomena. While, very heavy and heavy rain categories give lower rain attenuation. Based on Fig. 2 and Fig. 3, rain attenuation increases as rainfall rate increases. The attenuation and rain rate time series, shows some inconsistencies . This is due to the point rain rate database used in this study. It is expected that the rain coverage area used in this study, may not be able to be well represented by the point rain rate database. This phenomena is well shown in Fig. 5.

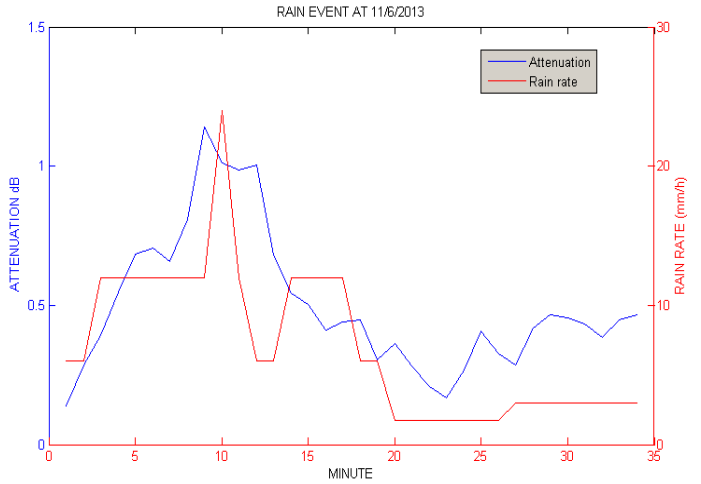


Fig.2 ;Rain event 11/6/2013 (heavy rain) between 4.0 mm/hour and 16.0 mm/hour.

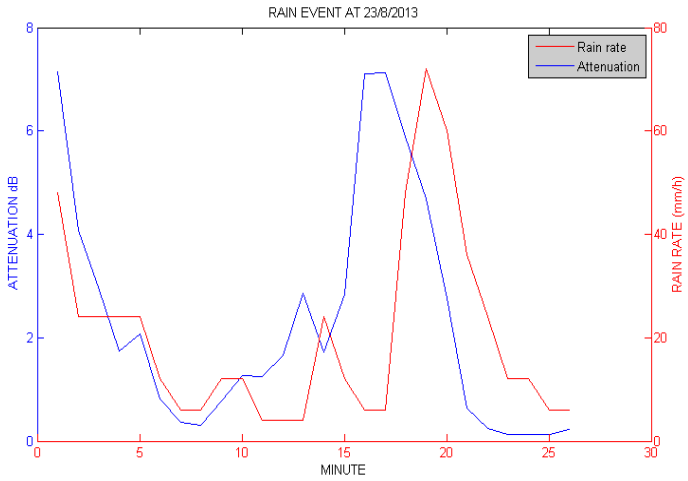


Fig.3; Rain event 23/8/2013 (very heavy rain) is between 16.0 mm/hour and 50 mm/hour.

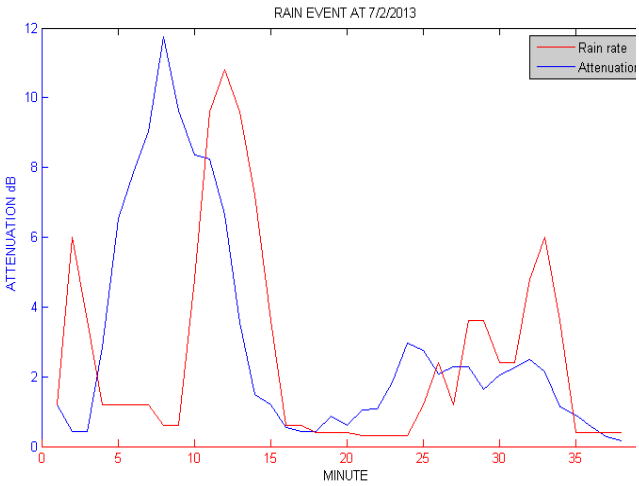


Fig.4; Rain event 7/2/2013 (extreme rain) precipitation rate > 50.0 mm/hour.

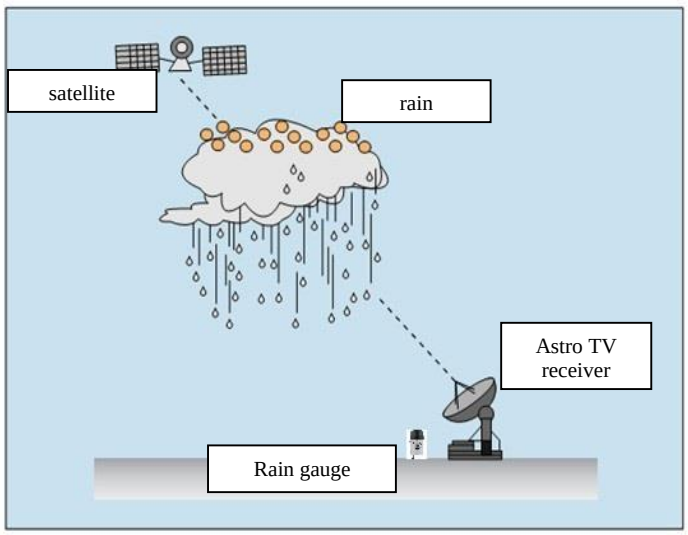


Fig.5; Rain event.

### *B. Availability*

In satellite propagation, it is a custom to offer a service availability of 99.99%. This is equivalent to a downtime of 0.01%. It is found that, the 0.01% downtime for a given year is equivalent to 53 minutes accumulated time period. Based on Table 3, rain margin exceeding 13.5 dB is corresponding to the 99.99% availability.

Table 3.Rain margin, time and availability.

| Rain margin dB | Total period of time(min) | Availability (%) |
|---|---|---|
| 7 | 299 | 99.943 |
| 7.5 | 267 | 99.949 |
| 8 | 237 | 99.955 |
| 8.5 | 196 | 99.963 |
| 9 | 170 | 99.968 |
| 9.5 | 154 | 99.971 |
| 10 | 140 | 99.973 |
| 10.5 | 119 | 99.977 |
| 11 | 105 | 99.980 |
| 11.5 | 93 | 99.982 |
| 12 | 80 | 99.985 |
| 12.5 | 73 | 99.986 |
| 13 | 61 | 99.988 |
| 13.5 | 55 | 99.990 |
| 14 | 42 | 99.992 |
| 14.5 | 34 | 99.994 |
| 15 | 27 | 99.995 |

## VII. CONCLUSIONS

In this paper, a propagation measurement campaign carried out in an equatorial region at Ku-band is presented. The rainfall categories based on rain rate has been adopted. Extreme rain events significantly affected the link performance. Rainfall occurs along the satellite path that not able to be recorded by the rain gauge, limits the study. For future studies, it is recommended to utilize a radar rain map to address this issue. Satellite availability has been analyzed. As the rain margin increases, the availability also increases. Result from this study will help service providers specify rain margin which will reduce the effect of link outage.

## REFERENCES

[1] G. N. Ezeh, N. S. Chukwuneke, N. C. Ogujiofor, and U. H. Diala,"Effects of Rain Attenuation on Satellite Communication Link," vol. 8, no. 22, pp. 1–11, 2014..

[2] A. D. Panagopoulos, P. Arapoglou, and P. G. Cottis, "SatelliteCommunications at Ku, Ka and V-bands : propagation impairments and mitigation techniques," IEEE Communications Survey & Tutorials, vol. 6, no. 3, pp. 2-14, 2004.

[3] M. C. Kestwal, S. Joshi, and L. S. Garia, "Prediction of rain attenuation and impact of rain in wave propagation at microwave frequency for tropical region (Uttarakhand, India)," Int. J. Microw. Sci. Technol., vol. 2014, 2014.K.

[4] M. M. Yunus, J. Din, H. Y. Lam and S. L. Jong, "Estimation of interfade duration for Ku- and Ka-band satellite communication system in equatorial Malaysia," *2016 URSI Asia-Pacific Radio Science Conference (URSI AP-RASC)*, Seoul, 2016, pp. 1967-1970..

[5] L. J. Ippolito, Satellite communications systems engineering: atmospheric effects, satellite link design and system performance. 2008.

[6] ITU-R, "Propagation data and prediction methods required for the design of Earth-space telecommunication systems," Recomm. ITU-R P.618-8, vol. 12, pp. 1–24, 2015.

[7] J. J. H. Ameen, "Rain Effect on Ku-Band Satellite System," vol. 28, pp. 116–124, 2016

[8] Availability. Retrieved from http;//en.wikipedia.org/wiki/Availability

[9] Geography of Malaysia https://en.wikipedia.org/wiki/Geography_of_Malaysia

[10] S. L. Jong, "Rain Fade Dynamics Characteristics for Ku-band Satellite Communication Systems in Malaysia," PhD. Thesis, Fac. Of Electrcial Eng., Universiti Teknologi Malaysia, 2015.

[11] M. D'Amico, S. L. Jong, and C. Riva, "Tipping bucket data processing for propagation application," *Electronics Letters*, vol. 49, no. 8, pp. 569–571, 2013.

[12] M. M. Yunus, J. Din, H. Y. Lam, and S. L. Jong, "Analysis of Inter-fade Intervals at Ku-Band in Heavy Rain Region," no. Rfm, pp. 14–16, 2015.

[13] H. Dao, M. R. Islam, K. Al-Khateeb, and S. Khan, "Preliminary analysis of Ku-band rain fade data for earth-to-satellite path measured in Malaysia," 2011 IEEE 10th Malaysia Int. Conf. Commun. MICC 2011, pp. 93–96, 2011.

[14] ITU-R Recomendation P.837-6, "Characteristics of precipitation for propagation modelling P Series Radiowave propagation," Radiowave Propag., vol. 6, 2012.

[15] J. E. Allnutt and F. Haidara,"Ku-band diurnal fade characteristics and fade event duration data from three, two-year, Earth-space radiometric experiments in equatorial Africa," International Journal of Satellite *Communications*, vol. 18, pp. 161-183, 2000

[16] Karasawa and Matsudo, "Characteristics of fading on low elevation earthspace paths where rain attenuation and scintillation occur concurrently", IEEE Trans. Antennas Propagation,Vol. 39, May 1991

[17] H. Dao, M. R. Islam, and K. A. S. Al-Khateeb, "Rain fade slope model in satellite path based on data measured in heavy rain zone," IEEE Antennas and Wireless Propagation Letters, vol. 12, pp. 50–53, 2013

[18] ITU-R, "Propagation data and prediction methods required for the design of Earth-space telecommunication systems," *Recomm. ITU-R P.618-8*, vol. 12, pp. 1–24, 2015.

# A MIMO Dielectric Resonator Antenna (DRA) for 4G Applications

Siti Salihah Binti Abd Rahim
*Faculty of Electrical Engineering*
*Universiti Teknologi Malaysia*
*Johor Bahru, Malaysia.*
*siti_salihah94@yahoo.com*

Mohd Haizal bin Jamaluddin
*Wireless Communication Centre (WCC)*
*Faculty of Electrical Engineering*
*Universiti Teknologi Malaysia*
*Johor Bahru, Malaysia.*
*haizal@fke.utm.my*

***Abstract*— A multiple-input-multiple-output (MIMO) dielectric resonator antenna (DRA) for 2.6GHz Long Term Evolution (LTE) application is investigated and presented in this article. The shape for the DRA is transform from basic shape that is rectangular to H-shaped DRA. There are two different feed mechanism has been proposed that is aperture coupled and coaxial probe. The DRA has been mounted in FR4 as a substrate. The measured impedance bandwidth for <-10 dB, Port 1 is 26 % (2.22-2.9 GHz) while port 2 is 13 % (2.2 –2.7 GHz). The gain provided for antenna at port 1 is 6.11 dBi and for port 2 is 6.63 dBi. The parameters, isolation and gain of the MIMO dielectric resonator antenna are studied and the result is obtained from the simulation in CST Microwave Studio Suite 2011.**

**Keywords—*dielectric resonator antenna; Multiple input multiple output; Long term evolution; 4G***

## I. INTRODUCTION

Wireless communication nowadays has been part of human life where people can send data information to communicate everywhere and anywhere with the high speed of transmission. Introducing the LTE with high speed of data transmission, data rates, throughput, and spectrum efficiency [1,2] make user's life easy where they can surf internet anytime with happily since it become necessary in our life. The use of devices such as smart phones, laptop and computers become more attractive [3].

Multiple-input–multiple-output (MIMO) technology has been developed to provide excellent channel capacity and high data rates for mobile wireless networks. MIMO is implemented by utilizing multiple antennas at the input and output side of the communication system to exploit multipath fading for improved capacity of the channel, data rates, link reliability, and network coverage. MIMO antenna for LTE is implemented as stated in [4].

Microstrip antennas is much been used in research to implemented MIMO antennas. In [5], an MIMO antennas for LTE and Wi-fi applications is presented with two planar inverted-F antennas (PIFAs) MIMO ferrite antenna is proposed at 720 MHz with isolation −16.4 dB. While in [6], a meander line MIMO antenna for mobile LTE handsets is proposed. The isolation obtained was 12 dB at 800 MHz.

A ceramic material with several attractive features is introduced and placed on top of the antenna radiating element. This antenna is called a dielectric resonator antenna (DRA). DRAs have several benefits for implementation in wireless communication system due to their small size, light weight, high radiation efficiency, small conductive loss, and ease of excitation and fabrication [6]. DRAs also have versatility and simplicity in shape [7]–[9] and feeding mechanisms [10]–[13]. Despite that, DRAs have not received much attention in MIMO technology, especially for LTE applications. A few research works have been reported in [6] and [14], which are based on MIMO DRA with dual polarization. Both of the proposed antennas produced good isolation of above 15 dB. Based on [15], a 700-MHz dual-mode MIMO DRA was proposed for LTE base stations. A compact MIMO antenna for LTE700 is proposed in [6]. The isolation obtained between two antennas is more than 12 dB. In [7], an MIMO rectangular dielectric resonator antenna (RDRA) for LTE applications which is excited using coplanar waveguide (CPW) for Port 1 and coaxial probe for Port 2 is proposed. It isolation is above 20 dB.

In this letter, an MIMO H-shaped dielectric resonator antenna (DRA) at 2.6 GHz is designed and fabricated for LTE applications. By removing several part of the DR, the effective permittivity of the whole volume is reduced and consequently the radiation Q-factor of DR is decreased, and hence it increases the impedance bandwidth (BW) of the proposed DRA [14]. In this article, two elements of such antennas are used for MIMO applications. The proposed structure obtains low mutual coupling and correlation coefficient due to the orthogonal polarization. Two orthogonal modes are excited in this design at port 1 and port 2. The parametric studies, simulated results including the performances of proposed antenna are discussed in the next section.

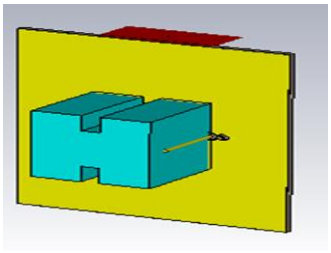

(a)

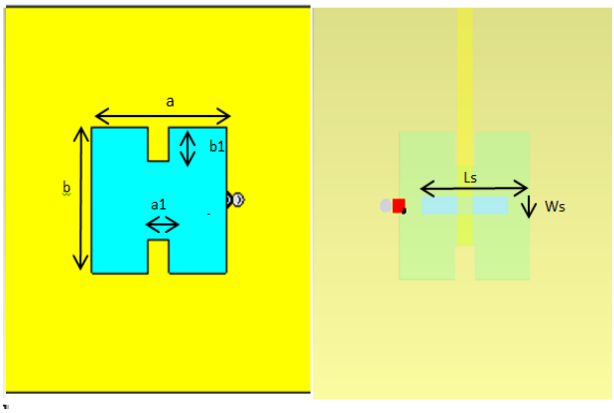


(b) (c)

Fig 1 : An MIMO H-shaped DRA geometry (a) perspective view (b) top view (c) back view.

## II. ANTENNA GEOMETRY

Basically the H shaped DRA is created from rectangular dielectric resonator antenna (RDRA). The design of the DRA is mounted on FR4 as substrate ($\varepsilon_r$=4.3) which has the size of 70 x 60 x 1.6 mm3 (Length x Width x Height ). The basic structure of rectangular DRA with dimension 26 mm x 26 mm x 24 mm is stated as figure 1. Then, the step to make the RDRA become H shaped is as fig.2 (a)-2(c). This step of making is to show the effect of antenna performance when several portions of RDRA with dimensions of a1 x b1 are removed. The selected value for the good impedance matching and isolation (S21) is as stated as a1= 4 mm and b1= 12mm. The result will be discussed in section IV.

Then, the antenna is modified by adding another port to make it MIMO antenna. Coaxial probe is chosen in this project as the second port while the first port is using aperture coupled feeding method. The length slot of aperture couple is Ls= 17mm and the width Ws=2mm. The radius for all the probe is, c1= 1.1mm, c2= 2.4mm, and c3 = 3.0mm. Height of c1, H=18 mm. The input impedance for both ports is 50 ohm.

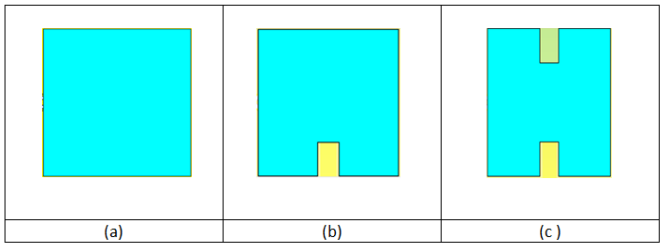


Fig 2. DRA cutting procedures. (a) Rectangular shaped (b) U-shaped and (c) H-Shaped

## III. METHODOLOGY

In this paper, the methodology used to obtain the result is by the software of CST Microwave studio Suite 2011. The result simulation will determine the frequency at 2.6GHz as what the objectives of this project. From the simulations, it will show the gains and the radiation pattern for E-plane and H-plane.

Antennas are used in a vast variety of applications, and thus take come in a vast variety of form factors and radiation mechanisms. The range of simulation methods in CST MWS allows the engineer to choose the best technique for each application. The transient solver could be best for wideband or planar antennas, the frequency domain solver may be more suitable for electrically small antennas. Powerful automated post-processing allows to extract every magnitude of interest for an antenna designer such as nearfield plots, SAR, phase center, directivity or farfield gain for single antennas or arrays - and to process those data further for use in parameter sweeps or optimizations in order to improve the performance of the design.

From the simulation, the result can be compare using the measurement. But in this paper, only one method have been use so that only simulated result is proposed. In this article, the material used for substrate is FR4 with the $\varepsilon_r$=4.3 and the ground plane of copper analead. For DRA, the material use with the permittivity of 10 is proposed.


Fig 3. CST Microwave Studio Suite 2011

## IV. RESULT AND DISCUSSION

Fig.4 show the good result simulations of S-parameters of the proposed antennas. The reflections for both coefficient reflection ($S_{11}$ and $S_{22}$) for both port is below -10dB which accepted in LTE applications [17].

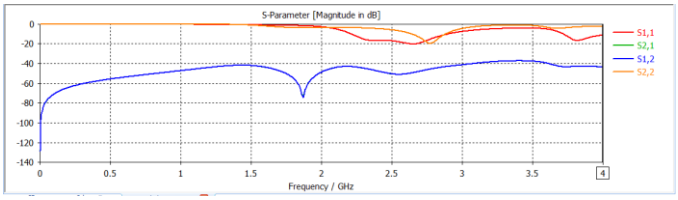


Fig 4. Simulated S-parameters of MIMO H-Shaped DRA

The measured impedance bandwidth for Port 1 is 26 % (2.22-2.9 GHz) while port 2 is 13 % (2.2 –2.7 GHz). The $S_{21}$ between two ports is -40 dB over the operating frequency due to orthogonal polarization.

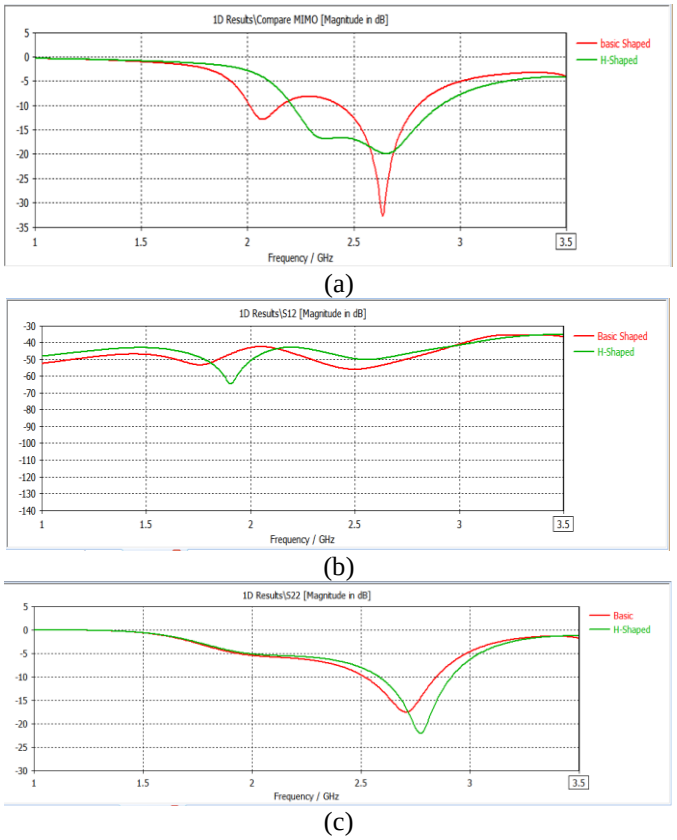


Fig 5. The comparison S-parameters between Basic shaped DRA and H-shaped DRA (a) $S_{11}$ parameters (b) $S_{21}$ parameters and (c) $S_{22}$ parameters.

From Fig 5 show that once the DRA has been cut from rectangular to H shaped, the bandwidth impedance increase from 12 % for basic shaped to 26 % for H shaped DRA.

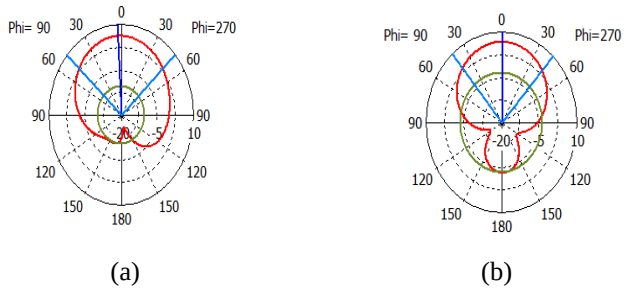


Fig 6. Simulated radiation pattern for directivity for both ports (a) Directivity for port 1 (b) Directivity for port 2

From the Fig 6, it shows that for port 1, the directivity is 6.11 dBi while for port 2 the directivity is 6.63 dBi. To get more information from this project, the radiation pattern for E-fields and H-fields are also stated as in Fig 7 and Fig 8.

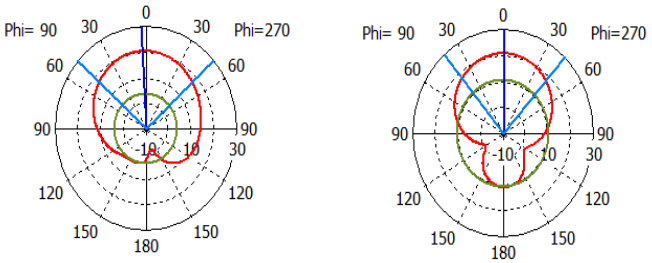


Fig 7. Radiation pattern for E-field for both ports (a) E- field for port 1 and (b) E-field for port 2

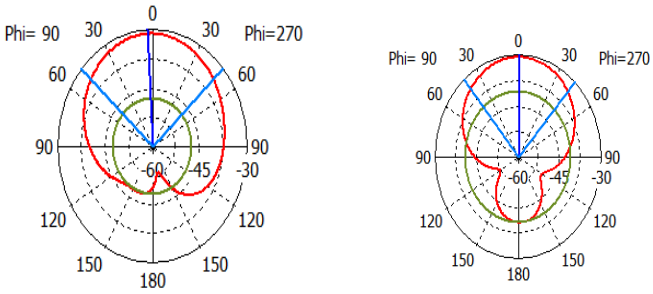


Fig 8. Radiation pattern for H-field for both ports (a) E- field for port 1 and (b) E-field for port

Fig 7 and 8 shows the simulated of E-plane and H-plane radiation pattern for both ports at 2.6 GHz. It can be seen that

simulated of the E-plane how the bidirectional pattern and for H-plane it nearly show to Omni-directional pattern.

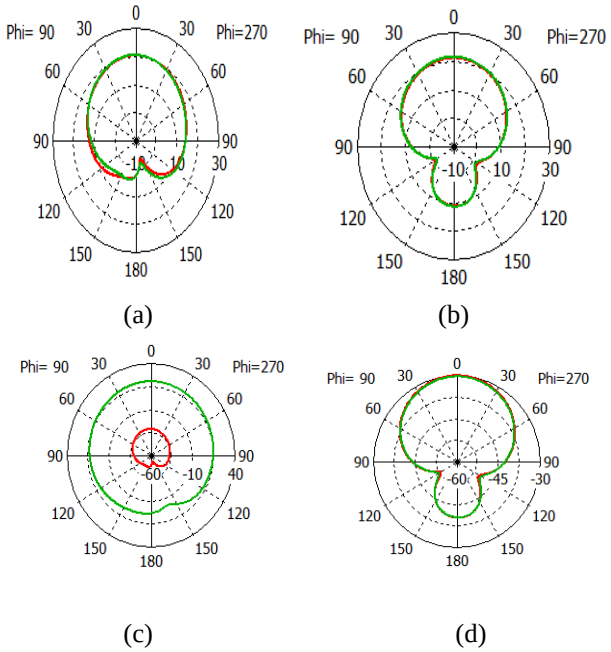


Fig 9. The comparison of radiation pattern for basic shaped and H-shaped. (a) and (b) E-fields for port 1 and port 2 respectively, (c) and (d) H-fields for port 1 and port 2 respectively.

From the picture above that is Fig 9, it show that for both shaped there is not much different and it can be said that they both have a good agreement.

## V. CONCLUSION

A MIMO H-shaped DRA for 4G applications is presented in this article. The H-shaped DRA was mounted on FR4 substrate in orthogonal polarization to obtained low mutual coupling and correlation coefficient. The antenna has a broadside and unidirectional radiation pattern, with reasonable gain for both antennas at the operating frequency. S11 < −10dB are 26 % (2.22-2.9 GHz) while port 2 is 13 % (2.2 –2.7 GHz). The gain provided for antenna at port 1 is 6.11 dBi and for port 2 is 6.63 dBi. Moreover, the presented results show that the proposed antenna is reasonable, efficient, and provides satisfactory performances for LTE applications. This research can be extended by reducing the height of the through.

## REFERENCES

[1] J. Lee, Y. Hong, S. Bae, G.S. Abo, W. Seong, and G. Kim, Miniature long-term evolution (LTE) MIMO ferrite antenna, IEEE Antennas Wireless Propag Lett **10** (2011), 603–606.

[2] H.S. Wong, M.T. Islam, and S. Kibria, Design and optimization of LTE 1800 MIMO antenna, Sci World J 2014, 1–10

[3] J.Lu and Z. Lin, Planar compact LTE/WWAN monopole antenna for tablet computer application, IEEE Antennas Wirel Propag Lett 12 (2013), 147–150.

[4] G.T. Jeong, S. Choi, K. Lee, and W.S. Kim, Low-profile dual-wideband MIMO antenna with low ECC for LTE and Wi-Fi applications, Int J Antennas Propag (2014), 1–6

[5] M.S. Sharawi, S.S. Iqbal, and Y.S. Faouri, An 800MHz 2 × 1 compact MIMO antenna system for LTE handsets, IEEE Trans Antennas Propag 59 (2011), 3128–3131

[6] H. Bae, F.J. Harackiewicz, M. Park, T. Kim, N. Kim, D. Kim, and B. Lee, Compact mobile handset MIMO antenna for LTE700 applications, *Microwave Opt Technol Lett* **52** (2010), 2419–2422.

[7] S.F. Roslan, M.R. Kamarudin, M. Khalily, and M.H. Jamaluddin, An MIMO rectangular dielectric resonator antenna for 4G applications, IEEE Antennas Wireless Propag Lett 13 (2014), 321–324.

[8] R.K. Chaudhary, R. Kumar, and K.V. Srivastava, Wideband ring dielectric resonator antenna with annular-shaped microstrip feed, IEEE Antennas Wireless Propag Lett 12 (2013), 595–598.

[9] R. Chair, A.A. Kishk, K.F. Lee, and C.E. Smith, Wideband flipped staired pyramid dielectric resonator antennas, Electron Lett 40 (2004), 13–14.

[10] M. Abedian, S.K.A. Rahim, and M. Khalily, Two-segments compact dielectric resonator antenna for UWB application, IEEE Antennas Wireless Propag Lett 11 (2012), 1533–1536.

[11] E.K.I. Hamad and H.A. Atallah, Bandwidth improvement of compact high permittivity RDRA using parasitic conducting strips, In: 6th European Conference on Antennas and propagation, Prague, 2012, pp. 5–8.

[12] A. Buerkle, K. Srabandi, and H. Mosallaei, “Compact slot and dielectric resonator antenna with dual-resonance, broadband characteristics,” IEEE Trans. Antennas Propag., vol. 53, no. 3, pp. 1020–1027, Mar. 2005

[13] T. A. Denidni and Z. Weng, “Hybrid ultrawideband dielectric resonator antenna and band-notched designs,” Microw., Antennas Propag., vol.5, no. 4, pp. 450–458, 2011.

[14] L. Zou, D. Abbott, and C. Fumeaux, “Omnidirectional cylindrical dielectric resonator antenna with dual polarization,” IEEE Antennas

[15] Wireless Propag. Lett., vol. 11, pp. 515–518, 2012.

[16] J.-B. Yan and J. T. Bernhard, “Design of a MIMO dielectric resonatorantenna for LTE femtocell base stations,” IEEE Trans. Antennas Propag., vol. 60, no. 2, pp. 438–444, Feb. 2012.

[17] P. Rezaei, M. Hakkak, and K. Forooraghi, “Design of wide-band dielectric

# Development of an Economical and High Sensitivity Fiber Optic Displacement Sensor

Muhammad Shafiq Bin Omar
*Faculty of Electrical Engineering*
*Universiti Teknologi Malaysia*
*Johor Bahru, Malaysia.*
*muhammadshafiqomar@gmail.com*

Nor Hafizah Ngajikin
*Department of Communication Engineering*
*Faculty of Electrical Engineering*
*Universiti Teknologi Malaysia*
*Johor Bahru, Malaysia.*
*nhafizah@fke.utm.my*

***Abstract*—This paper presents an improved sensor head configuration in order to increase the sensitivity of an economical fiber optic displacement sensor (FODS). FODS with single receiving fiber and multiple fiber configuration has been developed and characterize at millimeter distance. Both of the configuration used high power LED as light source and the sensor output is analyze from 0 mm to 13 mm displacement. The outcome of the research showed that the single receiving fiber configuration could detect displacement at 1.43 mV/cm sensitivity at 1.4 mm sensing range. However, multiple receiving fiber configuration could detect displacement at 5.38 mV/cm sensitivity at 2.6 mm sensing range. It showed that the sensitivity of reflective FODS can be enhanced by improving the sensor head configuration.**

***Keywords—fiber optic displacement sensor, intensity based sensor, fiber bundle***

## I. INTRODUCTION

Displacement sensor is an important device in industry that used for inspection, measurement, position detection and control application. Typical displacement sensor is work on capacitive, inductive, magnetic and eddy current concept [1]-[2]. Recently, displacement sensor based on optical technology has drawn increasing attention from industry and researcher since it has better performance in term of resolution, sensitivity, response time, range, size, weight and electromagnetic interference (EMI) immunity[3]. Fiber optic displacement sensor (FODS) are commonly classified into intensity based sensor (IBS) and phase-interferometry based sensor (PIBS). IBS offer better performance but it is a complex and expensive system [4]-[5]. IBS can be classified into two categories, microbend and reflective FODS.

In evaluating the reflective FODS, sensor's sensitivty has been analyzed. Sensitivity is defined as a change in sensor output, in term of refelected power or wavelegth peak, per unit change in displacement of target object [6]. High sensitivity reflective FODS can be achieved by improving the sensor head configuration. There are may type of sensor head configuration that have been proposed and developed for past few years. The first reflective FODS was introduced by W. E. Frank [7]-[8]. It has the simplest sensor head configuration which consist of one receiving fiber and one transmitting fiber as shown in Figure 1(a). Figure 1(b) shows the output for sensor developed by Frank. Distance of the sensor head and target object can be measure from the front slope region or back slope region (BC). Then, the sensor is improve by Jianli Zheng in 1998 by increasing the number of receiving fiber to develop a self-referenced reflective intensity modulated FODS [8]. Zheng improve the system by using both of the slope in order to increase the sensing range. Sensitivity of Frank and Zheng proposed sensor still can be improve since both of the sensor collect a small portion of reflected light.

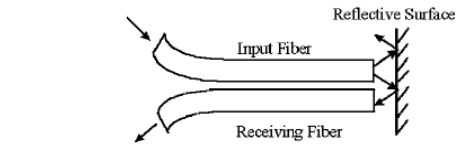


(a)

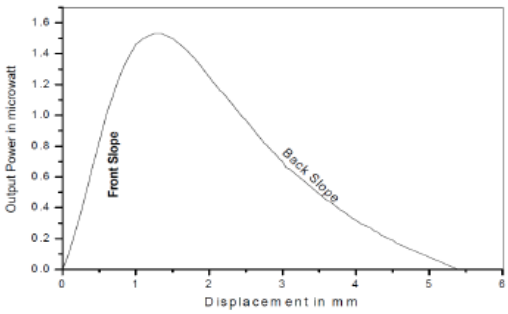


(b)

**Fig. 1** (a) W. E. Frank two-fiber displacement sensor configuration [8] (b) Two-fiber displacement sensor output

In 2015, Daing Hanum developed FODS for industrial application [9]. In the research, the FODS sensor are used to measure the concentration of Hydrocarbon, an organic water pollution. The sensor probe contain bundle of fiber optic that have two parts, one transmitting fiber and multiple receiving fiber. Receiving fibers are locate around the transmitting fiber However, Daing Hanum proposed sensor is expensive since she used Helium-Neon laser as light source. Therefore, in this paper, an economical and high sensitivity displacement sensor has been developed based on Daing Hanum sensor head configuration in [9] and light emitting diodie (LED) as light source.

## II. Receiving Fiber Position Using Snell's Law

In reflective FODS, the receiving channel position is change as the distance of the reflective surface change. Figure 2 shows the basic configuration of the reflective FODS. The equation of receiving fiber position in term of reflective surface distance can be obtain by using maximum launching angle and trigonometry formula.

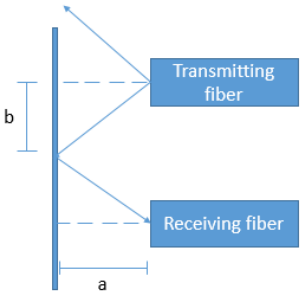


**Fig. 2** Basic configuration of the reflective FODS

Maximum launching angle of multimode fiber with 1.49 core refractive index and 1.46 cladding refractive index is given by

$$\theta max = sin^{-1}({n_1}^2 - {n_2}^2)^{1/2})$$
$$\theta max = sin^{-1}(1.49^2 - 1.46^2)^{1/2}$$
$$\theta max = 17.3° \quad (1)$$

Applying equation (1), the receiving fiber position can be expressed as

$$b = a \tan \theta max = a \tan(17.3°)$$
$$Receiving\ fiber\ position = c = 2a \tan(17.3°) \quad (2)$$

To obtain the relationship between receiving fiber and reflective surface distance, equation in (2) simulated using MATLAB. The distance of the reflective surface, $a$ is set from 0.1 mm to 5 mm.

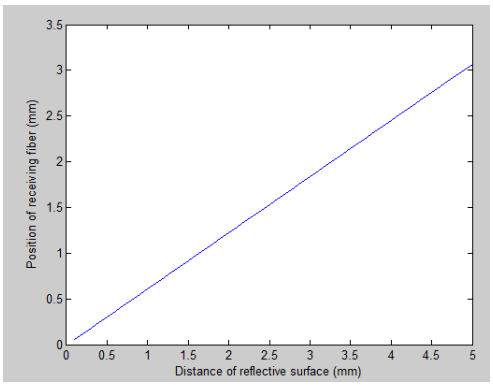


**Fig. 3** Relationship between receiving fiber and reflective surface distance

Figure 3 shows the outcome of the simulation. The graph shows that as the distance of the reflective surface increase, the position of the receiving fiber also increase.

## III. Experimental Setup

Before developing the proposed displacement sensor, several experiment has been carried out to determine the compatibility of component involved.

### A. Light Source Characterization

In this study, common low power LED with four different colour and high power led is characterized in term of wavelength, photon count and photodiode output voltage in order to determine the most suitable light source for displacement sensor application. For common LED, four different colour has been characterized which is blue, orange, white and green. Each of it is connected with 51 ohm resistor and 3 V power supply. For high power LED, only white colour is characterize and connected directly to 3.7 V and 0.68 A power supply. A Thorlab FDS 100 photodiode used to measure voltage that represent light intensity of LED with 1 mm air gap while wavelength and photon count is measured using optical spectrometer with 0 mm air gap.

### B. Fiber Characterization

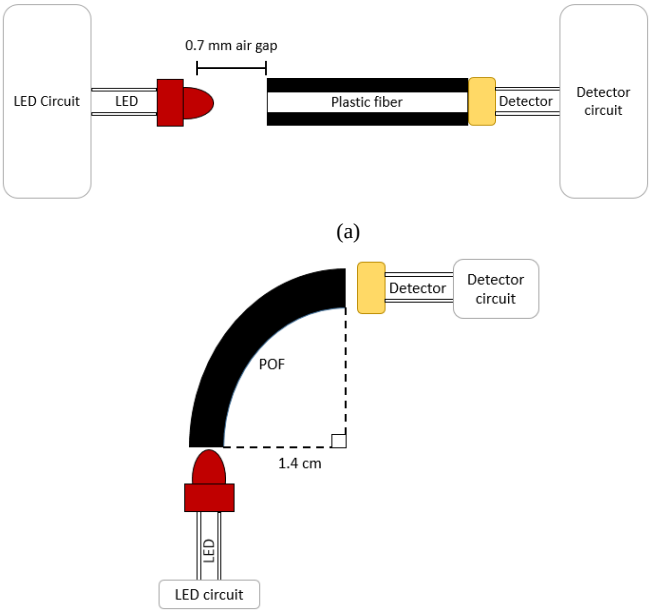


**Fig. 4** (a) Fiber length characterization setup (b) Bending loss analysis setup

Before develop the proposed displacement sensor, plastic optical fiber (POF) with 1 mm of core and cladding diameter in term of length and bending loss. POF is connected to high power LED with 0.7 mm air gap due to large amount of heat dissipate by light source. At the other end of POF is FDS 100 photodiode with 0 mm air gap. Photodiode voltage is measured for five different length of POF, from 6 cm to 10 cm with 1 cm increment. In bending loss analysis, each fiber is bend to 90° with 2.8 cm bend diameter. Both of the fiber characterization setup is illustrated in Figure 4. Then, the bending loss is calculated using

$$L = 20\log(\frac{v_1}{v_2}) \quad (3)$$

The average bending loss is given by

$$L_{ave} = \frac{L_1 + L_2 + .. L_n}{n} \quad (4)$$

### C. Sensor Characterization

There are two reflective FODS has been developed for this research which is ODS 1 and ODS 2. ODS 1 is reflective FODS based on Frank sensor head configuration in [7] while ODS 2 is the proposed sensor based on Daing Hanum sensor head configuration in [9]. Figure 5 shows the ODS 2 configuration. For both sensor, high power LED is used as light source and connected to the fiber with 0.7 mm air gap. Power supply for LED is set to 3.7 V and 0.68 A. The length of transmitting and receiving fiber is 6 cm and 3 cm respectively. Thin gold film is used as target object or reflective surface.

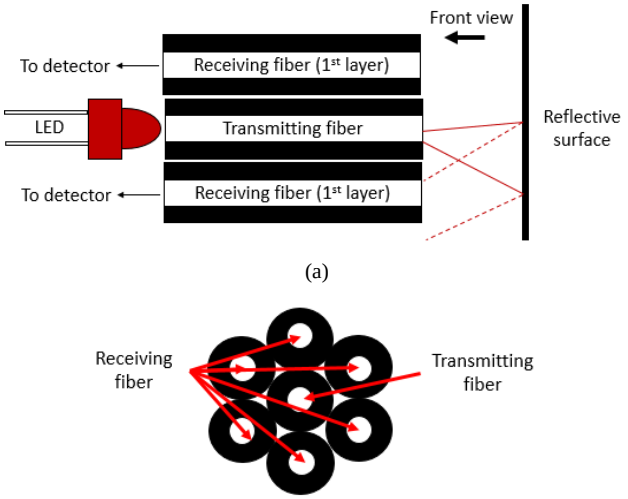


**Fig. 5** (a) ODS 2 configuration (b) ODS 2 sensor head from front view

Both of the sensor is characterize in term of distance between sensor head and target object. Initial distance between sensor head and gold film is set to 0 mm and increase to 13 mm with 0.1 mm increment. The reflected light intensity that pass through the receiving fiber or photodiode output voltage, *V* represent the distance between the sensor head and target object, *d*. Sensitivity of both sensor is given by

$$S = \frac{\Delta V}{\Delta \mathrm{d}} \quad (5)$$

## IV. Result And Discussion

### A. Light source characterization

Table 1 shows photodiode generated voltage for different LED. High power LED has highest output voltage compare to low power LED which is 10.8 V. The optical spectrometer output for all LED is shown in Figure 6. For low power light source, white LED has broad spectral bandwidth which is 154 nm while blue, green and orange LED has narrow spectral bandwidth which is 22 nm, 14 nm and 16 nm respectively. Besides, green LED has the lowest intensity which is 1821 photon count while white LED generate the highest light intensity which is 15630 photon count. For high power LED, it has broadest spectral bandwidth and largest photon count compare to other LED both of the value is unidentified due to spectrometer limitation.

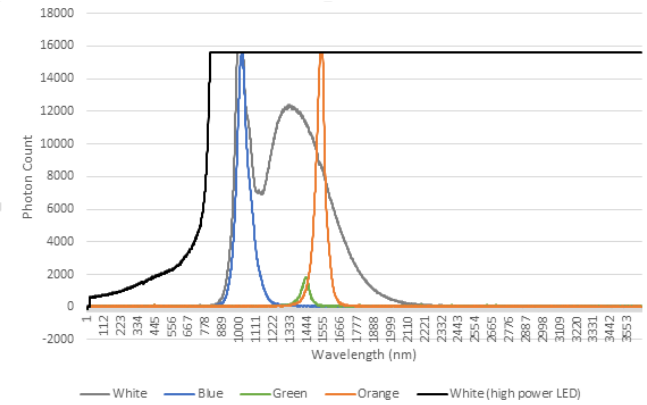


**Fig. 6** Spectrometer output

Data collected from spectrometer and photodiode shows that the output voltage in is depend on the area under the wavelength vs photon count curve. Since high power LED has very broad bandwidth and large photon count, more voltage is generated at the photodiode output. In optical displacement sensor, sensitivity is defined as change in the sensor output per unit change in displacement of target object. Therefore, high power LED is used for the proposed sensor to obtain high sensor output. Besides, narrow band light source is more suitable to use in other application that required to detect certain substances at specific wavelength, such as hydrocarbon sensor that proposed in [21] used 633 nm laser as light source at due to high absorption of hydrocarbon within the wavelength.

TABLE 1
PHOTODIODE OUTPUT VOLTAGE FOR DIFFERENT LED

| Type of LED | LED colour | Photodiode voltage (V) |
|---|---|---|
| Low power LED | Blue | 87 |
| | White | 301 |
| | Orange | 7 |
| | Green | 59 |
| High power LED | White | 10800 |

### B. Fiber characterization

POF characterization in term of length and bending loss is summarize in Table 2. The average voltage difference as the length increase is 22mV and the average loss is 0.425 dB. For bending loss, the average loss due to constant bend is 0.776 dB. Both result indicate that POF is acceptable to use since the maximum fiber length and maximum bending angle for the proposed sensor is 6 cm and 40° respectively.

TABLE 2
FIBER CHARACTERIZATION IN TERM OF LENGTH AND BENDING LOSS

| Fiber length (cm) | Voltage (mV) | Voltage due to bend (mV) |
|---|---|---|
| 6 | 498 | 471 |
| 7 | 481 | 439 |
| 8 | 451 | 433 |
| 9 | 408 | 361 |
| 10 | 407 | 352 |

### C. *Sensor Characterization*

As mention before, there are two reflective FODS has been developed for this research which is ODS 1 and ODS 2. Figure 7(a) shows the sensor output for ODS 1. The maximum sensor output generate by ODS 1 is 3 mV. From the output curve, there are 3 linear region with difference sensitivity and sensing range that can be used to measure displacement. The front slope sensitivity is 1.43 mV/cm, highest compare to other slope. However, it has shortest sensing range from 1 mm to 2.4 mm. The middle slope has worst sensitivity and medium sensing range compare to other slope which is 0.23 mV/cm and 2.4 mm to 6.8 mm respectively. Back slope has the best sensing range, it able to measure displacement from 6.8 mm to 13 mm. However, back slope has poor sensitivity compare to the front slope which is 0.32 mV/cm.

Figure 7(b) shows the ODS 2 output curve. The maximum sensor output generate by ODS 2 is 15 mV, 5 times larger compare to ODS 1. ODS 2 output consist of two linear curve that can be used to measure displacement which is front slope and back slope. Both of the slope has its own advantages. The front slope has the best sensitivity which is 5.38 mV/cm while back slope sensitivity is 1.36 mV/cm. However, the back slope has the best sensing range compare which is 8.1 mm while front slope sensing range is only 2.6 mm.

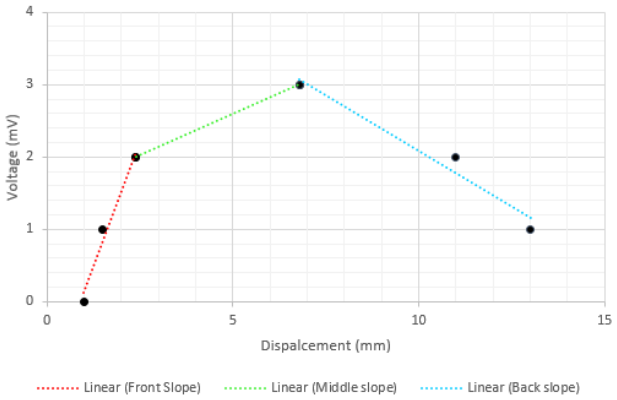


(a)

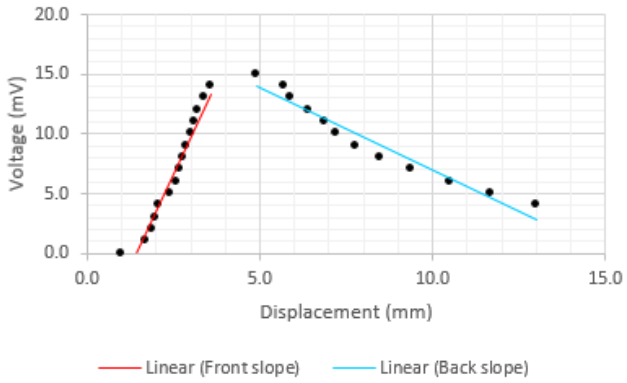


(b)

**Fig. 7** Sensor output (a) ODS 1 (b) ODS 2

Data collected from both ODS 1 and ODS 2 indicate that the sensitivity of reflective FODS can be improve by increasing the number of receiving fiber. As mention before, sensitivity is change in sensor output per unit change in displacement. ODS 2 front slope sensitivity is higher than ODS 1 because it has more receiving fiber that allow more reflected light receive by photodiode. Since ODS 1 has only single receiving fiber, the photodiode only measure small portion of reflected light. Therefore, even though laser FODS can offer better performance, the result obtained from sensor characterization shows that the ODS 2 is acceptable to use in the industry that required displacement sensor with low sensitivity and cost effectiveness.

## V. CONCLUSION

Economical reflective FODS with multiple receiving fiber is developed and presented in this paper. The developed sensor output is analyze from 0 mm to 13 mm of displacement and compared with a two fiber displacement sensor using the same light source and detector. From the experiment, FODS with multiple receiving fiber with sensitivity of 5.38 mV/cm and 2.6 mm sensing range is obtained. The application for this sensor configuration is targeted for application that require millimeter displacement and less precise equipment. The application of this FODS can be extended to wide range of application since it is immune to EMI and easy to implement.

## REFERENCES

[1] Chaurasiya H. Recent Trends of Measurement and Development of Vibration Sensors. International Journal of Computer Science Issues (IJCSI). 2012; 9(4). J. Clerk Maxwell, A Treatise on Electricity and Magnetism, 3rd ed., vol. 2. Oxford: Clarendon, 1892, pp.68-73.

[2] Santoso DR. A Simple Instrumentation System for Large Structure Vibration Monitoring. Indonesian Journal Of Elektrical Engineering. 2010; 8(3): 265-74.K. Elissa, "Title of paper if known," unpublished.

[3] Senior, J. M. Optical fiber communications: Principles and practice, 1985Y. Yorozu, M. Hirano, K. Oka, and Y. Tagawa, "Electron spectroscopy studies on magneto-optical media and plastic substrate interface," IEEE Transl. J. Magn. Japan, vol. 2, pp. 740-741, August 1987 [Digests 9th Annual Conf. Magnetics Japan, p. 301, 1982].

[4] G. Berkovic and E. Shafir. Optical methods for distance and displacement measurements. *Adv. Opt. Photon*, 2012. 4(4): 441–471.

[5] M. Życzkowski et al. Interferometric fiber optics based sensor for monitoring of the heart activity. *Acta Physica Polonica A*, 2011. 120(4): 782 –784

[6] N. Izzati Ismail and N. Hafizah Ngajikin. Development of fiber-based siglemode-multimode fiber with micro convex lens displacement sensor. Universiti Teknologi Malaysia. 2016

[7] W. E. Frank. Detection and measurement device having a small flexible fiber transmission line. U.S. Patent No. 3,273,447.

[8] J. Zheng and S. Albin. Self-referenced reflective intensity modulated fiber optic displacement sensor. *Opt. Eng*, 1999. 38 (2): 227–232.

[9] D. H. A. Munap, N. Bidin, S. Islam, M. Abdullah, and F. M. Marsin. Fiber optic displacement sensor for industrial applications. *IEEE Sensors J.*, May 2015. 15(9): 4882–4887.

# Wireless Power Bank

Anas Asyraf Lokmanulhakim
*Faculty of Electrical Engineering*
*Universiti Teknologi Malysia,*
*Johor Bahru, Malaysia*
Anasasyraf07@gmail.com

Chee Yen Leow
*Faculty of Electrical Engineering*
*Universiti Teknologi Malysia,*
*Johor Bahru, Malaysia*
bruceleow@fke.utm.my

***Abstract*—Conventional power bank requires cable connection to a mobile device for charging. The use of cable can be inconvenient. This paper proposes a wireless power bank using near field charging technique. Specifically, the system uses the inductive coupling between the wireless power bank and the mobile device to enable near-field wireless charging. The design follows the Wireless Power Consortium (WPC) Qi specification 1.2.2 and operating in the WPC compliant mode. The system requires a transmitter circuit and a transmitter coil at the power bank, and also receiver coil and receiver circuit at the target mobile device. The system is tested and analyzed for the end result. The highest output of the project is 1.19 watt where the receiver is allocated at the center of the transmitter.**

***#Keywords—Wireless charge; Portable wireless charge;***

## I. INTRODUCTION

Nowadays, charging mobile phone using AC supply or portable charging becomes an everyday routine. When travelling, power bank is preferred as a power source to charge a mobile device. Power bank requires a USB cable connection to charge a device. Common problem using a USB cable is that user has to align the cable connector with the charging port on the mobile phone before a connection can be made and the cable can be easily tangled. This has become a daunting task, especially for the elderly.

The wireless charging system is a promising solution for the above mentioned problem. Although wireless charging products exist, but there are shortcomings. Firstly, existing products are not portable as they require AC source from the power outlet. Secondly, the price of wireless charging is still quite expensive for the user, especially for the middle class.

The main objective of this paper is to develop a wireless power bank using inductive coupling which met the WPC specification. Based on the principle of electromagnetic, when the AC supply flowing through the transmitter coil, a time varying magnetic field is generated. When the receiver coil is placed in close proximity with the transmitter coil, the magnetic field induces an electric current through the receiver coil [1] [4].

The inductive coupling technique is a near field wireless charging method which operates at several hundred kHz during transfer the power. The small range of frequency limits the distance of power transfer to about several centimetres only [2]. This technique is easy to implement and produces high output efficiency [5]. Therefore, WPC has been formed to standardize this technology and its Qi charging standard is widely used in wireless charger for mobile devices.

The scope of the project is to design and develop a wireless power bank and to analyze the power transfer efficiency of the proposed system. The proposed wireless power bank uses DC as a power source and produces a 5V and 246 mA charging output.

## II. METHODOLOGY

### A. System Design

The IDT P9038 wireless power transmitter IC is selected as the main component at the transmitter. This IC operate 5V DC supply conforming to WPC-compliant mode and the integrated full bridge inverter supports until 8W power transfer. It has several protection features such as resistor programmable foreign object detection (FOD), built in over-current protection, and programmable over-voltage or over temperature protection.

The IDT P9025AC Qi compliant wireless power receiver IC is selected as the main component at the receiver. It operates with an AC power signal from the receiver coil and converts it into a regulated 5.3V output voltage. The receiver includes a high efficiency Synchronous Full Bridge Rectifier and 5.3V regulated output.

The transmitter coil in this project is WE 760308111. The coil has a low value of inductance, 6.3µH and operate at, 125kHz. The receiver coil used in this project is WE WPCC 760308103202 with a high Q-factor of 33. The size of the transmitter coil is larger than the receiver coil in order to reduce the misalignment issue.

The dimension of the transmitter and receiver are shown in Fig.1 and Fig.2 respectively.

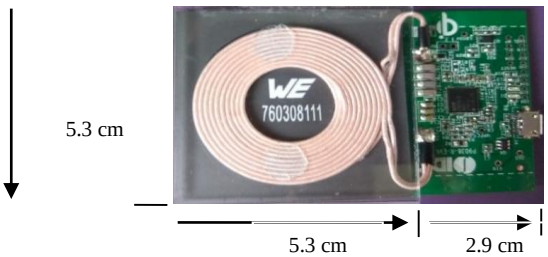


Fig. 1: Transmitter coil dimension

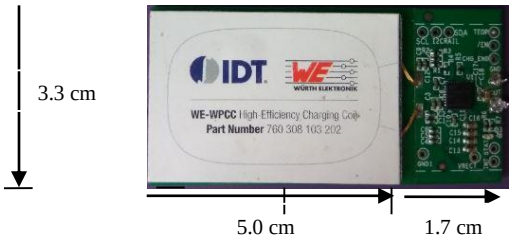


Fig. 2: Receiver dimension

### *B. Experiment Design*

An experiment is conducted to study the efficiency of the proposed wireless power bank. There are four scenarios considered in the experiment, i.e. starting position, separation distance, horizontal and vertical misalignment. The current and voltage are measured for each scenario in a 60 second time frame. For each scenario, three measurements will be taken and averaged to produce a final output. This step is repeated for each scenario. Since the output current expected is DC, so the first 10 second will be considered as transient stage before the steady state current is reached. The 60 seconds duration will be started after the first 10 seconds of transient current.

i) Starting Position

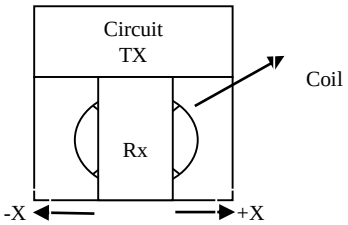


Fig. 3: Starting position

The first scenario is to define the best starting position where the highest output current and voltage can be obtained.

ii) Separation distance

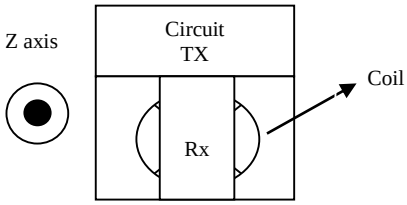


Fig. 4: Height of Receiver along Z-axis

For this scenario, both coils are aligned to the best starting position defined in the previous subsection. The received current is measured at various separation distances along the Z axis. It is important to make sure the transmitter and receiver coils are aligned. The separation distance is increased from 0.1 cm to the maximum height (before disconnection) and all the results are recorded.

iii) Horizontal Misaligment: Movement of receiver along X-axis

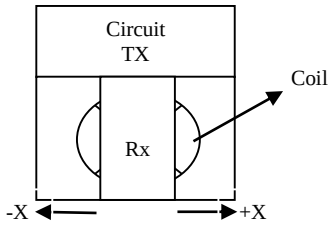


Fig. 5: Movement of receiver along X-axis

The best starting position mentioned in previous subsection II-B-I, will be the reference position. From the starting position the receiver moves along +X-axis in the step size of 0.1 cm. This step is repeated in the reverse direction, -X-axis. The changes of current and voltage for each position are recorded.

iv) Vertical Misalignment: Movement of receiver along Y-axis

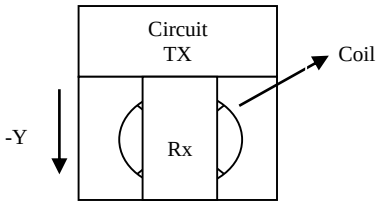


Fig. 6: Movement of receiver along Y-axis

From the best starting position mentioned in the previous subsection II-B-i the receiver is moved along the Y-axis at a step size of 0.1cm. This step is repeated in the reverse direction, -Y-axis. The changes of current and voltage for each position are recorded.

### *C. Indicator of System*

The transmitter circuit has two LED status indicators (green and red). A red LED indicates various Fault and FOD states. The green LED indicates active power transfer and charge complete state information. Upon power up, the two LEDs together may optionally indicate the standby state and remain in the state to another defined operational state occurs. Table 1 shows the status indicators at the transmitter.

TABLE I. STATUS INDICATORS AT TRANSMITTER

| **Condition** | **Green LED** | ***Red LED*** |
|---|---|---|
| Standby | On | On |
| Transfer | Blink 1 Hz | Off |
| Complete | One | Off |
| Power | Blink 2 Hz | Off |
| Fault | Off | Blink 4 Hz |

## III. RESULT AND DISCUSSION

In this section, all the measurement results of the experiment will be shown and discussed. The results include: starting position, separation distance, horizontal and vertical misalignment.

### A. *Starting Position*

Based on the result, at position 0 cm (where the receiver coil is aligned at the centre of the transmitter coil) produces the highest output current, about 246 mA. The current fluctuates when the receiver moves further from the centre. At the 0.6 cm, it achieves the second highest current around 237 mA. When the receiver is located at position greater than 0.8 cm or smaller than -0.8cm, there is no power transfer to the receiver.

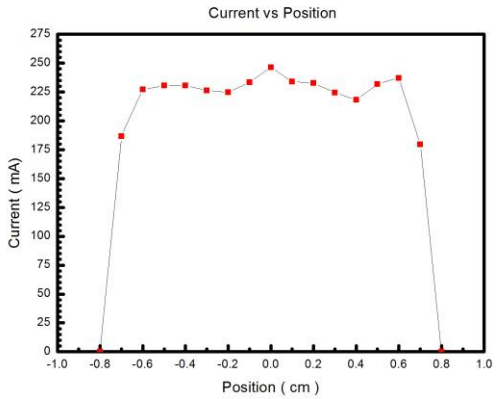


Fig. 7: Result of starting position

### B. *Separation Distance*

From the result, when the separation distance between the coil is increased the output current decreased. The best height of the receiver is at 0.2 cm (platform thickness) about 254 mA output current. This result shows that the best condition for the system transfer power is in the smallest separation distance. Besides that, after 0.4 cm the output current decreases steeply and reaches 0A (no power transfer) at a separation distance of 0.7 cm and above.

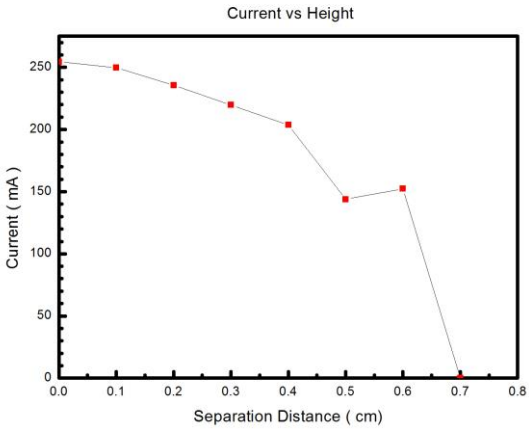


Fig. 8: Height of Receiver along Z-axis

### C. *Horizontal Misaligment: Movement of Receiver Along X-Axis*

When the misalignment is between -0.8 cm to 0.8 cm the output current maintains above the 200 mA. On the –X axis, the output current starts to decrease sharply at position smaller than -0.9 cm while on the +X axis starts to decrease at positions greater than 1cm. No power transfer to the receiver when the misalignment is beyond $\pm 1.2cm$. The result indicates that the system can tolerate $\pm 0.8cm$ of horizontal misalignment.

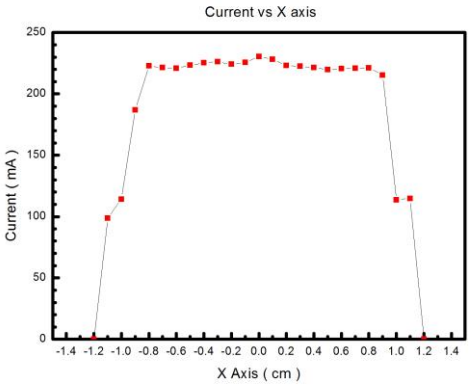


Fig. 9: Movement of receiver along X-axis

### D. *Vertical Misalignment: Movement of Receiver Along Y-Axis*

The result shows, that when the receiver moves toward the negative Y axis the output current decreases slowly at the beginning. When the receiver moves beyond -1.0 cm, the output current decreases drastically. At -1.8 cm, no power transfer is recorded.

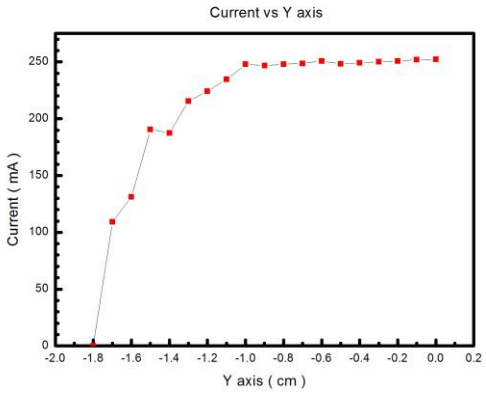


Fig. 10. Movement of receiver along Y-axis

In general, when the receiver coil is closer to the transmitter coil, the output current becomes higher and produces high power transfer. The power transfer can be calculated using the formula given by the following

$$P = I \times V \quad (1)$$

TABLE II. POWER FOR STARTING POSITION

| **Position (cm)** | **Current (mA)** | ***Voltage (V)*** | ***Power (W)*** |
|---|---|---|---|
| -0.8 | 0 | 0 | 0 |
| -0.7 | 186.67 | 4.62 | 0.86 |
| -0.6 | 227.22 | 4.66 | 1.06 |
| -0.5 | 230.5 | 4.68 | 1.07 |
| -0.4 | 230.69 | 4.65 | 1.07 |
| -0.3 | 226.43 | 4.74 | 1.07 |
| -0.2 | 224.72 | 4.73 | 1.06 |
| -0.1 | 233.45 | 4.75 | 1.11 |
| 0 | 246.53 | 4.83 | 1.19 |
| 0.1 | 233.89 | 4.75 | 1.11 |
| 0.2 | 232.78 | 4.71 | 1.10 |
| 0.3 | 224.48 | 4.66 | 1.05 |
| 0.4 | 218.33 | 4.63 | 1.01 |
| 0.5 | 231.93 | 4.67 | 1.08 |
| 0.6 | 237.22 | 4.80 | 1.14 |
| 0.7 | 179.67 | 4.78 | 0.86 |

The output voltage for the system is a regulated voltage in the range 4.5 to 5.3 Volt. The power transfer can be higher when the coupling coefficient K is higher [2]. This condition occurs if the distance of the receiver and the transmitter is closed to each other. Besides that, to increase power transfer efficiency of the system, it's important to design or use a coil with high quality factor [2]. By reducing the space between the coil, it will increase the value of quality factor [1].

The small value of coupling coefficient between resonators, will make the frequency separation decreases and continue until these two models converge to each other. This condition, also known as critical coupling points. It shows, the maximum distance for the power transfer efficiency still working. If the critical point bigger than the K value, the system is in under-couple. It's meant the power transfer to the load is inversely proportional to the separation distance [3].

## IV. CONCLUSION

As a conclusion, the proposed wireless power bank is able to support wireless charging of the mobile devices using the inductive coupling. From the measurements, the maximum power transfer occurred when the coil is perfectly aligned. Increase separation distance and misalignment effect the efficiency. The proposed system can transfer power when the separation distance is less than 0.6cm. The proposed system can also withstand a misalignment in the range of 0.8cm to 1cm before the performance starts to degrade severely.

.

## REFERENCES

[1] Akaa Agbaeze Enteng, Shahrul Kamal, Abdul Rahim and Chee Yen Leow "Wireless Nonradiative Energy Transfer", IEEE Antennas & Propagation Maganize JUNE 2015.

[2] Kiruthiga. G, Mahajan Yash Jayant, Sharmila.A "Wireless Charging for Low Power Application using Qi Standard" International Conference on Communication and Signal Processing, April 6-8, 2016, India

[3] B-J Jang1, S. Lee2, and H. Yoon3, "HF-BAND WIRELESS POWER TRANSFER SYSTEM ; CONCEPT, ISSUES AND DESIGN",Progress In Electromagnetics Research,Vol. 124, 211-231,2012

[4] Kurs, A., A. Karalis, R. Moffatt, J. D. Joannopoulos, P. Fisher, and M. Soljacic, "Wireless power transfer via strongly coupled magnetic resonances," Science, Vol. 317, 83–86, Jul. 2007.

[5] Xiou Lu, Ping Wang, Dusit Niyota, Dong In Kim, Zhu Han "Wireless Charging Technologies Fundamentals Standards, and Network Application" IEEE Communication Survey and Tutorial, VOL 18, NO 2, Second Quarter 2016

# Smart Investment Advisor

Yong Bang Xiang
*Faculty of Electrical Engineering*
*Universiti Teknologi Malaysia*
*Johor Bahru, Malaysia.*
*yongbangxiang@gmail.com*

Ahmad Shahidan Abdullah
*Department of Communication Engineering*
*Faculty of Electrical Engineering*
*Universiti Teknologi Malaysia*
*Johor Bahru, Malaysia.*
*ashahidan@utm.my*

***Abstract*—The financial market prediction is a lucrative field of interest with promising profit and covered with landmines for the unprecedented. The markets are complex, non-linear and chaotic in nature which poses huge difficulties to predict the prices accurately. In this paper, a stock trading system utilizing feed-forward deep neural network (DNN) to forecast price of 65 types of stocks and currency pairs in t days ahead is proposed and tested through market simulations on historical daily prices. There are 40 input nodes of DNN which are the past 10 days' opening, closing, minimum and maximum prices and consist of 3 hidden layers with 10 neurons per layer. The training algorithm used is stochastic gradient descent with back-propagation and is accelerated with multi-core processing. A trading system is proposed which utilizes the DNN forecasting results with defined entry and exit rules to enter a trade. DNN performance is evaluated using RMSE and MAPE. The overall trading system shows promising results with an overall profit factor of 18.67, 70.83% profitable trades and Sharpe ratio of 5.34 based on market simulation on test data.**

***Keywords: deep learning, stock market prediction, trading system***

## I. INTRODUCTION

Stock market and currency exchange prediction remains a lucrative field of research with promising profits for investors and researchers. The main motivation is to help investors and traders to analyze the market and help to make better informed decisions without watching the market constantly. However, there are challenges in predicting the financial markets accurately and precisely as the markets are complex, non-linear and chaotic in nature which calls for more powerful methods to tackle this problem. Many artificial intelligence methods have been employed to predict stock market prices. Artificial neural networks (ANN) remain a popular choice for this task and are widely studied [1] and have been shown to exhibit good performance [2]. More recently, deep learning has emerged an improved method over conventional neural networks for various applications such as recognition system, natural language processing and medical sciences and has shown astonishing results [3]. It has also been applied in financial markets for prediction of stock prices using textual news data and numerical data [4] [5]. Experiment has been conducted to test its profitability and performance as a trading system in the stock and commodity market [6]. However, there is still a lack of studies conducted on the usage of deep learning as an integral part of a trading system. In this paper, we propose a trading system for stock market which utilizes the prediction of DNN to generate trading signals, and evaluate its performance in the financial (stocks & forex) market as an attempt to convert the DNN predictions into a profitable system.

## II. METHODOLOGY

### A. Data sets

The data set used throughout this project are obtained from two major sources: daily stock data from Yahoo Finance and currency exchange rate from TrueFX which amounts to 19GB of data. The list of symbols for stocks and currency pairs with a total of 64 symbols used in this project are: EUR/USD, USD/JPY, GBP/USD, EUR/GBP, CAD/CHF, CAD/JPY, CHF/JPY, EUR/AUD, USD/CHF, EUR/JPY, EUR/CHF, USD/CAD, AUD/USD, GBP/JPY, AUD/CAD, AUD/CHF, AUD/JPY, AUD/NZD, EUR/CAD, EUR/NZD, GBP/CAD, GBP/CHF, NZD/JPY, NZD/USD, 5819.KL, 4677.KL, 4863.KL, 5225.KL, 5246.KL, 6012.KL, 2445.KL, 4197.KL, 6947.KL, 3182.KL, 4065.KL, 5347.KL, 1295.KL, 6033.KL, 1023.KL, 5235SS.KL, 3816.KL, 5681.KL, 1961.KL, 6399.KL, 1066.KL, 5183.KL, 1155.KL, 4162.KL, 3034.KL, 6888.KL, 4715.KL, 1082.KL, 3336.KL, 1015.KL, AAPL, GOOG, MSFT, TSLA, FB, TWTR, INTC, NATI, XOM, MCD, STI.

### B. Deep Neural Network

Deep neural network is a special type of artificial neural network characterized by its architecture which consists of higher number of hidden layers and neurons compared to conventional neural network. Higher number of hidden layers exhibits increased capability of high-level features extraction for every added hidden layer [7]. Hence, the raw input data is not required to be pre-processed using features extraction methods compared to conventional neural network. The principle for forecasting is based on windowing method, that is to use the opening, closing, maximum and minimum prices of n-1, n-2, … n-10 days as inputs to the DNN to output the

predicted closing price of *t* days ahead. The number of prior working days is selected based on [8] which has shown promising results. Multiple models need to be trained for every forecast of *t* days ahead.

In this paper, the architecture of DNN comprises of an input layer with 40 input nodes, 6 hidden layers with the composition of 10-10-10 neurons respectively and an output layer with a single node which outputs the stock price in *t* days ahead. The DNN architecture is depicted in Fig. 1.

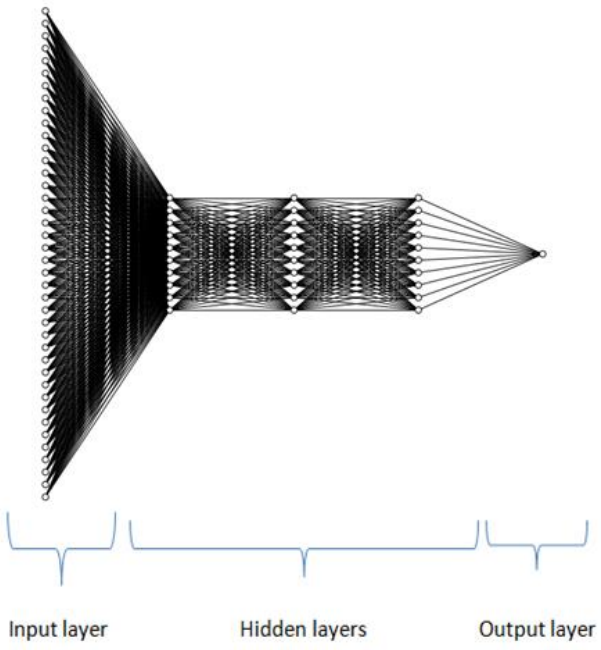


**Fig. 1.** Feed-forward deep neural network architecture used for prediction model of stock price of n+t day

### *C. Network Training*

Stochastic gradient descent and back-propagation is used as the learning algorithm. Training the DNN is an expensive process with 40 input variables and high number of neurons. To address this issue, multi-core processing method is used using Hogwild algorithm [9], which is a lock-free parallelization scheme whereby each core handles separate subsets of the training data. The result of training DNN is a forecast model which can be used to predict the closing price of n+t day.

### *D. Proposed Trading System*

The implementation of the algorithm (training and testing) for prediction is coded in R language, and the server is deployed in real-time, with the following flow scheduled to be done repeatedly for every tick: pull new data from source, evaluate trade signals and evaluate existing open signals.

The rules of a trading system tell the investor when to buy or sell the stocks which will result in a profitable trade. The proposed trading system uses the results of predicted closing stock prices of n, n+1 and n+2 days.

The proposed trading rules employ the logic of buying stocks when the forecasted closing price is higher than the current opening price, and selling all stocks (if any) in possession if the forecasted closing price is lower than current opening price. The effect of trading rules was investigated using different combination of n+t day forecast. Let $close_t$ be the predicted closing price at n+t day and *open* be the opening price of n-th day. Trading rules used are divided into entry and exit rules. Different entry rules are proposed to be tested on the trading system to compare the its performance. The trading rules used are as follows:

Entry rules:
1) Buy when $close_0 > open$
2) Buy when $close_0$ and $close_1 > open$
3) Buy when $close_0$ and $close_1$ and $close_2 > open$
4) Buy when $close_0$ and $close_1$ and $close_2$ and $close_3 > open$
5) Buy when $close_0$ and $close_1$ and $close_2$ and $close_3$ and $close_4 > open$

Exit Rule:
1) Sell all when $close_0 > open$

## III. RESULTS

The evaluation is conducted on two components namely the stock prediction model and performance of trading system. All evaluations are performed on the testing set. The predicted closing price for the testing sets are plotted on the graph to visualize the actual versus the predicted price as depicted in Fig 2.

### *A. Prediction Output*

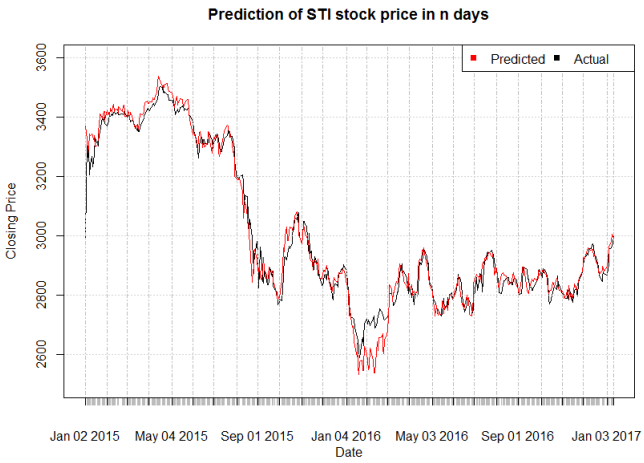


**Fig. 2. Prediction of STI stock price in n days**

The evaluation metrics used for the prediction models are the conventional root mean square error (RMSE) and mean absolute percentage error (MAPE) which is a statistical measure of prediction accuracy of a forecast model. Different models are compared for closing price of n, n+1, n+2, n+3, n+4 days and are shown in Table 1.

**Table 1.** RMSE of closing stock price prediction models of t days ahead.

| t (days) | RMSE | MAPE |
|---|---|---|
| 0 (Today) | 32.77 | 0.75 |
| 1 | 48.40 | 1.20 |
| 2 | 51.38 | 1.26 |
| 3 | 72.00 | 1.83 |
| 4 | 74.64 | 1.84 |

As the number of days increases for the forecast, the generalization error increases as well. This shows that it is less accurate to predict the price further into the future compared to more recent forecasts. Note that since the model uses windowing method, in the beginning of the time series where the past stock prices are not available, the prediction result is not available as well.

*B. Evaluation of Trading System*

The trading system is simulated on the test data using different entry rules as stated in the methodology. The metrics used are profit factor, Sharpe ratio and percentage of profitable trade and results are tabulated in Table 2.

**Table 2.** Performance of trading system using different entry rules

| Entry Rule | Profit Factor | Profitable Trades (%) | Sharpe Ratio |
|---|---|---|---|
| 1 | 2.54 | 47.37 | 2.13 |
| 2 | 4.92 | 52.08 | 3.21 |
| 3 | 14.32 | 67.74 | 4.69 |
| 4 | 15.31 | 65.52 | 4.80 |
| 5 | 18.67 | 70.83 | 5.34 |

It is shown that the best performance is exhibited by using the entry rule 5 which enters a buy trade only when the forecasted closing prices of n, n+1, n+2,… n+4 day are higher than the opening price of n-th day. This can be attributed to the higher chance of entering a profitable trade if there is an upward trend and ultimately increases the profit factor. This shows that the trading system which uses multiple steps of prediction from deep neural network can be profitable for the investors. The market simulation of the transactions made using the trading system and its cumulative return curve is shown in Fig. 3 where the green triangle depicts a buy signal and the red triangle depicts a sell signal.

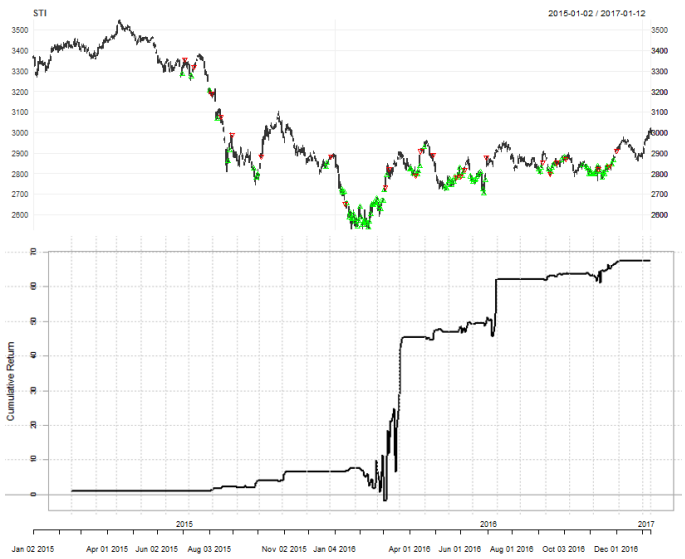


**Fig. 3.** Market simulation results of DNN trading system on test data

## 4 Conclusion

In this paper, a stock market trading system is proposed which uses deep neural network as part of its core components. The DNN uses historical data prices to forecast stock prices of t days ahead which is incorporated in the trading system to make buy and sell decisions. The effect of varying the number of steps of the forecast model was investigated and it is shown that the forecast further into the future yields less accurate results. The consequences of varying the trading rules were also studied and the trading system with best performance was determined to have a profit factor of 18.67, 70.83% profitable trades and Sharpe ratio of 5.34. In the future, different types of deep learning algorithm can be investigated such as Deep Boltzmann machine and Deep Q-networks. Better trading rules can also be investigated by using more advanced methods such as evolutionary programming. There is also potential for using different inputs of data such as correlated commodity and currency value, and

REFERENCES

[1] Vui, C.S., et al. A review of stock market prediction with Artificial neural network (ANN). in 2013 IEEE International Conference on Control System, Computing and Engineering. 2013.

[2] 2. Yetis, Y., H. Kaplan, and M. Jamshidi. Stock market prediction by using artificial neural network. in 2014 World Automation Congress (WAC). 2014.

[3] 3. Soniya, S. Paul, and L. Singh. A review on advances in deep learning. in 2015 IEEE Workshop on Computational Intelligence: Theories, Applications and Future Directions (WCI). 2015.

[4] 4. Akita, R., et al. Deep learning for stock prediction using numerical and textual information. in 2016 IEEE/ACIS 15th International Conference on Computer and Information Science (ICIS). 2016.

[5] 5. Day, M.Y. and C.C. Lee. Deep learning for financial sentiment analysis on finance news providers. in 2016 IEEE/ACM International

Conference on Advances in Social Networks Analysis and Mining (ASONAM). 2016.

[6] 6. Deng, Y., et al., *Deep Direct Reinforcement Learning for Financial Signal Representation and Trading.* IEEE Transactions on Neural Networks and Learning Systems, 2016. **PP**(99): p. 1-12.

[7] 7. Sun, Y., X. Wang, and X. Tang. Deep learning face representation from predicting 10,000 classes. in Proceedings of the IEEE Conference on Computer Vision and Pattern Recognition. 2014.

[8] 8. Moghaddam, A.H., M.H. Moghaddam, and M. Esfandyari, *Stock market index prediction using artificial neural network.* Journal of Economics, Finance and Administrative Science, 2016. **21**(41): p. 89-93.

[9] 9. Recht, B., et al. Hogwild: A lock-free approach to parallelizing stochastic gradient descent. in Advances in Neural Information Processing Systems. 2011.

# Optical Fiber Liquid Level Sensor

Wan Farhana Wan Ahmad Zamri
*Faculty of Electrical Engineering*
*Universiti Teknologi Malaysia*
*Johor Bahru, Malaysia.*
*wan_farhana@ymail.com*

Muhammad Yusof Bin Mohd Noor
*Department of Communication*
*Faculty of Electrical Engineering*
*Universiti Teknologi Malaysia*
*Johor Bahru, Malaysia.*
*yusofnor@fke.utm.my*

***Abstract*—This paper introduces a simple and stable Optical fiber liquid level sensor (OFSLLS). This liquid level sensor is utilizing an Optical Time Domain Reflectometer (OTDR) in order to ensure the sensor can measure up to 10km and able to detect multiple of liquid levels. The purpose of the project is to carry out a simple setup for OFLLS that capable to measure liquid levels in long distance simultaneously. The accomplishment of the OFLLS is studied by conducting a simple experiment to analyse the output signals of the OFLLS as per liquid level by using a 2×2 coupler. The end of the coupler is connected to different length of fiber reels, 10.26 km and 10.31 km. From the analysis, there is a difference in average amplitude of the reflection pulse for each fiber distance when the end of the fiber is exposed to different mediums. The findings show that an optical fiber liquid level sensor is easy to produce and can be used up to 10km.**

***Keywords—OTDR; Single Mode Fiber; liquid level sensor; reflectance power;***

## I. INTRODUCTION

Recently, communication is becoming a critical demand in human lives. The theory of guiding light with optical fiber by Dr. K. C. Kao and his colleagues in Standard Telecommunication Laboratories [1] were introduced to the world and has been applied to various fields such as telecommunication, medical and civil sector. The innovation of optical fiber based sensor is increased rapidly in every year and making their own path to replace the existing electrical based sensor.

Malaysia has two Inter-Monsoon is existed from April to May and September to October [2]. The aim to create an optical fiber liquid level sensor (OFLLS) is necessary in order to measure the liquid level in several locations in Malaysia such as Kelantan, Pahang and Terengganu which always hit by the flood especially of the monsoon season. In this case, electrical based sensor is not practical to be implemented in river bank or water dam due to the sensor has its limitation on robustness and sensitivity. This sensor is not only unable to withstand corrosive and harsh environment [3] but also does not have the ability to measure liquid level simultaneously because of the water level in a drainage, dams, irrigation system and drainage are changing in certain time. This means it is not practical to take the reading of water level by using bare eyes at the staff gauge. The existence of OFLLS sensor makes the precision of the liquid level reading is possible to obtain.

There are several OFLLS are designed using Single Mode Fiber (SMF), presented in the literature review based on reflection configuration [4-6]. A reflection based fiber optic sensor system using an OTDR technique is shown in [4]. The overall findings illustrate that the sensor is able to detect refractive index in a long distance at in particular concentration at one time. This explained the sensor is incompetent to measure a wide range of measurement. In 2015, water level and temperature dependence of the Fresnel Reflection is proposed in [5]. The optical power is linearly increased with the temperature of water and the proposal also proved water has greater reflectance signal than air due to the water temperature is higher than the ambient temperature because of the heat. A. Basgumus and co-workers [6] have applied fiber sensor based on Fresnel reflection technique for measuring the refractive index of several liquids as shown in Fig. 1. Nevertheless, the exact location of reflectance event is not mentioned. This can be improvised in the future.

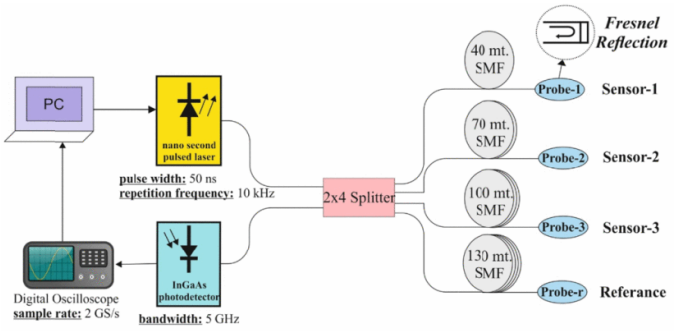


Fig. 1. Experimental of stable refractive index sensor system [6].

In this paper, the author is focusing on creating a new method to design the OFLLS by utilizing an OTDR. The sensor system is based on Fresnel Reflection for measuring the reflectance power. The OFLLS would be easy to setup, capable to operate in a wide range of distance, able to sense multipoint liquid levels.

## II. WORKING PRINCIPLE AND EXPERIMENTAL SETUP

The basic principle of OFLLS is based on the reflected pulse of the Fresnel reflection at the end of the probe. The OTDR emits laser light pulses into the fiber optic. As the pulses travel towards the fiber's flat end surface and the beaker, Rayleigh scattering and Fresnel reflection is existed. The end of the fiber is cut flat to guarantee a low loss in the transmission process. Variation of fiber density causes Rayleigh scatters. Fresnel reflection took place when the laser light pulse propagates to

fiber's end surface and there will be changes of medium density. The changes arose at splice and connectors where air gap is existed. After Fresnel reflection and backscattering signal arrived at the fiber end, the signals are reflected backward and will detect by the OTDR. According to Fresnel theory [7], the reflection happens between two different mediums with different refractive index.

Below are the experiments that have been conducted in constant laboratory temperature, 24°C. The liquid used for all experiments is tap water and the end of the fiber is cut flat. The refractive index of the liquid is 1.33 while the index of refraction of SMF fiber is 1.4682. A formula [8,9] was discovered to calculate the time taken for the pulse to launch and reflect back to the OTDR. The formula to calculate OTDR distance is given as:

$$d = \frac{c \times t}{2(IOR)} \quad (1)$$

Where,

| | |
|---|---|
| $c$ | is the speed of light |
| $t$ | is the round-trip travel time |
| $IOR$ | is the index of refraction of the fiber under test |

### A. *Experiment I – Verify Fresnel's Reflection Theory*

The experimental setup of the proposed OFLLS is shown in Fig. 2 and 3. This method is almost the same as a paper presented in [4] but reflectance pulse is becoming the main idea of this research. A stable optical pulse with a pulse width of 200 ns in generated by Optical Time Domain Reflectometer (*OTDR*) at 1550 nm wavelength. The pulse stream is traveled into 10.26 km single mode fiber (SMF) of fiber reel. Fresnel reflection can be observed and measured by using an OTDR (Anritsu MT9083A2-073). The first step of the experiment is to expose the end of the fiber to air. After data are taken, the same probe is immersed in water. After comparing the outputs results of probes at different medium, a conclusion has been made in the next topic.

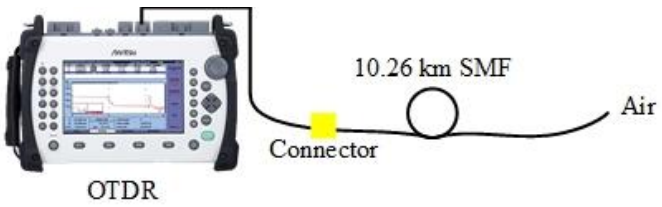


Fig. 2. Experimental setup when the end of 10.26 km SMF is exposed to air.

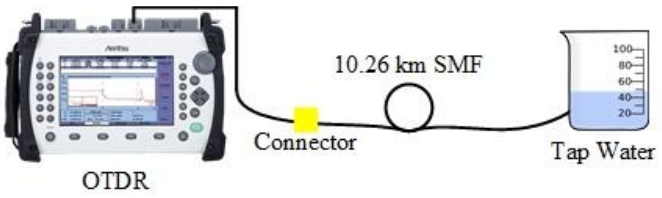


Fig. 3. Experimental setup when the end of 10.26 km SMF is immersed in water.

### B. *Experiment II – Optical Fiber Liquid Level Sensor with a 2×2 Coupler*

In this section, the experimental setup is different from the previous experiments. A 2×2 fiber-optic coupler is introduced in this research. The aim of this experiment is to prove that this sensor is able to measure liquid level simultaneously. The input from the OTDR (pulse) is divided into 2 ports with 50% splitting ratio. As OTDR is capable to measure very detail event signals and locations at the broad range of distance, two SMF reels which approximately have the same length are tested. This sensor is used for reflection measurements in different locations. Fig. 4 and 5 demonstrates the effect of the difference in fiber length on the output results. The reference data are taken when all probes are exposed to air.

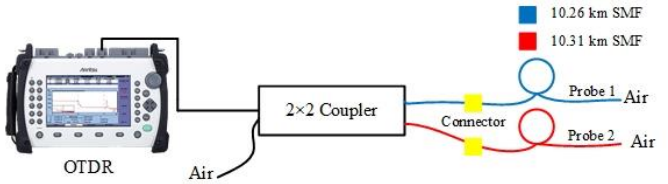


Fig. 4. Experimental setup of 2×2 coupler when both probes are exposed to air.

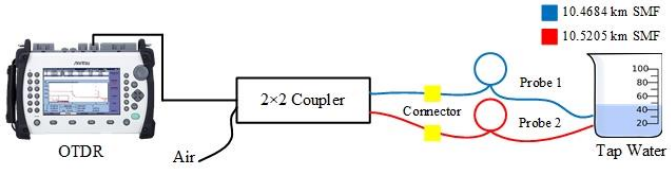


Fig. 5. Experimental setup of 2×2 coupler when both probes are immeresed in water.

### C. *Experiment III – Effect of Temperature on Optical Fiber Liquid Level Sensor*

In this section, the effect of temperature is tested on the sensor. Experimental setup is shown in Fig. 6. The function of Memmert Water Bath is to hatch water at a steady temperature over a long period of time. After, the Water Bath is filled with tap water, the knob is pressed and desired temperature is chosen. The volume of water is constant at 600ml. All data are taken starting from 25˚C until 70˚C. The interval between each temperature is 5˚C.

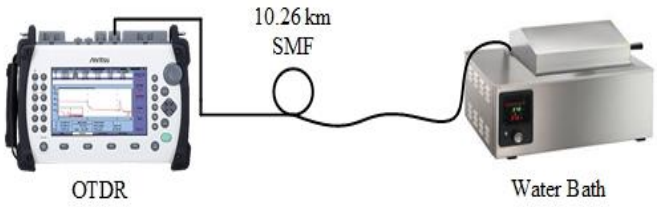


Fig. 6. Experimental setup to identify the effect of temperature the sensor.

## III. Result and Discussion

### A. Experiment I

According to Fresnel theory, the reflection happens between two different mediums with different refractive index. The light will be reflected and refracted. A light must enter the core within the acceptance angle to ensure it is propagated in the fiber. The reflection and refraction of the light can be determined by Snell's law [7]. The reflectance pulses are clearly shown in Fig 7. The OTDR output signal is originally displayed in Anritsu Traceview shows air reflectance power, -14.47 dBm and reflectance power of water, - 25.86 dBm. However, in this paper, the reflectance power graph is plotted using MATLAB R2013a. Average of amplitude reflection pulse was calculated and plotted as in Fig. 7. Fig. 8 demonstrates air has the higher amplitude pulse, -11.91 dBm than the reflectance power of water, -17.63 dBm. The reflective event took place at 10.26 km. The travel time for pulse for both events to launch and reflect to OTDR is 97, 880 nanoseconds.

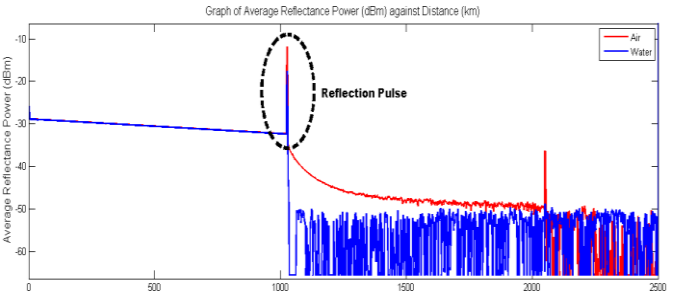


Fig. 7. Output Signal when probes in the air and water (Zoom out).

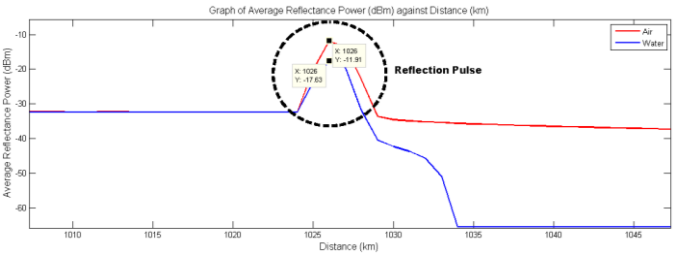


Fig. 8. Output Signal when probes in the air and water (Zoom in).

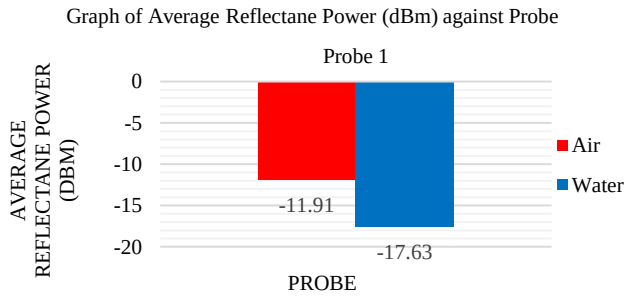


Fig. 9. Graph of average reflectance power (dBm) against probe.

In situation where lights travel into a different index of refraction, a large amount of light is reflected back and causes a spike in OTDR. Thus, these results are the evidences that fiber optic is an excellent liquid level sensor due to the sensor is successfully verified the Fresnel's theory as the sensor can detect the reflective event, Fig. 9 and at the same time capable to sense the changes of refractive index.

### B. Experiment II

This section shows the experimental results when using 2×2 coupler. Fig. 10 illustrates the difference of reflective events in water and air. All data in Fig. 10 are tabulated in Table 1.

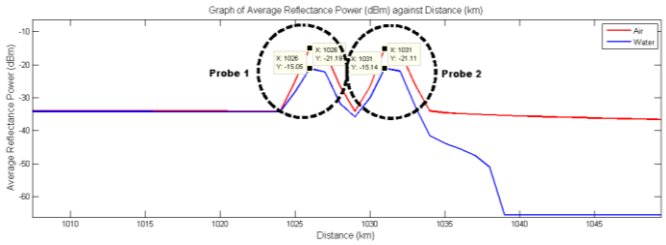


Fig. 10. Output Signal when probes in the air and water (Zoom in).

TABLE I. The Difference of Reflective Events in Water and Air at Different Location

| Experiment | Probe | Medium | Location of Reflectance Event (km) | Average of Reflectance Power (dBm) |
|---|---|---|---|---|
| 1 | 1 | Air | 10.26 | -11.05 |
| | 2 | Air | 10.31 | -11.14 |
| 2 | 1 | Water | 10.26 | -21.19 |
| | 2 | Water | 10.31 | -21.11 |

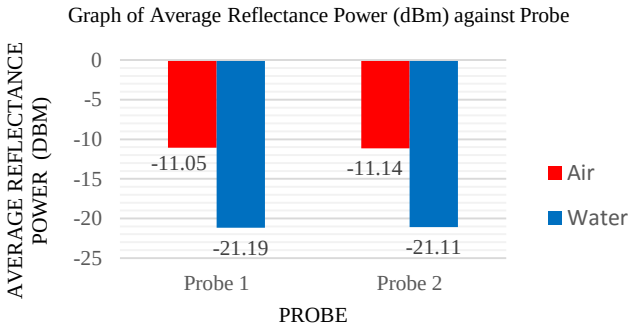


Fig. 11. Graph of average reflectance power (dBm) against 2 sensing probes.

According to OTDR distance calculation, the time taken for a reflection pulse in Fig.13 (a) for each probe length is 100,424.88 ns and 100,914.28 ns. As both probes in Fig. 11 are uncovered in the air the reflectance pulse of these probes is roughly the same which are -11.05 dBm and -11.14 dBm at 10.26 km and 10.31 km. The decrement of reflectance power can be seen as both probes submerged in the water which give the value -21.19 dBm and -21.11 dBm. By analyzing Table 1, if there are two different length optic fibers, the reflectance events would not overlap with each other. It can be deduced that this liquid level sensor has the ability to sense different medium and multiple level of water at the same time. The result of the demonstration declares that the sensing probes may be used as the liquid level detector due to the changes of reflection power of output signals in air and water. Therefore, this experiment is

an undefeated evidence as this sensor is able to measure liquid levels in long distance simultaneously.

### C. Experiment III

The data collected are tabulated in Table 2 and represented in Figure 12. Fiber optic is designed to withstand high temperature. Throughout this experiment, the theory has been justified due to there is a small change in peak of reflection pulse when the temperature is increased. Nevertheless, it is only insignificant changes in temperature which is less than 0.5 dBm between 25˚C and 70˚C.

TABLE II. DATA OF AMPLITUDE REFLECTANCE POWER (DBM) AND TEMPERATURE (˚C)

| Amplitude Reflectance Power (dBm) | Temperature (˚C) |
|---|---|
| -25.66 | 25 |
| -25.71 | 30 |
| -25.73 | 35 |
| -25.77 | 40 |
| -25.80 | 45 |
| 25.83 | 50 |
| -25.91 | 55 |
| -25.93 | 60 |
| -25.93 | 65 |
| -25.96 | 70 |

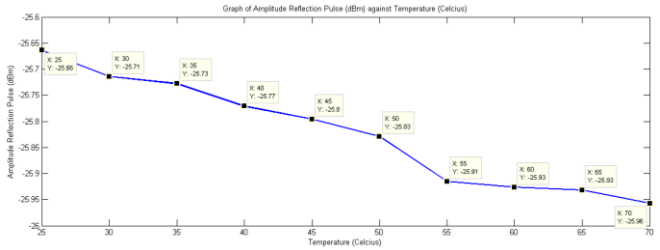


Fig. 12. Graph of amplitude reflectance power (dBm) against temperature (˚C)

## IV. CONCLUSION

The designed OFLLS has an easy measuring principle, stable, simple structure, able to measure at a wide range of measurement and immune to electromagnetic interference. The quality and performance of the sensor are compared from the previous researches and all the drawbacks from the studies are managed to resolve in this paper. This paper is successfully accomplished purpose of the project as manage to detect liquid levels in a long distance at multiple point. The sensing probes are succeeded to measure and distinguish the difference between air and water as the reflectance power will give the difference reading and can be seen in OTDR. The value of signal output when probes are immersed in water is lower that the probes which is exposed to air. The length of the sensing probe is very important because overlapping of optical peaks might be occurred. Hence, this sensor can be used to detect the other type of liquid such as gasoline, ethanol and methanol as the sensor is stable, can endure high temperature and easy to develop.

## ACKNOWLEDGMENT

Author expresses her appreciation to Dr. Muhammad Yusof Bin Mohd Noor for his advice, encouragement and guidance on the Optical Fiber Liquid Level Sensor project. Without his support, the above project will not possible to be completed.

## REFERENCES

[1] D. J. Richardson, “New Optical Fibres for High-Capacity Optical Communications,” United Kingdom: Optoelectronics Research Centre, University of SouthamptonPhil, p. 1, January 2016.

[2] A. Jamaluddin, The Weather and Climate of Malaysia, Malaysian Meteorological Department Ministry of Science, Technology and Innovation.

[3] B. Lee, Review of The Present Status of Optical Fiber Sensors. Optical Fiber Technology, vol. 9, No. 2, pp. 57-59.

[4] J. Yuan, C. Zhao, M. Ye, J. Kang, Z. Zhang, and S. Jin, “A Fresnel reflection-based optical fiber sensor system for remote refractive index measurement using an OTDR,” Photonic Sensor, vol. 4, No. 1, pp.48-52, March 2014.

[5] W. Yoo, H. Sim, S. Shin, K. Jang, S. Cho, J. Moon, and B. Lee, “A Fiber-Optic Sensor Using an Aqueous Solution of Sodium Chloride to Measure Temperature and Water Level Simultaneously,” Physical Sensor, vol. 14, No. 10, pp. 18823-18836, October 2014.

[6] A. Basgumus, F. Durak, A. Altuncu, and G. Yilmaz, “A Universal and Stable All-Fiber Refractive Index Sensor System,” IEEE Photonics Technology Letters, vol. 28, No. 2, pp. 171-174, January 2016.

[7] M. Senior. John, “Optical Fiber Communication”, 3rd Ed. Prentice Hall, 2009.

[8] C. H. Yeh, C. W. Chow, J. Y. Sung, P.C. Wu, W. T. Whang, and F. G. Tseng, “Measurement of Organic Chemical Refractive Indexes Using an Optical Time Domain Reflectometer” Sensors, vol. 12, No. 1, pp. 481-488, 2012.

[9] M. H. Younus, O. F. Ameen, R. K. R. Ibrahim and N. Redzuan, “Fuel Detection System using OTDR with Multimode Fiber,” Journal Teknologi (Sciences & Engineering), vol. 70, No. 3, pp. 107-112, December 2016.

# Dual Band Microstrip Patch Antenna using Artificial Magnetic Conductor

Nurul Shuhaila Binti Ismail
Faculty of Electrical Engineering
Universiti Teknologi Malaysia (UTM)
Johor, Malaysia.
nshuhaila.work@yahoo.com

Mohd Fairus Bin Yusoff
Communication Eng. Department
Faculty of Electrical Engineering
Universiti Teknologi Malaysia (UTM)
fairus@fke.utm.my

***Abstract*— Artificial Magnetic Conductor (AMC) is metamaterial that can mimic the characteristic of Perfect Magnetic Conductor (PMC) which it can introduced a zero phase reflection coefficient phase to incident waves. The combination of microstrip antenna with AMC structure help to improve several antenna characteristics performance. In this thesis, the dual-band microstrip antenna with and without AMC structure as a ground plane has been designed. Firstly, the dual-band microstrip antenna is designed to resonate at 2.4GHz and 5.8GHz using conventional ground plane. Then, the conventional ground plane of dual-band antenna has been replaced by AMC structure consist of 2x2 unit cell AMC. All of the simulations are been carried out using CST microwave Studio. The dual-band antenna and AMC structure are designed using FR4 substrate with dielectric constant 4.3 and thickness of 3.2mm and 1.6mm respectively. According to the results, dual-band microstrip antenna with AMC structure has shown several improvements. The return loss refined about -16 dB at both frequencies, the increment bandwidth at 5.8GHz with 248MHz and, higher maximum directivity of 6.18dBi at 2.4GHz. As conclusion, the presence of AMC structure as ground plane has improved microstrip antenna performances with compact size.**

***Index Terms*—Microstrip Patch Antenna; AMC; Dual band frequency;**

## I. INTRODUCTION

With the development in wireless communication, microstrip patch antenna is one of antenna type that commonly used for communication devices due to its excellent characteristic such as low cost in manufacturing, light weight, easy fabrication, and can be designed for multiple frequencies [1]. Indeed, the demand for a multiband antenna that can operate at multiple frequencies has increased in a recent development in wireless communication.

The concept of the microstrip antenna was first proposed in 1953. It is about 20 years before the practical antenna were produced. Since then, the interest in this kind of antenna was increasing rapidly. Around 1979, in New Mexico, first meeting on microstrip antenna was held [2].

Although microstrip patch antenna has many advantages [1]-[4], in most of the microstrip antenna was suffering from several limitations such narrow bandwidth, low gain, and limited input impedance. [1]- [4]. There are many related sorts of research have been led and explored over the world due to its wide consideration in communication system and to enhance the antenna performance by overcoming these limitations. [1]-[4].

Artificial Magnetic Conductor (AMC) is a type of metamaterial which metamaterial is a composite material that has property that not found in nature. The metamaterial is usually arranged in a repeating pattern and it drives their properties of the newly structure. The shape, size, and arrangement influence the properties that capable of manipulating the electromagnetic waves. There are many terms used for different application include Left Handed material, Double Negative material, Magneto dielectric, Artificial Magnetic Conductor and many more. All these terminologies are under Electromagnetic Bandgap (EBG). AMC that closely related to EBG is functioning to prevent or assists the electromagnetic wave in a specified band of frequency.

Usually, Perfect Electric Conductor (PEC) that used as conventional ground plane introduces image current with a different phase that will lead to attenuation and affecting the antenna efficiencies. Thus, AMC is an alternative way to the conventional ground plane, PEC as it can generate image current with zero reflection phase with an incident current wave to the antenna. Moreover, the performance of an antenna is potentially improved in term of bandwidth, radiation pattern and gain with the integration of AMC as a backed ground plane [3]. Therefore, in this thesis, a dual band microstrip patch antenna with the integration of AMC has been studied and designed.

## II. LITERATURE REVIEW

A micro strip patch antenna consists of radiating patch on top of the substrate with the thickness of h and permittivity $\varepsilon r$. It also consists of feeding transmission line and ground plane that are made from high conductivity metal and overview of micro strip antenna shown in Figure 1. Copper and gold are the typical conducting material used for ground plane and the patch.

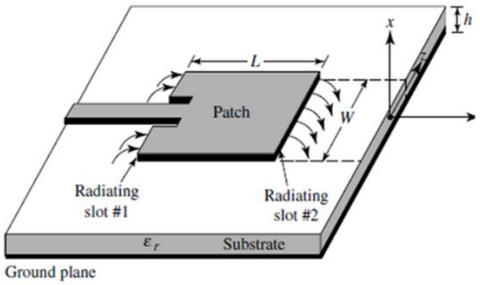


Figure 1 Basic Structure Microstrip Antenna

In the Figure 1 shows that the dimension of the patch is defined by length (*L*) and width (*W*). The length, *L* of the antenna patch will determined the frequency of operation.

In modern days, the design of antenna with dual or multiple frequencies is very important, especially in communication because anyone can use a single antenna with multiple frequency, instead of using two or more antennas to operate multiple frequencies. Besides, the dual frequency with bandwidth enhancement are recommended in current technologies [8]. Agarwal, Shaw, Das, Mukherjee (2012) [9] emphasized that dual frequency operations are important considerations for mobile transceiver applications.

There is a numerous way techniques to design multi band frequency, such as cutting the slot where in [4], by incorporating the slot in the patch result in size reduction about 65.8% and this dual band frequency antenna is suitable for WLAN and Wi-Max application [4]. Introducing slits on the patch, integrating the parasitic resonant ring SRR around radiating patch and two new short circuited microstrip antenna are other techniques used to achieve dual frequency.

There are lots of studies being conducted about patch miniaturization techniques. By using material substrate with high dielectric constant is one of the technique to minimize where it can reduce the guided wave propagates underneath the patch Besides, the use of electromagnetic band gap (EBG), the use of a quarter wavelength and photonic band gap (PBG) are several techniques that have been investigated to minimize the size of patch antenna.

In this paper, the alternative technique to miniaturize the antenna dimension is proposed by replacing the common ground plane of microstrip patch antenna with AMC structure. The AMC structure will introduce a zero reflection coefficient phase to the incident waves. The surfaces waves and the current have no propagation at certain frequency band thus making AMC it's very useful as ground plane. The surfaces is referred as s perfect magnetic conductor (PMC) by assuming no losses and zero reflection phase which complementary to a perfect electric conductor (PEC). In general, the useful bandwidth of AMC structure is between +90 to –90. The AMC structure has good radiation patterns without unwanted ripples due to the suppression of surface wave propagation presents within the band gap frequency range.

Thus, in this work, a dual band microstrip patch antenna has been designed with incorporating the AMC structure as ground plane with the aim to optimize several antenna characteristics such gain, bandwidth, radiation pattern and reflection coefficient. The proposed microstrip patch antenna and AMC structure are designed on a FR-4 substrate with dielectric constant 4.3 and thickness of 3.2mm and 1.6mm respectively.. The antenna have been designed and analyzed using CST software.

## III. Project Methodology

In order to achieve objectives, the required antenna specification has to be determined. The table 1 show the parameter specification that needs to be achieve by proposed antenna.

TABLE 1 Design Specification

| Parameter | Specification |
|---|---|
| Resonant frequency | 2.4GHz and 5.8GHz |
| Substrate Material | FR-4 |
| Dielectric constant of substrate | 4.3 |
| Feeding Technique | Microstrip line Feeding |
| Conductive Material | Copper/PEC |
| Directivity | 6 dBi |

### *A. Simulation Tools*

In this project antenna design and simulation is analyzed using Computer Simulation Technology (CST). It is specialist tool for the 3D EM simulation for high frequency component. This software as a solver that cover simulation for reflection coefficient, gain and radiation pattern.

### *B. Antenna Parameters Calculation*

The beginning step of antenna design determines all the parameter dimensions. Figure 2 show the basic antenna structure.

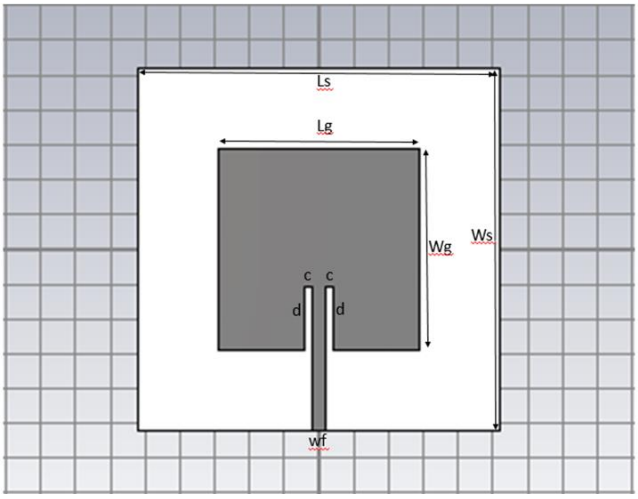


Figure 2 Basic Rectangular Patch Antenna

The antenna is designed to operate at 2.4GHz. All the step taken is shown as followed:

Step-1: The width of the patch antenna is derived using following equations:

$$W = \frac{C}{2fo\sqrt{\frac{\varepsilon r + 1}{2}}} \quad (1.1)$$

Where fo = 2.4GHz is the operating frequency.

Step-2: Calculating the effective dielectric constant (εeff):

$$\varepsilon eff = \frac{\varepsilon r+1}{2} + \frac{\varepsilon r+1}{2}\left[\frac{1}{\sqrt{1+\frac{12h}{W}}}\right] \quad (1.2)$$

Where h is the substrate thickness, w is calculated width of the patch, εr is the dielectric constant of the substrate material.

Step-3: Calculation of effective length (Leff):

$$Leff = \frac{C}{2fo\sqrt{\varepsilon eff}} \quad (1.3)$$

Step-4: Patch extension length calculation (ΔL):

$$\Delta L = 0.412h\frac{(eff+0.3)(\frac{W}{h}+0.264)}{(eff-0.258)(\frac{W}{h}+0.8)} \quad (1.4)$$

Step 5: Calculation of the actual length of the rectangular patch (L):

$$L = Leff - 2\Delta L \quad (1.5)$$

The equation (1.1) to (1.5) are generally used to design a microstrip antenna for a single radiating element of one resonant frequency that consists of a radiating patch, insert feed line, substrate and ground plane. However, the target of this project is to design the antenna that able to radiate at two resonant frequencies.

The next step is to obtain the second frequency at 5.8GHz. In this work, a slot has been introduced to a single radiating element. Figure 3 shows a single element dual band microstrip patch antenna operating at 2.4GHz and 5.8GHz respectively.

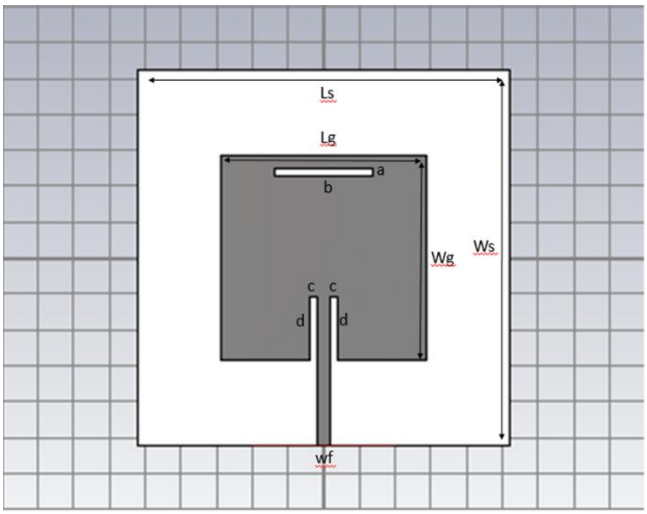


Figure 3 Dual Band Microstrip Patch Antenna with slot

For unit cell AMC, a rectangular shape is chosen due to simple design analysis. The first step, dimensions of length and width of single element AMC was calculated using equation (1.1) to (1.5). Then, to obtain a dual band AMC, second patch is introduced, thus the structure has two rectangular patches as shown in Figure 4. The outer patch operates at 2.4GHz and the inner patch operate at 5.8GHz respectively. The dimension of the gap is optimized to get the best result.

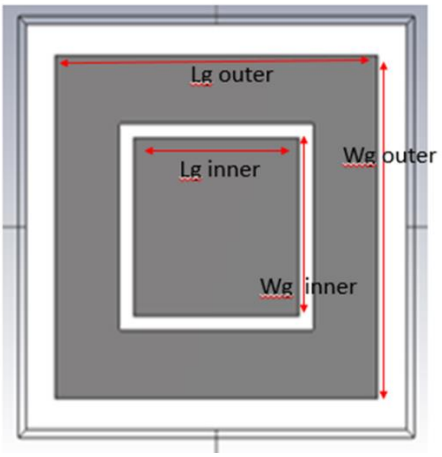


Figure 4 Dual Band unit cell AMC

In this work, the target is to analyze the microstrip patch with and without the presence of AMC. Therefore, a 2 x 2 unit cell AMC structure has been placed underneath the dual band microstrip patch antenna to replace the conventional ground plane as shown in Figure 5.

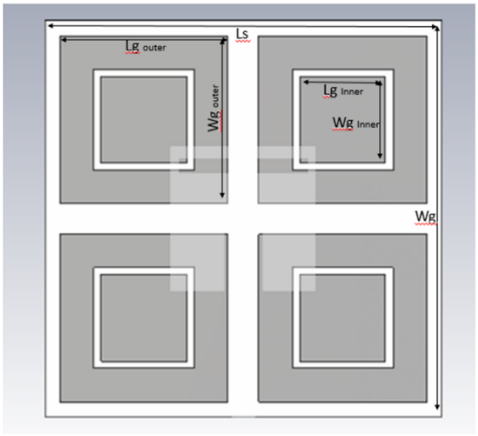


Figure 5 2x2 unit cell AMC as an antenna ground plane

## IV. Result And Discussion

Simulated results for the AMC unit cell, the proposed antenna in term of return loss and radiation pattern will be discussed in this section.

### A. *Unit cell AMC Design*

The unit cell AMC has been designed to exhibit zero reflection phase at 2.4GHz. Figure 6 shows the optimized geometries of unit cell. The dimension of Lg and Wg is 12.5mm and 11.9mm respectively.

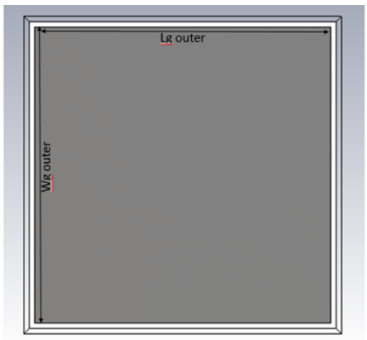


Figure 6 Geometry of single band unit cell AMC

Then, a gap was introduced for dual band unit cell AMC as shown in Figure 7.

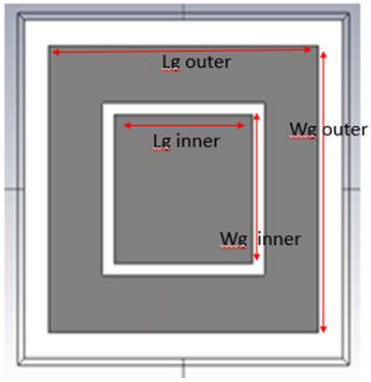


Figure 7 Dual Band unit cell AMC

Figure 8 shows the simulated reflection coefficient phase of a single band (green line) and dual band (blue line) unit cell AMC. It can be seen that the unit cell AMC exhibit zero reflection phase at 2.4GHz and 5.8GHz. The operating bandwidth of single band unit cell AMC at 2.4GHz is from 2.318GHz to 2.484GHz. The operating bandwidth of dual band unit cell AMC is from 2.362GHz to 2.428GHz and from 5.702GHz to 5.863GHz for 2.4GHz and 5.8GHz respectively.

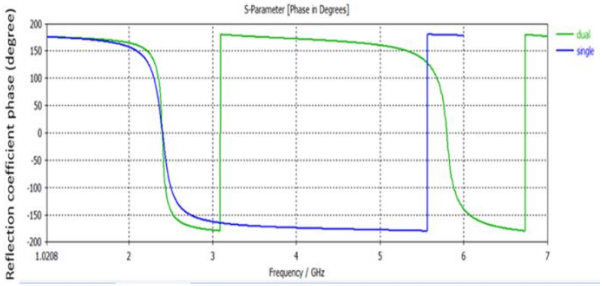


Figure 8 Simulated reflection coefficient phase of single band and dual band unit cell AMC

*B. Single band Microstrip Antenna*

Figure 9 shows the optimized geometries of single element microstrip patch antenna that operates at 2.4GHz.

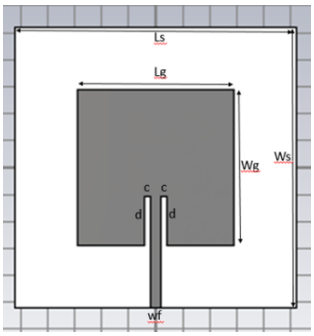


Figure 9 Geometry of single band of microstrip patch antenna

Figure 10 shows the simulated reflection coefficient (S11) of a single band microstrip patch antenna with a conventional ground plane. It can be seen that the antenna resonate at 2.4GHz and the reflection coefficient response about -15.1dB. As for -10dB bandwidth, at 2.4GHz, the simulation results show antenna bandwidth of 110MHz.

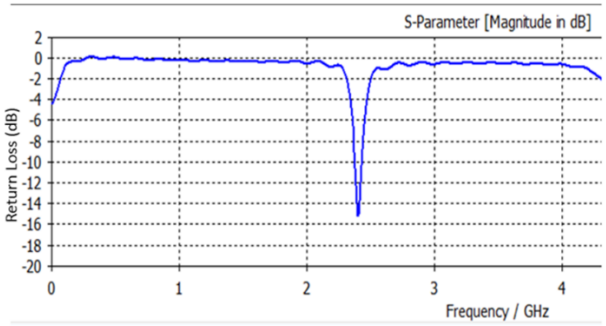


Figure 10 Simulated reflection coefficient of single microstrip patch antenna

*C. Dual Band Microstrip Antenna*

Then, a single element was transformed to dual band microstrip patch antenna by introduced a slot. A slot introduced second resonant frequency at 5.8GHz as shown in Figure 11.

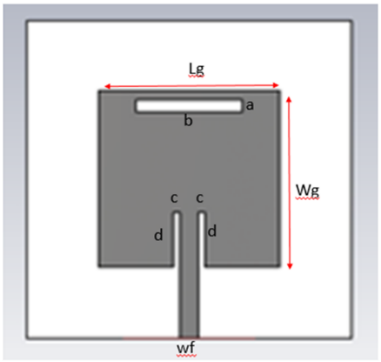


Figure 11 Geometry of dual band microstrip patch antenna

Figure 12 show the simulated reflection coefficient (S11) of a dual band microstrip patch antenna with a conventional ground plane. The reflection coefficient response is about -14.96dB and -15.35dB at 2.4GHz and 5.8GHz respectively. As

for -10dB bandwidth, the simulation results show antenna bandwidth of 114MHz and 156MHz.

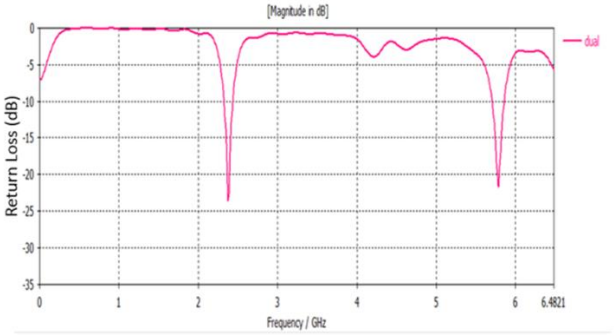


Figure 12 Simulated reflection coefficient of dual-band microstrip patch antenna

*D. Dual Band Antenna with AMC*

The unit cell AMC is then transformed to 2 x 2 units AMC structure with a size of the substrate is 52 x 52 mm as shown in Figure 13. Each square patch is positioned evenly and AMC structure is placed underneath the dual band microstrip patch antenna to replace the conventional ground plane.

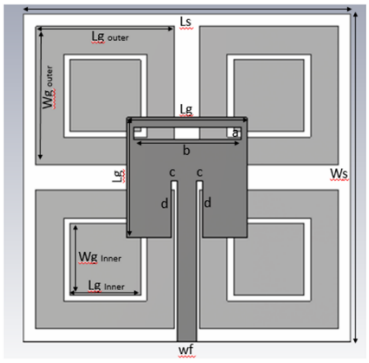


Figure 13 Geometry of 2 x 2 AMC structure underneath dual band microstrip patch antenna

Figure 14 show the reflection coefficient result of microstrip patch antenna with AMC as a ground plane. The resonant frequency at 2.4GHz after the presence of AMC are shifted to 1.8GHz while at 5.8GHz, it only has little shifted to the left. However, with the presence of AMC, another resonant frequency of 4GHz has been introduced.

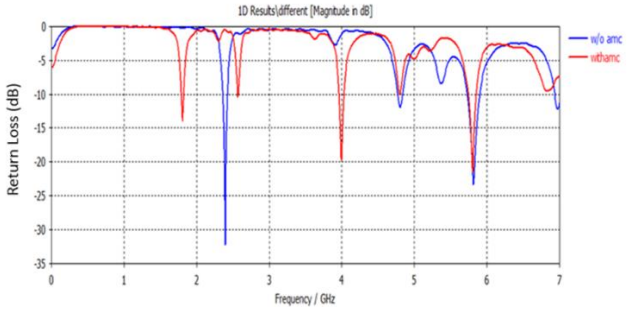


Figure 14 The return loss of microstrip patch antenna with AMC before altering the patch dimension

Figure 15 show the reflection coefficient of dual band microstrip patch antenna with AMC after optimization. The simulated result shows that after reduced several dimensions of a patch, the antenna managed to resonante at 2.4GHz and 5.8GHz. The reflection coefficient response is about -16.17dB and -16.38dB at 2.4GHz and 5.8GHz. As for the -10dB bandwidth, the results show antenna bandwidth is about 33MHz and 248MHz at 2.4GHz and 5.8GHz respectively. However, another resonant frequency is still happening at 4GHz.

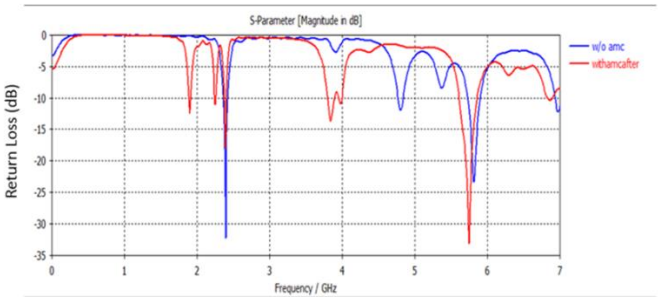


Figure 15 The return loss of microstrip patch antenna with AMC after optimization patch dimension

E. *Radiation Pattern*

The radiation pattern of dual band microstrip patch antenna at both frequencies of operation with and without the presence of AMC is shown in Figure 16 and Figure 17 respectively. Figure 16 represents the polar plot radiation pattern result at 2.4GHz while Figure 17 represents the polar plot radiation pattern result at 5.8GHz.

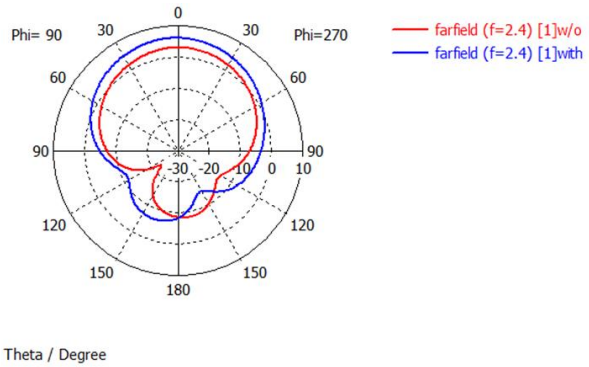


Figure 16 Polar plot of dual band microstrip antenna with and without AMC at 2.4GHz

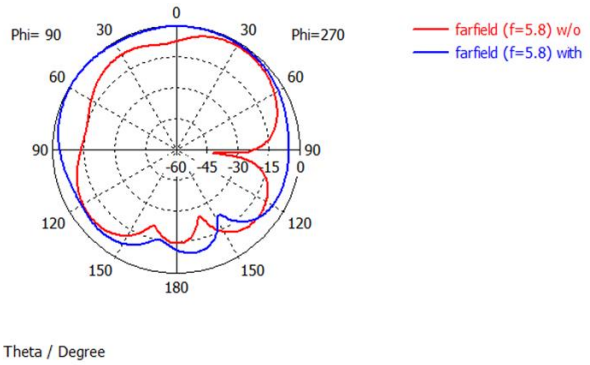


Figure 17 Polar plot of dual band microstrip antenna with and without AMC at 5.8GHz

It can be clearly observed that dual band microstrip patch antenna with AMC are more broadside with back lobe compared to the antenna without the presence of AMC. For 5.8GHz, the radiation pattern is more like Omni-directional meanwhile, at 2.4GHz, the result shows a more directive pattern.

TABLE 2 SUMMARIZED RESULTS OF DUAL BAND MICROSTRIP PATCH ANTENNA WITH AND WITHOUT AMC STRUCTURE

| **Properties** | **Dual band antenna without AMC** | | **Dual band antenna with AMC** | |
|---|---|---|---|---|
| Frequency | 2.4GHz | 5.8GHz | 2.4GHz | 5.8GHz |
| Return Loss (dB) | -14.96 | -15.35 | -16.17 | -16.38 |
| Bandwidth (MHz) | 114 | 156 | 33 | 248 |
| Maximum Directivity (dBi) | 6.14 | 5.34 | 6.18 | 4.66 |

It can clearly observe that, with the presence of AMC as a ground plane, the reflection coefficient response is better at both frequencies. Besides, the bandwidth also wider with the AMC as a ground plane at 5.8GHz while the maximum directivity at 2.4GHz has increased by 0.02dBi due to the effect of AMC structure as a ground plane. Moreover, with the presence of AMC as ground plane, the antenna patch size is more compact compared with the antenna patch size without AMC as a ground plane.

## V. CONCLUSION

This project proved that with the presence of AMC as a ground plane, the magnitude of return loss is much better with -16.17dB and -16.38dB compared with the antenna that using a conventional ground plane with -14.96dB and-15.35dB at 2.4GHz and 5.8GHz respectively. The maximum directivity has been recorded as 6.14dBi and 5.34dBi (without AMC) and 6.18dBi and 4.66dBi (with AMC) at 2.4GHz and 5.8GHz. The result shows at 2.4GHz, the maximum directivity increased. Meanwhile, the bandwidth also wider with the AMC structure as a ground plane at 5.8GHz.

## REFERENCES

[1] F. Rahmadani and A. Munir. Microstrip patch antenna miniaturization using artificial magnetic conductor. *6th International Conference on Telecommunication Systems, Services, and Applications (TSSA).* Oct 20-21, 2011. Bali: IEEE. 2011. 219-223.

[2] W.K.W. ALI. *Wide Band Micro strip Antenna for Land Based Vehicles*. UTM, RESEARCH VOT: 74038, 2004.

[3] M. Nafe, A. Syed and A. Shamim. Gain enhancement of low profile on-chip dipole antenna via Artificial Magnetic Conductor at 94 GHz. *9th European Conference on Antennas and Propagation (EuCAP)*. April 3-17, 2015. Lisbon: IEEE. 2015. 1-3.

[4] M. C. Tang, H. Wang and T. Deng. A compact dual-frequency patch antenna design. *IEEE 4th Asia-Pacific Conference on Antennas and Propagation (APCAP).* June 30 - July 3, 2015. Kuta: IEEE. 2015. 616-617.

[5] S. Bhunia, A. Roy and P. P. Sarkar. Compact wideband dual frequency (dual band) microstrip patch antenna for wireless communications. *URSI Asia-Pacific Radio Science Conference (URSI AP-RASC).* Aug 21-25, 2016 Seoul: IEEE. 2016.1357-1360.

[6] Agarwal, V. K., Shaw, A. K., Das, M. K., Mukherjee, J., & Mandal, K. *A Novel Compact Dual Frequency Micro strip Antenna. Procedia Technology*. 2012. 427 – 430.

[7] H. Malekpoor and S. Jam. Improved Radiation Performance of Low Profile Printed Slot Antenna Using Wideband Planar AMC Surface. *IEEE Transactions on Antennas and Propagation*. September 09, 2016. vol. 64, no. 11. 4626-4638.

[8] Feresidis, A. P., Goussetis, G., Wang, S., & Vardaxoglou, J. C. Artificial magnetic conductor surfaces and their application to low-profile high-gain planar antennas. *IEEE Transactions on Antennas and Propagation*. Jan, 2005. 53(1), 209-215.

# Dielectric Measurement of Thin Samples for Free-Space Technique from 12GHz to 15 GHz

Hafizah Mutadza
*Faculty of Electrical Engineering*
*Universiti Teknologi Malaysia*
*Johor Bahru, Malaysia.*
*hafizahmutadza@gmail.com*

You Kok Yeow
*Department of Communication Engineering*
*Faculty of Electrical Engineering*
*Universiti Teknologi Malaysia*
*Johor Bahru, Malaysia.*
*kyyou@fke.utm.my*

***Abstract*— In this paper, a free-space measurement system has been developed for thin planar material characterizations. The measurement system is operated in frequency range of 12 GHz to 15 GHz. The measurement consist of two standard gain horn antenna, network analyser, sliding guide, two antenna holder/stand, sample holder and two precision positioner. Most of the dimensions and the structure for the system components were designed by SolidWorks software and fabricated by 3D printer. Systematic errors due to multiple reflections along the measurement distance between antenna aperture and sample surface were calibrated by Thru-Reflect-Line (TRL) technique. The reflection/transmission coefficients of the sample was measured using Agilent E5071C ENA network analyzer. From the measured reflection/transmission coefficients, the relative permittivity of the sample can be predicted based on transmission phase shift concept. The thin planar well known samples that were used for this measurement for validation are the air, Teflon, PVC and FR4, respectively. In this study, the effect of thickness for the sample in permittivity prediction was also discussed and analysed in detail.**

**Keywords—Dielectric measurement, free-space, phase-shift transmission**

## I. INTRODUCTION

The measurement of complex dielectric properties of materials at radio frequency has gained interest because it importance especially in the research fields, such as material science, microwave circuit design, and to development of nowadays technologies. However one full set complete free space measurement system is very costly compare its usage. In this project,we want to build a free space measurement system that mostly its component is design in SolidWorks then we fabricate it to 3D as well as to do dielectric measurement from specific frequency to verify the system that we built. The importance of dielectric measurement because it can provide the electrical or magnetic characteristics of the materials, which proved useful in many research development field development of technologies [1].

Many methods have been created to measure these complex properties such as methods in time or frequency domain either with one port or two ports [1]. Every method must be followed its specific frequencies, materials and applications. With the advance of new technologies, the Methods can implement with a software program that measures the complex reflection and transmission coefficients with a suitable vector network analyser that later will convert the data into the complex dielectric property parameter.

Free-space methods are extremely well fit for the broadband measurement of the complex permittivity and permeability [2] .This technique is based on the measurement of the transmission coefficient and/or the reflection coefficient of planar samples for different polarization states, angles of incidence, frequencies, and thicknesses of the sample. Free-space methods are non-destructive and can be used for measuring a wide range of materials including gases, liquids, and solids [3].

However, there are two possibilities of inaccuracies in free space measurement technique. First the diffraction effects from the edge of samples and second the several reflections between two horns antenna through the surface of samples [2]. These two inaccuracies can be minimized if spot-focusing horn antennas are used and accurate calibration on the free space is done.

## II. LITERATURE REVIEW

### *A. Dielectric Measurement Technique*

Dielectric measurement can be determined by using resonance technique, free-space technique, open ended waveguide or one port reflection technique and two-port transmission and reflection technique. The differences between these techniques are material features that can be tested and its operating frequency. Resonance technique using small samples but it has high measurement accuracy for low loss materials at microwave frequencies. However it can be used in narrow band frequencies only. Open-ended waveguide using semi-infinite thickness of material and it is best for liquids or semi-solids. It is ease of measurement procedure however it has error in measurement due to improper contact between surface of sample and coaxial probe. Two-port transmission or reflection technique is best for material that has smooth, flat faces, perpendicular to long axis. It is suitable for magnetic material and for wideband frequency. Lastly, measurement technique for free space is for material that features large, flat, parallel-faced sample and specifically for magnetic materials.

### B. *Free Space Measurement Technique*

Free-space methods are extremely well fit for the broadband measurement of the complex permittivity and permeability. This technique is based on the measurement of the transmission coefficient and/or the reflection coefficient of planar samples for different polarization states, angles of incidence, frequencies, and thicknesses of the sample. Free-space methods are non-destructive and can be used for measuring a wide range of materials including gases, liquids, and solids. However, there are two possibilities of inaccuracies in free space measurement technique. First the diffraction effects from the edge of samples and second the several reflections between two horns antenna through the surface of samples. These two inaccuracies can be minimized if spot-focusing horn antennas are used and accurate calibration on the free space is done

### C. *TRL Calibration*

Internal calibration must be done on free space measurement to avoid rectangular and circular waveguide transitions due to multiple reflections as well as horn less antenna. Since free space method is used in this project, Thru-Reflect Line (TRL) calibration was chosen to calibrate the free space system as it is easier to implement compare to other calibration techniques. The TRL technique requires three standards of calibration, which are, a through connection, a short(reflect) circuit connected to each port, and a transmission line connected between the test ports[2] .These calibration standards are simpler to carry out in free space as compared with discrete impedance standards needed in other calibration techniques. T is referring to thru that means keeping the distance between two antennas equal twice the focal distance. R is reflect for port 1 and port 2 that connected to Vector Network Analyzer that are obtained by placing metal plate at focal plane. L is for line by moving the antenna away on a quarter wavelength then back in the original position.

## III. PROJECT METHODOLOGY

The measurement system of these free space is consists of two standard gain horn antenna that that have frequency from 12GHz to 15GHz,two precision positioner that function to adjust the distance of the horn ,sliding guide, two antenna holder/stand and sample holder. The horn antennas then connected to Vector Network Analyzer to determine the material under test (MUT) dielectric measurement. The material under test that was used are Teflon, PVC and FR4.All these materials have three different thickness 1mm,2mm and 3mm and being tested to determine whether different thickness give effect to dielectric value. Below are the overall process of project.

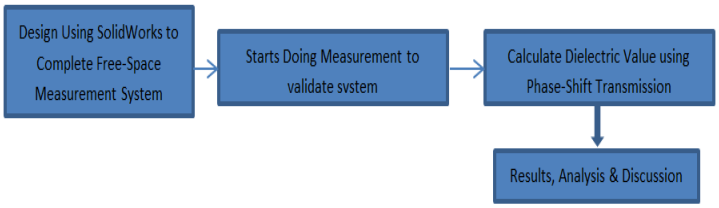


Fig. 1 Overall of the process

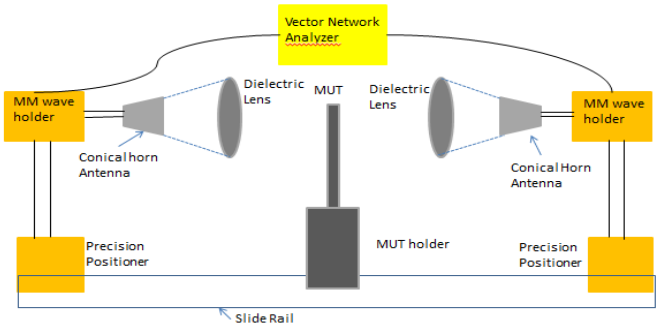


Fig.2 Illustration of free-space measurement technique [4]

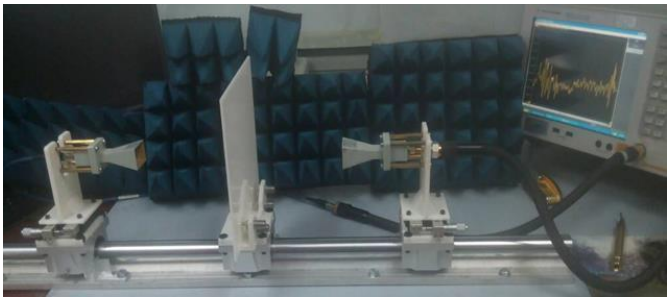

Fig.3 Real Free-Space Measurement system

### A. *Design in SolidWorks*

The precision positioner holder, horn holder/stand and sample holder were all design in SolidWorks and fabricate it to 3D.

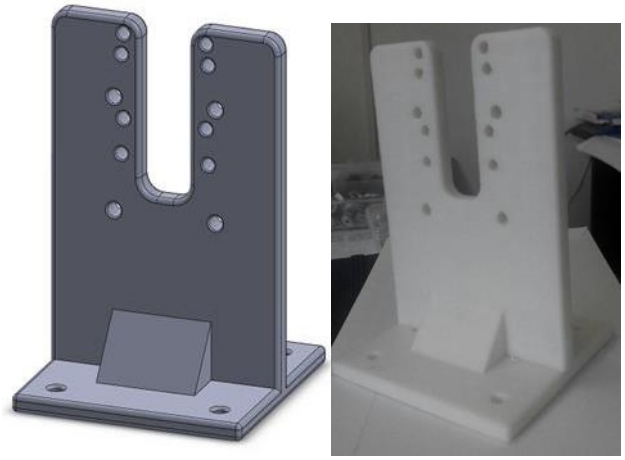

Fig.4 Horn Antenna holder/stand in SolidWorks and after it fabricate to 3D

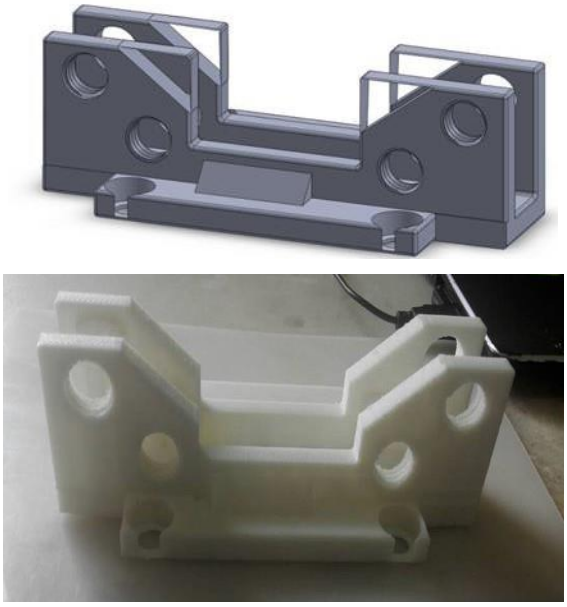

Fig.5 Sample holder in SolidWorks and after it fabricate to 3D

Fig.6 Precision positioner holder in SolidWorks and after it fabricate to 3D

*B.Formula Phase-Shift Transmission*

In this paper, transmission phase-shift (TPS) method is used as a formula to find the value of dielectric constant. The TPS method is a calibration-independent and material position-invariant technique, which can reduce the complexity of the de-embedding procedures without any iterative algorithm. Unlike NRW, the TPS can be applied for the thickness of the material which is exceeded λ/4. The indefinites of the forthcoming relative permittivity is high for the low-loss thin sample by using TPS method due to the reduce of the sensitivity for the transmitted wave through the sample [5].

The relative permittivity for material can be expressed as where $\varepsilon_r'$ for real part of permittivity and $\varepsilon_r''$ is imaginary part of permittivity [6]

$$\varepsilon_r' = \frac{1}{k_o^2}\left\{\left(\gamma_o + \frac{\emptyset_{21_{air}} - \emptyset_{21_{sample}}}{d}\right)^2 + \left(\frac{\pi}{b}\right)^2 - \alpha^2\right\} \quad (1)$$

$$\varepsilon_r'' = \frac{2\alpha}{k_o^2}\left(\gamma_o + \frac{\emptyset_{21_{-air}} - \emptyset_{21\_sample}}{d}\right) \quad (2)$$

$k_o$ is the propagation of free space

$$k_o = \frac{2\pi f}{c} \quad (3)$$

C is speed of light,3 x $10^8$, b(in meter) are the width of the aperture of the horn respectively, d(in meter) is the thickness of sample. The $\emptyset_{21\_air}$ and $\emptyset_{21\_sample}$ are the measured phase shift of the transmission coefficient in the air (without sample).The phase constant, $\gamma_o$ is given as

$$\gamma_o = \sqrt{k_o^2 - \left(\frac{\pi}{b}\right)^2} \quad (4)$$

While $|S_{11\_sample}|$, $|S_{21\_sample}|$,$|S_{11\_air}|$ ,and$|S_{21_air}|$ are the measured linear magnitudes of the reflection coefficient and the transmisssion coefficient for the air without sample.

$$\alpha \approx -1.15129254\left[\frac{1}{d}\log_{10}\left(|S_{11\_sample}|^2 + |S_{21\_sample}|^2\right) - \frac{1}{d_w}\log_{10}\left(|S_{11\_air}|^2 + |S_{21\_air}|^2\right)\right] \quad (5)$$

## IV.RESULT AND ANALYSIS

Taking only the results when thickness d=3mm the results is almost accurate when compared it to dielectric value of manufacturer. The uncertainty measurement is high for a thin sample due to the decreasing of the sensitivity for the transmitted wave through the sample, especially for transmitted waves that have longer wavelengths. Substitute the formula given in Matlab give almost accurate which is 1 while the value for FR4 between the value of 3.8 to 5.2.The value for Teflon is 1.8 to 2.4 and lastly for PVC is 2.2 to 2.7.The value of dielectric constant still in range but it will be slightly inaccurate if the samples is very thin such as for samples that has thickness d=1mm,2mm.It is due to the diffraction effects at the edge of sample and multiple reflections as the wave propagate since the samples is thin.

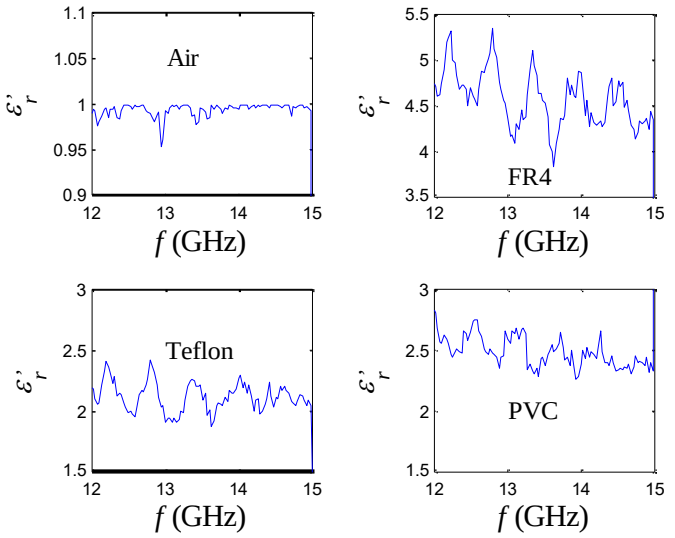


Fig.7 Dielectric Value for thickness 3mm

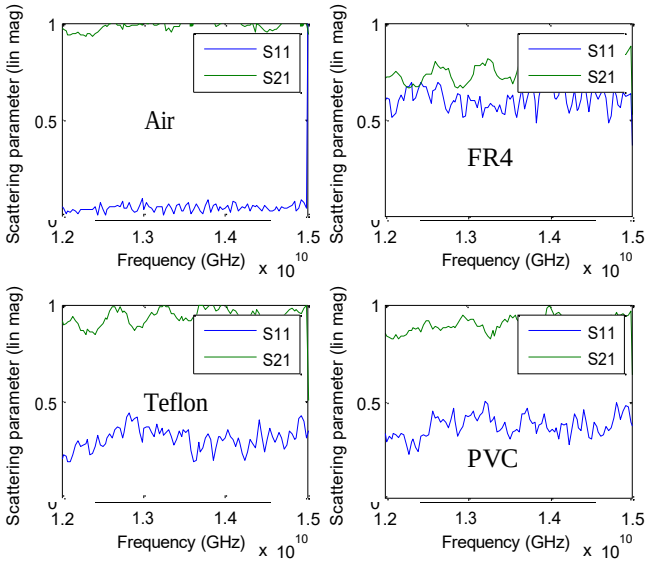


Fig.8 Scattering parameters for thickness 3mm

## V.CONCLUSIONS

The value of dielectric constant that being obtained is still in range of manufacturer dielectric value.It is proven that the free space measurement system can used in condition the thickness of sample should be exceeded λ/4.

## REFERENCES

[1] Measurement of Dielectric Material Properties. (n.d.). Retrieved May 15, 2017, from https://cdn.rohde-schwarz.com/pws/dl_downloads/dl_application/00aps_undefined/RAC-0607-0019_1_5E.pdf

[2] Ghodgaonkar, D., Varadan, V., & Varadan, V. (1989). A free-space method for measurement of dielectric constants and loss tangents at microwave frequencies. IEEE Transactions on Instrumentation and Measurement, 38(3), 789-793.

[3] Ghodgaonkar, D., Varadan, V., & Varadan, V. (1990). Free-space measurement of complex permittivity and complex permeability of magnetic materials at microwave frequencies. IEEE Transactions on Instrumentation and Measurement, 39(2), 387-394.

[4] ] Tosaka, T., Fujii, K., Fukunaga, K., & Kasamatsu, A. (2014). Development of Complex Relative Permittivity Measurement System Based on Free-Space in 220–330-GHz Range. IEEE Transactions on Terahertz Science and Technology, 1-8.

[5] K. Y. You, Y. S. Lee, L. Zahid, M. F. A. Malek, K. Y. Lee, E. M. Cheng, N. H. H. Khamis (2015). Dielectric Measurements For Low-Loss Materials Using Transmission Phase-Shift Method ,Jurnal Teknologi (Sciences & Engineering) 1-9.

[6] K. Y. You (2016). Effects of Sample Thickness for Dielectric Measurements Using Transmission Phase-Shift Method, International Journal of Advances in Microwave Technology (IJAMT),1-4.

$$\alpha + \beta = \chi. \qquad (1) \qquad (1)$$

# Sports Monitoring System

Rahmat bin Kamba
*Faculty of Electrical Engineering*
*Universiti Teknologi Malaysia*
*Johor Bahru, Malaysia.*
*Ramat_kay@yahoo.com*

Sharifah Kamilah binti Syed Yusof
*Department of Communication Engineering*
*Faculty of Electrical Engineering*
*Universiti Teknologi Malaysia*
*Johor Bahru, Malaysia.*

***Abstract*—Recent innovation of the technology in wireless sensor network (WSN) has eased the deployment of this type network in many applications such as monitoring system. This project presents a sports training monitoring system that is equipped with a set of advanced electronics, sensors and automated devices that is based on the technology in WSN. A steady and dependable sports monitoring observing framework is indispensable to build up a shrewd and effective sports administration program that can prompt to quality results. A sports training monitoring framework has been created and tried in a genuine preparing environment in a field. The system is designed based on a WSN that is linked to the cloud network on the Internet. Using TelG mote as the basis, customized sensor nodes that function as a forwarder node and the relay nodes are developed to establish the WSN. The TelG motes that have been customized to operate without the sensing unit operate using the ZigBee standard. A reliable system architecture for the sports training monitoring application is constructed according to the measurements conducted to investigate several factors that affect the packet loss rate. The components that are considered amid the estimations are the separation between the transmitter and the receiver, the tallness of receiver, the portability of the transmitter, the transmission force of the transmitter, and in addition the packet size and transmission rate. The system architecture consists of a base station, a forwarder node that is mounted on the body of sports player and receiver that are located at computer as base station where the positions are based on the results from the measurement. Several experiments are conducted in a real scenario in a field to measure the reliability of the system architecture. It is shown from the experiments that the proposed architecture is function very well even when the athletes is at a high speed. The packet loss for all of the experiments conducted is less than 2% which does not give huge impact to the data transmission.***

**Keywords—Sports monitoring system, zigbee, xbee pro**

## I. INTRODUCTION

Wireless Sensor Networks (WSN) include of various modest and low-control gadgets that are little in size and ordinarily controlled by battery [1]. These sensor gadgets cooperates to set up a shrewd situation that assembles vital information and data to be gotten to by human (coach, athlete, sport scientist) at whatever time and anyplace. Inferable from their straightforwardness and specially appointed arrangement highlights, WSNs have been connected to different fields of science and innovation, for example, medicinal services, military observation, thruway activity, environment monitoring likewise in sports monitoring[2]. Late best in class innovation of wireless sensor network has empowered the incorporation of the development of sensor nodes in the IoT region [3]. Utilizing the wireless sensor network as the premise, these brilliant sensors in Internet of Things team up specifically with no human intercession and convey another class of uses that further addition to the personal satisfaction.

A part of the primary errands of WSNs is information collection at the sensor field where the detected information are consistently gathered. This information can be handled firstly by sensor nodes before it is being sent through wireless correspondences to a base station for next step. The base station can be midway situated inside the sensor area, or someplace out of the detecting field. In the last case, a gateway need to connect the sensor node with the base station because the sensor nodes have constrained transmission extend. In the meantime, sensor nodes are regularly sent at the particular areas as required by the application. Since the span of the sensor node is little, the node can be joined at any area with insignificant aggravation to the encompassing surrounding. The adaptability offered by Wireless Sensor Network have diminished the expenses for organization. Therefore, this made the Wireless Sensor Network a focused approach for information accumulation when contrasted with its wired partner to the foundation based system.

## II. METHODOLOGY AND PROPOSED ARCHITECTURE (SYSTEM)

Chapter 3 examines on the review of proposed sports preparing monitoring framework and points of interest on the equipment advancement of the framework. Area 3.2 clarifies the general design of the framework and the stream of the proposed sports monitoring while Section 3.3 depicts the advancement periods of sports preparing observing framework.

### *A.* Proposed Sports Training Monitoring System

Sports preparing observing framework comprises of equipment segments, for example, server, door, sensor nodes and sensor gadgets. There are a few sorts of nodes that are utilized as a part of this framework which are sensors nodes, forwarder node, and base station node. Three sensor nodes are

utilized to acquire the information, for example, speed, heart rate and temperature. Figure 3.1 demonstrates the proposed framework engineering for the wireless sports monitoring framework. The sensor nodes that are connected to the athlete's body to deliver the information and transmit the information to the forwarder node. At that point, the forwarder node sends the information to the base station utilizing 802.15.4 innovation. The information are sent ceaselessly until the athletes quit preparing. The errand of the base station is to transfer the information to the server through cloud arrange. These information are then ready to be downloaded by the athlete, mentor and sports researchers from the server to be dissected. The extent of work required in this exploration is demonstrated by the specked box in Figure 3.1. The advancement of the cloud organizing and in addition the portable and graphical UI (GUI) applications are further created by the UTM-Mimos research center, Universiti Teknologi Malaysia. Figure 3.2 demonstrates the general stream diagram of the framework.

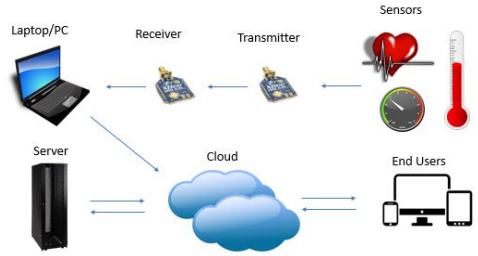


***Figure 3.1*** *Sports Training Monitoring System Architecture.*

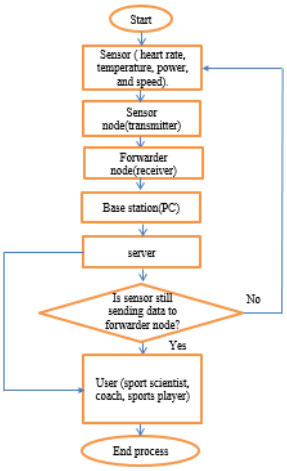


*Figure 3.1 Sports Training Monitoring System Flow Chart*

### *B. Development of Sports Training Monitoring System*

The examination stream for building up the sports monitoring system is appeared in Figure 3.3. The work is partitioned into three stages. The main stage is the preparatory review which included the writing audit on the current Wireless Sensor Networks applications and in addition the estimation frameworks and parameters for observing framework. The current execution identified with parcel misfortune estimation is additionally examined as talked about in points of interest in Chapter 2. Amid the principal stage, the equipment segments required for the arrangement of the sensor organize and reasonable gadgets to be utilized amid the estimation procedure are distinguished. In view of the reviews, TelG node that is produced by the Telematics Research Group, Universiti Teknologi Malaysia, is chosen to achieve the goals of the exploration [10]. Along these lines, the points of interest and particulars of this node are examined in subtle elements. Likewise, IEEE802.15.4 is picked as the wireless standard for information transmission in the system. The avocation of the choice to utilize both TelG node and IEEE802.15.4 standard has been clarified in Chapter 2. Endless supply of the preparatory review, the customization procedure of the TelG nodes that are utilized as sensor nodes as a part of the system is made inside this stage. The procedure incorporates outlining and programming of the TelG node. The packaging advancement process is likewise finished in this stage.

The following stage included the framework design estimations. At the point when outlining the sports monitoring system, calculates that can influence the bundle conveyance amid parcel transmission from the forwarder nodes or portal to the base station must be thought about. Because of the way that the transmission ability of the sensor node's handset shifts as per certain conditions, this estimation procedure is essential to guarantee the dependability of the framework. The genuine size of field and in addition its shape must be considered when outlining the entire framework as the instructional courses of athletes are typically held in field. The components connected with the estimation procedure are separation amongst transmitter and beneficiary, tallness and point of collector, transmission force of transmitter, and also bundle size and rate. Amid the estimation procedure, information are likewise gathered and broke down.

At last, in the third stage, the framework engineering is planned in light of the outcomes from estimation handle in the past stage. The execution assessment of the framework is then executed and results are investigated regarding parcel misfortune rate and end to end delay.


*Figure 3.3 System Architecture*

### *C. Measured Parameters*

In this estimation, there are different parameters that should be set contingent upon the estimation necessities. The parameters are set by components of the genuine item that is utilized as a part of the investigation. For instance, the transmission rate for every bundle to be transmitted is settled at 2 packets/second. This setting is connected for all estimations. The rate of 2 packets/second is picked in light of the fact that in the genuine item execution, every sensor node transmits a bundle in each 500ms interim. In the interim, the packet size is settled at 12 bytes for all estimations. The reason the estimation of 12 bytes is chosen as the packet size is on the grounds that this is the most extreme size permitted in the bundle transmission of a TelG node.

*Experiment A: Constant Distance (60m) with Different Speed*

Experiment A conducted to see rate of packet receive by the receiver from two transmitter, Transmitter A and Transmitter B. Experiment A conducted with the set of details show in Table 3.1. Different speed of transmitter A and B was set to see packet receive ratio with different speed of transmitter. Table 3.2 shows the data from experiment A and Figure 3.2 shows the graph plotted from the data.

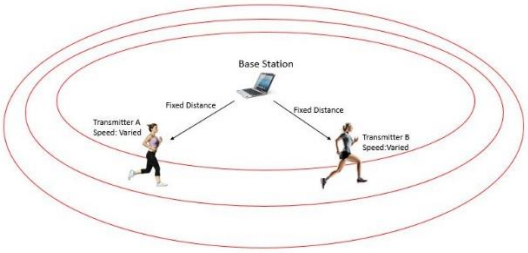


*Figure 3.2 Experiment A Setup*

| Parameters | Value |
|---|---|
| Transmission rate | 2 packets/second |
| Size of packet | 12 bytes |
| Speed of transmitter A and B | 10 to 23 km/h |
| Number of packets transmitted | 100 packets |

*Table 3.1 Parameters for Experiment A*

*Experiment B: Constant Speed (15kmph) with different Distance*

Experiment B conducted also to see the ratio of packet received by the transmitter. The speed of Transmitter A and Transmitter B both at the same speed which is 15km/h but with the different distance from the receiver. Details of the experiment are tabulated in table 3.3. Table 3.4 shows the data gain from the experiment. While Figure 3.4 shows the data plotted with the gained data.

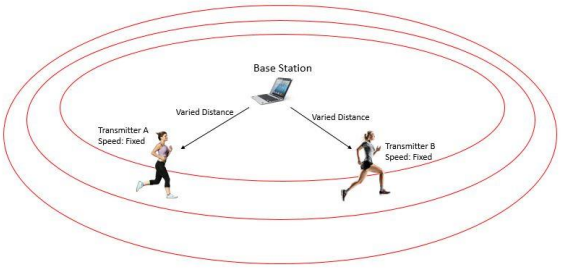


*Figure 3.3 Experiment B Setup*

| Parameters | Value |
|---|---|
| Transmission rate | 2 packets/second |
| Size of packets | 12 bytes |
| Distance between transmitter and receiver | 40 to 80 meter |
| Number of packets transmitted | 100 packets |
| Speed of Transmitter A and B | 15km/k (fixed) |

*Table 3.3 Parameters for Experiment B*

*Experiment C: Constant Distance (60meter) between Transmitter and Receiver with different distance between two transmitter (Transmitter A and Transmitter B) while Transmitter Static*

In Experiment C, the both transmitter are static but distance between Transmitter A and Transmitter B are varied from 5 to 13 meter to see what is the effect of the distance between the transmitter. Table 3.5 show the details of the parameter for Experiment C. While Table 3.6 shows the data gained from the measurement done.

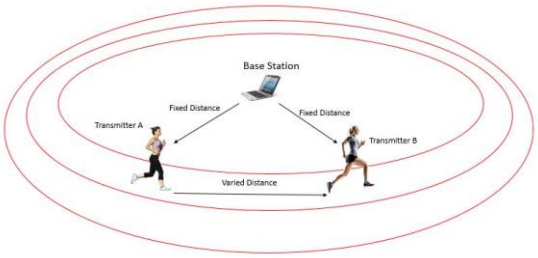


*Figure 3.6 Experiment C Setup*

| Parameters | Value |
|---|---|
| Transmission rate | 2 packets/second |
| Size of packet | 12 bytes |
| Distance of receiver to the transmitter path | 60meter (fixed) |
| Number of packets transmitted | 100 packets |
| Distance between Transmitter A and B | 5 to13 meter |

*Table 3.2 Parameter for Experiment C*

*Experiment D: Two transmitter in the same line to receiver with different distance to receiver (transmitter static)*

In this experiment, both of the transmitter also static same with Experiment C but these two transmitter are in the same line with the receiver. Figure 3.9 shows how the receiver and transmitter was set up. Table 3.7 show the details of the parameter in this experiment.

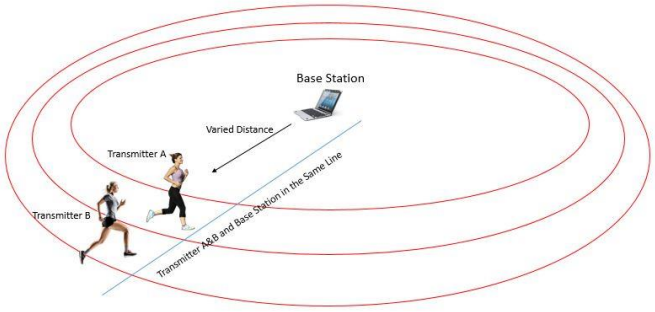


*Figure 3.8 Experiment D Setup*

| Parameters | Value |
|---|---|
| Transmission rate | 2 packets/second |
| Size of packet | 12 bytes |
| Distance of receiver to the transmitter path | 40 to 80 meter |
| Number of packets transmitted | 100 packets |

Table 3.7 Parameter for Experiment D

## III. Result and Analysis

### A. Result

*Experiment A*

| Speed (km/h) | Packet Receive Ratio |
|---|---|
| 10 | 0.96 |
| 15 | 0.96 |
| 17 | 0.94 |
| 20 | 0.92 |
| 23 | 0.91 |

*Table 3.2 Constant distance (60m) with different speed*

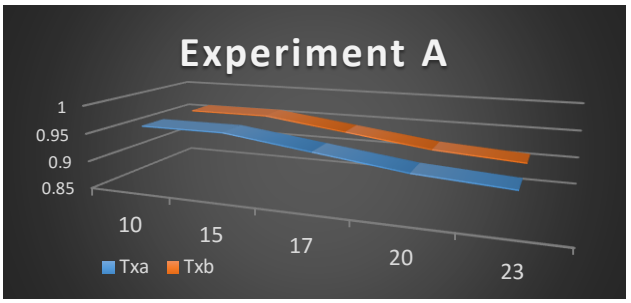


*Figure 3.2 Packet Receive Ratio for Experiment A*

Figure 3.2 demonstrates the results of the experiment. At the speed of 10 km/h, both transmitter shows the ratio of packet received are 0.96. While at 15km/h and 17km/h both shows ratio of 0.96 and 0.94 of packet received. At the speed of 17 and 23km/h shows the decrement of packet receive ratio to 0.92 and 0.91 due to higher speed set to the transmitter.

*Experiment B*

| Distance(meter) | Packet Receive Ratio |
|---|---|
| 40 | 1.00 |
| 50 | 1.00 |
| 60 | 0.96 |
| 70 | 0.93 |
| 80 | 0.88 |

*Table 3.4 Data from Experiment B*

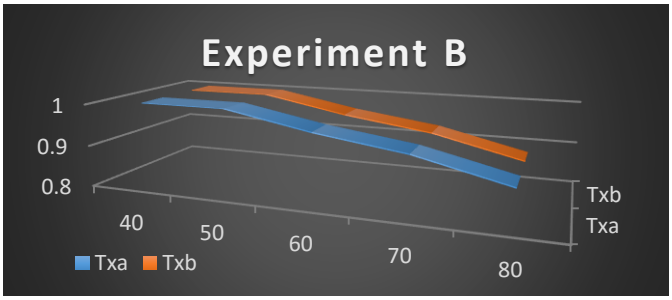


*Figure 3.5 Packet Receive Ratio for Experiment B*

Figure 3.5 shows the data where at the distance 40 and 50 meter, the transmitter send the packet with the ratio of 1 for both transmitter. Ratio of 1 means no packet loss at the receiver which is the base station. At 60, 70 and 80 meter shows the decrement of packet received ratio which is 0.96, 0.93, and 0.88. Due to the distance from receiver, signal from the transmitter become minimum for the receiver to get the packet send which is 100 packet.

*Experiment C*

| Distance (meter) | Packet Receive Ratio |
|---|---|
| 5 | 0.96 |
| 7 | 0.96 |
| 9 | 0.94 |
| 11 | 0.92 |
| 13 | 0.91 |

*Table 3.6 Data Gained from Experiment C*

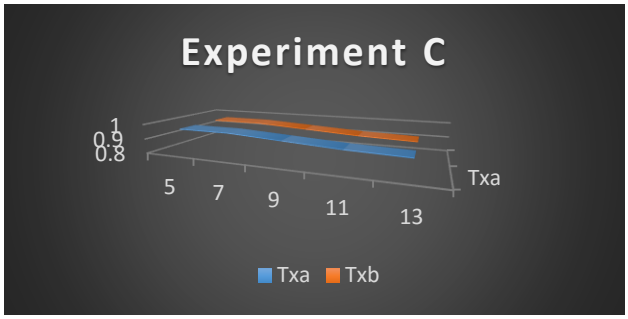


*Figure 3.7 Data Plotted for Experiment C*

Figure 3.7 show the data plotted from measurement C, where the Transmitter are static but with different distance from each of the transmitter. At distance 5 meter, ratio of packet received is 0.91. The larger the distance between two transmitters, the bigger the ratio of packet received. At distance of 7,9,11, and 13 meter from each other, the packet received ratio are 0.93, 0.93, 0.96, and 0.96. This data shows that if the transmitter are in the short distance with each other, the receiver will facing the problem getting the signal.

*Experiment D*

| Distance (meter) | Packet Receive Ratio |
|---|---|
| 40 | 0.96 |
| 50 | 0.96 |
| 60 | 0.96 |
| 70 | 0.92 |
| 80 | 0.87 |

*Table 3.8 Data from Experiment D*

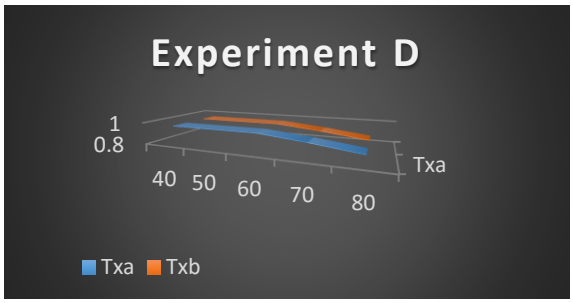


*Figure 3.9 Data plotted from Experiment D*

Figure 3.9 shows the data plotted from Experiment D. At distance 40 meter, 0.96 ratio of packet received by the base station. After distance 60 meter which is 70 and 80 meter, the graph shows the decrement of packet received ratio due to signal loss.

### B. *Discussion*

From the result, Experiment A shows that the faster the transmitter move, the bigger the packet loss. Due to high speed, the receiver facing the problem to receive the signal from transmitter directly cause the packet loss. As the result from Experiment B, the bigger the distance between transmitter and receiver, the bigger the packet loss due to lower signal strength if the transmitter move away from the receiver. In Experiment C, distance between Transmitter A and Transmitter B may cause effect to transmission of the data. The shorter the distance between Transmitter A and Transmitter B, the bigger the packet loss. This is due to overlapping signal and the receiver misunderstand the signal transmit make the receiver did not receive all the packet sent. While in Experiment D, position of the transmitter also things need to be consider. If the transmitter are stand in the same line to the receiver, the signal or the radiation from the antenna may be blocked by the transmitter whose stand nearer of in the front line of transmitter.

## IV. Conclusion

As the conclusion, from this experiment, to minimize the packet loss, hardware may be consider such as an antenna used in the transmitter may be replace with bigger radiation pattern from the antenna due to the signal blockage as the transmitter stand in the same line. Speed movement of the transmitter may be the things cannot be considered. But, to minimize the packet loss, this system may be used for suitable sport within the range of maximum speed for zero packet loss.

## References

1. Tubaishat M, Madria S. Sensor network: an overview. *IEEE Potentials*. 2013;22(2):20-23.

2. Wang F, Liu J. Networked Wireless Sensor Data Collection: Issues, Challenges, and Approaches. *IEEE Commun Surv Tutorials*. 2011;13(4):673-687.

3. Al-Fuqaha A, Guizani M, Mohammadi M, Aledhari M, Ayyash M. Internet of Things: A Survey on Enabling Technologies, Protocols, and Applications. *IEEE Commun Surv Tutorials*. 2015;17(4):2347-2376.

4. Armstrong S. Wireless connectivity for health and sports monitoring: a review.*British Journal of Sports Medicine*. 2007;41(5):285-289.

5. C. Young, P. R. Fleming, S. Dixon and MJC. Shoe signature monitoring for advanced running technique. *Eng Sport 7*. 2008;2(1):35-43.

6. S. K. Gharghan, R. Nordin and MI. A Survey on Energy Efficient Wireless Sensor Networks for Bicycle Performance Monitoring Application. *J Sensors*. 2014;1(1):2014.

# Refractive Index Measurements using Tapered Optical Fiber

Helal Ahmed Abdullah, Mohd Rashidi Salim, Nurul Ezaila Alias, Mohd Hafizi Ahmad, Mohd Amri Md. Yunus
*Faculty of Electrical Engineering, Universiti Teknologi Malaysia (UTM), UTM Skudai, Johor Bahru, Johor, Malaysia*
*alhelali44@gmail.com*

***Abstract*—Optical Fiber Sensors for monitoring the refractive index in liquids sample have been improved by modifying cladding part on the optical fiber. In this proposal, fabrication of a sensor using tapered fiber will be done to measure the refractive index of various liquids. We are going to analyze the characteristic change of the light transmission of the fiber when we use the fiber to sense a physical property from the external environment. Eight samples of the tapered fibers with different diameters is tested to analyze the performance and the responses of the samples. We fabricate a sensing region on the fiber optic using etching technique by dipping small part of the fiber optic into Hydrofluoric (HF) acid. The analytical results will be used to choose the most sensitive and fast response tapered optical fiber among the 8 samples. The main reason and significances why we want to manufacture this sensor using this technique are easy and safe fabrication, fast response and very sensitive to the external environment parameters. This sensor will be used as liquid refractive index sensor.**

***Keywords – Refractive Index; Single Mode Fiber; Multimode Fiber; Optical Fiber Sensor***

## I. INTRODUCTION

Optical fiber sensors (OFS) technology have become one of the most important devices for sensing during the last 10 years due to comparative advantages over other existence sensors technology. These advantages include rapid responsiveness, compact size, stability, safety, flexibility, capability for remote monitoring and also suitable to perform even in harsh and rough environment. OFS are designed to acquire the information through fiber optics. To make the optical fiber more sensitive to the external environment, the waveguide property is modified by some suitable techniques for example, etching the cladding. Many researchers working in OFS have suggested different techniques and methods to fabricate a sensing zone on the optical fiber elements [1]. Therefore, aside from adding accessory components to the system, we believe the enhancement of sensitivity relies heavily on the geometries of the tapered region itself [2]. A few studies have been done and adduced on the manipulation of the tapered optical fiber's dimensions that achieved a sensitivity value of 1913nm/RIU by sandwiching a tapered multi-mode fiber in between two single-mode fibers [3]. Another study used a single-mode tapered optical fiber as a transducer for biological sensors which achieved a sensitivity around 1500nm/RIU [4]. However, this work will describe the behavior of eight samples of tapered fiber optics with different diameters to manufacture a refractometry sensor which will have a high sensitivity. The main reason of the fiber optic sensor development over a conventional electrical based sensor is because of its ability to immune to electromagnetic interference. Meanwhile, it can also withstand the hazardous environment such as high temperature and corrosive liquid environment [5]. These features mentioned above yield a better result of analysis compared to the electrical based sensor which might give inaccurate measurement result. This happen since the electrical based sensor are built using discrete electronic component. Refractive index (RI) sensors is crucial and have been used extensively for many applications in the area of medical, biological and chemical industries. Hence, optical fiber based refractive index (RI) sensors has been attracted many scholars focusing on sensor to emphasize on this project due to its special roles and benefits in monitoring severe environment and medical analysis [6 ,7].

## II. LITERATURE REVIEW

The past studies will help in conducting the research and its results while some compassion are going to be done to emphasis our finding with previous literature content. An expected change in the light transmission characteristic of the fiber will occur when we use the fiber to sense a physical property from the external environment. Therefore, we have to consider the designing of the sensing element of the optical fiber sensors, the method of fabricating sensing element is also essential. To manufacture a tapered fiber optic sensor, the cladding of the fiber optic is removed or etched by using some techniques in some certain dimension, so that the core part would be very sensitive to the external environment. Among the most common methods to produce a tapered fiber optic are etching through hydrofluoric acid and heat and pull method. Selective previous studies are going to be highlighted and retrieved from the trusted resources of previous published books, journal papers, and conference papers.

The length of MMFC does not provide any change in the sensitivity when we use it to measure the refractive index, but the diameter makes a change in the transmission light which shows better sensitivity. Low sensitivity will occur when the diameter of the sensing zone is bigger. The refractive index with a larger MMFC diameter has a lower sensitivity compared to that with a smaller MMFC diameter. Experimental study proved the simulation records, the sensitivity has been achieved are 1815 and 1156 nm/RIU in the refractive index range from 1.431 to 1.437 and minimum sensitivity of 180 and 164 nm/RIU in the

refractive index range from 1.342 to 1.352 for refractive index with core diameters of 80 and 105 µm respectively. Since this SM fiber sensor structure based on refractive index has a high sensitivity. Sensitivity can be improved and achieved experimentally using an MMFC of 50 µm, provided that a reliable SMF-MMF splicing technique can be preferred [8].

Sensitivity around 1500nm/RIU has been achieved using an improved single mode tapered fiber optic sensor to monitor the refractive index of various liquids [4]. The proposed setup used to monitor the changes of RI when different concentrations of Sodium chloride (NaCl) applied to the tapered region. The changes of RI occurred because of the output interference spectrum shifting in response. Different environmental sensitivities were accomplished by manipulating the transition lengths of the tapered fiber. Experimental results depict RI sensitivities of 3914.7 nm/RIU (refractive index unit) and 3395.7 nm/RIU for taper profiles with down-taper transition lengths of 2 mm and 8 mm, respectively, which is higher than previously reported asymmetric taper RI sensors. This research has come out with advantages such as in low cost, reliable and simplified sensors [2].

## III. PROJECT METHODOLOGY

The method applied to produce a refractive index (RI) sensor based on reflection-type using tapered fiber optic as shown in Fig. 1 will be explained in this paper. The methods start from fabricating, testing and measuring of the sensor. The method mentioned above must be orderly follow for this project to be done systematically.

The literature review is needed in order to improve the determined problems from the previous project. Taking the previous project will assist us in planning and selecting suitable materials and solution to be utilized in our own experiments. Fabrication of the sensing zone will be done by etching the cladding layer of the fiber optic using hydrofluoric acid of the concentration of 49%. The performance measurements will be received and examined using the optical spectrum analyzer (OSA).

Numerous researchers have done different methods to fabricate fiber optical sensors, in this work, we are going to use one of methods that have been done but with different concepts. In this experiment, we are going to produce eight samples of fiber optic which have various diameters, each sample going to be tested after we make the experiment setup. The test will depend on the refractive index measurement to analyze the performance and sensitivity of all samples.

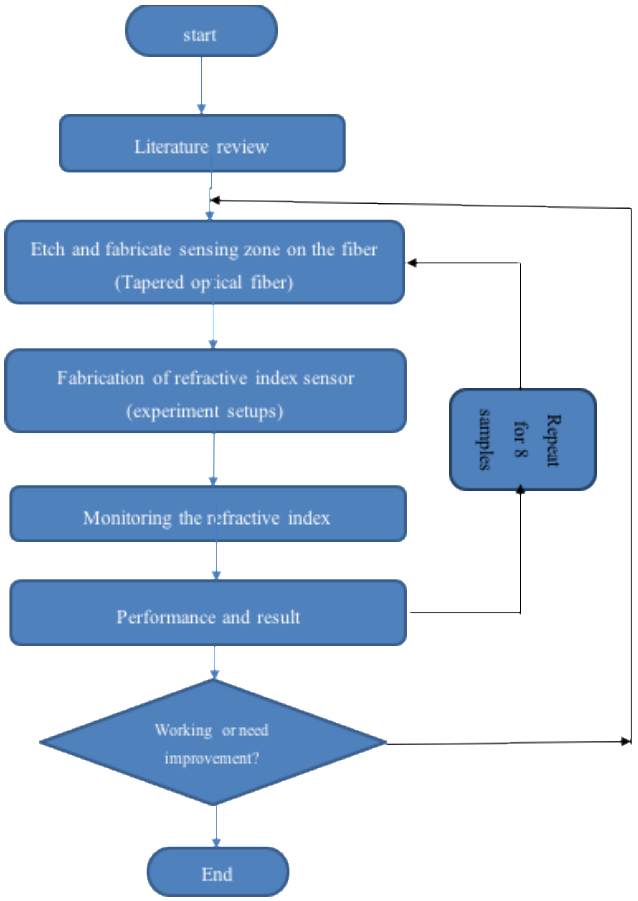


Fig. 1. Flow chart of Refractive Index Measurement

In this project, basic RI sensor structure is designed using one type of fiber optic which is multi-mode fiber (MMF). There are eight samples of the fiber that have different diameters along the sensing zone, which are 125µm, 110µm, 95µm, 80µm, 65µm, 50µm, 35µm, and 15µm to monitor the refractive index of the applied liquids. The design process of this sensor is very simple which are tapered zones on the multimode fiber (MMF) spliced with SMF as the two ends of the sensor, then the two ends of the SMF fiber was flat cleaved. The structure of the sensor after completed the designing process as shown in Fig. 2.

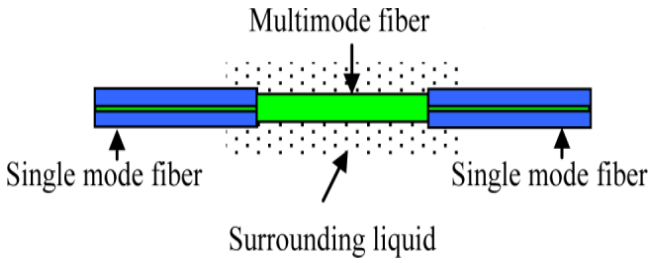


Fig. 2. Configuration of the SMF-MMF structure refractometer.

The fabrication process of this RI sensor was very simple. It only involved splicing, cleaving and etching process. The first step was getting rid of the coating of the sensing zone on the multimode fiber using stripper. The second step was to immerse the mean sensing zone into hydrofluoric acid with a concentration of 49% to acquire the desired diameters. Based on the experiment, the actual diameter of the MMF will lose $10\mu m$ after being etched with hydrofluoric acid for two minutes. The third step was to splice the MMF with two ends of SMF as shown in Figure 2. The fourth step is cleaving the end of the SM fiber using flatted cleaver. In this project, the stripped part of the fiber must be cleaned using task wiper with some isophoric alcohol to remove the dusts.

The refractive index measurement equipment was setup as Fig. 3 below. The first end in fiber was linked up to ASE C-banding light source with the input power of 10 to 20 dB while the lead out fiber was linked up to the optical spectrum analyzer. The fiber sensor was placed on the invisible plastic plate so that we can see the refractive index solution more clearly.

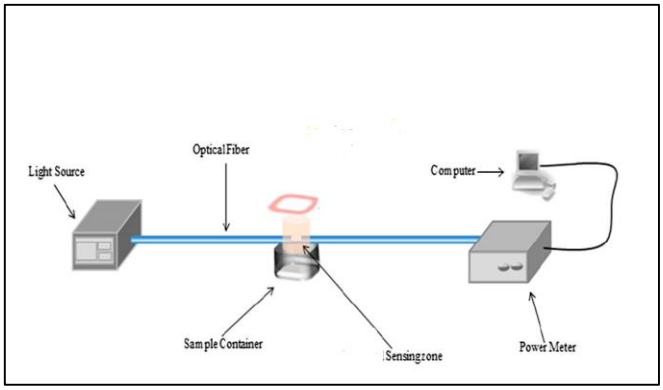


Fig. 3: The schematic diagram for refractive index measurement.

To start the experiment, the sensing zone of the fiber was cleaned by using distilled water in order to avoid contaminant or dust on the fiber sensor. Then, few drops of refractive index solution of 1.3900 was dropped on the sensing zone of the MMF and wait for approximately 30 seconds before the transmission output spectrum was observed and recorded. The procedure was repeated by using the refractive solutions which have different refractive indices. After that, the same procedure was repeated to measure RI for eight samples of the MMF-SMS sensor that have different diameters. Figure 4 shows the real experiment set up for RI sensor measurements, refractive index solution and the process of doping refractive index solution.

(a)

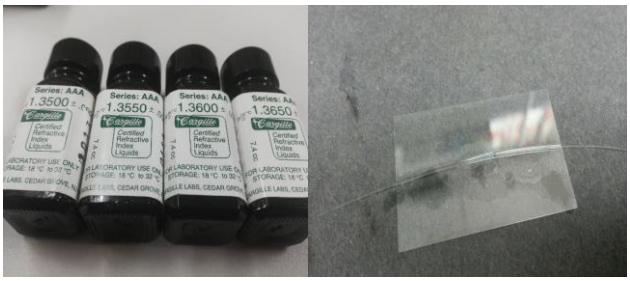


(b) (c)

Fig. 4: The process of refractive index measurement. (a) Refractive index. Measurement real experiment setup (b) Refractive index solutions (c) The process of dropping refractive index solution

To make sure the data was consistent, the sensing zone of the fiber was cleaned for every measurement with distilled water. However, the experiment process must be avoided from any surrounded disturbance such as vibration. Fig. 5 shows the change that happened to the sensor response when we modify a sensing zone on the MMF.

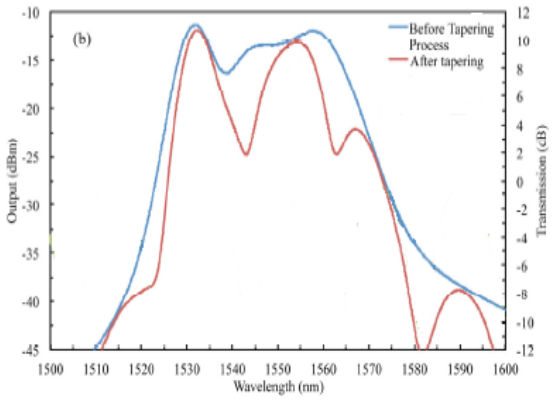


Fig. 5 Measured optical spectrum before and after tapering process

## IV. RESULT AND ANALYSIS

The outcome of this study will be described. This work has been carried in three different labs namely the PCB lab, the photonic research lab and the optical lab. Besides, the parameters used to design and fabricate the sensor will be explained accordingly. The analysis and performance of the measurement results will also be discussed by using Microsoft Excel.

During the experiment, the performances of these refractive index sensors have been monitored using the Optical spectrum analyzer (OSA). In this study, five different types of liquid with different refractive index were used to experiment the linearity and sensitivity of the sensing elements. The transmission spectrums, power and wavelength of this RI sensor displayed in the OSA will be observed and plotted in Microsoft Excel to be analyzed.

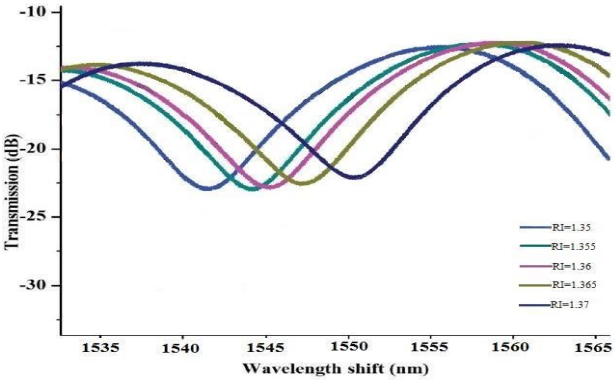


Fig. 6 Transmission spectra of SMTF sensor (D=15μm) with different RIs of liquids.

Fig. 6 shows the sample transmission spectrum of single mode tapered fiber sensor which has the diameter set at 15μm that had been analyzed from the data that observed on the optical spectrum analyzer. As it can be seen from the figures above, liquids with different refractive indices showed different transmission spectrum which proved this RI sensor sensitivity to identify RI. The interferences ripples exhibited by the transmission spectra of the device indicated that there were interferences of the cladding modes. By simply observed the variation of cladding mode power at a specific wavelength interval, the SRI can therefore be observed.

## V. CONCLUSION

As a conclusion, optical fiber sensors have gained escalating interest in the monitoring of various parameters in the surrounding due to its high sensitivity and selectivity. Moreover, the immune to electricity in the sensing system which make them suitable to work in harsh environment. This work investigated the prospect of tapered fiber as a highly sensitive refractive index sensor by analyzing eight samples of tapered fibers and their effects towards the changes of refractive index. This chapter concludes the overall works that have been executed to evolve this task and the recommendations for future research will be hashed out. Investigating process has been done in this project to examine whether the diameter gives any effects on the sensitivity of the sensing zone or not. As well, to test the linearity of the sensors. The outcome of the project founded is, the less diameter had given a better sensitivity. As well as all the sensors responses are linear.

## REFERENCES

[1] Hummad Habib Qazi, *D-Shape Optical Fiber Chemical Sensor For Multi Parameters Monitoring*. University Technology Malaysia, 2016.

[2] Kamil, Y. M., Mustapa, M. A., Bakar, M. A., Musa, B., Syahir, A., Yaacob, M. H., & Mahdi, M. A. (2015, April). Refractive index sensor with asymmetrical tapered fiber based on evanescent field sensing. In *Broadband and Photonics Conference (IBP), 2015 IEEE International* (pp. 35-39). IEEE.

[3] Wang, P., Brambilla, G., Ding, M., Semenova, Y., Wu, Q., & Farrell, G. (2011). High-sensitivity, evanescent field refractometric sensor based on a tapered, multimode fiber interference. *Optics Letters*, *36*(12), 2233-2235.

[4] Yadav, T. K., Narayanaswamy, R., Bakar, M. A., Kamil, Y. M., & Mahdi, M. A. (2014). *Single mode tapered fiber-optic interferometer based refractive index sensor and its application to protein sensing*. *Optics express*, *22*(19), 22802-22807.

[5] Fidanboylu.K, and Efendioglu.H.S (2009). Fiber Optic Sensors And Their Application. *5th International Advanced Technologies Symposium*. 13-15 May. Karabuk, Turkey. 1-6.

[6] Min Shao, X. Q., Haiwei Fu, Huidong Li, Zhenan Jia, and Hong Zhou (2014). "*Refractive Index Sensing of SMS Fiber Structure Based Mach–Zehnder Interferometer*." IEEE Photonics Technology Letters Vol. 26, NO. 5: 3.

[7] Hideki Fukano, T. H., and Shuji Taue (2014). "*Reflection-type Optical Fiber Refractive-Index Sensor Using a Multimode Interference Structure with High Sensitivity*." Japanese Journal of Applied Physics: 5.

[8] Wu, Q., Semenova, Y., Wang, P., & Farrell, G. (2011). *High sensitivity SMS fiber structure based refractometer–analysis and experiment*. *Optics Express*, *19*(9), 7937-7944

# Intelligent Bus Tracking System (IBTS)

Tee Kok Sheng
*Faculty of Electrical Engineering*
*Universiti Teknologi Malaysia*
*Johor Bahru, Malaysia.*
*tks_94@hotmail.com*

Kamaludin Bin Mohamad Yusof
*Department of Communication Engineering*
*Faculty of Electrical Engineering*
*Universiti Teknologi Malaysia*
*Johor Bahru, Malaysia.*
*kamalmy@utm.my*

***Abstract*— Public transport plays an important role in all the country and even environment nowadays as it brings a lot of benefits such as reduces traffic congestion, reduces gasoline consumption and carbon footprint, lowers accident rates, lowers rates of respiratory and heart disease, provides economic opportunities, drives community growth and so on. However, the number of public transport users in Johor do not reach a considerable level although Johor's government has proposed Bas Muafakat Johor to reduce the cost of living for Malaysian and increase the quality of bus transportation system. Due to inconvenient of current bus transportation system as the bus normally will not arrive at a certain bus stop by the expected time, citizens will not make public bus transport as their priority choice because they may face the difficulty in choosing an alternative way to reach the destination or continue waiting for the bus. Thus, Intelligent Bus Tracking System (IBTS) is proposed and will be implemented on Bas Muafakat Johor in solving this issue to increase the number of citizens who use public transport, yet reduce the carbon footprint and traffic congestion in Johor. Intelligent bus tracking system (IBTS) is a system that will provide users the exact location of a moving bus and the estimated time arrival (ETA) of a bus in user apps. GPS receiver in driver's smartphone will get the location of the bus from satellite. The data is then updated to the firebase database. Server will send the data to the user apps when the user apps request the current location of bus from the server. Then, user apps will display the exactly and updated location of the bus by activating symbolic representation of buses in the approximate geographic on map as well as the estimated time arrival (ETA) of the bus to the next bus stop. This system is convenience as it can be displayed on website and mobile apps.**

***Keywords—bus; location; estimated time arrival; server; website***

## I. INTRODUCTION

Public transport is a system of vehicles such as buses and trains that operate at regular times on fixed routes and are used by the public. Public transport brings a lot of benefits to all the countries such as reduces traffic congestion, lowers accident rates, reduces gasoline consumption, reduces carbon footprint, lowers rates of respiratory and heart disease, provides economic opportunities, drives community growth and so on [1]. However, there is only 8% of citizens in Johor who use public transport including Bas Muafakat Johor. Bas Muafakat Johor is a free public bus transportation for whole Malaysian and it is provided by Johor's government. The purpose of implementing Bas Muafakat Johor is to reduce the cost of living for Malaysian and increase the quality of bus transportation system [2]. One of the reason citizens do not make public transports as their priority choice because they do not satisfy with current bus transportation system. Unpredictable and inaccuracy time for a bus to reach certain bus stop will cause citizens face the decision of whether it would be faster to wait for the next bus or find other alternative ways to reach the destination. Thus, intelligent bus tracking system (IBTS) is proposed in solving this issue to increase the number of citizens using public transport, yet reduce the carbon footprint and traffic congestion in Johor.

Intelligent bus tracking system (IBTS) is a system that will provide users the exact location of a moving bus and the estimated time arrival (ETA) of a bus. This system required global positional system (GPS) to function as navigation by providing geolocation and time information to a GPS receiver in all weather conditions. GPS is a constellation system which consists of a network of 32 satellites orbiting the earth at an altitude of about 20,000 km above the earth's surface [3]. Among these 32 satellites, 24 of them are active to provide global coverage whist 8 of them are used as backup purpose. GPS receiver on earth will track the different signals broadcasted by each satellite and analyse it to determine the precise location. Although the signal will not affect by all weather conditions, it cannot penetrate through solid, thus the GPS receiver will give the best performance when there is a clear view of sky.

## II. LITERATURE REVIEW

### *A. Intelligent Bus Monitoring and Management System [4]*

This research paper is authored by M. A. Hannan, A. M. Mustapha, A. Hussain, and H. Basri. In this research, authors use radio frequency identification (RFID) as well as integrated sensing technologies such as global positioning system (GPS), general packet radio service (GPRS) and geographic information system (GIS) in implementing an intelligent bus monitoring system. Authors implement RFID in their system because RFID can improve the overall performance of a monitoring system at affordable prices [5]. In their project, RFID reader, GPS and GPRS transmitter is placed in a black box which is located in the moving bus whereas RFID tag or RFID transponder is inserted at the bus station. The distance between RFID reader and RFID tag will decrease as the bus approaching the bus station, thus result in interaction between them. Data will be produced and circulated by this communication and is being sent to the monitoring centre through GPRS. At the meantime, GPS module is activated to detect the location of the bus. By using web server over the GPRS network, the data from RFID and GPS will be sent to the database. After connection of network is established, data of RFID and GPS will be stored in

database including the location of bus and estimated time arrival (ETA). The stored data will be retrieved by user interface and updated accordingly. Figure 1 manifests the system architecture for the bus identification and monitoring system.

Fig. 1. Architecture of bus identification and monitoring system

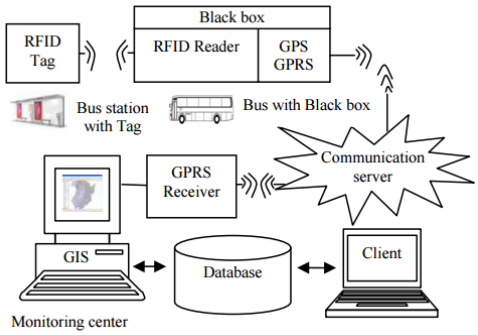


### *B. UTMbus: Real Time Bus Tracking Application [6]*

This project was done by Muhamad Aizzat, UTM (2016) [6]. In this project, it consists of two android application, one is for the bus driver and another one is for users. By using GPS feature in phone, driver apps will get current location of bus and the data will be updated to the Ubidots database by accessing internet connection. Data will be stored in Ubidots database and user apps will request the data from database using internet connection. Estimated time arrival (ETA) will be calculated and distance of bus from the next bus station will be displayed in user apps. Figure 2 illustrates the overall system of the project.

Fig. 2. Overall system of Real Time Bus Tracking System


For the bus driver apps, it displays the current coordinate of bus. The bus driver has to update the location of bus by pressing a start button on the driver apps. For the user apps, it shows distance between moving bus and selected bus stop as well as estimated time arrival. The author fix the route along Jalan Lingkaran Ilmu and Jalan Amal as well as the speed of bus at 30 km/h. Thus, there are only four choices (bus station) can be chosen from user apps.

The author calculates the distance between current location of bus and the next bus stop by using a formula:

$$\Delta d_{estimated} = \frac{\Delta d_{bus\_nxtstop}}{\Delta d_{nxtstop\_prvstop}} \times \Delta d_{actualnxtstop\_prvstop}$$

Where

$\Delta d_{estimated}$ : Calculated distance between bus location and next bus stop

$\Delta d_{bus\_nxtstop}$ : Straight line distance between bus location and next bus stop

$\Delta d_{nxtstop\_prvstop}$ : Straight distance between next and previous bus stop

$\Delta d_{actualnxtstop\_prvstop}$ : Actual distance between next and previous bus stop

The estimated time arrival of the bus is calculated by the author using the formula below.

$$Time_{busarrival} = \frac{\Delta d_{estimated}}{v_{bus}}$$

Where

$Time_{busarrival}$ : Time taken for the bus to arrive next destination (minutes)

$\Delta d_{estimated}$ : Calculated distance between bus location and next bus stop

$v_{bus}$ : Speed of bus (Assume 30 km/h)

## III. METHODOLOGY

Intelligent Bus Tracking System consist of four main part, that is GPS on driver's smartphone, Firebase database, user apps in android smartphone as well as website. Figure 3 displays the architecture of Intelligent Bus Tracking System.

Fig. 3. Architecture of Intelligent Bus Tracking System

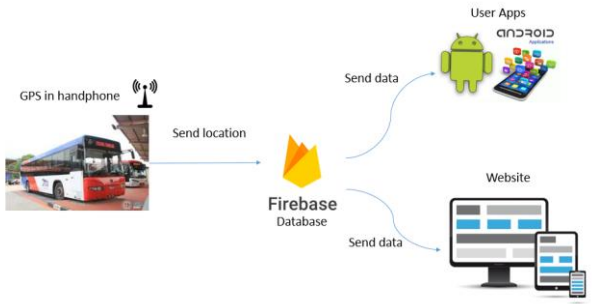


GPS receiver in driver's smartphone will get the location of the bus from satellite. Then, it will update the data to the Firebase database continuously. When the user apps request the current location of bus from Firebase, it will send the data to the user apps. Thus, user apps can display the exactly and updated

location of the bus in maps as well as the estimated time arrival (ETA) of the bus to the next bus stop.

### A. *GPS in driver smartphone*

Global Positioning System (GPS) is a constellation system consists of a network of 24 active satellites orbiting the earth at an altitude of about 20,000 km above the earth's surface and it functions as navigation by providing geolocation and time information to a GPS receiver in all weather conditions. GPS in driver's smartphone will get the location of bus from satellite and display in bus's apps in google map. Google map API is obtained before the bus's apps is created. Bus's apps will send current location of bus to firebase and store in its database.

### B. *Firebase as database*

Firebase is a mobile and web application development platform. It is also a real time database which provide an API and allows developers to store and sync data across multiple clients. Some information is stored in Firebase such as latitude and longitude of bus, bus's plate number, distance of bus from next bus station as well as estimated time arrival (ETA) of bus to the next bus station. Location of bus and ETA will be sent and shown in user's website or user's apps if they request these information from Firebase.

### C. *Website and user apps*

The web user interface is developed using Atom, a source coder editor which supports CSS and HTML programming language used for this system. Ionic framework, a complete open source SDK for hybrid mobile apps development is used to transform the website to user apps. The user apps can be viewed by using any web browser. When the website or user's apps is initiated, it will request location of bus as well as estimated time arrival of bus to reach next bus station from Firebase and show in the interface of website or apps.

## IV. Result And Discussion

When the bus is moving, GPS receiver in android smartphone of the driver will send the bus location to Firebase and store in database. When user apps request data from it, it will send the data to user website. User website will display the location of bus by activating symbolic representation of buses in the approximate geographic on map and time estimated time arrival (ETA).

### A. *GPS in driver smartphone*

Figure 4 shows the display of bus driver's apps which can show the exact location of bus in google maps and sent the data to firebase.

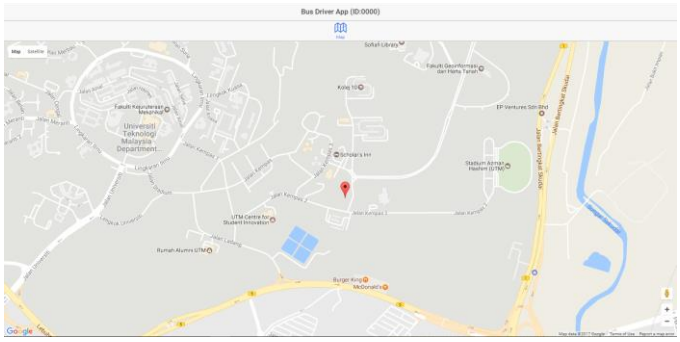


Fig. 4. Interface of bus driver's apps

### B. *Firebase as database*

Figure 5 shows the display of Firebase database which contain the information of bus such as latitude and longitude of bus, estimated time arrival of bus to next bus station, and plate number of bus.

Fig. 5. Display of firebase database

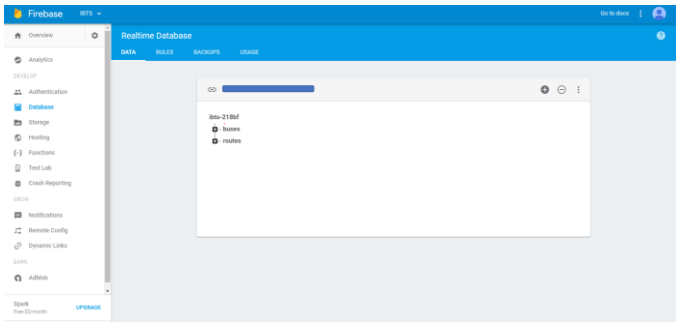


### C. *User website and user apps*

Figure 6 and figure 7 show the GUI of the user website and location of bus position displayed on user website. When we click on the GUI of user website, google map will be activated and location of bus can be shown in google map.

Fig. 6. GUI of user's website

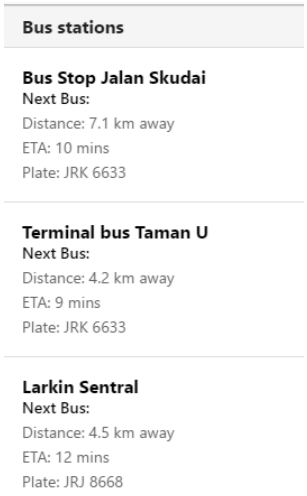


Fig. 7. Location of the bus position displayed on user website

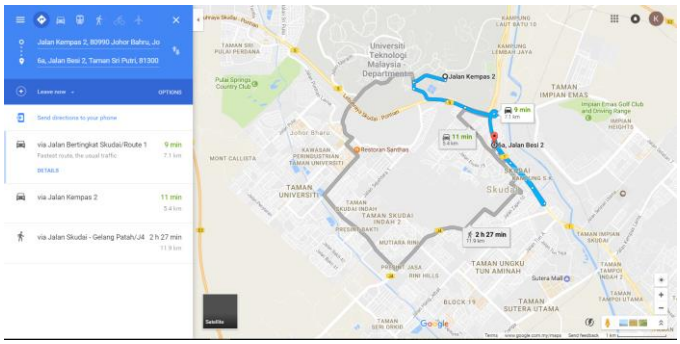


## V. CONCLUSION

Intelligent Bus Tracking System (IBTS) is a system which brings a lot of convenience for citizens. By using the user website or apps, citizens can easily know the exactly location of the bus by observing the activating symbolic representation of buses in the approximate geographic on map as well as the estimated time arrival of bus. This can prevent the passengers waste their time in waiting the bus at the bus station. After the citizens feel convenient and satisfy with this system, the number of citizens who use Bas Muafakat will increase. This will directly and indirectly reduce the traffic congestion as well as the carbon footprint in Johor.

## VI. ACKNOWLEDGEMENT

I would like to express the highest gratitude and deepest appreciation to my supervisor, Dr Kamaludin Bin Mohamad Yusof for his support and helpful suggestion all the way through this research. His brilliant advices, ideas and tolerance encourage me to be more determination in completing this project. I would also wish to express my warmest regards to my families, expecially my parents for their encouragement and boundless support. Last but not least, I would like to acknowledge with much appreciation to my friends and everyone that had made this report a success.

## REFERENCES

[1] American Public Transportation Association. *The leading force in advancing public transportation*. 2014

[2] Perbadanan Pengangkuatan Awam Johor (PAJ). *Mengenai Bas Muafakat Johor*. 2016.

[3] University of Tasmania. 2014. How GPS Works.

[4] M. A. Hannan, A. M. Mustapha, A. Hussain and H. Basri. (2012). Intelligent Bus Monitoring and Management System. World Congress on Engineering and Computer Science. Vol II.

[5] T. C. Poon, K. L. Choy, Henry Lau C. W., Felix Chan T. S., K. C. Ho. (2009). A RFID case-based logistics resources management system for managing order-picking operations in warehouses. Expert Systems with Applications. vol. 36, no. 4, p. 8277-8301.

[6] Muhamad Aizzat (2016).. *UTMbus: Real Time Bus Tracking Application* Bachelor's Degree Project Report. UTM

# Bus Tracking System using Speed and Location for Estimation Time Arrival

Nor Zahirah Zainol
*Faculty of Electrical Engineering*
*Universiti Teknologi Malaysia*
*Johor Baharu, Malaysia.*
*zahirahzainol9@gmail.com*

Nurzal Effiyana Ghazali
*Department of Communication Engineering*
*Universiti Teknologi Malaysia*
*Johor Baharu, Malaysia.*
*nurzal@utm.my*

***Abstract*—Public transport systems in Universiti Teknologi Malaysia (UTM) campus, the most important transport is UTM's bus. Students need bus if they want to go anywhere around the campus. Certain faculties far from students' college. Usually they need the bus to attend their classes. However, not a substantial effort is done in order to improve the existing public transport, UTM's buses. This project will present the development of an Internet of Thing (IoT) based on bus tracking system (UTMBus). The development will be new technologies has enable the development of various Intelligent Transport System (ITS). By providing the IoT solution, database of real time bus tracking system for efficient transport management has become viable. The database that going to develop will provide the information of the bus which is ETA of the bus. User's smartphone must equip with internet connection and GPS function. Every UTM bus has been installed with GPS system. The database from server will keep update the location and speed of the bus. MYSQL is used as database to store bus information. The user app will request the information from database and calculating the ETA of the bus. The ETA of the bus will display on database.**

***Keywords— ETA; bus tracking system; Internet of Thing (IoT); vehicles tracking device.***

## I. INTRODUCTION

In the daily operation of public transport systems in Universiti Teknologi Malaysia (UTM) campus, the most important transport is UTM's bus. Students need bus if they want to go anywhere around the campus. Certain faculties far from student's college. Usually they need the bus to attend their classes. They need to wait the bus at particular time for the bus to arrive at their destination. However, they do not have idea what time the bus will arrive. Although, every bus stop have the bus schedule, but still the bus not arrive at the destination on time. Sometime bus delay and sometime bus come too early at destination. In order to improve the UTM's bus transportation, this project will develop an application that offer reliable bus arrival time information for UTM's student. In this proposed project, the database of the system will be developed to display ETA for the bus. Every UTM bus has been installed with GPS system. Data that obtain from the GPS, which is the location and speed of the bus will be stored in database. To connect this devices will be use 3G or 4G network. The user will request data from database and calculate the distance between bus location and user's location. The user and bus must have at least 3G connection to request and send data.

The main goal of this project is to offer reliable bus arrival time for UTM's students. The specific objective of the project ais to apply algorithm using bus location and bus speed and to develop database of ETA to store the bus information. So the user can access the database on their smartphone.

The aim of this paper is to present a bus tracking system for UTM's bus. The devices that going to develop can track the location of the bus and speed of the bus. The use of this system is to make sure the location of the bus and the user can predict the time for bus arrive at their destination.

The rest of this paper is organized as follows. In section II, The literature review on previous research based. In section III, is the methodology. In the methodology will discuss on method to implementation the devices, architecture, flow chart and algorithm of the devices will present. Section IV the results from the developed service are presented. Finally, in section V concludes the paper and provides suggestions for future work.

## II. LITERATURE REVIEW

This literature review will discuss on previous research based. All previous work that related to this project including hardware and software will be reviewed. The aim of this research methodology is to make sure current project can be successful as the planning. This chapter is like references to implement the overall system. All the citation are extracted from the articles, journals, paper and thesis founded from UTM library and Internet.

### *A. Bus Tracking System*

By referring to the research conducted by Lau [1] in UCSI University, Kuala Lumpur, most of the tracking system are using General packet Radio Service (GPRS) network. However, bus tracking system also give bus information for selected route. In this research, use the Light-Emitting Diodes (LED) panel to display the bus information. Bus information will be displayed on LED panel that have located on each bus stop and also will be displayed on smartphone apps. Real-time bus tracking system will give more beneficial to student with larges campuses. Another research conducted by Wengping [2] from Huazhong University. By providing the reliable services, there are many transit agencies or used GPS enable in vehicles devices. Furthermore, GPS based tracking and ETA in real world have limitation. In this paper, using powerful tool named Signal Voronoi Diagram (SVD) to partition the radio frequency (RF)

signal space of WiFi Access Point (APs) [2].In this research paper from author Shiv. H. Sutar, et al [3], MIT college of engineering. Intelligent Transportation System (ITS) provide solution for the problem occur such as increase the number of accidents and various other traffic related issues by modified existing technologies. The world become more technology on cellular network, that may be benefit to get real time vehicle tracking more efficient.

### I. *GPS Tracking System*

By referring this research from MA .et al [4]. Automated Fare Collection (AFC) system also known as Transit Smart Card System (SCS) that provide manual fare collection system. In this system, all public transport are fully equipped with GPS tracking. The GPS technology is being more efficiency towards tracking and schedule of the buses. This paper focusing on the implementation of bus monitoring system, by installing the GPS on buses. This device will enable to obtain GPS data which is bus locations. Data from GPS will be transfer to centralized control unit. Another research from Pham [5], the development of vehicle tracking system use GPS and GSM. Aim of using both device are enable users to locate their vehicles and in convenient manner. This paper present that system will control remotely using mobile network. GPS device were using to obtain the coordinate of the vehicle and transmit data to GSM modem. Nowadays, GPS navigation system is widely used in vehicle tracking device [6]. GPS can be used in tracking the distance traveled , vehicle mileage and speed. GPS also keep update the driving activity, include location of vehicle [6].

### II. *RFID*

RFID is technology that similar with a bar code scanning. An RFID system include of tags, which use radio frequency signals to transmit location to reader. Usually sends information to server to process the request from user. By placing RFID tags in the buses and every bus stops the system can track the bus in the city [7]. RFID technology consist three component: tags, reader and Middleware logic for interaction with the back-end database continuously. This technology can be used effectively for this type of application [8].

### III. *Hardware Based*

Hardware based that widely used to solve problem of bus tracking system and scheduling. Which is use same approaches such as microcontroller, GPS module, GPRS/GSM Modem. GPS module collect data location and sent to the micro controller which in turn is sends it to the GPRS/GSM modem [3]. According to research Pham, Michael, Chi [5], the suggestion of this report is vehicle tracking system consist the GPS module, use to obtain vehicle's coordinate and GSM modem, used to transmit location of the vehicle to user's smartphone. GSM is the Global System from Mobile communication.

### IV. *Database Server*

Database server is technology that used to refer to the back-end system of database application by using client/server architecture. Database server will perform all tasks such as data analysis, storage and etc. In this project, database server is used to store the all information that obtained from GPS into database. Database server consist server module and client module.

a) *Server Module*

According to research on Shiv. H. Sutar [3], web server module is the core of their system. Serves as the back-end tool. This server contains all information about the routes of all the buses as well as the intermediate bus stops on the route. Server will process the request from a client regarding ETA of the bus at particular bus stop. Android application will install on the bus to send information to the server. Data information will store in server database called name MYSQL.

b) *Client Module*

The implementation towards bridging the communication gap between a regular user and the information generate from the system. Their proposed is to develop an application on client side that can be used to track the location of the bus and availability at a particular bus stop with ETA [3].

## III. METHODOLOGY

This chapter discusses on the methods of the proposed project. In addition, the architecture of this project also illustrated as shown in Figure 1. The flow chart will be illustrated to show how the system working.

### A. *Architecture*

The architecture of the proposed project is illustrated in Figure 1. It required GPS module and GPRS/GSM module. All UTM's bus are installed with GPS device requires by the owner of the bus. Therefore, need to develop own database to store the information that obtain from GPS. Information data from GPS such as location and speed of the bus will be send to server database by using 3G and 4G cellular network. Information data that stored in database can be retrieved by the user using WiFi, 3G or 4G. So, the ETA of the bus will display on database.

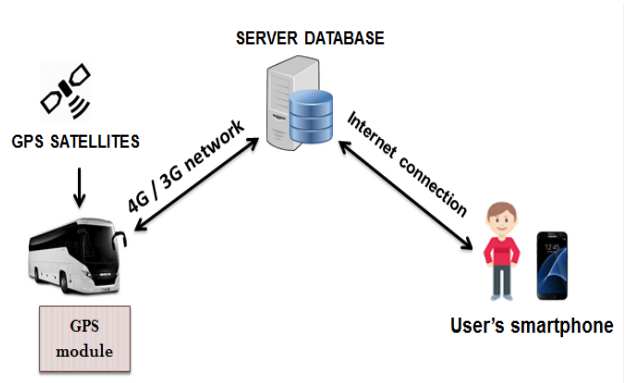


Fig.1. Architecture of (UTMBus)

Furthermore, user's smartphone must have internet connection to use the application and receive data from the server database.

### B. *Flow Chart*

Figure 2 shows the flow chart for overall bus tracking system (UTMBus).

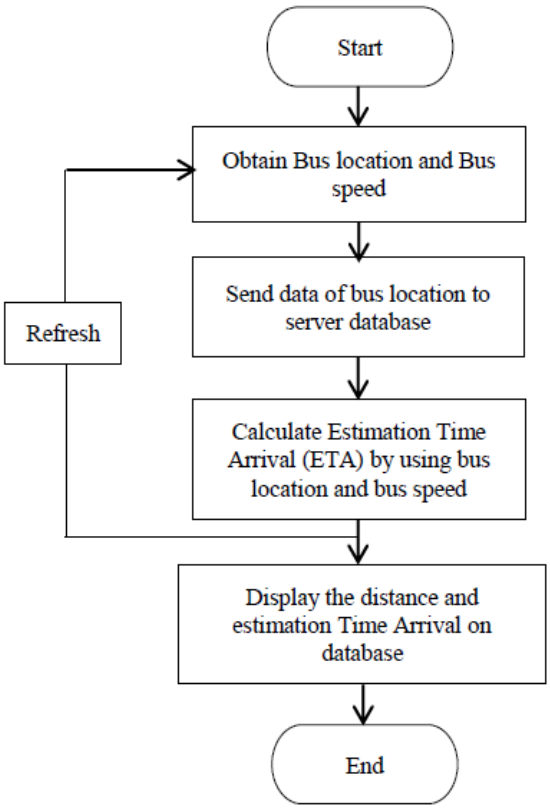


Fig 2. Flow chart of the (UTMBus)

The flow chart shows from starting process until the apps can display ETA of the bus. Firstly, information data will obtain from GPS. Then, the information from GPS will be send to server and stored to the database. Calculate ETA using suitable algorithm that will discuss later. Lastly, the information will be send to user's smartphone. The request from user will be displayed on smartphone. The algorithm will be applied on stage of calculate ETA by using bus location and bus speed. Algorithm will be discussed on next section.

### C. *Algorithm*

The equation shows the way to calculate the speed for current segment, $V_f$ The real-time velocity and average velocity of the bus should be obtained before the speed for the current segment can be calculated.

$$\textit{Speed for current segment, } V_f = \frac{d1Vreal + d2\,Vaverage}{d1 - d2} \qquad (1)$$

*d1Vreal = Real velocity of bus from GPS*

*d2Vaverage = Average Velocity From Apps*

*d1= Distance from current location to end of the segment*

*d2= Distance from beginning location to current location*

The main goal stated before, which is to offer reliable time bus arrival time for UTM's student. To achieve that objective, this suitable algorithm will be applied on this system. After getting information data from previous algorithm, then calculate ETA of the bus.

$$\textit{Time Arrival Bus, } T = \left[\frac{D_i}{V_f} + \frac{D_{i+1}}{V_{i+1}} + \frac{D_{i+2}}{V_{i+2}} + \cdots + \frac{D_k}{V_k}\right] \qquad (2)$$

$D_i$ *= distance of current segment*

$D_k$ *= distance to destination segment*

$D_{i+1}, D_{i+2}, \ldots D_{k-1},$ *= distance of intermediate segment*

$V_{i+1}, V_{i+2},$ *= predicted speed of intermediated segment*

$V_k$ *= predicted speed to destination segment*

6By applying both algorithm in this project, the ETA can be considered as reliable. Segment is the path between one station to another station. This segment will going to divided by three segments:-

1) First Segment is from FAB to Jalan Amal
2) Second Segment from Jalan Amal to Jalan Kempas2
3) Third segment from Jalan Kempas 2 to Kolej 10

Figure 3 shows the full route for selected route. The selected route is from FAB bus stop go through Jalan Amal to Kolej 10. This route only take 8 minutes to reach the destination without traffic. Distance from FAB bus stop to Kolej 10 only 3.1km.

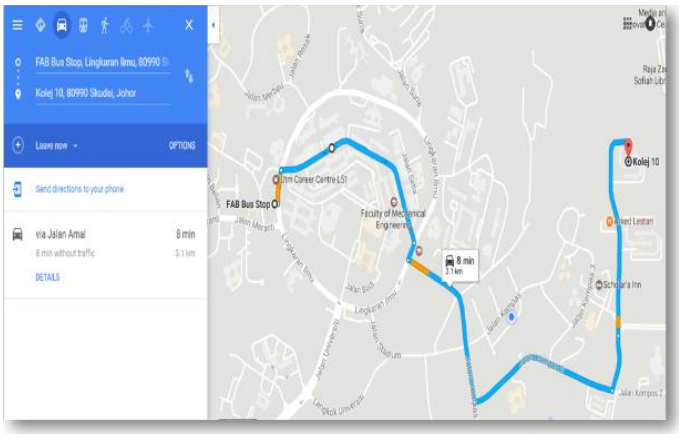


Fig 3. Selected route for this project

This map was obtained from Google map. The Fig.4 shows is first divided segment. This segment consists from FAB bus stop off to Jalan Amal. The distance from beginning of the segment to end of the segment are 900meter. It going take only 2 minutes by car without traffic.

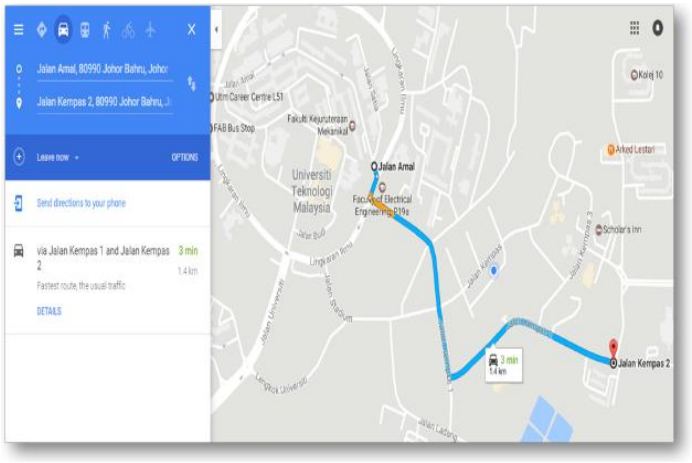


Fig 4. First segment from FAB to Jalan Amal

Fig.5. shows the second segment will be taken as the selected route. By consider this route have normal traffic. The time taken from Jalan Amal to end off Jalan kempas 2 are 3 minutes. Distance from end of segment 1 to end of segment 2 is 1.4 km.

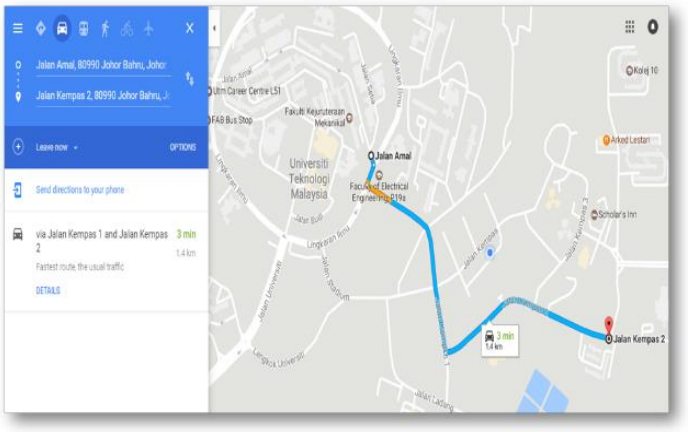


Fig.5. Second segment from Jalan Amal to Jalan Kempas

Fig.6. shows the last segment will be considered. This segment will covered from Jalan Kempas 2 to Kolej 10. It will take 3 minutes to reach last destination.

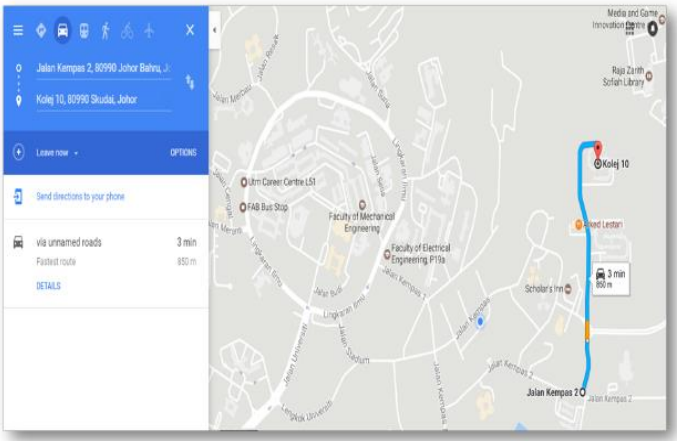


Fig. 6. Third segment from Jalan Kempas to Kolej 10

All of the segment above will be considered to make the system more easy to calculate the speed of the segment.

## IV. Result and Discussion

Table I and Table II is the initial result of this project that have been obtained. Route that involve in this project is from FAB until Kolej 10. There are several important point such as FAB, going through FKM, Jalan Amal, FKE, Kolej 10 and lastly Kolej 9. Table I shows the initial result compared actual time and schedule time.

TABLE I. Initial result compared actual time and schedule time

| *Arrival/ Leaving FAB (Schedule)* | *Arrival/Leaving FAB (Actual)* |
|---|---|
| - | 7.58 am |
| 12.00 pm | 12.04pm |
| 4.00 pm | 4.06 pm |
| 10.00 pm | 10.10 pm |

From the Table I that have obtained, the comparison between schedule and actual of arrival/leaving FAB. The result of arrival/leaving FAB from actual shows some delay compare to table. The delay will affect the time of student arrive their destination such as faculty.

Fig.7 shows the bus stop that will the bus go through before reach the destination, Kolej 10.

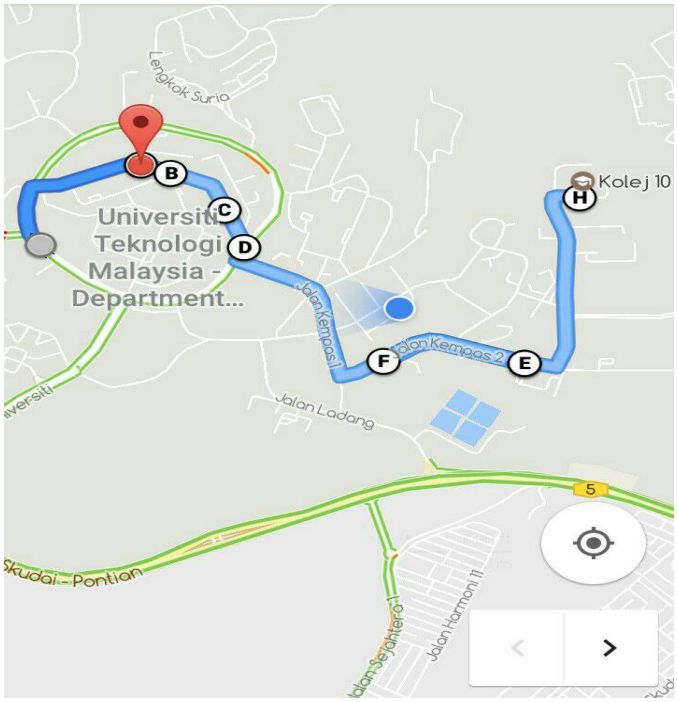


Fig 7. The bus stop around selected route

TABLE II. AVERAGE TIME FOR BUS TO REACH AT EVERY BUS STOP

| *TIME* | IN / OUT FAB | D01 | D06 | FKE | S40 | S15 | S43 | K10 |
|---|---|---|---|---|---|---|---|---|
| 8 AM | 7.58 AM | 7.59 AM | 7.59 AM | 8.02 AM | 8.04 AM | 8.04 AM | 8.06 AM | 8.13 AM |
| 12 PM | 12.04 PM | 12.05 PM | 12.05 PM | 12.06 PM | 12.09 PM | 12.10 PM | 12.12 PM | 12.20 PM |
| 4 PM | 4.08 PM | 4.08 PM | 4.09 PM | 4.10 PM | 4.12 PM | 4.13 PM | 4.15 PM | 4.22 PM |
| 10 PM | 10.06 PM | 10.06 PM | 10.07 PM | 10.08 PM | 10.09 PM | 10.10 PM | 10.12 PM | 10.17 PM |

Table II shows the average time for bus to reach at every bus stop. This results have been obtained after ride the bus every peak of time. Every peak time, 8.00am starting of classes, 12.00pm time for rest and lunch, for 4.00 pm student back to their college and the last bus at 10.00 pm. Every peak time, the results have been recorded by three times. Based on the result current bus schedule is not reliable compare to the initial results that have been obtained.

Table III shows the average speed for bus to reach the last destination.

TABLE III. AVERAGE SPEED FROM APPS AND DEVICES

| Speed From Apps | Speed From Devices |
|---|---|
| 1) 37 km/h | • 39km/h |
| 2) 40 km/h | • 38 km/h |
| 3) 38 km/h | • 39.5 km/h |

This results have been obtained after ride the bus every peak of time and the speed from apps was obtained by using speedometer. The speedometer can download from play store. Speed from devices which mean speed that get from the hardware that be implemented.

## V. CONCLUSION

As the conclusion, the structure will bring changes in bus tracking system (UTMBus) by tracking the ETA of the buses. By using the database that going to develop, students can access the timetable anywhere and anytime. Student will get information from database. By adding the bus speed, the ETA can be considered reliable. The next stage to implement this project, firstly develop database server. Then, apply the algorithm that have been discuss before. The data of the bus location and bus speed can get from the implementation devices. For the future work, the reliable of this system can be improved by adding the others parameter that can be measure such as the distance from one point to another point. Once the system is complete, the bus tracking system has the high potential to be commercialized as standalone product.

## REFERENCES


[1] Lau, E. C.-W. Simple Bus Tracking System. Journal of Advanced Computer Science and Technology Research, Vol3, 2013. (1).

[2] Liu, W., Liu, J., Jiang, H., Xu, B., Lin, H., Jiang, G. and Xing, J. WiLocator: WiFi-Sensing Based Real-Time Bus Tracking and Arrival Time Prediction in Urban Environments. Distributed Computing Systems (ICDCS), 2016 IEEE 36th International Conference on. IEEE. 2016. 529–538.

[3] Sutar, S. H., Koul, R. and Suryavanshi, R. Integration of Smart Phone and IOT for development of smart public transportation system. Internet of Things and Applications (IOTA), International Conference on. IEEE. 2016. 73–78.

[4] Ma, X.-l., Wang, Y.-h., Chen, F. and Liu, J.-f. Transit smart card data mining for passenger origin information extraction. Journal of Zhejiang University SCIENCE C, 2012. 13(10): 750–760. ISSN 1869-196X. doi:10.1631/jzus. C12a0049.

[5] Pham, H. D., Drieberg, M. and Nguyen, C. C. Development of vehicle tracking system using GPS and GSM modem. Open Systems (ICOS), 2013 IEEE Conference on. IEEE. 2013. 89–94.

[6] El-Rabbany, A. Introduction to GPS: The Global Positioning System Artech.Boston, MA, 2006.

[7] Anu, V. M., Sarikha, D., Keerthy, G. S. and Jabez, J. An RFID based system for bus location tracking and display. International Confernce on Innovation Information in Computing Technologies. IEEE. 2015. 1–6

[8] Oberli, C., Torres-Torriti, M. and Landau, D. Performance Evaluation of UHF RFID technologies for real-time passenger recognition in intelligent public transportation systems. IEEE transactions on intelligent transportation systems, 2010. 11(3): 748–753.

[9] T. Charoenporn, T. Sunate, P. Pianprasit, S. Kesphanich, A. Bunpeng and A. On-uean, "Selection model for communication performance of the bus tracking system," 2016 International Computer Science and Engineering Conference (ICSEC), Chiang Mai, 2016, pp. 1-5.

[10] M. N. Z. Juhari and H. Mansor, "IIUM Bus on Campus Monitoring System," 2016 International Conference on Computer and Communication Engineering (ICCCE), Kuala Lumpur, 2016, pp. 138-143.

[11] A. Shingare, A. Pendole, N. Chaudhari, P. Deshpande and S. Sonavane, "GPS supported city bus tracking & smart ticketing system," 2015 International Conference on Green Computing and Internet of Things (ICGCIoT), Noida, 2015, pp. 93-98.

[12] K. Sujatha, P. V. N. Rao, K. J. Sruthi and A. A. Rao, "Design and development of android mobile based bus tracking system," 2014 First International Conference on Networks & Soft Computing (ICNSC2014), Guntur, 2014, pp. 231-235.

[13] S. Sankarananrayanan and P. Hamilton, "Mobile enabled bus tracking and ticketing system," 2014 2nd International Conference on Information and Communication Technology (ICoICT), Bandung, 2014, pp. 475-480.

[14] L. Singla and P. Bhatia, "GPS based bus tracking system," 2015 International Conference on Computer, Communication and Control (IC4), Indore, 2015, pp. 1-6

# Low-Cost Wireless Sensor Network Device for Automatic Meter Reading System

Muhamad Arifzaqwan bin Md Faudzi
Electronic communication Engineering Department
Faculty of Electrical Engineering, UTM
81310 Skudai, Johor
Arifzaqwan3006@gmail.com

Dr. Noor Asmawati binti. Samsuri
Radio Communication Engineering Department (RaCED)
Faculty of Electrical Engineering, UTM
81310 Skudai, Johor
Asmawati@fke.utm.my

***Abstract*—This study is related to automatic energy meter reading system which enable real-time monitoring of the electricity consumption for the consumers and utility provider. The system enable utility provider to reduce meter reader required for collecting electricity usage from houses to another houses and hence, it will reduce labor cost. There are many approaches or techniques used by researchers in order to develop automatic energy meter reading system for example, Wi-Fi, GSM, and radio frequency (RF) module. This study is focuses on developing a low-cost automatic energy meter reading based on wireless sensor network (WSN). The proposed system consists of node device and base station. The node device consists of LM393 light sensor, Arduino Nano and NRF24L01 wireless transceiver that will be installed at power meter. The pulse on power meter will be measured and the data will be transmitted to base station via NRF24L01. At the base station, the NRF24L01 wireless transceiver and Raspberry Pi 3 model B will receive data from node devices and upload the data into the web server.**

***Keywords—Automatic meter reading (AMR); wireless sensor network(WSN); node device, base station..***

## I. INTRODUCTION

Power meter is a device that measure the amount of the electricity usage by the residential, industrial, or the electrically power devices. In Malaysia, Tenaga Nasional Berhad (TNB) are the electrical entity that supply power energy, install the power meter and standardize the amount of the electricity supply. In 2012, TNB has launched power meter replacement programmed [1] for the residential houses to change the electromechanical energy meter to the digital power meter which improve the energy meter reading accuracy and avoid electricity theft. The digital energy meter had been improved in its design and function. For example, the digital display (kWh) and pulse LED (imp/kWh) have been installed as the indicator for the energy consumed by the customers.

The introduction of automatic meter reading (AMR) can reduce labor cost, eliminate human operator in collecting electricity usage and billing process, avoid electricity theft and improve billing process system. AMR technology consist of Global System for Mobile Communication (GSM), General Packet Radio System (GPRS), Wireless Fidelity (Wi-Fi) and Radio Frequency (RF) module to transmit wirelessly the electricity usage by consumer to utility provider. In Malaysia, AMR had been introduced for large power consumer (LPC) industry using Global System for Mobile communication (GSM) and General Packet Radio Service (GPRS) in 2005 [2]. In 2014, TNB had successful done pilot project in Malacca by installing smart meter at 85 houses and in March 2017, TNB will implement advanced metering infrastructure (AMI) in Malacca to about 400000 customers over five years [3].

The aim of the project is to develop a low-cost real time power meter reading system using the NRF24L01+2.4GHz wireless transceiver and the Raspberry Pi. The objective of the project is to develop low-cost wireless sensor network (WSN) that transmit real-time electricity usage to electricity provider and to improve the conventional energy meter reading technique by having real-time reading for the electric energy usage where user can access their usage at any time. The proposed system was done by interfacing light sensor of node device into LED pulse on single phase power meter to count the power where every 800 pulse of LED pulse of power meter is equal to 1 kilowatt-hour (kWh) and it will transmit the electricity usage to base station every 1 kWh. At the base station, the electricity usage will be uploaded into the online web server (ubidots) and web server will store the data.

## II. L ITERATURE REVIEW

There are several research studies have been conducted which related to the automatic meter reading system. There are a lot of research studies that have been reviewed in obtaining information that related to develop the project based on the automatic meter reading technology. The implementation system for this project also obtain from the research studies on the AMR system

### *A. Research on Automatic meter reading system (AMR)*

From the research studies, there are five different type of wireless communication devices for Automatic Meter Reading System which is Wireless Fidelity (Wi-Fi) module, radio frequency (RF) module, the Global system for Mobile (GSM), ZigBee module and hybrid. In Wireless fidelity (Wi-Fi), Wi-Fi module is used as the communication medium between energy meter and the service provider. Wi-Fi module provides the wireless local area network based on IEEE802.11 standard and mainly used in an electronic device [4]. Users need to install and subscribe the Wi-Fi router in implementing AMR based on Wi-Fi module in their house. For AMR based on Radio Frequency

(RF) module [5] [6], RF module is low-cost wireless communication that is used to transmit and receive the radio signals between RF transmitter and RF receiver module. RF transmitter and RF receiver module can communicate with each other if it has the same operating and carrier frequencies. Some RF modules will ignore the line-of-sight (LOS) between the RF transmitter module and RF receiver module [5]. In order to implement the system, further research needs to be done in order to improve the accuracy of the RF module [6] due to the sensitivity of RF module to the noise. On the other hand, the Global System for Mobile (GSM) for AMR system [7] [8] provides wide coverage of communication which is up to 35 km with suitable ISM band (Industrial, Scientific and medical radio band). In Malaysia, GSM technology normally operates at 900 MHz and 1800 MHz frequency bands. GSM technology provides more efficient, reliable and secure network communication. The main focus of AMR system based on GSM module is to implement the system at a dense or rural area and for long distance data transmission because it provides wide coverage of communication and services such as Short Message Service (SMS) and GPRS for requesting and retrieving data to the utility provider from consumer houses. However, the implementation of this system is expensive due to GSM module and the network traffic will occur if many data being transmitted to the server at same time [7]. In ZigBee module based AMR system [9] [10], ZigBee module able to transmit the data directly to the utility provider base station from node device because each ZigBee module have two-way wireless communication protocol that able to perform star network communication [10], tree network communication and even mesh network communication when operates in full function device (FFD). ZigBee also facilitates wireless personal area network (WPAN) based on IEEE 802.15.4 standard where it will provide the low power consumption with low cost and low data rate at 250kbps in 2.4 GHz frequency band [10]. However, the weakness of this system is it need to configure and monitor regularly to make sure the node device can communicate with another node device. Lastly, Hybrid based AMR system is a combination of two communication technology to perform monitoring and remote energy metering system. For example, ZigBee module and the global system for mobile (GSM) communication [11]. The system has a systematic and effective system because the AMR system will be divided into several parts and every part has a specific task. For example, the node device only monitors and transmit the data of electricity consumption to the base station.

### *B. The proposed AMR system*

From the studied that had been done on the automatic metering system using GSM, Wi-Fi, ZigBee, RF module and Hybrid system, it was found that all the automatic meter reading system focuses on how to produce the systematic and effective metering system based on the current technology on which suitable system to be implemented and developed in all area included dense and rural area. The cost of implementing the automatic meter reading system also need to be accounted. Therefore, the proposed technique that suitable to implement that related to the low-cost power meter reading system based on wireless network sensor is the hybrid based automatic meter reading system [11]. In this system, the wireless communication medium between the node device and base station is NRF24L01 wireless transceiver compare to [11] that consists of ZigBee modules as their wireless communication device. It is because the cost of NRF24L01 wireless transceiver much cheaper compare to ZigBee module. The NRF24L01 wireless transceiver also provides 1 to 2Mbps data rate and distance range up to 1 km by adding additional power amplifier (PA) and low-noise amplifier (LNA) on the wireless transceiver. The base station consists of Raspberry Pi 3 model B and NRF24L01+ PA+LNA wireless transceiver compare to [11] that consist of ZigBee and GSM module. The base station will upload the data from the node device to web server as shown in Fig. 1. So, all technique of the system will be combined to implement the proposed system that will be installed on the energy meter with the systematic, effective and low-cost device.

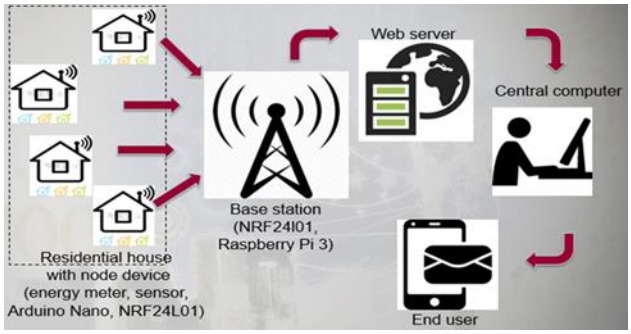


Fig. 1. The proposed system of the AMR system

## III. METHODOLOGY

### *A. Hardware development*

This project is divided into two main parts which are hardware and software components. The hardware component consists of base station and node device. Node device uses LM393 light sensor, Arduino Nano and NRF24L01 +2.4 GHz wireless transceiver. Base station used NRF24L01+PA+LNA+2.4 GHz wireless transceiver. Arduino software (IDE) and Python 3 have been used in software development.

Fig. 2 shows the overall hardware development process. When the node device and base station are activated, they will try to communicate with each other. If the node device and base station was communicating, the sensor will count the number of pulse. If the sensor detect a pulse on the power meter, the sensor will count the number of pulse until it reaches the maximum number of pulse. The data on the node device will be transmitted to the base station and upload the data to web server when the number of pulse at maximum value. The sensor will recount the number of pulse and follow with other steps.

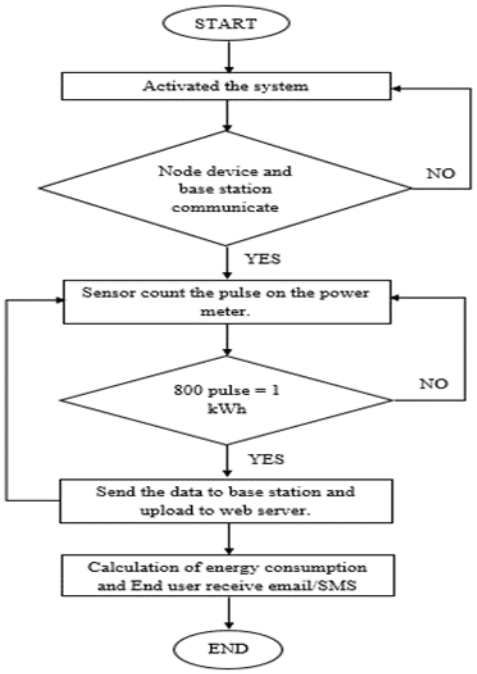


Fig. 2. The flowchart of the hardware component.

### *B. Software development*

The software that being used is Arduino software (IDE) and Python 3 programming language. In the Arduino software, the pulse sensor will be programed using c language programming to count the pulse on energy meter and transmit the data to base station. The code will read the input and count the input until it reaches maximum number of pulse. NRF24L01 on node device will transmit the data to the base station. In the python 3 programming language, the code design to receive and translate the data from node device before upload it to web server.

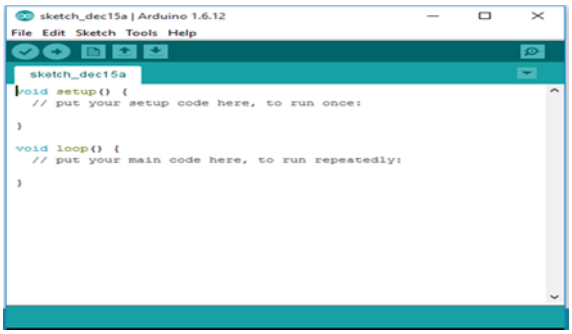


Fig. 3. Arduino sketch for Arduino software [12].

## IV. RESULT AND DISCUSSION

### *A. The implementation cost of the project*

The development of this project consists of the node device and the base station and the comparison in the cost implementation is done between this project and the Hybrid based Automated Meter reading (AMR) system [11]. Table I and II shows the implementation cost of the project. Table I shows the implementation cost for the node device that consists of Arduino Nano, Light sensor and NRF24L01 wireless transceiver and Table II shows the implementation cost for the base station that consists of Raspberry Pi 3 model B and NRF24L01+PA+LNA wireless transceiver.

TABLE I. THE IMPLEMENTATION COST FOR THE NODE DEVICE

| No | Node device | | |
|---|---|---|---|
| | ***Component*** | ***Quantity*** | ***Cost*** |
| 1. | Arduino Nano | 1 | RM15.70 |
| 2. | Light sensor | 1 | RM6.80 |
| 3. | NRF24l01 wireless transceiver | 1 | RM 8.50 |
| | TOTAL | | RM 31.00 |

TABLE II. THE IMPLEMENTATION COST FOR THE BASE STATION

| No | Base station | | |
|---|---|---|---|
| | ***Component*** | ***Quantity*** | ***Cost*** |
| 1. | Raspberry Pi model B | 1 | RM198.00 |
| 2. | NRF24l01+PA+LNA | 1 | RM22.00 |
| | TOTAL | | RM220.00 |

Table III and IV shows the implementation cost of the Hybrid based Automated Meter reading (AMR) system. Table III shows the implementation cost for the node device that consists of PIC16f628A and ZigBee module and Table IV shows the implementation cost for the base station that consists of ZigBee module and GSM module.

TABLE III. THE IMPLEMENTATION COST FOR THE NODE DEVICE [11]

| No | Node device | | |
|---|---|---|---|
| | ***Component*** | ***Quantity*** | ***Cost*** |
| 1. | PIC16F628A | 1 | RM16.00 |
| 2. | ZigBee module | 1 | RM180.00 |
| | TOTAL | | RM196.00 |

TABLE IV. THE IMPLEMENTATION COST FOR THE BASE STATION [11]

| No | Base station | | |
|---|---|---|---|
| | ***Component*** | ***Quantity*** | ***Cost*** |
| 1. | ZigBee module | 1 | RM180.00 |
| 2. | GSM module | 1 | RM90.00 |
| | TOTAL | | RM270.00 |

From the implementation cost, it shows that the project cost implementation for the low-cost automated power meter

reading based on WSN is much cheaper compared to the Hybrid based Automated Meter Reading system.

*B. The node device*

Fig. 4(a). Represents the node device that consist of light sensor, Arduino Nano and NRF24L01. Before interfacing the sensor with the power meter, the potentiometer of the sensor needs to be setup in order to get the accurate reading of the LED pulse on the power meter.

When the node device is activated, the serial monitor displays the radio detail and start communicate with base station. The radio detail shown the channel used, the number of payload, the data rate and etc. At this state, the light sensor is in low state and start to count the number of LED pulse.

When the light sensor detects the LED pulse, the sensor start to count down the LED pulse as shown in Fig. 4(b). On the serial monitor, it will represent the number of LED pulse that has been count down. If the number of Led pulse equal to zero, the node device start to transmit the data which is 1kWh to the base station and displayed 1kWh at the serial monitor. When the data has been received at the base station, the serial monitor has displayed the sentence “data was received”.

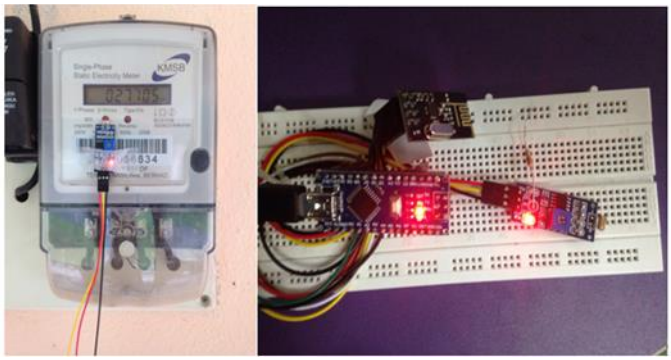

(a)

```
LOW-COST WIRELESS SENSOR NETWORK FOR POWER METER READING
STATUS            = 0x0e RX_DR=0 TX_DS=0 MAX_RT=0 RX_P_NO=7 TX_FULL=0
RX_ADDR_P0-1      = 0xf0f0f0f0d2 0xf0f0f0f0e1
RX_ADDR_P2-5      = 0xc3 0xc4 0xc5 0xc6
TX_ADDR           = 0xf0f0f0f0d2
RX_PW_P0-6        = 0x20 0x20 0x00 0x00 0x00 0x00
EN_AA             = 0x3f
EN_RXADDR         = 0x02
RF_CH             = 0x4c
RF_SETUP          = 0x0f
CONFIG            = 0x0f
DYNPD/FEATURE     = 0x00 0x00
Data Rate         = 2MBPS
Model             = nRF24L01+
CRC Length        = 16 bits
PA Power          = PA_MAX
```

(b)

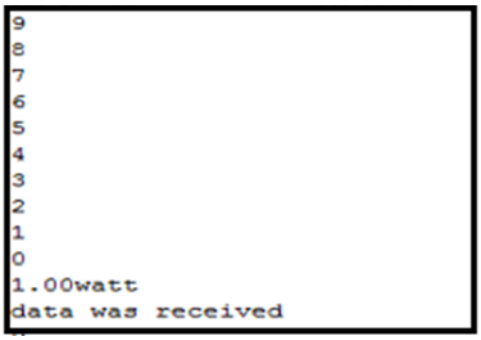


(c)

Fig. 4 (a) Power meter and node device, (b) System activated, (c) Sensor count the LED pulse.

*C. The base station*

Base station that consist of NRF24L01+PA+LNA and Raspberry Pi 3 has received the data from node device as in Fig. 5(a). The terminal of Python 2 has displayed the radio details and system activated.

Fig 5(b). Represent the data has received and displayed it on the terminal of Python 2 which is “Power: 1.00Watt”. It also has displayed the Uniform Resource Locator (URL) of online server that has uploaded by base station which is http://things.ubidots.com/api/vt.6/values/5911d54e7625423d3f3258d0. The accuracy of the data transmission was investigated by comparing the current electricity consumption that displays on the power meter with the Python 2 terminal.

(a)


(b)

Fig. 5 (a) Base station, (b) Base station received data from node device.

### *D. Online server*

*Ubidots* represent the data being upload by the base station and consist of the daily of electricity power usage, the monthly of electricity usage and the graph electricity power of 1kWh power over time as shown in Fig. 6(a). *Ubidots* sends email and short message service (SMS) to users at the end of the month of their electricity consumption as shown in Fig. 6(b.)

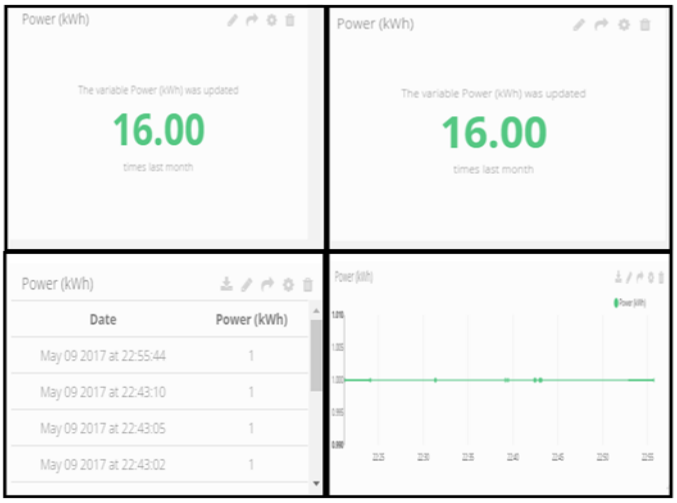


(a)

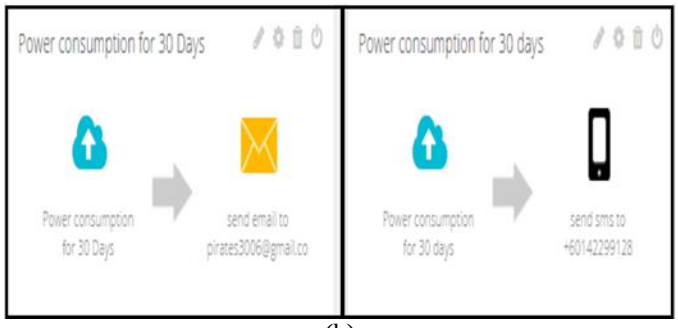


(b)

Fig. 6 (a) Display of power consumption, (b) Email/received sent to users.

## V. CONCLUSION

The hardware and software developments had successfully done and tested. The node device and base station is running and working properly. This project provide low-cost automated meter reading system based on wireless sensor network (WSN) from the comparison on the cost implementation between the project and the Hybrid based AMR systems. The experiment was successfully conducted in order to get the correct result of power meter reading. The suitable distance range of the node device and the base station. The future improvement needs to improve is by replacing the light sensor module to another device that able to be install in the power meter and the further studies on the interference during the data transmission.

## REFERENCES

[1] "TNB Better. Brighter.", TNB Better. Brighter., 2012. [Online]. Available: https://www.tnb.com.my/residential/meter-replacement-programme.

[2] M.K. Abdul Latif,"Development of smart energy meter system for low voltage residential premises in Malaysia", 2014.

[3] "Smart Meter First Phase To Roll Out Next Year In Malacca". NST Online. N.p., 2016. Web. 5 Dec. 2016.

[4] D. Thanh and M. Borole, "Wi-Fi Based Smart Energy meter", 2015.

[5] Prachi Agrawal "Radio Frequency based automatic meter reading system" ,May 2014.

[6] A.Ali,N.H.Saad,N.A.Razali and N.Vitee"implementation of automatic meter reading using radio frequency (RF) module" December 2012.

[7] S. Palaniappan, R. Asokan, S. Bharathwaj and S. N, "Automated Meter Reading System - A Study", International Journal of Computer Applications, vol. 116, no. 18, pp. 39-46, 2015.

[8] Asahna. K and Sudhish N George "GSM based Automatic Energy Meter Reading System with Instant Billing", National Institute of Technology, Calicut, India, 673601, 2013.

[9] Champ Prapasawad, Kittitach Pornprasitpol and Wanchalerm Pora "Development of An Automatic Meter Reading System Based on ZigBee Pro Smart Energy Profile IEEE 802.15.4 Standard", *IEEE*, 2012.

[10] Dipti Yeolekor, H. H. Kulkarni and Dr. D. G. Bhardwaj "Real Time AMR and Control of Household Energy Meter with ZigBee Communication", *IEEE*, 2015.

[11] Mohd Yunus Nayan, Aryo Handoko Primicanta and Mohammad Awan, "Hybrid Automated Meter Reading System", *IEEE*, 2009.

[12] "Arduino - Software". *Arduino.cc*. N.p., 2009. Web. 9 Dec. 2016.

# Lossless Image Compression with Variable Block Sizes

Muhammad Afiq bin abdul Rahim
Faculty of Electrical Engineering
Universiti Teknologi Malaysia
(UTM) Johor, Malaysia.
afiqrahim20@yahoo.com

En Samura bin Ali
Telecommunications Eng. Department
Faculty of Electrical Engineering
Universiti Teknologi Malaysia (UTM)
samura@fke.utm.my

***Abstract*—Nowadays, many people tend to take pictures for hobbies, event, travel and even for professional job of photographer. But all this kind of images need a huge amount of space or data size to saved and it will fully fill up the hard disk or any storage devices. The big data size of the image will takes longer times to be transfer to other platform and it will be troublesome if the information need at that moment. Image compression is the technique to solve this situation as in telecommunication and medical area, the use of lossless image compression tend the image not loss any information and image quality while reduce the file size. The data missing from the original image will leads to misunderstanding as the information from the compressed image received not exactly identical to the original image. This thesis proposed image compression technique by using Huffman coding. The mechanism of multiple Huffman coding is it will compress the block by using all available table inside Number of Symbol(NOS).This will enlarged the size of the transmitted data. Differential pulse code modulation (DPCM) used as predictor which numbers of bits can be reduced while sustain the acceptable visual. This thesis proposed image compression technique by compare the compression ratio of block size from 8x8,16x16,32x32, 64x64, 128x128 and 256x256.The design then verified by an experiment on the compression varied by compression process with selected tested images. The experiment on image compression is validated via computer simulation and coding using MATLAB.**

***Index Terms*— Multiple Huffman Table; Block Sizes; DPCM; Lossless Image Compression; Number of Table; Number of Symbol.**

## I. INTRODUCTION

Images transmitted over the internet are brilliant example of why data compression is vital to people. Suppose we need to download a digitized color photograph over a computer's. If the image is not compressed it will contain about for example 600 kilo bytes of data. When the image is compressed using a lossless technique, it will be about half the original image size, or about 300 kilo bytes. Thus, the compressed image will be transmit much faster to the storage medium such as pen drive, hard disk and other electronic devices. It also saves a lot of space for storing data or information in the future when the images have been compressed.

Compression refers to minimize the quantity of data used to represent a file, image or video content without extremely decrease the quality of the original data. It also reduces the number of bits needed to store and/or transfer digital media. To compress something means that you have a piece of data and you reduce its size. There are diverse techniques to do that and they all have their specific advantages and disadvantages. Huffman coding is a lossless image compression technique used in this project. Huffman coding is built based on the frequency of occurrence of a data, for example, pixel in images. The technique is to use a lower number of bits to encode the data into binary codes that arises more frequently. The suitable image format for Huffman coding is in bitmap.

## II. LITERATURE REVIEW

There are two types of compression which is lossless image compression and lossy image compression [1]. Lossless image compression offer no data loss of data after the data compressed and the data size be much smaller. Thus the image retain its information and also in compact size and the information exactly similar to the original image. Lossy image compression also reduce the data size but there are some information loss when compare the original image. The data slightly alter from the original data when the decompression process occur. For sound and images, the compression have small alteration and it is not a big deal but for text, the data loss cannot be tolerate as there will be misguided information that will occurred. For this project, lossless image compression method will be used to give optimized results. Lossless image compression method includes Differential Pulse Code Modulation (DPCM) and Huffman Coding. DPCM gives predictive of future value meanwhile Huffman coding gives high, simple and effective compression.

The focus of this project is to compress image with Multiple Huffman coding but before perform this method, the vital element of lossless image compression methods which is Differential Pulse Code Modulation (DPCM). DPCM is effective techniques of predictive ways which is lossless or error free approach where inter-pixel redundancies of nearby pixel are eliminated. Previously coded neighboring pixel has been used by the predicted value of target pixel and illustrated in Figure 1 and the formula to find Pixel Error is shown in

(1).The difference between the actual and predictive value is entitled pixel error as shown in Figure 2 and Figure 3.

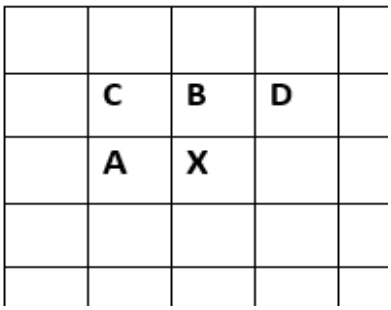


Fig. 1. Predictor and neighboring pixels

$$\text{Pixel Error} = X - [\, a*A + b*B + c*C \,] \quad (1)$$

where X is origin of image gray pixel with A, B and C which are neighbor of origin images gray pixels and a=0.5, b=0.3, c=0.2

```
>> image_grayI(1:8,1:8)

ans =

   162   162   162   161   162   157   163   161
   162   162   162   161   162   157   163   161
   162   162   162   161   162   157   163   161
   162   162   162   161   162   157   163   161
   162   162   162   161   162   157   163   161
   164   164   158   155   161   159   159   160
   160   160   163   158   160   162   159   156
   159   159   155   157   158   159   156   157
```

Fig. 2. Original image gray value

```
>> PixErr(1:8,1:8)

ans =

     0     0     0    -1     1    -5     6    -2
     0     0     0    -1     1    -3     3    -2
     0     0     0    -1     1    -3     3    -2
     0     0     0    -1     1    -3     3    -2
     0     0     0    -1     1    -3     3    -2
     2     1    -5    -7     1    -1    -2    -2
    -4    -3     3     0     0     2    -1    -4
    -1    -1    -7    -2     0    -2    -5     0
```

Fig. 3. Pixel Error Value

Huffman code is one of the widely use method among data compression. Huffman coding is a simpler encoder algorithm in building a variable length codes to symbolize different number of symbols (NOS). A number of symbols which have higher probability of redundancies gives shorter variable length code compare with the lesser probability of redundancies gives lengthier variable length codes. Results of the number of pixels to be used to represent the HSO can be optimized and reduced by used that code that will create a table of Huffman to represent number of symbols in Huffman Stream Output (HSO). A binary tree must be created to build such codes which called Huffman tree that build using number of symbols occurred and their probabilities of all the possible symbols.

The Huffman tree is build using the number of symbols occurred and their probabilities of all the potential symbols. The table dictionary is built by using a binary tree. At first, the symbols form an input arranged in order of decreasing probabilities of occurrences. Then, a new node is formed result of combined two lowest probabilities number of symbols. Then the new nodes formed before combine with the next symbols follow the increasing order to get an additional new nodes beside current node. This process is repeated until all nodes have been processed. Afterwards, one branch as '0' and '1' done tagged of traversal from the final node back to the tree. Traversal from the final node back to the originating node would give you the code words for the all symbols and create a so-called Huffman table dictionary for one definite number of symbols.

By definition, the compression ratio (CR) is ratio of original image size ($I_{uncomp}$) to the compressed image size ($I_{comp}$) as shown in (2), thus:

$$Compression\ Ratio = \frac{Original\ Image}{Compressed\ Image} \quad (2)$$

## III. Project Methodology

There are several image compression coding technique applied in compression images. In lossless image compression, entropy coding has two method which are Huffman coding and Arithmetic coding. Huffman coding is selected for this project because it is the most effective entropy coding compared to Arithmetic coding.

There are three parts in encoding process. First stage is to perform the predictor or called as Differential Pulse Code Modulation (DPCM) which has been discussed in Chapter Two. Pixel Error is form from the predictor and also called the output DPCM. The second stage is pixel error is changed to pixel number using pixel number converter to make Huffman coding encoding procedure much easier. Lastly, the third stage where entropy coding is perform by using the Multiple Huffman table (MHT) that has been built manually. Both table code and the Huffman stream output was ready to be transmit to the receiver. Flowchart 1 show the proposed lossless image compression algorithm.

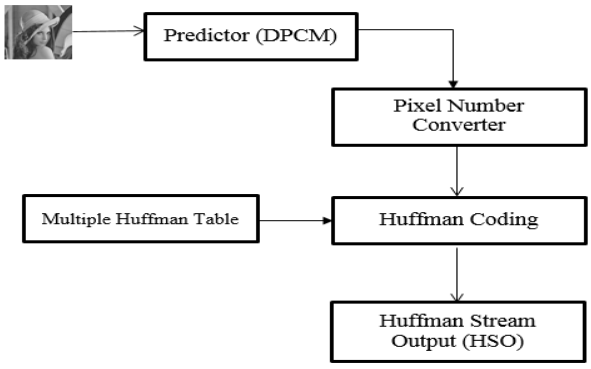


Flowchart. 1. Proposed lossless image compression

In this project, DPCM is referred as lossless DPCM or lossless predictive coding. Prediction error or pixel error produced will near zero and has lower zero order compared to its original image in theory fact. This process is effective because when the compress near zero or zero itself for the pixel value, it could minimize the pixel need to be compressed The predictor was modified to produce all positive value by converting negative and positive pixel error values to all positive pixel number or pixel value from the predictive value of pixel error which whole are not entirely positive. Figure 4 show the integer converter theory.

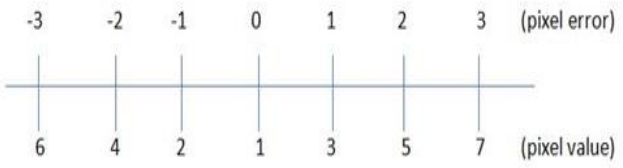


Fig. 4. Integer converter theory

As Huffman coding is a method on reducing code redundancy, the produce code word which is the final code word acquired from the Huffman coding is stored in a code table and being moved together with the compressed data as a reference for decompression process. The code table have the information on the symbols exists in source data and from coded word is created its probability. Generally, the early stage of Huffman coding is to develop the Huffman tree. Below are steps needed to develop a binary tree.

1. Find the probabilities for image by finding its histogram.
2. Arranged the probabilities in increasing order which is smaller or largest.
3. At the smallest two of probabilities are combined by addition.
4. Go to steps 2 until only two probabilities are left.
5. By working backward along the tree, generate the code by alternating assign 0 and 1.
6. Sort the code word with its probabilities to create code word table.

Single table Huffman coding is the basic to the multiple table Huffman coding. Flowchart 2 show the compression engine for Huffman Table and Flowchart 3 show the decompression engine for Huffman Table.

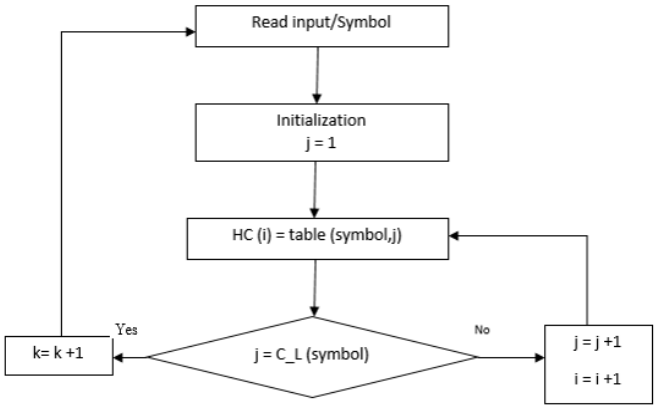


Flowchart. 2. Compression engine for Huffman table

Example on conventional Huffman encoding are shown in Figure 5 below:

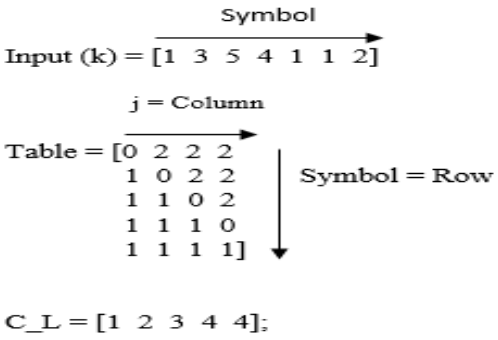


Fig. 5. Huffman Table encoding

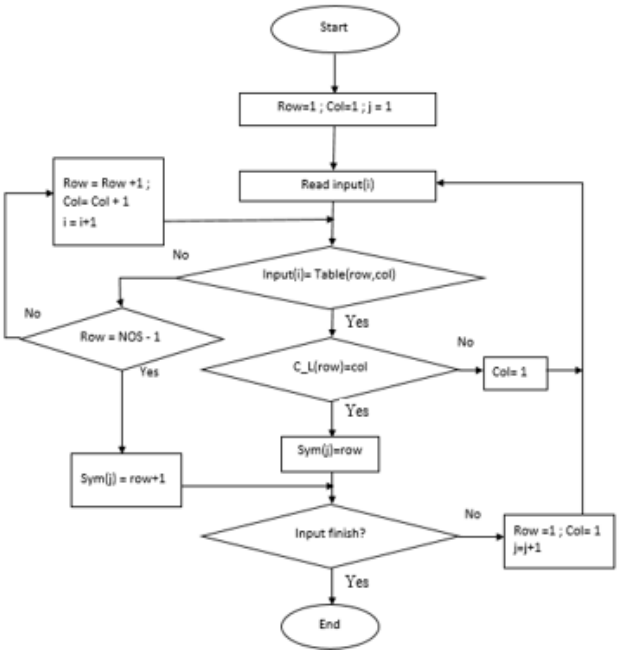


Flowchart. 3. Decompression engine for Huffman table

To perform the Multiple Huffman Table, codebook must be created manually. This table is created same as the conventional but for Huffman table the table code are fix for each number of

symbols (NOS). The step to create the Normal Multiple Huffman table are below:

1. Assign the binary tree follows number of symbols occurred.
2. By tracing along the node of the tree, generate the code by alternating assignment 0 and 1.
3. Read the code by follow node into their number of symbols.
4. The length of each code word were saved for reference in compression.
5. Repeat step 1 until 4 for different shape of binary tree. For number of symbols more than three had more than one binary tree.
6. The number of table for each NOS are until 511.

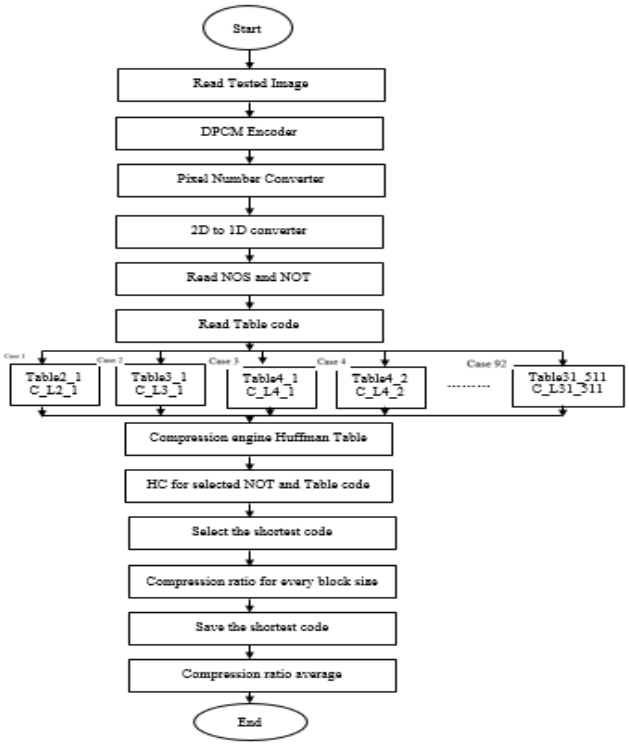


Flowchart. 4. DPCM and Huffman Table encoder compression

Flowchart 4 show the process of DPCM and Huffman Table encoding compression. Firstly, select the tested image and it goes to DPCM encoder. Then it goes to Pixel Number Converter which convert the Pixel Error that has positive and negative value to positive value. We must convert the 2D input to 1D for the Huffman compression to be process successfully. Then we can varies the block size wanted from 8x8, 16x16, 32x32, 64x64, 128x128 and 256x256. Next it goes to read NOS and NOT which NOS is maximum value in 1D input and NOT is the number of table for specific NOS. For example, the NOS obtain is 14 and the number of table (NOT) for NOS 14 is 6 which from table14_1 to table14_6. Second example is NOS obtain is 22 and the number of table (NOT) for NOS 22 is 1 at table21_30. Next, the process continue by read Table code which is the case for every table from NOS 2 to NOS 511. For example, at NOS 14, we get six table of NOT and at table code, the case of NOS 14 is from 43 to case 48. Next example, at NOS 22, we get one table of NOT and at table code, the case of NOS 22 is at case 91 which has table21_30 and C_L21_30. The process will select the case and it goes to Huffman Table encoding compression which has been discuss in Flowchart 2. The output of this Huffman encoder is Huffman code (HC) which based on the selected NOT and Table code and the input process by refer to case selected. Next, the program select the shortest code length and perform the compression ratio for every block. All HC which has the shortest code length will be saved based on NOT. Lastly, the compression ratio average calculated by find the mean of all compression ratio.

## IV. Result and Analysis

All the compression algorithm are used to create the design.Images of black and white ‘Lena’, ‘Barbara’, ‘Goldhill’, ‘Airplane’, ‘Pepper’, ‘Baboon’ and ‘Boat’ were used with the resolution of 512x512 as the input of the data with bitmap(.bmp) format. The compression done into 8x8, 16x16, 32x32, 64x64, 128x128 and 256x256. After the compression, the output go to decompression algorithm to decompress the Huffman Stream Output. Table 1 show the result of the compression ratio for each variable block size using seven tested images.

Table 1. Result for tested images of various block size for compression ratio

| | Compression Ratio | | | | | | |
|---|---|---|---|---|---|---|---|
| Block size | Lena | Airplane | Baboon | Barbara | Boat | Goldhill | Pepper |
| 8x8 | **1.78** | 1.16 | 0.66 | **1.05** | **1.32** | **1.04** | **1.26** |
| 16x16 | 1.63 | 1.40 | **0.69** | 1.03 | 1.22 | 1.03 | 1.25 |
| 32x32 | 1.62 | **1.47** | 0.65 | 1.01 | 1.17 | 1.02 | 1.17 |
| 64x64 | 1.46 | 1.40 | 0.65 | 1.03 | 1.14 | 1.02 | 1.13 |
| 128x128 | 1.28 | 1.29 | 0.62 | 1.04 | 1.08 | 1.03 | 1.16 |
| 256x256 | 1.30 | 1.28 | 0.61 | 1.02 | 1.01 | 1.01 | 1.16 |

From Table 1, for Lena, block size 8x8 has higher compression ratio. For Airplane, block size 32x32 has greater compression ratio. Block size 16x16 has greater compression ratio for image Baboon. Block size 8x8 for image Barbara has higher compression ratio. For Boat, block size 8x8 has greater compression ratio. For Goldhill, block size 8x8 has larger compression ratio.Lastly, block size 8x8 has highest compression ratio for image Pepper. The higher compression ratio, the better the performance. Thus the block size selected for Lena is 8x8, Airplane with block size 32x32, Baboon with block size 16x16, Barbara, Boat, Goldhill and Pepper with block size 8x8 respectively.

## REFERENCES

[1] Ida Mengyi Pu. (2006). Fundamental Data Compression. Great Britain. Butterworth-Heinemann.

[2] C. Wu and C.- C.J. Kuo. (2001) “Efficient multimedia encryption via entrophy codec design”, SPIE international symposium on electronic imaging, San Jose.

[3] C. Wu and C.-C.J. Kuo. (2000) “Fast encryption methods for audio visual data confidentially”,SPIE Photonics East – Symposium on Voice, Video and Data Communications, Boston.

[4] Paul, G. Howard, and Jeffrey, Scott, Vitte (1993). Fast And Efficient Lossless Image Compression. 351-360. IEEE.

[5] Marcelo, J. Weinberger, Gadiel, Seroussi, and Guillermo, Sapiro (2000). The LOCO-I Lossless Image Compression Algorithm: Principles and Standardization into JPEG-LS. 9 (8), 1309-1324. IEEE Transactions On Image Processing.

# Wireless Heartbeat Monitoring System (WHMS)

Nur Mariam binti Abdul Rahim
Faculty of Electrical Engineering
Universiti Teknologi Malaysia
Skudai, Johor, Malaysia
mariamrahim19@yahoo.com

Mohamad Kamal A. Rahim
Communication Engineering Department
Universiti Teknologi Malaysia
Skudai, Johor, Malaysia
mkamal@fke.utm.my

***Abstract*— This paper describes the development of wireless technology into medical appliances that is applicable in hospitals. This integration results in a monitoring system that involves the usage of Raspberry Pi 3 and a pulse oximeter. This project involves the usage of both hardware and software. Two major parts of this project includes interjection between the pulse oximeter with the Raspberry Pi 3 and an algorithm that transmits the data from Raspberry Pi 3 to a database. The final result is then being displayed on a monitoring station powered by XAMPP known as a localhost. The purpose of this project is to initiate a system that is capable of collecting data from the hardware components and display the data collected at the monitoring station. The distance between Raspberry Pi 3 to the access point affects the signal strength during data transmission where a distance of 1m and 16m will result in -52 dBm and -64 dBm respectively. The transmitted data is stored in a database and displayed at a user-friendly GUI.**

***Keywords*— Monitoring system, Pulse oximeter, localhost, XAMPP, Raspberry Pi 3, GUI***

## I. INTRODUCTION

The broad usage of technology today have made a huge impingement in different industries in the world including the medical field. For instance, the application of an oximeter has made easy by simply placing on a patients' finger to monitor his pulse rather than having to analyze manually. In the past years, bioengineers have increased their efforts to create a large amount of devices that is able to detect the human heart rate. The pulse oximetry is one of the devices that is capable of doing so. The pulse oximeter is easy to apply thus making it beneficial for doctors and nurses. Despite the low complexity, users must acquire basic knowledge in conducting the device to ensure a better understanding on how data can be interpreted.

In America, there were 71 300 000 adults facing Cardiovascular Disease (CVD) of which 27 400 000 were estimated to be above 65 years old [National Health and Nutrition Examination Survey 1999-2002]. This CVD disease is a condition where plaque, a waxy substance is built up inside the arteries. A heart attack is triggered once the oxygen fails to reach the heart due to the blockage of oxygen paths. This is also known as artherosclerosis [1]. There are also other factors that affects the chances of a CVD such as physical activities, overweight and obesity and also the presence of other internal diseases [1].

A huge mistake that is common among patients is the lack of awareness of the danger of a certain disease. Patients are not aware that this may later lead to other problems which can in the end be the cause of death [2] [3]. The implementation of wireless network in medical field has improved the approach on health monitoring. The technological advancements in hospitals have now become crucial for early disease detection of patients. Bioengineers play a big role in applying new advancements in both clinics and hospitals to allow clinicians monitor the health of patients.

However, medical surveillance does not limit its usage to only clinics and hospitals, it can also be used at our homes. An integration of wireless communication into a health monitoring system allows users to monitor their health within a distance. The functionality of a Raspberry Pi allows users to do so as long as it is connected to the internet. This approach is beneficial as it is low-cost and is portable allowing users to check their health condition at any time and any place.

## II. LITERATURE REVIEW

### *A. Principles of Pulse Oximetery*

Our blood contains hemoglobins which are consisted of oxygenated and deoxygenated hemoglobins. The concept behind the pulse oximetery is the transmission of light through our blood which will determine the concentration of both the types of hemoglobin [1]. Light-Emitting Diode (LED) and (IR) are chosen to be exposed to our skin as they have wavelengths smaller than the red skin pigmentation in our bodies that is able to absorb wavelengths around 660nm [4]. The oxygenated hemoglobin absorbs more infrared light as compared to red light. The result will oppose when we calculate the concentration of deoxygenated hemoglobin.

The concept behind the acquiring the beats per minute or bpm value is obtained by calculating the time between 2 beats. This is also known as inter beat interval (IBI). By collecting the 10 IBI values, the bpm can be calculated as shown in (1).

$$bpm = \frac{60000}{IBI} \quad (1)$$

### B. *Raspberry Pi 3 as the brain of the system*

The Raspberry Pi is an advancement of small computers developed by Eben Upton [5]. This device has the same functionality as a modern PC but with lower power consumption level. What differentiates a Raspberry Pi from other microcontrollers such as Arduino is that it is a fully functional Linux computer. There are several generations of the Raspberry Pi but the most recent is Raspberry Pi 3. The latest edition is proved to be 80% faster than the old editions [10] plus having extra features like 2.4 GHz WiFi and Bluetooth.

Since the pulse oximeter can only transmit analog signals, and the Raspberry Pi can only read digital inputs, an external circuit is needed to be included to convert the analog to digital. For this purpose, an analog-to-digital converter (ADC) MCP3008 is used. This ADC is an 8 channel converter with benefits of low-cost. The schematic layout is showed in Fig. 1.

### C. *Localhost development*

XAMPP is a shorter form of Cross-Platform (X), Apache (A), MYSQL (M) PHP (P) AND PERL (P) [6]. MySQL enables user to search, store, sort and retrieve data [10]. With relevance to the purpose of this project, a server needs to be connected to the system to ensure the data collected can be gathered and stored in one spot. By utilizing XAMPP, all data can be stored and allow hospitals to have their patients' data stored in a server.

## III. WHMS Development

This project is an integration of two algorithms built between the pulse oximeter and the Raspberry Pi 3, and also between the Raspberry Pi 3 to the server. Fig. 1 shows the process flow of the whole system.

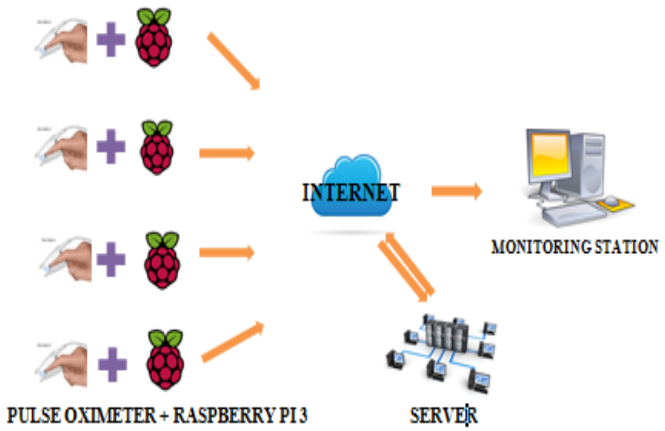


Fig. 1 Process flow from pulse oximeter to monitoring station

Since this system consists of two main parts, the framework of the development can also be divided into 2. The first part of this project requires knowledge on python language as that is the main language used to configure a Raspberry Pi. External hardware was used to connect the sensor to the controller because the sensor can only transmit information in analog form. Hence an analog to digital converter is required to convert into readable information. Fig. 2 shows the flowchart of the progress of initiating a connection between the pulse oximeter and Raspberry Pi 3.

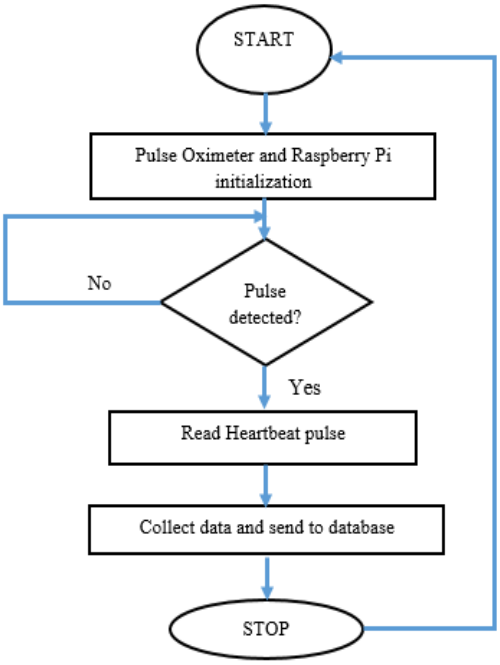


Fig 2. Framework of the collection of data on the Raspberry Pi and the transmission of data to a database

As for the second part, the framework will show the progress in developing a connection between the Raspberry Pi 3 to the server as shown in Fig. 3. With relevance to this projects' objective, this process allows the data to be stored for future reference. However, a larger database is required if the data stored exceeds the limit of storage.

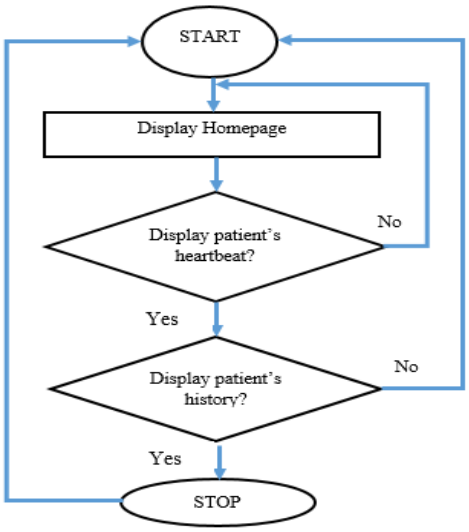


Fig 3. Framework of the capturing data from database to Localhost

At the end of this process is where the data will be stored into a server. XAMPP allows user to store and call data whenever needed and be displayed on a localhost. As for the designing of the localhost, it is quite similar to web designing as it uses HTML and PHP language. Users are able to read their data on the localhost as long as they are connected to the same network as the raspberry Pi. A same IP address is required to allow the transmission of data.

## IV. Results And Discussions

To attain the read data from pulse oximeter, the hardware is needed to be connected. After the hardware connections were done, the reading could be displayed on the Raspberry Pi. Python language was used to configure the hardware elements. A few modifications were done to the program to ensure a more precise reading is captured.

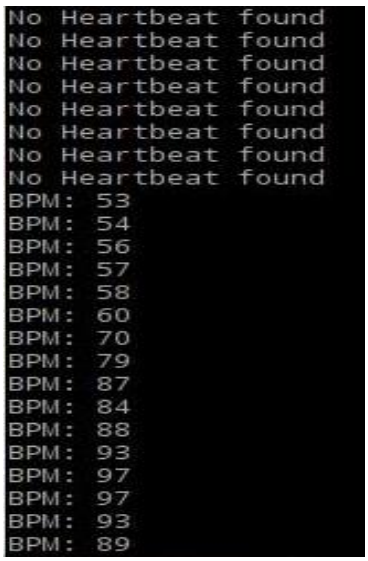


Fig 4. Output from pulse sensor displayed on Raspberry Pi 3

This stream of data is displayed every time a beat is detected. Further calculations can be obtained from the sensor file. The upper limit of this output is set to 240 BPM to avoid high frequency noise. As shown in Fig. 4, the output can determine the BPM whenever it is in contact with human skin. However, this result depends on the sensitivity of the surrounding.

After the hardware configurations and capturing of data are settled, next is the transmission of data to a database. This step requires the connection of Raspberry Pi to the internet. The setup of the measurement system has been done in the laboratory. The signal strength of the system is analyzed in the Research Room at P18 Faculty of Electrical. The different length was set as a reference to interpret the change in strength with relevance to distance to the access point. Table 1 displays the signal strength obtained at different distances.

Table 1: Signal strength measurement at different distance

| **Indoor Signal Strength** | | |
|---|---|---|
| Distance (m) | Signal Strength (dB) | |
| | Waiting for data | Transmitting data |
| 1 | -49 | -52 |
| 6 | -51 | -53 |
| 9 | -50 | -55 |
| 11 | -54 | -57 |
| 16 | -59 | -64 |

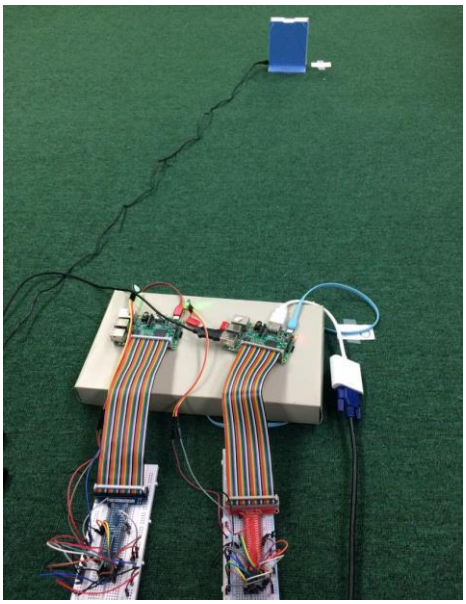

Fig 5. Signal strength of a multiple node system at 1 m distance

In Phpmyadmin, we are able to store data collected from Raspberry Pi. The first step to store these data is to build a table based on the information received. Fig. 6 shows the table in database with the information stored.

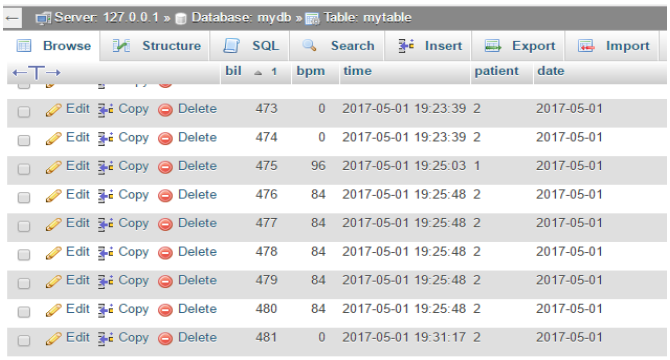


Fig 6. Data obtained from Raspberry Pi of patient 2 stored in database PHPmyadmin

The localhost developed was to call and display the data stored in the database. As seen in Fig. 6, the table is made up of 5 columns consisting of bil, bpm, time, patient and date. All these information will be used later to be displayed on the GUI. In the web development stage, HTML and php language were used to ensure a user-friendly GUI. The output displayed on the localhost will be in real-time.

The main page of the GUI is displayed as shown in Fig. 7. Fig. 8 shows the layout for each patient where it will display the time and BPM of patient. The main page displays the title of the project and other related information. At the bottom of the content page, there is a button where it leads to a page that displays a table containing the average bpm for both men and women. Below this is where users can choose which patient to monitor. The amount of buttons will increase if there is an additional amount of patients connected to the system.

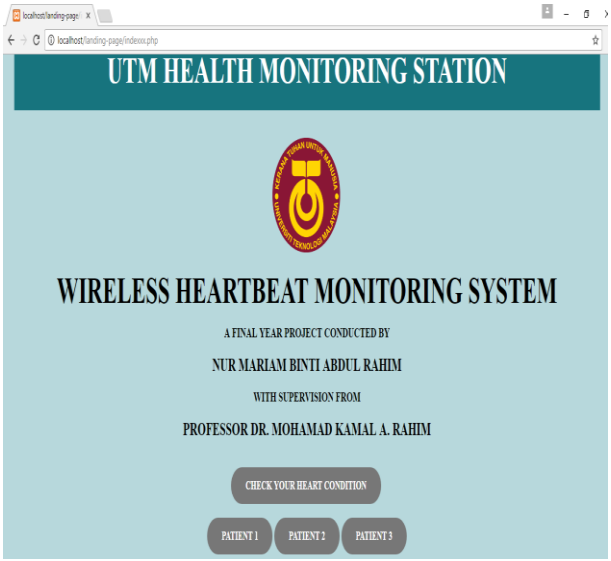


Fig 7. Main page of Monitoring Site

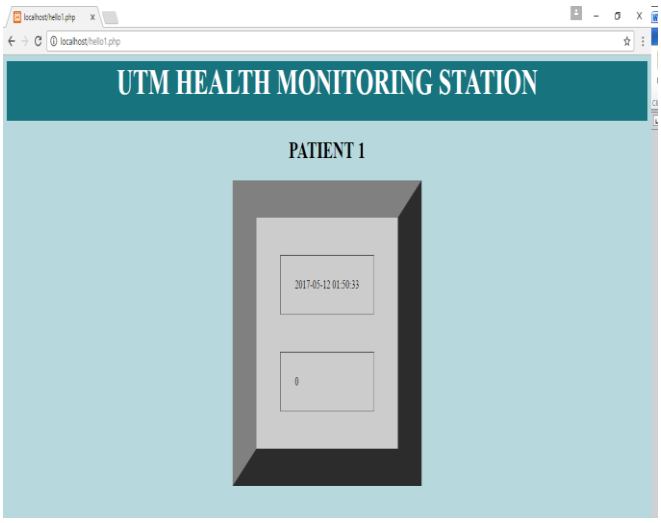


Fig 8. Layout for each patient current heartbeat

The lower row of button on the main page is where users can pick which user to monitor at a certain time. The higher the number of patients, the higher the number of buttons displayed on main page. In this case, only two patients can be monitored at a certain time. This part of the program needed the initialization between the database and the page. The php initialization is as shown in Figure 9.

```
DEFINE('DB_USER','root');
DEFINE('DB_PASSWORD', 'root');
DEFINE('DB_HOST', '');
DEFINE('DB_NAME', 'mydb');

$dbc = @mysqli_connect(DB_HOST, DB_USER, DB_PASSWORD, DB_NAME)
OR die('Could not connect to MYSQL: ' .
    mysqli_connect_error());
```

Figure 9: PHP initialization between database and monitoring page

The integration of hardware and software in this system showed excellent results. However, there were a few setbacks on the hardware development. The reading from the pulse showed a fluctuating BPM. According to pulsesensor.com, the developer of the pulse oximeter used, this condition is normal as we have different periods before our next pulse is formed. However, this will be hard to interpret for users with no medical knowledge as there is no graph displayed. A better approach would be to include the pulse waveform to understand how the BPM is calculated. The pulse oximeter is developed by World Famous Electronics llc is almost precise to the ECG used in hospitals. However, the circuitry on the back side of the sensor is needed to be protected from touch to avoid any shortage of current. The 3.3V power source connected from the Raspberry Pi 3 to the pulse sensor was sufficient enough to operate the pulse sensor.

As for the software development, the transmission of data showed a slightly delayed transmission. This is due to the data being sent every time a pulse is detected. However, this data will only show a delay on the server side. The result collected on the Raspberry Pi will remain the same with no delay. This theoretical information is only valid when both the Raspberry Pi and server are connected to the internet. Therefore it is crucial to ensure that both have a very good connection to the WiFi connected. This system is planned to be implemented in hospitals or used at homes. Due to that this system works well indoors as long as it is connected to WiFi. The build in WiFi in the Raspberry Pi 3 makes it easier to connect to the internet rather than having to use a WiFi dongle.

The signal strength of line-of-sight was determined by varying the distance of Raspberry Pi to access point. Figure 10 shows the distance that was varied. The sample location chosen to conduct this experiment is Masjid Sultan Ismail (MSI), UTM. This location was chosen because of the spacious factor besides it was isolated from the UTM WiFi.

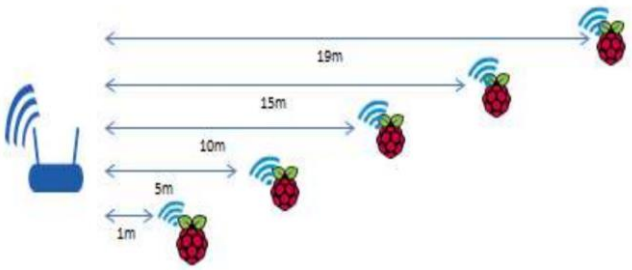


Figure 10 : Different lengths between Raspberry Pi 3 to access point

Figure 11 shows the result from signal strength at different lengths for both single node and double nodes. The result obtained showed that the signal strength of the signal node had a stronger signal as compared to double nodes at all distances. The pattern of the results showed that the shorter distance had a better signal. However, the results showed some fluctuations but the average would range in between -50 dB to -60 dB. The results started to differ after exceeding 19 meters in length where the signal strength started to go below -60 dB. It is assumed that a distance larger than 19 meters will result in a reduction of signal strength. However, this does not affect the data transmission as there is still internet connection. The distance between bed and access point needs to be taken into consideration.

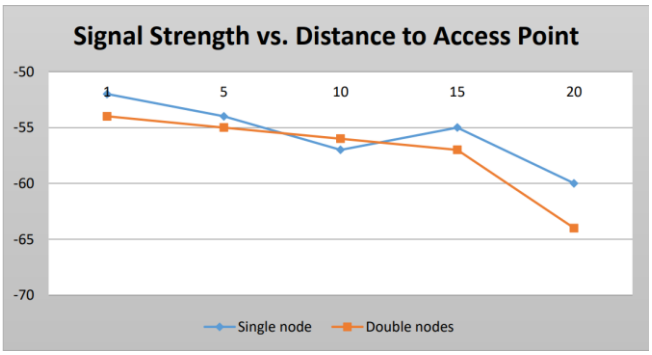


Figure 11: Relationship between signal strength and distance to access point for single and multiple nodes

Observing the different arrangements in hospitals makes it important to understand the signal strength for non-line-of-sight data transmission. The sample location chosen for this experiment is block S09, Kolej Tuaku Canselor, UTM. The arrangement of rooms are as pictured in Figure 12. This block has different rooms that is suitable for non-line of sight configurations. One access point is located in one room while another 5 raspberry is located at 5 different rooms. There is no line of sight in this condition. The signal strength is taken for each distance of the sensor node

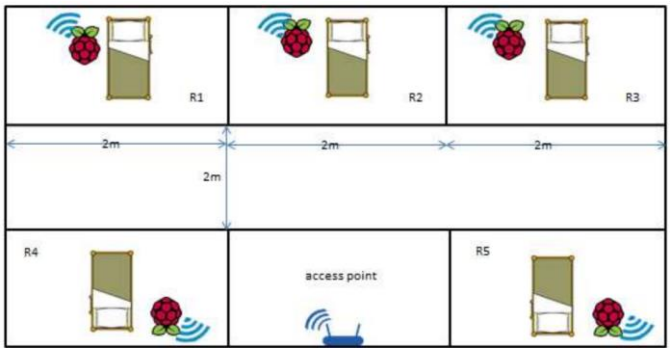


Figure 12: Room arrangements with different distance to access point

Table 1 shows the results obtained at different rooms. From the results obtained, it is observed that the rooms placed opposite of the access point had a lower signal strength as compared to the rooms placed directly next to the access point. This is mainly due to the distance between the rooms to the access points. As stated before, a shorter distance will result in a better signal strength. Comparing the results of line-of-sight and non-line-of-sight, the arrangement with lesser obstacles showed a better result. The signal strength for non-line-of sight was low due to the obstacles between Raspberry Pi 3 to the access point. Obstacles such as walls, doors and furniture may cause a reduction in signal strength due to their high densities.

Table 1: Signal strength at different rooms

| ROOM | SIGNAL STRENGH (dB) |
|---|---|
| 1 | -71 |
| 2 | -71 |
| 3 | -73 |
| 4 | -66 |
| 5 | -62 |

## V. CONCLUSION

This is a portable and easy to use system that can be implemented in hospitals. The completed system is able to display a real-time pulse monitoring system. To allow the transmission of data from patients' bed to the monitoring station, both systems needed to be connected to the same network. As long as the same network is connected to both sides, the data transmission will be smooth throughout the process. The first part of the system consisted of hardware development connecting the pulse sensor to the Raspberry Pi 3. The collected data from Raspberry Pi 3 is transmitted to the database. A large distance between the transmitters to the access point will result in a lower signal strength. On the second part, an online web

application, XAMPP is used to store and display data on the self-developed localhost. A user-friendly GUI is designed to allow users to handle the system without any issues. The signal strength measurement for indoors and outdoors has been measured and it shows that more obstacle will show the result of signal strength will be decreased for the non-line of sight condition

## REFERENCES


[1] T. L. Rusch, R. Sankar, J. E. Scharf, 'Signal Processing Methods for Pulse Oximetry', Computing Biomedical Jurnal, Vol 26 pp 143-159, 1996.

[2] Shirokov, Slesareva, Korepanov, 'The device for remote monitoring of human's heartbeat', 2010 5th International conference on Ultrawide and Ultrashort Impulse Signals, pp 195-197, 2010.

[3] Mark V. R., John F. B., 'The defense medical surveillancesystem and the department of defense serum repository: Gllimpse of the future of public health surveillance', Am J Public Health, pp 1900 – 1904, Dec. 2002.

[4] Mehta A., 'Introduction to the Electromagnetic Spectrum and Spectroscopy', Pharma Change, 2008.

[5] Halfacree G., Upton E., 'Raspberry Pi user Guide', Wiley and Sons, Sept. 2012.

[6] Er. Saurabh Walia, Er. Satinderjit K.G., 'A Framework for Web Based Student Record Management System using PHP', International Journal of Computer Science and Mobile Computing (IJCSMC) Vol.3, No. 8, 2014.

[7] American Heart Association Statistics Committee and Stroke Statistics Subcommittee,'Heart Disease an Stroke Statistics', 2006.

[8] Sin Tong Kok, "Sustainable wireless densor device for heartbeat monitoring with energy harvesting", Bachelor Project Report, Departmentof Electrical-Meachotronics Universiti Teknologi Malysia, 2013.

[9] Muhammad Hazmi Bin Mokhtar '*Multiuser Wireless Pulse Oximeter For Medical Care Monitoting System*. Bachelor Project Report, Department of Electrical-Telecommunication, Universiti Teknologi Malaysia, July 2011/2012.

[10] Luke W.,Laura T., 'PHP and MySQL Web Development', 4th edition, 2009.

# Sound Manipulation using Acoustic Metamaterial

Siti Nur Nashya Azlika binti Hamidon
*Faculty of Electrical Engineering*
*Universiti Teknologi Malaysia*
*Skudai, Johor*
*nashya_azlika94@yahoo.com*

Siti Zaleha binti Abd Hamid
*Department of Communication Engineering*
*Universiti Teknologi Malaysia*
*Skudai, Johor*
*szaleha@fke.utm.my*

***Abstract*—This paper proposes the development and application of acoustic metamaterial in sound manipulation. The main advantage of this study is improving sound manipulation in noise control of conventional materials through the use of metamaterial. A unit cell of the metamaterial is developed using calculative analysis to come up with the measurement and design of the metamaterial using resonant structures. The unit cells are arranged in a 100 millimeters square acoustic enclosure inner faces. Then, the metamaterial is fabricated using 3D printing method with poly lactic acid plastic as the filament type with 5millimeters thickness of unit cells to observe the sound wave response. This acoustic enclosure undergoes testing of sound reduction towards sine wave varied from 200 to 1000 Hertz. Based on this experiment, the acoustic enclosure with metamaterial reduced the sound level as compared to acoustic enclosure without metamaterial and 900 Hertz showed a significant amount of sound level reduced by the acoustic enclosure.**

***Keywords—acoustic enclosure, metamaterial, poly lactic acid, sound manipulation***

## I. INTRODUCTION

Noise control material is commonly seen in buildings, bridges, cooling towers and heavy industrial area [19]. These large noise sources providing communities with noise in terms of both high frequency and low frequency. Before taking solution in overcoming these problems, one should consider the understanding of these noises where high frequency noise is a form of sound we are able to hear and it can possibly be attenuated completely as it travels through the air. Conventional materials use as noise absorber such as concretes, woods, foams and glasses is widely used in building to reduce noise in our surroundings. However, these conventional materials exhibit very low capability to absorb low frequency noise [2] due to long wavelength [18] exist in this waves therefore a massive unit area and thickness of sound absorbing material is needed to absorb such low frequency. Advancement of technology in sound absorption to overcome noise level in community has been growing in acoustic engineering. Sound absorption materials for low frequency such as fibrous and porous materials are heavy and more costly [13]. Therefore, metamaterial is introduced in this field to provide better low frequency sound absorption [11], replacing the conventional bulky materials with less weight and cost. Acoustic metamaterial in the study of sound absorption could be built manually or digitally printed using materials include polyester, polyamide and poly lactic acid. Proving acoustic metamaterial as better noise control compared to traditional material requires answer to questions include: what specific material is needed to build metamaterial with better noise control? How the structure of repeating patterns in metamaterial influenced its performance in noise control? This paper investigates the effect of these two factors on performance of metamaterial in noise control as compared to conventional materials.

## II. LITERATURE REVIEW

The central theme of this study is to design and characterize the acoustic metamaterial for potential application in low frequency sound absorption. This chapter is organized into three sections, comprising the current section which intends to give a brief introduction of the acoustic metamaterial, as well as the other three chapters organized as following:

- Sound manipulation of low frequency noise
- Acoustic properties for sound manipulation of low frequency noise
- Design of unit cell acoustic metamaterial

Metamaterial have demonstrate tremendous potential covering many science and technology fields due to the high demand of ability to manipulate light as well as sound waves which properties are not found in nature. Generally, metamaterial responsible to replace molecules of conventional materials with man-made structures on a scale much less than the required wavelength to be used [14]. In acoustic engineering, the use of metamaterial is undoubtedly capable of transforming existing technology in many applications. Unlike light waves, sound waves are certainly different which acoustic wave is longitudinal wave; pressure and particle velocity are the essential parameters used to describe the wave [20][2].

### *A. Sound manipulation of low frequency noise*

Noise can be defined as unwanted sound or non-meaningful sound that should be lowered so it will not be harmful to human ears [19]. There are two sources of noise; natural and artificial. Natural sources are related with natural phenomena such as lightning, thunder, volcanic eruption, earthquake, and sound of the ocean waves which impact is limited and did not bring much harm to human ears. Meanwhile, artificial noise sources is a man-made noise which brings more harm to human ears

especially noise produced by industry, holding responsibility for noise pollution.

Air traffic noise is also one of the most troublesome sources [17] of noise pollution. In our environment, human are more attracted to consider artificial noise from human itself, where people talking in the middle of the night which is not meaningful to be heard as well as noise from the surrounding such as industrial and automotive noises include rattling sound of machines and vehicles. For example, a study [17] has been conducted to observe level of annoyance of the community living near airport areas; Los Angeles International Airport and Minneapolis-St Paul International Airport towards low frequency noise from the aircraft, defined as experiencing rattling sounds and vibration. Results from this study show that almost half of the respondents stated that they were annoyed by the vibrations and rattling sounds induced by the aircraft in their homes. Similarly, almost half of the respondents reported that they noticed the occurrence of vibrations and rattling sounds in their homes. This study shows that low frequency noise did not harm our ears as what high frequency noise did as explained in the previous paragraph but it causes vibration and rattling sound in the building we live in which brings more harm to a peaceful environment than high frequency noise.

Low frequency noise covers both infrasonic defined as frequency below 20 Hz and audible ranges from 20 Hz to 20,000 Hz [11]; considered as the resulting frequency range from about 10Hz to 200Hz. The frequency is not fixated in boundaries of 10 Hz to 200 Hz but this is where the low frequency is difficult to be optimized in terms of controlling noise. Active noise control [19] is defined as the noise reduction by purposely adding another sound to eliminate the existing noise. The introduced noise may achieve the required noise reduction by way of any one or combination of four different physical mechanisms. Active noise control is a very demanding discipline and its successful implementation requires a detailed knowledge of engineering noise-control principles. In the design of a practical active noise control system, there are three primary components that must be designed specifically for each implementation. These are the control system that generates noise cancelling signals, the sensor system that provides inputs to the controller and the actuator system that converts the signals generated by the controller into sound or vibration [13][13]. Principles of noise control are essential to provide a conducive environment with good management of acoustic.

### *B. Acoustic properties for sound manipulation of low frequency noise*

Noise in our environment, be it natural or artificial noise, is able to be controlled and reduced by employing sound absorbing materials. In phenomenon of sound absorption, sound absorber is a material that will reduce acoustic energy of a sound wave as the wave passes through it. This material is capable of counteracting undesirable effects of sound reflection and reducing reverberant noise levels. Sound absorptive materials could be categorized commonly as fibrous and porous materials [15] [18]. A porous material can be defined as a solid that allows sound waves to enter through them which contains cavities, channels or interstices. Based on their microscopic configurations, porous absorbing materials can be characterized by the capability of its small holes or openings on their surfaces to allow sound waves to enter the materials, thus determining its acoustical properties. While fibrous material can be classified as natural or synthetic which artificially made from minerals and polymers. Synthetic fibrous material has wide applications in sound absorption and thermal isolation. However, it holds significant amount of carbon footprints [20] due to its production involves high-temperature extrusion and industrial processes which based on synthetic chemicals, often from petrochemical sources.

Performance of these fibrous and porous materials could be determined by absorption coefficient, reflection coefficient, acoustic impedance, propagation constant, normal reduction coefficient and transmission loss of sound. However, to specifically determine acoustic performance of sound absorbing materials, parameters include sound absorption coefficient, $\alpha$, and acoustic impedance is considered. $\alpha$ is the measure of acoustical energy of sound wave absorbed by material as sound wave passes through it. This measure depends on angle of incident sound wave to the material with certain sound frequency [7]. It is equal to ratio of amount of total reflected sound intensity to total incident sound intensity. Whereas, acoustic impedance is sound pressure acting on a surface of material divided by velocity of associated particle normal to the surface. In terms of noise control as discussed earlier in this chapter, noise reduction coefficient is widely used as single number index to compare the performance of sound absorbing efficiency of a material. Noise reduction coefficient (NRC) is a measure of capability of materials to prevent sound from reflecting when sound waves hit the materials surface thus presenting the percentage of sound which the materials able to absorb.

For fibrous materials, fiber size, airflow resistance, density and compression are the factors that influence performance of fibrous materials in sound absorption. Diameter of fiber determines sound absorption coefficient of a material, where a decrease in diameter will cause an increase in sound absorption coefficient. Airflow resistance is ratio of specific flow resistance to unit thickness of material. Density is also an important aspect in sound absorption. Middle and higher frequency (more than 2000Hz) has higher sound absorption when material used have high density. Whereas in lower frequency sound absorption [11], structure of fibrous material must be less dense than in middle and higher frequency. High density means that the number of fiber per unit area is abundant. If surface area of material used is large, there will be an increase in energy loss which escalates the sound absorption. While for porous materials, porosity, tortuosity and thickness play an important role to determine its performance in sound absorption. Porosity is the quality of a material being porous, or full of tiny holes and pores.

Meanwhile, tortuosity is the measure of elongation of passage way through pores to identify how far the pores are able to elongate from normal. Internal structure of this porous material is the key that determines behavior of high frequency in sound absorption. For low frequency, effective sound

absorption can be obtained by deciding material thickness equal to one tenth of wavelength of incident sound. At one-quarter wavelength of incident sound, this is where peak absorption occurs [5].

### *C. Design of unit cell acoustic metamaterial*

Throughout the years, researchers have developed methods to build devices especially the passive ones which is operable without the need of power supply to operate to reduce the noise level we hear, such as earplugs or sound absorbing panels. These types of devices are traditionally a material made from soft rubbers or fabrics that exhibits spongy feelings which determine their sound absorbing properties based on the materials they are made of. They are effective at absorbing sound, but these materials absorb sound with equal potential [10] from different possible direction resulting a material to possess identical values of acoustic properties in all directions and such material are referred to as isotropic. This property is not applicable in a situation where the source of sound you are interested to hear is in unidirectional, while the source of the noise also being unidirectional, only differed by sound direction because these traditional sound absorbers will not differentiate these sounds into meaningful sound for you or not. Traditional sound absorbing materials are visually seen in non-transparent, disabling them to be used for transparent applications.

Unfortunately, physical nature of the materials influence the limitation of many qualities of the material to perform as the best sound absorbers. This calls for the need to develop material capable in sound absorption regardless of the type of material. In recent years, a new material has been developed for acoustical applications referred to as acoustic metamaterial which utilize the acoustic motion of its scrupulous designed small-scale structure to create a material with extraordinary acoustic properties which is not found in traditional material made from natural sources. These utmost properties are the focus of current research, and are being optimized to develop novel, new applications such as acoustic cloaking and super-resolution lenses that reaching resolution beyond what ordinary lens can achieve.

Therefore, these losses is utilized using resonant structures [5][4] in acoustic metamaterial has become an interest to make better sound absorbers. Similar to situation of ringing a bell, the resonant structures are excited at a single frequency or tone and functional over a very limited frequency range in the tone vicinity. Alternatively, another approach to overcome the limited frequency range is established through the use of repeated equal distribution of small metals in air called sonic crystals. Sonic crystals is capable to work as an ordinary sound absorber by themselves with varying arrangement and design to build structures with extreme acoustic properties [10]. It is observed in this study that peak of sound absorption coefficient decreases in frequency as the thickness of the air layer is increased. The air volume below and within the sonic crystals which hold properties similar to a stiff spring with inverse dependent on cavity size.

Besides designing acoustic metamaterial using sonic crystals, another method of using perforated plates [16] with an array of hole is available to perform as porous metamaterial. By using the Transformation Acoustics [9] approach, anisotropic properties of the material can be achieved by varying densities and bulk modulus in two dimensions on a structure. However, fabrication of these materials could be challenging for some applications as these material parameters may have values that could be difficult to implement in practice without causing changes in the metamaterial performance. As an alternative approach, bulk metamaterial design [10] is taken into consideration to include a stack of perforated plates made of an acoustically hard material, separated by a sound-supporting fluid such as air to allow sound waves propagate towards metamaterial. Basically, this design use hole array as its main component, having transmission properties of sub-wavelength control over sound waves suitable for novel phenomena such as sound shielding near a diffraction onset or as sound absorbers beyond capability of naturally occurring materials. Besides, such acoustic metamaterial also do not rely on diffraction to achieve negative refraction, in contrast to sonic crystals. Due to inherent high acoustic impedance, traditional porous materials exhibit poor low-frequency noise absorption characteristics which results to high reflection coefficient thus leaving absorption coefficient with low percentage. This study shows that the effective range of sound absorption can be extended to lower frequencies by application of acoustic metamaterial principles to porous materials using finite element numerical models of porous foam samples with and without acoustic metamaterial layers. The results based on experimental method involving impedance tube test shows that effective sound absorption between 100-400 Hz is achieved by using four layers acoustics metamaterial foam system.

A study is carried out to experimentally imply another approach using a geometric principle to develop metamaterial with utmost dispersion by coiling up space on the metamaterial surface [7]. As a result of this approach, negative refraction for acoustic metamaterial with an isotropic property is demonstrated with airborne sound. Using the same geometric principle, double-negative metamaterial is also implied specifically for microwaves with possibility of cut off-free wave-guiding occurrence, while varying the lattice constant and wavelength ratio. This study is crucial to design metamaterial with further improvement showing extreme conical dispersion in order to control and manipulate propagation of slow sound wave in a finer resolution of broadband of frequencies with constant sound speed.

Another recent study has shown the innovation of acoustic metamaterial sound absorbing panels for interiors using slow sound concepts and critical coupling to demonstrate a lightweight and super thin materials as perfect absorbers [6][7]. Adding to this innovation is the ability of this metamaterial to control and manipulate sound waves in almost independent of the incident angle upon the surface which is the first material that exhibits such behavior. This sound absorbing panels for interiors are equipped with systematic repeated distribution of very thin closed slits [15] and the upper wall is filled with Helmholtz Resonators (HR) to provide resonating cavity [12] so the sound passing through the metamaterial will go through

the propagation slowly, suitable for low frequency sound using deep sub-wavelength. It is comprehensible that the slit and the HRs geometrical characteristics responsible as the variable in this study so that the sound waves can be controlled in a wide range of angles directional. Results of this study revealed that this metamaterial has achieved perfect sound absorption at 338.5Hz without porous material added to the configuration of this metamaterial.

## III. METHODOLOGY

### A. Design of Unit Cell of Metamaterial

Designation of acoustic metamaterials is carried out using range of frequency selected from 200 Hz to 1000Hz to improve absorption of low frequency noise [8] coming from vehicles; road traffic and air traffic. Based on this frequency range, a parameter to build unit cell of acoustic metamaterial is developed for the three-dimensional model. In order to obtain effective sound absorption, thickness of material used for sound absorption must be one tenth of the wavelength of incident sound [11]. Therefore, from this properties, thickness of sample design is calculated as shown below.

$$\lambda = v / f \quad (1)$$

$$v = d / t \quad (2)$$

(1)

One-quarter wavelength of incident sound is said to be the resonant frequency which peak absorption will take place. The new frequency will determine dimension of model design as shown below. Metamaterial design for this study is based on Helmholtz resonator which holds equation that will determine dimension of unit cell design. Based on Helmholtz equation,

$$f_H = c / 2\pi \times \sqrt{} ( A_{neck} / ( V_{cavity} \times h_{eq}$$

)) (3)

$$\alpha + \beta = \chi. \quad (1)$$

(1)

$$A_{neck} = V_{neck} / h_{eq} \quad (4)$$

(1)

$$h_{eq} = h_{neck} + 0.3\mathrm{D} \quad (5)$$

(1)

$$D = ( 2 \times l_{neck} \times w_{neck} ) / l_{neck} + w_{neck}$$

) (6) (1)

These assumptions are considered in calculation of parameters of unit cell acoustic metamaterial.

$$l_{neck} = 1 / 3\ l_{cavity} \quad (7)$$

$$h_{neck} = 1 / 6\ h_{cavity} \quad (8)$$

$$w_{neck} = 1 / 2\ w_{cavity} \quad (9)$$

### B. Fabrication of Acoustic Enclosure

In order to design the metamaterial, the procedures are broken into few parts to ease the development of the metamaterial using 3D design TinkerCAD. This software is easier to be used for beginner to learn basic 3D sketching and drawing.

### C. Testing of Acoustic Enclosure

The acoustic enclosure undergoes a testing of sound reduction by isolating the source of sound in the acoustic enclosure. This test is to provide comparison between acoustic enclosures built using poly lactic acid plastics without and with metamaterial. The experimental setup include equipment such as sound level meter, wireless speaker, different acoustic enclosures, and weighing system.

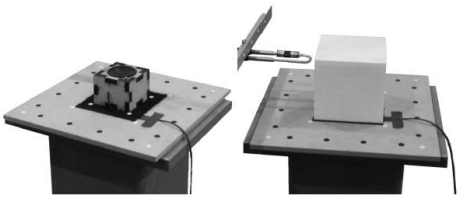

Fig. 1. Experimental setup

## IV. RESULTS AND DISCUSSIONS

### A. Results

Both Fig. 1 and Fig. 2 shows the sample results of sound level measured on acoustic enclosure responds to 900 Hz sine wave.

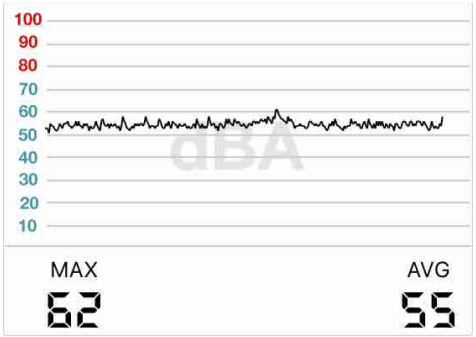


Fig. 2. Sound level of acoustic enclosure without metamaterial.

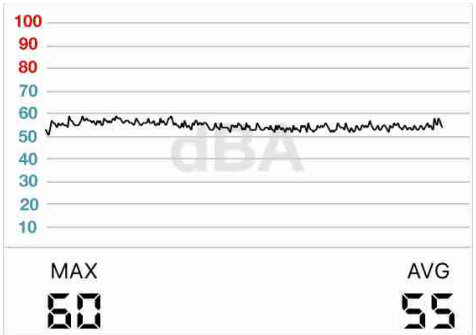


Fig. 3. Sound level of acoustic enclosure with metamaterial.

TABLE I. RESULTS OF SOUND PRESSURE LEVEL USING ACOUSTIC ENCLOSURE

| Frequency (Hz) | | 200 | 300 | 400 | 500 | 600 | 700 | 800 | 900 | 1000 |
|---|---|---|---|---|---|---|---|---|---|---|
| SPL max (dB) | Without MMR | 74 | 72 | 71 | 70 | 69 | 68 | 66 | 62 | 65 |
| | With MMR | 74 | 72 | 71 | 70 | 69 | 68 | 65 | 60 | 63 |
| SPL avg (dB) | Without MMR | 71 | 69 | 69 | 67 | 67 | 66 | 63 | 55 | 61 |
| | With MMR | 71 | 69 | 69 | 67 | 67 | 66 | 63 | 55 | 61 |

### *B. Discussions*

Based on the results shown in previous section, acoustic enclosure with metamaterial shows the highest reduction in maximum sound level compared to acoustic enclosure without metamaterial differed by 2 dB during 900 Hz sound wave subjected to the material. The resonant structure of unit cell metamaterial is specifically designed based on 200-1000 Hz low frequency sound range in order to provide alternative material to replace the conventional material, wood, conducted by previous study using same dimension that shows result of 81.8 dB of sound level reading using same frequency.

Future study should improve this study by using different materials with better noise control properties such as polyamide and polyethylene using either 3D printing or laser sintering method, depending on the suitability to develop the material. Different patterns and structure of unit cell could also be used in order to obtain better sound reduction thus providing the community with the best noise control device using metamaterial.

## V. CONCLUSION

Comparing both previous study to the result this paper provides, it is best to conclude that this paper successfully achieved its objectives to design an acoustic enclosure metamaterial-based with better noise control.

## REFERENCES


[1] Chin, C. (2016, July 21). *Drowning out the noise*. The Star Online. Retrieved November 27, 2016, from http://www.thestar.com.my/news/nation/2016/07/31/drowningoutthenoise/ 4/

[2] Guenneau, S., & Craster, R. V. (2013). *Fundamentals of Acoustic Metamaterials*. Acoustic Metamaterials Springer Series in Materials Science, 1-42. doi:10.1007/978-94-007-4813-2_1

[3] Hansen, C. H. (2005). *Current and future industrial applications of active noise control*. Noise Control Engineering Journal,53(5), 181. doi:10.3397/1.2839255

[4] *Helmholtz resonator*. (n.d.). AccessScience. doi:10.1036/1097-8542.006400

[5] Herrero-Durá, I., Picó, R., Sánchez-Morcillo, V., Garcia-Raffi, L. M., & Romero-García, V. (2015). *Vibroacoustic effects of resonant sonic crystals in sound absorption*. European Acoustics Association Journal. Retrieved December 13, 2016, from http://www.sea-acustica.es/fileadmin/Oporto16/110.pdf

[6] Jiménez, N., Huang, W., Romero-García, V., Pagneux, V., & Groby, J. P. (2016). *Ultra-thin metamaterial for perfect and quasi-omnidirectional sound absorption*. Applied Physics Letters, (109), 121902nd ser. doi:10.1063/1.4962328

[7] Liang, Z., Feng, T., Lok, S., Liu, F., Ng, K. B., Chan, C. H., Li, J. (n.d.). (Rep. No. 3:1614). doi:10.1038/srep01614

[8] Luxon, L. M., & Prasher, D. (2007). *Noise and its effects*. Retrieved September 19, 2016, from http://catdir.loc.gov/catdir/toc/ecip0620/200602847 6.html

[9] Molerón, M., & Daraio, C. (2015). *Acoustic metamaterial for subwavelength edge detection*. Nature Communications,6, 8037. doi:10.1038/ncomms9037

[10] Sanchez-Dehesa, J., Chocano, V. M., & Guild, M. D. (2014). *Recent results on sonic crystals for sound guiding and acoustic absorption*. The Journal of the Acoustical Society of America,136(4), 2076-2076. doi:10.1121/1.4899452

[11] Simon, F. (2013). *Low frequency sound absorption of resonators with flexible tubes*. The Journal of the Acoustical Society of America,133(5), 3265. doi:10.1121/1.4805288

[12] Sood, D., & Tripathi, C. C. (2015). *A wideband wide-angle ultra-thin metamaterial microwave absorber*. Progress In Electromagnetics Research M,44, 39-46. doi:10.2528/pierm15082903

[13] Takahashi, Y. (2009). *Vibratory sensation induced by low-frequency noise: A pilot study on the threshold level*. Low Frequency Noise, Vibration and Active Control,28(4), 245-253. doi:10.1260/0263-0923.28.4.245

[14] *Test method for sound absorption and sound absorption coefficients by the reverberation room method*. (n.d.). doi:10.1520/c0423

[15] U.S.Cong. (2016). *Potential of sound absorbers based on acoustic metamaterials* (Y. Bobrovnitskii, T. Tomilina, K. Morozov, & B. Bakhtin, Authors) [Cong. Rept. from International Congress on Sound & Vibration Cong., 23rd sess.]. Moscow. Retrieved December 13, 2016, from http://www.iiav.org/archives_icsv_last/2016.../full_paper_825_20160530175723879.pdf

[16] U.S.Cong., Gopal Mathur. (2016). *Novel sound absorptive materials based on acoustic metamaterials principles* (C. Fuller, Author) [Cong. Doc. from International Congress on Sound & Vibration Cong., 23rd sess.]. New York, NY: Acoustic Metamaterials Inc.

[17] U.S.Cong., InterNoise. (2000). *Studies of the annoyance of low frequency aircraft noise at two civil airports* (L. Silvati, S. Fidell, K. Pearsons, R. Howe, & M. Sneddon, Authors) [Cong. Doc. I-INCE Classification: 6.6 from International Congress and Exhibition on Noise Control Engineering Cong., 29th sess.]. Canoga Park, CA: BBN Technologies.

[18] Wang, Q. (2008). *Studies On The Relationship Between Sound Absorption*. Acta Polymerica Sinica,008(6), 517-521. doi:10.3724/sp.j.1105.2008.00517

[19] Wise, S., & Leventhall, G. (2010). *Active noise control as a solution to low frequency noise problems*. Low Frequency Noise, Vibration and Active Control, 29(2), 129-138. doi:10.1260/0263-0923.29.2.129

[20] Zhang, S. (2010). *Acoustic metamaterial design and applications* (Unpublished doctoral dissertation). University of Illinois. Retrieved September 19, 2016, from http://web.mit.edu/nanophotonics/projects/Dissertation_Shu.pdf

# IoT-based Irrigation System

Noor Hazira binti Yusof
*Faculty of Electrical Engineering*
*Universiti Teknologi Malaysia*
*Johor Bahru, Malaysia.*
*noorhazirayusof@yahoo.com*

Nik Noordini binti Nik Abd Malek
*Department of Communication Engineering*
*Faculty of Electrical Engineering*
*Universiti Teknologi Malaysia*
*Johor Bahru, Malaysia.*
*noordini@utm.my*

***Abstract*—As a population is growing, the agriculture activities are highly needed. In addition, the home agriculture activities are useful for economical and healthy living. An automated irrigation system was developed to optimize water use for agriculture. Other than that it is suitable for the people who are living in a city and busy with work. Irrigation system is a method of allowing water and drip slowly to the roots of plants, either onto the soil surface or directly onto the root zone, through a network of valves. This paper suggests an economical and easy-to-use IoT Based Irrigation System. The irrigation system has been covered in small home garden area by implementing Particle Photon integrated with multi-sensors such as soil moisture sensors, ultrasonic sensors, temperature sensors and light sensors. This proposed project is managed to reduce cost, minimize waste water and reduce physical human interface.)**

***Keywords— Particle Photon; Soil moisture sensor; IoT, Wi-Fi; Thingspeak; IFTTT***

## I. INTRODUCTION

According to the official portal from Department of Statistics Malaysia, agriculture sector continued to expand in 2015 with a contribution of 8.9 per cent to the Gross Domestic Product (GDP). Oil palm was a major contributor to the GDP of agriculture sector at 46.9 per cent followed by other agriculture (17.7%), livestock (10.7%), fishing (10.7%), and rubber (7.2%) as well as forestry & logging (6.9%) in 2015 [1]. From this analysis it is shown that the agriculture sector in term of plantation and crop production field is one of the important sectors in Malaysia.

In worldwide, 85% of available freshwater resources have been used in the agriculture sector which is in irrigation system. Due to the increase of food demand and population growth, this percentage will continue to be dominant in water consumption. So for sustainable use of water for a long term including technical, agronomic, managerial, and institutional improvements, there is a critical need to create strategies that is based on science and technology [2]. In the irrigation system, water plays an important role to increase the population of crop. So, the usage of water needs to be maintained to produce more healthy and good production of plants. There are many ways to achieve water savings which is from the basic technology to the advance technology. One of the ways is to minimal the usage of water in the crop field. So, it is necessary to implement the project that can reduce the usage of water. By doing this, the water usage can be reduced, and the water can be used for another sector and activity.

Green technology is one of the good factors to produce a healthy crop production. Green technology means it is more environmentally friendly based on its production process. This technology is more focusing on the traditional ways and less harmful and it is less harmful to the environment. By using this type of technology it is suitable for the people who are busy with their live and does not have much time to watering their plants. Green technology is an application which is to control, conserve and monitor plant, either food crops or any crops with the negative impacts of human involvement. It is use electronic devices, green chemistry, environmental monitoring and environmental science to monitor the condition of the plant and to watering the plant.

All crops need a sufficient nutrient to make it growth well. This type of nutrient is such as water and fertilizer. A sufficient fertilizer is not enough for a crop, it also needs sufficient water every day. Lack of water will give an effect to the plant which it will die and not grow effectively. Sufficient water will prevent it from dying. The efficiency by solenoid irrigation are exceeds 90% where by sprinkler system is only 50-70%. It is the best to calculate the amounts of fertilizer, water and schedule to applying them through an irrigation system because every type of plant have different need of fertilizer and water. Another factor, a good lighting also help plant to grow well and faster. By using green technology, light sensor is really needed to help crop grow well. For the green technology, the crop does not receive enough light to make it grow well. So, with the help of light sensor, it will detect the current ambient light level. Other than that, the humidity of the surrounding also gives an effect to the plant. So, all these things need to be monitor and control to make a plant growth well in a short time.

Internet of Things (IoT) is a shared network which can interact with each other. It is a shared network between anything such as objects or things. It only needs an internet connection to interact with each other. By using IoT, agriculture industry can feed 9.6 billion people on the Earth until 2050. Thus, it plays a significant role in agriculture sector. Smart Agriculture helps to increase the crop yield and thereby helps to reduce wastage and effective usage of fertilizer. This system is more efficient by 92% than the conventional approach thus it will be more useful in areas where water is in inadequate [3]. IoT is the heart of digital agriculture. The electronic system will need to have the

capability to connect to cloud network via internet, and transmit sensor data for storage.

For this project Raspberry Pi is being replaced with the Particle Photon which is a microcontroller embedded with WiFi. It is more small and robust. The Particle board only needs WiFi connection and power, the rest are done via web interface. So, no application is required to be downloaded for the development. Then, code compilation and flashing the microcontroller are done Over-The-Air (OTA). By using this microcontroller people can control it with the computer that is connected wirelessly as long as there is internet connection. Beside that this microcontroller is less expensive than using microcontroller (Raspberry Pi or Arduino) with ESP8266 WiFi module.

## II. Literature Review

A new technology has been developed in terms of automatic irrigation system. This is occurring in order to improve the standard agriculture for advance and better agriculture system. The reason for this development in the agriculture irrigation process is to reduce the water energy source and for farmer's convenient need [4]. The water usage needs to be reduced due to the lack of water in the earth. Other than that, greenhouse is one of the popular systems in the agriculture sector. So this system was integrated with many technologies due to the specific prerequisite that can improve its quality in the crop productions [5]. This irrigation system is developed not only in farm area, but home garden also has been developing with these small irrigation systems [6]. So, the purpose of this new technology is to monitor the plant growth and controlling the system by using IoT with various platforms. The other improvement also has been developed in irrigation system such as the controlling GSM module [7] in greenhouse system and the development of Android application [8] in irrigation system monitoring.

The research paper from School of Electronics Engineering, VIT University Vellore has develop an IoT automate irrigation system. This paper discuss about the growth in technology made humans to search for new methods or technology where one could meet the same old requirements with less human effort and less interaction. This system uses a motor as it switching button. So, the process of switching ON or OFF of a motor has become a problem. It has become very difficult for user to look after the motor every time, to overcome this situation it has come up with an idea of using IoT [9]. The platform that is used by this paper is temperature sensor, soil moisture sensor, ultrasonic sensor, Analog to Digital converter (MCP3008) and Raspberry Pi. Then, the final values are place on the web page that has been designed by HTML script (notepad++ editor). Other than that this paper using third-party site to show the data. So, the address of the third party side needs to be type to view the reading on the webpage. So, this can be controlled through IoT. The power button which is button for ON and OFF of the motor is being controlled by the sensor that has been integrated along. When the moisture of the soil is below the pre-set value, the sensor will automatically switch on the power button and it is switch off automatically as required for a specified soil. The advantage of this system it will save the electricity and it is efficiency to the crop as well. Other than that it also involve in surrounding environmental conditions such as temperature.

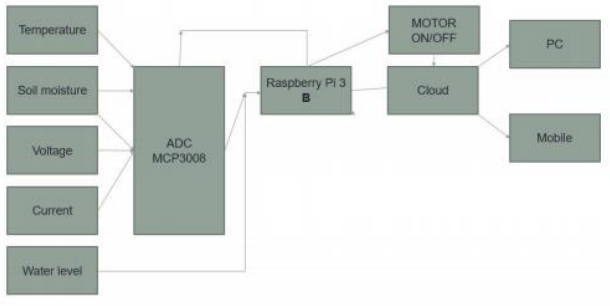


Fig. 1. Block Diagram of Proposed System

The drawback of this system is it using multiple type of sensor. Soil moisture sensor and the temperature sensor give an analog output, but the values that microcontroller Raspberry Pi takes only digital values. So, in order to convert the analog to digital values, need to use Analog to Digital Converter (ADC). Other than that, to measure the power consumed by the motor, the voltage measured must be stepping down using step down converter from 240V to 12V. Then, this voltage will be step down again to 3.3V by bridge rectifier circuit. After this it is connect to the channel of Analog to Digital Converter.

Another research from Department of Electronics and Communication, Amrita School of Engineering, India using soil moisture sensor and temperature sensor as it sensing module. By using soil moisture sensors it estimates the soil volumetric water content based on the dielectric constant (soil bulk permittivity) of the soil. The dielectric constant can be thought of as the soil's ability to transmit electricity. The dielectric constant of soil increases as the water content of the soil increases. This response is because of the fact that the dielectric constant of water is much larger than the other soil components, including air. Thus, measurement of the dielectric constant gives a predictable estimation of water content. It consists of a pair of electrodes to measure the resistance of the soil. Greater the resistance, lower the moisture content of the soil. While the temperature sensor has Resistance Temperature Detector (RTD) is used to measure temperature as a function of resistance. As the temperature of the soil increases, the resistance of the soil also increases. According to this study RTDs readings are more accurate and more repeatable [10].

## III. Methodology

The propose system design shown in Fig. 2. has illustrate the block diagram of whole system for Automatic Irrigation System. All sensor nodes which are soil moisture sensor, temperature sensor, light sensor and ultrasonic sensor are connected to microcontroller which is Particle Photon. Soil moisture sensor will sense the humidity of the soil and temperature sensor that will sense the temperature of the surrounding. Meanwhile light sensor will detect the current ambient light level. This microcontroller is using web interface to place the coding and program. Then, the data that has been collected will be transferred to the cloud which is ThingSpeak. This system use IoT as it platform. From this, the data can be analyzed to see the humidity of the soil and temperature. At certain critical

condition, user will be notified by message application from IFTTT.

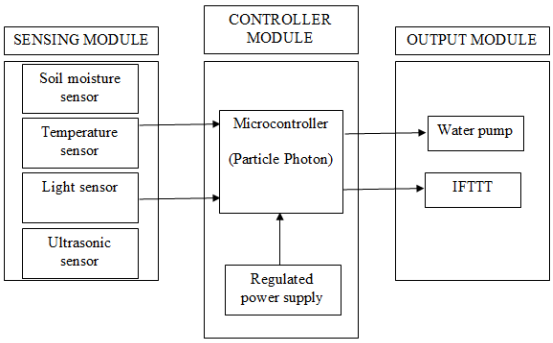


Fig. 2. Block Diagram for Each Module

The water will flow out from the solenoid valve to the plant. Other than that, this system is an automated system. So, it will supply the water according to the time that has been programmed in the web interface. The amount of the water that will receive by the plant also has been programmed at the web interface. It is an automatic system that has been set at the microcontroller. This system can be control by change the programming at IDE web. IDE web is an open source webpage enable for coding for particle photon. Other than that, if the soil humidity is higher which it reach certain critical condition, the solenoid will not watering the plant.

This system is using IFTTT application. IFTTT give a meaning which is if this then that. It is launched in 2010 both and has the slogan "Put the Internet to work for you". Other than that, it is a website and a mobile application. The idea is that the use of IFTTT to automate everything from favorite apps and websites to app-enabled accessories and smart devices. By using this it will give a notification to the user. Next, the integration works between hardware and software parts has been done in this next semester. For the next phase, the system has been tested after both system developments and troubleshoots for the system error is integrated. By doing this, the performance of the system can be analyzed and finalized it the form of documentation work.

### *A. Development of Microcontroller and Sensor Module*

Particle's IoT hardware development kit will provides everything to build a connected project. This microcontroller has combined a powerful 120 MHz ARM Cortex M3 micro-controller with a Broadcom Wi-Fi chip in a tiny thumbnail-sized module called the PØ (P-Zero). The core of the whole electronic system is the Particle Photon board. It is a 1 inch by half inch microcontroller with Wi-Fi module embedded in it. Particle products are ideal for IoT deployments. It has very low current usage demand, with only the Wi-Fi module drawing 30mA when operational. Additional coding can put the WiFi module to sleep, and then it will only draw 1mA current per second. The circuit alone can be powered either by power-bank via USB-B type connector, or either 5V through VIN pin, or through its 3V3 pin. It input and output pins are sufficient for up to ten plants. For this plant monitoring module, the specifications require to sense ambient temperature, light, the amount of water in the tank and plant soil humidity.

This Photon comes with access to the Particle Cloud, a free cloud service. The Particle Cloud has many great features for creating a project such as over-the-air firmware updates, an easy to use REST API and firmware development supported by web and local IDEs. Particle Photon is a new microcontroller. It is easy to use for many project developments instead of using other microcontroller such as Arduino and Raspberry Pi. It is because its low cost and the size is very small, like a match box.

For this project, it uses many type of sensor module. First is soil moisture sensor. It is known as hygrometer sensor and it detects moisture level of soil. This sensor reads resistance of soil to get its moisture level. The soil with much water has less resistance while dry soil has more resistance. Temperature sensor will sense the temperature of the surrounding. Ultrasonic sensor uses sonar and capable to determine the distance of object, not easily affected by sunlight. It is also packaged with transmitter and receiver. Meanwhile, light sensor detects the current ambient light level of surrounding. The entire sensor module connects to the Particle Photon. Then the solenoid valve also connected to the Particle Photon.

### *B. Software Development*

In this project, the software development is divided into 3 parts, i.e. particle.io for Particle Photon, simple programming for Thingspeak and applet code for IFTTT. User needs to login the system in particle.io by sign in in the webpage through smartphone or computer to make a programming or to change the programming. From ThingSpeak, user can see the pattern of the graph of multiple sensors and analyse the pattern of the sensor. Then user can change the programming in the particle.io according to the humidity of the soil. At certain critical condition level, the system will notify user by sending a message notification through an IFTTT app if there is damage in the hardware part. This system is an automate system which is it watering the plant according to the time that has been set at the microcontroller.

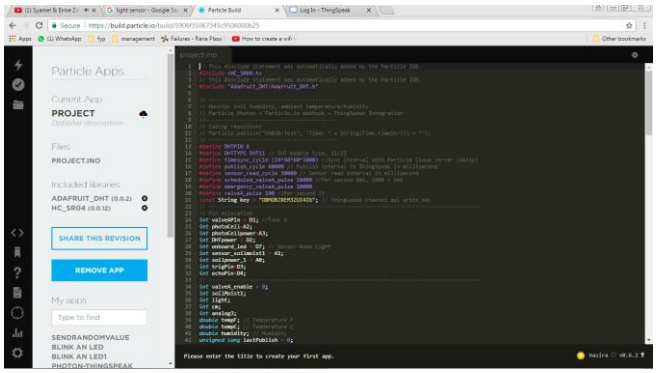


Fig. 3. Particle.io Cloud Storage

### *C. Operation*

The developed program is loaded to the completed circuit for testing purposes before being attached to the real system. Once reliability is proven, the system is then placed outdoors to gather data. When the Particle Photon is connected to cloud, it will display a pulsing blue light. The Particle boards once bound to an account, all of them will publish data to the same online console, allowing programmers to view the output of all boards

under the programmers control. This function can be extended to perform fault monitoring of the board and sensors when they are deployed in the field.

For end-users, it will push the data to ThingSpeak cloud. It is free, and it provides visualization that eases viewing of data. Time frame of data can be set up to 1 month. From this user can analyze the condition of the soil. The changes can be made if user want to change the pattern of the watering scheduled.

## IV. Result and Discussion

Fig. 4. shows the completed hardware setup for the IoT-Based Automatic Irrigation System using Particle Photon that has been connected to the microcontroller which is ThingSpeak and solenoid valve. In this part, the entire sensor module is connected to the motherboard of this project which is Particle Photon. The sensor module that has been used in this project is soil moisture sensor that will detect the humidity of the soil, temperature sensor that will detect the surrounding temperature, light sensor that will detect the ambient level of light and ultrasonic sensor that will detect the distance of the water. After that, the microcontroller will be connected to the relay and solenoid valve. This project is an automate irrigation system. So, it will water the plant according to the program has been set at the programming section. The blue light at the Particle Photon act as LED that indicates the system is function.

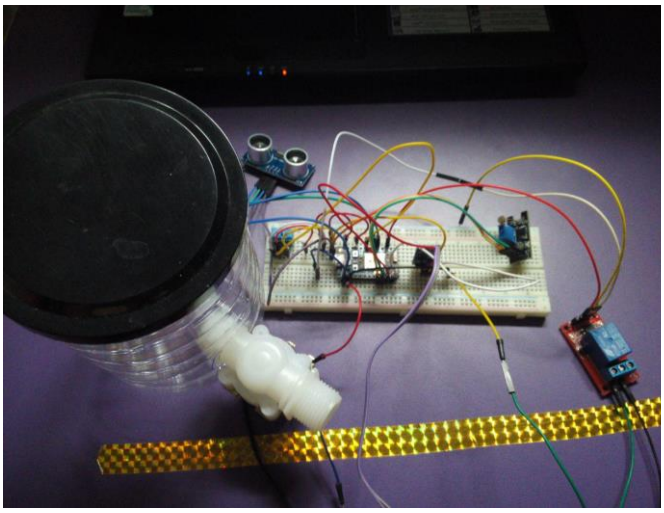

Fig. 4. Hardware Setup

After all the hardware components have been set up, The Particle Photon is connected to the internet by login to its website. Then, simple program code is developing in ThingSpeak. The purpose is to link between ThingSpeak cloud and particle.io. Next, a programming code for ThingSpeak cloud is develop in particle.io for send the data to ThingSpeak and publish it in the graph form. The data will be display in ThingSpeak in term of graph. For Particle Photon, the blue colour indicates that it is connected to the cloud.

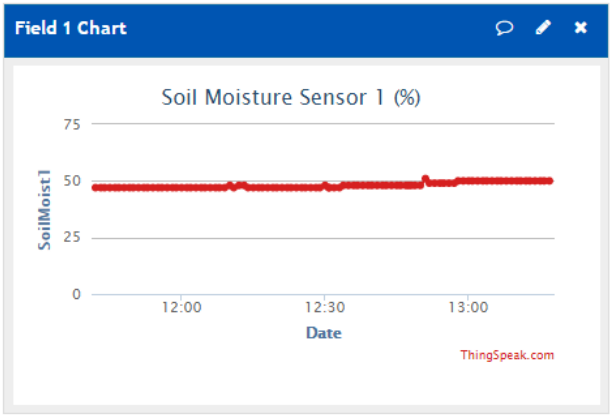


Fig. 5. Graph for Soil Moisture Sensor

## V. Conclusion

As a conclusion, IoT-Based Automatic Irrigation System is developed with Particle Photon by connecting it with the sensor module which is soil moisture sensor, temperature sensor, light sensor, and ultrasonic sensor and the data is send to the cloud which is ThingSpeak. Other than that, this controller can be programmed wirelessly. This board is mainly programmed through internet, not through wire interface. The coding and all the configurations are placed on the cloud. It is means the programmer can just login from any computer to make changes. All sensors have a good measurement of parameters at surrounding.

For further development work, this irrigation system project can be implemented in the large area of garden or farm. This implementation can be done with many microcontrollers due to this microcontroller can be connecting together. So that it can be controlled wirelessly. With this technology it is hope that it will reduce the farmer physical interface and decrease the number of worker. At the same time, the garden or farm owner can reduce the cost from recruitment new worker by using this system. Basically need to install the Wi-Fi module at the garden or farm. So that this microcontroller can function really well.

## References

[1] "Department Of Statistics Malaysia Official Portal". Dosm.gov.my. N.p., 2017. Web. 8 May 2017.

[2] Gutierrez, Joaquin et al. "Automated Irrigation System Using A Wireless Sensor Network And GPRS Module". IEEE Transactions on Instrumentation and Measurement 63.1 (2014): 166-176.

[3] P. Rajalakshmi, S. Devi Mahalakshmi. "IOT Based Crop-Field Monitoring And Irrigation Automation". Intelligent Systems and Control (ISCO), 2016 10th International Conference on (2016)K. Elissa, “Title of paper if known,” unpublished.

[4] A. Ramya, G. Ravi. "Efficient Automatic Irrigation System Using Zigbee". Communication and Signal Processing (ICCSP), 2016 International Conference on (2016).

[5] Chaudhary, D., Nayse, S., & Waghmare, L. (2011). Application Of Wireless.

[6] Sagi, M., Mijic, D., Milinkov, D., & Bogovac, B. (2012, 20-22 Nov. 2012). “Smart Home Automation”. Paper presented at the Telecommunications Forum (TELFOR), 2012 20th.

[7] Teymourzadeh, R., Ahmed, S. A., Kok Wai, C., & Mok Vee, H. (2013, 13-15 Dec. 2013). “Smart GSM Based Home Automation System”. Paper presented at the Systems, Process & Control (ICSPC), 2013 IEEE International Conference on

[8] Li, X., Qin, L., Lu, L., & Wu, G. (2015, 28-30 July 2015). “Design And Implementation Of Modern Greenhouse Remote Monitoring System Based On The Android System”. Paper presented at the Control Conference (CCC), 2015 34th Chinese.

[9] M Sri Phanindra Sarma. "Automatic Irrrigation And Weather Monitoring System Using IoT". International Journal of Research in Engineering and Technology 05.11 (2016): 15-19.

[10] "Smart Irrigation System". IOSR Journal of Electronics and Communication Engineering (IOSR-JECE) 10.3 (2015): 32-36. Web. 8 May 2017.

# IoT based Access and Security System for UTM College

Herianto bin Udin
*Faculty of Electrical Engineering*
*Universiti Teknologi Malaysia*
*Johor Bahru, Malaysia.*
*heriantobinudin@gmail.com*

Mohd Adib bin Sarijari
*Department of Communication Engineering*
*Faculty of Electrical Engineering*
*Universiti Teknologi Malaysia*
*Johor Bahru, Malaysia.*
*madib@utm.my*

***Abstract*—Internet-of-Things (IOT) technology had been growth rapidly in these few years. IOT is a technology that can helps to improve the conventional system in many fields. Among them is to provide users with remote monitoring, management and control of their devices at any times and anywhere. This paper presents an IOT based system for security and access management at UTM residential/college building. The IOT system is developed based on the IOTWave platform which consist of three main components: the Things, the Network, and the Cloud. The main objective of the system is as the solution to the unauthorized access at UTM student's residential building, in particular of Siswi (women) residence. The developed IOT-based system consists of management and monitoring the access of the residence, and detecting intruder to the student's residential building. We then work to investigate and address the quality-of-service (QoS) issue, i.e., in term of latency, on the proposed IOT-based Smart Access and Security System.**

## I. INTRODUCTION

The security and access system that currently in development progress is using NFC that already built-in in the UTM student and staff matric card as the user authentication. The NFC reader that connected to the raspberry Pi that acts as a gateway will read the data from the NFC car then transferring it the raspberry pi internal database that is synchronous to the cloud. Any date updated at the cloud will directly transfer to the raspberry pi and otherwise. The building administrator will provide the enterprise services with user-friendly UI and the Android-based apps to manage the system.

### *A. Internet of Thing(IoT)*

Atzori et al. (1) define, Internet of Things can be present in three paradigms—semantic-oriented (knowledge), internet-oriented (middleware), and things oriented (sensors or actuators). However, there is no specific definition for IoT even though many researchers use their definition. The group known as RFID defines the IoT as:

- The worldwide network of the interconnected things is unique can be addressed based on standard communication protocols known as IP address. The Cluster of European research projects on the IoT state that
- The 'Things' is active component that participates in a specific process in a working system. They have the capability of communicating with each other and exchange the information among them. Moreover, it can be functioning autonomously in the to do specific process without needing direct human control or monitor it all over the time.

According to Forrester, a smart environment –

- Utilizes data and interchanges innovations to make the basic facilities segments and administrations of a city's organization, sports training, human services, real estate, transportation, and utilities more aware, intuitive and productive.

The objective of this project is to develop IoT-based security and access system for UTM residential college building. Therefore, it is important to do background study about the Internet of Things and the related technology. The first section will explain about Internet of Thing and general framework. Secondly, about the related technology that related to security gand access system will be discussed. Finally, the comparison about related work done in security and access system.

The building access and security system are developed to be implemented at student residential building G07, Kolej Rahman Putra, Universiti Teknologi Malaysia (UTM). It provides IOT-based system that allows real-time monitoring and access. The admin (e.g., the collage office) can access the data whenever they need to and get the notification when something happen. Moreover, it also provides the data history of the user that access the building and it very useful when some occur in the building and reference proposes. Compare to the current situation that no system implement at the building make it difficult to identify the factor of the problem if something happens because no data of people that access the building recorded during problem happened. Therefore, the system develops also reduce the workforce of the guard and college officer to monitoring the college.

### *B. LITERATURE REVIEW*

Ying-Wen Bai and Shi-Chang Chen has done the research on Design and Implementation of Home Intercom and Security Control Systems for Buildings (5). The common intercom system is only can be used for small scale building house and cannot handling thousands of building at the same time. It their paper they are proving the system that can control up to thousand building at the same time with the low cost, high stability and simple architecture. As the intercom consists of many futures such as monitoring video, call request and image capture they were designed multi-layer application to handled all the intercom system futures. It is including, physical layer, data link layer, and OSI/ISO standard covering layer. they were using wired connection network that is RS-485 communication network to lowering the cost and easy building. The system is combination of P2P communication, and master and slave to achieve real-time data transmission and full fill the user requirement. (5) However, the using of wireless network is better in term of cost and reliability.

An access system for buildings based on smart cards (4) one of the existing system that based on IoT.This system the developed by the writer(4) is the system that used a smart card that is NFC or RFID to access the building. The door connected to the access point that connected to the server via the internet. The access point will read the data from the user smart card who want to access the certain building or room in the building. Then it will pass data to the server, and the server will make decisions and also sent the command to open the door if the user is authorized.However when the connection lost system will stop working. (4)

## II. SYSTEM DESIGN ARCHITECTURE AND HARDWARE REQUIREMENT

Generally, the framework or architecture the Access and Security System for UTM College system platforms are relatively similar to other IoT systems. The proposed system architecture is shown in Figure 1 consists of three major components listed as follows the Thing, the Cloud and the network

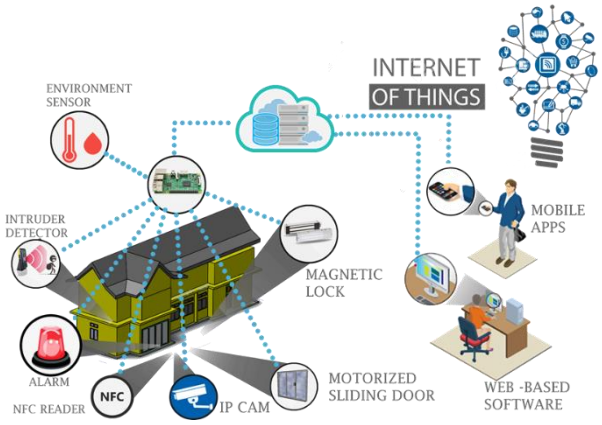


Figure 1 Overall system architecture

### *A. The Thing*

The Thing in IOT is any items or object, and it can be a car, the animal, or even a chair that can be set to an address for it by a unique ID such as using the IPv6. Therefore, it can be identified through the internet. The thing also can communicate to each other depends on its application. In the proposed system, the Thing refers to the building and the motoring devices which is the smartphone and the PC in this case. In the building, there are three major components required for the system to work and another add-on to improve the system so it can be more efficient and reliable.

- Use raspberry pi for the main controller and the gateway: Raspberry PI is small one board computer that only size of a credit card. It very popular among the hobbies because of its small size and computing capabilities. Other than that, it also a low-priced computer that only around RM200 and below. There several series of Raspberry Pi version and the latest one is Raspberry Pi 3. Raspberry Pi 3 is very high-performance board on it price level and has capabilities and futures like the standard computers has such as Ethernet port, Wi-Fi, Bluetooth, USB port, HDMI port, and extra IO port that use for electronic programming. Therefore, it is suitable to use in the electronic project especially in the IoT-based project. In this project, Raspberry Pi was chosen to be the gateway due to it high processing capability and its built-in future that need in the project.

- Other platforms commonly used in electronic projects such as Arduino board, the previous version of Raspberry Pi and Intel Galileo board. However, Raspberry Pi 3 has the upper hand compare to Arduino and the earlier version raspberry pi in term of processing speed and the future add in one board of raspberry pi 3. Intel Galileo board has very future with raspberry pi 3

and it also more powerful compared to Raspberry Pi 3 but the price is higher.

- User Authentication Technology - In the security and access system the user authentication is one important component that to identify the user. In this section, the two common user authentication technology that is Radio-Frequency Identification(RFID) and Near Field Communication (NFC) will be discussed

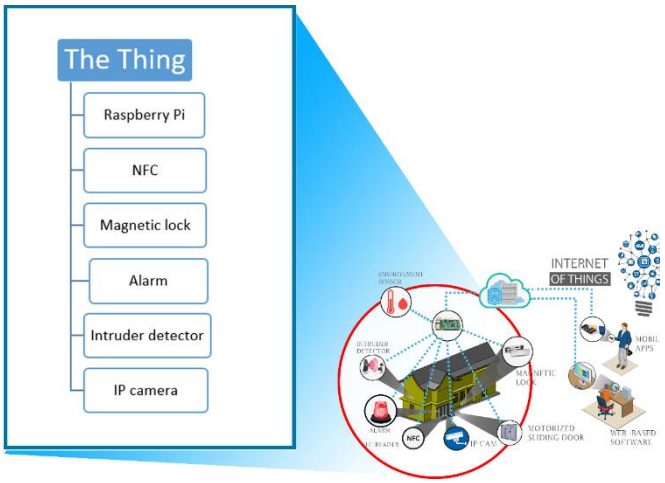


Figure 2 The Things

.

## B. *The Cloud*

The cloud is including server, database and enterprise services where people will refer or access to get or sent the information. In general, the server will get information or data then store it to the database if it is necessary. The cloud needs to setup fist to be functioning. It has required enterprise services to enable people to access it from the browser. There several tools and software required to setup the cloud. The software and the tools requirement will be show in figure 2 and in table 1

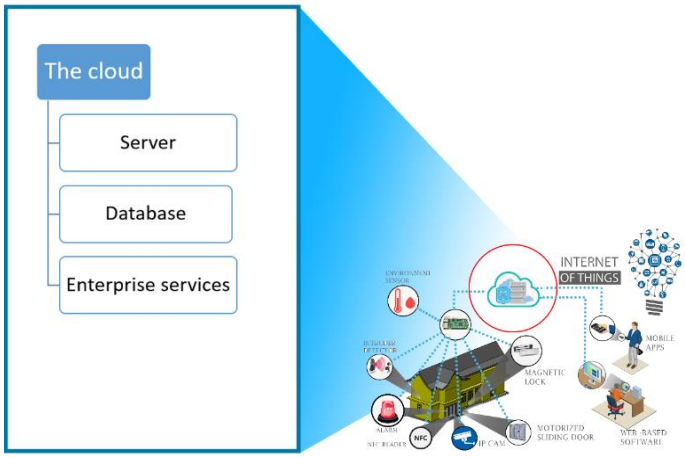


Figure 3 The cloud

Table 1:Cloud

| Cloud | Discription | Example |
|---|---|---|
| Server | An access manager that centralized the source of a program or services | Digital, ocean,local server |
| Database | The place where data collected or stored and can retrieve and control | MySQL,Mongodb |
| Enterprise services | SAP's term for services that have the proper scope to play a productive role in automating business processes in enterprise computing | Website |

## C. *The Network*

The network is the interconnection better the cloud and the Things. It is the technology that were using to communication in other words it is a data transmission medium. In this system, the raspberry pi will connect to the

cloud by using the Ethernet technology or also can using Wi-Fi since raspberry Pi has built in Wi-Fi and Ethernet port. For the software part the raspberry Pi using socket IO to communicate to the server since it need to communicate with the server all over the time. Figure 3 show the example included in the network layer.

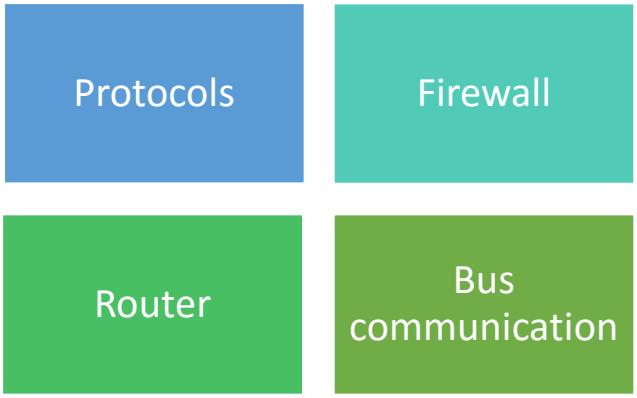


Figure 4 The Network

## III. RESULT

### A. *Hardware*

#### *1) Printed Circuit Board Design*

After finalize the main component that need in the circuit, the process was continue to the other part that is circuit design. In this part I was using proteus 8 software to design the circuit. The design was include design of circuit connection, designing of the PCB board, and the simulation of the board. All of this process done using proteus 8 software. The following figure 5 to 6 show the full schematic of this ras design :

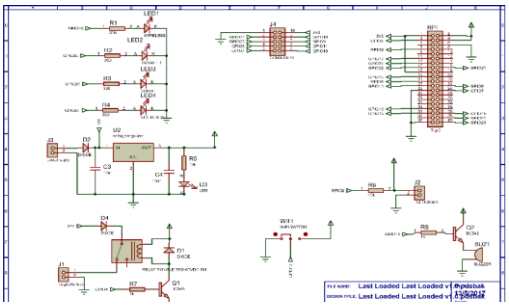

Figure 5 Raspberr Pi Extension Board schematic

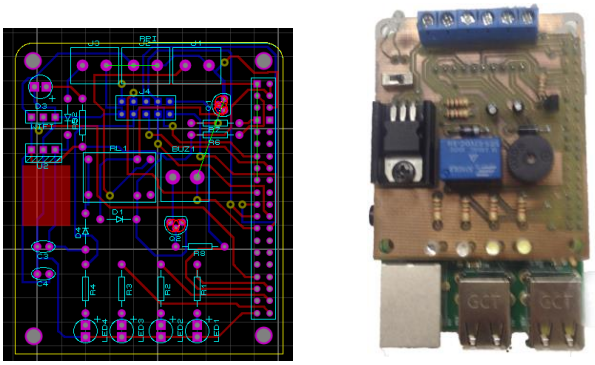

Figure 6 PCB design in proteus and PCB board

### B. *Software*

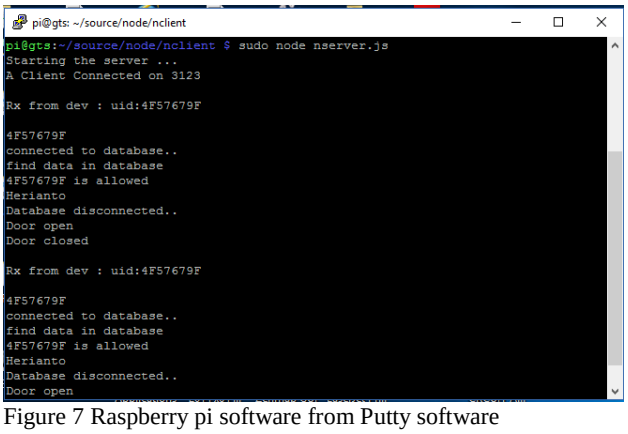


Figure 7 Raspberry pi software from Putty software

The software part is include imbedded coding in the raspberry pi that be the main device, local and server database, and website services are able work as the designed. The devise card is able read the id in the student Matrix card and any other NFC card. Then ,it will decide to open the door or not based on the data it store in the database. Figure 7 show the device allow a user to access the door from the putty software view.

For the administrative part the of these system, the admin website as show as figure 8 are able to view student log activities and manage the data in the database.

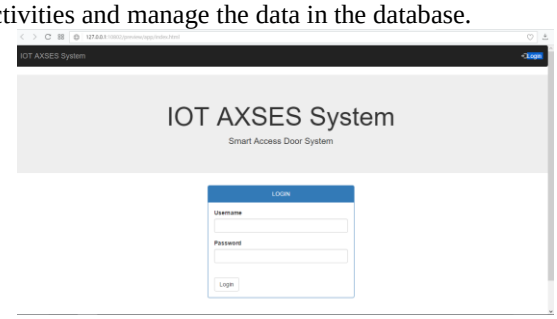


Figure 8 Administrative website

## IV. CONCLUSION

The project also includes the investigating the QoS problem of the developed system in term of latency. The system must have the lower latency; the system will be more efficient and reliable.

These systems help to solve unauthorized access cases in UTM residential building and will improve the security system. Moreover, it will make data manange of the building more efficient and will reducing the workforce to monitoring the building all over the time beside reducing operation cost to pay more guard. For the next part of this project, the focus will be on developing the hardware and provide complete solution for the system.

## REFERENCES

[1] 1. L. Atzori, A. Iera, G. Morabito,. The Internet of Things: a survey. s.l. : Computer networks 54, 2010. 2787–2805.

[2] 2. IoT-based Home Intercom System. AZMAN, NUR ZAFIRAH BINTI. s.l. : University Teknologi MalaysiaUTM), 2016.

[3] 3. Shayan, Nalbandian. .A survey on Internet of Things: Applications and challenges. Department of Information Technology, Islamic Azad University. Mashhad,Iran : IEEE, 2015.

[4] 4. M. Popa,H. Ciocarlie. An access system for buildings based on smart cards. "Politehnica" , Faculty of Automation and Computers,University of Timisoara. Timisoara : IEEE, 2011. p. Romania.

[5] 5. Ying-Wen Bai,Shi-Chang Chen. Design and Implementation of Home Intercom and Security Control Systems for Buildings. Department of Electronic Engineering, Fu Jen Catholic University. Taipei, Taiwan : IEEE, 2007.

# Double Cladding Fiber Structure Based Sensor for Simultaneous Measurement of Refractive Index and Temperature

Nur Fatiha binti Amat Bari
*Faculty of Electrical Engineering*
*Universiti Teknologi Malaysia*
*Johor Bahru, Malaysia.*
nurfatiha.ab@gmail.com

Asrul Izam bin Azmi
*Department of Communication Engineering*
*Faculty of Electrical Engineering*
*Universiti Teknologi Malaysia*
*Johor Bahru, Malaysia.*
asrul@fke.utm.my

***Abstract*—For the past few years, optical fiber has been chosen as one of the prominent "" applied in both biological and chemical industries. As optical fiber provides various advantages such as small size, light weight, small temperature dependence, all-fiber structure and high sensitivity, it gained so much interests in sensing applications. Double-cladding fiber (DCF) currently is considered as one of the most efficient, robust, and cost effective light sources available on the market. It offer large volumes for optical pumping. This paper presents the simultaneous refractive index and temperature sensor based on SMF-MMF-DCF. The result shows good and reliable performances. This sensing performance together with the advantages of optical fiber sensor is highly desirable by many application fields.**

***Keywords— double-clad fiber; simultaneous refractive index and temperature sensor***

## I. INTRODUCTION

Since a few years ago, fiber optic has been widely used in the field of sensors involving many parameters such as temperature, refractive index, vibration and other physical parameters. Fiber optic sensors serve many advantages compare to other type of sensors. Some of the advantages are freedom from EMI (Electromagnetic Interference), wide bandwidth, geometric versatility and economy, and can withstand high temperature and harsh environment.

Optical fiber was first used to explore the inside of human body. It is function by allowing voice, video and data transmission to occur with ever-increasing quality. With some advance changes in optical fiber, they are used to communicate with a sensor device or use a fiber as the sensor to conduct continuous monitoring physical, chemical and biological changes in the subjects. The information from optic fiber sensor is primarily conveyed by a change in either phase, polarization, frequency and intensity. In sensing, fiber act as modulator and also transducer. When fiber act as transducer, it converts measurement data such as temperature, stress, strain, rotation, electric and magnetic current into corresponding changes in optical radiation.

The structure of Double-Clad fiber (DCF) consisting of three layers of optical materials instead of two; the core, inner cladding and outer cladding. The three layers are made up of materials with different refractive index. The refractive index of the core is equal to the outer cladding, while the inner cladding has lower refractive index compare to the core and outer cladding.

Fiber optic refractive index (RI) measurement has become one of most important techniques in biosensor and chemical sensor system. However, the temperature cross-sensitivity usually causes imprecise determination of RI. Thus, it is necessary to measure the temperature simultaneously with the ambient RI. Different structures of optic fiber sensor have been proposed by some studies involving simultaneous measurement of temperature and refractive index by using fiber Bragg gratings (FBGs) and long-period gratings (LPGs). However, FBG is usually insensitive to ambient RI, while LPGs are strongly influenced by ambient RI.

On the other hand, in term of cladding mode, the cladding mode is sensitive to both SRI and temperature, while the core only sensitive to temperature. Hence, for simultaneous RI and temperature measurement, typical fiber sensor sensitive to both RI and temperature. It is not possible to be done because of error.

Thus, a simultaneous temperature and refractive index sensor based on SMF-MMF-DCF is being designed to develop simultaneous temperature and refractive index sensor and to overcome the cross sensitivity problem in optical fiber sensor.

## II. LITERATURE REVIEW

### *A. Optical Fiber Sensor*

Over the past few years, many product revolutions have taken place due to the growth of the optoelectronics and fiber optic communication industries. The reasons of optic fiber have been used widely in industries because it comes with many advantages which are small size, light weight, immunity to electromagnetic interference (EMI), high temperature performance, large bandwidth, high sensitivity, environmental ruggedness and the ability of distributed sensing [1].

The information of fiber optic sensors is primarily transmitted in all optical sensors by a change in either phase, polarization, frequency, intensity or a combination thereof. In

communication system, the signal that passing through a fiber is already modulated, whereas for sensing, the fiber itself act as a modulator. Other than that, fiber also can act as transducer and converts measurements data such as temperature, stress or strain.

### B. *Basic Concept for Fiber Optic Sensor*

Basically, fiber optic sensors can be loosely grouped into two basic classes which are extrinsic or hybrid fiber optic sensor, and intrinsic or all fiber sensors. Extrinsic fiber optic sensors consist of optical fibers that lead up to and out of a "black box" that modulates the light beam passing through it in response to an environment effect. While intrinsic fiber optic sensors rely on the light beam propagating through the optical fiber being modulated by the environment effect either directly or through environmentally induced optical path length changes in the fiber itself [2].

### C. *Fiber Intereferometer Sensor*

The use of interferometers in optical communication has widely established for many years. Interferometric sensors can provide the maximum in sensitivity when the technique is used in a way that is appropriate for the measurement of certain particular physical parameters, although cross sensitivity problem arise [4].

### D. *Freshnes'sl Reflection*

Fresnel's reflection can be defined as the reflection of a portion of light incident on a planar interface between two homogenous media having different refractive index. Fresnel's reflection occurs at the air-glass interfaces at entrance and exit ends of the optical fibers.

### E. *Temperature and Refractive Index Sensing*

In recent years, multimode fiber interference have been widely used for development of sensors, for example using a single-mode-multimode-single-mode (SMS) fiber structure [7] and a multimode-coreless-multimode (MCM) fiber structure [8]. However, all of these approaches proposed are single parameter measurement the SMS fiber structure proposed are basically transmission-type which is difficult to immerse the multimode fiber (MMF) into the measured material.

### F. *SMF-MMF Based Sensor*

A single-mode-multimode (SM) fiber structure was proposed before to measure simultaneous refractive index and temperature. There is formation of interference between the different modes in the multimode fiber. The wavelength of the interference minimum will vary the temperature of the solution. While the reflected intensity will vary with the RI of the solution due to the Fresnel reflection at the interface between the MMF and the solution. Hence, the simultaneous measurement of temperature and refractive index could be achieved [9].

## III. PROJECT METHODOLOGY

The design is determined by consider the design specifications required to achieve the goal of this project. The suitable structure of double-cladding based sensor is designed in the early stage. Then, it follows by the fabrication process involving cleaving, splicing and using microscope to construct the sensor. After that, the sensors are tested by conducting experiment which engross both refractive index and temperature measurements. All the data was then analysed by using Matlab or Microsoft Excel. Data analysis is done to observe the findings or final sensitivity of the proposed sensors.

### A. *Sensor Fabrication Process*

In this project, double-cladding fiber based sensor for simultaneous measurement of refractive index and temperature is designed. In fabrication process, Single-mode fiber (SMF), multi-mode fiber (MMF) and double-cladding fiber (DCF) is splice to each other by SMF-MMF-DCF order.

First and foremost, the design of double-cladding fiber based sensor for simultaneous measurement of refractive index and temperature is carried out. The schematic diagram of the proposed sensor is shown in Figure 1. Basically, SMF, MMF and DCF is fabricated by splicing to the order of SMF-MMF-DCF.

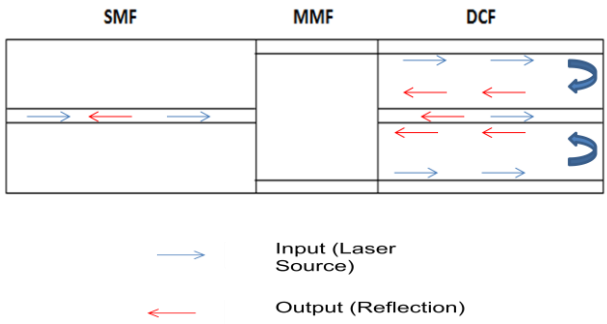


Fig. 1. Schematic Diagram of Double-Cladding Fiber Based Sensor For Simultaneous Measurement Of Refractive Index And Temperature

For this experiment, length of SMF and DCF will be constant while the length of MMF will be varied into three sample which are 0.4mm, 0.8mm and 1.2mm

Figure 2 shows the process of splicing process in order to complete the proposed structure sensor. First, the cable has to be stripped, removed the coats, and other protection layer, leaving the optical fibers naked. Then clean the fibers by using an optic clean wipe soaked with isorophyl alcohol. The fibers should be cleaned properly in order to remove dust that have the potential to increase the splicing loss as it can scatter and absorb light.

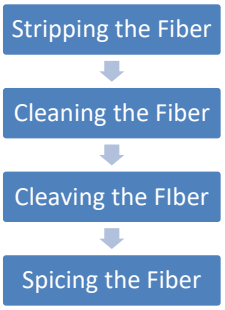


Fig. 2. The Process of Optic Fiber Fabrication

The end of the fibre was cleaved before the splicing process. It is necessary to make sure the condition of the cleaved fibre end face is totally flat and perpendicular to the fibre axis. The splicing loss will be lower when the cleave angle is near to 90°C.

Next, the SMF will be spliced to MMF and then spliced to the DCF. The splicing machine will estimate and display the optical loss of the splicing based on digital image processing technique.

### B. Experiment Setup

Figure 3 shown the experimental setup of double-cladding fiber based sensor for simultaneous measurement of refractive index and temperature. The sensor is connected to the Broadband Source (BBS) and an optical spectrum analyzer (OSA) by using circulator. The ASE source emitted wavelength at range from 1520 to 1580 nm .Illumination was provided through a Amplified Spontaneous Emission (ASE) light source., working in the L-band, and a circulator, being the output signal collected by an optical spectrum analyzer (OSA). The light from the broadband light source was passed through the SMF-MMF-DCF structured sensor. The light transmitted from the SMF-MMF-DCF will eventually received by an OSA and the transmission spectrum was then recorded.

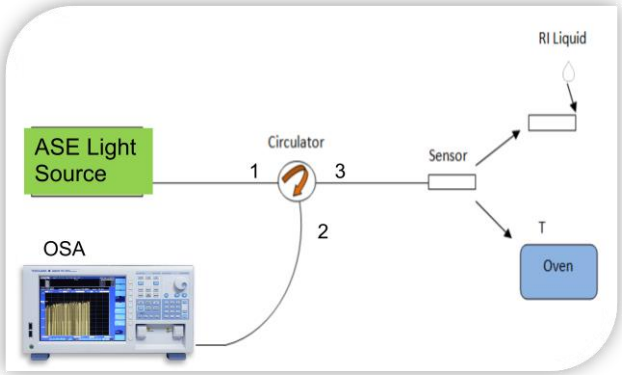


Fig. 3. Experimental Setup of double-cladding fiber based sensor for simultaneous measurement of refractive index and temperature

### C. Sensor Testing

For refractive index testing process, the end part of DCF is immersed with different value of refractive index solution. which are 1.35, 1.36, 1.37, 1.38 and 1.39. Whereas, for temperature testing process, the sensor will be testing by continuous heating of the sensor in a dry oven from 30 °C up to 100 °C. A digital thermometer was also used as a reference reading. Readings from thermometer and the corresponding transmission spectrum acquired by the OSA will be recorded.

### D. Experiment Control

The surrounding temperature were regulated by air conditioning system, hence ensuring that the measurements were taken under minimum ambient influence. During experiment, the surrounding temperature was kept in range between 22 °C and 28 °C. Also, the sensor was fixed in one place during the experiment to avoid any unnecessary

## IV. RESULT AND ANALYSIS

### A. Calculation

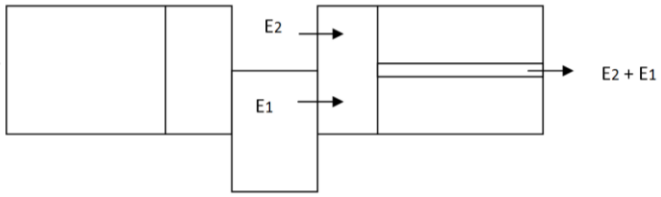


Fig. 4. Schematic Diagram of SMF-MMF-DCF Sensor

$$E1 = E01\, e^{-j(k1r - \Phi1)} \quad (1)$$

$$E2 = E02\, e^{-j(k2r - \Phi1)} \quad (2)$$

Where k = k0n = $\frac{krn}{\lambda}$ is wave vector, n is the refractive index of material, r is vector position.

Detected irridence or intensity of optical signal by photodetector is given by:

$I(r) = E(r)^2$

For this case, $E = E1 + E2$ (3)

$I = E1 + E2^2$

$= (E1 + E2)(E1 + E2)^*$

$= E1E1^* + E1E2^* + E2E1^* + E2E2^*$ (4)

Substitute (1) and (2) into (4) and cancel out:

$I = Eo1^2 + E02^2 + E01E02\,(e^{-j[(k1-k2)r-(\Phi1-\Phi2)]} + e^{j[(k1-k2)r-(\Phi1-\Phi2)]}$

$= Eo1^2 + E02^2 + 2E01E02 \cos[(k1-k2)r - (\Phi1 - \Phi2)]$

$Eo1^2 = I1$ , $E01 = \sqrt{I1}$

$E02^2 = I2$ , $E02 = \sqrt{I2}$

$\Rightarrow E01E02 = \sqrt{I1I2}$

For 2 optical wave originated from same source ($\lambda1 = \lambda2 = \lambda$) propagated through 2 different RI with same length:

$I = I1 + I2 + 2\sqrt{I1I2} \cos(k1r - k2r)$

$= I1 + I2 + 2\sqrt{I1I2} \cos(\frac{2\pi n1L}{\lambda} - \frac{2\pi n2L}{\lambda})$ , assume $\Phi1 = \Phi2$

$= I1 + I2 + 2\sqrt{I1I2} \cos(\frac{2\pi(n1-n2)L}{\lambda})$

$= I1 + I2 + 2\sqrt{I1I2} \cos(\frac{2\pi\Delta nL}{\lambda})$

$= I1 + I2 + 2\sqrt{I1I2} \cos\delta$, $\delta = \frac{2\pi\Delta nL}{\lambda}$

$I1 + I2 + 2\sqrt{I1I2} \cos\delta$

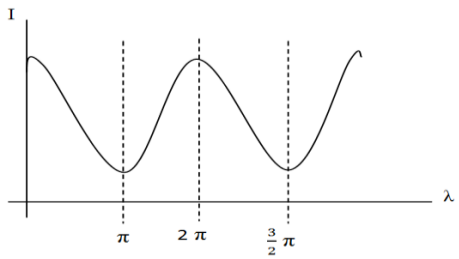


Dip occur every (2N + 1) π , N= 0,1,2 (integer)

Peak occur every 2N π , N= 0,1,2….

$\delta = \frac{2\pi\Delta nL}{\lambda}$ , where $\frac{2\pi\Delta nL}{\lambda}$ must be multiple of (2N + 1) π to reach minimum value / dip.

Condition to dip wavelength:

$\frac{2\pi\Delta nL}{\lambda} = (2N + 1)\,\pi$

Condition for peak wavelength:

$\frac{2\pi\Delta nL}{\lambda} = 2N\pi$

$\lambda dip = \frac{2\pi\Delta nL}{(2N-1)\pi}$ , $\lambda peak = \frac{2\pi\Delta nL}{2N\pi}$

Free spectral range (FSR) between 2 successive transmitted $\lambda$: (i.e $\lambda seperation$)

$\delta = \frac{2\pi\Delta nL}{\lambda}$

$\frac{d\delta}{d\lambda} = \frac{2\pi\Delta nL}{\lambda}$

$d\delta = \frac{2\pi\Delta nL}{\lambda^2} d\lambda$ (remove negative sign )

Substitute dδ = 2π (because the phase difference between 2 peak is 2π )

$2\pi = \frac{2\pi\Delta nL}{\lambda^2} d\lambda$

$d\lambda = \frac{\lambda^2}{\Delta nL}$

RI sensitivity:

$\lambda dip = \frac{2\pi\Delta nL}{(2N-1)\pi}$

$= \frac{2(n1-n2)L}{(2N-1)}$

Only n2 is changed,

$\frac{d\lambda dip}{dn2} = \frac{-2L}{2N-1}$

$$d\lambda dip = \frac{-2L}{2N-1}\, dn2$$

Temperature sensitivity:

$d\lambda N = [\frac{1}{\Delta n}\frac{d(\Delta n)}{dT} + \frac{1}{L}\frac{dL}{dT}]\ \Delta T\ (\lambda N)$

## B. *Result Analysis for Refractive Index Sensor*

The liquid samples which having refractive indices of 1.35, 1.36, 1.37, 1.38 and 1.39 were used for the refractive index measurement. Figure 5 shows the transmission spectra of the refractive index sensor with different surrounding refractive indices.

When the refractive index was varied from 1.35 to 1.39, peak wavelength did not show any differences. All the peak power land on 1539 nm. However, there are shift in power value for every refractive index value. Figure 6 shows the power value for peak and dip of different refractive index. The higher the refractive index value, the lower the power.

For refractive index sensor, ΔP should be maximum and Δλ should be minimum. As for this experiment, the value of ΔP is $0.85x10^{-6}$ W while Δλ is 0.12nm.

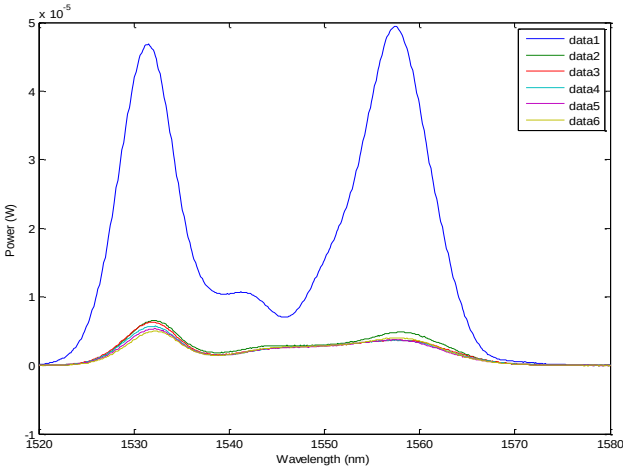


Fig. 5. Transmission spectra of the refractive index sensor based on SMF-MMF-DCF with different refractive indices

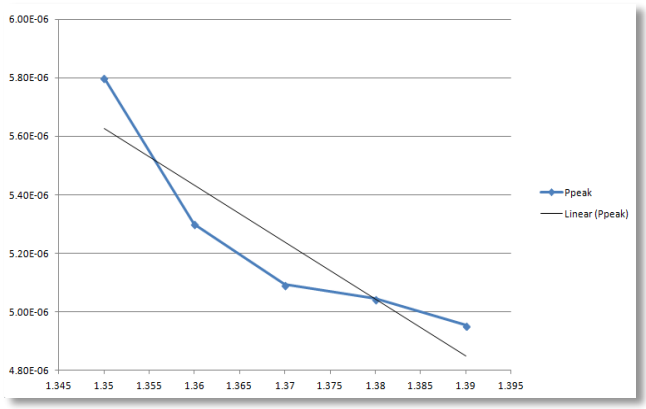


Fig. 6. Power shift of simultaneous refractive index and temperature sensor based on SMF-MMF-DCF versus refractive index

## C. *Analysis of Sensor Temperature Sensitivity*

Figure 7 shows the wavelength shift of the peaks with the increase of oven temperature. The shift of the peak in the

transmission spectra can be observed as the refractive index of the sensor is temperature dependent.

When the temperature was increased from 30 to 100 °C, the center wavelength of the first peak was changed from 1542.08 nm to 1544.66 nm, corresponds to the total wavelength shift of 2.58 nm. The shifted of the wavelength of the first peak is plotted in Figure 8. The result shows that the sensor has a linear relationship with the temperature.

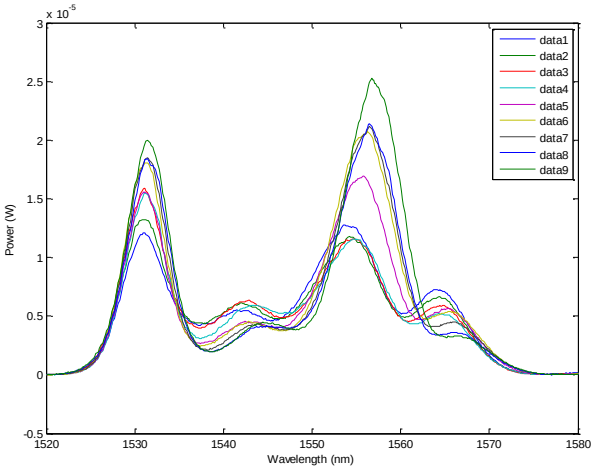


Fig. 7. Transmission spectra of simultaneous refractive index and temperature sensor based on SMF-MMF-DCF with different temperature

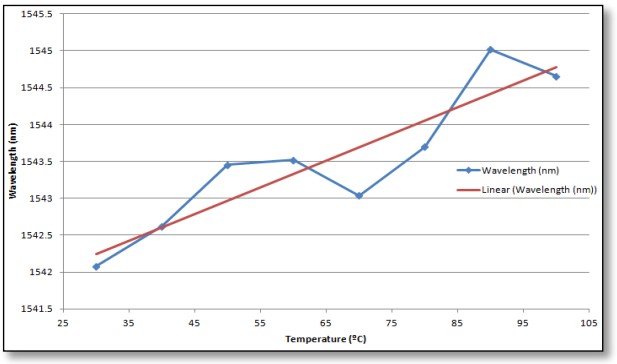


Fig. 8. Wavelength shift of simultaneous refractive index and temperature sensor based on SMF-MMF-DCF versus temperature

Although the sensor marked small temperature sensitivity, the result obtained for refractive index measurement was unaffected by temperature effect as the experiment was conducted in temperature controlled environment.

## V. CONCLUSION

This project has presented the simultaneous refractive index and temperature based on SMF-MMF-DCF. With suitable techniques, this sensor can provide sensitivity that are suitable for various applications. The results showed promising and reliable performance. This type of sensor is very attractive since it can be simply conducted in any optical laboratory. Moreover, the proposed refractive index sensor has the advantages such as reusable, small and flexible size, simple and convenient fabrication, it opening to future prospect in the chemical and biological sensing fields

## REFERENCES

[1] [1] G. Bahareh and N Hooman (2008). Fiber Optic Sensors. World Academy of Science, Engineering and Technology 42.

[2] [2] T. S. Y. Francis and Y. Shizuo (2002). Fiber Optic Sensors, Marcel Dekker Inc. , United States of America

[3] [4] L. S. Grattan and B. T. Meggit (2013). Optical Fiber Sensors Technology: Fundamentals, Springer Science and Business Media, New York

[4] Q.Wu, A. M. Hatta, P. Wang, Y. Semenova, and G. Farrell, Use of a Bent Single SMS Fiber Structure for Simultaneous Measurement of Displacement and Temperature Sensing, IEEE Photon. Technol. Lett. , Vol. 219, pp. 130-132, 2011

[5] Y. Jung, S. Kim, D. Lee, and K. Oh, Compact Three Segmented Multimode Fibre Modal Interferometer for High Sensitivity Refractive Index Measurement, Meas. Sci. Technol., Vol. 17, pp. 1129-1133, 2006

[6] X. Hongchao, M. Hongyun, W. Wei, X. Rui, Y. Qiqi, and H. Ben, Single-Mode-Multimode Fiber Structure Based Sensor for Simultaneous Measurement of Recractive Index and Temperature, IEEE Sensors Journal, Vol. 13, pp. 4220-4223, 2013

# Design of Optical Coupler Based on MMI Structure

Muhammad Irfan bin Tarmizi
*Faculty of Electrical Engineering*
*Universiti Teknologi Malaysia*
*Johor Bahru, Malaysia.*
*irfantarmizi94@gmail.com*

Ahmad Sharmi bin Abdullah
*Department of Communication Engineering*
*Faculty of Electrical Engineering*
*Universiti Teknologi Malaysia*
*Johor Bahru, Malaysia.*
*sharmi@utm.my*

***Abstract*— In optical communication system, optical coupler has become main attraction in research due to the interest of its effect in integrated optics and its advantage. From this statement, it is very important to design and develop optical coupler with high performance and low power consumption with low crosstalk. In recent years, the interest towards Multimode Interference (MMI) effects has been increase drastically in integrated optics. The unique properties of MMI such as low crosstalk, large optical bandwidth and excellent fabrication process make it has more potential to be used in many applications such as couplers, switches, filters and routers. Different types of materials such as silica, polymers and silicon are being used to prove that different materials can give different performance of optical switch. The optical coupler is designed on the 2x2 MMI cross coupler architecture of optical switch based on general interference mechanism. The propagation of light and characteristics of waveguide had been simulated by using BeamPROP software which is based on Beam Propagation Method.**

***Keywords—optical, multimode interference, BeamPROP, coupler, crosstalk***

## I. INTRODUCTION

As development of optical fiber communications and integrated optical electronics scale up, the popularity for research work in this area are increasing as well. The population of telecommunication system leads to the demand for increasing bandwidth capacity. This is the main reason why the world needs telecommunications system that can fit on the flexibility and configurability. The problem can be overcome by introducing new communication revolution based on photonic technology. The implementation of optical communication system as medium to transmit data has become major concern in communication field due to its advantage in performance. The main advantage of using photonic application is its extremely large information carrying capacity and low transmission losses.

There are several structure of optical coupler and the most common one is Directional Coupler which produces devices with large dimensions. The MMI Couplers based on self-imaging principle has many advantages compared to other structure such as low optical loss, small and compact in size. This characteristic of coupler makes it the best option to be choose in optical circuit.

Materials with different advantages have been explored and being used for fabrication of waveguide. The materials include silica, silicon and various types of polymers with different refractive index. All of these materials have their own advantages and disadvantages to their counterpart. Due to their ability to produce at lower cost, polymeric materials had been extensively used in optical switch development (Yao et al., 2002). It is believed that excellent performance of optical switch can be achieved by combination of suitable material such as polymer and superior structure like MMI structure.

In this project we have designed the MMI Coupler for its advantage which were enhanced to diminish losses and reduced the crosstalk at the output waveguide.

## II. LITERATURE REVIEW

### *A. Optical Waveguide Analysis*

This chapter presents the fundamentals and brief concepts of optical waveguide theory and the techniques used. Other than that, the types of optical waveguide were also introduced in this chapter.

Optical waveguide and optical fibre consist of a core, in which light is confined, and a cladding, or substrate surrounding the core [1]. Optical waveguide can be defined as physical medium which trap light locally and guide it in a specific direction [2]. It is very difficult to construct waveguide mainly from metal because the characteristics of metal itself which having a complex permittivity with large absolute value. This is the main reason why waveguides are constructed by joining appropriate dielectrics.

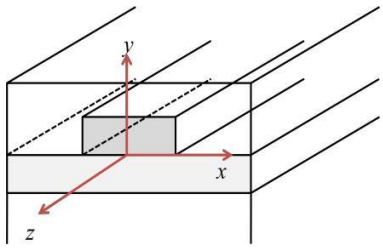


**Fig. 1**: Basic Optical waveguide structure [2]

Figure 2.1 above shows the basic structure of optical waveguide. It consists of thin film which has higher refractive index compared to substrate and upper cladding. Basically, optical waveguide can be classified into two main categories which are planar/slab waveguide (2D) and channel waveguide (3D). Planar/slab waveguide confine light propagation only in 1 dimension, another dimension will lead light to propagate indefinitely.

*1) Waveguide Parameter*

*a) Refractive Index* : In optical, the refractive index, n, of a substance (optical medium) is describes as how light or any other radiation propagates through a certain medium.

There are a law that describe the refractive index which is Snell's law of refraction, $n_1 \sin \theta_1 = n_0 \sin \theta_0$.

*b) Total Internal Reflection* : Basically, the guiding of light is a consequence of a total internal reflection from the interface between the core and cladding by the fact that the refractive index of core is higher than cladding. The equation below describe total internal reflection :

$$n_1 \sin \left(\frac{\pi}{2} - \emptyset\right)$$

For total internal reflection, angle of incident light must be greater than critical angle where $n_1$ is the index of the core and $n_2$ is the index of cladding

*2) Channel Optical Waveguide*

In integrated optics, the most practical structure is channel waveguide. This type of structure allows the flexible routing of light around the waveguide surface [3]. In order to facilitate the construction of optical integrated circuits, various types of channel waveguide which traps light in both x and y directions have been devised [2].

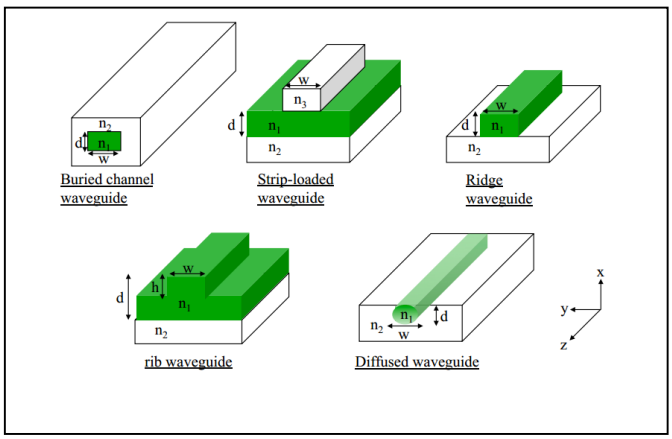


**Fig. 2**: Most common structure for channel waveguide [4]

For this project, ridge waveguide was used as the main optical waveguide structure in the simulation. A ridge waveguide structure is a waveguide that looks like a strip waveguide but the ridge (on top of its planar) has high index and it is actually the waveguide core.

## *B. Optical Coupler*

Optical fiber couplers are one of the key components of an optical fiber system since it has the ability to transfer light from one fiber to another. An optical coupler also could be used as a splitter that allows light signal to be shared between multiple fibers. Generally, the couplers can be categorized such as bi-directional coupler, star coupler and multimode interference coupler (MMI). MMI coupler can split the power among more than two waveguides [15].

MMI couplers are widely used in many PLCs application such as power splitter [16], optical switches [17] and ring laser [18]. MMI couplers are based on self-imaging principle and offer some advantages of the compact size, low crosstalk and low power imbalance. Other than that, MMI structure show superior in scalability since they do not need to be cascaded to achieve large port counts.

*1) Materials used in Optical Coupler*

To design and develop a good and functional optical coupler, it usually needs to know the materials that were used for fabrication. Many researchers have been investigated variety types of materials for optical waveguide. It is desirable to fabricate all the components on silicon substrate for integrated optics [5]. For this research, polymeric material has been chosen due to its advantage which is ease of fabrication process and its properties.

There are several inorganic materials capable of multiple functions are under research including Silica (SiO2), Silicon (Si), Sol-Gels and Polymers. Among all of these materials, polymeric materials offer advantages over the aforementioned materials. They have attracted lot of attention in optical network because they have potential to produce at low cost. The switching time of the polymer based optical switch is faster since it can react faster with the heat applied. A number of polymers have been shown to demonstrate capability in a variety of demanding applications [6]. However, polymers have its drawback such as prone to aging problems, poor mechanical resistance and low thermal stability which can reduce its long-term reliability [7].

## *C. Structure of Optical Coupler*

The Multi-Mode Interference (MMI) consists of multi-mode waveguide regions and one or more single mode input/output waveguide [10]. The MMI device generally consists of three parts: input ports (or left ports), a MMI area output ports (or right ports). A typical MMI device is usually an M-input-and-N-output device with tapered functions. The property of MMI coupler is based on the principal of the self-imaging effect [12-13]. The principle can be stated as the input is reproduced in single or multiple images at periodic intervals along the propagation direction of the guide [14]. MMI thermo-optic couplers consume less power. Switching device based on MMI

are also generally robust against processing intolerance compared to MZI and directional coupler (DC) counterparts.

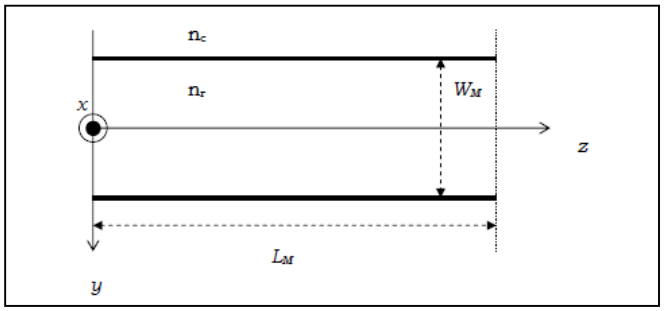


**Fig. 3**: Basic configuration of MMI structure

Couplers based on MMI structure have been realized and being used in many materials such as $SiO_2$, GaAs and from that material, excellent performance had been reported. An MMI coupler is based on the self-imaging principle of a multimode waveguide. There are 3 types of MMI structures according to the different position of the input waveguide. They are general Multimode Interference (GMMI), Paired Multimode Interference (PMMI) and Symmetric Multimode Interference (SMMI) [19].

**Table 1**: Comparison of three MMI structures

| Structure of MMI | GMMI | PMMI | SMMI |
|---|---|---|---|
| Position of input waveguide | $w_e/(N+1)$ | $w_e/3$ and $2w_e/3$ | At the center of the multimode waveguide |
| Length of multimode waveguide | $3L_\pi/N$ | $L_\pi/N$ | $3L_\pi/(4N)$ |

For MMI coupler with straight configuration, the length is directly proportional to the square of the width of multimode waveguide. Usually, the width of the multimode waveguide in a straight MMI is determined by the number of ports and the space between different ports. Increasing the number of ports by a factor of two will result a corresponding double of the MMI width and the length of the MMI will be quadrupled.

There are 2 types of cross couplers that can be designed and simulated which is general interference and restricted interference. Restricted interference can be further divided into paired and symmetric interference. In general interference, single images of the input field will be formed at the following locations:

$L_M = p(3L_\pi)$ with p = 0,1,2,3,……

p= periodic nature of imaging along multimode structure

$L_\pi = \frac{\pi}{\beta 0 - \beta 1}$

## III. Methodology

Before starting this project, the planning and methodology has been taken into account and all of the steps to complete this project were done carefully. To get better understanding, each steps starting from data gathering until thesis writing was planned. Other than that, methodology also will help us to always keep the research on track.

For this project, first of all, during semester one for FYP 1 the simulation was done to get the basic knowledge of ridge waveguide structure. This is to ensure that we can understand the basic knowledge first before doing the complicated which is optical coupler. However, to do the simulation part, the refractive index value for each material must be obtained first. From literature review, the exact value of refractive index for each material was taken and used in the simulation.

From the simulation, the simplest structure of the ridge waveguide was fabricated and the materials were varied to investigate their performance. The optical coupler for this project will be designed in semester two and the main focus for this semester is to design the ridge waveguide and investigate their performance when different materials are used as their core. The waveguide will be used as input and output ports for MMI optical coupler later.

During semester two, the optical coupler is designed and simulated using BeamPROP software to investigate their performance using different types of materials. The materials used for core and substrate are changed but the couplers are based on the same configuration. The important part for this project is to calculate the width and length of the multimode region to be used. There are 2 input waveguide and 2 output ports that will be used for the coupler that will become 2x2 configuration.

## IV. Result and Discussion

This section will discuss and explain about the result of BeamPROP simulation for ridge waveguide and optical coupler MMI. The main material that is used for core of the waveguide is polymer.

The fabrication of ridge waveguide focuses mainly on single mode propagation structure. The main objective to simulate the ridge waveguide is to make sure the waveguide that will be used later for designing the coupler are single mode waveguide which will only allow one mode to propagate through it.

As a coupler, several performance parameters, the crosstalk and insertion loss should be evaluated and calculated. The crosstalk is defined as a ratio of the undesired power output ($P_u$) to desired power outputs ($P_d$) while insertion loss can be described as ratio of the input power to the output power at one of the output ports of the coupler.

One of the most critical issues when designing the MMI structure is the width of the multimode. The width must be obtained first to get the optimum length of MMI.

For this project, the wavelength of light propagate through the waveguide is fixed to 1550nm throughout all of the couplers. For communication wavelengths near 1550nm, polymers waveguide are popular among others because they are simple to process, cost effective and has low optical loss.

The decision to choose what materials that needed for fabrication of coupler is highly depending on criteria on that specific material such as easy processing, high stability and low cost processing. There are 2 main materials that were used in this project as the core material of the coupler. A BenzoCyclobutene (BCB 4024-40) polymer and photosensitive hybrid sol-gel material known as VTT are used with difference refractive index to measure which one has high performance in optical devices. Both of this material has their own advantages and disadvantages for the use in optical application.

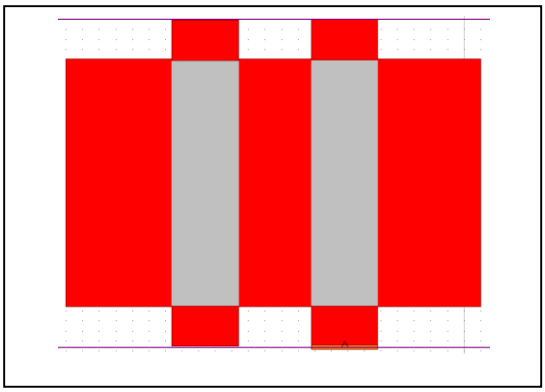

**Fig 4:** Schematic layouts of 2x2 cross coupler

Fig.4 above shows the layout of optical cross coupler with VTT material with refractive index of 1.4860 as a core, quartz substrate with refractive index of 1.4442 and surrounded by air (refractive index=1) cladding. The dimension of the single input and output waveguide structures were 3µm x 4µm of height by width respectively. The width of MMI region was 25µm. The length of MMI region was then obtained by using the equation and the length for this structure was 2463.9µm.

The MMI optical coupler was then simulated using BeamPROP software. The MMI coupler was designed with 2x2 configuration based on paired interference mechanism. The single mode waveguides were placed at the input and output ports. The simulation result are shown in Fig. 5.The right figure shows normalized optical power monitored along the propagation of MMI waveguide structure and the left shows the top view of optical propagation inside the cross coupler structure.

For MMI optical cross coupler, the performances are fundamentally characterized by the insertion loss and the crosstalk. Average insertion loss about 1.26 dB and crosstalk of about -1.11 dB were found in this MMI cross coupler.

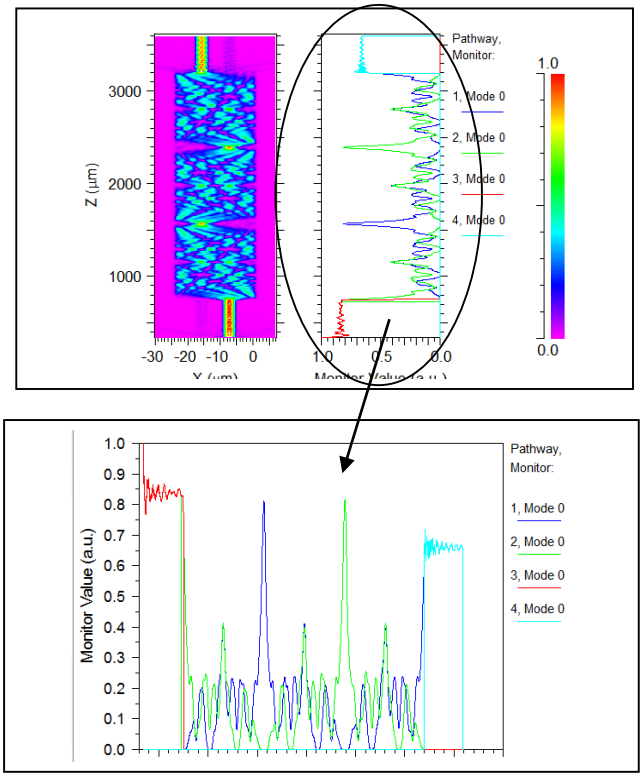


**Fig. 5:** Optical propagation in 2x2 MMI coupler

## V. CONCLUSION

According to the main objective of this project, the previous chapter has briefly explained the important issue in development of optical waveguide and Multimode Interference (MMI) based on several materials, BenzoCyclobutene (BCB 4024-40) polymer and mixture of sol-gel organic-inorganic material, VTT. Self-imaging principle has been briefly stated prior to the further discussion of MMI effect. MMI optical coupler based on paired interference were successfully designed using polymer and sol-gel material and both of them show different performance parameter, crosstalk and insertion loss. To be effectively employed in optical application, the MMI cross coupler should exhibit low crosstalk and low insertion loss. Both of this parameter were evaluated and calculated in the previous chapter

## REFERENCES


[1] Okamoto, K. (2006). Fundamentals of Optical Waveguides. Japan: Academic Press

[2] Koshiba, M. (1992). Optical Waveguide Analysis. New York: McGraw-Hill

[3] Zappe H.P. (1995). Introduction to Semiconductor Integrated Optics. Artech House Publisher. Boston. London

[4] Jia Ming Liu. Photonic Devices, Chapter 2

[5] H. Ma, A. K. Y. Jen, L. R. Dalton, "Polymer Based Optical Waveguides: Materials, Processing and Devices," Advanced Materials, Vol. 14, pp. 1339-1365, 2002.

[6] Louay Eldada, Polymer Integrated Optics. Promise vs. Practicality. Proc. SPIE. 4642: 11-22. 2002

[7] P. Coudray et al., "Integrated optics based on organic-material materials," Materials Science in Semiconductor Processing, Vol. 3, pp 331-337, 2000

[8] Giuseppe Coppola, Luigi Sirleto, Ivo Rendina, Mario Iodice (2011) "Advanced in Thermo-optical Switches: Principles, Materials, Design and Device Structure," Opt. Eng. 50(7), 071112 (May 05, 2011)

[9] Georgios I. Papadimitriou, "Optical Switching: Switch Fabrics, Techniques and Architectures," IEEE Journal of Lightwave Technology., Vol. 21, No 2, February 2003

[10] Tarek S. El-Bawab. (2006). Optical Switching. United States of America, Springer Science + Business Media, Inc

[11] Samdin et al., "Crosstalk Improvement of Polymer in Glass Thermo-Optical Multimode Interference Switch," Telkomnika, Vol. 10, No. 2, June 2012, pp. 371-378

[12] Bryngdahl O. Image formation using self-imaging technique. Journal of the Optical Society of America. 1973; 63: 416-419

[13] Ulrich R and Ankele G. Self-imaging in Homogenous Planar Optical Waveguides. Applied Physics Letters. 1975. 27; 337-339

[14] Soldano LB and Penning MC. Optical Multi-Mode Interference Devices Based on Self- Imaging: Principle and Application. IEEE Journal of Lightwave Technology. 1995; 13: 615-627

[15] H. G. Van Zyl, "Modeling of integrated optic components for lightwave communications systems using the beam propagation method," M.Eng.dissertation, Rand Afrikaans University, Johannesburg, Republic of South Africa, 2001.

[16] L. B. Soldano, F. B. Veerman, M. K. Smit, B. Verbeek, A. H. Dubost, and E. C. M. Pennings, "Planar monomode optical couplers based on multimode interference effects," *Journal of Lightwave Technology*, vol. 10, no. 12, pp. 1843–1850, 1992.

[17] F. Wang, J. Yang, L. Chen, X. Jiang, and M. Wang, "Optical switch based on multimode interference coupler," *IEEE Photonics Technology Letters*, vol. 18, no. 2, pp. 421–423, 2006.

[18] Y. Shi, "Design, simulation of characterization of some planar lightwave circuits (PLC)," Ph.D. dissertation, KTH School of Information and communication Technology, Stockholm, Sweden, 2008.

[19] Lucas. B. Soldano and Erik C. M. Pennings, "Optical Multi-mode Interference Based on self-imaging:principle and application"s, .1. Of Lightwave Technol, 1995 l3(4):615-627

ISBN 978-967-0194-94-3

UTM
UNIVERSITI TEKNOLOGI MALAYSIA

Faculty of
Electrical Engineering